Title
Setting the Record Straight: Bottom-Up Carbon Nanostructures via Solid-State Reactions

Author
Jordan, Robert Stanley

Publication Date
2017

Peer reviewed|Thesis/dissertation

UNIVERSITY OF CALIFORNIA

Los Angeles

Setting the Record Straight:

Bottom-Up Carbon Nanostructures via Solid-State Reactions

A dissertation submitted in partial satisfaction of the

requirements for the degree Doctor of Philosophy

in Chemistry

by

Robert Stanley Jordan

2017

ABSTRACT OF THE DISSERTATION

Setting the Record Straight:

Bottom-Up Carbon Nanostructures via Solid-State Reactions

by

Robert Stanley Jordan

Doctor of Philosophy in Chemistry

University of California, Los Angeles, 2017

Professor Yves F. Rubin, Chair

Chapter 1 describes the development and spectroscopic investigation of a novel synthetic route to *N*=8 armchair graphene nanoribbons from polydiacetylene polymers. Four distinct diphenyl polydiacetylene polymers are produced from the crystal-phase topochemical polymerization of their corresponding diphenyl-1,4-butadiynes. These polydiacetylene polymers are transformed into spectroscopically indistinguishable *N*=8 armchair graphene nanoribbons via simple heating in the bulk, solid-state. The stepwise transformation of polydiacetylenes to graphene nanoribbons is examined in detail by the use of complementary spectroscopic methods, namely solid-state nuclear magnetic resonance, infrared, Raman and X-ray photoelectron spectroscopy. The final morphology and width of the nanoribbons is established through the use of high-resolution transmission electron microscopy. Chapter 2 chronicles the implementation of a similar approach to *N*=12 armchair graphene nanoribbons from a dinaphthyl substituted polydiacetylene polymer. The mild nature of the process and pristine structure of the nanoribbons is again confirmed with

the use of spectroscopic and microscopic methods. The chapter concludes with preliminary electrical measurements of the nanoribbons confirming that they are indeed conductive. Chapter 3 details the development of a synthetic route to diaryl *trans*-enediynes as structural models of individual reactive units within a polydiacetylene polymer. The *trans*-enediynes described are found to undergo three distinct annulation reactions depending on reaction conditions. Finally, the synthetic routes developed are utilized to access diethynyl [5]helicenes and phenanthrenes which fueled studies on the mechanism of the Bergman polymerization reaction.

The dissertation of Robert Stanley Jordan is approved.

Richard B. Kaner

Jorge R. Barrio

Yves F. Rubin, Committee Chair

University of California, Los Angeles

2017

This dissertation is dedicated to my family,

Mom, Dad, Richard and Stephanie

TABLE OF CONTENTS

LIST OF TABLES, FIGURES AND SCHEMES

Introduction

Chapter 1

Chapter 2

Chapter 3

LIST OF ABBREVIATIONS

ACN	acetonitrile
CHD	1,4-cyclohexadiene
COSY	correlation spectroscopy
CNT	carbon nanotube
CP/MAS	cross-polarization magic angle spinning
DART	direct analysis in real time
DCC	dicyclohexylcarbodiimide
DCM	dichloromethane
DFT	density functional theory
DIPEA	diisopropyl ethyl amine
DMAP	dimethyl amino pyridine
DMF	dimethyl formamide
Et_3N	triethylamine
Et_2O	diethyl ether
FET	field-effect transistor
FFT	fast Fourier transform
FT-IR	Fourier-transform infrared spectroscopy
FVP	flash vacuum pyrolysis
GIAO	gauge-independent atomic orbital
GC-MS	gas chromatography mass spectrometry
GNR	graphene nanoribbon
$_A$GNR	armchair graphene nanoribbon
$_Z$GNR	zig-zag graphene nanoribbon
HMBC	heteronuclear multiple-bond correlation spectroscopy
HMPA	hexamethylphosphoramide
HRMS	high-resolution mass spectrometry
HRTEM	high-resolution transmission electron microscopy
HSQC	heteronuclear single-quantum correlation spectroscopy
LiHMDS	lithium hexamethyldisilylazide
MALDI-TOF	matrix assisted laser desorption ionization time of flight

MeOH	methanol
MeI	methyl iodide
MOM	methoxymethyl
n-BuLi	*n*-butyl lithium
NOESY	nuclear Overhauser effect spectroscopy
NMR	nuclear magnetic resonance
OTS	octadecyltrichlorosilane
PDA	polydiacetylene
ppt	percipitate
PTA	polytriacetylene
SAED	selected-area electron diffraction
SEM	scanning electron microscope
SSFVP	solution spray flash vacuum pyrolysis
SM	starting material
STM	scanning tunneling microscopy
TBAF	tetra *n*-butyl ammonium fluoride
TEM	transmission electron microscopy
TfOH	trifluoromethanesulfonic acid
TIPS	triisopropylsilyl
THF	tetrahydrofuran
TLC	thin layer chromatography
TOCSY	total correlation spectroscopy
TMEDA	tetramethylethylenediamine
UV	ultraviolet
UV-Vis	ultraviolet-visible
UV-vis-NIR	ultraviolet-visible-near infrared
XRD	X-ray diffraction
XPS	X-ray photoelectron spectroscopy

ACKNOWLEDGEMENTS

This dissertation would not have been possible without the love, friendship and support of many people. I will attempt futilely to name most of them here, but for those of you I miss, you are not forgotten.

Firstly, I would like to thank my teachers throughout my education, without your help, inspiration and patience none of this would have been possible.

I would like to thank my undergraduate mentors, Prof. Don Deardorrf and Prof. Michael Hill of Occidental College. It was you who first got me interested in actually doing science and you who supported me in this formational time in my life. You went out of your way to help me find my path in this life and for that I am deeply thankful.

I would like to thank Prof. Patrick Harran of UCLA. The years I spent working under Patrick made me the synthetic chemist I am today. Prof. Harran's deep knowledge and love for synthesis left a deep mark on the way I look at problems, and the beauty and opportunity often present within them.

I would like to thank my colleagues,

Andrew G. Roberts for taking me under his wing when I entered UCLA. His patient mentorship and support provided me with a tremendous opportunity to learn the art of synthetic chemistry. Tristin Rose for challenging me with hard-hitting questions and always demanding excellence.

Nicholas Knutson, Robert Thompson, Simon Kervyn, and Yolanda Li for making me feel at home in the Rubin lab.

Ryan McCurdy for asking challenging questions, providing a pair of hands, and being a great friend to have around in lab.

Jessica Wang, Chris Turner, Matt Kowal and Cheng-Wei Lin of the Kaner lab at UCLA. You introduced me to materials chemistry and a different way to look at the molecules I make.

My friends in climbing, chemistry and beyond.

My family, mom, dad and Richard. You have supported me and believed in me since my birth. Thank you.

Stephanie Quan, our relationship has been a consistent positive force in my life and I look forward to planning trips, climbing, and watching shows with you in the future.

Finally, I would like to thank my graduate advisor Prof. Yves Rubin. Yves and I met at a distinct turning point in my life, and I will never forget the opportunity that he gave me. Yves provided me with a space to do science and a constant flow of interesting ideas. Most importantly, he gave me the freedom to try my own ideas and solve problems on my own. My relationship with Yves has transformed me into the scientist that I am today and I am deeply grateful for his mentorship and support these past four years.

Chapter 1 is a version of [Jordan, R. S.; Li, Y. L.; Lin, C-W.; McCurdy, R. D.; Lin, J. B.; Brosmer, J. L.; Marsh, K. L.; Houk, K. N.; Kaner, R. B.; Rubin, Y. *J. Am. Chem. Soc.* **2017**, *in press*] Yolanda Li assisted in the preparation and characterization of compounds. Cheng-Wei Lin conducted HRTEM studies. Ryan McCurdy assisted in compound synthesis. Janice B. Lin performed DFT calculations. Jon Brosmer supported preliminary Raman experiments. Kristopher Marsh obtained XPS data.

Chapter 2 is a version of [Jordan, R. S.; Wang, Y.; McCurdy, R. D.; Yeung, M. T.; Marsh, K. L.; Khan, S. I.; Kaner, R. B.; Rubin, Y. *Chem* **2016**, *1*, 78-90.] Yue Wang performed HRTEM, electrical measurements and assisted in writing the manuscript. Ryan McCurdy assisted in the synthesis and characterization of compounds. Michael Yeung performed heating experiments. Kristopher Marsh obtained XPS data. Saeed Khan performed X-ray analysis.

FINANCIAL ACKNOWLEDGMENT

This work was supported by the NSF, Grant NSF-CHE-1608957 and NSF-CHE-1125054 to YR, as well as an NMR Instrumentation grant from the NSF (NSF-CHE-9974928).

Curriculum Vita

Education

Occidental College	Chemistry	B.S. (2010)

Professional Experience:

10/2014 – 08/2017	Graduate Researcher, Chemistry Department, UCLA Advisor: Yves Rubin Research Specialization: New Synthetic Approaches to Carbon Nanostructures from Polyalkyne Precursors
07/2010 – 09/2014	Graduate Researcher, Chemistry Department, UCLA Advisor: Patrick G. Harran Research Specialization: Synthesis of Macrocylcic Peptidomimietics via Multi-Stage Electrophiles
10/2008 – 06/2010	Undergraduate Researcher, Chemistry Department, Occidental College. Advisor: Donald Deardorff Research Specialization: Enantioselective Synthesis Utilizing Enzymatically formed Cyanohydrins

Selected Awards and Honors

Aldrich-UCLA Dissertation Award for Advances in Organic Synthesis (2016)
Session Chair, Division of Organic Chemistry, ACS San Diego (2016)
2nd Place Poster Prize – Seaborg Symposium, UCLA (2015)
Dr. L. Reed Brantley Scholarship (2009-2010)
McMenamin Scholarship (2008-2009)
Occidental College Scholarship (2007-2010)

Peer-reviewed Publications

Jordan, R.S.; Rubin, Y. "The Allure of Metallic Stripes: Single-Sized Narrow Ribbons of Graphene", *Chem,* **2017**, *2*, 11-19.

Jordan, R. S.; Wang, Y.; McCurdy, R. D.; Yeung, M. T.; Marsh, K. L.; Khan, S. I.; Kaner, R. B.; Rubin, Y. "Synthesis of Graphene Nanoribbons via the Topochemical Polymerization and Subsequent Aromatization of a Diacetylene Precursor", *Chem*, **2016**, *1*, 78-90.

Jordan, R. S.; McCurdy, R. D.; Li, Y.; Brosmer, J.; Marsh. K.; Rubin, Y. "Synthesis of $N = 8$ Armchair Graphene Nanoribbons from Four Distinct Polydiacetylenes" <u>*Submitted*</u>

Publications in preparation

Jordan R. S.; McCurdy R. D.; Rubin Y. "Expedient Access to Triphenylenes and Benzohelicenes via Bergman Cyclizations" *in preparation*

Patents

Kaner, McVerry, Rao, Jordan "Energy Providing Device and Applications Thereof" U.S Provisional Application 62/428,899 (Dec. 2016)

Rubin, Jordan, Kervyn de Meerandre, Wang, McCurdy "Synthesis of Graphene Nanoribbons From Monomeric Molecular Precursors Bearing Reactive Alkyne Moieties" UCLA Invention Disclosure (Nov. 2016)

Teaching and Mentoring

2015 - 2017	Mentored graduate student colleagues: Robert Thompson, Yolanda Li, Nick Knutson, Shane Bradner
2015 - 2017	Mentored undergraduate student: Ryan D. McCurdy (Ph.D. cand. at Berkeley)
2015	Mentored CSST summer student: Yang Song (Ph. D. cand. Lin Group, U of Chicago)
2011- 2013	Mentored undergraduates: Jeffery Shin, Jennifer K. Matsui (Ph.D. cand. Molander Group, UPenn)
2010- 2016	Organic Chemistry (Lab/Lecture)
09 -12/2013	Biochemistry (Lab)
2010 - 2015	General Chemistry (Lab)

Public Presentations

1. "*Convergent Access to 8-AGNR via Two Distinct Polydiacetylenes*" Presentation, ACS National Meeting, San Francisco (April 2017)
2. "*8-AGNRs via Polydiacetylenes"* Poster, ACS National Meeting, San Francisco (April 2017)
3. "*Nanoribbons in a Flash*" Presentation, Organic Graduate Symposium, UCLA (June 2016)
4. "*Bottom-up synthesis of graphene nanoribbons via the topochemical polymerization of diacetylenes"* Presentation, ACS National Meeting, San Diego (March 2016)
5. "*Bottom-up GNRs from Polydiacetylenes"* Poster, UCLA Research Showcase, ACS National Meeting, San Diego (March 2016)
6. "*Bottom-up synthesis of graphene nanoribbons via the topochemical polymerization of diacetylenes"* Poster, Seaborg Symposium, UCLA (Nov. 2015)

Introduction:

Section 1: Low-dimensional carbon materials

Carbon based materials have played an integral part in the development of human culture, such as the use of pitch to form tools by early humans 200,000 years ago or the development of nylon-6,6 in the 1930s.[1] Accordingly, the controlled synthesis of carbon materials has been a constant focus of research since the birth of modern chemistry with Sir Robert Boyle. Organic chemistry, named for the class of compounds derived from the processing of organs, has provided humanity with many transformational technologies be they pharmaceuticals, plastics, or new fuels. Accordingly, the synthesis of complex, three-dimensional carbon-based structures has been the principle focus of synthetic organic chemistry during the 20th century.

In contrast to the carbon materials produced by humanity, carbon structures produced by the planet, classically underground under high heat and pressure, typically display uniform bond hybridization, structure and long-range order, as the sp^3 hybridized diamond or sp^2 hybridized graphite exemplify.[2] In the early 1990s a major shift in synthetic chemistry occurred with a growing number of organic chemists fascinated with the controlled synthesis of carbon frameworks of low-dimension and uniform bond hybridization (Figure 1). The isolation and structural elucidation of the zero dimensional buckminsterfullerene (C_{60}) in 1985, and one dimensional carbon nanotubes (CNTs) in 1991, led to a new vigor within the synthetic community to develop targeted syntheses of such compounds.[3,4] Expanding into the 21st century, graphene nanoribbons (GNRs) have generated large amounts of theoretical and synthetic interest as *the* futuristic carbon based electronic material.

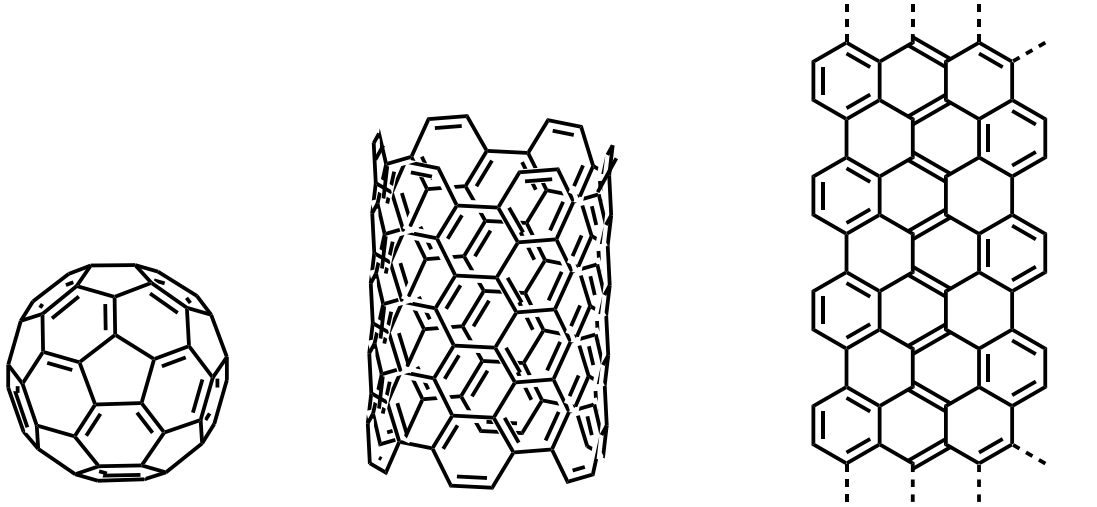

Figure 1. Examples of low-dimensional carbon based materials (fullerene, CNT and GNR).

Section 2: Graphene nanoribbons

Graphene nanoribbons were first described theoretically in 1996 by Fujita and Dresselhaus.[5] They found that constriction of a graphene sheet to narrow ribbon led to the opening of a bandgap that was width and edge dependent. Two prototypical edge-structures of GNRs were described, either armchair ($_A$GNR) or zig-zag ($_Z$GNR), with the former being semi-conducting with a bandgap that increases inversely with ribbon width and the latter having no bandgap. Even before the isolation of single-layer graphene by Geim and Novoselov in 2004, a number of groups had targeted the synthesis of "graphite ribbons" in the 1990s (Figure 2).[6] Mallory in a series of papers described the development of a synthesis of $[4]_A$GNR, the narrowest armchair graphene nanoribbon, using a key stilbene cyclization approach that his lab developed.[7,8,9] Swager had also targeted the synthesis of a graphite ribbon in 1994, utilizing an acid-promoted Friedel-Crafts annulation of poly-phenylene polymers.[10] These syntheses illustrate that the peculiar, extended

aromatic structure of GNRs attracted synthetic chemists long before their exciting material properties were known.

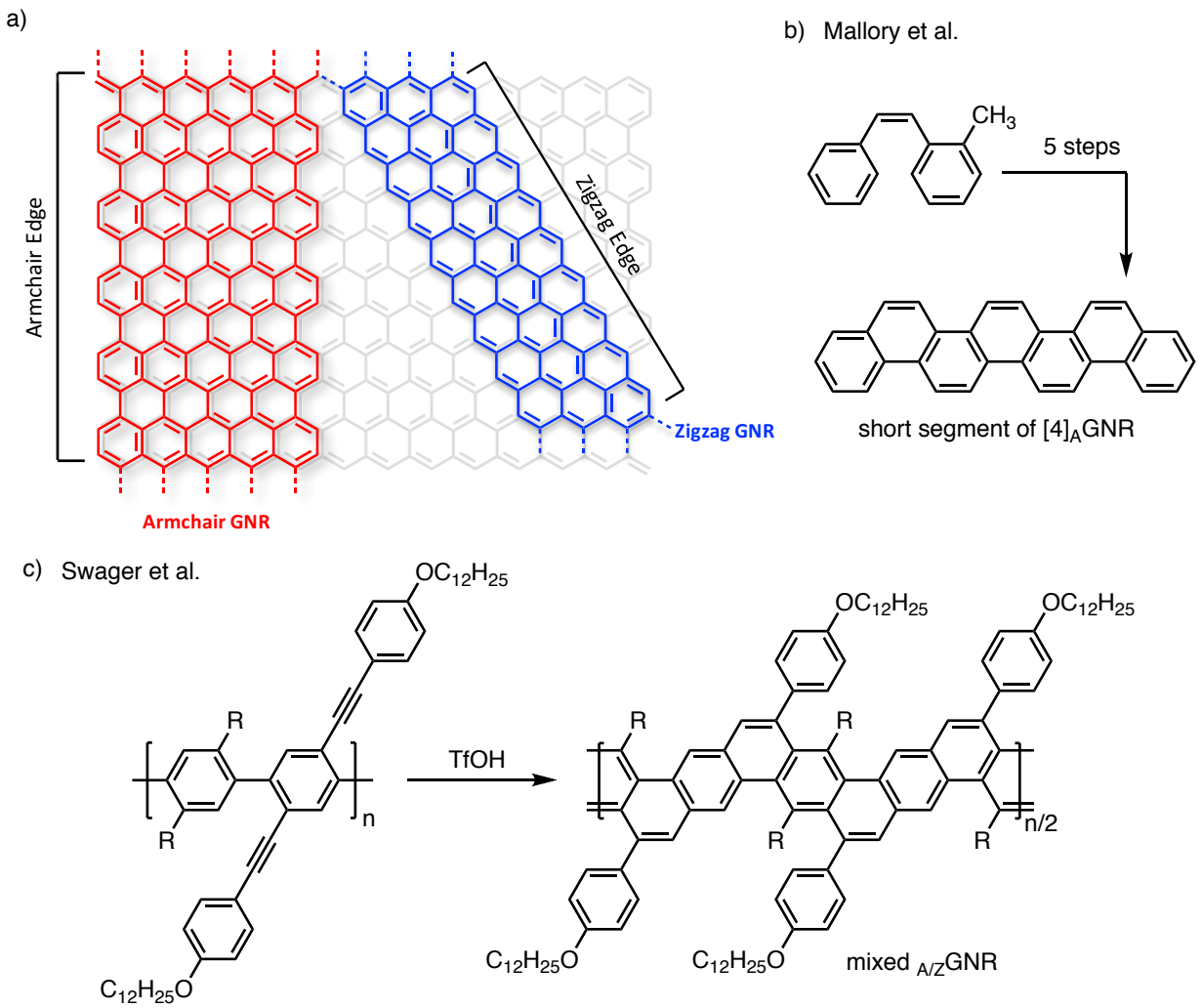

Figure 2. a) GNRs have two prototypical edge structures; armchair or zig-zag. b,c) Early GNR syntheses by Mallory and Swager in the mid 1990s before the isolation of single layer graphene.

While initial syntheses of GNRs and segments of GNRs can be found in the 1990s, synthetic interest in GNRs would explode in the first decade of the second millennium. In general, the controlled synthesis of GNRs fall into either "top-down" or "bottom-up" approaches.[11] Top-

down approaches focus on the synthesis of GNRs from larger sp^2 hybridized carbon structures such as graphene, single and multi-walled carbon nanotubes. GNRs have been synthesized from sonochemical cutting or lithographic etching of a pristine graphene sheet as well as oxidative "unzipping" of multi-walled carbon nanotubes.[12,13,14] Initial top-down syntheses of GNRs provided experimental evidence of the predicted electrical properties of GNRs as well as the inverse relationship between bandgap size and nanoribbon lateral width. While top-down approaches significantly advanced our initial understanding of the potential and real material properties of GNRs, they have substantial hurdles to overcome.

The principal issue limiting the application of top-down approaches to the synthesis of GNRs is their inability to reliably produce ribbons with widths below 10 nm. It should be noted that for an armchair GNR to have a similar bandgap to that of silicon, the principal semiconductor behind nearly all modern electronic devices, it would need to be approximately 1-2 nm in width.[15] Also, nearly all top-down approaches struggle to produce ribbons with atomically precise, regular edges. Without a well-defined, regular edge the electronic properties of the resulting GNR cannot be reliably predicted or targeted. Thankfully, these two over-arching problems can be addressed using a step-wise bottom up approach.

Section 3: Bottom-up syntheses of graphene nanoribbons

Bottom-up syntheses of GNRs utilize the power and precision that synthetic chemistry affords to build narrow ribbons atom-by-atom. Until 2016, all published bottom-up syntheses of GNRs fell into one of two categories, utilizing either in-solution or on-surface methods (Figure 3). On-surface synthesis of GNRs was first reported by Müllen and Fasel in 2010 utilizing a scanning-

tunneling microscope (STM) to image the intermediates and resulting $[7]_A$GNR.[16] Their synthesis exploited the Au(111) surface-promoted dehalogenation, polymerization and cyclodehydrogenation of 10,10'-dibromo-9,9'-bianthracene monomers to form pristine nanoribbons that could be directly imaged with STM. This process highlighted the pristine edges and narrow width that could be achieved from well-designed bottom-up strategies. This process has been subsequently expanded upon to form a large number of GNRs, including $_Z$GNRs,[17] with different widths and edge structure while imaging with STM.[18]

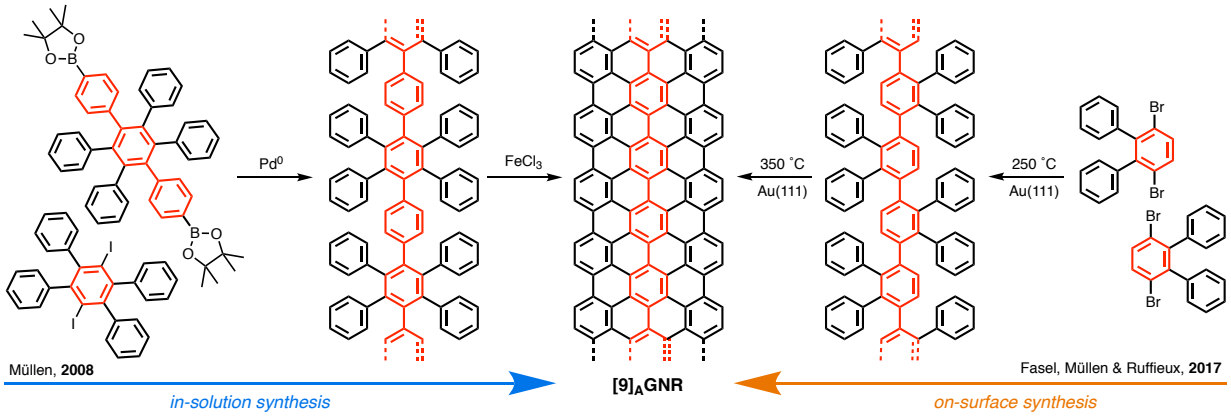

Figure 3. Contrasting bottom-up syntheses of $[9]_A$GNRs utilizing either in-solution or on-surface methods with common poly-phenylene backbone highlighted in red.

While on-surface methods have flourished in the past few years, they have several drawbacks. Firstly, because the chemistry relies on surface contact for monomer organization and orientation during the reactions, flat 2-dimensional monomers with predictable surface orientation are necessary. The addition of branching chains to improve solubility or trans-annular rings to prevent ribbon-ribbon stacking would be nearly impossible to incorporate. Because of this, the GNRs produced typically contain no solubilizing functionality and therefore are difficult to

separate from the surface, although elaborate methods have been developed.[19] The largest limitation for the application of on-surface synthesis to bulk synthesis of GNRs is the small, limited amount of material produced. Reactions are performed on a small (typically 1 cm x 1 cm) surface and a sub-monolayer of GNRs is produced. The ideal use case for on-surface GNR synthesis would be the controlled growth of GNRs between two contacts in a real device, but this goal is far from being achievable in a commercially viable setting.

In-solution syntheses benefit from the ability to produce large amounts of material (grams) and no fundamental restrictions on the topology of monomers. As noted above, targeted, solution synthesis of GNRs can be traced to the mid 1990s and even further back to the 1970s in some cases.[20,21] In-solution syntheses of GNRs typically utilize well-developed polymerization methodologies such as transition metal-catalyzed cross-couplings or Diels-Alder reactions. These reactions are utilized to create poly-phenylene type backbone polymers which are subsequently aromatized to GNRs under oxidative conditions (Figure 3).[22,23] The GNRs produced can incorporate solubilizing groups to aid in material transfer for the creation of devices based on such GNRs. Recently, the groups of Dichtel and Chalifoux have developed innovative new strategies to create GNRs in solution using benzannulation reactions after initial metal-catalyzed polymerization (Figure 4). In seeking to expand the collection of bottom-up syntheses of GNRs, solid-state reactions provide an interesting platform to explore GNR synthesis. One of the most well understood and robust solid-state transformations is the topochemical polymerization of 1,4-butadiynes to form polydiacetylene polymers.

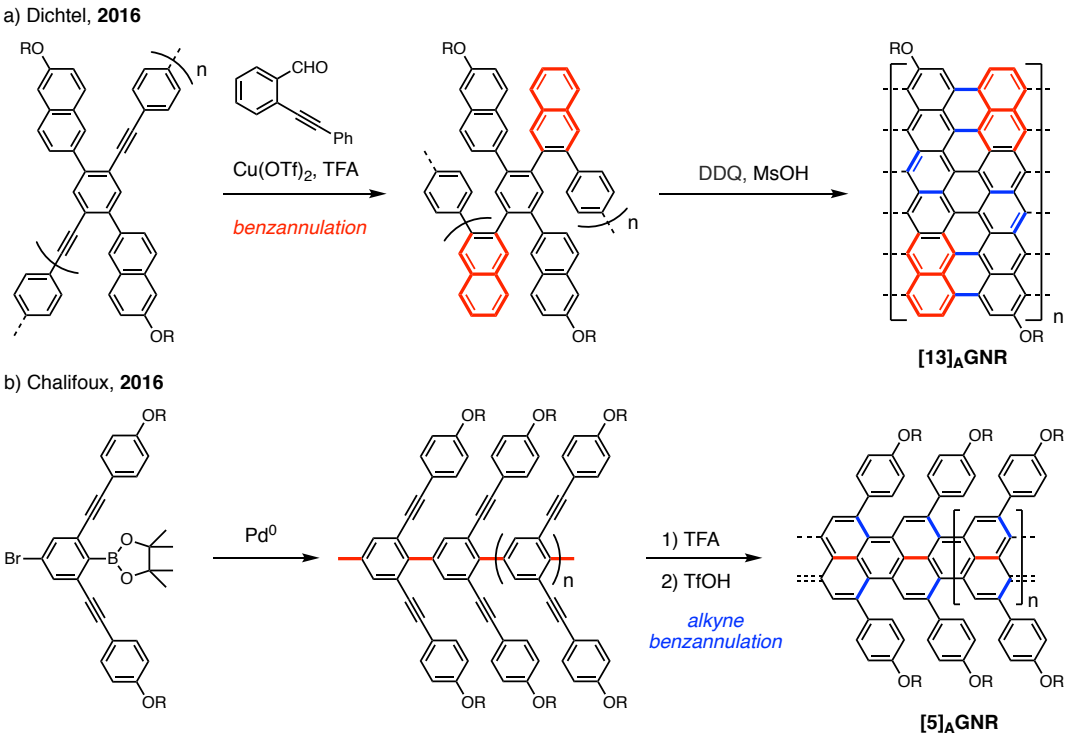

Figure 4. Unique benzannulation reactions utilized during the in-solution synthesis of GNRs by Dichtel and Chalifoux.

Section 4: Topochemical polymerization of 1,4-butadiynes

Polydiacetylenes (PDAs) have a rich history of synthesis and solid-state design due to their intriguing crystal-phase formation through the topochemical polymerization of 1,4-butadiynes.[24] The solid-state parameters required for 1,4-butadiynes to undergo topochemical polymerization were thoroughly studied in the 1970s by Wegner.[25] He found that crystal-phase polymerization readily took place when the terminal ends of the 1,4-butadiynes were within their Van der Waals' radii (≤3.5 Å) and offset by a short regular distance (≤5 Å). Excitation of crystalline 1,4-butadiynes displaying favorable packing parameters with either UV light, heat or γ-rays promoted polymerization to the corresponding PDA polymers. To date a wealth of PDA polymers have been

produced utilizing these simple guidelines for crystal-phase packing. These PDA polymers have largely been investigated for the interesting thermochromic properties that they display.[26]

Despite the large amount of PDA polymers described in the literature, few groups have attempted to utilize the formed PDA backbone in further chemistry. In 1994, Kojima and coworkers described the reaction of diphenylbutadinye at 210 ˚C under high pressure (50-500 MPa) as a neat solid (Figure 5a).[27] Upon reaction, a gas was produced as well as material that was characterized spectroscopically (CP/MAS ^{13}C NMR, IR, Raman). They concluded that the material was graphitic in nature but were unable to establish an exact structure based on information collected. They concluded that the structure contained a mixture of unreacted mono-substituted phenyl rings as well as larger graphitic areas. Importantly, the lack of any spectroscopic evidence of an alkyne led them to conclude that the diphenyl PDA polymer was not a likely intermediate.

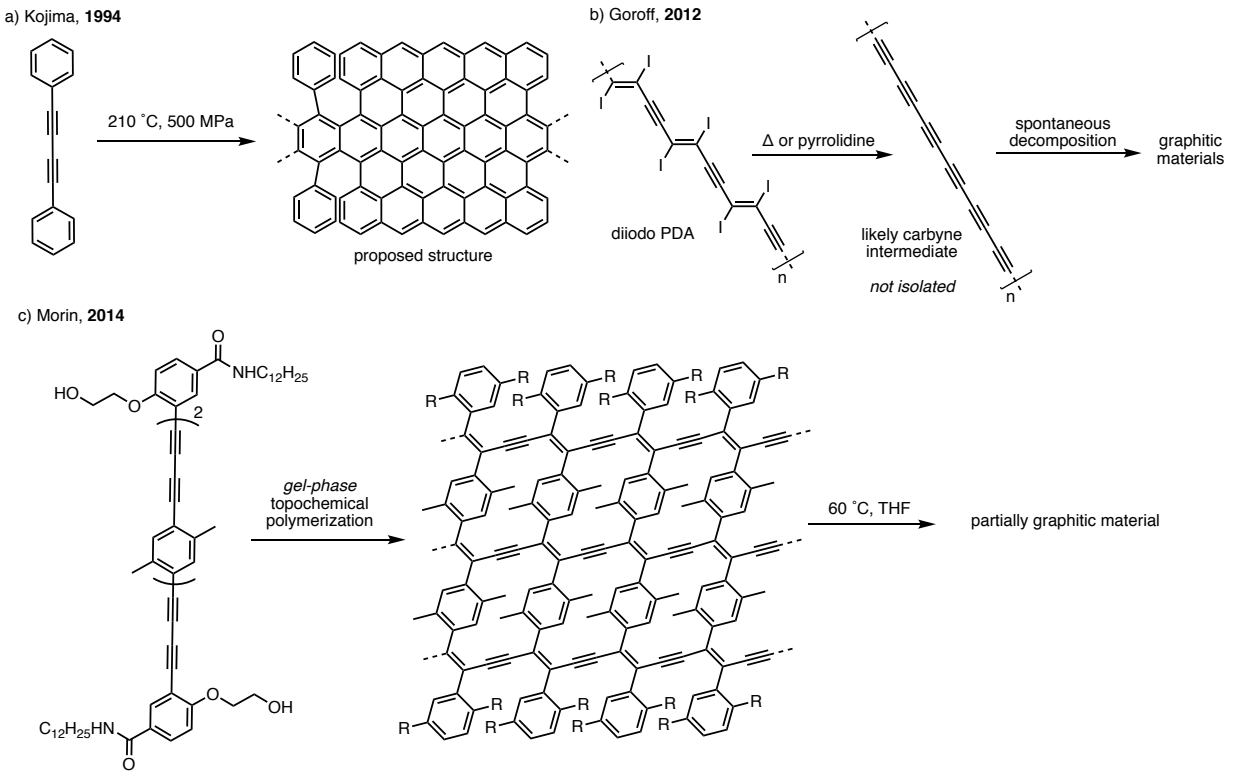

Figure 5. Attempted graphitization of 1,4-butadiynes and polydiacetylenes.

More recently, Goroff and coworkers have described the thermal decomposition of diiodopolydiacetylene at 900 ˚C (Figure 5b).[28] They subsequently reported that a similar decomposition pathway could be promoted by treatment with pyrrolidine, a Lewis base.[29] They investigated the resulting materials by Raman spectroscopy and observed broad D and G bands, spectroscopic fingerprints of graphitic materials. This particular decomposition is intriguing in that the most likely intermediate after loss of iodine is the one-dimensional carbon allotrope carbyne, which to date has eluded direct synthesis and isolation.[30] Due to this, the reaction observed by Goroff is most likely thermal or Lewis base promoted loss of iodine to produce carbyne, and then reaction of carbyne to form random, networked graphitic structures.

The group of Morin has developed the topochemical polymerization of 1,4-butadiynes containing molecules in pre-formed xerogels.[31] Their key discovery was an amphiphilic head group on the butadiynes that promoted efficient gelation. In a subsequent report, they found that mild heating (60 ˚C) of a diaryl polydiacetylene, produced using the amphiphile noted above, promoted conversion to a graphitic material (Figure 5c).[32] Due to the methyl substituents on the internal aryl rings of their PDA polymers, these materials will not be able to fully graphitize to a GNR. Characterization by Raman spectroscopy and transmission electron microscopy (TEM) showed the material to contain a thin-layered structure of graphitic sheets, but the authors were unable to discretely determine the structure of the graphitized material.

Section 5: Bottom-up synthesis of GNRs via solid-state reactions

Since 2010, the Rubin group has published reports that target the controlled synthesis of carbon nanotubes via the topochemical polymerization of [24]dehydroannulenes.[33,34] In the course of their research, only one [24]dehydroannulene derivative was found to undergo topochemical polymerization, under high pressure. Also, one drawback of using [24]dehydroannulenes is that they can stack in a non-productive fashion if they do not stack completely in-register, leading to a networked structure instead of individual columnar stacks. In contrast, diphenyl-1,4-butadiynes have only one possible stacking dimension, and can only lead to discrete, non-crosslinked polymers. Topochemical polymerization of diphenyl-1,4-butadiynes would produce diphenyl PDAs that would be ideal precursors to GNRs if promoted to undergo aromative cyclization reactions (Figure 6).

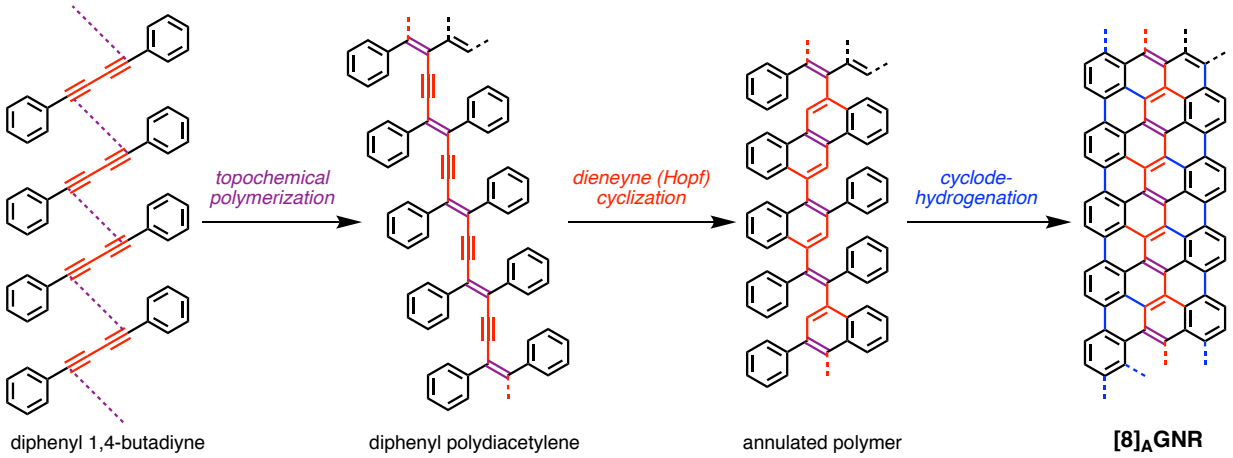

Figure 6. Bottom-up synthesis of GNRs from 1,4-butadiynes via solid state reactions.

Key to the transformation of PDAs to GNRs would be (1) the cyclization of an enyne unit of the polymer backbone onto a pendant aromatic ring in a classical dienyne cyclization and (2) cyclodehydrogenation of the resulting annulated polymer. The pericyclic reaction of dieneynes to form new aromatic rings is named the Hopf cyclization after its pioneer, Henning Hopf.[35] Until the Rubin groups' initial report in 2016, the Hopf cyclization utilizing the enyne backbone of a PDA polymer had not been discretely investigated.[36] Since then, a number of PDA systems that undergo such a transformation have been identified and studied by the Rubin group. Also, the Rubin group has been able to show that simple heating of annulated PDA polymer indeed promotes thermal cyclodehydrogenation to produce $_A$GNRs. Studies detailing the development, implementation and spectroscopic investigation of this pathway to GNRs from PDAs, are detailed in the following chapters.

Chapter 1 describes the development of the PDA to GNR pathway and its investigation using a combination of spectroscopic and microscopic methods. Spectroscopic investigation (CP/MAS ^{13}C NMR, IR, Raman, XPS) was instrumental in examining the PDA to GNR process in detail. Furthermore, the PDA to GNR process is revealed to be general through the successful

conversion of four distinct PDA polymers to $[8]_A$GNR. Chapter 2 chronicles the elaboration of the solid-state PDA to GNR process to access $[12]_A$GNR from a dinaphthyl PDA polymer. Investigation of the bulk electrical properties of the formed $[12]_A$GNR confirm that they are indeed conductive. Chapter 3 details a synthetic route toward diaryl *trans*-enediynes as model systems for the internal Hopf cyclization proposed as a key step on the PDA to GNR pathway. It is shown that model diaryl *trans*-enediynes do undergo thermal Hopf cyclization at temperatures relevant to those seen in the bulk PDA to GNR process. Furthermore, in the course of research diaryl *trans*-enediynes were found to be optimal platforms for the formation of diethynyl [5]helicenes and phenanthrenes. Mechanistic studies of the Bergman polymerization of such *cis*-enediynes are described in detail.

References

[1] Roebroeks, W.; Villa, P. *P. Natl. Acad. Sci.* **2011**, *108,* 5209-5214.

[2] Greenwood, N. N.; Earnshaw. A. *Chemistry of the Elements*; Butterworth-Heinemann: Oxford, 2006.

[3] Kroto, H. W.; Heath, J. R.; O'Brien, S. C.; Curl, R. F.; Smalley, R. E. *Nature* **1985**, *318*, 162-163.

[4] Sumio, I. *Nature* **1991**, *354*, 56-58.

[5] Nakada, K.; Fujita, M.; Dresselhaus, G.; Dresselhaus, M. *Phys. Rev. B.* **1996**, *54*, 17954-17961.

[6] Novoselov, K. S.; Geim, A. K.; Morozov, S. V.; Jiang, D.; Zhang, Y.; Dubonos, S. V.; Grigorieva, I V.; Firsov, A. A. *Science*, **2004**, *306*, 666-669.

[7] Mallory, F. B.; Butler, K. E.; Evans, A. C.; Mallory, C. W. *Tetrahedron Lett.* **1996**, *37*, 7173-7176.

[8] Mallory, F. B.; Bulter, K. E.; Evans, A. C.; Brondyke, E. J.; Mallory, C. W.; Yang, C.; Ellenstein, A. *J. Am. Chem. Soc.* **1997**, *119*, 2119-2124.

[9] Mallory, F. B.; Butler K. E.; Bérubé, A.; Luzik, E. D. Jr.; Mallory, C. W.; Brondyke, E. J.; Hiremath, R.; Ngo, P.; Carrol, P. J. *Tetrahedron* **2001**, *57*, 3715-3724.

[10] Goldfinger, M. B.; Swager, T. M. *J. Am. Chem. Soc.* **1994**, *116*, 7895-7896.

[11] Tour, J. M. *Chem. Mater.* **2014**, *26*, 163-171.

[12] Li, X.; Wang, X.; Zhang, L.; Lee, S.; Dai, H. *Science* **2008**, *319*, 1229-1232.

[13] Sommer, B.; Sonntag, J.; Ganczarczyk, A.; Braam, D.; Prinz, G.; Lorke, A.; Geller, M. *Sci. Rep.* **2015**, *5*, 7781.

[14] Kosynkin, D. V.; Higginbotham, A. L.; Sinitskii, A.; Lomeda, J. R.; Dimiev, A.; Price, B. K.; Tour, J. M. *Nature* **2009**, *458*, 872-876.

[15] Son, Y-W.; Cohen. M. L.; Louie, S. G. *Phys. Rev. Lett.* **2006**, *97*, 216803.

[16] Cai, J.; Ruffieux, P.; Jaafar, R.; Bieri, M.; Braun, T.; Blankenburg, S.; Muoth, M.; Sietsonen, A. P.; Saleh, M.; Feng, X.; Müllen, K.; Fasel, R. *Nature,* **2010**, *466*, 470-473.

[17] Ruffieux, P.; Wang, S.; Yang, B., Sánchez-Sánchez, C.; Liu, J.; Dienel, T.; Talirz, L.; Shinde, P.; Pignedoli, C. A.; Passerone, D.; Dumslaff, T.; Feng, X.; Müllen, K.; Fasel, R. *Nature* **2016**, *531*, 489-492.

[18] Talirz, L.; Ruffieux, P.; Fasel, R. *Adv. Mater.* **2016**, *28*, 6222-6231.

[19] Koch, M.; Ample, F.; Joachim, C.; Grill, L. *Nat. Nanotechnol.* **2012**, *7*, 713-717.

[20] Stille, J. K.; Noren, G. K.; Green, L. *J. Polym. Sci. A-1, Polym. Chem.* **1970**, *8*, 2245-2254.

[21] Hurley, S. A.; Dutt, P. K.; Marvel, C. S. *J. Polym. Sci. A-1 Polym. Chem.* **1972**, *10*, 1243-1261.

[22] Yang, X. Dou, X.; Rouhanipour, A.; Zhi, L.; Räder, H. J.; Müllen, K. *J. Am. Chem. Soc.* **2008**, *130*, 4216-4217.

[23] Narita, A.; Verzhbitskiy, I. A.; Frederickx, W.; Mali, K. S.; Jensen, S. A.; Hansen, M. R.; Bonn, M.; De Feyter, S.; Casiraghi, C.; Feng, X.; Müllen, K. *ACS Nano* **2014**, *8*, 11622-11630.

[24] Ogawa, T. *Prog. Polym. Sci.* **1995**, *20*, 943-985.

[25] Wegner, G. *Makromolekul. Chem.* **1972**, *154*, 35-48.

[26] Park, I. S.; Park, H. J.; Kim, J-M. *ACS Appl. Mater. Interfaces* **2013**, *5*, 8805-8812.

[27] Kojima, Y.; Tsuji, M.; Matsuoka, T.; Takahashi, H. *J. Polym. Sci. A-1 Polym. Chem.* **1994***, 32*, 1371-1376.

[28] Luo, L.; Wilhelm, C.; Young, C. N.; Grey, C. P.; Halada, G. P.; Xiao, K.; Ivanov, I. N.; Howe, J. Y.; Geohegan, D. B.; Goroff, N. S. *Macromolecules* **2011**, *44*, 2626-2631.

[29] Luo, L.; Resch, D.; Wilhelm, C.; Young, C. N.; Haladan, G. P.; Gambino, R. J.; Grey, C. P., Goroff, N. S. *J. Am. Chem. Soc.* **2011**, *133*, 19274.

[30] Chalifoux, W. A.; Tykwinski, R. R. *Nat. Chem.* **2010**, *2*, 967-971.

[31] Néabo, J. R.; Rondeau-Gagné S.; Vigier-Carrière, C.; Morin, J-F. *Langmuir,* **2013**, *29*, 3446-3452.

[32] Levesque, I.; Néabo, J. R.; Rondeau-Gagné S.; Vigier-Carrière, C.; Daigle, M.; Morin, J-F. *Chem. Sci.* **2014**, *5*, 831.

[33] Suzuki, M.; Comito, A.; Khan, S. I.; Rubin, Y. *Org. Lett.* **2010**, *12*, 2346-2349.

[34] Suzuki, M.; Khosrowabadi, J. F.; Khan, S. I.; Rubin, Y. *J. Am. Chem. Soc.* **2016**, *138*, 5939-5956.

[35] Prall, M.; Krüger, A.; Schreiner, P. R.; Hopf, H. *Chem. Eur. J.* **2001**, *7*, 4386-4394.

[36] Jordan, R. S.; Wang, Y.; McCurdy, R. D.; Yeung, M. T.; Marsh, K. L.; Khan, S. I.; Kaner, R. B.; Rubin, Y. *Chem* **2016**, *1*, 78-90.

Chapter 1: Synthesis of $N = 8$ Armchair Graphene Nanoribbons from Four Distinct Polydiacetylenes

Section 1.1: Abstract

We demonstrate a highly efficient thermal conversion of four differently substituted poly(1,4-diphenyl)butadiyne polymers (polydiacetylenes, PDAs **1** and **2a–c**) into indistinguishable $N = 8$ armchair graphene nanoribbons ($[8]_A$GNR). We characterize the clean, stepwise transformation of these substituted PDAs, initially into partially annulated intermediates, and subsequently into $N = 8$ armchair graphene nanoribbons following full aromatization and side-chain losses. The four distinct PDAs **1** and **2a–c** are obtained in 7, 11, 23, and 15% yield, respectively, upon photochemically initiated topochemical polymerization of the *para* or *meta*-substituted 1,4-diphenylbutadiynes (**3** and **4a–c**) within their crystal phases. The overall yield is substantially increased upon recycling of the leftover starting material (e.g. diyne **3** produces 24% yield of PDA **1** over four cycles). The subsequent clean, quantitative transformation of PDAs **1** and **2a–c** into $N = 8$ armchair graphene nanoribbons occurs via a series of Hopf pericyclic reactions, followed by aromatization reactions of the annulated polycyclic aromatic intermediates, as well as homolytic bond fragmentation of the edge functional groups upon heating up to 600 ˚C under an inert atmosphere. The thermal conversion of PDAs **1** and **2a–c** gives essentially identical samples of $[8]_A$GNR, as characterized by complementary spectroscopic techniques (CP/MAS ^{13}C NMR, Raman, FT-IR, and XPS), and by high-resolution transmission electron microscopy (HRTEM). This novel approach to GNRs exploits the power of crystal engineering and solid-state reactions by

targeting very large organic structures through programmed chemical transformations. It also affords the first reported near-zero bandgap $[8]_A$GNR, which can now be synthesized on a large scale via two operationally simple and discrete solid-state processes.

Section 1.2: Introduction

While graphene displays a number of remarkable properties, its zero bandgap makes it unsuitable for most semiconductor applications.[1] However, graphene nanoribbons (GNRs), which are narrow strips of graphene with widths below 10 nm, display defined bandgaps in addition to ballistic charge transport thanks to the lateral confinement of charge carriers.[2] Not surprisingly, the designed synthesis of GNRs has quickly gained prominence in this field.

Graphene nanoribbons are classified as either armchair, zigzag, or chiral, depending on the topology of the repeating units within their long edges.[3] Armchair graphene nanoribbons ($_A$GNRs),[4] which are the most interesting type of GNR in terms of semiconductor applications, can be divided into three classes defined by the number of carbon atoms within their width. These classes comprise 3p, 3p + 1, and 3p + 2 carbon atoms, where p is in an integer. Armchair GNRs that fall into the 3p or 3p + 1 classes (e.g. [6] and $[7]_A$GNRs) are predicted to be semiconducting, with a bandgap that increases as ribbon width narrows.[5] On the other hand, the 3p + 2 class (e.g. $[8]_A$GNR) is predicted to be metallic with a near zero bandgap. The smallest member of the 3p + 2 class, $[5]_A$GNR, was first synthesized using on-surface chemistry, and subsequently, in-solution.[6,7,8,9] Since then, many graphene nanoribbons of the other classes have been synthesized, although the next smallest member of the 3p + 2 class, $[8]_A$GNR, has yet to be reported via either solution or surface chemistry.

While graphene nanoribbons are quickly gaining importance, there is only a limited number of methods to generate them. These methods fall either into "top-down" or "bottom-up" strategies.[10] Top-down strategies include cutting a large piece of graphene with an electron beam, unzipping of carbon nanotubes, or sonochemical tearing of graphene sheets.[11,12,13] A major limitation of the top-down strategies is that they do not provide homogeneous ultra-narrow ribbon widths (<10 nm) as well as atomically precise edges. By contrast, bottom-up strategies rely on the precision and control afforded by synthetic chemistry to construct ribbons molecule-by-molecule. Until recently, only two marginally differing bottom-up approaches had been described: (1) Surface assisted coupling and cyclodehydrogenation of dihalo polycyclic arenes, or (2) metal-catalyzed solution-phase polymerization of similar precursors, including alkynylarenes, to form polyarylene backbone polymers, followed by their subsequent, typically oxidative, aromatization to GNRs (Figure 1.1).[14,15,16,17,18] Recently, the groups of Dichtel and Chalifoux have described key strategic innovations in this area. Their approaches both utilize benzannulation reactions performed after metal-catalyzed polymerization.[18,19]

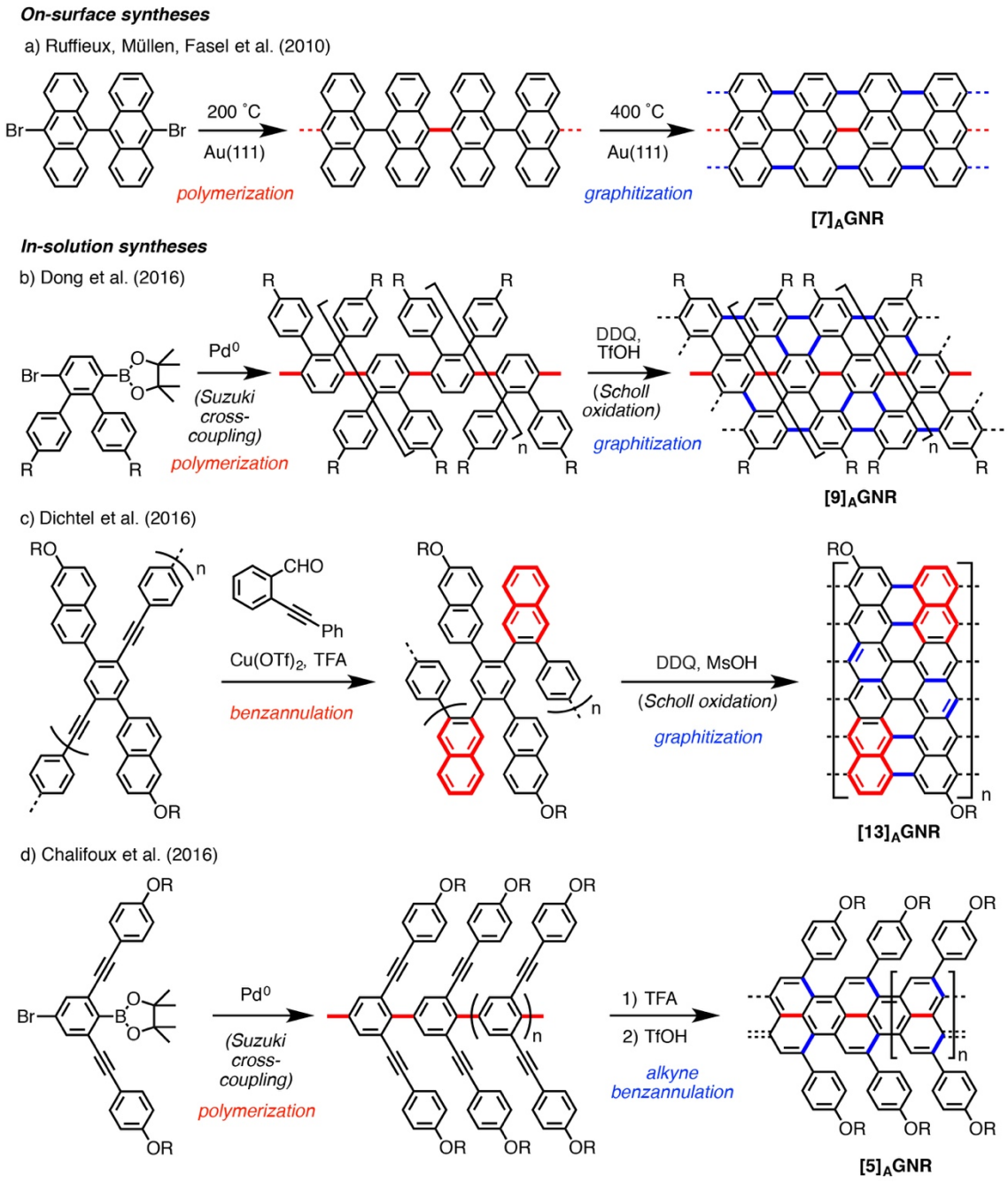

Figure 1.1. Examples of bottom-up syntheses of GNRs. a,b) Most approaches take advantage of the metal-catalyzed polymerization of arene monomers, either on-surface or in-solution, and subsequent oxidation of the ensuing polymers to the corresponding GNRs. c,d) By contrast, Dichtel and Chalifoux have developed ingenious new benzannulation strategies to access GNRs.

Section 1.3: Results and Discussion

The broad bandgap semiconducting polydiacetylene polymers (PDAs) have a rich history of synthetic design, spectroscopy, and applications in materials science, with a recent focus on their thermochromic properties.[20,21,22] However, synthetic strategies that directly utilize their polyenyne backbone functionality for further synthetic transformations have only been described recently and are still rare.[23,24,25] Following our initial studies seeking the formation of nanotubular PDAs through topochemical polymerization of [24]dehydroannulenes,[26,27] our own approach to GNRs originated from the intriguing prospect of exploiting the rehybridization energy of *sp* carbons within the alkyne units of aryl-substituted polydiacetylenes. By coercing them to expand their coordination using known thermal reactions involving the aryl substituents, the rehybridization and aromatization energies gained from each cyclizing alkyne unit should be energetically favorable and give polycyclic aromatic structures.[28] We postulated that aryl substituents on the PDA backbone would engage their adjacent *trans*-dienyne moieties into a series of Hopf pericyclic reactions to provide annulated polycyclic aromatic intermediates (Figure 1.2).[28,29] Full cyclodehydrogenation of the resulting adjacent polycyclic aromatic rings, which would initially be a random mix of 2-phenylnaphthalene, chrysene, 1,2-diphenylethene units, or larger, should ultimately fully aromatize to 8-armchair graphene nanoribbons (Figure 1.2).

Hopf cyclizations have been experimentally shown to take place via three distinct mechanisms dependent on the reaction temperature: 1) 6π electrocyclization, 2) rearrangement of the alkyne to a vinylidene carbene followed by aryl C-H insertion, and 3) cyclization via initial radical addition to the alkyne.[30] Hopf has shown that electrocyclization is the predominant mechanism for a gas phase reaction below 550 ˚C.[30] All polymers discussed here undergo backbone cyclizations

below 500 ˚C in the solid state, therefore it is likely that the backbone cyclization process occurs via a 6π electrocyclization pathway.

To model the energetics of the Hopf cyclization stage for PDAs **1** and **2a**, we carried out DFT calculations on the *trans*-enediynes **5** and **6** as model systems for the keto and amido functionalized PDAs **1** and **2a** (Figure 1.3). We base our mechanistic study on previous work by Hopf *et al.*,[29] in which the thermal cycloisomerization pathway of *cis*-hexa-1,3-dien-5-yne was explored computationally. The authors established that the Hopf cyclization proceeds through the initial 6π-electrocyclization, which is followed by two consecutive [1,2]-H shifts, with the first H-shift being the rate-determining step. Structures were optimized in the gas-phase using B3LYP/6-31G(d),[31] and single-point calculations were performed using M06-2X/6-311+G(d,p)[31d] to obtain free energy values.[32] Transition state geometries of the Hopf cyclization (**5a**, **6a,c**) and first H-shift (**5b**, **6b,d**) steps are shown in Figure 1.3.

The activation free energies are 52.6 and 58.4 kcal mol^{-1} for **5a** and **5b**, respectively. Similar reaction barriers of 52.5 and 57.5 kcal mol^{-1} are found for the *meta*-amide model system undergoing cyclization *para* to its amide side chain (**6a,b**). The barriers to *ortho* cyclization (**6c,d**) are higher than for *para* cyclization by 2.9 and 6.8 kcal mol^{-1}, respectively. In all cases, the barriers for the first H-shift are higher than that for the Hopf cyclization, a finding that is in line with the work of Hopf *et al.*[29]

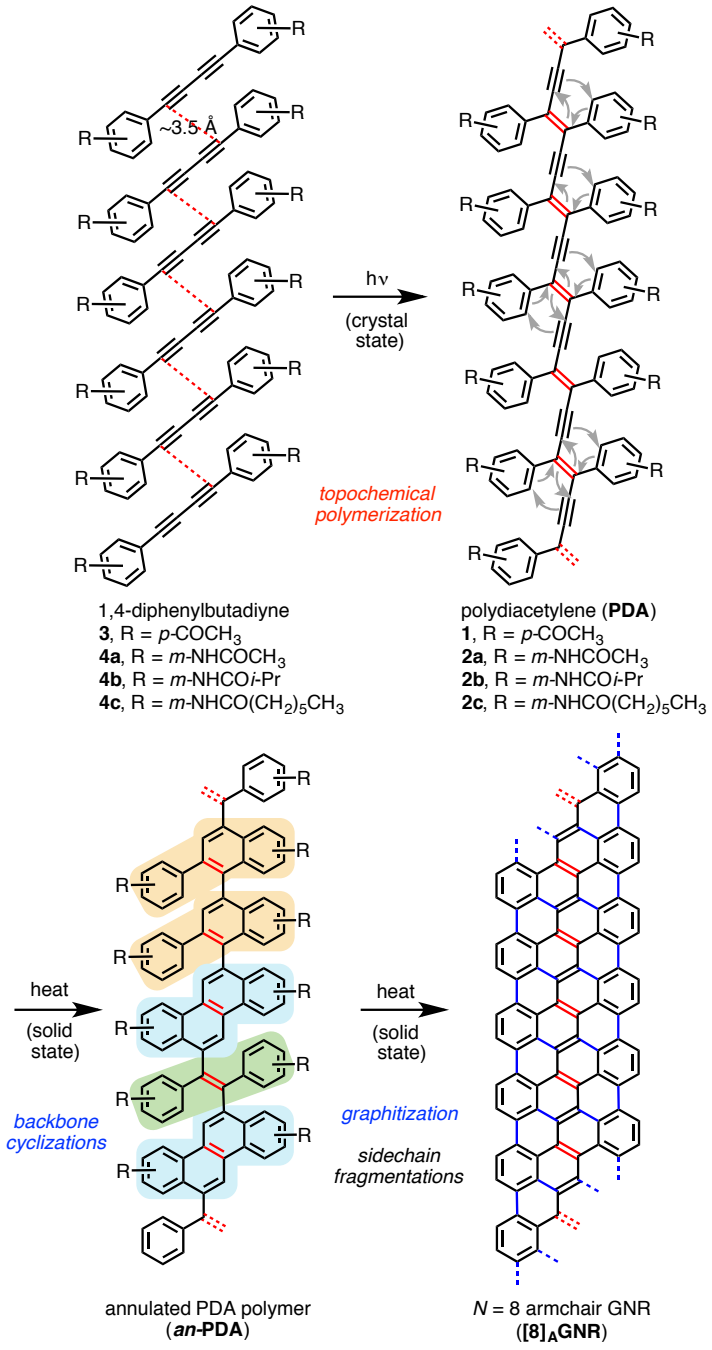

Figure 1.2. Our synthetic approach to $[8]_A$GNR from substituted 1,4-diphenylbutadiynes via the crystalline-state topochemical polymerization of substituted 1,4-diphenylbutadiynes, followed by a separate solid-state thermal aromatization and fragmentation of side-chains. Likely steps in the series of random Hopf cyclizations include the formation of 2-phenylnaphthalene units (orange shaded area), as well as chrysene (cyan) and 1,2-diphenylethene units (green).

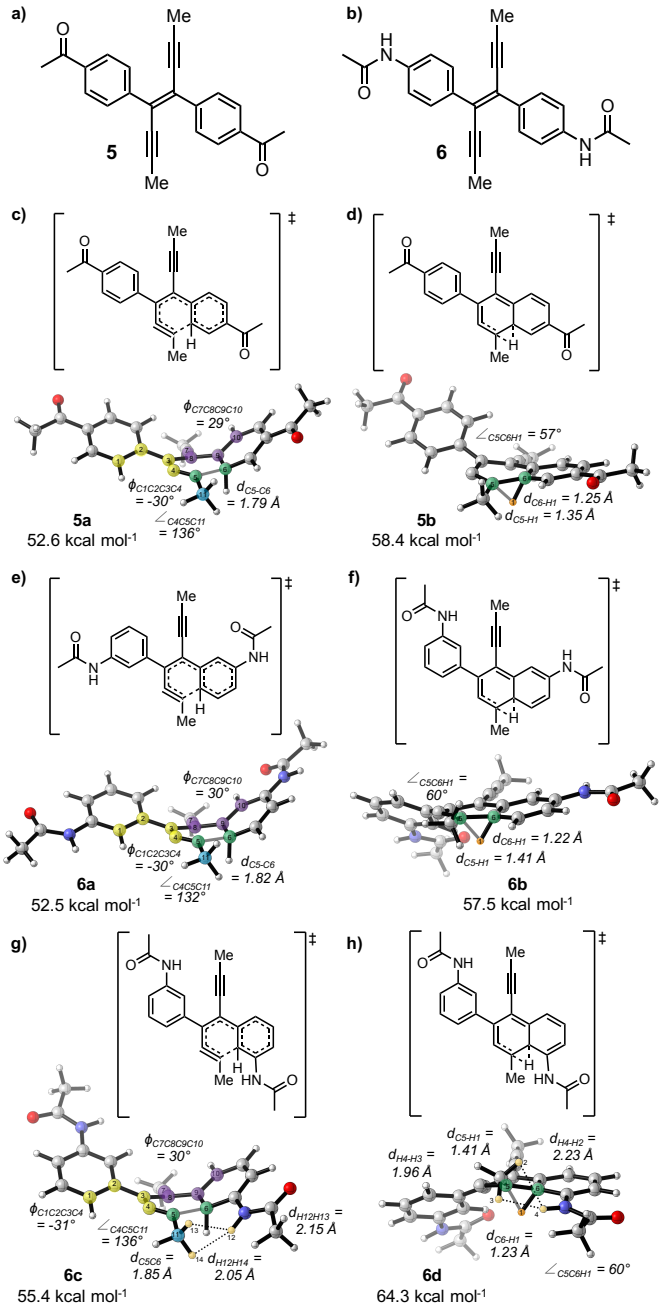

Figure 1.3. Transition state geometries and free activation energies of the 6π-electrocyclization and subsequent H-shift for model systems **5** and **6**. Structures were optimized in the gas phase using B3LYP/6-31G(d) and single-point energies were performed using M06-2X/6-311+G(d,p). Frequency analysis was performed at 350 ˚C.

The geometries of each of the transition structures are similar. The π-system of the alkynes is planar in each of the Hopf cyclization transition states, while the flanking aryl groups are out of plane by approximately 30˚. In the H-shift step, the forming naphthyl ring is planar, and the C6-H1 bond stretches to about 1.23-1.25 Å from its normal C-H bond length of 1.09 Å (Figure 3d,f,h). In both *ortho* transition states **6c** and **6d**, the close proximity of the amide and methyl groups at the forming C-C bond leads to higher barriers. This results in an intrinsic preference for the *para* pathway over the *ortho* pathway by 6.8 kcal mol^{-1}.

For both models **5** and **6**, the reaction barriers of the rate-determining H-shift are >14 kcal mol^{-1} higher than that of *cis*-hexa-1,3-dien-5-yne. This increase in reaction barrier can be attributed to the benzannulation within the π-systems of **5** and **6** compared to *cis*-hexa-1,3-dien-5-yne, which requires disrupting the aromatic π-system at the transition state.[33] In addition, while these gas-phase energies are useful for understanding the intrinsic barriers to cyclization, we acknowledge the limit of these simple models in accounting for the solid-state behavior and polymer conformational influence on the large scale graphitization process within PDAs **1** and **2a**.

During the conceptual development of this work, we identified that diphenylpolydiacetylene polymers should produce $[8]_A$GNRs if they could be triggered to undergo internal backbone cyclization and cyclodehydrogenation (Figure 1.2). As demonstrated herein, the diphenylpolydiacetylene polymer motif has proven itself to be an ideal platform to access these graphene nanoribbons. We show that four differently substituted diphenyl PDA polymers with either *para*- or *meta*-substituents (PDAs **1** and **2a**) all produce pristine $[8]_A$GNRs quantitatively via simple heating. This process is readily applicable to bulk synthesis thanks to the inherent ease with which solid-state transformations can be scaled up. This operationally simple, two-step synthesis of $[8]_A$GNRs does not require any external reagents or solvents and should be applicable to a range

of device manufacturing techniques. As detailed in this report, these transformations are not limited by edge substituents and should provide access to a variety of different edges and widths, including the incorporation of heteroatoms. Herein, we discuss the elaboration of these four synthetic transformations, detailed spectroscopic analysis of the conversion of 1,4-diphenylbutadiynes to PDAs and then GNRs, and structural investigation of the formed nanoribbons.

Monomer Synthesis: A key to our methodology was to identify monomers that have: 1) phenyl substituents on both ends of the butadiyne unit, and 2) undergo the proper crystalline-state organization that promotes topochemical polymerization. In our previous investigations of the solid-state packing of [24]-dehydroannulenes, we noted that carbamate groups could be exploited to achieve tight, in-register crystal packing of the internal butadiyne units.[27] While designing monomers to access $[8]_A$GNRs, we anticipated that either amide, carbamate, or urea functionalities would be suitable to promote tight, in-register packing of simple diphenylbutadiynes. Interestingly, three systems related to our design had been reported to undergo topochemical polymerization, namely bis-*para*-acetophenone butadiyne (**3**) bis-(*meta*-acetylamidophenyl) butadiyne (**4a**) and bis-(*meta*-heptanoylamidophenyl) butadiyne (**4c**).[34,35,36] Our own synthesis and characterization of both **3**, **4a** and **4c** confirmed their predisposition to undergo topochemical polymerization. We also synthesized a range of diphenylbutadiynes containing a number of different amide substituents in their *meta* position and were delighted to find that many of them, including amide **4b**, provide crystals that undergo topochemical polymerization.

While diynes **3** and **4a–c** differ in their substitution, the position and nature of these substituents is not critical in the PDA to GNR conversion process. For diyne **3**, there is only one possible Hopf cyclization pathway because of the inherent axial symmetry of its *para*-substitution

(Figure 1.3). For diynes **4a–c**, the *meta*-amido group is predicted, as discussed above, to have a significant *para*-directing effect in preference to *ortho* in the Hopf cyclizations. Thus, annulated polymers with primarily *edge* amido substituents should be formed initially according to our calculations. However, should a small fraction of Hopf cyclization reactions take place at *ortho* positions, this should not be an issue because all side-chains are ultimately lost in the final conversion of PDAs **1** or **2a–c** to $[8]_A$GNR. Thanks to this design feature, nearly any emergent edge group can now be used to promote organization of the internal butadiyne monomer units without worry of its effect on the resulting GNR structure. In addition, GNRs with heteroatom doping (B, N, O, or S) can be targeted through the specific incorporation of heteroaromatic rings as substituents of the butadiyne, which we are currently pursuing.

The synthesis of monomer **3** was carried out in three steps from commercially available 4-bromoacetophenone following the method of Szafert et al.[34] Crystals of monomer **3** turn rapidly blue upon standing, which is indicative of their propensity to undergo topochemical polymerization. Monomeric amides **7a–c** were synthesized in two steps from commercially available 3-ethynylaniline (Scheme 1.1). Amide bond formation between the amino group and either acetyl chloride, isobutyric acid (via activation with *N,N'*-dicyclohexylcarbodiimide (DCC)), or heptanoic anhydride, produced the highly crystalline amides **7a–c**. Oxidative dimerization of these alkynyl aryl amides under the Hay conditions produced the corresponding butadiynes monomers (**4a–c**) in good yields. Recrystallization from an appropriate solvent gave crystals suitable for topochemical polymerization in each case.[33] All syntheses are very efficient (66%, 69%, 71%, and 84% overall yields for monomers **3**, **4a**, **4b** and **4c**, respectively, from the commercially available starting materials) and allowed us to generate tens of grams of the respective diynes **3** and **4a–c** within a few days.

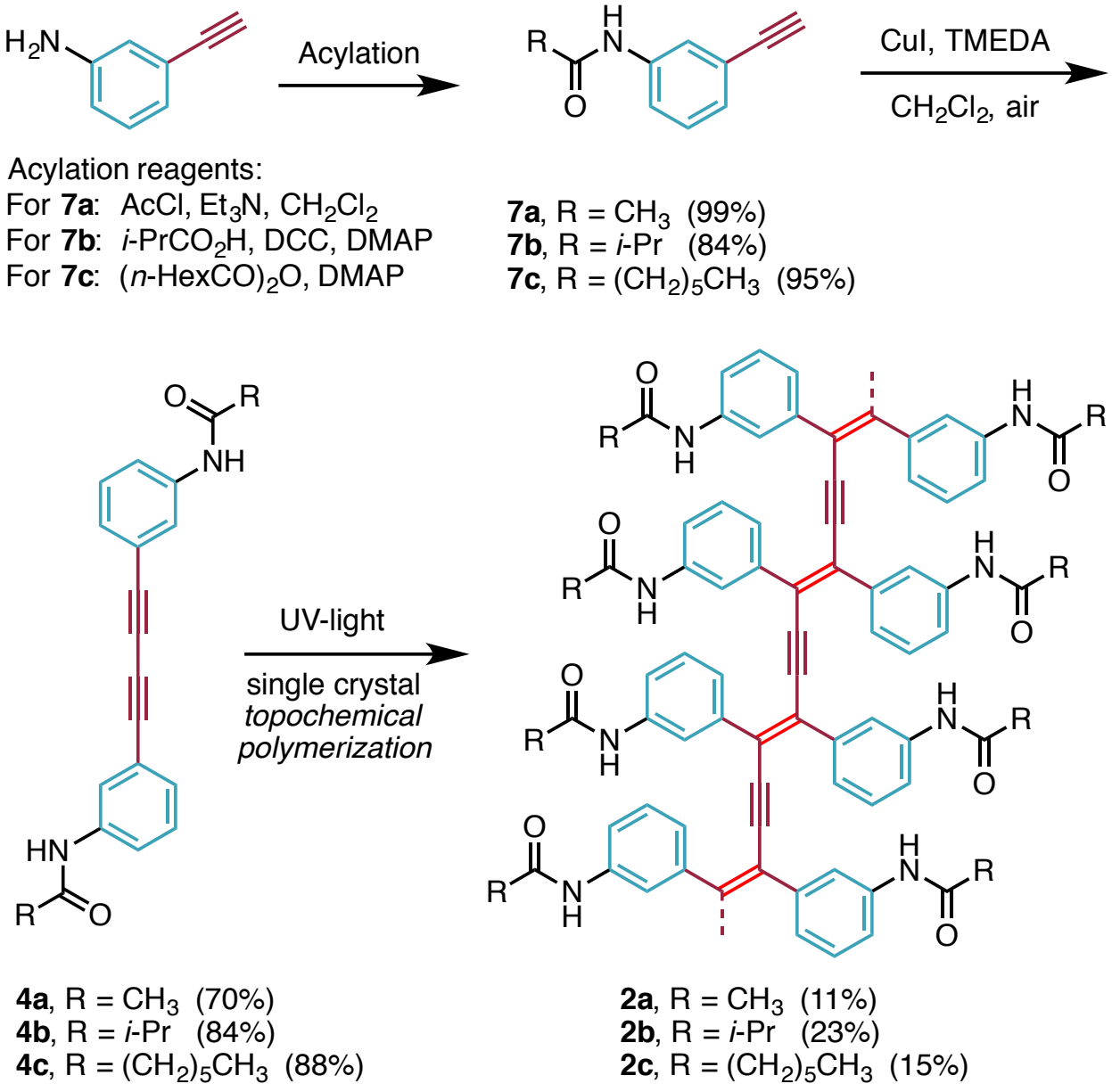

Scheme 1.1. Syntheses of the PDAs **2a–c**.

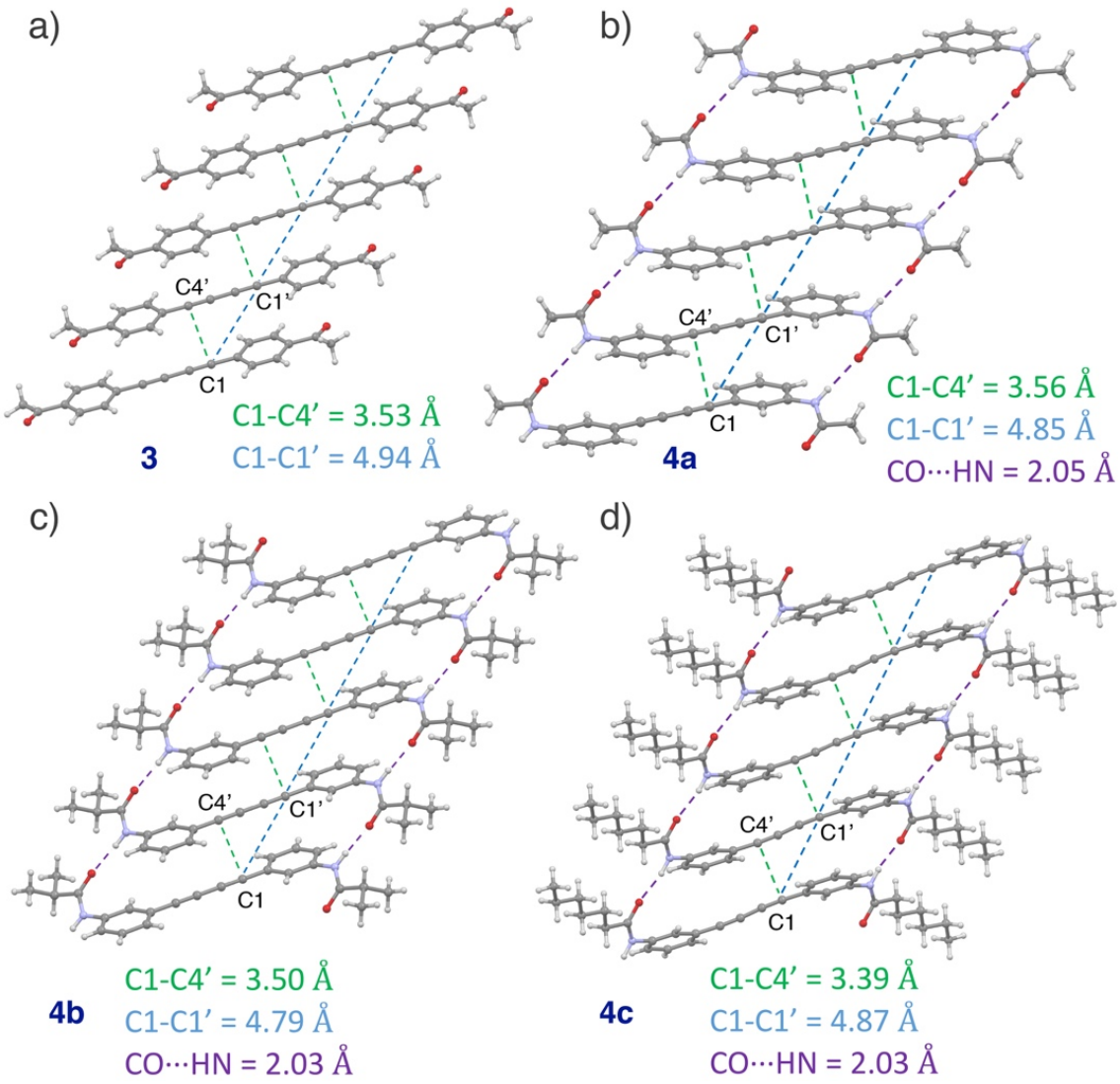

Figure 1.4. Crystal packing structures of diynes **3** and **4a–c** showing close contact distances C1–C4' (≤3.5 Å) and C1–C1' (≤5 Å) crucial for topochemical polymerization.

*Topochemical Polymerization of Diynes **3** and **4a–c***: For butadiyne units to undergo topochemical polymerization, their termini need to be within close to van-der-Waals contact (≤3.5 Å), and also offset by a short repeat distance (≤5 Å).[37] As can be seen from the X-ray crystal structures (Figure 1.4a–d), diynes **3** and **4a–c** all display ideal close-contacts between the terminal carbons of their

butadiyne units, which should favor topochemical polymerization. Accordingly, all four crystalline diynes (**3** and **4a–c**) readily undergo topochemical polymerization at room temperature upon exposure to ambient light. Polymerization is clearly noted by the deep blue color that appears within the crystals upon standing in an unshielded container. Topochemical polymerization can be accelerated by irradiation of the crystals with a high powered Hanovia lamp, typically overnight, producing a deep purple/black color within the crystals. Dissolution of the polymerized crystals to dissolve any unreacted monomer provides the pristine polydiacetylenes **1** and **2a–c** as bulk fibrous powders after filtration. The recovered monomer solutions can be concentrated, recrystallized and subjected again to irradiation to provide further amounts of PDA. Repeating this process allowed us to produce gram quantities of PDAs **1** and **2a–c** in only a few days. As an example, the recycling polymerization reaction of the lowest yielding diyne **3** produced 24% of PDA **1** overall after four cycles (first cycle: 7%).

Characterization of the Polydiacetylenes: Polydiacetylene polymers **1** and **2a–c** were characterized by solid state CP/MAS ^{13}C NMR, XPS, IR, and Raman spectroscopy. Utilizing cross-polarization magic angle spinning (CP/MAS) ^{13}C NMR spectroscopy, the structure and purity of all four polymers could be established unequivocally. While full assignment of each carbon of the aryl or alkyl groups is difficult via solid-state NMR due to the inherently large ^{1}H dipolar couplings in this method, key features can be identified (Figure 1.5). For example, the alkyne carbons in the PDA backbone can be clearly seen at 102 ppm for **1**, and 101 ppm for **2a**, **2b**, and **2c**. The position of these peaks matches well with other reported PDAs and supports the symmetric structure of the polymer backbone.[38,39] Other discernable features of PDA **1** are the ketone carbonyl carbon, appearing at 198 ppm, and the methyl carbon present at 26 ppm. On the other hand, the carbonyl

carbon for the amide containing PDAs **2a–c** appears at 169, 177, and 172 ppm, respectively. The alkyl side chains in these amides appear as discrete carbon peaks in the alkyl region (10-50 ppm). Further investigation of the PDA structure was carried out by analysis of the infrared absorption spectra of all four polymers (Figures 1.6, A1-A8). As will be discussed later, detailed assignment of the unreacted PDAs' IR spectra was key to determining subtle structural changes within the polymers upon heating. PDA **1** displays a strong absorption at 1676 cm^{-1} corresponding to the carbonyl stretch of its ketone functional group. Furthermore, strong absorption bands centered around 831 cm^{-1} correspond to the in-phase out-of-plane (oop) C-H wagging motion of two adjacent C–H bonds on the *para*-substituted phenyl rings.[40] A medium strength in-plane ring bending mode can be identified at 1400 cm^{-1}, attributed to the *para*-substituted phenyl ring in PDA **1**. Infrared analysis of PDAs **2a–c** reveals a medium strength N-H stretch centered around 3300 cm^{-1}, as well as strong carbonyl absorptions at 1665, 1652 and 1660 cm^{-1}, respectively, confirming the presence of the amide sidechains (Figure 1.6). The well-defined in-phase oop C–H wagging motion of the *meta*-substituted phenyl ring can be identified by the strong absorptions at 888, 783, and 694 cm^{-1} for PDA **2a**, 873, 774, and 698 cm^{-1} for PDA **2b**, and 870, 783, and 698 cm^{-1} for PDA **2c**, respectively.[40] The stretching vibration at ~ 880 cm^{-1} corresponds to the oop C-H wagging motion of a single, isolated aromatic C–H bond, whereas the stretching vibration at ~ 780 cm^{-1} results from the oop C-H wagging motion of the three adjacent hydrogens between the *meta* substituents.[40] The strong absorption at ~700 cm^{-1} is a ring bending mode characteristic of asymmetrically substituted (*meta*) phenyl rings.[40] In combination, these stretches provide strong support for the *meta*-substituted nature of the aryl rings in PDAs **2a–2c**.

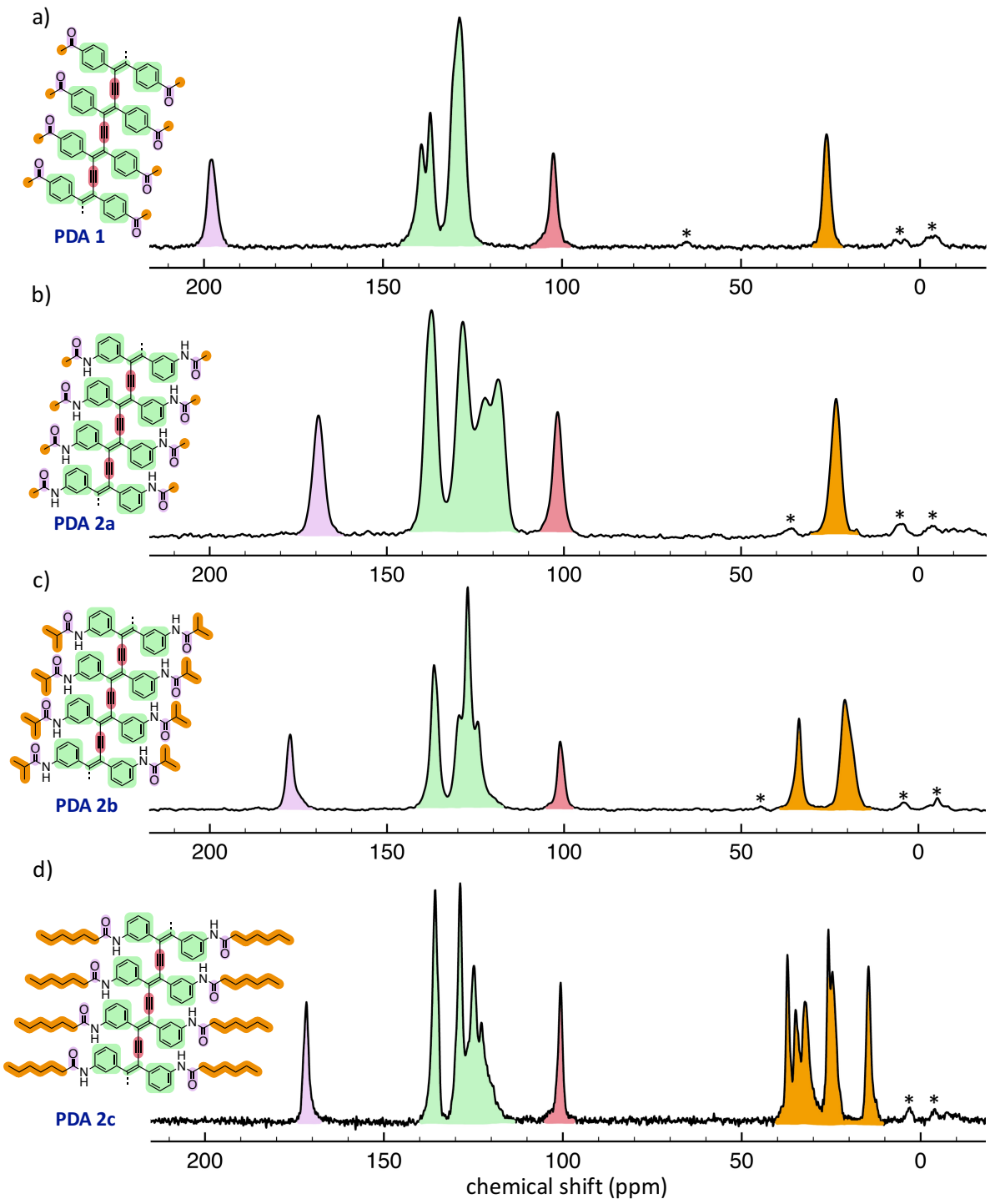

Figure 1.5. Cross polarization magic angle spinning (CP/MAS) solid state ^{13}C NMR spectra of PDAs **1** and **2a–c**. Characteristic regions are color-shaded to guide the eye. Asterisks denote spinning sidebands (10 kHz).

Due to the symmetric nature of the PDA backbone, Raman spectroscopy is another technique of choice for its characterization. Excitation of the polymers in the form of pressed pellets using a 514 nm Argon laser produces intense peaks at 1466 cm^{-1} and 2113 cm^{-1} for PDA **1**, 1471 cm^{-1} and 2120 cm^{-1} for PDA **2a,** 1483 cm^{-1} and 2133 cm^{-1} for PDA **2b,** and 1480 cm^{-1} and 2110 cm^{-1} for PDA **2c** (Figure 1.7). These peaks correspond to symmetric stretching vibrations for the alkene (1466, 1471, 1483, and 1480 cm^{-1}) and alkyne (2113, 2120, 2133 and 2110 cm^{-1}) moieties of the polydiacetylene backbone. Importantly, lack of any absorption at 2200 cm^{-1}, corresponding to monomeric butadiynes **3** and **4a–c**, confirms the absence of any monomer contamination in the polymer samples.

X-ray photoelectron spectroscopy analysis of PDAs **1** and **2a–c** shows distinct C1s spectra with two well defined peaks (Figures A9-A12).[33] The single peaks centered at 284.5, 284.7, 284.6 and 284.5 eV in the spectra of PDAs **1**, **2a**, **2b** and **2c**, respectively, reflect the combination of sp, sp^2, and sp^3 hybridized carbons engaged in the carbon-carbon bonding throughout the structure. The peaks centered at 287.2, 287.9, 287.7, and 287.5, respectively, correspond to the sp^2 hybridized carbonyl carbon of the PDA side chains.

Thermal Conversion of the Polydiacetylenes to Graphene Nanoribbons: With large quantities of the PDA polymers easily available, their conversion to $[8]_A$GNR was carried out by heating of the bulk polymers in a programmable tube furnace under argon flow. PDA polymers **1** and **2a–c** were placed in an aluminum oxide boat within a quartz tube and heated at various temperatures for 1 hour. The resulting materials were characterized by CP/MAS ^{13}C NMR, Raman, XPS and FT-IR to follow the PDA to GNR conversion process (Figures 1.5–1.8, A1-A16).[33] Successful transformation of the PDAs to $[8]_A$GNR relies on three thermally promoted reactions, namely (1)

backbone Hopf cyclization, (2) exhaustive cyclodehydrogenation of the nanoribbon core, and (3) removal of the edge groups (ketone or amide). From the gathered spectroscopic data, we can conclude that for all PDAs presented here, Hopf cyclizations along the poly-enyne backbone are completed before the other two steps at the range of temperature between 400 and 500 ˚C. Accordingly, we present below spectroscopic evidence for all three steps of the PDA to GNR pathway.

Initial Step, Backbone Cyclization (Hopf reaction): As described above, the CP/MAS ^{13}C NMR spectra provide unambiguous assignments for the internal alkyne carbons of each PDA (101-102 ppm). Heating of the PDA polymers to either 500 ˚C (**1**) or 400 ˚C (**2a–c**) for 1h results in complete loss of the backbone alkyne carbons in the CP/MAS ^{13}C NMR spectra (Figure 1.8). Concomitant with this change is a transformation of the aryl region (100-150 ppm) from the well-defined spectra of the unheated PDAs to a broader cluster with two main peaks at 127 and 135 ppm for **1**, and 127 and 137 ppm for **2a–c**, respectively. Interestingly, the spectra of the heated polymers are remarkably similar, which highlight a common cyclization pathway among all of the polymers.

Raman analysis of the heated polymers also confirms the absence of any remaining backbone alkynes (Figures A13-A16).[33] Most importantly, analysis of the IR spectra obtained for these heated polymers details discrete changes in their out-of-plane (oop) bending modes (Figure 1.6). The oop bending modes are the key spectroscopic signatures of the substitution patterns within the aryl rings in the starting material, intermediate structures, and final $[8]_A$GNR product.[17,18]

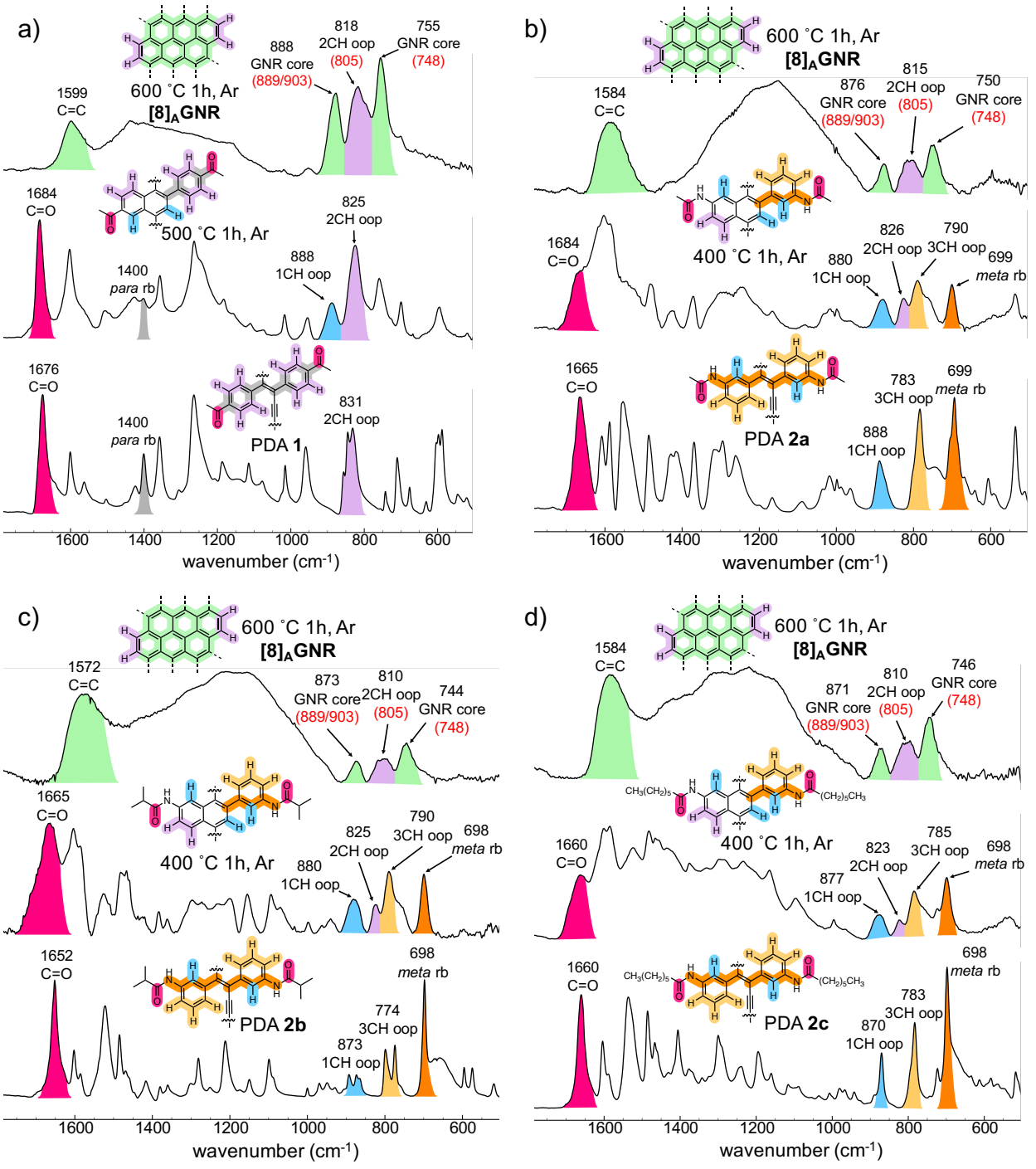

Figure 1.6. Detailed infrared analysis of the conversion of PDAs **1** and **2a–2c** to $[8]_A$GNR via annulated intermediate polymers. Characteristic stretches have been denoted and colored to guide the eye. Experimentally measured vibrations have been marked in black with corresponding calculated (DFT) vibrational modes[33] denoted in red where applicable.

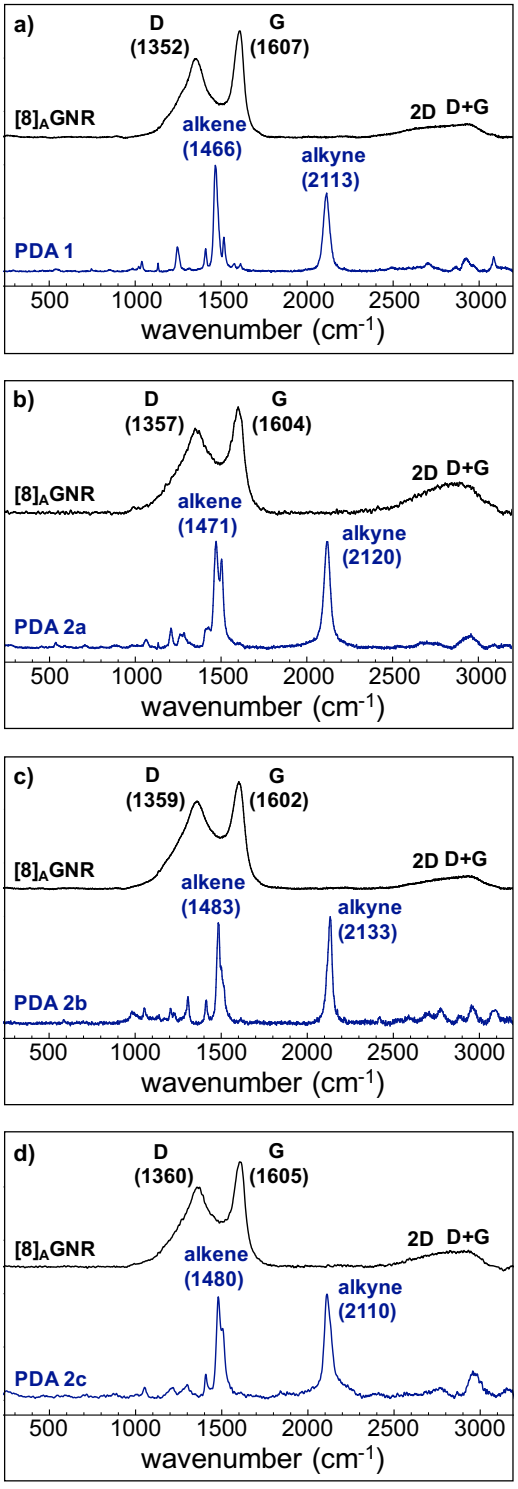

Figure 1.7. Raman spectra of PDAs **1** and **2a**-**2c** and the corresponding $[8]_A$GNR samples produced after thermal conversion. Specific vibrations corresponding to the enyne backbone of the PDA polymers, as well as the D and G peaks characteristic of GNRs, are labeled.

The IR data for PDA **1** heated to 500 ˚C shows the appearance of a new C–H oop bending absorption at 889 cm^{-1}, characteristic of a lone aryl C–H with no adjacent hydrogens, which can only appear if an annulated ring such as naphthalene or chrysene is formed, which is also supported by our frequency calculations (Figures 1.2 and 1.6a).[33,40] Furthermore, the strong phenyl ring bending mode characteristic of *para* substituted rings at 1400 cm^{-1} has been attenuated, lending further support to an annulated intermediate structure. Very similar changes can be noted in the IR spectra of samples of **2a–c** heated to 400 ˚C (Figures 1.6b-d). In all three IR spectra, a new oop C–H bend characteristic of two adjacent aryl hydrogens appears at 826, 825, and 813 cm^{-1} for PDAs **2a**, **2b**, and **2c**, respectively.[40] Importantly, this specific oop C–H bend should only occur if polymers **2a–c** underwent cyclization *para* to their amido substituents.

The combined CP/MAS ^{13}C NMR, IR, and Raman data provide strong evidence that the PDA polymers have undergone successful cyclization of the backbone alkyne units to form annulated polycyclic aromatic structures (Figure 1.2). While the spectroscopic data does not directly point to a specific mechanism of backbone cyclization, it is highly likely that formal Hopf (dieneyne) cyclizations are occurring as designed.

Steps 2 and 3, Exhaustive Cyclodehydrogenation and Side Chain Removal: The remaining two thermal steps, cyclodehydrogenation of the nanoribbon core and side chain removal, both occur upon heating of PDAs **1** and **2a–c** up to 600 ˚C for 1h. Evidence for thermal cyclodehydrogenation is again found through analysis of the CP/MAS ^{13}C NMR, IR and Raman data (Figures 1.6–1.8). The CP/MAS ^{13}C NMR spectra obtained after heating PDAs **1** and **2a–c** to 600 ˚C for 1h show a clean convergence to the uniform spectra of $[8]_A$GNR (Figure 1.8). In all spectra, resonances

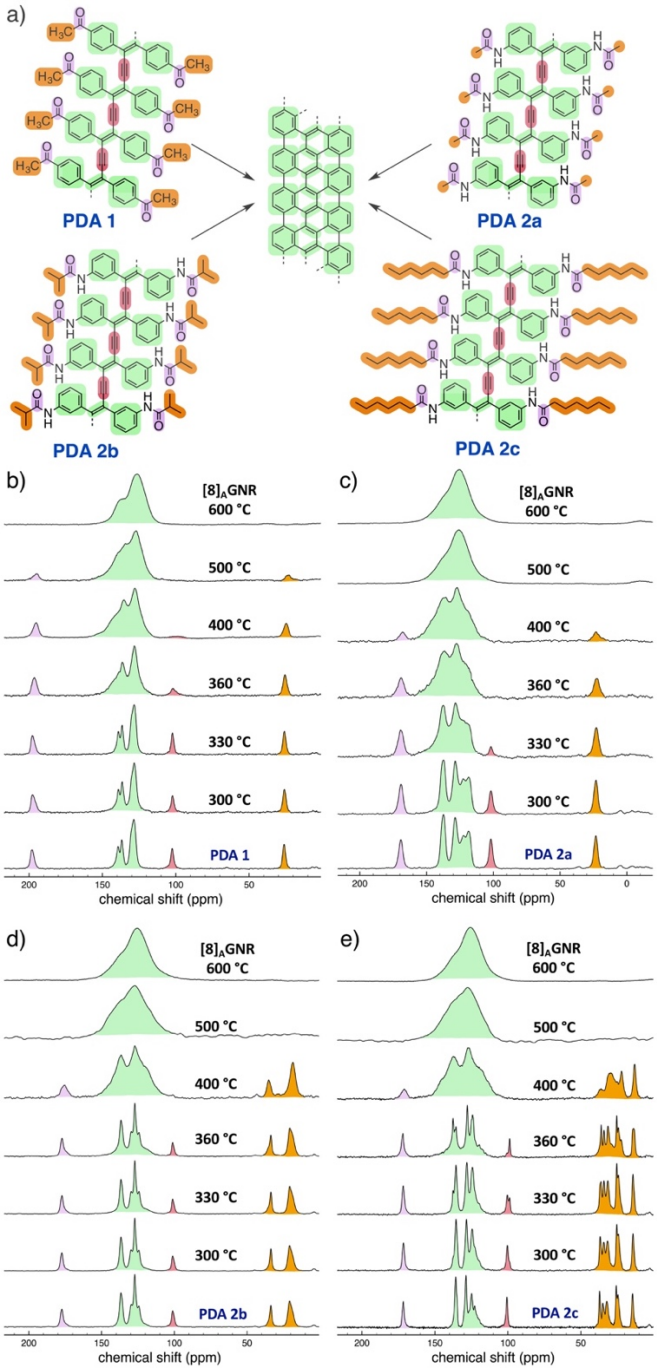

Figure 1.8. CP/MAS ^{13}C NMR spectra for the conversion of PDAs **1**, **2a–2c** to $[8]_AGNR$. a) Overview of the thermal conversions of PDAs **1**, **2a–2c** to $[8]_AGNR$. b–e) Spectra corresponding to the different samples obtained after heating at the temperatures shown, each for one hour. All spectra are normalized for comparison, and spectral acquisition data are included in Appendix A.

corresponding to the carbonyl and alkyl carbons of the PDA side chains are absent, indicating complete removal. Furthermore, the aryl region has simplified dramatically and all spectra of [8]-$_A$GNR exhibit a principal peak centered at 126 ppm, along with a prominent shoulder at 137 ppm. The position of the principal peak is in good agreement with calculated and experimental data for graphene-like systems.[41]

In this context, reagent-less, thermal cyclodehydrogenation reactions to produce annulated polycyclic aromatic hydrocarbons have been shown to occur in polycyclic aromatic systems upon simple heating. For example, Clar synthesized hexabenzocoronene via a high-yielding thermal cyclodehydrogenation of a penultimate intermediate at 482 ˚C.[42] Coronene was also shown to undergo dimerization, ultimately leading to polymerization, through cyclodehydrogenation at its edges upon heating to 530 ˚C.[43]

The spectra of [8]$_A$GNR produced from the different PDAs vary slightly with respect to their peak width at half height, which we attribute to the differences in morphology of the samples (Figure 1.8). In CP/MAS experiments, the intensities of carbon peaks are directly related to the amount of cross-polarization that they experience. In all our CP/MAS experiments, we used a long cross-polarization contact time (5 ms) to eliminate any distance dependence and its effect on the height or ratio between individual peaks. The relative ratio of the shoulder at 137 ppm to the main peak at 126 ppm in all three spectra is ~1:3 (Table 1.1). Due to the highly symmetric nature of the graphene nanoribbons, there should be only four carbons with distinct chemical shifts in [8]$_A$GNR; which include the edge C–H carbons and three quaternary interior carbons (Figures A17 and A18).[33] Deconvolution of the experimental spectra of [8]$_A$GNR obtained from PDAs **1** and **2a** using four equal intensity curves provides the values shown in Table 1. The chemical shifts of the individual carbons of [8]$_A$GNR produced from PDA **1** are centered at 137.6, 129.8, 126.4, and

121.8, while the $[8]_A$GNR produced from PDA **2a** has chemical shifts of 136.3, 128.9, 124.9, and 119.5 respectively. The shoulder peak (137 ppm) can be attributed to the quaternary carbon of the bay region (second row), similar to other well-known polycyclic aromatic hydrocarbons,[44] which is also evidenced by the calculated model for a large section of $[8]_A$GNR (B3LYP//6-31G* level of theory) (Table 1.1 and Figure A19).[33] The NMR shielding tensors were computed with the Gauge-Independent Atomic Orbital (GIAO) method. Overall, the calculated chemical shifts are in rather good agreement with the deconvoluted chemical shifts for the four types of carbons (Table 1.1 and Figure A19).[33]

As was detailed earlier, analysis of the oop CH wag region (1000-700 cm^{-1}) for heated samples of the PDAs confirms the successful cyclization of alkynes on the backbone of PDAs **1** and **2a–c**. Upon heating of the polymers to 600 ˚C , we obtain IR spectra with remarkably similar features which we assign to $[8]_A$GNR (Figure 1.6). The CH oop region is transformed further upon heating to 600 ˚C, producing three distinct peaks. The intensity and shape of the peaks are similar in all samples of $[8]_A$GNR and occur at similar wavenumbers. Critically, all samples of $[8]_A$GNR display an oop CH wagging mode for two adjacent (*ortho*) hydrogens at 818, 815, 810, and 810 cm^{-1} for $[8]_A$GNR produced from PDAs **1** and **2a-c**, respectively. This stretch is consistent with the presence of two adjacent hydrogens at the edges of $[8]_A$GNR. The two other distinguishable peaks in the oop region are centered around 875 cm^{-1} and 750 cm^{-1} for all samples. Frequency analysis performed on a model system slightly shorter than that shown in Table 1.1 gives a finger-print region similar to the experimental spectrum (Figure A22).[33] Analysis of the calculated vibra-tional modes provides insight into the molecular origin of the three fingerprint stretches observed

Table 1.1. Comparison of the fitted experimental spectral curves with calculated ^{13}C NMR chemical shifts (B3LYP/6-31G(d)) for the model $[8]_A$GNR molecule shown in a). b) Deconvolution analysis of the ^{13}C CP/MAS NMR spectrum $[8]_A$GNR obtained from PDA **1** using a set of four curves with equal heights.[45]

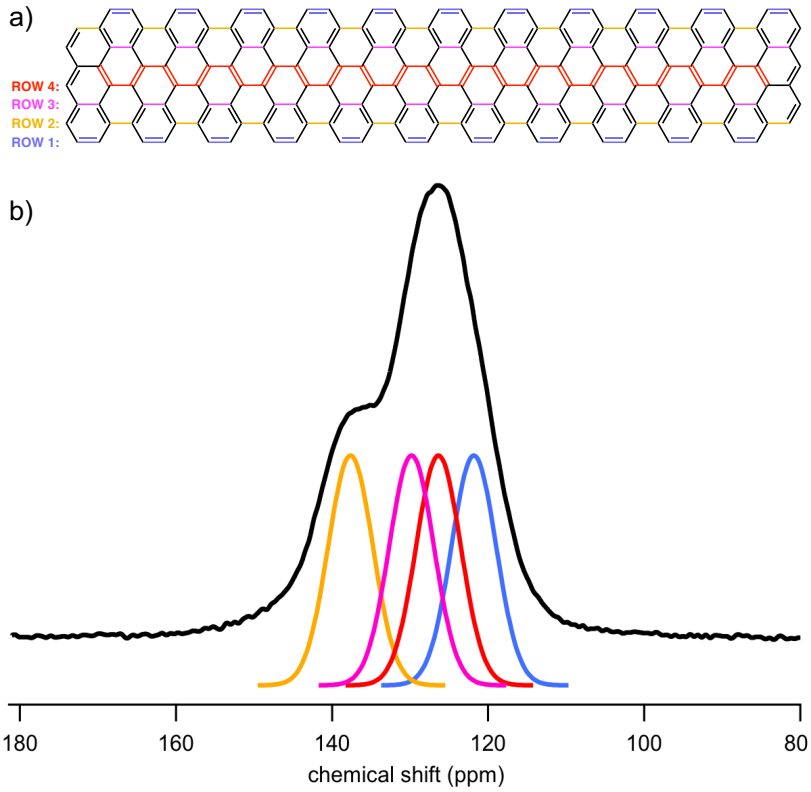

Carbon row	**1**	**2**	**3**	**4**
Deconvoluted (ppm) (PDA **1**)	136.3	128.9	124.9	119.5
Deconvoluted (ppm) (PDA **2a**)	137.6	129.8	126.4	121.8
Calculated (B3LYP) (a)	130.0	125.2	124.4	122.5

in all experimental spectra. The experimental absorption at ~750 cm^{-1} can be attributed to an asymmetric ring stretching mode for the C=C bonds within the $[8]_A$GNR core, calculated to occur at 748 cm^{-1}. Furthermore, the oop CH wagging mode for the edge protons is calculated to occur at 805 cm^{-1} and is observed experimentally around 815 cm^{-1}. Finally, the strong absorption at ~ 875 cm^{-1} is calculated as two modes at 905 and 890 cm^{-1}, which are in-plane rocking modes for the edge CH bonds.

Further confirmation of successful cyclodehydrogenation and side-chain removal is evidenced by the Raman spectra of the respective samples of $[8]_A$GNR (Figure 1.7). Raman spectra of all PDA polymers after heating to 600 ˚C for 1h clearly exhibit D and G peaks, which are spectroscopic signatures for GNRs (Figures 1.7 and A13-A16).[33,46] The $[8]_A$GNRs produced from either **1** or **2a**, **2b** or **2c** display a large D peak at 1352, 1357, 1359, and 1360 cm^{-1} and a base G peak at 1607, 1604, 1602 and 1605 cm^{-1}, respectively. In all four cases, the G peak is slightly upshifted and broadened compared to the G peak for pristine few-layer graphene, which occurs at 1581 cm^{-1}.[47] This shift is consistent with a narrowing of a graphene sheet into "nanographene".[48] Additionally, the overtone 2D and D+G peaks can clearly be identified and display significant broadening. The broadening of these peaks is attributed to π-π^* interactions between multiple layers, a consequence of the stacked nature of our GNRs in bulk samples (see below for TEM section).[49] Importantly, the appearance of the D and G peaks and their overtones provides spectroscopic evidence that exhaustive cyclodehydrogenation has taken place along the PDA nanoribbons to give the $[8]_A$GNRs.

All four samples of $[8]_A$GNR produced from PDAs **1** and **2a–c** to $[8]_A$GNR were also examined by XPS to ensure the complete removal of side-chains as evidenced by the loss of a C=O peak (Figures A9-A12).[33] All C1s spectra of $[8]_A$GNRs display a single peak centered at 284.6 eV, characteristic of sp^2 hybridized carbons engaged in C-C and C-H bonding. All spectra also show significant narrowing of their main C1s peak, due to the absence of any sp or sp^3 hybridized carbons, further confirming that backbone cyclization and side-chain removal is complete.

Transmission Electron Microscopy: The morphology of the PDA polymers and the ensuing GNRs was investigated by high-resolution transmission electron microscopy (HRTEM, Figure 1.9). All four PDA polymers have a thin fibrous nature with uniform thickness, and show large regions of agglomeration (Figure 1.9a). After thermal aromatization to $[8]_A$GNR, all samples display tight (0.34 nm) co-facial graphitic stacking and can clearly be seen by HRTEM (Figure 1.9b). Additionally, the long length and flexibility of the stacked GNRs can be distinctly visualized. The stacked nature of our GNR samples appears reinforced by the initial preorganization of the PDA polymers as they are formed within crystals, which leads to in-register columnar stacks that remain strongly associated after aromatization. This supports the Raman data gathered from the samples and helps to explain the broadening of the 2D and D+G bands as a consequence of tight nanoribbon stacking.[49] Importantly, individual ribbons can be identified and measured (Figures 1.9c,d). Figure 1.9c clearly shows a number of individual $[8]_A$GNRs, produced from thermal aromatization of PDA **2b**, aligned horizontally with respect to each other. Their uniform width (1.2 nm) is confirmed through a plot profile of pixel intensities across a number of GNR bundles (see Figure A23).[33] This value is in close agreement with their calculated width of 1.3 nm.[33]

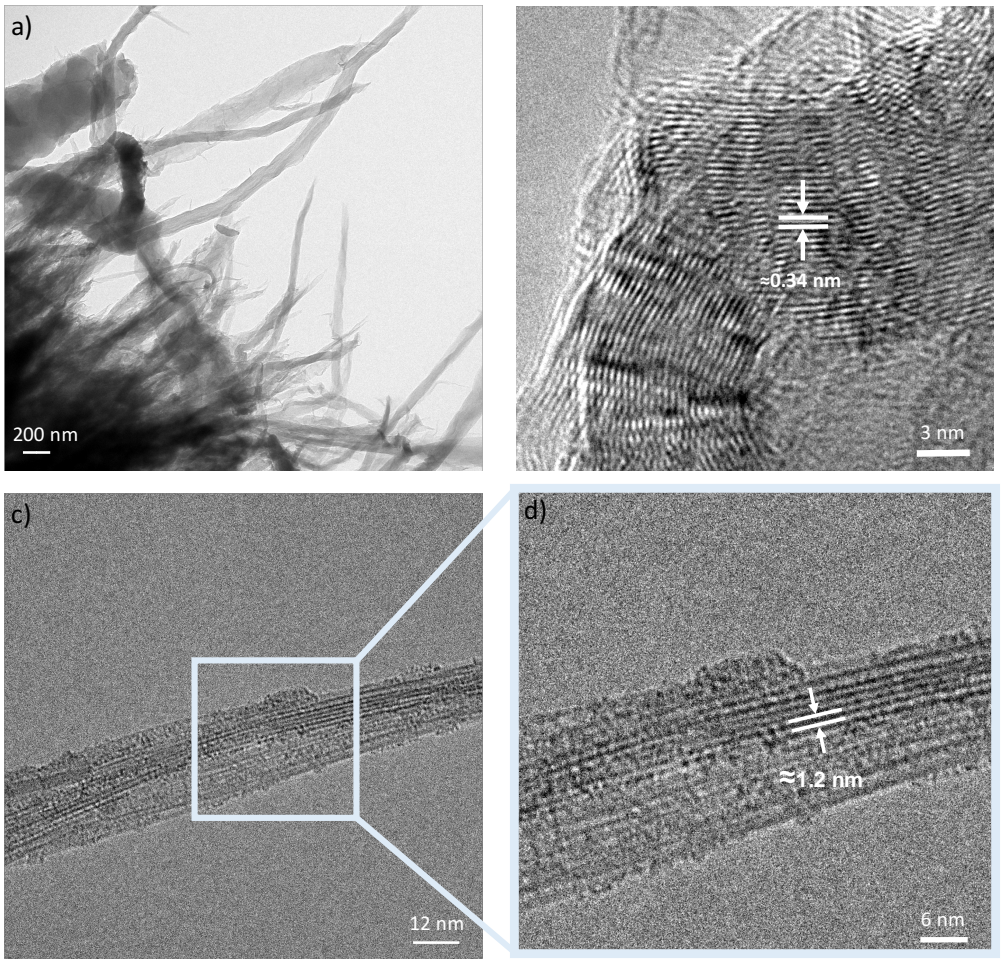

Figure 1.9. TEM and HRTEM analysis of PDA polymers and the $[8]_A$GNRs produced from their solid-state graphitization. a) TEM analysis of PDA polymer **1** showing the thin, layered and fibrous nature of the polymer. b) HRTEM analysis of the resulting $[8]_A$GNR produced from heating of PDA **1**. The tight (0.34 nm) co-facial π-π (002) graphitic stacking of the GNRs can clearly be seen. c,d) HRTEM analysis of $[8]_A$GNR produced from PDA **2b**. Individual GNRs of width ≈ 1.2 nm can clearly be seen.

Section 1.4: Conclusion

We have described here parallel synthetic routes to $[8]_A$GNRs from four distinct, differently substituted 1,4-diphenyl polydiacetylenes. PDA polymers **1** and **2a–2c** can be readily synthesized in bulk quantities via a solid-state topochemical polymerization. Heating of all four PDAs at 600 ˚C under Ar for 1h promotes their conversion to $[8]_A$GNRs in the solid state, without the need for additional reagents. This process occurs via a cascade of thermally promoted reactions including (1) backbone cyclization, (2) exhaustive cyclodehydrogenation, and finally (3) side chain thermolysis, as highlighted by the spectroscopic data. This solid-state reaction cascade is remarkably efficient, as evidenced yields in the PDA **1** and **2a–2c** to GNR conversion process being quantitative in all cases. Accordingly, the quality of this complex transformation can be viewed as a highlight of designed solid-state reaction pathways. Our approach should be expandable to GNRs of different widths and structure (including heteroatoms) via judicious design of the starting diarylbutadiyne monomers. Further studies on the synthetic and mechanistic aspects of these conversions are currently underway and will be communicated in due time.

Acknowledgements: We thank Prof. Yue (Jessica) Wang (UC Merced) for invaluable discussions and advice on the TEM data. We would like to thank Dr. Christopher Turner (Prof. Richard Kaner group) for assistance with the GNR heating experiments and Drs. Ta-Chung Ong and Robert Taylor (UCLA MIC instrumentation facility) for assistance with the NMR experiments. Prof. Jeffery I. Zink assisted in preliminary Raman work and discussions. This work was supported by grants from the National Science Foundation to YR (NSF-CHE-1608957) and to KNH (DMR-1335645

and CHE-1254897). This work used computational and storage services associated with the Hoffman2 cluster provided by the UCLA Institute for Digital Research and Education's Research Technology Group, the NSF-supported Extreme Science and Engineering Discovery Environment (XSEDE) (OCI-1053575), and high performance research computing resources provided by Texas A&M University (http://hprc.tamu.edu).

Section 1.5: Experimental

Topochemical polymerizations were carried out using a high powered Hanovia lamp inside a quartz immersion well for cooling. All PDA heating experiments were carried out in alumina boats inside a programmable tube furnace under a positive argon flow. Solid state CP/MAS ^{13}C NMR experiments were performed on a Bruker DSX300 instrument operating at 300 MHz, utilizing a 4mm zirconia rotor spinning at 10 KHz. Raman spectra were obtained using a laser excitation wavelength of 514 nm with a maximum output of 40mW. IR spectra were obtained using an ATR-IR. TEM and HRTEM samples were prepared by drop-casting of dispersed PDA samples onto Si wafers. The PDA coated Si wafers were then heated at 600 ºC for 1h under argon flow to promote graphitization. The newly formed GNRs were then mechanically transferred to a TEM grid by brushing of the grid against the GNR coated surface. All TEM images were collected on a Tecnai G^2 TF20 (FEI). Figure 1.9a,b were collected at 200 kV on TEM grids with formvar films and lacey carbons grids. Figure 1.9c,d were acquired at 200 kV with low-dose technique on TEM grids with only lacey carbon. Figure 1.9d was processed using ImageJ.

General Procedures: Unless stated otherwise, reactions were performed under an argon atmosphere in flame-dried glassware. Tetrahydrofuran (THF), methylene chloride (CH_2Cl_2), di-

ethyl ether (Et_2O), toluene (C_7H_8), and acetonitrile (CH_3CN) were passed through activated alumina columns prior to use. Chemical reagents were obtained from commercial sources and used without further purification. Reaction temperatures were controlled using an IKA magnetic stirplate with a temperature modulator and oil bath. Procedures were performed at room temperature (~23 ˚C) unless otherwise indicated. Column chromatography was performed on Silicycle (Siliflash P60) silica gel 60 (240-400 mesh). Thin layer chromatography utilized pre-coated plates from E. Merck (silica gel 60 PF254, 0.25 mm).

4'-Ethynylacetophenone and compounds **3**, **7c**, and **4c** were prepared according to their previously reported syntheses.[50,51] All spectra of known compounds matched their reported values and are tabulated below. For new compounds that were synthesized for this study (namely compounds **7a**, **4a**, **7b**, and **4b**), their ^1H and ^{13}C NMR spectra are included in Figures **A28–A35**.

4'-Ethynylacetophenone

4'-Bromoacetophenone (10.5 g, 52.8 mmol, 1 eq) was added to a round bottom flask with a stirbar under argon. THF (160 mL, 0.33M) was added, followed by bis(triphenylphosphine)palladium dichloride (1.85 g, 2.6 mmol, 0.05 eq) and copper(I) iodide (1.01 g, 5.28 mmol, 0.1 eq) in one portion. This mixture was sparged with argon for 30 min and then trimethylsilylacetylene (10.4 g, 105 mmol, 2 eq) was added and the mixture heated to reflux until judged complete by ^1H NMR (typically overnight). The mixture was cooled to room temperature and potassium fluoride (6.13 g, 105 mmol, 2 eq) was added along with methanol (110 mL) and the mixture allowed to stir open in the air. Once the deprotection was complete as judged by NMR, the mixture was filtered over celite, and concentrated. The crude residue was purified by filtration over SiO_2 eluting with

CH_2Cl_2. Recovered 6.2 g (81%) of 4'-ethynylacetophenone as a deep yellow oil. **Spectral data:** ^{1}H NMR (400 MHz, $CDCl_3$): 2.60 (s, 3H), 3.24 (s, 1H), 7.57 (d, J = 8.6 Hz, 2H), 7.90 (d, J = 8.6, 2H); ^{13}C NMR (100 MHz, $CDCl_3$): 26.65, 80.35, 82.76, 126.93, 128.20, 132.31, 136.80, 197.27. HRMS (DART) Calculated for $C_{10}H_8O$ [$M^{\bullet+}$]: 144.05751; found 144.05872.

1,1'-(Buta-1,3-diyne-1,4-diylbis(4,1-phenylene))bis(ethan-1-one) (3)

4'-Ethynylacetophenone (6.2 g, 43 mmol, 1 eq) was added to a round bottom flask with a stirbar and dissolved in CH_2Cl_2 (200 mL, .2M). To this mixture was added copper(I) iodide (820 mg, 4.3 mmol, 0.1 eq) and TMEDA (500 mg, 4.3 mmol, 1 eq) in one portion. Air was bubbled into the mixture and allowed to react at room temperature until complete as indicated by TLC. Upon completion, the mixture was diluted with water and partitioned via a separatory funnel. The aqueous layer was extracted with fresh CH_2Cl_2 three times, organics pooled, washed with 0.5M HCl, brine, dried over $MgSO_4$, filtered and concentrated *in vacuo* to give the crude product as a crystalline solid. The crude product was immediately recrystallized from boiling ethanol via hot filtration and the receiving flask covered from ambient light to limit polymerization of the forming crystals. Recovered 5.1 g (83%) of **3** as clear crystals which rapidly turn blue upon standing in ambient light. **Spectral data:** ^{1}H NMR (400 MHz, $CDCl_3$): 2.61 (s, 3H), 7.62 (d, J = 8.6 Hz, 2H), 7.94 (d, J = 8.6, 2H); ^{13}C NMR (100 MHz, $CDCl_3$): 26.67, 76.56, 81.98, 126.26, 128.31, 132.71, 137.12, 197.06. HRMS (DART) Calculated for $C_{20}H_{14}O_2$ [$M^{\bullet+}$]: 286.09938; found 286.098676.

N-(3-Ethynylphenyl)acetamide (7a)

Acetyl chloride (4.15 g, 78.50 mmol, 1.2 eq) dissolved in CH_2Cl_2 (20 mL, 2.5M) was added to a solution of 3-ethynylaniline (5.20 g, 44.39 mmol, 1.0 eq) and triethylamine (5.83 g, 57.71

mmol, 1.3 eq) in CH_2Cl_2 (150 mL) at 0°C. The mixture was allowed to warm to room temperature and stirred until complete by TLC. The reaction mixture was washed twice with an aqueous $NaHCO_3$ solution before passing the organic layer over a SiO_2 plug. A total of 7.23 g (99%) of **7a** was recovered as a yellow solid. **Spectral data:** ^{1}H NMR (400 MHz, $CDCl_3$): 2.17 (s, 3H), 3.05 (s, 1H), 7.21 (td, J = 1.8 Hz, 4.0 Hz, 1H), 7.26 (t, J = 8.0 Hz, 1H), 7.43 (br, 1H), 7.53 (td, J = 1.8 Hz, 4.0 Hz, 1H), 7.61 (t, J = 1.8 Hz, 1H); ^{13}C NMR (100 MHz, $CDCl_3$): 24.59, 77.47, 83.16, 120.44, 122.82, 123.24, 128.02, 129.03, 137.94, 168.48; HRMS (DART) Calculated for $C_{10}H_9NO$ [$M^{\bullet+}$]: 160.07569; found 160.07540.

N,N'-(Buta-1,3-diyne-1,4-diylbis(3,1-phenylene))diacetamide (4a)

N-(3-Ethynylphenyl)acetamide (7.07 g, 44.39 mmol, 1.0 eq), copper (I) iodide (845 mg, 4.44 mmol, 0.1 eq) and TMEDA (2.58 g, 22.193 mmol, 0.5 eq) was dissolved in CH_2Cl_2 (134 mL, 0.33M) . Air was bubbled through the mixture and allowed to stir at room temperature overnight. The insoluble product was filtered and washed with water before hot recrystallization from acetone. 4.91 g (70%) of **4a** was isolated as clear crystals which rapidly turn blue. **Spectral data:** ^{1}H NMR (400 MHz, DMSO): 2.02 (s, 3H), 7.23 (td, J = 1.4 Hz, 4.0 Hz, 1H), 7.32 (t, J = 8.0 Hz, 1H), 7.56 (td, 1.4 Hz, 4.0 Hz, 1H), 7.84 (t, J = 1.4 Hz, 1H), 10.06 (br, 1H); ^{13}C NMR (100 MHz, DMSO): 24.49, 73.60, 82.25, 121.04, 122.55, 127.47, 129.92, 140.13, 169.13; HRMS (DART) Calculated for $C_{20}H_{16}N_2O_2$ [$M^{\bullet+}$]: 317.12845; found 317.12841.

N-(3-Ethynylphenyl)isobutyramide (7b)

3-Ethynylaniline (5.00 g, 42.68 mmol, 1.0 eq), isobutyric acid (3.756g, 42.68 mmol, 1.0 eq), N,N'-dicyclohexylcarbodiimide (8.79 g, 42.68 mmol, 1.0 eq) and DMAP (677 mg, 5.55 mmol,

0.13 eq) were dissolved in CH_2Cl_2 (200 mL, 0.22M) and stirred at room temperature overnight. The resulting mixture was filtered and the filtrate concentrated *in vacuo* before purification by column chromatography with SiO_2 eluting with CH_2Cl_2. Recovered 6.67 g (84%) of **7b**. **Spectral data:** ^{1}H NMR (400 MHz, $CDCl_3$): 1.25 (s, 3H), 1.26 (s, 3H), 2.49 (septet, J =6.9 Hz, 1H), 3.05 (s, 1H), 7.10 (br, 1H), 7.22 (ddd, J = 0.6 Hz, 1.1 Hz, 8.0 Hz, 1H), 7.27 (t, J = 8.0 Hz, 1H), 7.57 (ddd, J = 0.6 Hz, 1.1 Hz, 8.0 Hz, 1H), 7.64 (dd, J = 0.6 Hz, 1.1 Hz, 1H); ^{13}C NMR (100 MHz, $CDCl_3$): 19.58, 36.76, 77.41, 83.13, 120.28, 122.83, 123.12, 127.87, 129.04, 138.02, 175.22; HRMS (DART) Calculated for $C_{12}H_{13}NO$ [$M^{\bullet+}$]: 187.09917; found 187.09986.

N,N'-(Buta-1,3-diyne-1,4-diylbis(3,1-phenylene))bis(2-methylpropanamide) (4b)

N-(3-Ethynylphenyl)isobutyramide (659 mg, 3.52 mmol, 1.0 eq) was dissolved in CH_2Cl_2 (10 mL. 0.33M) before copper (I) iodide (67 mg, 0.35 mmol, 0.1 eq) and TMEDA (41 mg, 0.35 mmol. 0.1 eq) were added to the flask. Air was bubbled through the mixture and allowed to stir at room temperature overnight. The insoluble product was filtered and washed with water before recrystallization by hot filtration from THF. 549 mg (84%) of **4b** was recovered as clear crystals which rapidly turn blue. **Spectral data:** ^{1}H NMR (400 MHz, DMSO): 1.06 (s, 3H), 1.07 (s, 3H), 2.55 (heptet, J = 6.9 Hz, 1H), 7.23 (ddd, J = 0.6 Hz, 1.1 Hz, 8.0 Hz, 1H), 7.33 (t, J = 8.0 Hz, 1H), 7.61 (ddd, J = 0.6 Hz, 1.1 Hz, 8.0 Hz, 1H), 7.86 (dd, J = 0.6 Hz, 1.1 Hz, 1H), 9.95 (br, 1H); ^{13}C NMR (100 MHz, DMSO): 19.89, 35.47, 73.57, 82.23, 121.02, 121.28, 122.72, 127.46, 129.91, 140.26, 176.05; HRMS (DART) Calculated for $C_{24}H_{24}N_2O_2$ [$M^{\bullet+}$]: 372.1833; found 372.17976.

***N*-(3-Ethynylphenyl)heptanamide (7c)**

3-Ethynylaniline (3.5 g, 30 mmol, 1 eq) was added to a round bottom flask with a stirbar and reflux condenser, pyridine (150 mL, 0.2M) was added followed by heptanoic anhydride (10.9 g, 45 mmol, 1.5 eq) and finally dimethylaminopyridine (DMAP) (367 mg, 3 mmol, 0.1 eq). The resulting mixture was heated to 100 °C. After stirring overnight, the reaction was complete as indicated by TLC. The mixture was concentrated *in vacuo*, partitioned between Et_2O/H_2O, aqueous extracted x2 with fresh Et_2O, organic pooled, washed with 0.5M HCl x2, brine, dried over $MgSO_4$, filtered and concentrated *in vacuo* to give a crude residue. The residue was purified by column chromatography on SiO_2 utilizing a gradient of 0% to 20% EtOAc in hexanes. Recovered 6.6 g (95%) of **7c** as an oil. **Spectral data:** ^{1}H NMR (400 MHz, $CDCl_3$): 0.88 (t, J = 7 Hz, 3H), 1.32 (m, 6H), 1.7 (q, J = 7.5 Hz, 2H), 2.34 (t, J = 7.5 Hz, 2H), 3.05 (s, 1H), 7.21 (dt, J = 7.7, 1.5 Hz, 1H), 7.25 (t, J = 7.7 Hz, 1H), 7.36 (br, 1H), 7.55 (dt, J = 7.7, 1.7 Hz, 1H), 7.63 (m, J = 1.7, 1.5 Hz, 1H); ^{13}C NMR (100 MHz, $CDCl_3$): 14.04, 22.50, 25.55, 28.93, 31.56, 37.78, 77.40, 83.18, 120.40, 122.80, 123.23, 127.88, 129.00, 138.02, 171.64. HRMS (DART) Calculated for $C_{15}H_{19}NO$ [$M^{\bullet+}$]: 229.14666; found 229.14354.

***N*,*N*'-(Buta-1,3-diyne-1,4-diylbis(3,1-phenylene))diheptanamide (4c)**

N-(3-Ethynylphenyl)heptanamide (6.6 g, 28.7 mmol, 1 eq) was added to a round bottom flask with a stirbar and dissolved in CH_2Cl_2 (100 ml, 0.33M). To this mixture was added copper(I) iodide (550 mg, 2.8 mmol, 0.1 eq) followed by TMEDA (325 mg, 2.8 mmol, 0.1 eq). Air was bubbled through the mixture and allowed to react at room temperature overnight. In the morning a large amount of insoluble product had formed and the percipitate was filtered over a fritted funnel. The filtrate was added back to the reaction flask and allowed to continue to react. The filtered

product was washed with CH_2Cl_2 and dried. Repeating of this process until the reaction was complete produced a large amount of white precipitate product which turned blue upon standing. The product was recrystallized from boiling isopropanol via hot filtration and the receiving flask was covered to block out ambient light during cooling. Recovered 5.8 g (88%) of **4c** as clear crystals which rapidly turned blue upon standing in ambient light. ^{1}H NMR (400 MHz, DMSO): 0.86 (t, J = 7.2 Hz, 3H), 1.29 (m, 6H), 1.58 (q, J = 7.3, 2H), 2.31 (t, J = 7.3 Hz, 2H), 7.26 (ddd, J = 8, 1.1, 1.8 Hz, 1H), 7.36 (t, J = 8 Hz, 1H), 7.61 (ddd, J = 1.8, 1.1, 8 Hz, 1H), 7.89 (t, J = 1.8 Hz, 1H), 10.04 (s, 1H); ^{13}C NMR (100 MHz, DMSO): 13.94, 21.99, 24.97, 28.31, 31.04, 36.43, 73.12, 81.77, 120.56, 120.64, 122.14, 126.97, 129.46, 139.69, 171.66. HRMS (DART) Calculated for $C_{30}H_{36}N_2O_2$ [$M^{\bullet+}$]: 456.27768; found 456.27679.

General procedure for topochemical polymerizations:

The crystals to be irradiated were placed into a suitable Erlenmeyer flask and suspended in hexanes with a stir bar. The flask was capped and placed inside a photoreactor equipped with a water-jacketed quartz immersion well with a high-powered Hanovia lamp inside. The flask was placed on a stirplate with stirring to ensure the crystals would mix in the liquid to expose all faces to UV light. The lamp was turned on and the crystals were allowed to react overnight. In the morning, the crystals typically took on a deep purple or black color. The crystals were filtered to remove hexanes and then dissolved in a solvent that readily dissolved the monomer. This solution was boiled to ensure complete dissolution of the monomer from the crystals, resulting in a suspension of the PDA polymer. The hot mixture was filtered over a Buchner funnel with a filter paper and the polydiacetylene "paper" produced was further washed with fresh solvent. The PDA paper could be easily peeled away from the filter paper and further dried under vacuum to give pure

polymer. Due to the insolubility of the polymers, their purity was routinely checked by CP/MAS ^{13}C NMR, as the internal alkyne carbon (≈100 ppm) can easily be distinguished from the monomeric butadiyne (≈70-80 ppm). Utilizing the above procedure, specifically, boiling of the solvent while dissolving the reacted crystals, we rarely observed any monomer impurities in our recovered polymer samples. The recovered monomer solution was concentrated and recrystallized to produce more monomer crystals for further polymerization. As an example, 11.6 g of diyne **3** was subjected to UV irradiation overnight, dissolved and filtered to produce 807 mg (7 %) of PDA **1**. The dissolved monomer solution was concentrated and recrystallized to produce 10.6 g of crystalline diyne **3**. Repetition of this process 3 more times produced a total of 2.8 g (24 % overall yield) of PDA **1** from 11.6 g of diyne **3**.

Diyne 3:

Polymerization yield: 960 mg of PDA **1** was recovered from 14 g of crystals (7%)

Solvent: Boiling $CHCl_3$ is an ideal solvent for dissolution of the monomer

Recrystallization: Boiling ethanol and hot filtration

Diyne 4a:

Polymerization yield: 185 mg of PDA **2a** was recovered from 1.7 g of crystals (11%)

Solvent: Boiling THF is an ideal solvent for dissolution of the monomer followed by additional boiling of the crude PDA in DMF, filtering, and washing with diethyl ether

Recrystallization: Boiling acetone and hot filtration

Diyne 4b:

Polymerization yield: 363 mg of PDA **2b** was recovered from 1.56 g of crystals (23%)

Solvent: Boiling in a 1:1 solution of THF:acetone is an ideal solvent for dissolution of the monomer followed by additional boiling of the crude PDA in DMF, filtering, and washing with diethyl ether

Recrystallization: Boiling THF and hot filtration

Diyne 4c:

Polymerization yield: 540 mg of PDA **2c** was recovered from 3.6 g of crystals (15%)

Solvent: Boiling THF is an ideal solvent for dissolution of the monomer

Recrystallization: Boiling isopropanol and hot filtration

General procedure for the graphitization experiments:

For the conversion of the PDA polymers **1** and **2a–c** to $[8]_A$GNR, a programmable tube furnace (MTI OTF-1200X-S-NT) was used. A quartz tube with internal diameter of 2 inches was used, and the PDA to be heated was placed in an alumina boat inside the quartz tube in the middle of the hot zone. End caps were clamped onto the tube to provide a positive flow of Argon. The program used for the heating experiments is as follows: heat over 40 min to the target temperature, hold at target temperature for 1 h, then cool to room temp over 40 min. Due to the thermal mass of the tube, cooling of the system from higher temperatures (>400 ˚C) could take long times, but the system rapidly cooled from the higher temperatures (>400 ˚C) to below 250 ˚C at the end of the 40 min cooling period. After the system had cooled to 25 ˚C, the material was removed from the alumina boat and immediately weighed to quantify mass loss and yield, as reported in Table A1.

Section 1.6: Appendix A

The yields for the graphitization process were determined by measuring the amount of material recovered after thermal aromatization of the respective PDAs (Table A1). The expected theoretical mass recovery after complete graphitization of the PDAs **1**, and **2a-2c** was 68%, 62%, 53%, and 43% respectively. After heating of PDAs **1**, and **2a–2c** to 600 ˚C for 1h under argon, the experimental mass recovery matched the theoretical mass recovery in all cases. This implies that the yield for the overall PDA to GNR conversion process is quantitative for all cases presented here.

Table A1. Mass and percent mass recovery for the thermal conversions of PDAs **1** and **2a–c** to $[8]_A$GNR.

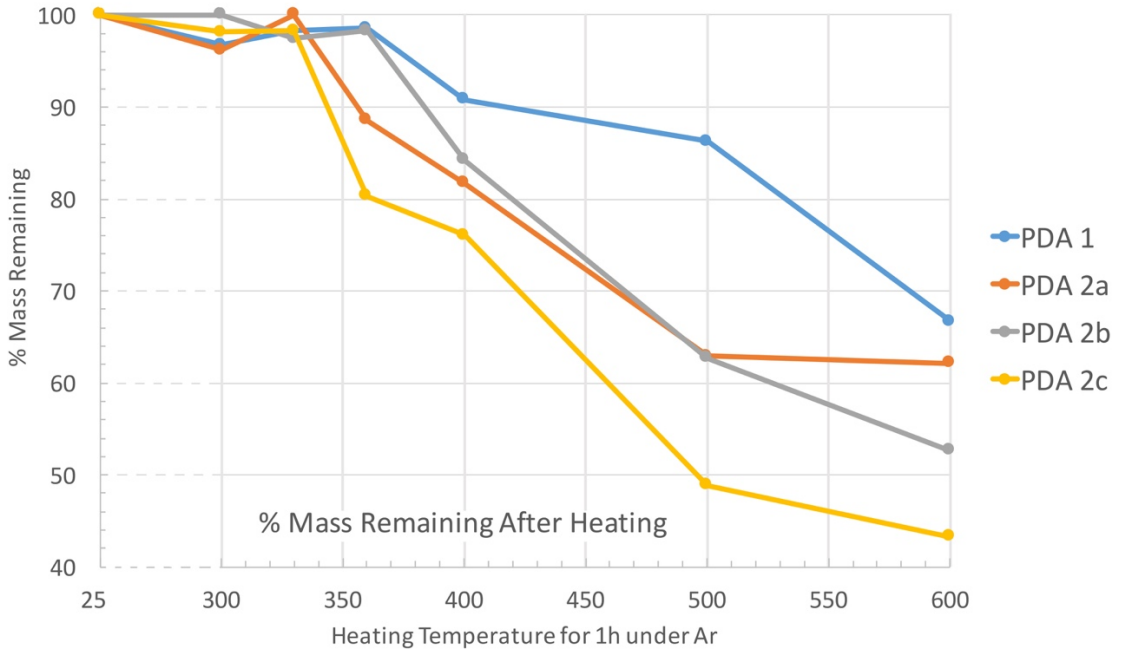

Temperature (˚C)	Amount (mg) at:	1	2a	2b	2c
25	starting mass	62	52	66	53
300	final mass	60	50	66	52
	mass % remaining[1]	97%	96%	100%	98%
25	starting mass	57	37	78	59
330	final mass	56	37	76	58
	mass % remaining[1]	98%	100%	97%	98%
25	starting mass	71	35	59	66
360	final mass	70	31	58	53
	mass % remaining[1]	99%	89%	98%	80%
25	starting mass	76	93	76	71

400	final mass	69	76	64	54
	mass % remaining[1]	91%	82%	84%	76%
25	starting mass	80	143	134	135
500	final mass	69	90	840	66
	mass % remaining[1]	86%	63%	63%	49%
25	starting mass	318	148	76	141
600	final mass	212	92	40	61
	mass % remaining[1]	67%	62%	53%	43%
	theoretical mass % remaining[2]	68%	62%	53%	43%
	$[8]_A$GNR yield[3]	99%	100%	100%	100%

[1] The mass percent remaining was calculated by dividing material mass before and after a heating experiment. [2] The theoretical mass percent remaining was calculated by comparing the molecular weight of a pristine PDA monomer unit to that of $[8]_A$GNR (after undergoing side-chain loss and exhaustive cyclodehydrogenation). [3] The overall yield for the PDA to $[8]_A$GNR process was determined by dividing the experimental and theoretical mass percentages for product remaining after heating to 600 ˚C.

Supplementary spectroscopic data for PDAs **1**, **2a–2c** and $[8]_A$GNR

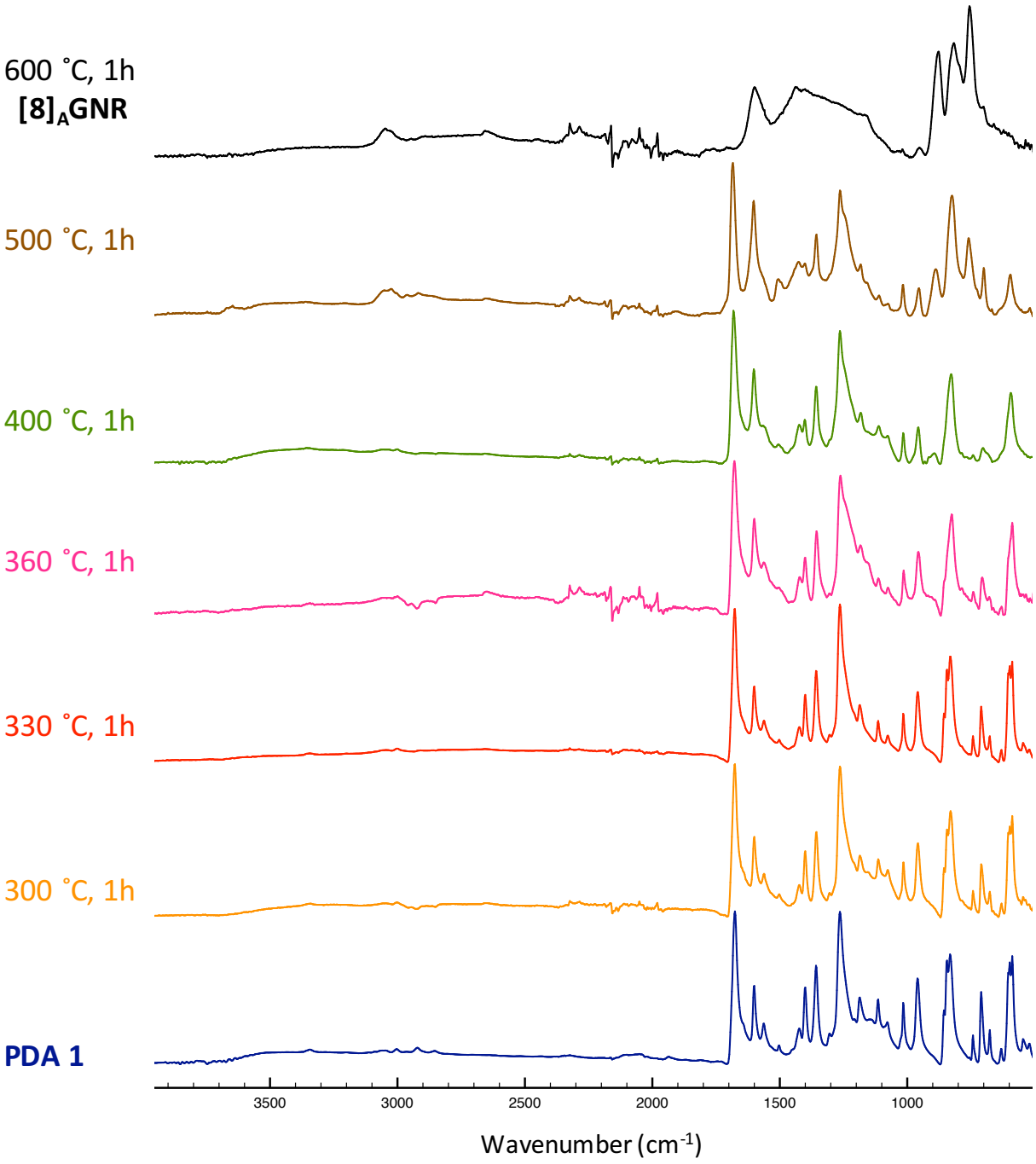

Figure A1. Full width infrared spectrum detailing the conversion of PDA **1** to $[8]_A$GNR.

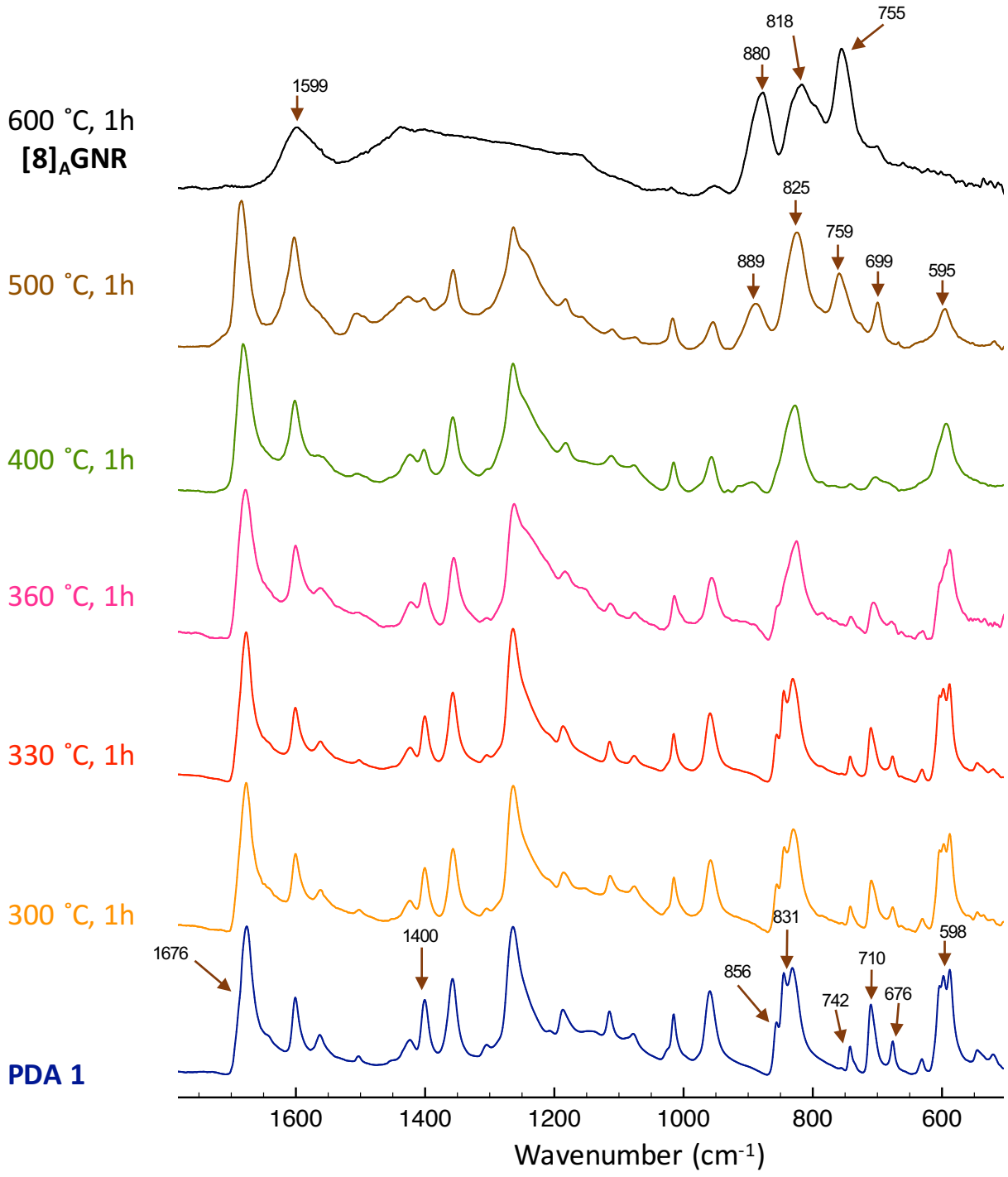

Figure A2. Fingerprint region expansion of infrared spectrum detailing the conversion of PDA **1** to $[8]_A$GNR.

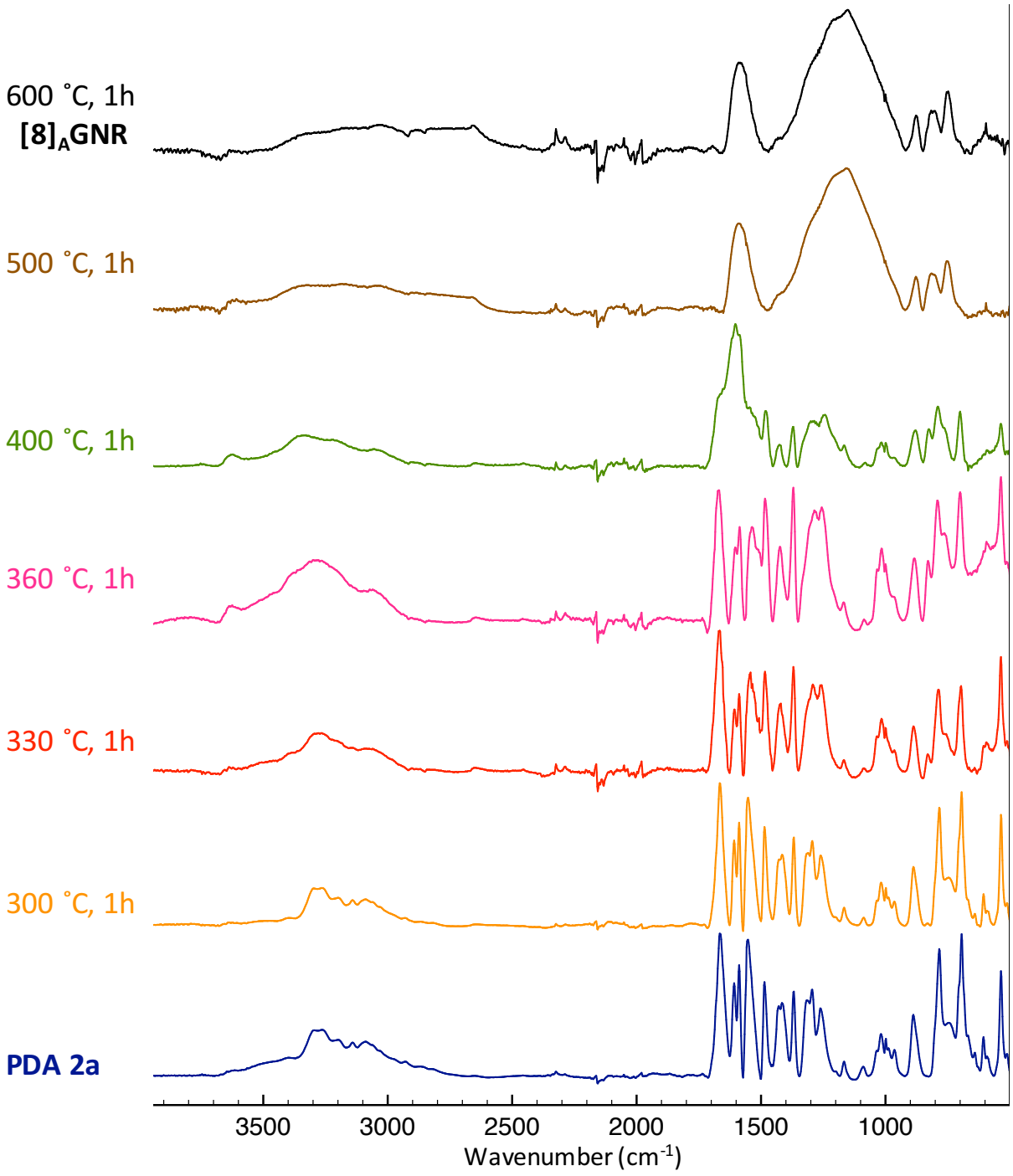

Figure A3. Full width infrared spectrum detailing the conversion of PDA **2a** to $[8]_A$GNR.

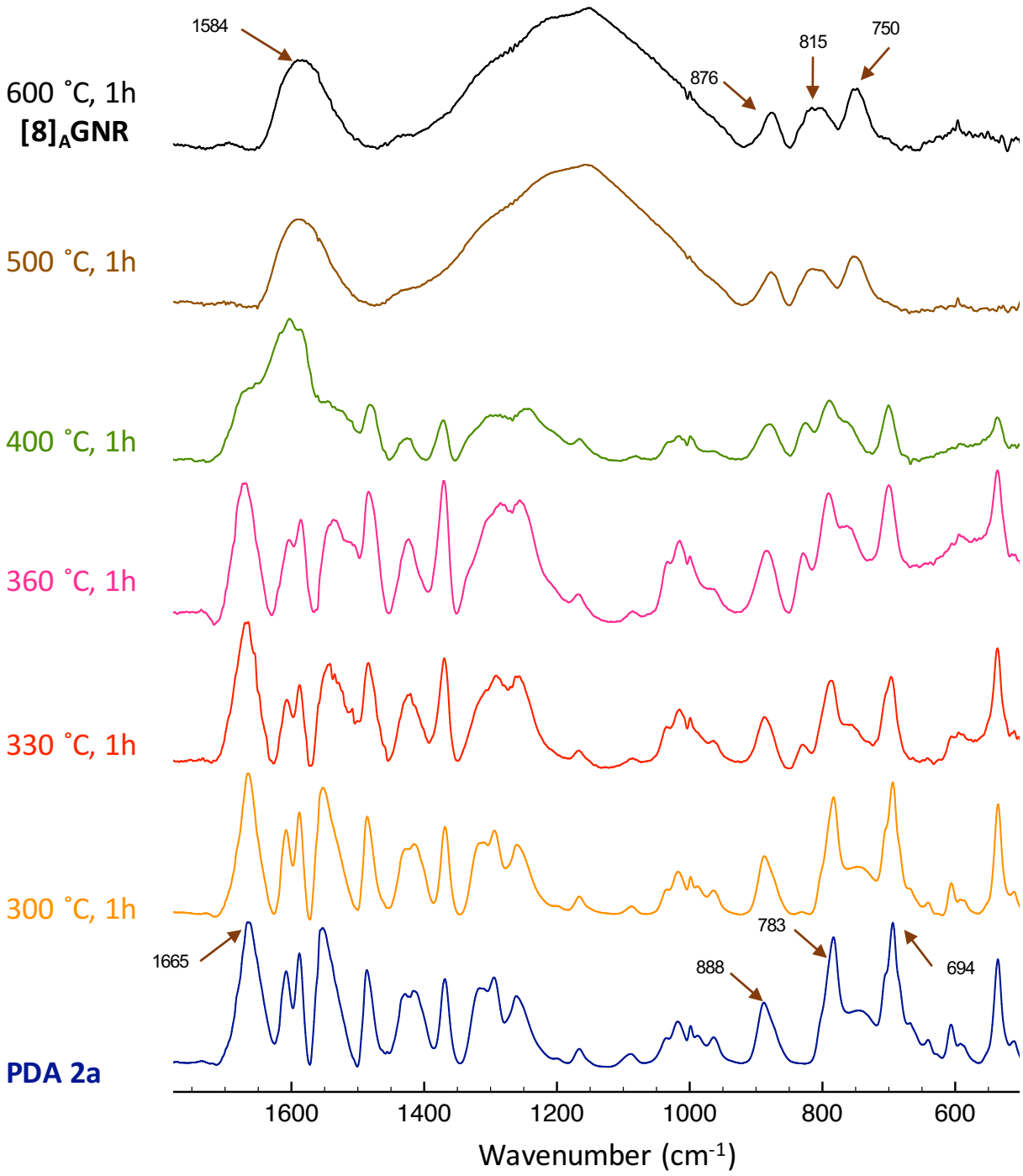

Figure A4. Fingerprint region expansion of infrared spectrum detailing the conversion of PDA **2a** to $[8]_A$GNR.

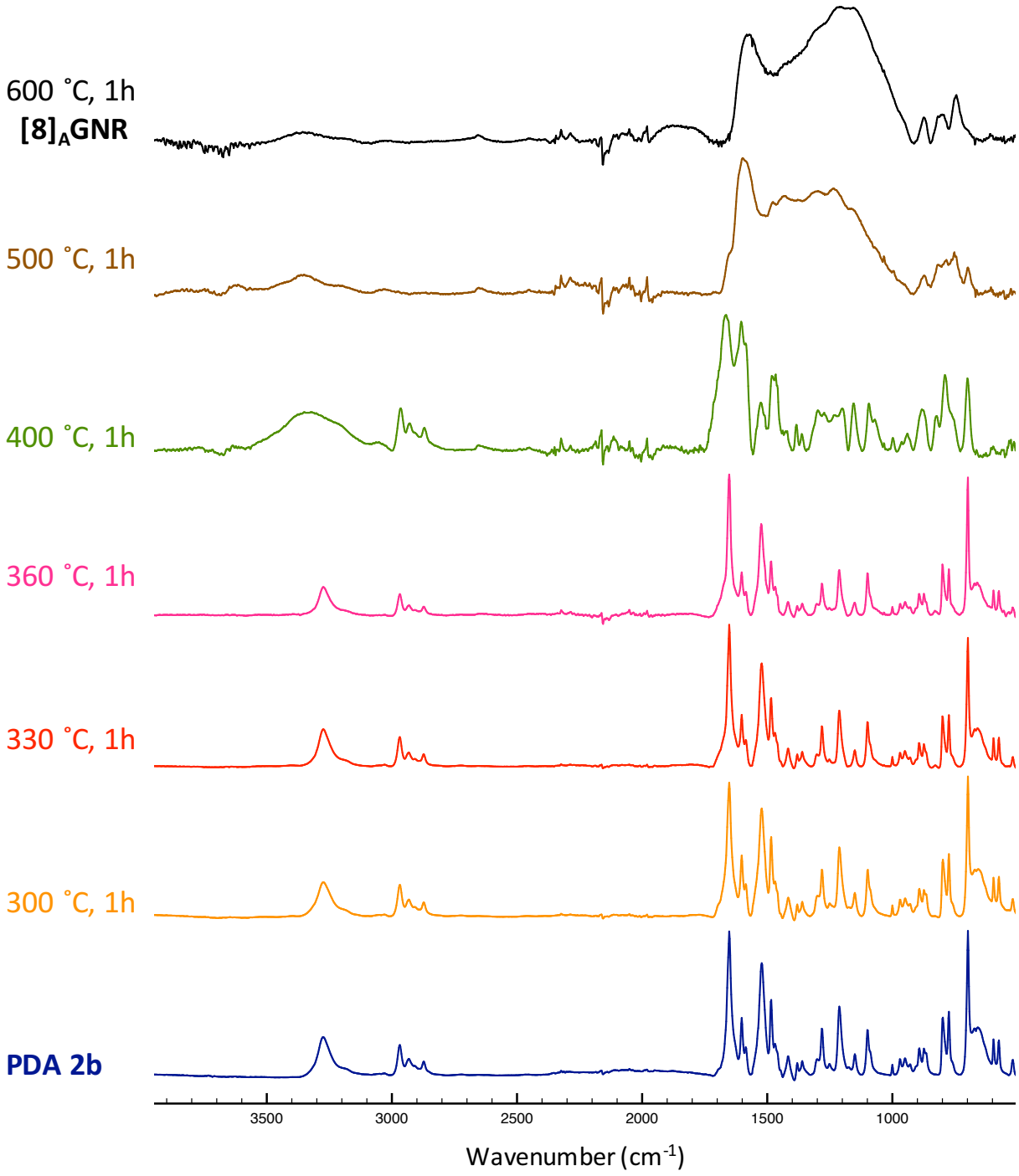

Figure A5. Full width infrared spectrum detailing the conversion of PDA **2b** to $[8]_A$GNR.

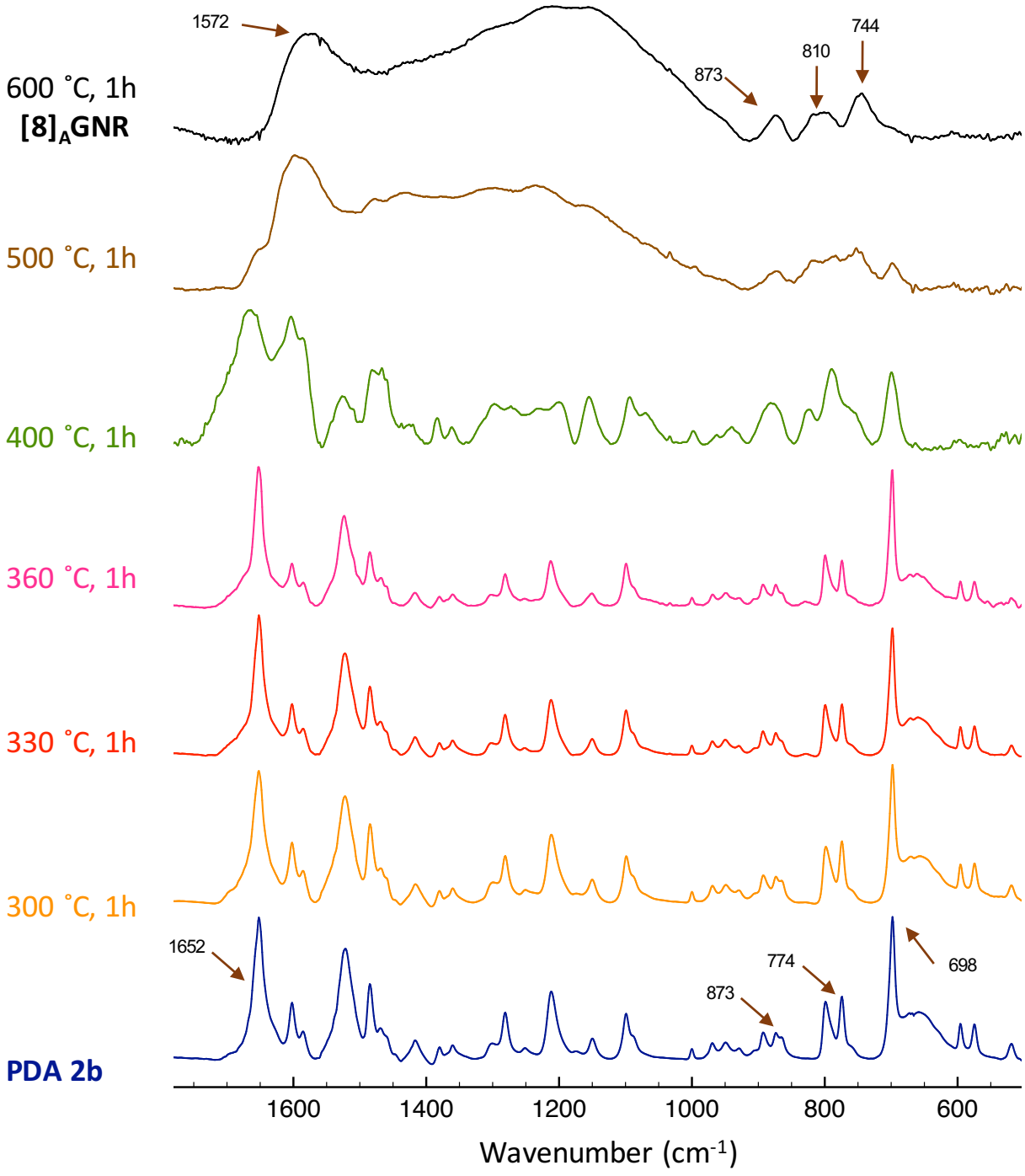

Figure A6. Fingerprint region expansion of infrared spectrum detailing the conversion of PDA **2b** to $[8]_A$GNR.

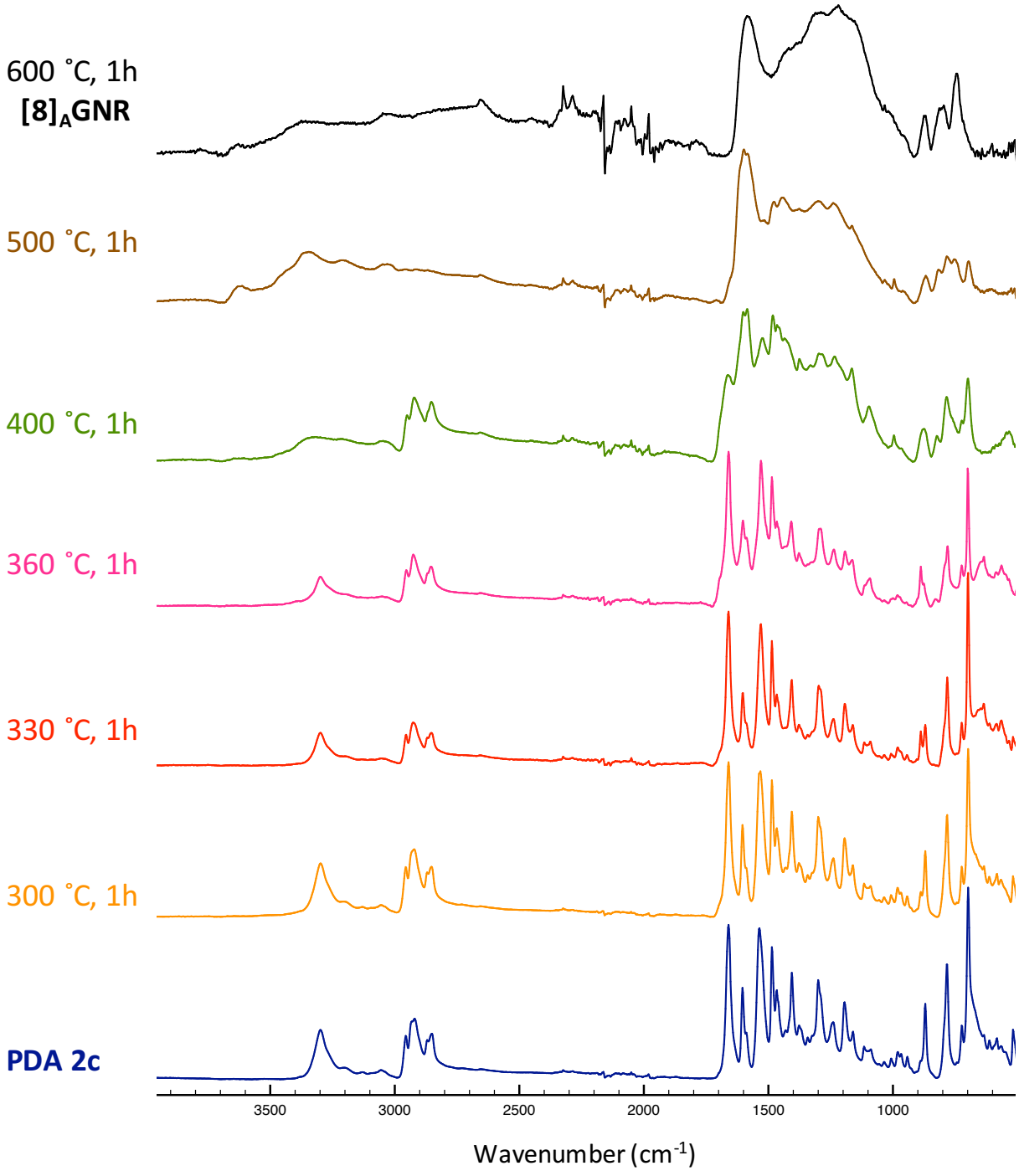

Figure A7. Full width infrared spectrum detailing the conversion of PDA **2c** to $[8]_A$GNR.

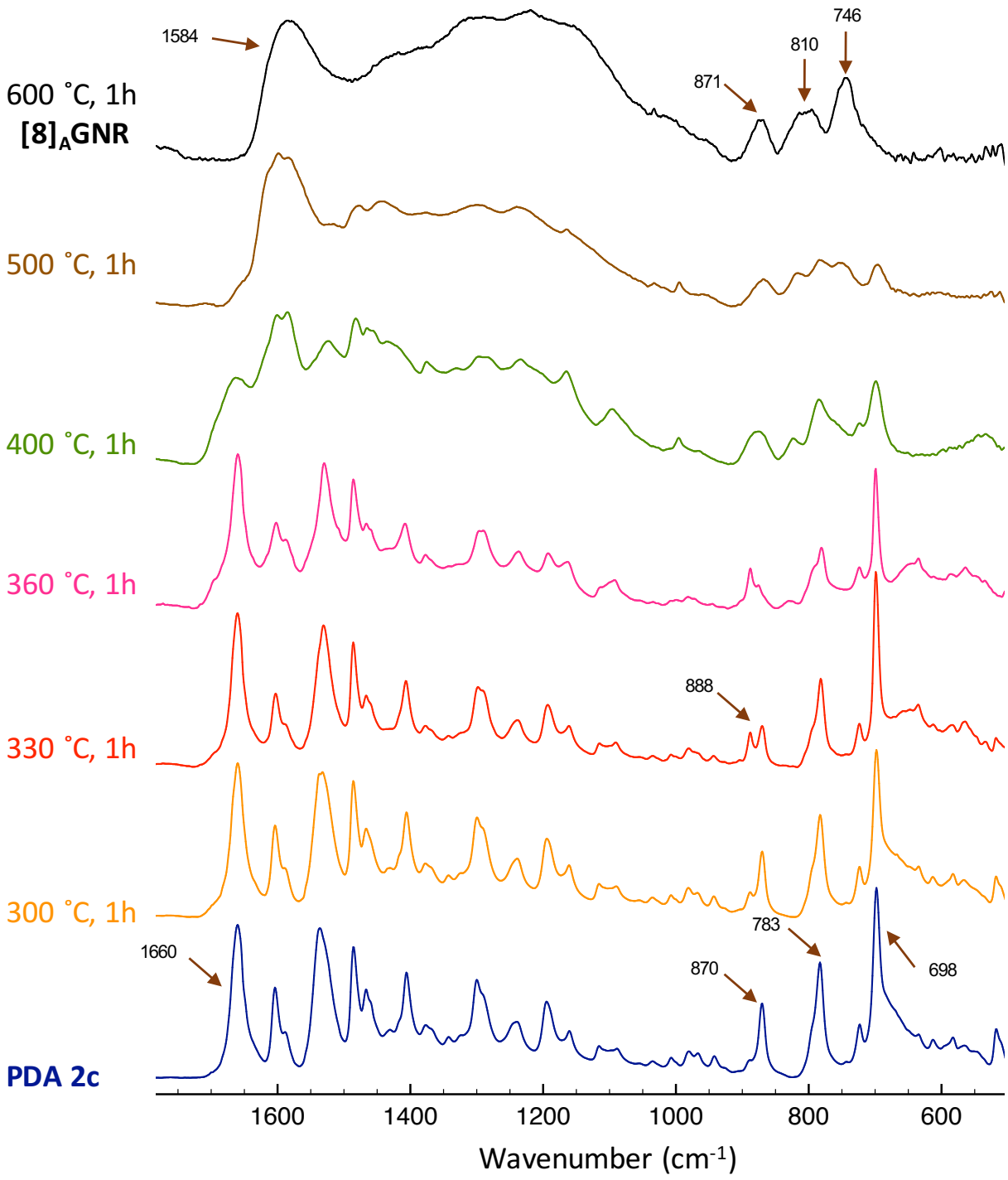

Figure A8. Fingerprint region expansion of infrared spectrum detailing the conversion of PDA **2c** to $[8]_A$GNR.

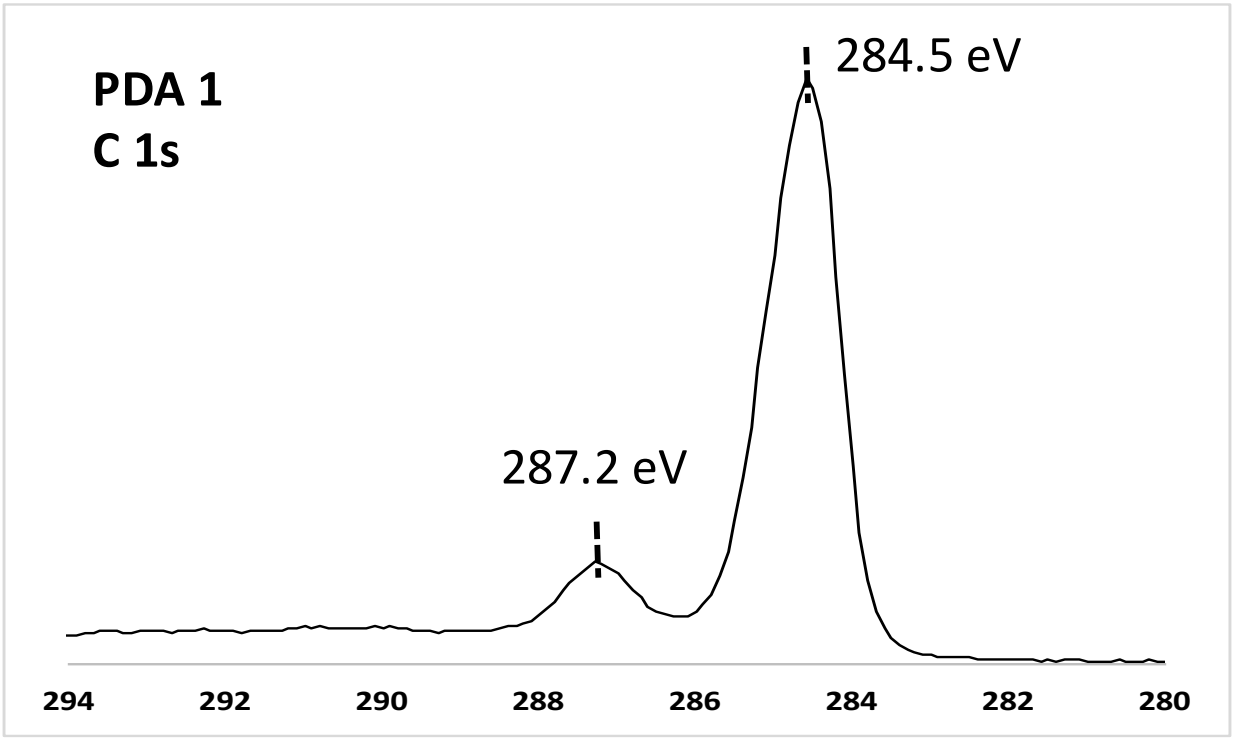

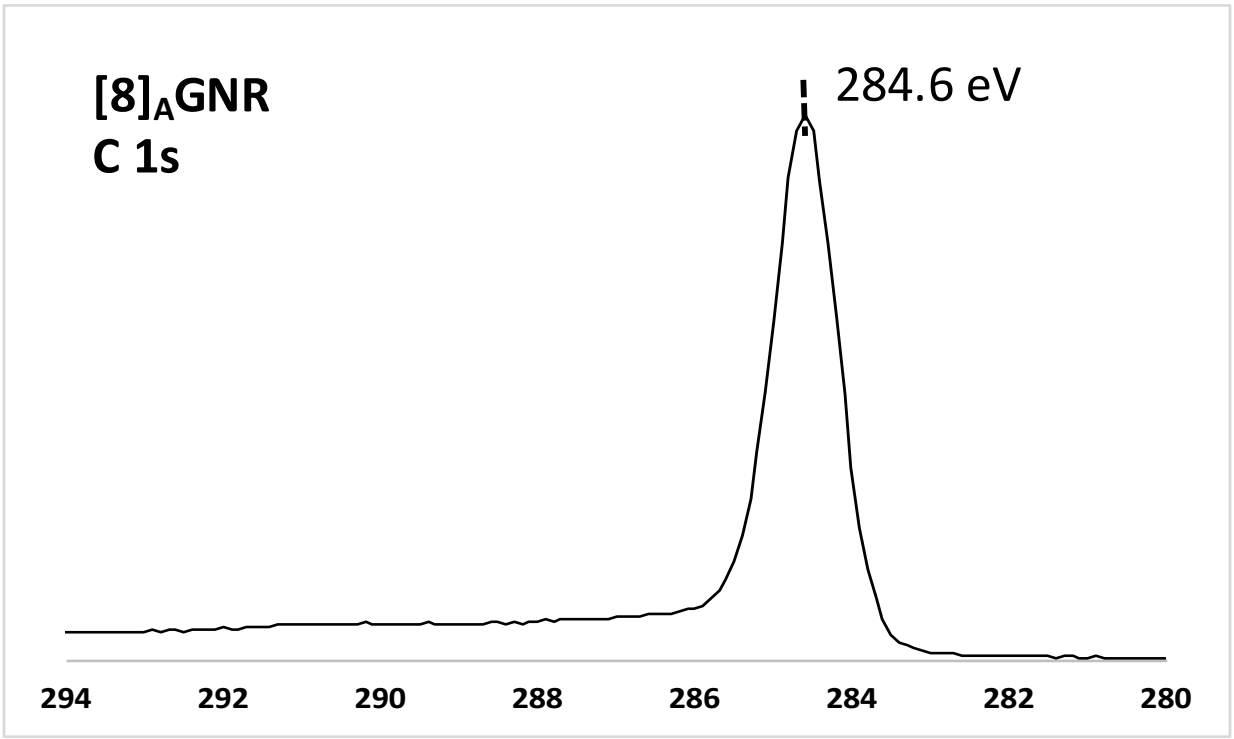

Figure A9. XPS spectra showing the conversion of PDA **1** to $[8]_A$GNR.

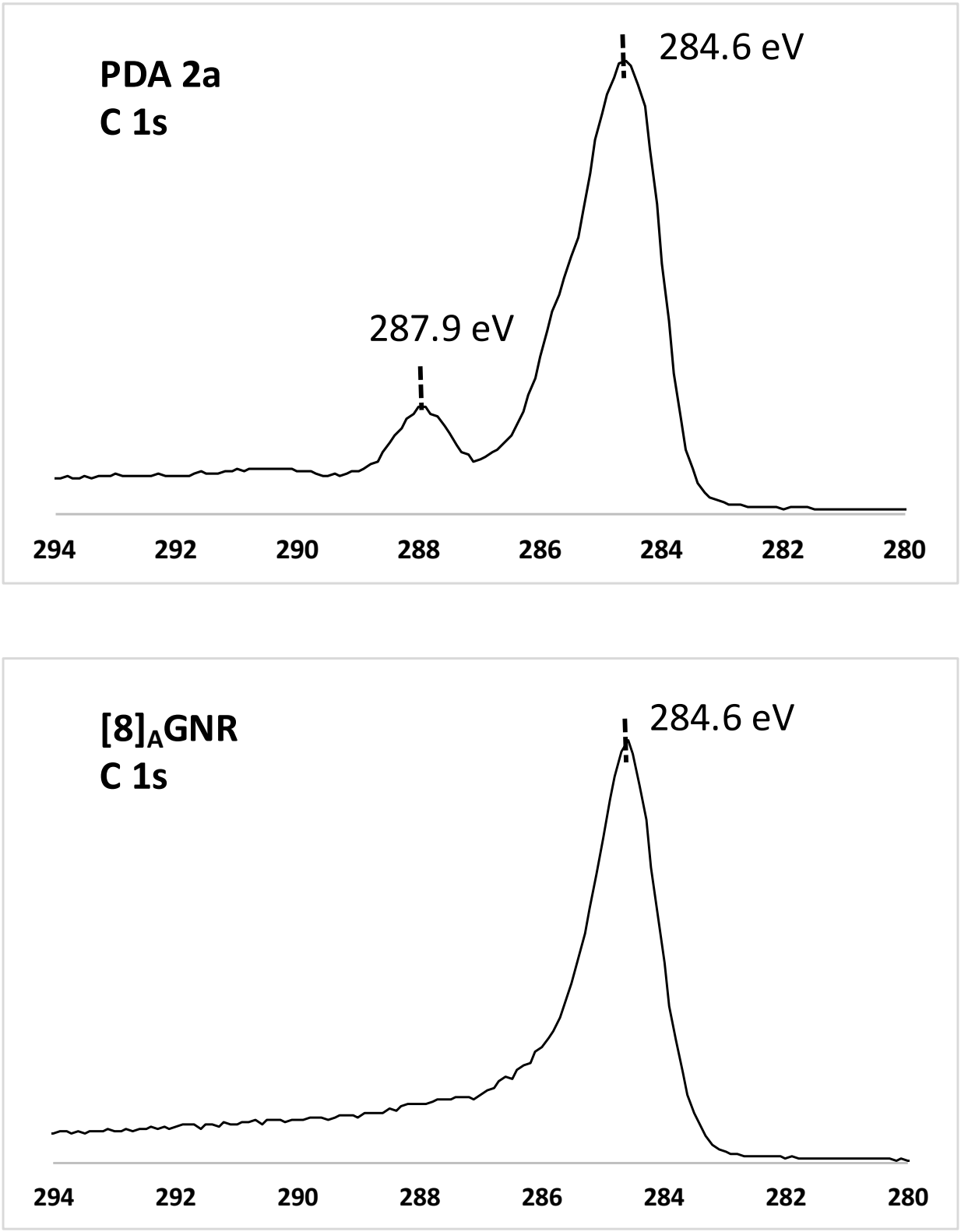

Figure A10. XPS spectra showing the conversion of PDA **2a** to $[8]_A$GNR.

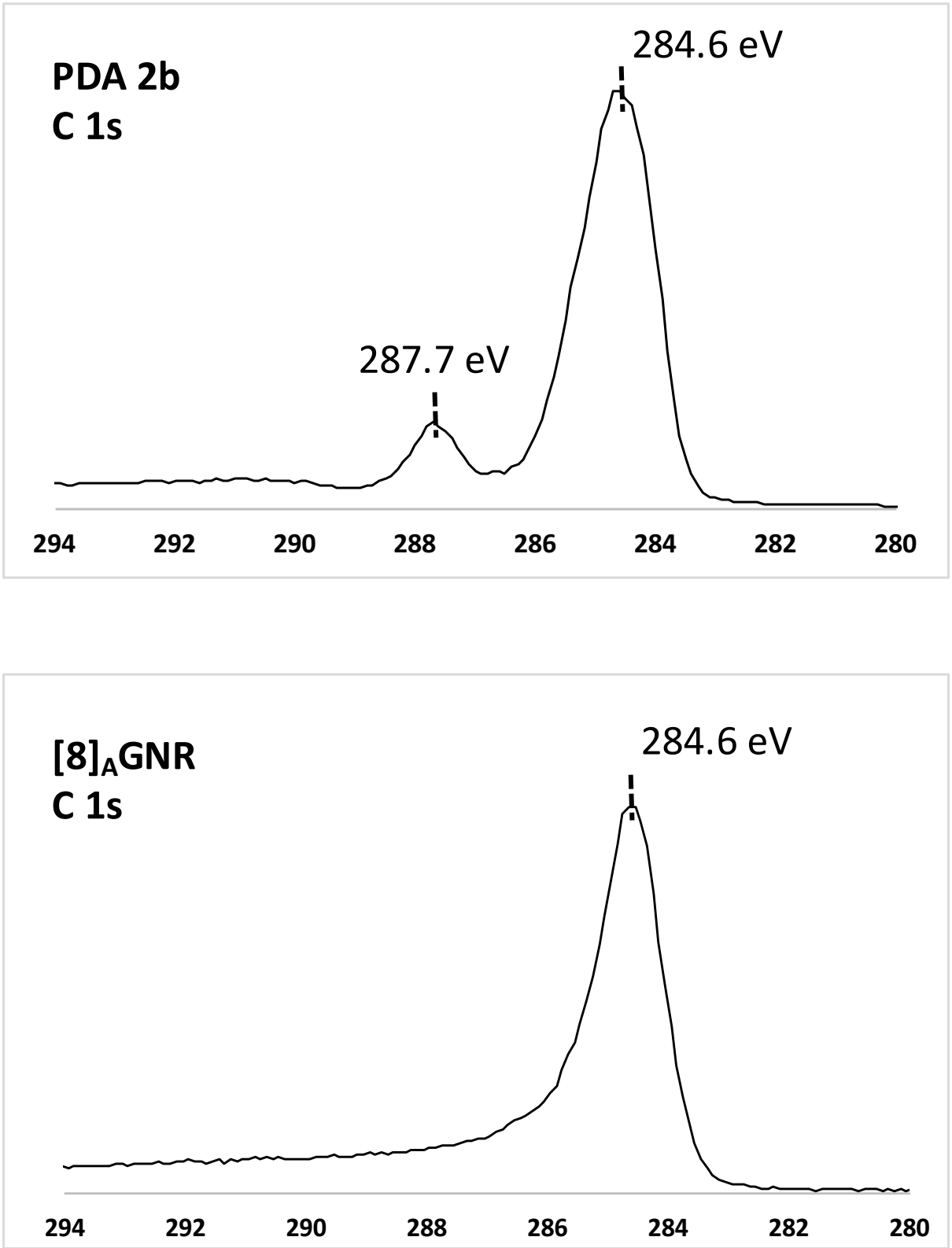

Figure A11. XPS spectra showing the conversion of PDA **2b** to $[8]_A$GNR.

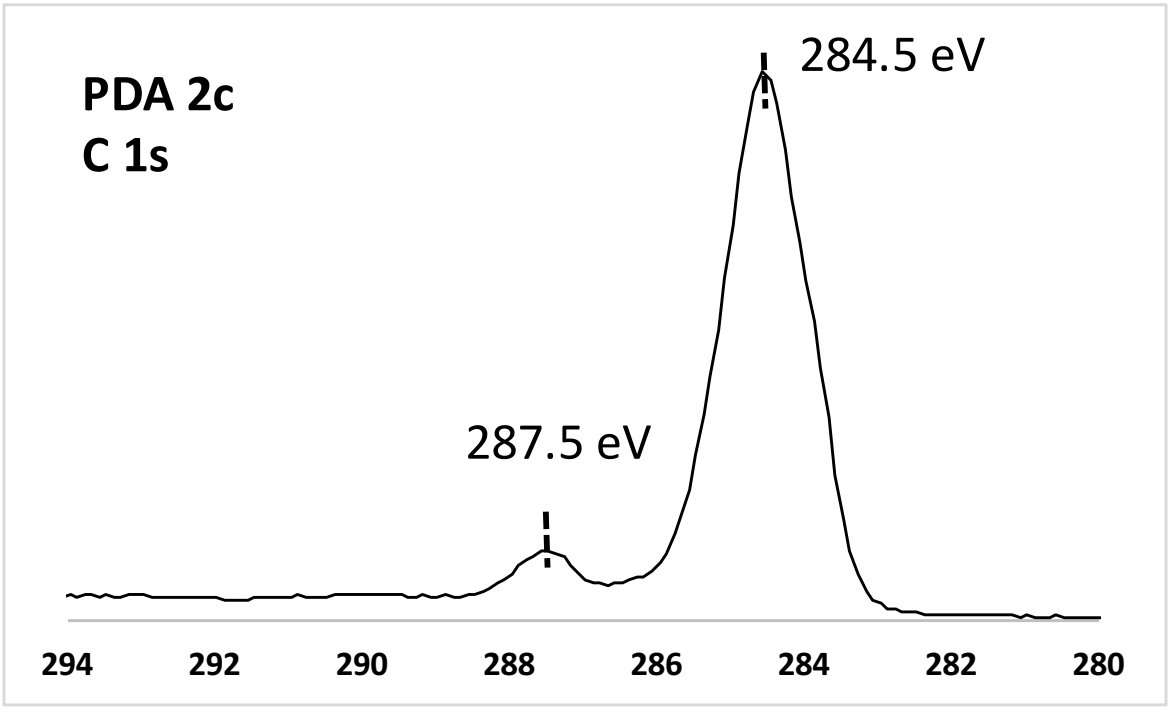

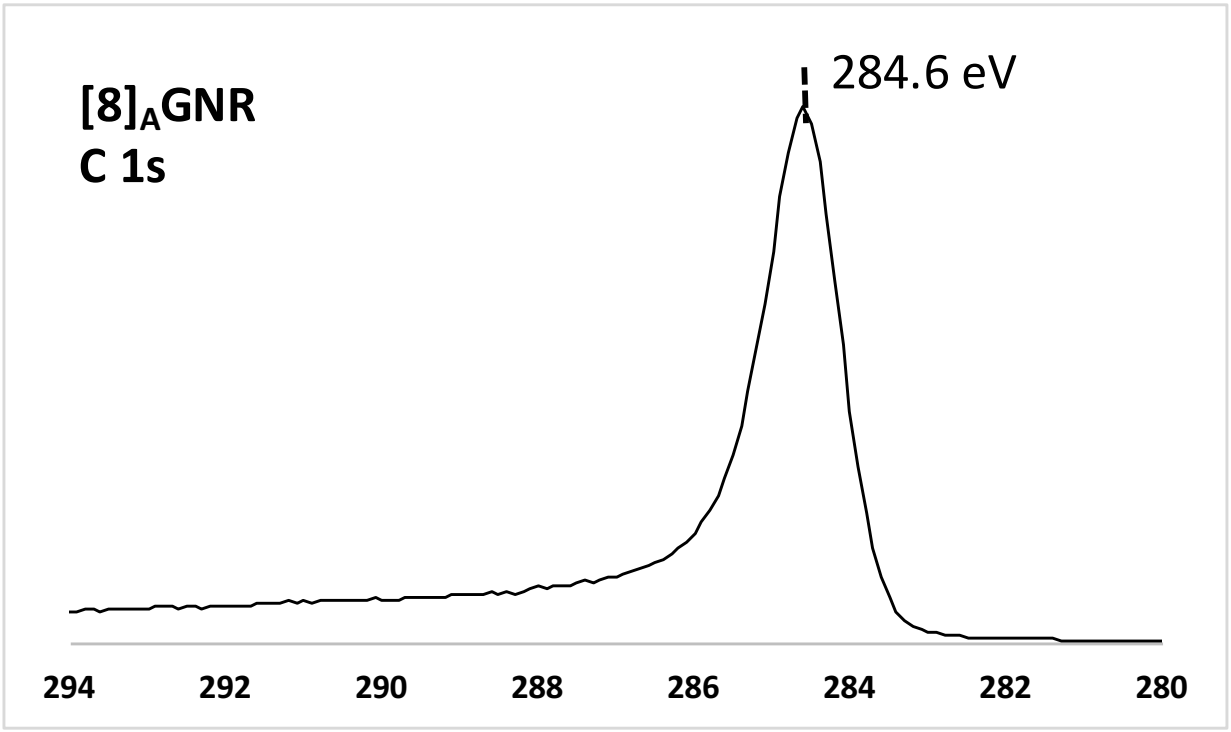

Figure A12. XPS spectra showing the conversion of PDA **2c** to $[8]_A$GNR.

Raman spectra are displayed stacked without baseline correction to highlight the photoluminescence background that occurs in a number of the annulated intermediate polymers produced upon heating. We attribute this background to the formation of larger polycyclic aromatic moieties (naphthalene, chrysene, etc) along the polymeric backbone. Such polycyclic aromatic compounds have been shown to fluoresce at the excitation wavelength (514 nm) and interfere with Raman measurements.[52] Noticeably, upon full graphitization to $[8]_A$GNR upon heating to 600 ˚C for 1h, the photoluminescence decreases to a large extent in all cases due to fusion of the isolated polycyclic aromatic units along the polymer backbone into $[8]_A$GNR.

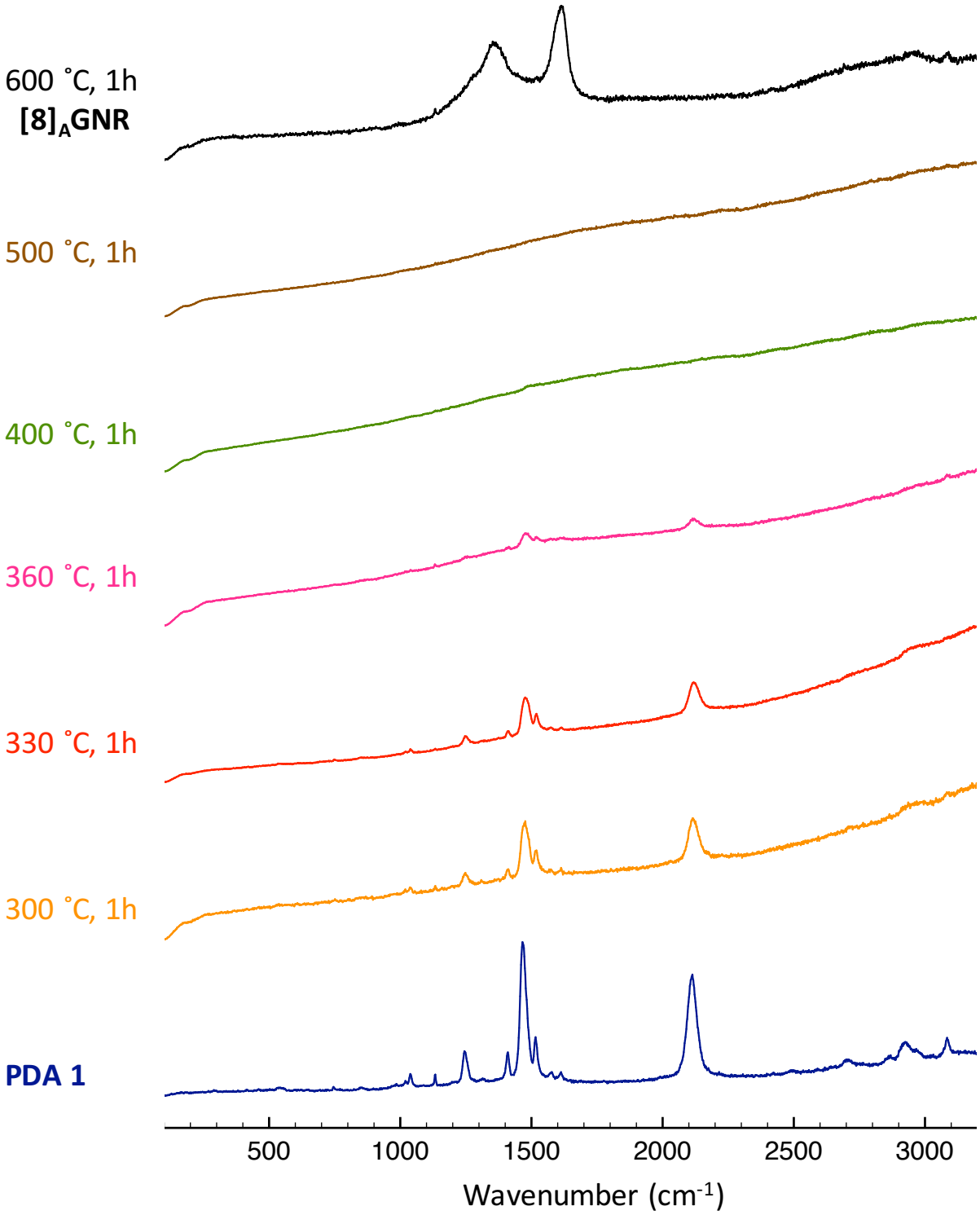

Figure A13. Raman spectra (514 nm excitation wavelength) showing the conversion of PDA **1** to $[8]_A$GNR.

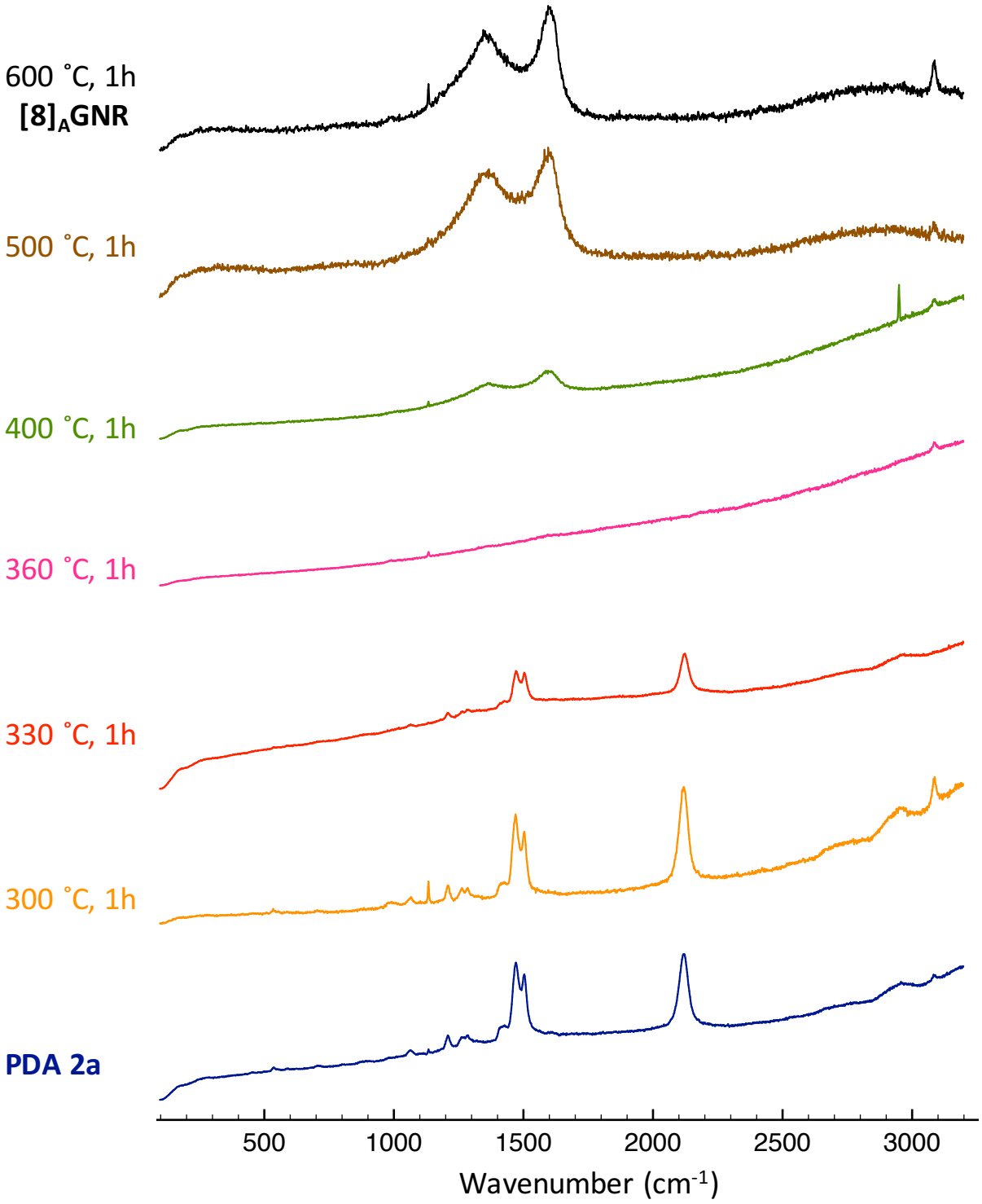

Figure A14. Raman spectra (514 nm excitation wavelength) showing the conversion of PDA **2a** to $[8]_A$GNR.

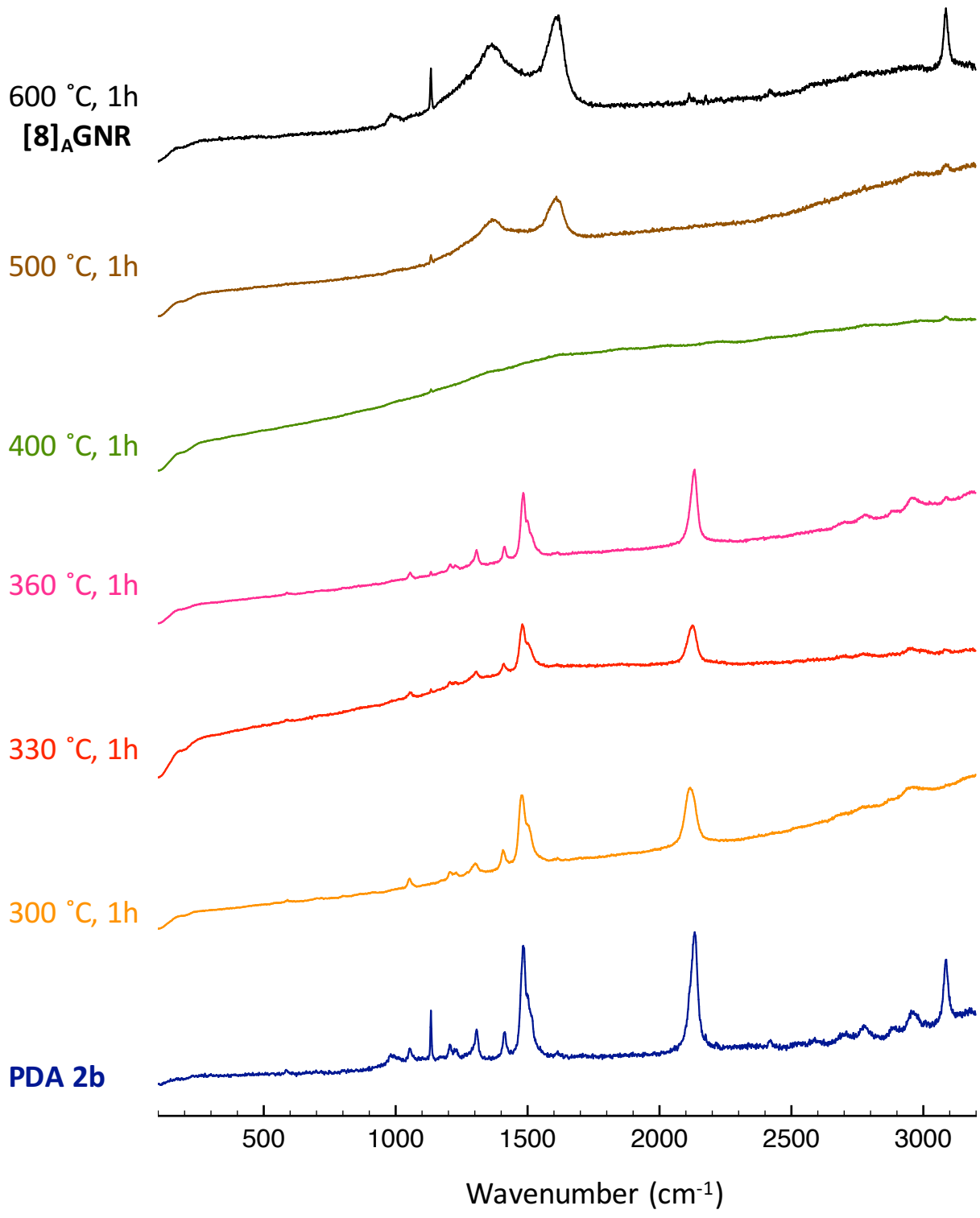

Figure A15. Raman spectra (514 nm excitation wavelength) showing the conversion of PDA **2b** to $[8]_A$GNR.

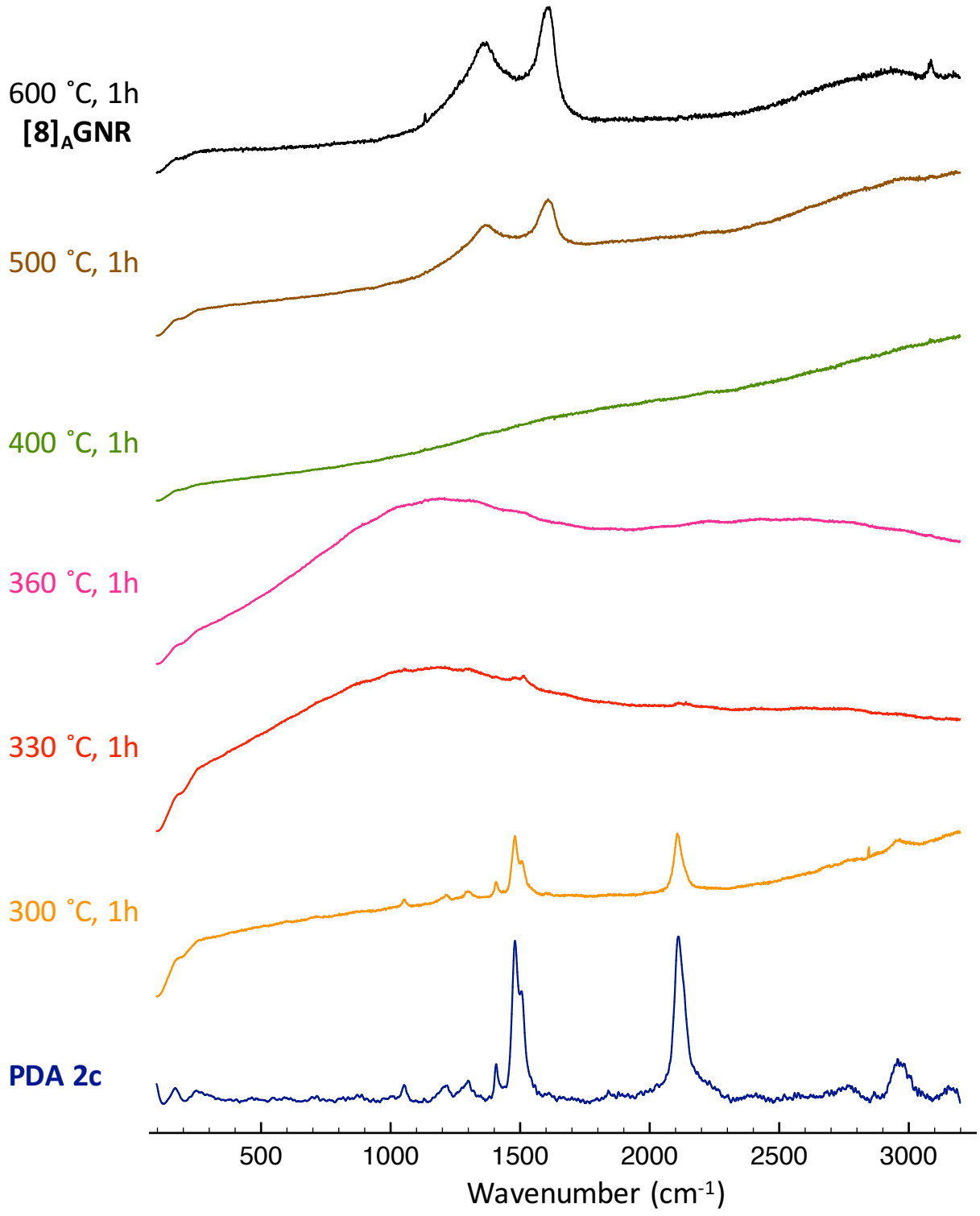

Figure A16. Raman spectra (514 nm excitation wavelength) showing the conversion of PDA **2c** to $[8]_A$GNR.

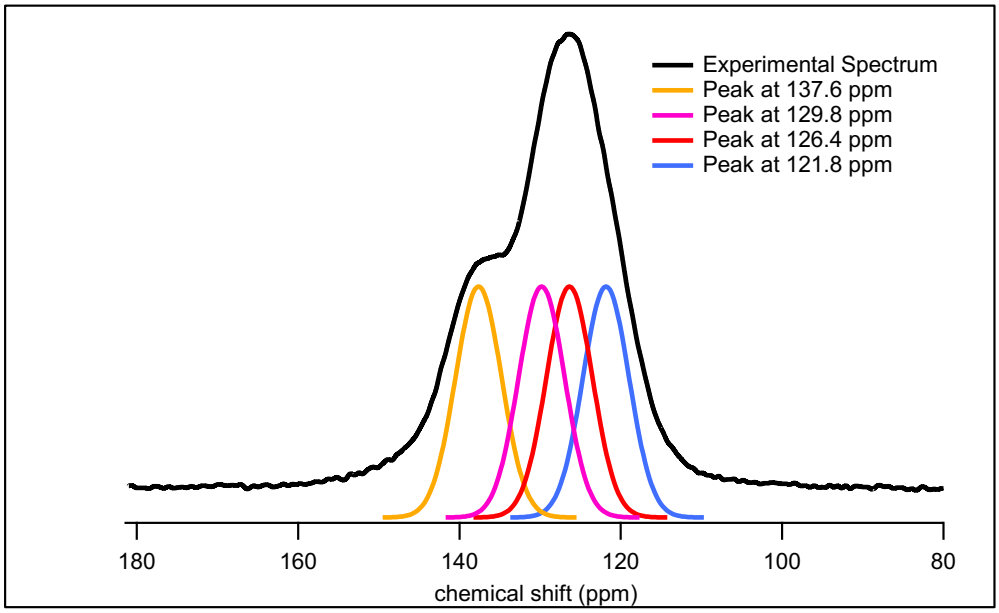

Figure A17. Calculated curve fitting of CP/MAS ^{13}C NMR data for $[8]_A$GNR produced from thermal aromatization of PDA **1**.

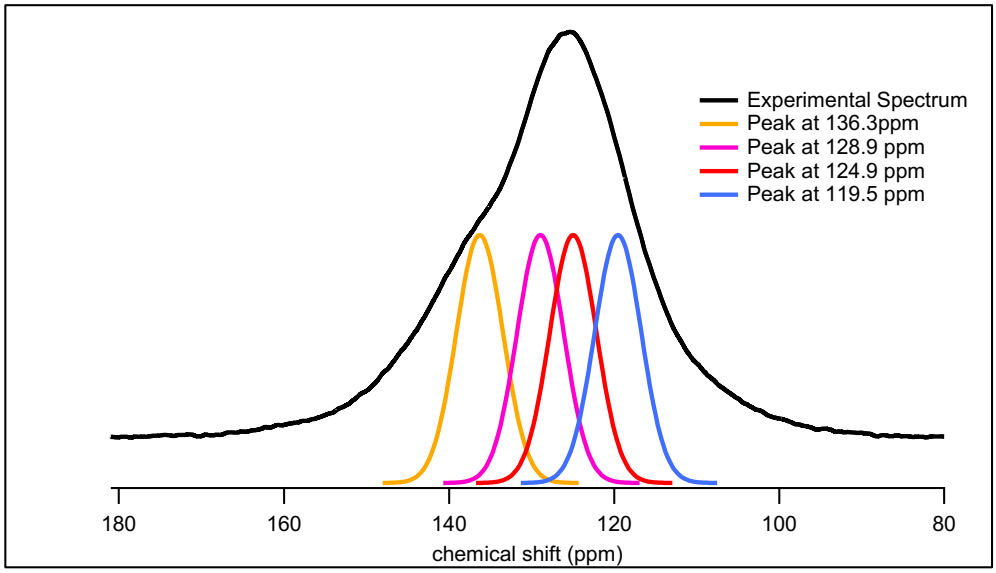

Figure A18. Calculated curve fitting of CP/MAS ^{13}C NMR data for $[8]_A$GNR produced from thermal aromatization of PDA **2a**.

Peak fitting was accomplished using the Multipeak Fitting 1.4 package in Igor Pro 6.37. The experimental spectra were fit to four peaks over the region of interest using a Gaussian line shape. As each GNR is composed of four distinct carbons of equal weighting, the amplitude and width of each fit was held constant during the fitting process. The results show four distinct functions whose centers were taken to be the chemical shift of the carbons in question.

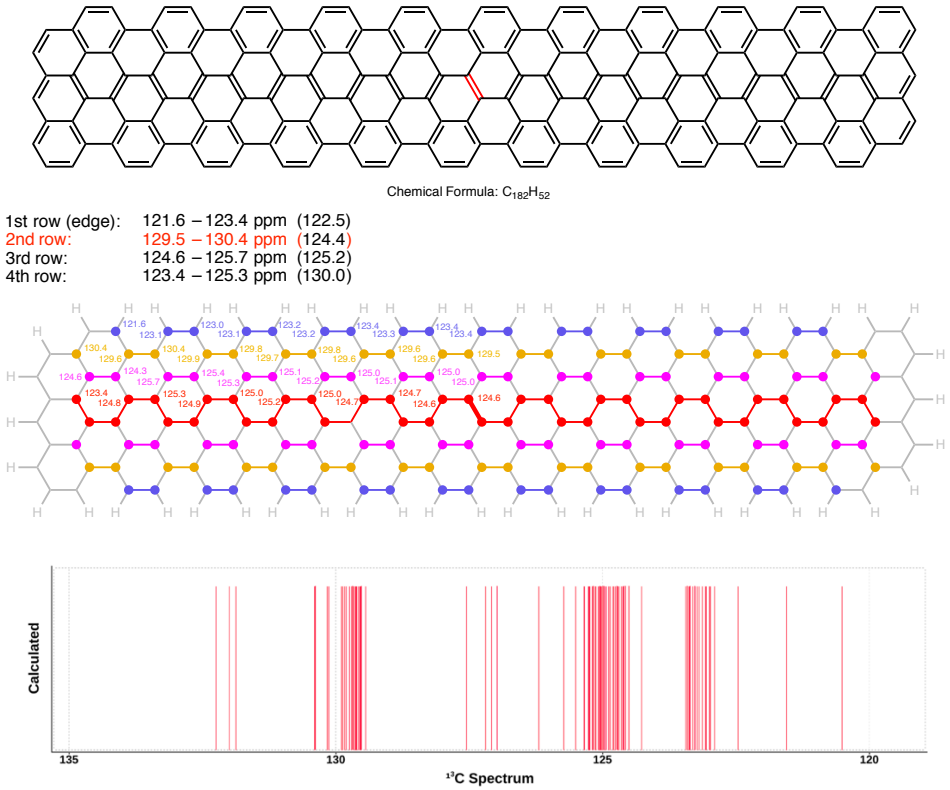

Figure A19. a) Chemical structure and b) ^{13}C NMR chemical shifts δ (ppm) for a large section of [8]$_A$GNR calculated at the B3LYP//6-31G* level of theory. NMR shielding tensors were computed with the Gauge-Independent Atomic Orbital (GIAO) method. The calculation was performed with the MacSpartan 16 package.[53] The ^{13}C NMR chemical shifts that are displayed here are all within ±1 ppm of each other in each of the four different rows of carbons. Thus, the 2nd

row of carbons should roughly have a relative intensity of 1:3 with those carbons within rows 1, 3, and 4. c) Plot of all the ^{13}C NMR chemical shifts obtained in the B3LYP//6-31G* calculation for this model compound using Spartan 16.

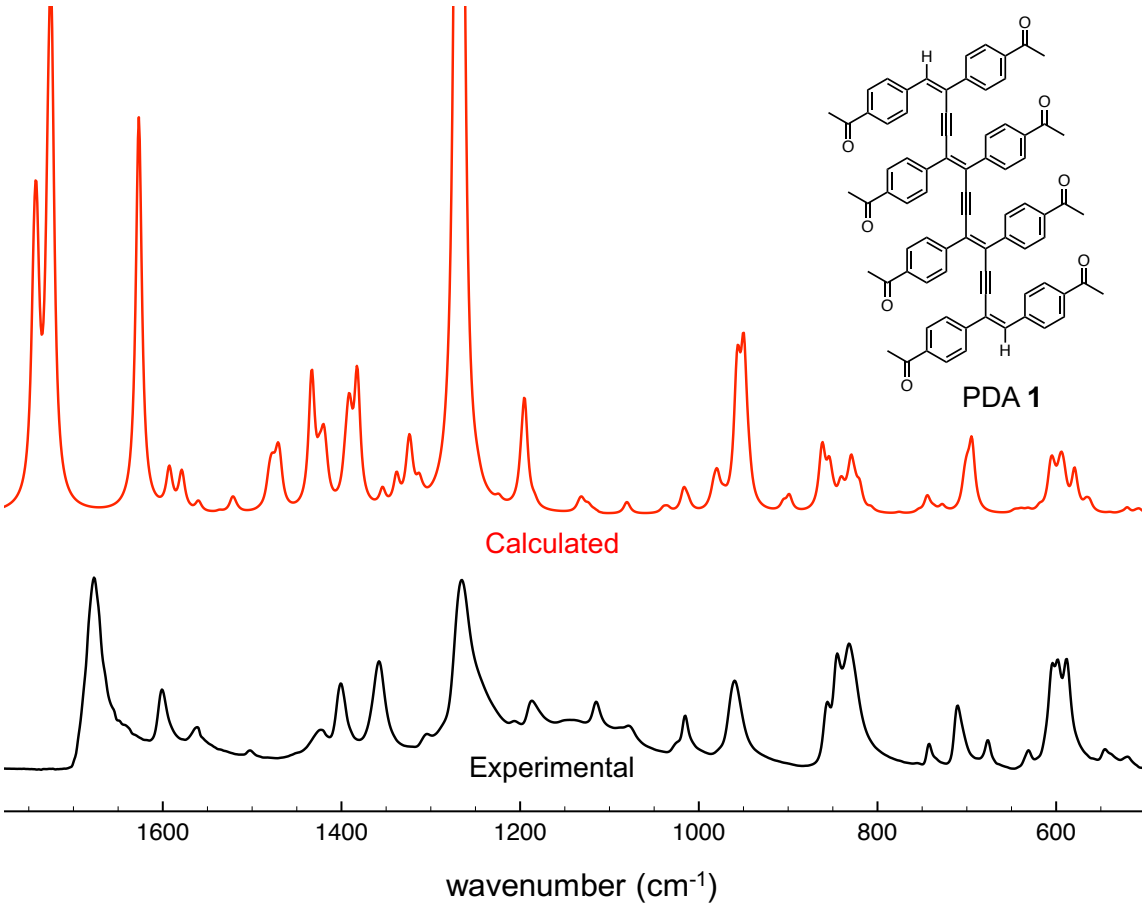

Figure A20: Comparison of calculated and experimental IR spectra for PDA polymer **1**.

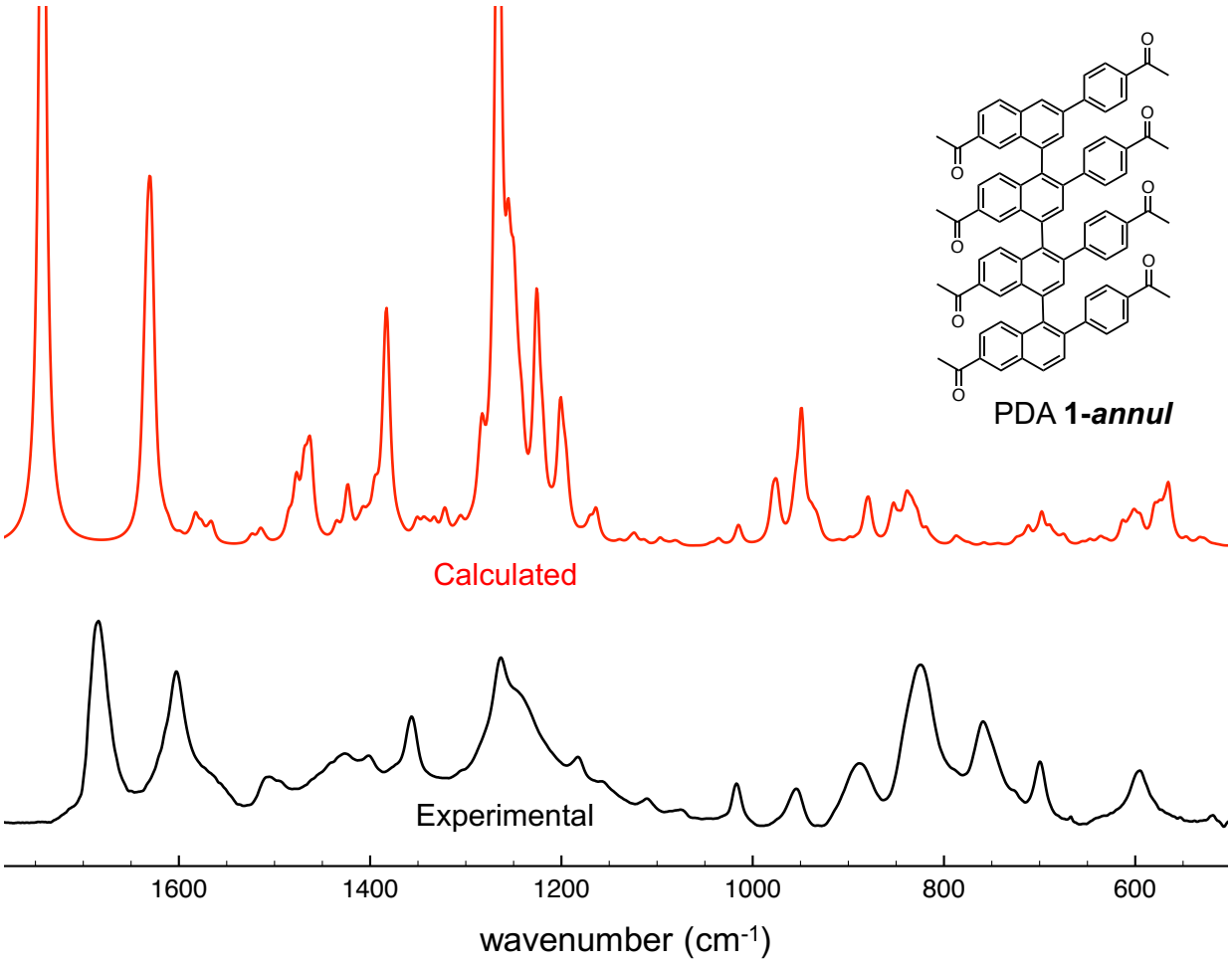

Figure A21: Comparison of calculated IR spectra of a possible structure for the annulated polymer (PDA **1**-***annul***) resulting from thermal treatment of PDA **1** and comparison to experimental data.

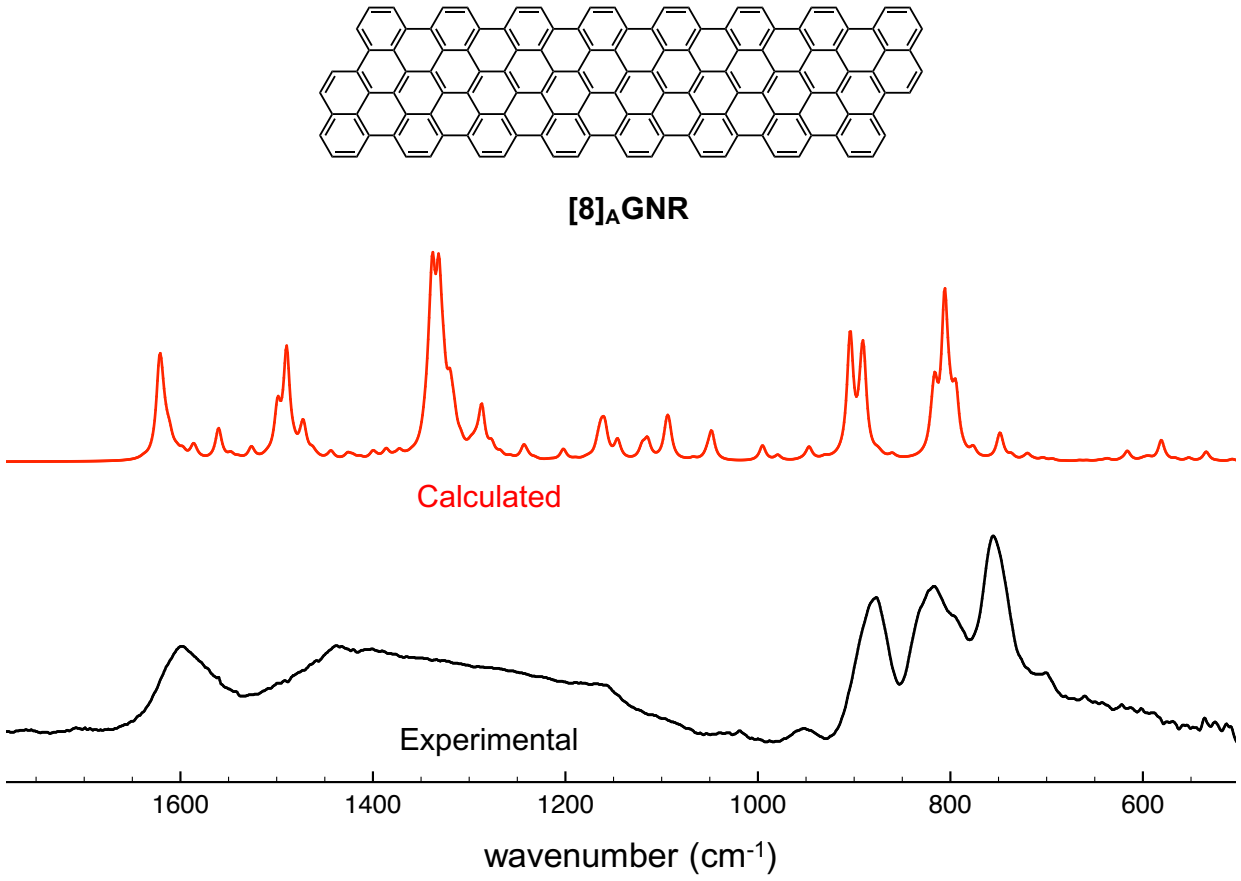

Figure A22. Comparison of calculated and experimental IR spectra for $[8]_A$GNR produced from thermal aromatization of PDA **1**. In light of computational resources a small section of $[8]_A$GNR was used as a surrogate for the spectrum of an infinite ribbon. The ribbon is 34 carbons in length and its structure is shown inset in the figure.

The width of an individual $[8]_A$GNR ribbon was calculated using the optimized geometry of the model segment described in Fig. S22. Distance from the center of an edge hydrogen to the center

of the edge hydrogen horizontally across the ribbon was measured using GuassView as 10.47 Å. To account for the Van der Waals radii of the edge hydrogen (1.2 Å), 2.4 Å was added to the measured width to produce the calculated ribbon width of ≈12.9 Å (1.29 nm).

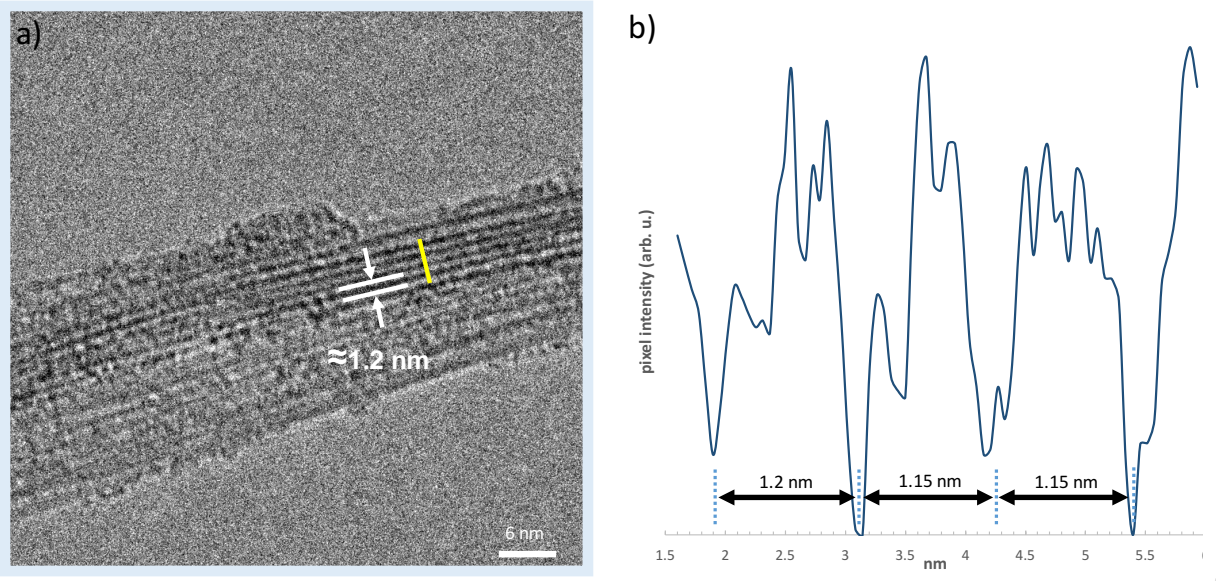

Figure A23. Plot profile analysis (yellow line) of HRTEM image of $[8]_A$GNR produced from thermal graphitization of PDA **2b**.

CP/MAS ^{13}C NMR experiments were performed on a Bruker DSX300 operating at 300 MHz and at 298 K. A 4mm zirconia rotor with a Kel-F cap was used spinning at 10 KHz in all experiments. A 5 ms cross-polarization contact time was utilized in all experiments. To ensure that a good signal-to-noise ratio was achieved for all spectra, the number of scans collected was increased as

necessary. Below is a table listing the specific number of scans collected for all spectra described in Fig 8 of the paper. A 50 Hz line broadening was applied to all spectra except for the spectra of PDAs **2b** and **2c** after heating to 500 ˚C where a 100 Hz line broadening was used.

PDA	No heating (# of scans)	300 ˚C, 1h (# of scans)	330 ˚C, 1h (# of scans)	360 ˚C, 1h (# of scans)	400 ˚C, 1h (# of scans)	500 ˚C, 1h (# of scans)	600 ˚C, 1h (# of scans)
1	2048	2048	2048	2048	19456	12288	12288
2a	2048	2048	2048	2048	24576	24576	24576
2b	2048	2048	2048	2048	24576	24576	24576
2c	2048	2048	2048	2048	17408	40960	32768

Interestingly, amide-containing PDAs **2a–2c** underwent a dramatic loss of CP/MAS signal upon conversion to the annulated intermediate polymers (heating to either 400 or 500 ˚C, see Fig. 2 in paper) en-route to $[8]_A$GNR. The CP/MAS signal returned upon final aromatization to $[8]_A$GNR. This behavior was not noted in *para*-acetophenone PDA **1**. To showcase this phenomenon, a series of spectra were acquired where the number of scans was held constant at 2048 and peak heights were not normalized. These four series of spectra are shown in Figures A24–A27 below. The origin of this phenomenon is currently under investigation in our group.

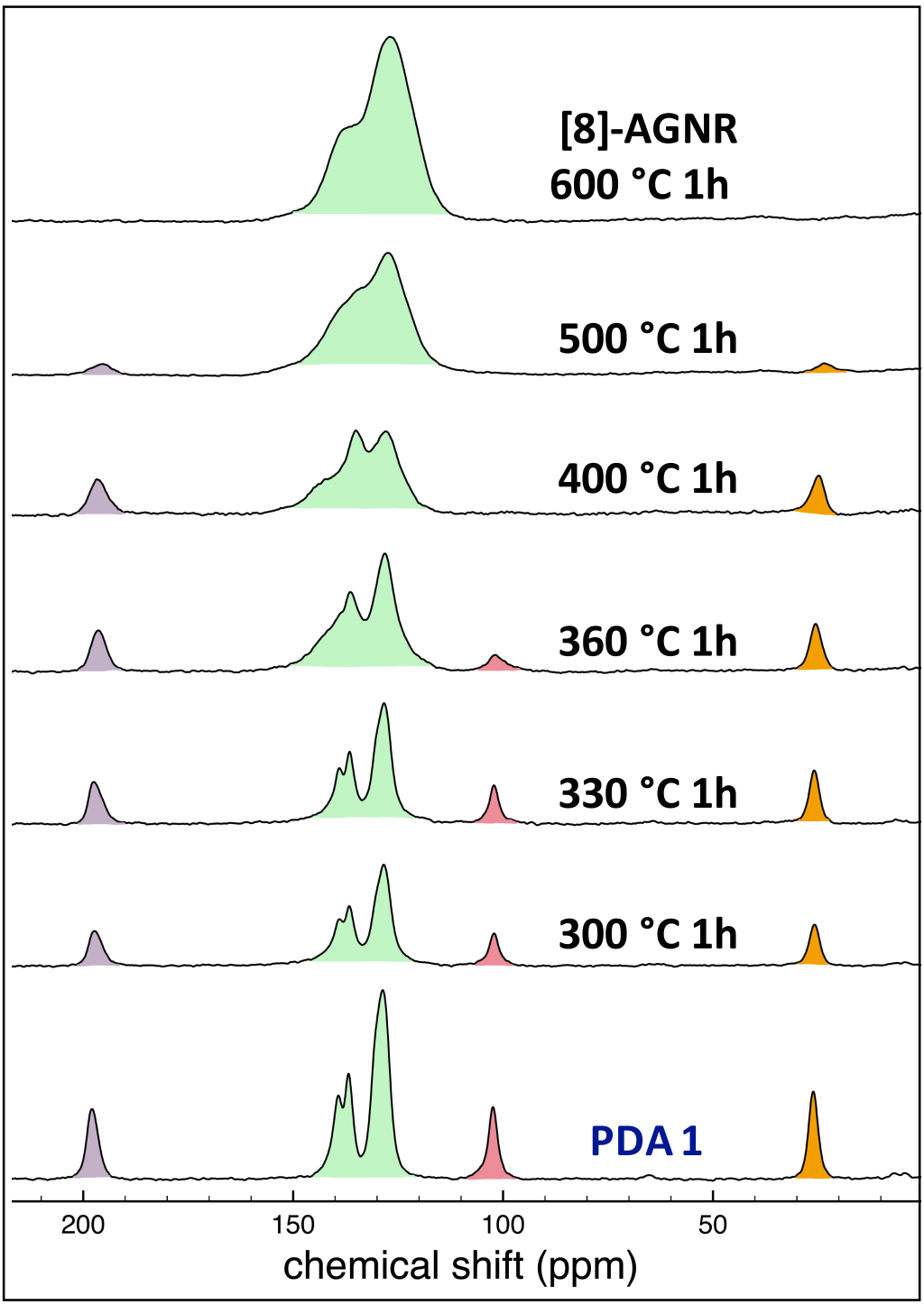

Figure A24. Stacked CP/MAS ^{13}C NMR spectra of the conversion of PDA **1** to $[8]_AGNR$ with consistent number of scans (2048) and no peak height normalization. No significant loss of signal was noted for this system.

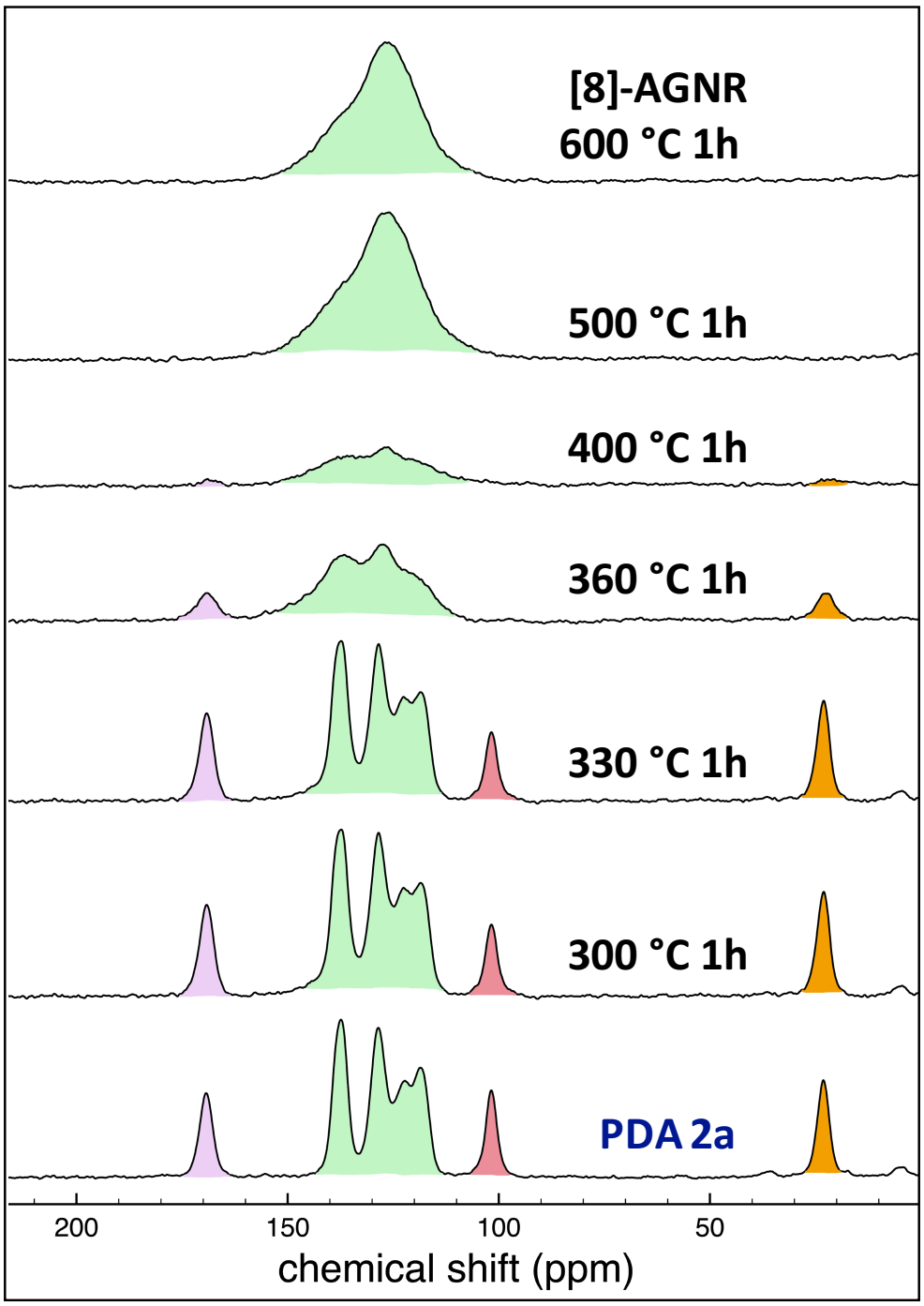

Figure A25. Stacked CP/MAS ^{13}C NMR spectra of the conversion of PDA **2a** to $[8]_A$GNR with consistent number of scans (2048) and no peak height normalization. Note the dramatic reduction and regain in signal upon heating from 360 to 500 ˚C.

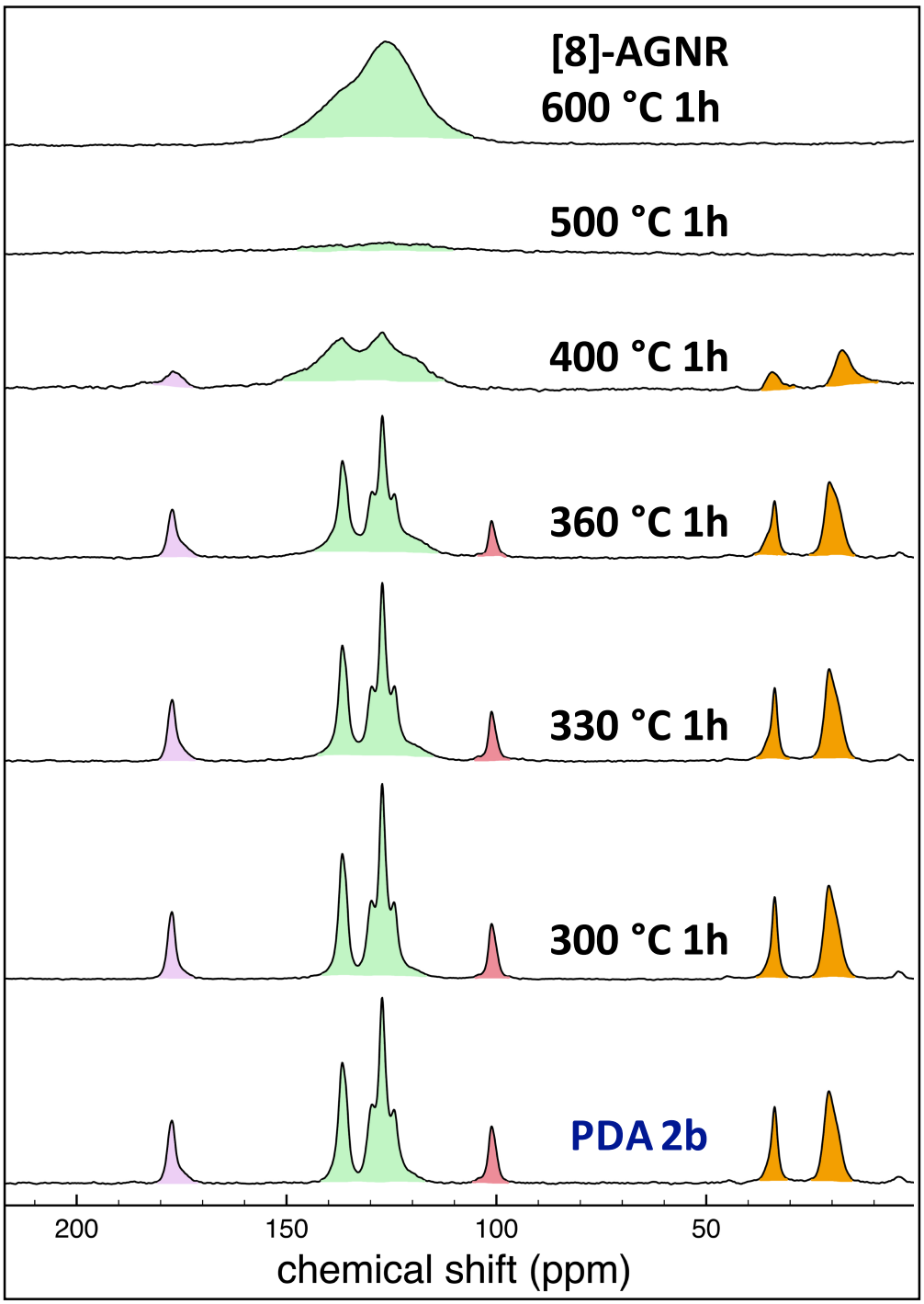

Figure A26. Stacked CP/MAS ^{13}C NMR spectra of the conversion of PDA **2b** to $[8]_A$GNR with consistent number of scans (2048) and no peak height normalization. Note the dramatic reduction and regain in signal upon heating from 400 to 600 ˚C.

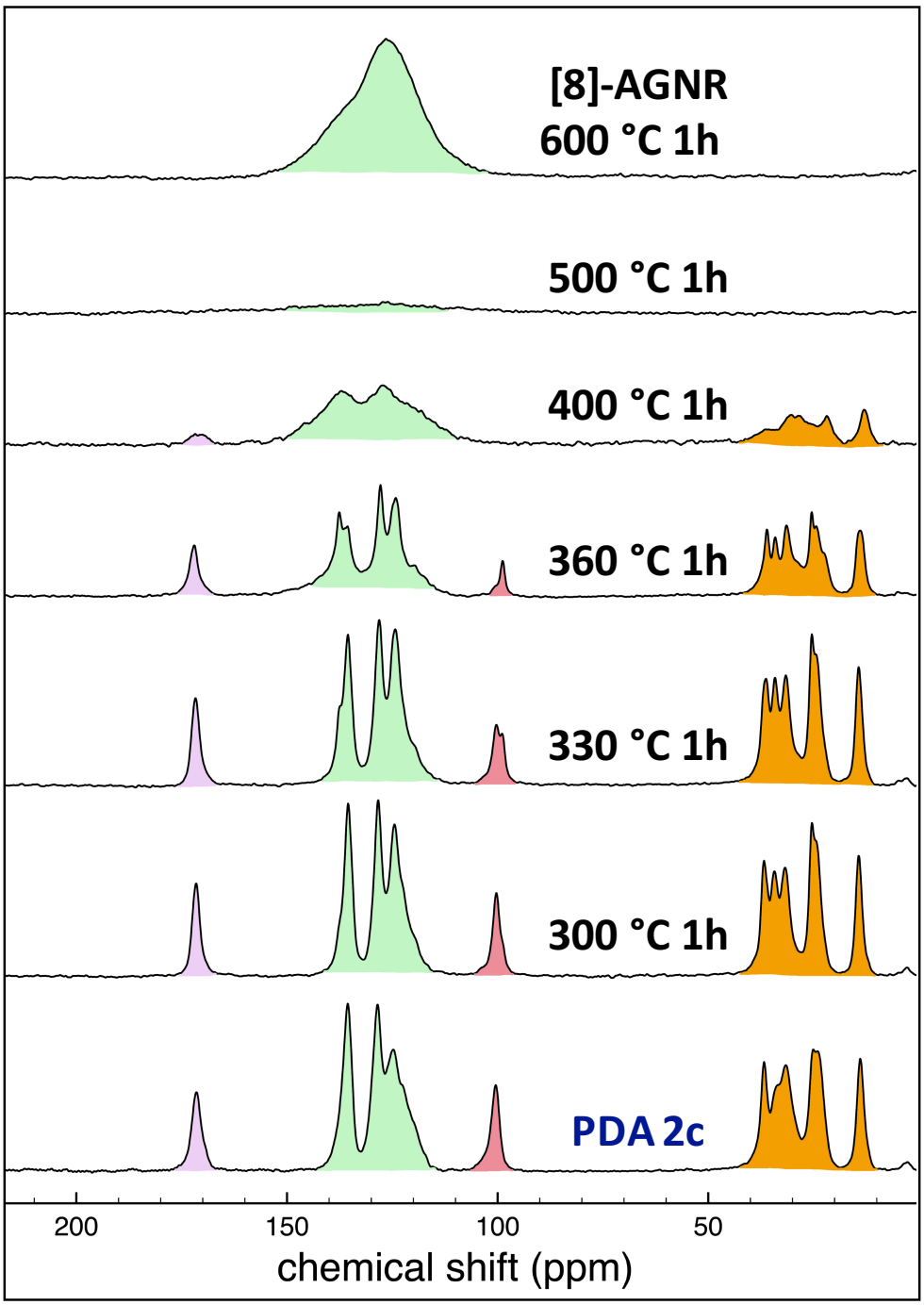

Figure A27. Stacked CP/MAS ^{13}C NMR spectra of the conversion of PDA **2c** to $[8]_A$GNR with consistent number of scans (2048) and no peak height normalization. Note the dramatic reduction and regain of signal in samples heated up to 400, 500, and 600 ˚C.

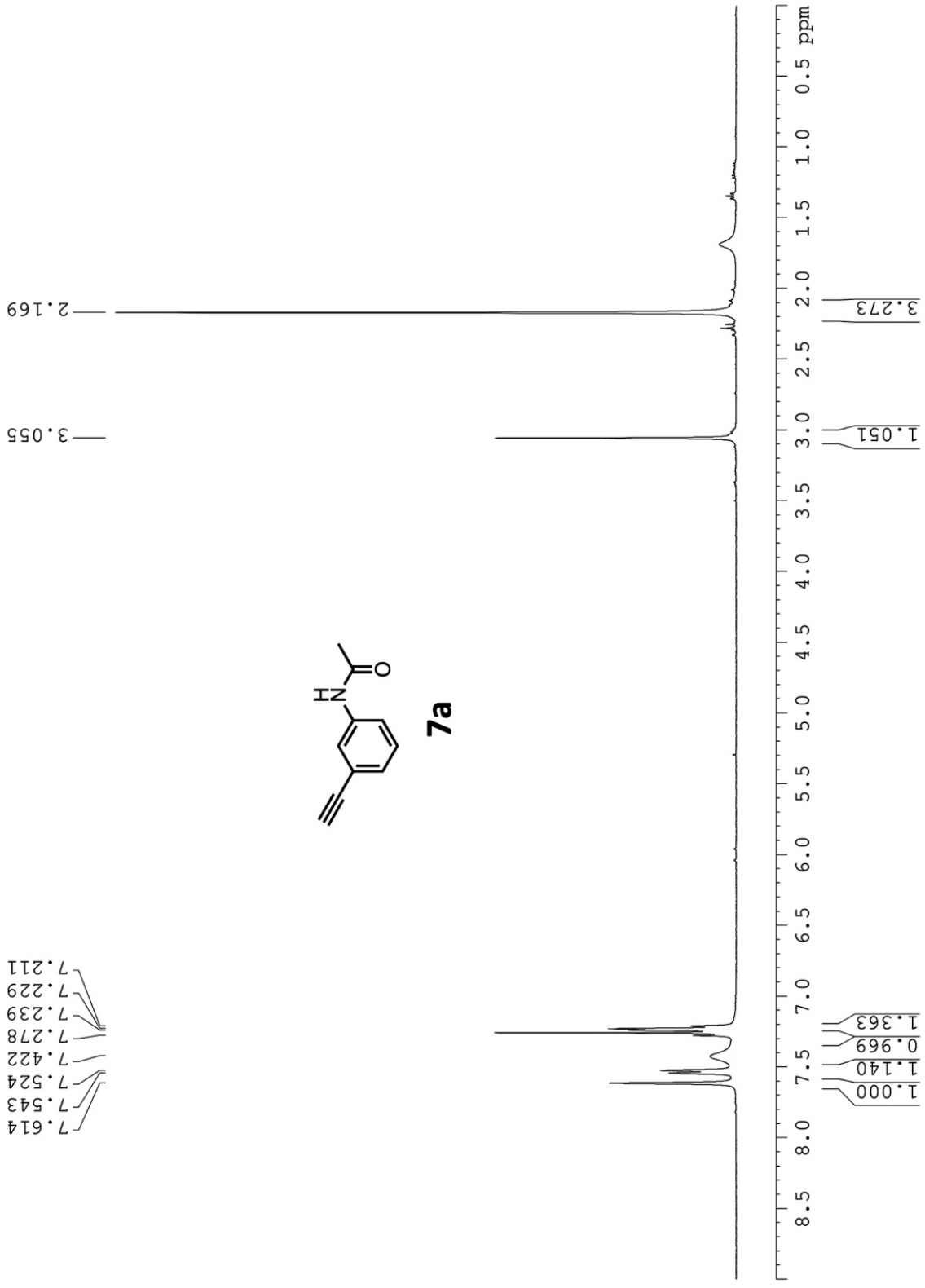

Figure A28: ^{1}H NMR spectrum of compound **7a**.

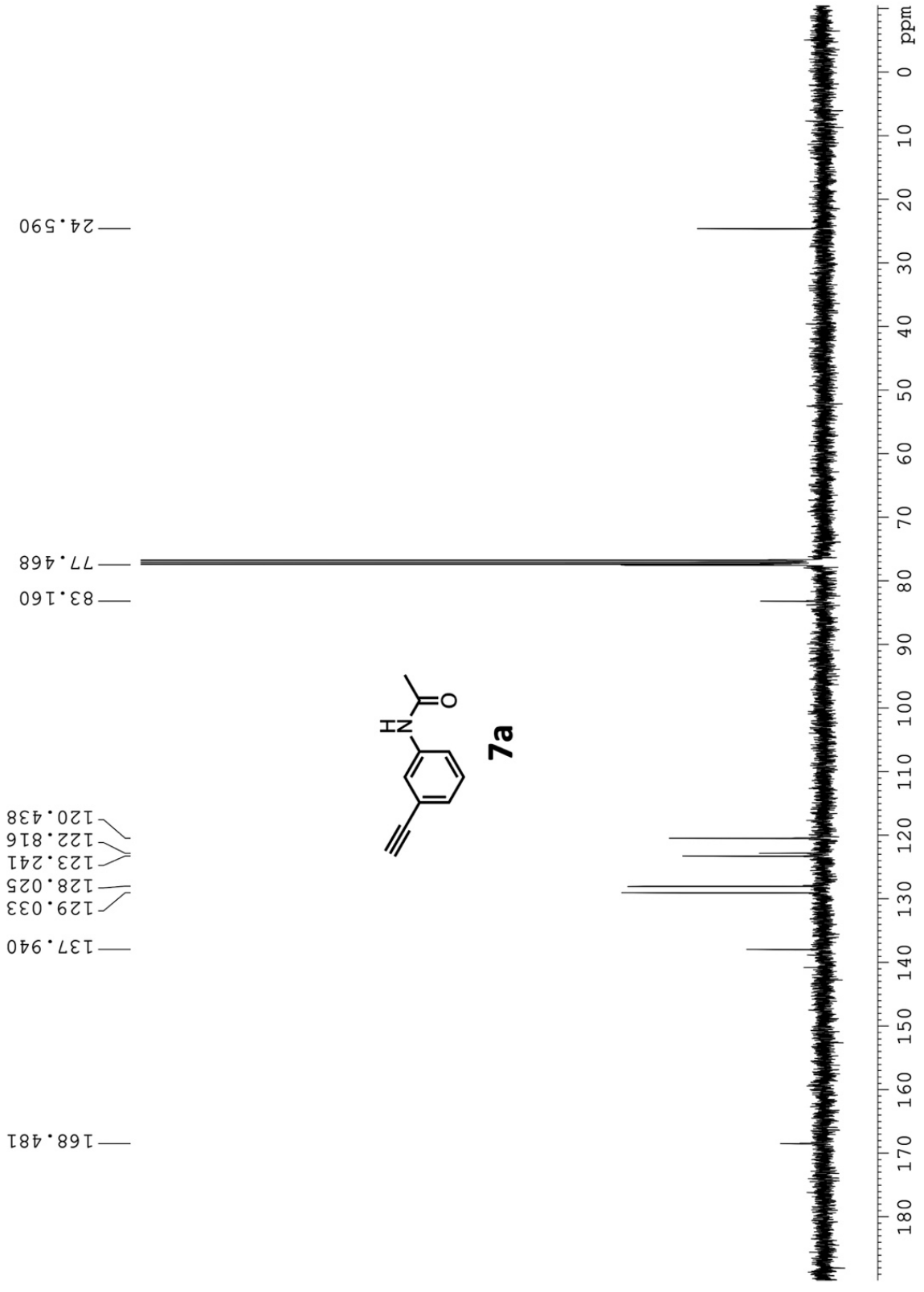

Figure A29: ^{13}C NMR spectrum of compound **7a**.

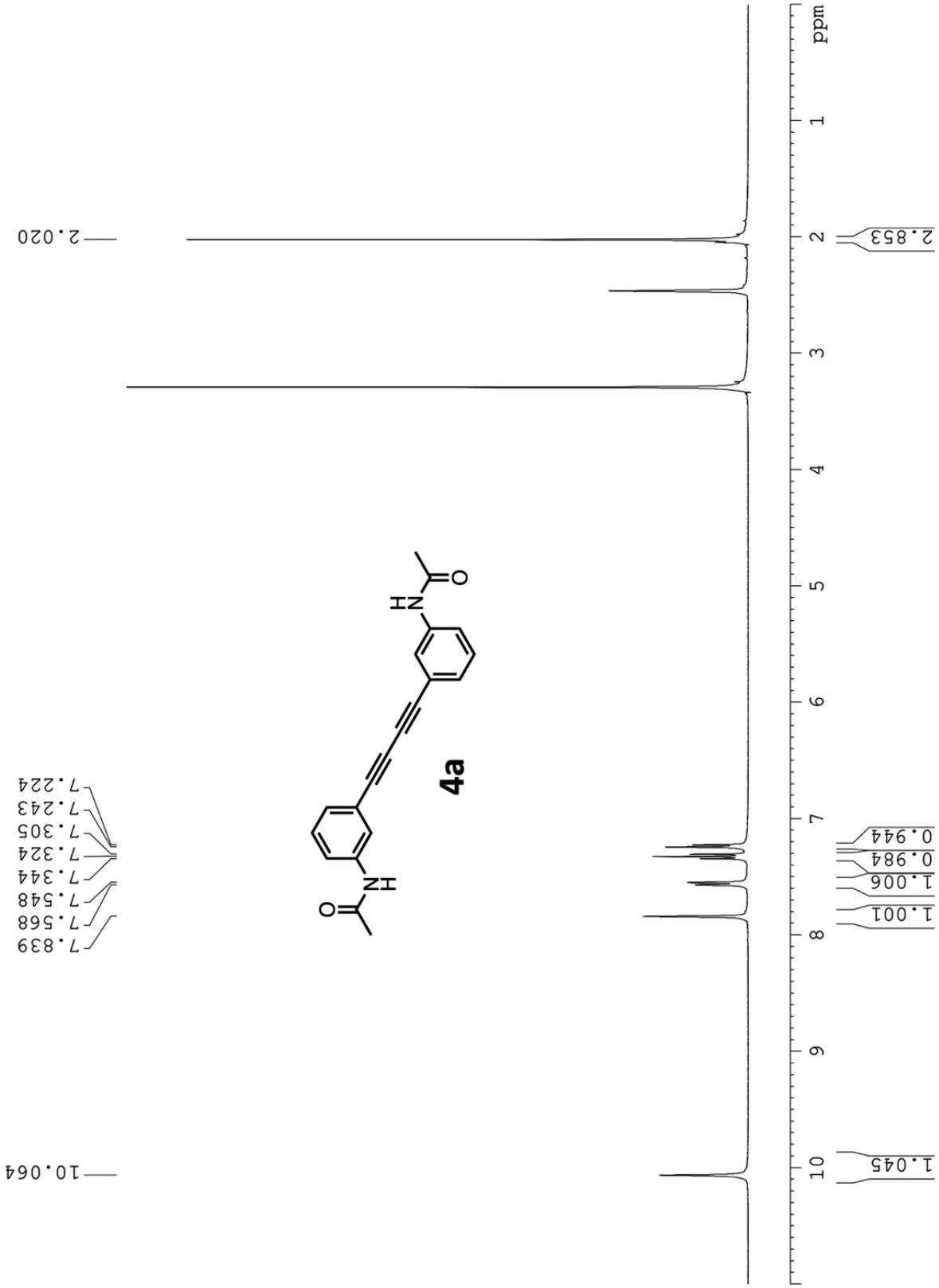

Figure A30: ^{1}H NMR spectrum of compound **4a**.

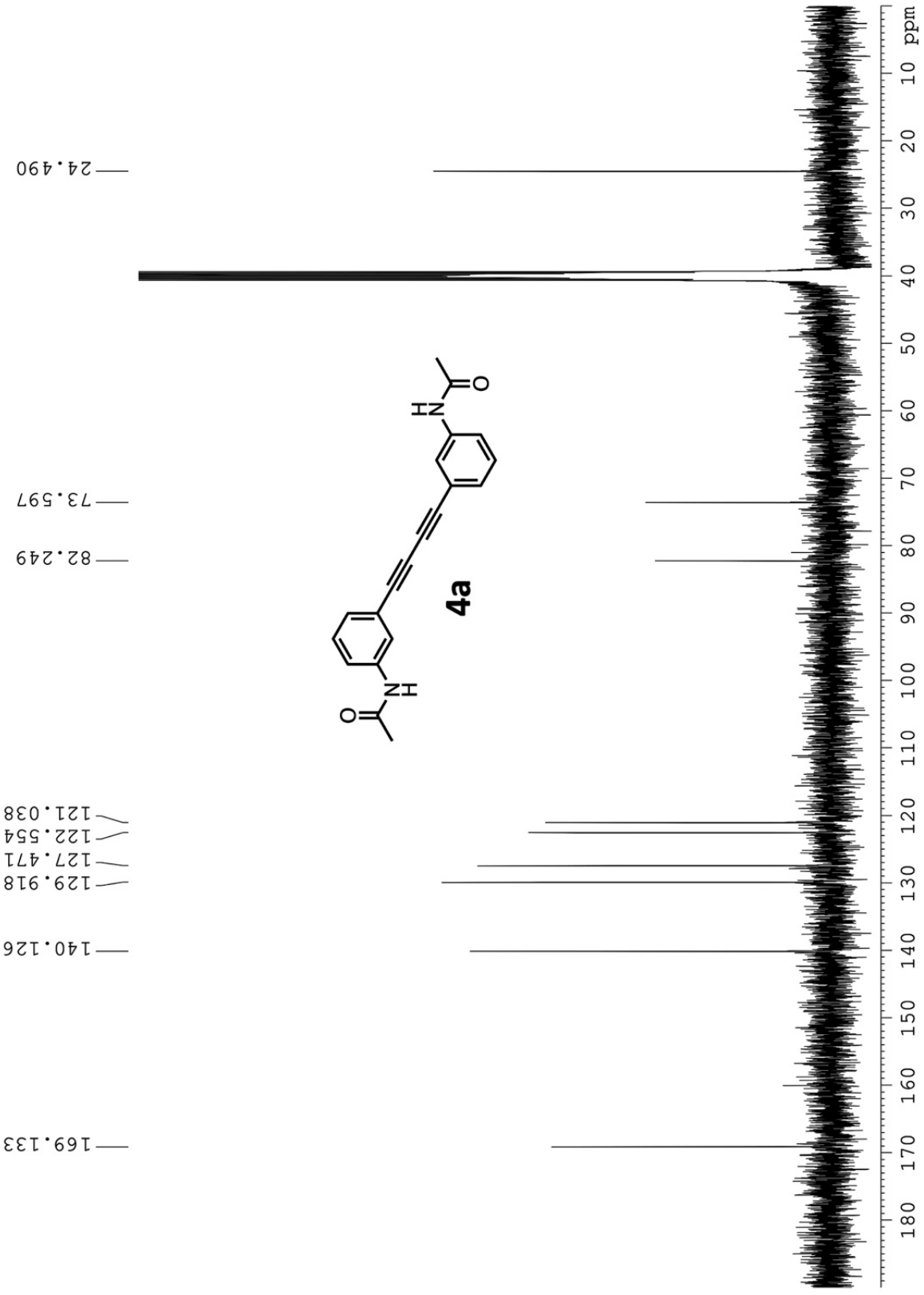

Figure A31: ^{13}C NMR spectrum of compound **4a**.

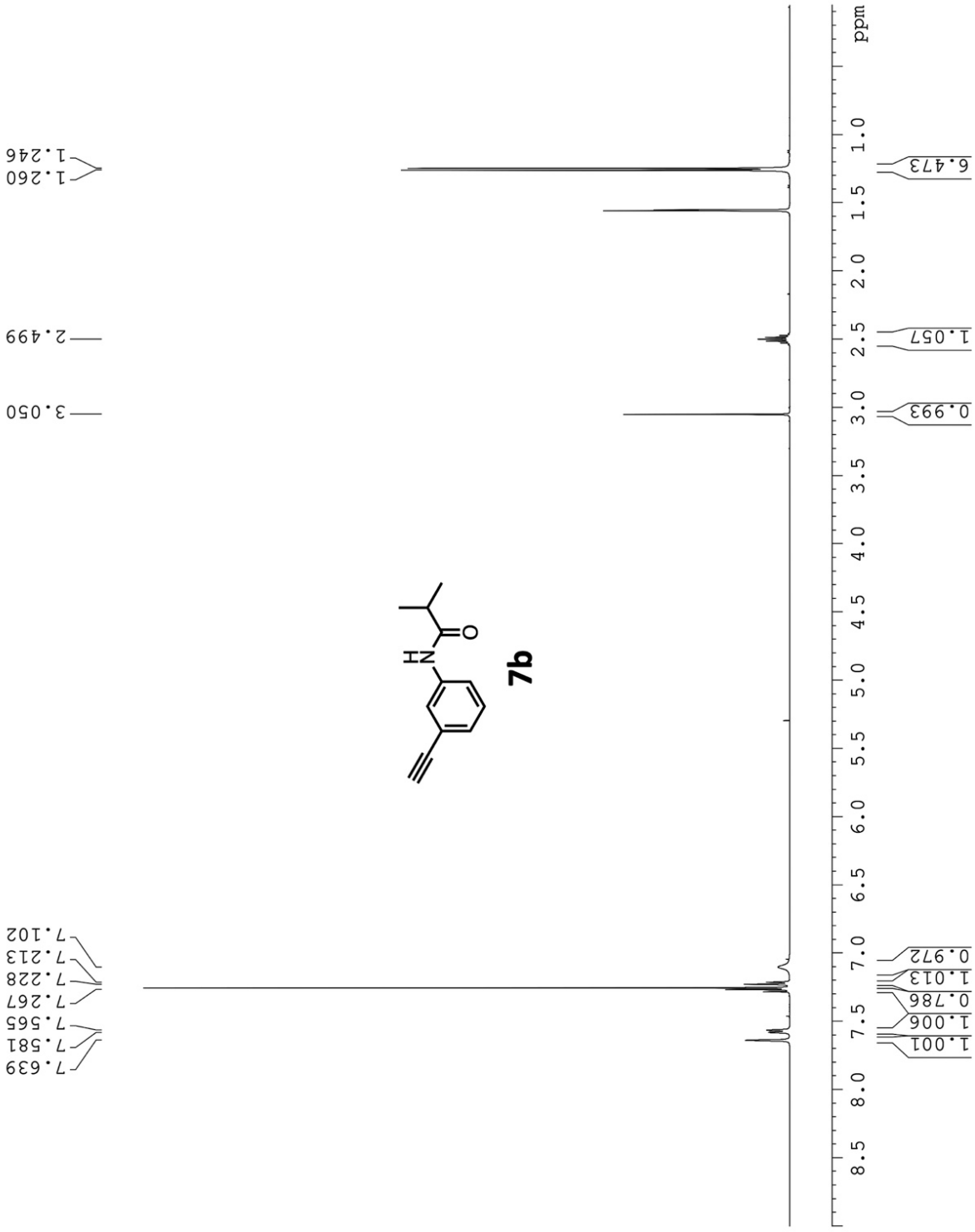

Figure A32: ^{1}H NMR spectrum of compound **7b**.

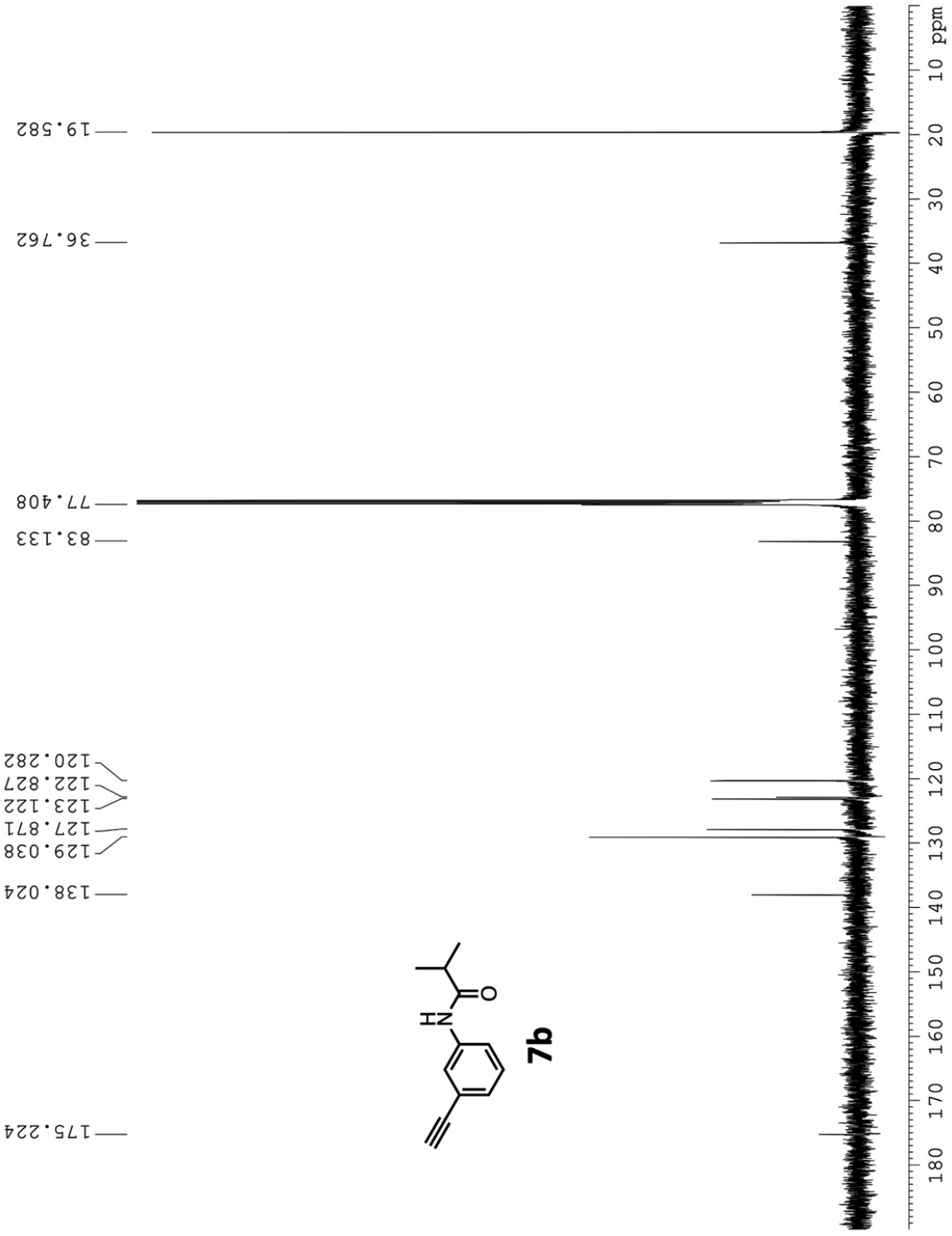

Figure A33: ^{13}C NMR spectrum of compound **7b**.

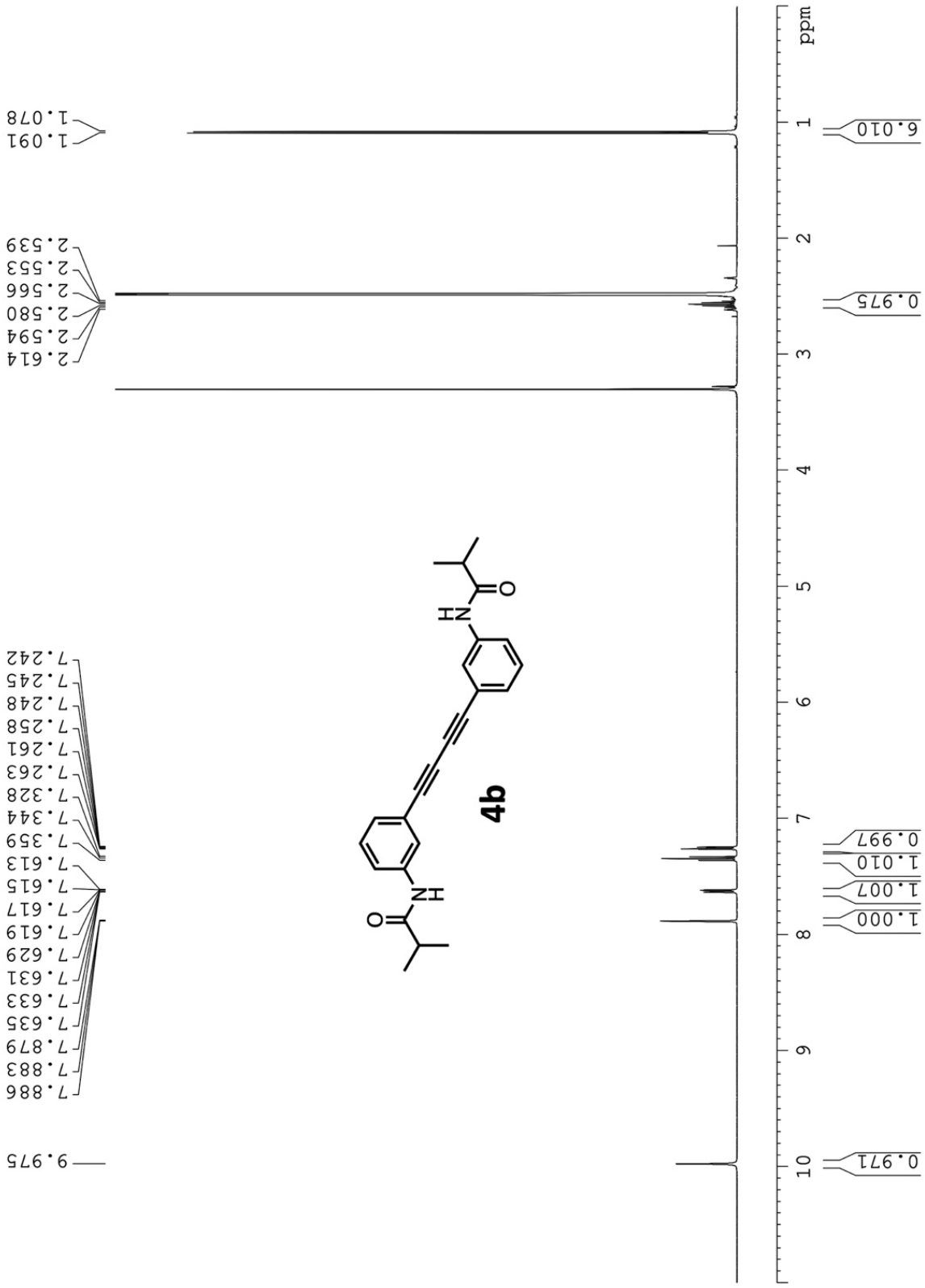

Figure A34: ^{1}H NMR spectrum of compound **4b**.

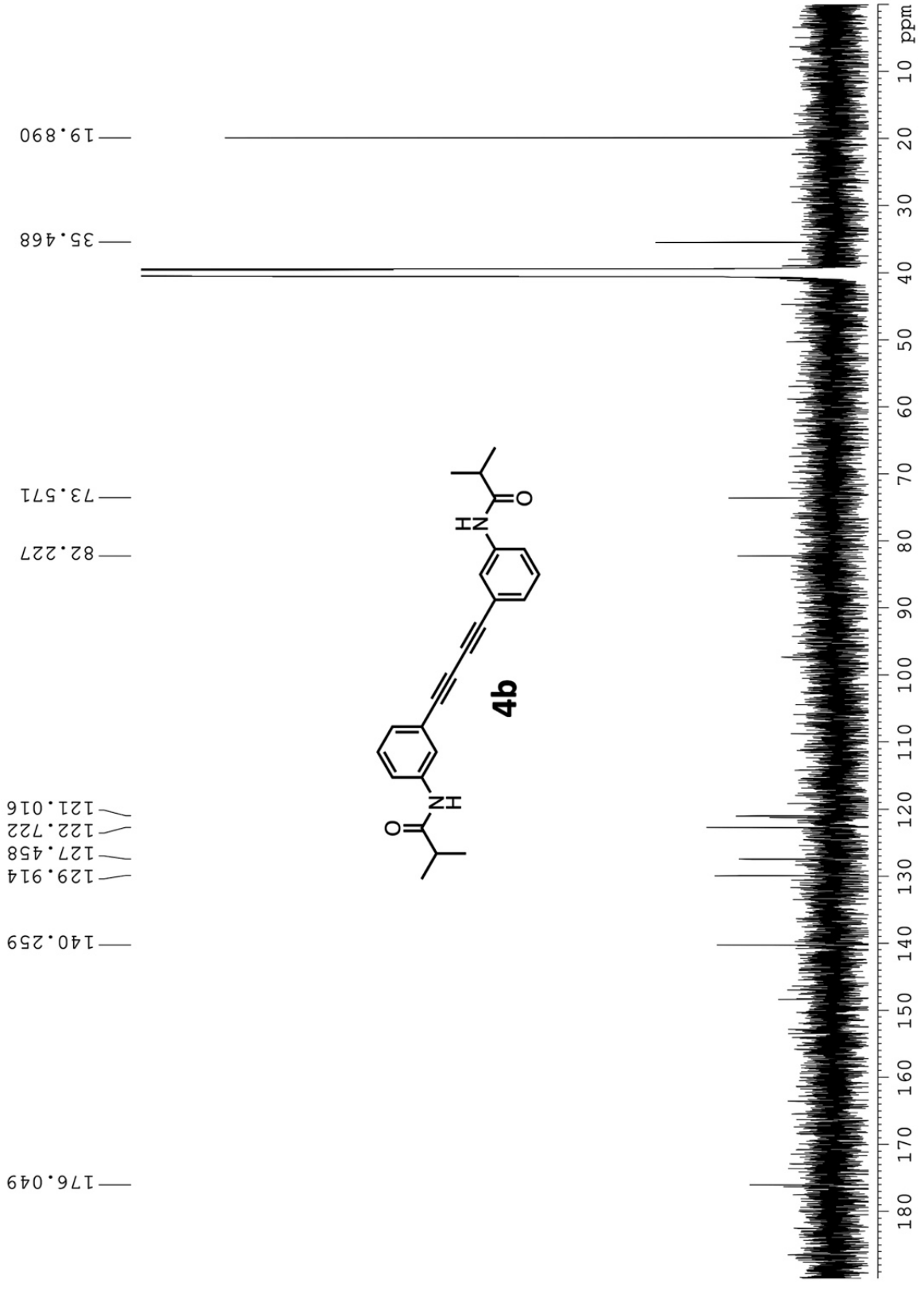

Figure A35: ^{13}C NMR spectrum of compound 4**b**.

All geometries were fully optimized at the B3LYP/6-31G(d) level of theory in the gas phase.[54,55,56,57] All optimized geometries were verified by frequency computations as minima (no imaginary frequencies) or transition structures (one imaginary frequency). Frequency analysis was performed at 623.15 K, and frequency values discussed in the text were scaled using a factor 0.98.[58,59] Free energy corrections were calculated using Truhlar's quasiharmonic approximation, which sets all the real vibrational frequencies that are lower than 100 cm^{-1} to 100 cm^{-1} to correct entropies for the breakdown of the harmonic oscillator approximation. [60,61] Subsequent single-point energy calculations on the optimized structures were performed using the M06-2X/6-311+G(d,p) level of theory. The thermal corrections calculated from the scaled vibrational frequencies at the B3LYP/6-31G(d) level on the optimized geometries were then added to the M06-2X/6-311+G(d,p) electronic energies to obtain the Gibbs free energies. All quantum chemical computations were performed using Gaussian 09.[62] All graphics on optimized structures were generated with CYLview.[63]

Conformational searches were carried out with *MacroModel* from *Schrödinger* using OPLS_2005 and an energy window of 10.0 kcal mol^{-1}.[64] A redundant conformer elimination was performed using an energy window of 10.0 kcal mol^{-1} and a maximum atom deviation cutoff of 0.5 Å. The lowest energy conformers were optimized with B3LYP/6-31G(d) to locate the global minimum for each reaction.

The cycloisomerization of PDA model compounds **5** and **6** is expected to proceed through a 6-π electrocyclization pathway, the favored pathway of dienynes for reaction temperatures under 550°C.[65] Previously, Prall *et al.*[66] computed the mechanistic pathway of the thermal cyclization of hexa-1,3-dien-5-yne **8a** (Scheme A1). The initial 6π electrocyclization forms isobenzene intermediate **8a-*cycl***, which subsequently undergoes two consecutive [1,2]-H shifts and rearomatizes to the final product benzene. This study established the first [1,2]-H shift (**8a-*H-shift***) from the allenic intermediate as the rate-determining step,

with an enthalpic barrier of 38.4 kcal mol^{-1} relative to the starting dieneyne (computed using BCCD(T)/cc-pVCZ//BLYP/6-31G(d)). The results are tabulated in Table A2.

Scheme A1. Mechanistic pathway of hexa-1,3-dien-5-yne (**8a**).

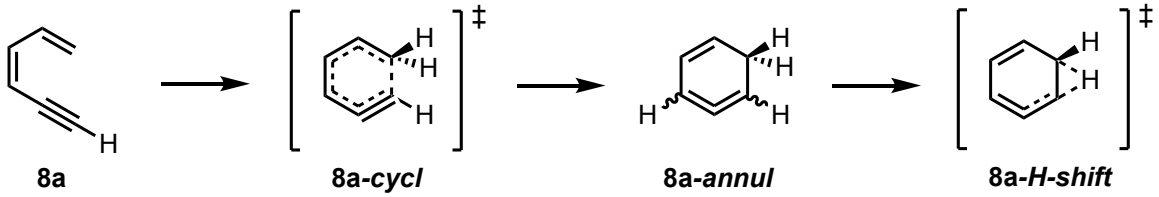

We sought to explore a set of four test structures **8a–11a**, the former two in order to validate our method compared to calculations by Prall *et al*. (Schemes A1 and A2), and the latter two to probe the effect of π-extension of **8a** on reaction barriers (Schemes A3 and A4). We computed the reaction barriers to **8a-*cycl*** and **8a-*H-shift***, which are 40.2 and 44.0 kcal mol^{-1}, respectively (Table A2). For the benzannulated system **9a** (Scheme A2), the barriers for **9a-*cycl*** and **9a-*H-shift*** increase to 46.6 and 51.1 kcal mol^{-1}, respectively, as would be expected to due to the breaking of aromaticity necessary for cyclization to occur. Enthalpies of rate-determining barriers for **8a** and **9a** are within 3 kcal mol^{-1} of those calculated by Prall *et al*.

Scheme A2. Mechanistic pathway of 1-ethynyl-2-vinylbenzene (**9a**).

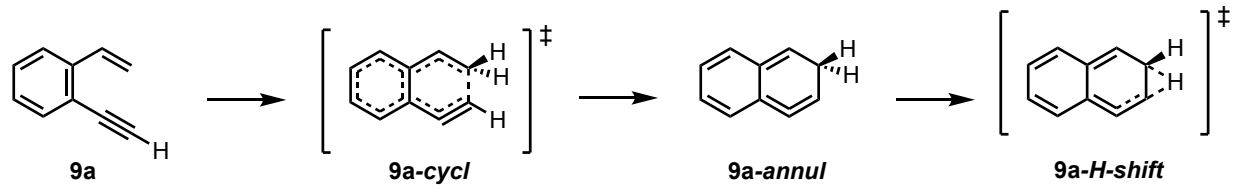

Next, we explored the effect of extending the π-system, as is the case in the PDAs. Phenyl fusion at the 3,4-positions of (*E*)-hexa-3,5-dien-1-yn-3-ylbenzene (**10a**) does not affect the reaction barriers, which stay approximately the same as those for **8a** (37.6 and 46.3 kcal mol^{-1} for **10a-*cycl*** and **10a-*H-shift***, respectively).

However, (*Z*)-but-1-en-3-yn-1-ylbenzene **11a** (Scheme A4) has much high reaction barriers of 54.1 and 58.4 kcal mol^{-1} for **11a-*cycl*** and **11a-*H-shift***, respectively. The increases in the energetic barriers of the rate-determining steps of **9a** and **11a** are due to the necessity to interrupt the aromaticity of the benzene ring.

Scheme A3. Mechanistic pathway of (*E*)-hexa-3,5-dien-1-yn-3-ylbenzene (**10a**).

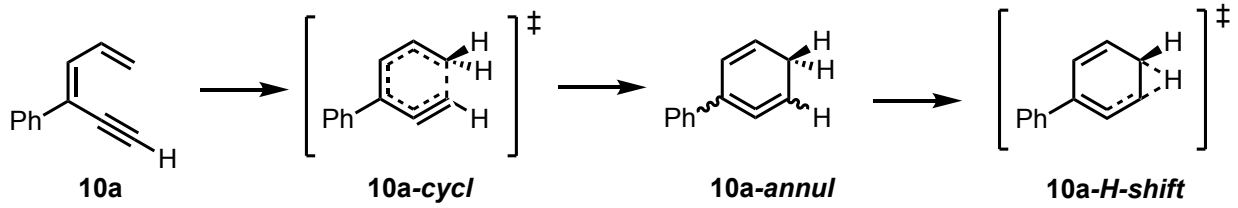

10a **10a-*cycl*** **10a-*annul*** **10a-*H-shift***

Scheme A4. Mechanistic pathway of *cis*-2-ethynyl-1-phenylethene (**11a**).

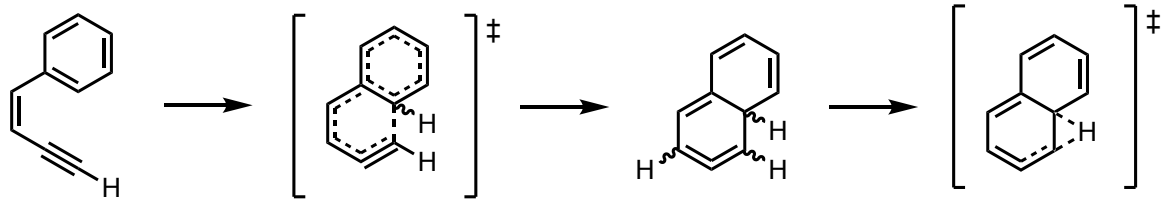

11a **11a-*cycl*** **11a-*annul*** **11a-*H-shift***

Table A2. Computed energetics of pathway intermediates in kcal mol^{-1} relative to starting dieneynes **8a**, **9a**, **10a**, and **11a**.

		cycl	*annul*	*H-shift*
8a	$\Delta H/\Delta H^{\neq}$ [a]	31.7	7.9	39.4
	$\Delta H/\Delta H^{\neq}$	34.5	11.8	36.7
	$\Delta G/\Delta G^{\neq}$	40.2	17.5	44
9a	$\Delta H/\Delta H^{\neq}$ [a]	36.4	25.5	46
	$\Delta H\Delta H^{\neq}$	41.3	32.9	44.4
	$\Delta G/\Delta G^{\neq}$	46.6	37.6	51.1
10a	$\Delta H\Delta H^{\neq}$	32.4	34	39.7
	$\Delta G/\Delta G^{\neq}$	37.6	39.3	46.3
11a	$\Delta H\Delta H^{\neq}$	48.9	44.7	52.7
	$\Delta G/\Delta G^{\neq}$	54.1	48.4	58.4

[a] Computed by Prall et al[66] using BCCD(T)/cc-pVDZ//BLYP/6-31G(d).

Scheme A5. Mechanistic pathway for the *trans*-enediyne **5** model system.

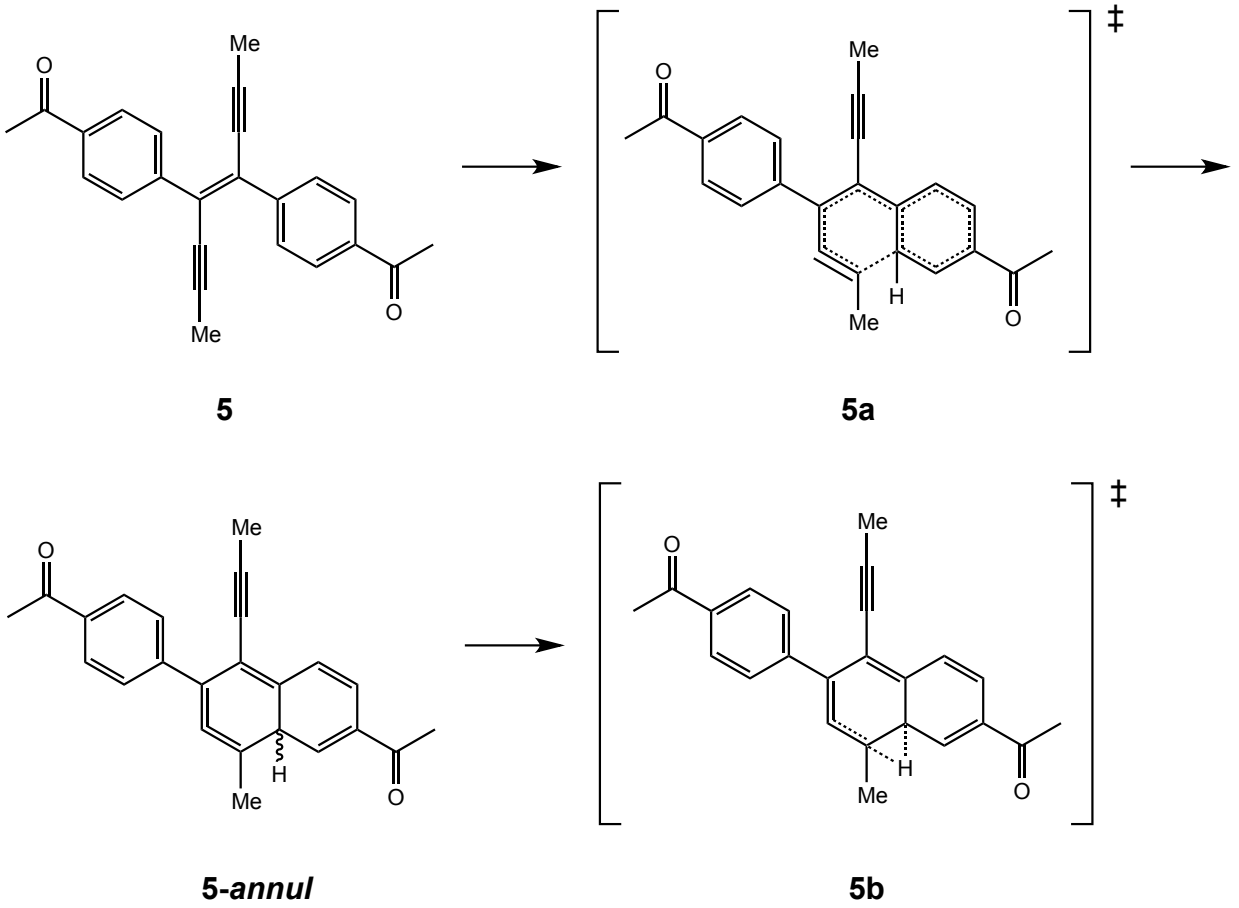

Table A3. Computed energetics in kcal mol^{-1} relative to *trans*-enediyne 5.

Structure	$\Delta H/\Delta H^{\neq}$	$\Delta G/\Delta G^{\neq}$
5a	47.5	52.6
5-*annul*	41.6	45.5
5b	52.9	58.4

Scheme A6. Mechanistic pathway of *trans*-enediyne **6** model system.

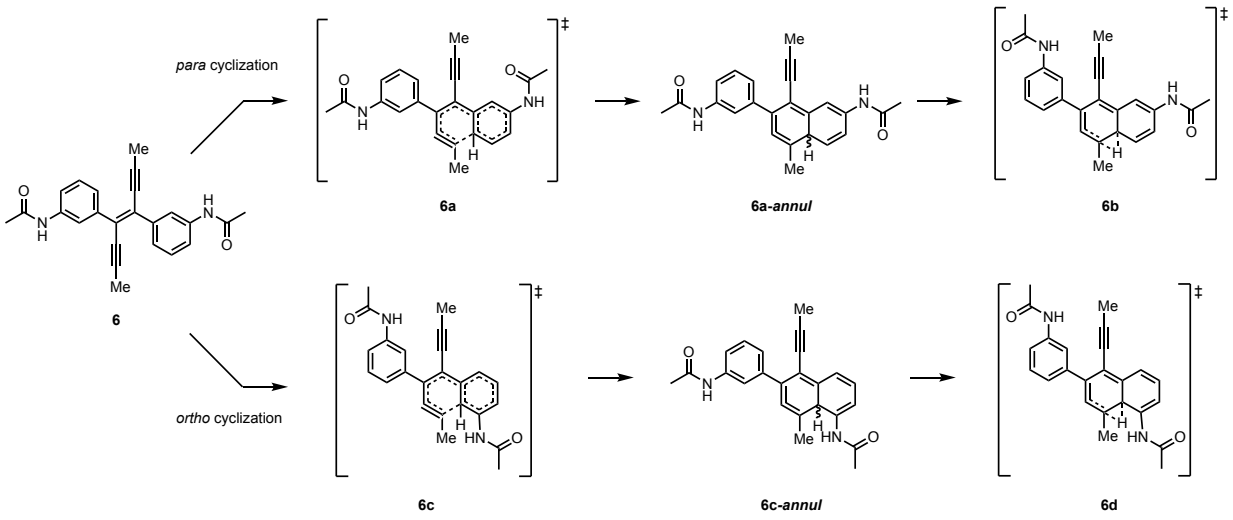

Table A4. Computed energetics in kcal mol^{-1} relative to *trans*-enediyne **6**.

Structure	$\Delta H/\Delta H^{\neq}$	$\Delta G/\Delta G^{\neq}$
6a	48.2	52.5
6a-*annul*	38.6	42.0
6b	52.3	57.5
6c	50.5	55.4
6c-*annul*	37.8	41.5
6d	58.8	64.3

Frequencies and IR intensities

Calculated IR spectra were obtained using DFT. Optimization of ground state structures were performed in the gas phase using B3LYP/6-31G(d), and subsequent frequency calculations were performed at the same level of theory. Frequency values were subsequently scaled according to the previously determined scale factor of 0.98 for B3LYP/6-31G(d).[58,59] Each frequency (cm^{-1}), scaled frequency (cm^{-1}), IR intensity, and vibrational mode symmetry for $[8]_A$GNR, PDA **1**, and PDA **1-*annul*** is tabulated below.

$[8]_A$GNR model system (computed structure described in Fig. A22)

3.7591, 3.6839, 0.0126, A
10.8839, 10.6662, 0.0000, B
11.6690, 11.4356, 0.0000, A
14.5886, 14.2968, 0.0000, B
18.2999, 17.9339, 0.0038, A
23.2288, 22.7642, 0.0201, A
26.4301, 25.9015, 0.0000, B
33.9612, 33.282, 0.0000, B
35.1583, 34.4551, 0.0002, A
42.0545, 41.2134, 0.0011, A
42.6379, 41.7851, 0.0000, B
43.8158, 42.9395, 0.0763, B
47.5128, 46.5625, 0.0000, B
48.2518, 47.2868, 0.0003, A
49.4408, 48.452, 0.1252, A
49.7479, 48.7529, 0.0000, B
76.1991, 74.6751, 3.0455, A
80.3517, 78.7447, 0.0000, B
86.2615, 84.5363, 0.6570, A
93.5868, 91.7151, 0.0000, A
93.9562, 92.0771, 0.0000, B
99.5475, 97.5566, 0.0000, A
104.1331, 102.0504, 0.5201, A
114.0138, 111.7335, 0.0000, B
122.5015, 120.0515, 0.0074, A
135.5879, 132.8761, 0.0000, B
152.5565, 149.5054, 0.1740, B
153.7651, 150.6898, 0.1639, A
168.9970, 165.6171, 0.0000, B
177.5502, 173.9992, 0.1212, A
182.4801, 178.8305, 0.0000, B
184.1532, 180.4701, 0.9670, A
185.2072, 181.5031, 0.0000, B
188.9498, 185.1708, 0.0397, A
192.6506, 188.7976, 5.9351, B
192.6852, 188.8315, 0.0018, B
194.3778, 190.4902, 0.0000, B
194.4768, 190.5873, 0.0105, A
203.9246, 199.8461, 0.0000, A
232.8023, 228.1463, 0.0121, A
233.3387, 228.6719, 0.0000, B
245.9956, 241.0757, 0.0000, B
249.1636, 244.1803, 0.0000, A
249.7145, 244.7202, 0.3948, B
249.9368, 244.9381, 0.9146, A
264.1529, 258.8698, 0.1562, A
272.5594, 267.1082, 0.0000, B
276.9627, 271.4234, 1.4216, B
279.7361, 274.1414, 0.0000, A
286.7408, 281.006, 0.0000, A
287.4821, 281.7325, 0.0000, B
294.9906, 289.0908, 0.7120, A
310.9867, 304.767, 0.0000, A
313.5329, 307.2622, 0.0000, B
313.9190, 307.6406, 0.3408, A
316.4644, 310.1351, 0.1147, B
329.5677, 322.9763, 1.0994, A
333.8510, 327.174, 0.0000, B
334.8777, 328.1801, 1.2636, B
338.1115, 331.3493, 0.0000, A
341.6509, 334.8179, 0.0705, A
345.2419, 338.3371, 0.0000, B
346.2704, 339.345, 7.1672, B
349.9989, 342.9989, 0.0000, B
350.2446, 343.2397, 0.0044, A
350.2551, 343.25, 4.9191, B
350.5981, 343.5861, 0.0000, A
352.2443, 345.1994, 0.0000, B
357.0980, 349.956, 0.0000, A
357.1480, 350.005, 5.7770, A
361.1008, 353.8788, 1.0260, A
366.6995, 359.3655, 0.2860, A
367.2729, 359.9274, 0.0000, B
369.6219, 362.2295, 0.0000, A

376.4362, 368.9075, 0.0000, B
381.8717, 374.2343, 4.8560, B
386.3403, 378.6135, 0.0243, A
388.6468, 380.8739, 0.0001, B
393.1716, 385.3082, 1.8966, B
401.1684, 393.145, 0.0000, B
401.6419, 393.6091, 0.0091, A
401.7257, 393.6912, 0.0001, A
404.3065, 396.2204, 0.5854, B
406.5664, 398.4351, 0.3339, A
422.3602, 413.913, 0.0000, A
440.1450, 431.3421, 0.0000, B
446.7792, 437.8436, 0.0000, A
452.3757, 443.3282, 0.0000, A
453.5989, 444.5269, 0.1769, B
456.4595, 447.3303, 0.2985, B
459.2374, 450.0527, 0.2156, A
462.3576, 453.1104, 0.0000, B
471.9556, 462.5165, 1.7063, B
476.0943, 466.5724, 0.0012, A
477.3425, 467.7956, 0.7125, B
478.5801, 469.0085, 0.0000, A
496.6771, 486.7436, 0.0001, B
497.4026, 487.4545, 5.0884, B
498.7857, 488.81, 0.0000, A
498.9805, 489.0009, 0.0001, B
499.2230, 489.2385, 0.4767, A
500.2216, 490.2172, 0.0000, A
501.3032, 491.2771, 0.3861, A
507.0061, 496.866, 0.0000, B
509.6238, 499.4313, 0.0000, B
513.2479, 502.9829, 0.0372, A
515.5001, 505.1901, 0.0035, A
517.5113, 507.1611, 2.8243, B
520.3471, 509.9402, 0.0000, B
521.8552, 511.4181, 0.0000, A
528.7574, 518.1823, 0.0000, B
529.6322, 519.0396, 0.0148, A
530.0907, 519.4889, 0.0000, B
533.3298, 522.6632, 0.4724, B
540.9562, 530.1371, 0.0593, A
543.2185, 532.3541, 0.0000, A
545.1332, 534.2305, 13.1894, B
549.1266, 538.1441, 0.0000, B
550.7969, 539.781, 0.0000, A
552.1976, 541.1536, 0.0004, A
555.8190, 544.7026, 0.0000, B
560.9573, 549.7382, 0.0114, A
563.5558, 552.2847, 4.2220, B
565.3737, 554.0662, 0.0000, A
570.0412, 558.6404, 0.0126, A
570.2190, 558.8146, 0.0000, B
573.6140, 562.1417, 0.0034, A
576.1594, 564.6362, 0.0000, B
577.8978, 566.3398, 2.7637, B
580.4089, 568.8007, 0.0000, B
583.6118, 571.9396, 0.0000, A
584.2918, 572.606, 0.1380, B
587.0477, 575.3067, 0.5039, B
589.1559, 577.3728, 0.0000, A
589.3474, 577.5605, 0.1026, A
592.7261, 580.8716, 28.8549, B
593.1048, 581.2427, 0.0000, A
593.1269, 581.2644, 0.0000, B
603.9262, 591.8477, 0.0000, A
604.7560, 592.6609, 1.8705, B
605.8853, 593.7676, 0.1025, A
607.8722, 595.7148, 3.1958, A
610.4395, 598.2307, 0.0000, A
610.7472, 598.5323, 0.0000, B
611.7044, 599.4703, 2.2019, A
613.5443, 601.2734, 0.0000, B
615.2864, 602.9807, 0.5971, B
618.1732, 605.8097, 0.1081, A
619.0734, 606.6919, 0.0000, B
623.6230, 611.1505, 0.2398, A
625.1653, 612.662, 0.0583, A
625.6214, 613.109, 0.0000, B
628.7107, 616.1365, 13.6543, B
629.0733, 616.4918, 0.0000, A
635.1430, 622.4401, 1.1676, B
638.9920, 626.2122, 0.0000, A
639.1632, 626.3799, 0.0000, B
643.0124, 630.1522, 0.0000, A
643.5365, 630.6658, 0.1967, B
644.7215, 631.8271, 0.0000, B
648.4611, 635.4919, 0.0000, A
649.7076, 636.7134, 3.0663, B
652.1903, 639.1465, 0.0000, A
653.7435, 640.6686, 0.8471, A
658.5373, 645.3666, 0.4219, A
658.6728, 645.4993, 0.6009, B
659.4952, 646.3053, 0.0000, B
660.6409, 647.4281, 0.0000, B
661.8493, 648.6123, 0.1538, A
665.3076, 652.0014, 0.0000, A
670.5431, 657.1322, 0.2593, A
671.9723, 658.5329, 0.8113, B
673.7102, 660.236, 0.0000, B
678.8123, 665.2361, 0.0000, B
679.6176, 666.0252, 1.1043, A
688.1951, 674.4312, 0.0000, A
693.5983, 679.7263, 0.0673, B
695.4233, 681.5148, 0.2805, A
695.4700, 681.5606, 0.0000, B
708.1646, 694.0013, 2.6308, B
709.3357, 695.149, 0.0000, A
715.5111, 701.2009, 0.0000, B
717.8584, 703.5012, 2.1038, A
718.5596, 704.1884, 1.6357, A

720.5653, 706.154, 0.0000, B
720.7186, 706.3042, 0.0299, A
721.4551, 707.026, 0.0000, B
721.7214, 707.287, 0.0000, A
723.8436, 709.3667, 0.2435, A
725.9343, 711.4156, 0.0000, B
726.8826, 712.3449, 0.0000, B
728.6187, 714.0463, 1.3008, B
728.6614, 714.0882, 0.1145, A
734.3201, 719.6337, 0.0012, A
734.5021, 719.8121, 8.6358, A
736.8139, 722.0776, 0.0000, B
738.7250, 723.9505, 1.2750, A
745.2001, 730.2961, 0.0000, B
747.7613, 732.8061, 0.0000, A
751.6202, 736.5878, 6.0615, B
755.6521, 740.5391, 0.0000, A
758.3163, 743.15, 0.4256, B
763.0804, 747.8188, 24.8056, A
763.0809, 747.8193, 0.0001, B
764.9479, 749.6489, 13.9904, B
778.0750, 762.5135, 0.4567, B
785.8264, 770.1099, 0.0000, A
789.8066, 774.0105, 0.0000, A
792.0736, 776.2321, 0.0000, B
792.0754, 776.2339, 12.3643, A
802.7927, 786.7368, 2.0508, B
808.6675, 792.4941, 0.0003, A
810.4191, 794.2107, 69.0274, A
810.4347, 794.226, 0.0000, B
810.9817, 794.7621, 5.3575, A
811.2008, 794.9768, 0.0000, B
812.2162, 795.9719, 0.0000, B
812.7188, 796.4644, 3.7300, A
814.1237, 797.8412, 7.2283, A
814.8360, 798.5393, 0.0000, B
816.7531, 800.418, 0.0000, B
817.6703, 801.3169, 29.8940, A
819.8887, 803.4909, 0.0725, A
820.4873, 804.0776, 0.0000, B
821.9562, 805.5171, 0.0000, B
821.9674, 805.5281, 0.7357, B
822.4023, 805.9543, 208.1540, A
832.8949, 816.237, 0.0001, B
832.8985, 816.2405, 80.8806, A
835.8092, 819.093, 19.3441, B
837.5469, 820.796, 0.0001, A
860.1695, 842.9661, 0.0000, A
867.6021, 850.2501, 0.0016, B
873.7732, 856.2977, 0.0000, A
875.5550, 858.0439, 0.0013, A
875.6173, 858.105, 0.0000, B
877.8762, 860.3187, 5.5877, B
890.8357, 873.019, 0.0000, B
890.8543, 873.0372, 2.6255, A
893.4871, 875.6174, 0.0000, A
893.8305, 875.9539, 4.6603, B
899.0747, 881.0932, 0.0982, A
900.9841, 882.9644, 0.0000, A
902.3163, 884.27, 0.0001, B
908.4103, 890.2421, 113.3481, B
908.9469, 890.768, 0.0030, B
910.7514, 892.5364, 52.2533, B
911.4576, 893.2284, 0.1425, A
920.2437, 901.8388, 0.0010, A
922.1167, 903.6744, 0.0010, B
922.5767, 904.1252, 169.6376, B
926.8561, 908.319, 0.0000, A
930.7609, 912.1457, 0.0000, A
930.8569, 912.2398, 0.0000, B
932.2854, 913.6397, 0.1347, A
939.5236, 920.7331, 0.0855, A
940.6880, 921.8742, 0.0000, B
943.8008, 924.9248, 0.0000, A
945.4834, 926.5737, 0.0000, B
946.5485, 927.6175, 0.1256, A
947.9434, 928.9845, 0.8612, A
948.4752, 929.5057, 0.0000, B
949.9708, 930.9714, 2.2446, B
963.7810, 944.5054, 0.0000, B
963.7840, 944.5083, 0.2602, A
963.8266, 944.5501, 0.0000, A
966.2117, 946.8875, 17.2154, B
970.4424, 951.0336, 1.0751, A
970.4428, 951.0339, 0.0000, B
975.4580, 955.9488, 0.5992, B
978.6605, 959.0873, 0.0000, A
987.4800, 967.7304, 0.0000, A
999.3008, 979.3148, 7.2191, B
1002.6138, 982.5615, 0.0000, A
1015.5149, 995.2046, 21.1473, B
1047.5127, 1026.5624, 0.0000, A
1069.5069, 1048.1168, 38.9335, B
1073.6857, 1052.212, 7.4746, B
1074.5941, 1053.1022, 0.0000, A
1087.7803, 1066.0247, 0.0000, A
1089.0046, 1067.2245, 2.8861, B
1097.5181, 1075.5677, 0.3876, B
1099.9257, 1077.9272, 0.0000, A
1104.9907, 1082.8909, 0.0000, A
1114.6829, 1092.3892, 34.7705, B
1117.2137, 1094.8694, 34.8758, B
1128.2744, 1105.7089, 0.0000, A
1131.8029, 1109.1668, 0.0000, A
1137.4547, 1114.7056, 25.4519, B
1142.9855, 1120.1258, 16.8871, B
1151.9990, 1128.959, 0.0000, A
1162.3133, 1139.067, 0.0000, A
1169.1535, 1145.7704, 26.0421, B
1177.1845, 1153.6408, 0.5399, B

1177.5009, 1153.9509, 0.0000, A
1182.5447, 1158.8938, 0.0000, A
1182.8531, 1159.196, 39.6620, B
1184.6902, 1160.9964, 0.0000, A
1186.7207, 1162.9863, 28.7250, B
1190.0209, 1166.2205, 13.9881, B
1191.8305, 1167.9939, 0.0000, A
1196.5315, 1172.6009, 0.0000, A
1199.1930, 1175.2091, 1.9384, B
1203.3881, 1179.3203, 1.8250, B
1205.6390, 1181.5262, 0.0000, A
1210.9321, 1186.7135, 0.0000, A
1213.5536, 1189.2825, 1.6277, B
1215.6452, 1191.3323, 0.0000, A
1216.3527, 1192.0256, 0.2796, B
1222.6826, 1198.2289, 0.0000, A
1226.6485, 1202.1155, 15.2653, B
1231.2560, 1206.6309, 0.0000, A
1237.5004, 1212.7504, 0.0000, A
1238.9580, 1214.1788, 0.7622, B
1242.5889, 1217.7371, 0.6213, B
1249.8837, 1224.886, 0.0000, A
1255.9049, 1230.7868, 0.0000, A
1257.1945, 1232.0506, 2.5414, B
1258.9315, 1233.7529, 0.0000, A
1264.7923, 1239.4965, 3.4302, B
1265.6432, 1240.3303, 0.0000, A
1268.5556, 1243.1845, 18.9320, B
1282.9896, 1257.3298, 3.1079, B
1284.4752, 1258.7857, 0.0000, A
1289.1254, 1263.3429, 0.0132, B
1293.3587, 1267.4915, 6.8945, B
1294.0897, 1268.2079, 0.0000, A
1297.0894, 1271.1476, 0.4350, B
1302.7669, 1276.7116, 16.5782, B
1304.6400, 1278.5472, 0.0000, A
1306.0261, 1279.9056, 0.0000, A
1310.6189, 1284.4065, 0.0000, A
1313.1087, 1286.8465, 65.0143, B
1315.1584, 1288.8552, 0.0001, A
1316.6596, 1290.3264, 8.0458, B
1319.5037, 1293.1136, 0.0000, A
1320.3052, 1293.8991, 9.9251, B
1324.5322, 1298.0416, 10.2248, B
1326.9308, 1300.3922, 0.0000, A
1328.8131, 1302.2368, 2.3175, B
1328.9346, 1302.3559, 0.0000, A
1335.0010, 1308.301, 0.0000, A
1335.5571, 1308.846, 12.4717, B
1338.5499, 1311.7789, 0.0000, A
1340.7402, 1313.9254, 0.0000, A
1342.5504, 1315.6994, 31.3160, B
1346.8417, 1319.9049, 66.8891, B
1350.6821, 1323.6685, 0.0000, A
1353.8896, 1326.8118, 60.0231, B
1358.5438, 1331.3729, 0.0000, A
1358.6516, 1331.4786, 196.8522, B
1361.5338, 1334.3031, 0.0000, A
1365.4517, 1338.1427, 199.1285, B
1368.3878, 1341.02, 0.0000, A
1368.8014, 1341.4254, 47.2962, B
1372.7546, 1345.2995, 11.4972, B
1373.4538, 1345.9847, 5.6660, B
1374.2603, 1346.7751, 0.0000, A
1376.1652, 1348.6419, 2.5696, B
1378.6128, 1351.0405, 0.0000, A
1381.0600, 1353.4388, 0.0000, A
1382.2668, 1354.6215, 0.7467, B
1382.5636, 1354.9123, 0.0000, A
1387.3889, 1359.6411, 2.1722, B
1387.6301, 1359.8775, 0.0000, A
1388.4527, 1360.6836, 0.2734, B
1392.9599, 1365.1007, 0.0000, A
1393.7515, 1365.8765, 0.7431, B
1393.8438, 1365.9669, 0.0000, A
1396.1704, 1368.247, 0.2078, B
1396.9490, 1369.01, 0.0000, A
1398.7897, 1370.8139, 0.0000, A
1400.5694, 1372.558, 8.9656, B
1400.7835, 1372.7678, 0.0000, A
1406.1442, 1378.0213, 1.9332, B
1406.9554, 1378.8163, 0.0000, A
1413.1813, 1384.9177, 0.0000, A
1414.4529, 1386.1638, 12.2458, B
1418.4415, 1390.0727, 0.5499, B
1420.3349, 1391.9282, 0.0000, A
1420.8634, 1392.4461, 0.0000, A
1421.4269, 1392.9984, 0.0707, B
1423.7956, 1395.3197, 0.2105, B
1425.0740, 1396.5725, 1.4918, B
1425.2167, 1396.7124, 0.0000, A
1428.5485, 1399.9775, 10.1056, B
1431.7669, 1403.1316, 0.0000, A
1434.3617, 1405.6745, 0.0000, A
1442.3443, 1413.4974, 3.2183, B
1443.6929, 1414.819, 0.0000, A
1450.0418, 1421.041, 4.6558, B
1455.2953, 1426.1894, 7.8157, B
1458.6523, 1429.4793, 0.0000, A
1469.1562, 1439.7731, 0.0000, A
1473.0274, 1443.5669, 11.0348, B
1473.1459, 1443.683, 0.0000, A
1477.1706, 1447.6272, 0.2998, B
1481.6713, 1452.0379, 0.0000, A
1484.4928, 1454.8029, 0.0000, A
1487.7470, 1457.9921, 0.2651, B
1488.1902, 1458.4264, 1.5294, B
1489.6459, 1459.853, 0.0000, A
1492.5818, 1462.7302, 9.0163, B
1495.7817, 1465.8661, 0.0143, B

1496.6593, 1466.7261, 0.0000, A
1500.9506, 1470.9316, 0.0000, A
1502.3548, 1472.3077, 43.7952, B
1504.5719, 1474.4805, 0.0000, A
1505.3468, 1475.2399, 5.3686, B
1510.6054, 1480.3933, 0.0000, A
1512.8061, 1482.55, 6.6379, B
1514.0615, 1483.7803, 0.0000, A
1520.0573, 1489.6562, 147.5679, B
1524.2614, 1493.7762, 0.0000, A
1529.5547, 1498.9636, 0.0000, A
1529.6481, 1499.0551, 66.0466, B
1539.9529, 1509.1538, 2.7353, B
1543.0544, 1512.1933, 0.8943, B
1543.7699, 1512.8945, 0.0000, A
1555.6949, 1524.581, 0.0000, A
1557.3576, 1526.2104, 16.4498, B
1558.6531, 1527.48, 0.0000, A
1568.1594, 1536.7962, 0.0000, A
1568.4291, 1537.0605, 0.3749, B
1571.5742, 1540.1427, 2.5076, B
1578.8337, 1547.257, 0.0000, A
1579.1334, 1547.5507, 7.1232, B
1581.5180, 1549.8876, 0.0000, A
1585.1600, 1553.4568, 0.0338, B
1588.4618, 1556.6926, 0.0000, A
1592.1882, 1560.3444, 43.6554, B
1601.1842, 1569.1605, 0.0000, A
1605.4974, 1573.3875, 0.0000, A
1606.6057, 1574.4736, 0.0692, B
1608.1387, 1575.9759, 0.0000, A
1610.1695, 1577.9661, 0.1981, B
1612.2536, 1580.0085, 0.0000, A
1613.0396, 1580.7788, 0.4667, B
1613.4623, 1581.1931, 0.0000, A
1617.1418, 1584.799, 5.5943, B
1619.0062, 1586.6261, 15.1028, B
1624.3643, 1591.877, 0.0000, A
1627.9112, 1595.353, 0.0000, A
1630.1975, 1597.5936, 9.4375, B
1636.3458, 1603.6189, 6.6330, B
1636.8688, 1604.1314, 0.0000, A
1640.0849, 1607.2832, 2.9227, B
1640.3931, 1607.5852, 0.0000, A
1644.2835, 1611.3978, 22.5058, B
1645.4007, 1612.4927, 0.0000, A
1647.6527, 1614.6996, 0.0000, A
1648.2624, 1615.2972, 16.0325, B
1649.7827, 1616.787, 0.0000, A
1651.6518, 1618.6188, 25.4206, B
1653.3032, 1620.2371, 36.9385, B
1654.3689, 1621.2815, 0.0000, A
1655.1440, 1622.0411, 93.8649, B
1655.4873, 1622.3776, 0.0000, A
1657.7648, 1624.6095, 0.0000, A
1657.9144, 1624.7561, 0.0674, B
1659.5137, 1626.3234, 0.0000, A
1659.5592, 1626.368, 0.9751, B
1671.6004, 1638.1684, 0.0000, A
1671.6013, 1638.1693, 2.0077, B
3184.0417, 3120.3609, 18.8822, B
3184.0443, 3120.3634, 0.0000, A
3187.7679, 3124.0125, 16.4511, B
3187.7682, 3124.0128, 0.0000, A
3193.1555, 3129.2924, 200.2975, B
3193.1844, 3129.3207, 0.0000, A
3201.7053, 3137.6712, 349.5977, B
3201.7414, 3137.7066, 0.0001, A
3212.8041, 3148.548, 0.0000, A
3212.8206, 3148.5642, 133.4451, B
3214.1214, 3149.839, 1.2382, B
3214.1485, 3149.8655, 0.0000, A
3216.2432, 3151.9183, 0.0000, A
3216.2606, 3151.9354, 0.9699, B
3219.1951, 3154.8112, 5.2449, B
3219.2157, 3154.8314, 0.0000, A
3222.4551, 3158.006, 0.0000, A
3222.5026, 3158.0525, 6.2913, B
3224.0510, 3159.57, 7.4216, B
3224.1058, 3159.6237, 0.0000, A
3226.5668, 3162.0355, 0.0000, A
3226.5875, 3162.0557, 12.9654, B
3229.7148, 3165.1205, 3.0521, B
3229.7189, 3165.1245, 0.0000, A
3235.7129, 3170.9986, 20.5269, B
3235.7151, 3171.0008, 0.0000, A
3238.3680, 3173.6006, 19.6238, B
3238.3739, 3173.6064, 0.0000, A
3241.5840, 3176.7523, 0.0000, A
3241.5855, 3176.7538, 22.5947, B
3244.6125, 3179.7203, 5.7147, B
3244.6283, 3179.7357, 0.0000, A
3246.3930, 3181.4651, 0.0000, A
3246.4202, 3181.4918, 193.9567, B
3247.4700, 3182.5206, 53.2751, B
3247.5289, 3182.5783, 0.0001, A
3249.3532, 3184.3661, 0.0000, A
3249.3746, 3184.3871, 147.3290, B
3250.5959, 3185.584, 246.8701, B
3250.7269, 3185.7124, 0.0001, A

PDA **1**

4.6611, 4.5679, 0.1432, A
6.9889, 6.8491, 0.1551, A

8.4223, 8.2539, 0.2416, A
11.2147, 10.9904, 0.0676, A
15.9201, 15.6017, 0.0423, A
17.2367, 16.892, 0.4053, A
19.9120, 19.5138, 0.2877, A
22.7655, 22.3102, 0.3102, A
24.7994, 24.3034, 0.5824, A
26.1330, 25.6103, 0.2746, A
26.6106, 26.0784, 1.6231, A
27.5668, 27.0155, 1.1030, A
30.8649, 30.2476, 1.4259, A
31.9242, 31.2857, 0.4138, A
32.8979, 32.2399, 0.2513, A
36.9863, 36.2466, 1.3351, A
37.9438, 37.1849, 0.5224, A
39.9331, 39.1344, 1.7550, A
42.7919, 41.9361, 0.7399, A
49.4646, 48.4753, 0.9346, A
52.8586, 51.8014, 0.6203, A
57.2596, 56.1144, 1.8237, A
59.5767, 58.3852, 2.3638, A
61.7084, 60.4742, 3.4279, A
64.5021, 63.2121, 1.0637, A
68.5749, 67.2034, 4.1255, A
71.3683, 69.9409, 6.8983, A
72.0762, 70.6347, 0.7919, A
72.2683, 70.8229, 1.5959, A
73.5206, 72.0502, 0.2642, A
76.0208, 74.5004, 1.3786, A
76.3257, 74.7992, 2.4876, A
80.7638, 79.1485, 0.2770, A
81.8660, 80.2287, 5.0401, A
84.2358, 82.5511, 1.4147, A
92.1781, 90.3345, 3.4734, A
94.2099, 92.3257, 3.0242, A
95.7170, 93.8027, 0.0759, A
102.6371, 100.5844, 0.3992, A
105.4323, 103.3237, 0.6977, A
112.0857, 109.844, 1.0698, A
121.6466, 119.2137, 0.0693, A
127.5331, 124.9824, 0.2949, A
128.2857, 125.72, 1.6831, A
130.8528, 128.2357, 0.8744, A
136.5965, 133.8646, 0.1351, A
143.8584, 140.9812, 1.6345, A
156.4861, 153.3564, 0.4246, A
157.4803, 154.3307, 1.1386, A
157.6735, 154.52, 0.3313, A
162.1909, 158.9471, 0.4960, A
165.0440, 161.7431, 0.1726, A
166.0414, 162.7206, 0.7245, A
168.0929, 164.731, 0.5047, A
173.6145, 170.1422, 0.8725, A
179.7704, 176.175, 7.2593, A
180.9681, 177.3487, 1.6059, A
184.3473, 180.6604, 2.1135, A
188.7399, 184.9651, 2.2571, A
190.6164, 186.8041, 1.1757, A
191.9129, 188.0746, 4.7408, A
192.7503, 188.8953, 0.5714, A
199.1083, 195.1261, 0.8099, A
204.9374, 200.8387, 0.5593, A
217.3462, 212.9993, 9.4053, A
221.7300, 217.2954, 9.2414, A
237.0731, 232.3316, 0.0966, A
237.4538, 232.7047, 1.1926, A
254.5843, 249.4926, 0.8490, A
256.5080, 251.3778, 3.6165, A
258.2755, 253.11, 5.1298, A
265.4718, 260.1624, 1.1031, A
271.7238, 266.2893, 0.6194, A
277.4337, 271.885, 0.5136, A
287.6564, 281.9033, 6.1052, A
291.5157, 285.6854, 0.5849, A
297.7980, 291.842, 0.5739, A
311.7958, 305.5599, 10.6864, A
329.4237, 322.8352, 0.4911, A
333.1340, 326.4713, 4.9412, A
337.5218, 330.7714, 0.1651, A
344.7567, 337.8616, 0.4447, A
353.7960, 346.7201, 1.5385, A
360.3043, 353.0982, 5.2101, A
370.8439, 363.427, 2.2679, A
380.2675, 372.6621, 2.4773, A
387.0991, 379.3571, 1.8672, A
394.3452, 386.4583, 0.7524, A
396.2100, 388.2858, 0.4000, A
398.7017, 390.7277, 0.2609, A
403.7919, 395.7161, 3.8771, A
409.7537, 401.5586, 6.3715, A
414.3535, 406.0664, 1.3617, A
415.4895, 407.1797, 1.0483, A
418.3759, 410.0084, 0.1768, A
419.1456, 410.7627, 0.6729, A
419.8822, 411.4846, 0.8331, A
419.9500, 411.551, 0.2172, A
420.1854, 411.7817, 0.4413, A
422.8413, 414.3845, 0.7174, A
426.5569, 418.0258, 1.2153, A
440.5194, 431.709, 0.3222, A
452.3853, 443.3376, 0.9774, A
454.4641, 445.3748, 6.7723, A
460.7995, 451.5835, 1.4564, A
461.8428, 452.6059, 1.9097, A
469.6513, 460.2583, 26.9171, A
473.2693, 463.8039, 8.9460, A
475.0057, 465.5056, 3.2815, A
484.1454, 474.4625, 0.8802, A
485.5634, 475.8521, 0.9719, A
493.2098, 483.3456, 2.9618, A

499.2543, 489.2692, 1.1880, A
501.1894, 491.1656, 2.4494, A
502.2351, 492.1904, 1.0896, A
516.4907, 506.1609, 0.9765, A
517.3357, 506.989, 4.8329, A
520.8802, 510.4626, 2.9511, A
531.1625, 520.5393, 8.7468, A
537.1812, 526.4376, 0.9857, A
539.5837, 528.792, 0.6194, A
550.9635, 539.9442, 1.4156, A
567.1835, 555.8398, 0.2542, A
574.1083, 562.6261, 13.0643, A
578.0839, 566.5222, 11.1328, A
587.7841, 576.0284, 4.1786, A
591.2547, 579.4296, 57.9544, A
601.3561, 589.329, 1.7322, A
602.9898, 590.93, 22.6235, A
603.8055, 591.7294, 4.8560, A
605.8601, 593.7429, 38.9255, A
607.9779, 595.8183, 7.1272, A
608.5258, 596.3553, 19.6409, A
609.8583, 597.6611, 2.4052, A
611.3455, 599.1186, 3.0884, A
614.2037, 601.9196, 14.3990, A
616.4718, 604.1424, 24.4403, A
617.9568, 605.5977, 20.0635, A
618.2376, 605.8728, 2.8352, A
619.3540, 606.9669, 25.1313, A
631.1694, 618.546, 6.8207, A
642.5164, 629.6661, 0.3713, A
643.8167, 630.9404, 0.5237, A
644.4060, 631.5179, 2.8992, A
644.7500, 631.855, 0.6533, A
647.9449, 634.986, 0.5477, A
650.6292, 637.6166, 1.2343, A
651.5834, 638.5517, 1.1590, A
653.2073, 640.1432, 2.5908, A
657.6755, 644.522, 2.4111, A
660.4957, 647.2858, 2.8113, A
701.0040, 686.9839, 0.6059, A
706.1887, 692.0649, 6.9051, A
707.8782, 693.7206, 9.9042, A
708.6981, 694.5241, 82.5468, A
713.7312, 699.4566, 36.0434, A
716.8679, 702.5305, 31.7452, A
736.1078, 721.3856, 0.9703, A
742.3104, 727.4642, 9.8947, A
746.9639, 732.0246, 1.0419, A
751.9708, 736.9314, 4.6666, A
754.2210, 739.1366, 0.1012, A
755.4094, 740.3012, 1.1095, A
756.2115, 741.0873, 0.7087, A
758.5064, 743.3363, 4.4754, A
759.2257, 744.0412, 2.9629, A
759.7905, 744.5947, 17.5212, A
769.3279, 753.9413, 3.5351, A
769.9218, 754.5234, 0.0492, A
791.6188, 775.7864, 2.0249, A
823.7488, 807.2738, 5.4698, A
836.0588, 819.3376, 10.1550, A
837.0800, 820.3384, 22.3693, A
842.3471, 825.5002, 20.8920, A
845.9993, 829.0793, 20.7626, A
846.5669, 829.6356, 39.9115, A
849.6474, 832.6545, 6.4286, A
849.7397, 832.7449, 3.1100, A
851.5339, 834.5032, 3.2063, A
854.5880, 837.4962, 2.5369, A
856.6754, 839.5419, 15.1487, A
858.7037, 841.5296, 20.4111, A
860.3099, 843.1037, 1.4303, A
866.7581, 849.4229, 7.0895, A
867.6269, 850.2744, 0.2874, A
869.0145, 851.6342, 4.0286, A
871.1197, 853.6973, 42.0998, A
872.1741, 854.7306, 14.2831, A
878.5369, 860.9662, 39.0246, A
879.5294, 861.9388, 32.1607, A
880.9884, 863.3686, 27.1989, A
917.1040, 898.7619, 23.2102, A
923.7518, 905.2768, 12.3740, A
963.0479, 943.7869, 23.5152, A
965.7197, 946.4053, 10.3983, A
967.6088, 948.2566, 41.7741, A
968.0763, 948.7148, 6.6036, A
968.4749, 949.1054, 2.7432, A
969.0256, 949.6451, 16.5436, A
969.3529, 949.9658, 137.0426, A
969.5738, 950.1823, 5.5017, A
969.8311, 950.4345, 1.1983, A
971.1226, 951.7001, 4.1552, A
974.1332, 954.6505, 7.9629, A
974.5022, 955.0122, 17.4174, A
974.9962, 955.4963, 31.8086, A
975.9404, 956.4216, 18.9600, A
976.4220, 956.8936, 53.0014, A
976.8046, 957.2685, 1.5403, A
977.5117, 957.9615, 81.9414, A
991.6370, 971.8043, 7.4751, A
993.0078, 973.1476, 2.7177, A
994.5560, 974.6649, 1.3567, A
996.9542, 977.0151, 0.9900, A
997.1829, 977.2392, 4.6863, A
999.5738, 979.5823, 38.7077, A
1002.3730, 982.3255, 5.7206, A
1003.6809, 983.6073, 19.3875, A
1008.3651, 988.1978, 1.6665, A
1026.1797, 1005.6561, 0.5957, A
1032.1113, 1011.4691, 4.0064, A
1032.3890, 1011.7412, 4.6345, A

1034.0591, 1013.3779, 5.7551, A
1035.9730, 1015.2535, 2.3043, A
1037.4591, 1016.7099, 20.8913, A
1038.3914, 1017.6236, 8.6576, A
1039.0048, 1018.2247, 0.8570, A
1050.1174, 1029.1151, 0.3107, A
1055.3918, 1034.284, 1.9696, A
1055.5795, 1034.4679, 1.8432, A
1056.2848, 1035.1591, 1.6781, A
1056.5551, 1035.424, 1.2747, A
1058.6999, 1037.5259, 0.8409, A
1059.5499, 1038.3589, 1.3359, A
1060.8270, 1039.6105, 2.9793, A
1061.1525, 1039.9294, 2.7916, A
1095.5135, 1073.6032, 0.1935, A
1099.9300, 1077.9314, 0.7882, A
1101.3904, 1079.3626, 2.3885, A
1101.4213, 1079.3929, 2.7215, A
1102.7284, 1080.6738, 5.1198, A
1102.8964, 1080.8385, 4.1270, A
1103.6960, 1081.6221, 3.5456, A
1104.2441, 1082.1592, 0.1151, A
1120.5983, 1098.1863, 0.0730, A
1139.6666, 1116.8733, 2.7295, A
1144.6506, 1121.7576, 2.3217, A
1146.6587, 1123.7255, 6.6166, A
1147.8611, 1124.9039, 1.8603, A
1152.0561, 1129.015, 2.5970, A
1152.7594, 1129.7042, 3.4008, A
1154.2002, 1131.1162, 1.7019, A
1155.0417, 1131.9409, 12.8989, A
1157.6768, 1134.5233, 5.4310, A
1207.9576, 1183.7984, 8.3764, A
1215.5517, 1191.2407, 1.5673, A
1216.3227, 1191.9962, 0.9874, A
1218.7952, 1194.4193, 37.1387, A
1219.1142, 1194.7319, 28.7602, A
1219.5999, 1195.2079, 82.6519, A
1221.2486, 1196.8236, 0.6786, A
1221.6477, 1197.2147, 6.7604, A
1223.0658, 1198.6045, 27.4695, A
1243.9742, 1219.0947, 0.1638, A
1248.8517, 1223.8747, 8.3748, A
1264.0039, 1238.7238, 0.0905, A
1271.6201, 1246.1877, 5.4431, A
1274.4871, 1248.9974, 4.5609, A
1287.7182, 1261.9638, 42.8027, A
1289.7508, 1263.9558, 127.5961, A
1290.3690, 1264.5616, 388.7070, A
1291.7158, 1265.8815, 76.9464, A
1292.6704, 1266.817, 124.7521, A
1294.0472, 1268.1663, 425.7966, A
1295.7343, 1269.8196, 1046.7376, A
1298.0948, 1272.1329, 100.1248, A
1299.6289, 1273.6363, 100.3767, A
1307.8967, 1281.7388, 4.2105, A
1334.7958, 1308.0999, 2.4176, A
1337.7380, 1310.9832, 1.3309, A
1339.7118, 1312.9176, 23.8071, A
1340.7762, 1313.9607, 2.4856, A
1342.6355, 1315.7828, 0.8135, A
1346.6428, 1319.7099, 1.0092, A
1348.0185, 1321.0581, 5.8251, A
1349.1268, 1322.1443, 3.6962, A
1349.9258, 1322.9273, 11.5897, A
1350.8091, 1323.7929, 61.5903, A
1351.1234, 1324.1009, 3.9746, A
1351.8376, 1324.8008, 0.9118, A
1351.9241, 1324.8856, 0.3401, A
1353.1035, 1326.0414, 20.4506, A
1365.6397, 1338.3269, 44.0619, A
1366.7922, 1339.4564, 0.4074, A
1381.6433, 1354.0104, 25.8289, A
1409.4997, 1381.3097, 56.8591, A
1410.6895, 1382.4757, 76.2982, A
1411.1928, 1382.9689, 64.3224, A
1417.9754, 1389.6159, 25.8964, A
1418.9936, 1390.6137, 32.2588, A
1419.6142, 1391.2219, 14.0296, A
1420.7739, 1392.3584, 34.0241, A
1420.8633, 1392.446, 33.1540, A
1423.5955, 1395.1236, 11.5090, A
1424.7096, 1396.2154, 23.5278, A
1445.7740, 1416.8585, 13.6075, A
1447.0079, 1418.0677, 18.7845, A
1448.5137, 1419.5434, 32.0286, A
1449.5069, 1420.5168, 40.3911, A
1453.6416, 1424.5688, 37.5928, A
1454.6036, 1425.5115, 3.8674, A
1461.4853, 1432.2556, 57.0713, A
1462.9107, 1433.6525, 149.1810, A
1498.3358, 1468.3691, 10.7375, A
1498.6904, 1468.7166, 10.0286, A
1499.3743, 1469.3868, 8.1869, A
1499.5501, 1469.5591, 20.0370, A
1501.0461, 1471.0252, 2.8043, A
1501.2655, 1471.2402, 6.6791, A
1501.3408, 1471.314, 25.8852, A
1502.7393, 1472.6845, 13.9769, A
1506.3002, 1476.1742, 8.6311, A
1506.3465, 1476.2196, 9.1804, A
1507.8556, 1477.6985, 9.4889, A
1508.2305, 1478.0659, 11.1410, A
1508.9928, 1478.8129, 13.9714, A
1510.6728, 1480.4593, 8.2092, A
1511.0636, 1480.8423, 9.4407, A
1511.9571, 1481.718, 12.5694, A
1521.9665, 1491.5272, 0.5904, A
1545.9839, 1515.0642, 0.7125, A
1548.4646, 1517.4953, 0.6344, A

1548.7018, 1517.7278, 0.7270, A
1550.9028, 1519.8847, 1.2698, A
1551.1889, 1520.1651, 7.5789, A
1552.9133, 1521.855, 0.4111, A
1553.0734, 1522.0119, 9.4095, A
1553.6534, 1522.5803, 6.0641, A
1567.7824, 1536.4268, 2.2642, A
1590.9462, 1559.1273, 5.2846, A
1592.3478, 1560.5008, 10.3129, A
1609.1593, 1576.9761, 0.6070, A
1610.2790, 1578.0734, 14.2555, A
1610.7168, 1578.5025, 22.3548, A
1611.5468, 1579.3159, 19.7975, A
1612.3328, 1580.0861, 1.0684, A
1614.0411, 1581.7603, 1.1719, A
1624.2226, 1591.7381, 20.1976, A
1625.6437, 1593.1308, 42.0803, A
1657.8240, 1624.6675, 8.2370, A
1658.4727, 1625.3032, 7.0945, A
1658.8222, 1625.6458, 13.8556, A
1659.2359, 1626.0512, 15.8032, A
1659.6480, 1626.455, 1.4245, A
1659.9772, 1626.7777, 467.4437, A
1660.6475, 1627.4345, 68.6613, A
1661.2540, 1628.0289, 23.3909, A
1759.5342, 1724.3435, 352.8441, A
1760.5105, 1725.3003, 277.2710, A
1762.6843, 1727.4306, 62.9877, A
1763.6760, 1728.4025, 113.8520, A
1763.8246, 1728.5481, 97.7625, A
1776.6349, 1741.1022, 217.7765, A
1777.0752, 1741.5337, 94.6879, A
1779.8486, 1744.2516, 207.1766, A
2211.4741, 2167.2446, 2.0712, A
2246.5795, 2201.6479, 0.4329, A
2270.7382, 2225.3234, 0.1384, A
3050.6327, 2989.62, 5.1142, A
3050.6381, 2989.6253, 5.1693, A
3051.7490, 2990.714, 3.3968, A
3052.7112, 2991.657, 2.5292, A
3053.7404, 2992.6656, 3.5168, A
3053.7550, 2992.6799, 4.1883, A
3054.0480, 2992.967, 1.9999, A
3054.1715, 2993.0881, 2.0008, A
3111.5048, 3049.2747, 3.3068, A
3111.8323, 3049.5957, 9.5237, A
3112.3344, 3050.0877, 3.9259, A
3113.3949, 3051.127, 8.4099, A
3113.4871, 3051.2174, 8.4079, A
3113.6879, 3051.4141, 5.6188, A
3114.3783, 3052.0907, 3.0920, A
3116.4048, 3054.0767, 3.7908, A
3168.2014, 3104.8374, 9.5317, A
3168.3342, 3104.9675, 17.9799, A
3168.4470, 3105.0781, 9.7947, A
3169.0672, 3105.6859, 15.3489, A
3169.3328, 3105.9461, 12.7755, A
3170.5188, 3107.1084, 16.3888, A
3170.8761, 3107.4586, 16.2145, A
3171.2687, 3107.8433, 15.1233, A
3179.6531, 3116.06, 4.0531, A
3180.4029, 3116.7948, 7.3286, A
3187.0201, 3123.2797, 14.7124, A
3187.2261, 3123.4816, 16.6014, A
3199.4268, 3135.4383, 4.6180, A
3199.9361, 3135.9374, 2.6707, A
3201.1184, 3137.096, 3.2931, A
3203.5706, 3139.4992, 2.7060, A
3204.0637, 3139.9824, 2.6636, A
3204.6299, 3140.5373, 2.8632, A
3207.4012, 3143.2532, 2.2185, A
3209.9895, 3145.7897, 6.9993, A
3211.7659, 3147.5306, 32.0251, A
3212.3499, 3148.1029, 32.5491, A
3214.5589, 3150.2677, 3.8754, A
3215.5274, 3151.2169, 4.1164, A
3215.8070, 3151.4909, 15.9850, A
3218.6523, 3154.2793, 0.1258, A
3219.9440, 3155.5451, 9.3879, A
3221.0442, 3156.6233, 8.0698, A
3221.1906, 3156.7668, 1.2631, A
3223.7432, 3159.2683, 0.8166, A
3224.2032, 3159.7191, 5.4049, A
3225.2085, 3160.7043, 0.7384, A
3225.7057, 3161.1916, 3.9348, A
3226.9990, 3162.459, 3.0012, A
3228.4107, 3163.8425, 7.4397, A
3229.3958, 3164.8079, 4.8466, A
3230.2679, 3165.6625, 0.8412, A
3232.0032, 3167.3631, 0.3714, A
3235.5490, 3170.838, 2.1028, A
3235.7740, 3171.0585, 0.3845, A
3259.4131, 3194.2248, 1.2606, A
3266.6129, 3201.2806, 0.7875, A

PDA **1-*annul***

3.6990, 3.625, 0.0067, A
6.4261, 6.2976, 0.0042, A
7.7767, 7.6212, 0.0054, A
9.2040, 9.0199, 0.0721, A
11.5251, 11.2946, 0.0045, A
18.6093, 18.2371, 0.0620, A
19.7030, 19.3089, 0.4385, A
20.4653, 20.056, 0.1143, A

22.7231, 22.2686, 0.3915, A
24.6340, 24.1413, 0.6540, A
25.6647, 25.1514, 0.2612, A
27.6193, 27.0669, 0.5064, A
31.6870, 31.0533, 0.2823, A
32.4531, 31.804, 1.8834, A
33.3181, 32.6517, 2.9664, A
34.8188, 34.1224, 1.5982, A
37.4829, 36.7332, 0.8401, A
40.3281, 39.5215, 0.7745, A
43.2525, 42.3874, 0.2316, A
45.4552, 44.5461, 4.4539, A
47.8029, 46.8468, 3.1652, A
52.3504, 51.3034, 0.9327, A
53.3620, 52.2948, 3.2635, A
57.8376, 56.6808, 3.5628, A
60.1065, 58.9044, 1.7061, A
70.6514, 69.2384, 0.3589, A
71.2225, 69.798, 2.4686, A
73.9062, 72.4281, 1.7276, A
75.6217, 74.1093, 0.7060, A
78.1840, 76.6203, 1.0184, A
80.3886, 78.7808, 0.0440, A
81.0384, 79.4176, 0.6016, A
84.5693, 82.8779, 0.2490, A
85.0017, 83.3017, 0.6013, A
98.5413, 96.5705, 0.5766, A
103.3541, 101.287, 1.6494, A
111.7429, 109.508, 0.2065, A
113.3812, 111.1136, 0.1212, A
122.0081, 119.5679, 0.7158, A
136.7481, 134.0131, 4.6313, A
146.8561, 143.919, 0.3248, A
156.6741, 153.5406, 1.4895, A
159.8334, 156.6367, 0.7602, A
161.0790, 157.8574, 1.3524, A
162.4748, 159.2253, 0.1651, A
163.9000, 160.622, 0.2513, A
167.2836, 163.9379, 0.1798, A
167.9330, 164.5743, 0.2354, A
171.9608, 168.5216, 0.1904, A
173.5558, 170.0847, 0.2965, A
173.8815, 170.4039, 0.0878, A
174.1959, 170.712, 0.3664, A
176.0461, 172.5252, 0.0589, A
177.0714, 173.53, 0.4036, A
183.0668, 179.4055, 1.4113, A
183.5250, 179.8545, 0.4135, A
185.8077, 182.0915, 0.2235, A
187.3008, 183.5548, 0.9907, A
189.7467, 185.9518, 0.4775, A
191.6464, 187.8135, 2.5262, A
197.7306, 193.776, 1.6008, A
203.7805, 199.7049, 3.6838, A
210.5878, 206.376, 4.0402, A
216.5005, 212.1705, 3.0565, A
224.8797, 220.3821, 0.3653, A
238.3021, 233.5361, 1.1799, A
246.5290, 241.5984, 1.3881, A
254.1450, 249.0621, 5.0520, A
260.2631, 255.0578, 2.6028, A
264.7205, 259.4261, 2.0051, A
268.3638, 262.9965, 0.4787, A
282.7096, 277.0554, 1.0344, A
300.7009, 294.6869, 1.3339, A
304.1110, 298.0288, 1.3232, A
316.6868, 310.3531, 2.5107, A
320.5860, 314.1743, 0.9402, A
331.4440, 324.8151, 0.0135, A
337.6106, 330.8584, 0.2975, A
339.3336, 332.5469, 0.6476, A
339.4858, 332.6961, 0.7123, A
358.2759, 351.1104, 0.5204, A
368.8766, 361.4991, 0.4760, A
386.7953, 379.0594, 6.1161, A
395.2633, 387.358, 4.9172, A
402.9035, 394.8454, 1.9195, A
409.1514, 400.9684, 0.9044, A
412.5883, 404.3365, 0.4140, A
416.7775, 408.4419, 0.6078, A
417.5625, 409.2113, 0.1944, A
417.7736, 409.4181, 0.4684, A
418.1406, 409.7778, 0.9285, A
418.4007, 410.0327, 0.0831, A
422.2569, 413.8118, 0.4236, A
427.2582, 418.713, 0.6712, A
432.4326, 423.7839, 1.1434, A
439.0194, 430.239, 0.9802, A
448.7198, 439.7454, 2.6860, A
456.0316, 446.911, 0.4394, A
462.4606, 453.2114, 5.7821, A
474.0200, 464.5396, 2.9262, A
478.4097, 468.8415, 0.8018, A
482.4837, 472.834, 6.3149, A
483.5819, 473.9103, 1.4518, A
487.1557, 477.4126, 2.8426, A
489.3905, 479.6027, 0.4392, A
492.6220, 482.7696, 1.0942, A
501.9325, 491.8938, 1.3688, A
505.3613, 495.2541, 0.5170, A
507.3735, 497.226, 0.4424, A
509.8872, 499.6895, 0.2394, A
522.9137, 512.4554, 1.0216, A
527.9845, 517.4248, 1.3933, A
533.4026, 522.7345, 0.9530, A
534.0230, 523.3425, 0.0739, A
535.9272, 525.2087, 1.5901, A
538.5531, 527.782, 5.5637, A
541.4092, 530.581, 0.8246, A
543.8548, 532.9777, 7.6026, A

549.6522, 538.6592, 0.9661, A
557.6524, 546.4994, 8.1115, A
573.2366, 561.7719, 4.7738, A
576.6745, 565.141, 69.6451, A
581.2382, 569.6134, 22.7758, A
586.2132, 574.4889, 30.0851, A
591.1581, 579.3349, 20.4268, A
592.3083, 580.4621, 19.8049, A
602.4563, 590.4072, 1.2422, A
605.9063, 593.7882, 2.7557, A
606.5967, 594.4648, 18.5751, A
607.1666, 595.0233, 4.5591, A
610.5074, 598.2973, 9.0434, A
613.0303, 600.7697, 4.9528, A
613.6521, 601.3791, 18.9132, A
615.5955, 603.2836, 7.0472, A
616.7598, 604.4246, 2.8060, A
619.2586, 606.8734, 12.8486, A
623.7080, 611.2338, 2.4225, A
626.0629, 613.5416, 25.2471, A
643.0337, 630.173, 4.3626, A
648.4614, 635.4922, 6.3707, A
650.0234, 637.0229, 0.0526, A
650.5954, 637.5835, 4.4316, A
654.0530, 640.9719, 0.8710, A
660.7145, 647.5002, 6.9782, A
668.9073, 655.5292, 3.8331, A
687.9169, 674.1586, 6.0418, A
688.7078, 674.9336, 6.4138, A
692.6949, 678.841, 3.0487, A
697.6557, 683.7026, 6.1325, A
699.9225, 685.924, 0.9524, A
703.4379, 689.3691, 18.5646, A
711.6127, 697.3804, 24.3510, A
712.5595, 698.3083, 17.8056, A
718.2738, 703.9083, 6.5220, A
726.2987, 711.7727, 21.1534, A
729.4942, 714.9043, 3.6579, A
734.3058, 719.6197, 4.8877, A
739.0688, 724.2874, 7.6165, A
756.1431, 741.0202, 0.9339, A
756.8690, 741.7316, 0.2802, A
759.2082, 744.024, 1.8798, A
763.6211, 748.3487, 1.0101, A
773.6572, 758.1841, 4.3766, A
789.4735, 773.684, 2.3735, A
791.1472, 775.3243, 0.8872, A
795.6536, 779.7405, 2.2671, A
799.2396, 783.2548, 4.1767, A
803.2526, 787.1875, 5.7459, A
803.8987, 787.8207, 5.2144, A
807.0501, 790.9091, 1.0892, A
825.7002, 809.1862, 1.6088, A
829.2643, 812.679, 3.3359, A
834.9948, 818.2949, 16.5821, A
843.7891, 826.9133, 11.8045, A
845.1379, 828.2351, 16.1627, A
848.3082, 831.342, 11.5646, A
851.0248, 834.0043, 27.5122, A
854.9518, 837.8528, 6.4991, A
855.3865, 838.2788, 27.3069, A
857.7613, 840.6061, 25.6275, A
864.0426, 846.7617, 16.1551, A
865.8582, 848.541, 2.6247, A
870.1474, 852.7445, 15.4298, A
870.2684, 852.863, 26.2590, A
873.8868, 856.4091, 10.4640, A
894.7537, 876.8586, 4.4860, A
896.0663, 878.145, 35.7566, A
898.2777, 880.3121, 18.4319, A
900.3028, 882.2967, 21.7496, A
909.8198, 891.6234, 4.1231, A
917.2427, 898.8978, 6.6245, A
927.7628, 909.2075, 3.4062, A
930.3759, 911.7684, 0.3856, A
931.9017, 913.2637, 0.9222, A
949.7887, 930.7929, 10.6426, A
952.8361, 933.7794, 19.2589, A
956.9516, 937.8126, 3.8000, A
957.3138, 938.1675, 15.7313, A
959.5834, 940.3917, 7.8307, A
967.4408, 948.092, 49.9975, A
968.5353, 949.1646, 52.6478, A
968.6845, 949.3108, 53.4424, A
968.7998, 949.4238, 21.5398, A
970.9757, 951.5562, 1.1474, A
971.6784, 952.2448, 0.4238, A
971.9760, 952.5365, 0.3371, A
973.6190, 954.1466, 1.7498, A
973.6996, 954.2256, 1.2633, A
974.6441, 955.1512, 39.9063, A
976.5967, 957.0648, 5.1075, A
977.3902, 957.8424, 2.0459, A
978.6969, 959.123, 3.9004, A
980.2614, 960.6562, 0.5047, A
993.3640, 973.4967, 2.1068, A
994.1592, 974.276, 36.6707, A
995.0286, 975.128, 20.5748, A
995.8049, 975.8888, 4.2620, A
996.6580, 976.7248, 1.8028, A
997.6967, 977.7428, 2.0614, A
998.8533, 978.8762, 34.1694, A
999.4472, 979.4583, 15.5076, A
1034.7468, 1014.0519, 6.7845, A
1034.7741, 1014.0786, 5.2686, A
1035.5317, 1014.8211, 7.3039, A
1036.5921, 1015.8603, 10.4096, A
1055.9804, 1034.8608, 1.3025, A
1056.0939, 1034.972, 0.7746, A
1056.4472, 1035.3183, 0.8401, A

1056.6942, 1035.5603, 0.8260, A
1056.8131, 1035.6768, 1.6385, A
1056.8699, 1035.7325, 1.1780, A
1056.9418, 1035.803, 1.2867, A
1057.0552, 1035.9141, 1.3087, A
1059.5969, 1038.405, 0.9561, A
1060.6525, 1039.4394, 0.0872, A
1065.0875, 1043.7858, 3.0246, A
1081.4237, 1059.7952, 0.2564, A
1097.1824, 1075.2388, 0.1583, A
1098.1631, 1076.1998, 0.1209, A
1099.6971, 1077.7032, 1.6438, A
1101.4087, 1079.3805, 1.9284, A
1103.6351, 1081.5624, 3.1010, A
1104.5170, 1082.4267, 1.1371, A
1108.5811, 1086.4095, 1.3308, A
1112.9692, 1090.7098, 2.4209, A
1119.2299, 1096.8453, 10.0957, A
1136.1628, 1113.4395, 5.2300, A
1146.4029, 1123.4748, 11.2674, A
1147.3627, 1124.4154, 1.0192, A
1147.6971, 1124.7432, 1.3236, A
1150.8549, 1127.8378, 4.8545, A
1162.4289, 1139.1803, 4.1750, A
1187.4123, 1163.6641, 41.4323, A
1194.0953, 1170.2134, 21.7298, A
1198.4782, 1174.5086, 2.6844, A
1199.8202, 1175.8238, 0.9073, A
1203.4560, 1179.3869, 3.5912, A
1218.9629, 1194.5836, 22.5670, A
1219.4818, 1195.0922, 34.2280, A
1219.6392, 1195.2464, 2.2411, A
1221.3359, 1196.9092, 25.7841, A
1225.6091, 1201.0969, 160.3739, A
1235.2144, 1210.5101, 9.9931, A
1244.5162, 1219.6259, 82.8407, A
1249.6650, 1224.6717, 84.0947, A
1251.2303, 1226.2057, 231.6436, A
1266.8449, 1241.508, 88.3159, A
1271.3034, 1245.8773, 72.1270, A
1275.3684, 1249.861, 205.1784, A
1276.1487, 1250.6257, 11.5074, A
1280.5561, 1254.945, 92.8939, A
1281.1684, 1255.545, 136.2324, A
1282.5414, 1256.8906, 29.9352, A
1290.5598, 1264.7486, 169.8789, A
1291.1017, 1265.2797, 297.8894, A
1291.5106, 1265.6804, 52.1725, A
1292.5698, 1266.7184, 551.5905, A
1295.0162, 1269.1159, 86.6705, A
1308.9222, 1282.7438, 58.5266, A
1309.8623, 1283.6651, 43.7348, A
1312.5850, 1286.3333, 21.8634, A
1321.2030, 1294.7789, 5.2787, A
1332.0726, 1305.4311, 16.8179, A
1333.5762, 1306.9047, 1.2299, A
1335.6481, 1308.9351, 2.8992, A
1337.2513, 1310.5063, 2.0154, A
1347.9915, 1321.0317, 6.9933, A
1348.5596, 1321.5884, 8.4480, A
1348.6813, 1321.7077, 16.7778, A
1350.6509, 1323.6379, 8.3251, A
1360.2542, 1333.0491, 21.9753, A
1367.0197, 1339.6793, 10.3987, A
1371.4454, 1344.0165, 18.8270, A
1378.5187, 1350.9483, 22.6996, A
1382.1199, 1354.4775, 1.9369, A
1394.8783, 1366.9807, 3.0823, A
1398.5477, 1370.5767, 4.5696, A
1402.1531, 1374.11, 2.6542, A
1404.8991, 1376.8011, 3.0014, A
1407.3936, 1379.2457, 2.4182, A
1409.2658, 1381.0805, 34.0166, A
1409.9741, 1381.7746, 50.2152, A
1410.4154, 1382.2071, 43.9769, A
1410.7639, 1382.5486, 39.0445, A
1411.7243, 1383.4898, 93.0019, A
1412.1850, 1383.9413, 39.2989, A
1413.4856, 1385.2159, 35.6222, A
1413.7763, 1385.5008, 20.1657, A
1421.7120, 1393.2778, 11.3872, A
1423.9424, 1395.4636, 44.5812, A
1430.8993, 1402.2813, 15.0603, A
1435.3435, 1406.6366, 5.5268, A
1436.6960, 1407.9621, 21.7271, A
1441.1824, 1412.3588, 9.0427, A
1452.2115, 1423.1673, 60.3113, A
1453.1922, 1424.1284, 10.4471, A
1454.2009, 1425.1169, 7.6839, A
1464.4961, 1435.2062, 21.2916, A
1491.6551, 1461.822, 62.1177, A
1492.4412, 1462.5924, 29.4861, A
1494.2566, 1464.3715, 40.6804, A
1498.4837, 1468.514, 22.3973, A
1498.5567, 1468.5856, 5.3391, A
1498.5736, 1468.6021, 7.6355, A
1498.6535, 1468.6804, 9.0692, A
1498.8158, 1468.8395, 14.4919, A
1499.1917, 1469.2079, 6.7815, A
1499.4756, 1469.4861, 9.0572, A
1499.6688, 1469.6754, 8.7948, A
1506.4871, 1476.3574, 8.6736, A
1507.0662, 1476.9249, 9.4025, A
1507.2521, 1477.1071, 9.5081, A
1507.5772, 1477.4257, 9.4495, A
1507.5939, 1477.442, 8.0866, A
1507.7029, 1477.5488, 9.9935, A
1507.8401, 1477.6833, 9.8252, A
1507.8602, 1477.703, 9.1387, A
1515.4291, 1485.1205, 27.9216, A

1541.0073, 1510.1872, 3.1241, A
1543.2146, 1512.3503, 3.3931, A
1544.8808, 1513.9832, 1.6616, A
1545.7341, 1514.8194, 15.4945, A
1554.2987, 1523.2127, 5.4191, A
1554.4784, 1523.3888, 1.6912, A
1554.7501, 1523.6551, 0.6661, A
1555.9238, 1524.8053, 4.4851, A
1597.6179, 1565.6655, 22.9323, A
1599.8455, 1567.8486, 5.0627, A
1602.3012, 1570.2552, 4.5335, A
1608.5090, 1576.3388, 18.3715, A
1613.5466, 1581.2757, 5.1814, A
1614.9203, 1582.6219, 22.4421, A
1615.7329, 1583.4182, 8.0721, A
1620.2262, 1587.8217, 4.7315, A
1631.3367, 1598.71, 5.8946, A
1636.1827, 1603.459, 0.4612, A
1644.1638, 1611.2805, 11.8861, A
1649.9832, 1616.9835, 10.4355, A
1659.9117, 1626.7135, 63.2932, A
1660.8477, 1627.6307, 7.7528, A
1661.2870, 1628.0613, 1.2364, A
1661.7487, 1628.5137, 35.8611, A
1662.2173, 1628.973, 164.2694, A
1662.8668, 1629.6095, 101.0912, A
1665.9620, 1632.6428, 233.2598, A
1669.3028, 1635.9167, 105.8606, A
1776.5894, 1741.0576, 119.5989, A
1777.2221, 1741.6777, 122.2058, A
1777.4571, 1741.908, 220.8851, A
1777.7285, 1742.1739, 373.1200, A
1778.2156, 1742.6513, 95.7929, A
1778.6065, 1743.0344, 231.3459, A
1779.2949, 1743.709, 107.3472, A
1781.3921, 1745.7643, 140.4035, A
3052.3956, 2991.3477, 2.4043, A
3052.5248, 2991.4743, 2.7417, A
3052.6382, 2991.5854, 2.5008, A
3052.6731, 2991.6196, 2.5753, A
3053.4234, 2992.3549, 2.8031, A
3053.6112, 2992.539, 2.3929, A
3053.9813, 2992.9017, 2.2559, A
3054.0101, 2992.9299, 2.5184, A
3111.2609, 3049.0357, 7.5568, A
3111.4477, 3049.2187, 6.3915, A
3111.5482, 3049.3172, 7.8762, A
3111.6251, 3049.3926, 7.9459, A
3112.2261, 3049.9816, 10.2101, A
3112.9646, 3050.7053, 8.3231, A
3113.1159, 3050.8536, 8.6230, A
3113.1992, 3050.9352, 7.6434, A
3169.9700, 3106.5706, 19.9513, A
3170.3161, 3106.9098, 14.2802, A
3170.5280, 3107.1174, 12.4851, A
3170.5952, 3107.1833, 20.7420, A
3170.6551, 3107.242, 8.7583, A
3170.7807, 3107.3651, 16.2824, A
3170.9601, 3107.5409, 12.2899, A
3170.9934, 3107.5735, 16.6361, A
3186.9809, 3123.2413, 4.4334, A
3190.4108, 3126.6026, 7.1175, A
3190.9632, 3127.1439, 9.5153, A
3193.3696, 3129.5022, 11.5511, A
3193.6781, 3129.8045, 4.7095, A
3195.9346, 3132.0159, 6.8117, A
3197.1500, 3133.207, 8.7792, A
3197.7994, 3133.8434, 8.6572, A
3199.6562, 3135.6631, 7.6506, A
3204.9159, 3140.8176, 5.7693, A
3205.4139, 3141.3056, 7.0089, A
3206.0615, 3141.9403, 4.4658, A
3207.8090, 3143.6528, 6.0549, A
3208.6014, 3144.4294, 1.8883, A
3208.7423, 3144.5675, 6.8195, A
3209.8156, 3145.6193, 13.2218, A
3209.9586, 3145.7594, 4.2433, A
3210.3217, 3146.1153, 3.3826, A
3212.3436, 3148.0967, 6.9902, A
3214.5523, 3150.2613, 7.2762, A
3217.1559, 3152.8128, 24.2294, A
3217.2863, 3152.9406, 4.6816, A
3222.4174, 3157.9691, 5.7174, A
3222.8669, 3158.4096, 6.1385, A
3225.8221, 3161.3057, 1.4723, A
3226.2174, 3161.6931, 1.3714, A
3226.5742, 3162.0427, 1.9263, A
3227.1881, 3162.6443, 4.1579, A
3228.6509, 3164.0779, 1.8079, A
3228.7657, 3164.1904, 4.0620, A
3229.8703, 3165.2729, 11.5973, A
3230.4286, 3165.82, 8.1191, A
3231.3708, 3166.7434, 9.0718, A
3240.1361, 3175.3334, 0.2289, A

Computed structures of model systems **8a**-**11a** and *trans*-enediynes **5** and **6.**

8a

C	0.85140	1.05021	0.15302
C	-0.48259	1.21077	-0.00210
C	-1.54317	0.23936	-0.27690
C	1.73185	-0.12226	-0.00506
C	1.46713	-1.40263	-0.20157
C	-1.70647	-0.96486	0.28868
H	-1.02632	-1.34106	1.04669
H	0.62226	-2.06801	-0.29824
H	1.40808	1.96201	0.36601
H	2.79293	0.14589	0.02759
H	-0.83601	2.24186	0.05087
H	-2.55640	-1.59345	0.03749
H	-2.31343	0.58925	-0.96690

SCF energy: -232.086400774 hartree
Zero-point correction: 0.093293 hartree
Enthalpy correction: 0.118480 hartree
Free Energy correction: 0.015218 hartree
Quasiharmonic Free Energy correction: 0.016069 hartree

8a-*cycl*

C	1.33065	-0.64496	0.00925
C	1.17036	0.73851	0.16029
C	-0.06582	1.36979	-0.07520
C	0.18962	-1.43244	-0.04445
C	-1.06120	-1.24066	-0.11102
C	-1.33195	0.77277	0.05111
H	-1.62539	0.38837	1.02446
H	-1.98079	-1.68391	0.23237
H	2.31176	-1.02413	-0.26822
H	2.06879	1.35251	0.12334
H	-2.16091	1.25706	-0.46798
H	-0.00347	2.33207	-0.58390

SCF energy: -232.028325883 hartree
Zero-point correction: 0.093140 hartree
Enthalpy correction: 0.115378 hartree
Free Energy correction: 0.022025 hartree
Quasiharmonic Free Energy correction: 0.022025 hartree

8a-*annul*

C	1.24096	-0.78486	0.16536
C	1.24185	0.64816	-0.21400
C	0.07210	1.30149	-0.05671
C	0.06168	-1.37752	-0.02418
C	-1.15488	-0.86631	-0.18065
C	-1.25238	0.59112	0.24495
H	-1.53242	0.78576	1.29461
H	-1.92984	-1.29915	-0.80972
H	2.04942	-1.17950	0.77852
H	2.16618	1.18335	-0.41932
H	-2.05220	1.04832	-0.35281
H	0.04283	2.38875	-0.09992

SCF energy: -232.0668176 hartree
Zero-point correction: 0.095286 hartree
Enthalpy correction: 0.117757 hartree
Free Energy correction: 0.024329 hartree
Quasiharmonic Free Energy correction: 0.024329 hartree

8a-*H-shift*

C	1.20183	0.68315	0.04767
C	0.00365	1.38799	-0.03404
C	-1.19938	0.65696	-0.06751
C	1.22626	-0.72290	-0.01300
C	0.09008	-1.56467	-0.04582
H	-0.01674	2.47222	-0.07701
H	-1.23801	-0.04363	1.01504
C	-1.12825	-0.82649	-0.01829
H	-2.09899	-1.32731	0.00518
H	-2.16304	1.15290	-0.18065
H	2.13530	1.24289	0.10493
H	2.21629	-1.18134	-0.08159

SCF energy: -232.022839771 hartree
Zero-point correction: 0.092172 hartree
Enthalpy correction: 0.113358 hartree

Free Energy correction: 0.022563 hartree
Quasiharmonic Free Energy correction: 0.022563 hartree

9a

C	-2.47978	0.53132	-0.00003
C	-0.03671	0.77542	0.00002
C	1.07445	1.74076	-0.00007
C	2.39986	1.54171	0.00013
C	0.07462	-0.64411	0.00004
C	1.31751	-1.35126	-0.00004
C	-1.33472	1.32063	-0.00005
H	0.73047	2.77538	-0.00027
H	3.07088	2.39623	0.00002
C	-2.35929	-0.85904	0.00004
C	-1.09300	-1.43270	0.00007
H	-1.43654	2.40311	-0.00009
H	-3.46037	0.99923	-0.00007
H	-3.24207	-1.49200	0.00006
H	-0.98137	-2.51255	0.00009
C	2.31341	-2.04039	-0.00011
H	3.20607	-2.62366	-0.00012
H	2.85471	0.56022	0.00039

SCF energy: -385.717403355 hartree
Zero-point correction: 0.139785 hartree
Enthalpy correction: 0.176506 hartree
Free Energy correction: 0.046969 hartree
Quasiharmonic Free Energy correction: 0.049497 hartree

9a-*cycl*

C	-2.44480	0.72394	0.06479
C	0.00122	0.68850	0.07209
C	1.23233	1.35220	-0.20234
C	2.49373	0.79979	0.07112
C	-0.04590	-0.77044	0.03307
C	1.18011	-1.47804	0.00832
C	-1.23150	1.38752	0.09963
H	1.17115	2.23400	-0.83847
H	3.34880	1.26849	-0.41971
C	-2.48310	-0.67731	-0.04553
C	-1.30163	-1.40086	-0.08204
H	-1.21185	2.47155	0.17937
H	-3.37141	1.28977	0.11301
H	-3.43804	-1.19306	-0.09489
H	-1.32051	-2.48376	-0.15418
C	2.39005	-1.07430	-0.03913
H	3.36455	-1.45949	0.21938
H	2.71428	0.56653	1.11567

SCF energy: -385.648220935 hartree
Zero-point correction: 0.139373 hartree
Enthalpy correction: 0.173141 hartree
Free Energy correction: 0.054553 hartree
Quasiharmonic Free Energy correction: 0.054553 hartree

9a-*annul*

C	2.43451	0.71146	0.04634
C	0.00448	0.69551	0.00288
C	-1.22268	1.38589	-0.09943
C	-2.42438	0.67587	-0.05165
C	0.00062	-0.75496	-0.01304
C	-1.18300	-1.56379	-0.03034
C	1.24309	1.39793	0.04913
H	-1.23248	2.46530	-0.22190
H	-2.44881	0.04935	1.03093
C	2.45064	-0.70561	-0.01290
C	1.26771	-1.40870	-0.04952
H	1.23303	2.48518	0.09074
H	3.37399	1.25730	0.08276
H	3.40291	-1.22914	-0.02685
H	1.25118	-2.49374	-0.08564
C	-2.37779	-0.83411	0.02598
H	-3.35664	-1.30806	0.10643
H	-3.38232	1.17706	-0.18123

SCF energy: -385.663816316 hartree
Zero-point correction: 0.141176 hartree
Enthalpy correction: 0.175386 hartree
Free Energy correction: 0.055793 hartree
Quasiharmonic Free Energy correction: 0.055793 hartree

9a-*H-shift*

C	-2.44096	0.69551	0.07760
C	-0.01100	0.70249	0.17083
C	1.16112	1.31200	-0.17979
C	2.47104	0.58555	-0.33374
C	-0.01595	-0.78483	0.10514
C	1.19593	-1.40391	0.28722
C	-1.28319	1.38451	0.27916
H	1.15006	2.36632	-0.45041
H	2.86457	0.74432	-1.35450
C	-2.42359	-0.71013	-0.22658
C	-1.25385	-1.42161	-0.22023
H	-1.29885	2.44659	0.51188
H	-3.39786	1.20697	0.14138
H	-3.36528	-1.21482	-0.42501
H	-1.24956	-2.49661	-0.37735
C	2.39978	-0.83967	0.19901
H	3.28723	-1.24398	0.68376
H	3.21370	1.07181	0.31854

SCF energy: -385.641337517 hartree

Zero-point correction: 0.138366 hartree
Enthalpy correction: 0.171267 hartree
Free Energy correction: 0.054843 hartree
Quasiharmonic Free Energy correction: 0.054843 hartree

10a

C	-3.52508	-0.17372	-0.02276
C	-2.77440	-1.27647	0.38964
C	-2.86857	0.99560	-0.41049
C	-1.47669	1.06012	-0.39351
C	-1.38257	-1.21349	0.40583
C	0.78255	0.01765	-0.01572
C	1.53283	-1.09450	-0.26771
C	2.97698	-1.28332	-0.31049
C	1.35773	1.30316	0.21970
C	1.77754	2.42217	0.42074
C	3.96267	-0.42987	0.02020
H	5.00087	-0.73710	-0.06890
H	-0.81427	-2.06584	0.76599
H	-3.44159	1.86292	-0.72788
H	-0.97303	1.97342	-0.69461
C	-0.70812	-0.04869	-0.00051
H	-3.27362	-2.18536	0.71527
H	0.96623	-1.99281	-0.50054
H	2.17069	3.39655	0.60312
H	-4.61061	-0.22182	-0.03041
H	3.27137	-2.27416	-0.65592
H	3.77478	0.57236	0.38436

SCF energy: -463.10241976 hartree
Zero-point correction: 0.172961 hartree
Enthalpy correction: 0.217754 hartree
Free Energy correction: 0.069287 hartree
Quasiharmonic Free Energy correction: 0.072079 hartree

10a-*cycl*

C	-3.58784	0.00522	-0.12818
C	-2.88055	-1.19702	-0.21525
C	-2.89045	1.19773	0.06994
C	-1.50300	1.18613	0.19375
C	-1.49263	-1.20787	-0.10765
C	0.69622	0.03093	0.22778
C	1.48350	-1.11980	0.42266
C	2.82258	-1.20703	0.00451
C	1.40203	1.20926	-0.05020
C	2.58267	1.55089	-0.34060
C	3.72910	-0.14341	-0.12787
H	3.95652	0.45822	0.74721
H	-0.96334	-2.14852	-0.22406
H	-3.42871	2.13928	0.14130
H	-0.95929	2.10844	0.37522
C	-0.77456	-0.01537	0.10581
H	-3.41207	-2.12988	-0.38462
H	0.96546	-2.05758	0.61174
H	3.26935	2.37139	-0.22257
H	-4.67098	0.01041	-0.21538
H	3.11491	-2.17589	-0.40230
H	4.60581	-0.31383	-0.75473

SCF energy: -463.047680368 hartree
Zero-point correction: 0.172750 hartree
Enthalpy correction: 0.214658 hartree
Free Energy correction: 0.075697 hartree
Quasiharmonic Free Energy correction: 0.077304 hartree

10a-*annul*

C	3.51072	0.01952	0.29520
C	2.77845	1.20881	0.27452
C	2.86034	-1.19507	0.05908
C	1.49428	-1.21867	-0.20253
C	1.40827	1.18749	0.02360
C	-0.70545	-0.09194	-0.45428
C	-1.52626	1.12909	-0.65724
C	-2.69764	1.17935	0.00718
C	-1.45974	-1.19986	-0.27478
C	-2.71759	-1.30746	0.14099
C	-3.30923	-0.02980	0.71211
H	-3.22151	0.10851	1.80368
H	0.84723	2.11694	0.03972
H	3.42410	-2.12437	0.06365
H	0.98624	-2.15309	-0.42277
C	0.73943	-0.02874	-0.21316
H	3.27571	2.15724	0.46068
H	-1.13084	2.00316	-1.17008
H	-3.38046	-2.13102	-0.11882
H	4.58052	0.03962	0.48506
H	-3.24445	2.11798	0.07913
H	-4.39013	-0.05134	0.51557

SCF energy: -463.047680368 hartree
Zero-point correction: 0.175277 hartree
Enthalpy correction: 0.217183 hartree
Free Energy correction: 0.078686 hartree
Quasiharmonic Free Energy correction: 0.080044 hartree

10a-*H-shift*

C	-3.56733	-0.01513	0.10598
C	-2.84251	-1.19900	0.26217
C	-2.88841	1.18418	-0.12405
C	-1.49846	1.20016	-0.20921
C	-1.45150	-1.18316	0.18019
C	0.72554	0.06518	-0.15561

C	1.44448	-1.10322	-0.46757
C	2.82444	-1.15827	-0.17957
C	1.38716	1.31922	0.04308
C	2.77196	1.27009	0.21737
C	3.51051	0.06285	0.23969
H	3.02514	-0.86846	1.06658
H	-0.89992	-2.10550	0.34219
H	-3.44624	2.10973	-0.24305
H	-0.94462	2.11656	-0.38489
C	-0.75565	0.01478	-0.06552
H	-3.36097	-2.13373	0.46052
H	0.96772	-1.99132	-0.87560
H	3.35379	2.18978	0.30903
H	-4.65250	-0.02745	0.16912
H	3.41497	-2.05267	-0.35686
H	4.58127	0.01698	0.43132

SCF energy: -463.033762525 hartree
Zero-point correction: 0.171357 hartree
Enthalpy correction: 0.212317 hartree
Free Energy correction: 0.075910 hartree
Quasiharmonic Free Energy correction: 0.077237 hartree

11a

C	2.23238	-1.06461	0.00021
C	0.91851	-1.39546	0.00029
C	-0.28851	-0.56749	0.00015
C	2.82545	0.22464	-0.00014
C	3.41581	1.28395	-0.00050
C	-0.28841	0.84210	0.00042
H	0.65255	1.37837	0.00066
H	3.91365	2.22679	-0.00068
H	2.94533	-1.88827	0.00028
H	0.71524	-2.46530	0.00036
C	-1.53359	-1.22800	-0.00025
C	-2.73068	-0.51739	-0.00037
C	-2.71214	0.87844	-0.00009
H	-3.67673	-1.05220	-0.00069
C	-1.48683	1.55057	0.00030
H	-3.64347	1.43839	-0.00018
H	-1.46458	2.63727	0.00051
H	-1.55396	-2.31555	-0.00045

SCF energy: -385.721282245 hartree
Zero-point correction: 0.140578 hartree
Enthalpy correction: 0.176707 hartree
Free Energy correction: 0.048771 hartree
Quasiharmonic Free Energy correction: 0.050886 hartree

11a-*cycl*

C	-2.42634	-0.69522	-0.24200
C	-1.30849	-1.34331	0.27338
C	-0.04831	-0.68908	0.33433
C	-2.41301	0.69879	-0.37337
C	-1.45617	1.53602	-0.14576
C	0.04097	0.77453	0.44549
H	-0.33177	1.13161	1.41660
H	-1.45151	2.58142	0.13484
H	-3.21903	-1.30323	-0.67519
H	-1.31190	-2.43193	0.31533
C	1.12876	-1.42666	0.05151
C	1.32136	1.37871	0.11393
C	2.39834	0.62276	-0.25975
H	3.33804	1.10192	-0.52241
C	2.31562	-0.79686	-0.25604
H	1.06103	-2.51127	0.00742
H	1.40914	2.45993	0.19143
H	3.18955	-1.38642	-0.51841

SCF energy: -385.639673951 hartree
Zero-point correction: 0.139756 hartree
Enthalpy correction: 0.173075 hartree
Free Energy correction: 0.055512 hartree
Quasiharmonic Free Energy correction: 0.055512 hartree

11a-*annul*

C	2.54217	0.52317	0.12789
C	1.34705	1.34621	-0.13768
C	0.13098	0.75017	0.01393
C	2.35572	-0.77454	-0.13519
C	1.22489	-1.46250	-0.27341
C	0.04792	-0.77275	0.37228
H	0.14552	-0.77932	1.47823
H	1.06824	-2.25879	-1.00100
H	3.39204	0.94481	0.66149
H	1.42081	2.42044	-0.29341
C	-1.12308	1.47005	-0.04245
C	-1.30183	-1.39062	0.09052
C	-2.40196	-0.63172	-0.04607
H	-3.37635	-1.09323	-0.18641
C	-2.31651	0.82467	-0.05029
H	-3.23874	1.39624	-0.11531
H	-1.08719	2.55361	-0.13258
H	-1.35652	-2.47670	0.07172

SCF energy: -385.648570857 hartree
Zero-point correction: 0.140757 hartree
Enthalpy correction: 0.175166 hartree
Free Energy correction: 0.055373 hartree
Quasiharmonic Free Energy correction: 0.055373 hartree

11a-*H-shift*

C	2.46984	0.66443	-0.08367
C	1.28770	1.37077	0.09429
C	0.02857	0.72763	0.08528
C	2.56140	-0.75466	-0.19292
C	1.36605	-1.43010	-0.00777
C	0.00612	-0.72064	0.10830
H	0.62206	-1.06593	1.10720
H	1.28765	-2.51416	0.09254
H	3.37555	1.25958	-0.22006
H	1.29926	2.46042	0.13619
C	-1.20622	1.42515	0.01463
C	-1.26240	-1.39864	0.01260
C	-2.42096	-0.67624	-0.08964
H	-3.37257	-1.19272	-0.18353
C	-2.39935	0.74736	-0.07660
H	-3.33408	1.29567	-0.14734
H	-1.18661	2.51224	0.01418
H	-1.27578	-2.48554	0.01383

SCF energy: -385.631734333 hartree
Zero-point correction: 0.138075 hartree
Enthalpy correction: 0.171114 hartree
Free Energy correction: 0.054335 hartree
Quasiharmonic Free Energy correction: 0.054335 hartree

5

C	4.74218	-0.09486	-0.07201
C	3.94099	0.78983	-0.81016
C	4.11592	-1.11983	0.65287
C	2.73098	-1.25136	0.64132
C	2.55769	0.66777	-0.81194
C	0.44233	-0.52326	-0.07009
C	-0.44234	0.52324	0.07000
C	-1.92591	0.34947	0.07447
C	0.00017	-1.86791	-0.24294
C	-0.29050	-3.03391	-0.41811
C	-2.55766	-0.66787	0.81186
C	-3.94095	-0.78994	0.81015
C	-4.74217	0.09483	0.07213
C	-4.11598	1.11988	-0.65269
C	-2.73104	1.25141	-0.64120
H	-2.26006	2.05688	-1.19609
H	-4.70628	1.82548	-1.22926
H	-1.95853	-1.35286	1.40031
H	1.95861	1.35271	-1.40050
H	4.70615	-1.82539	1.22958
H	2.25997	-2.05676	1.19627
C	1.92589	-0.34949	-0.07449
C	0.29048	3.03390	0.41792
C	-0.00019	1.86789	0.24280
C	0.68382	4.42237	0.62816
H	0.54835	4.71850	1.67594
H	1.73849	4.57878	0.37129
H	0.08342	5.10371	0.01285
C	-0.68385	-4.42236	-0.62841
H	-1.73799	-4.57923	-0.36965
H	-0.55030	-4.71783	-1.67663
H	-0.08209	-5.10390	-0.01465
H	-4.43219	-1.56728	1.38641
H	4.43225	1.56712	-1.38647
C	-6.22768	-0.09292	0.10365
C	6.22769	0.09294	-0.10351
C	7.10674	-0.87067	0.67843
H	6.86192	-0.85094	1.74718
H	6.96843	-1.90160	0.33104
H	8.14987	-0.58066	0.54178
C	-7.10661	0.87076	-0.67831
H	-8.14979	0.58099	-0.54156
H	-6.96802	1.90171	-0.33105
H	-6.86184	0.85085	-1.74707
O	-6.72770	-1.00475	0.74611
O	6.72766	1.00479	-0.74600

SCF energy: -1076.75960768 hartree
Zero-point correction: 0.357835 hartree
Enthalpy correction: 0.455985 hartree
Free Energy correction: 0.171968 hartree
Quasiharmonic Free Energy correction: 0.192017 hartree

5a

C	-4.56731	-0.39550	0.56719
C	-3.71355	0.66721	0.90858
C	-4.05140	-1.44582	-0.20511
C	-2.72797	-1.42505	-0.63310
C	-2.39335	0.68877	0.48520
C	-0.46079	-0.42989	-0.74327
C	0.38685	0.70615	-0.90094
C	1.79298	0.53893	-0.64545
C	0.13648	-1.68987	-0.86391
C	1.34716	-2.11524	-0.95613
C	2.48597	-0.72905	-0.92443
C	3.76852	-0.92982	-0.28522
C	4.35032	0.02161	0.52013
C	3.72051	1.29520	0.64484
C	2.50178	1.54706	0.05263
H	2.01810	2.50701	0.20026
H	4.18755	2.07635	1.23589
H	2.54441	-0.92093	-2.00493
H	-1.75187	1.50712	0.78793
H	-4.68146	-2.28490	-0.48406
H	-2.33527	-2.23423	-1.24020
C	-1.87041	-0.35724	-0.30371
C	-0.54031	3.15533	-1.22420
C	-0.12977	2.02834	-1.03286
C	-1.06999	4.49620	-1.44579

H	-2.07263	4.60245	-1.01385
H	-0.42614	5.25993	-0.99308
H	-1.14512	4.72003	-2.51738
C	2.01024	-3.36633	-1.42664
H	2.62747	-3.19048	-2.31874
H	2.66990	-3.78582	-0.65616
H	1.25362	-4.11577	-1.67262
H	4.30966	-1.85483	-0.46004
H	-4.11272	1.46596	1.52529
C	-5.98368	-0.35613	1.05055
C	5.66295	-0.30545	1.17276
C	6.34717	0.76238	2.00970
H	6.56708	1.65361	1.40941
H	5.70695	1.08054	2.84153
H	7.27869	0.35454	2.40552
C	-6.91284	-1.50714	0.69743
H	-7.89423	-1.30886	1.13158
H	-7.01219	-1.61570	-0.38927
H	-6.52940	-2.45806	1.08635
O	-6.38910	0.58396	1.71896
O	6.17164	-1.40722	1.03316

SCF energy: -1076.680287 hartree
Zero-point correction: 0.356840 hartree
Enthalpy correction: 0.452307 hartree
Free Energy correction: 0.182927 hartree
Quasiharmonic Free Energy correction: 0.196489 hartree

5-*annul*

C	-4.31239	-0.56099	0.65555
C	-3.43016	0.44060	1.09546
C	-3.90220	-1.40297	-0.38929
C	-2.65575	-1.23858	-0.98281
C	-2.18210	0.60097	0.51289
C	-0.43437	-0.15777	-1.16054
C	0.44974	1.01178	-1.02000
C	1.77331	0.70533	-0.70677
C	0.16312	-1.25486	-1.70338
C	1.44025	-1.59076	-1.80785
C	2.39836	-0.63455	-1.06053
C	3.40429	-1.11482	-0.06847
C	4.04690	-0.24848	0.75726
C	3.69821	1.16094	0.71922
C	2.62283	1.61413	0.01400
H	2.31222	2.65129	0.09577
H	4.26679	1.86437	1.31897
H	3.02592	-0.37119	-1.94326
H	-1.51377	1.36830	0.88589
H	-4.56041	-2.18468	-0.75660
H	-2.35048	-1.87022	-1.81096
C	-1.76564	-0.24044	-0.54010
C	-0.47609	3.48084	-0.97102
C	-0.04108	2.34680	-0.96703
C	-1.01857	4.83499	-0.97534
H	-2.08697	4.83222	-0.72801
H	-0.50714	5.47277	-0.24416
H	-0.90667	5.30500	-1.96055
C	2.03125	-2.58103	-2.77456
H	2.76914	-2.11117	-3.44031
H	2.55081	-3.39671	-2.25184
H	1.24369	-3.02750	-3.38741
H	3.69233	-2.16214	-0.06511
H	-3.74967	1.08067	1.91146
C	-5.64745	-0.67666	1.32173
C	5.10747	-0.79558	1.67384
C	5.83973	0.16722	2.59270
H	6.36523	0.93941	2.01723
H	5.13886	0.68188	3.26139
H	6.56252	-0.39420	3.18693
C	-6.60829	-1.76070	0.85848
H	-6.85732	-1.64118	-0.20276
H	-6.16723	-2.75735	0.97972
H	-7.52105	-1.69510	1.45306
O	-5.96314	0.08493	2.22491
O	5.37376	-1.98701	1.68007

SCF energy: -1076.69151475 hartree
Zero-point correction: 0.357847 hartree
Enthalpy correction: 0.454264 hartree
Free Energy correction: 0.181844 hartree
Quasiharmonic Free Energy correction: 0.196334 hartree

5b

C	-4.69019	-0.34522	0.45588
C	-3.80783	0.61700	0.97522
C	-4.17254	-1.34912	-0.37662
C	-2.81763	-1.38180	-0.69027
C	-2.45691	0.58654	0.66165
C	-0.48951	-0.51647	-0.50647
C	0.36305	0.63389	-0.55233
C	1.75377	0.45831	-0.29980
C	0.03845	-1.79772	-0.73332
C	1.41036	-2.02166	-0.73285
C	2.33708	-0.87599	-0.34134
C	3.70589	-1.04832	0.05921
C	4.48876	0.02994	0.39849
C	3.93265	1.34638	0.34822
C	2.62143	1.54704	-0.00023
H	2.20480	2.54853	-0.01455
H	4.54994	2.20294	0.59780
H	2.12778	-1.20227	-1.52520
H	-1.79378	1.32732	1.09469
H	-4.82679	-2.11115	-0.78981
H	-2.40803	-2.15871	-1.32631
C	-1.93355	-0.41090	-0.18599
C	-0.54650	3.06535	-1.03386

C	-0.13050	1.95102	-0.78866
C	-1.08954	4.38909	-1.31617
H	-0.97821	4.64441	-2.37741
H	-2.15748	4.43700	-1.07180
H	-0.57533	5.16343	-0.73411
C	2.01562	-3.38024	-1.02519
H	2.96655	-3.32755	-1.56997
H	2.20523	-3.92536	-0.09122
H	1.30006	-3.96368	-1.60929
H	4.14485	-2.03952	0.09061
H	-4.21079	1.37798	1.63575
C	-6.13826	-0.25372	0.82153
C	5.91381	-0.23669	0.80310
C	6.79183	0.93768	1.19727
H	6.88518	1.65485	0.37263
H	6.36622	1.47776	2.05173
H	7.78132	0.56221	1.46277
C	-7.10011	-1.30038	0.28012
H	-7.10613	-1.30222	-0.81644
H	-6.81177	-2.30699	0.60574
H	-8.10314	-1.07531	0.64661
O	-6.54642	0.64520	1.54355
O	6.35165	-1.37617	0.81422

SCF energy: -1076.66931677 hartree
Zero-point correction: 0.354557 hartree
Enthalpy correction: 0.449956 hartree
Free Energy correction: 0.181560 hartree
Quasiharmonic Free Energy correction: 0.194812 hartree

6

C	4.46146	0.82345	0.54123
C	3.66477	1.85923	1.02858
C	3.83783	-0.33623	0.05752
C	2.44044	-0.42985	0.07301
C	2.27428	1.77417	1.03276
C	0.15569	0.45973	0.54710
C	-0.71125	1.44239	0.12270
C	-2.20214	1.31630	0.14698
C	-0.30304	-0.79979	1.02855
C	-0.62090	-1.89773	1.43880
C	-2.97184	2.43695	0.50188
C	-4.36140	2.35707	0.52607
C	-5.00474	1.17092	0.18683
C	-4.24928	0.05053	-0.18786
C	-2.85087	0.12458	-0.21387
H	-2.28561	-0.74125	-0.51977
H	-2.47432	3.36557	0.76062
H	1.67878	2.58773	1.42960
H	1.95670	-1.33559	-0.28544
C	1.64317	0.62139	0.54075
C	0.10496	3.74838	-0.87123
C	-0.22760	2.68246	-0.39429
C	0.55344	5.01479	-1.43921
H	0.40007	5.04155	-2.52554
H	0.00592	5.86276	-1.00896
H	1.62197	5.17622	-1.25083
C	-1.08849	-3.20586	1.88003
H	-1.43592	-3.17241	2.92073
H	-1.92243	-3.53506	1.24878
H	-0.29145	-3.95738	1.82311
H	-4.95013	3.22441	0.81214
H	4.14664	2.75099	1.42115
H	-6.09138	1.11192	0.20947
H	5.53981	0.89244	0.53666
N	-4.96676	-1.11484	-0.55146
N	4.54864	-1.44648	-0.45157
C	-4.51055	-2.39829	-0.73615
C	5.90770	-1.61945	-0.58962
H	-5.96621	-0.98532	-0.62524
H	3.96671	-2.21304	-0.75964
O	-3.33612	-2.73345	-0.64466
O	6.74462	-0.78788	-0.26721
C	-5.59511	-3.41184	-1.07936
H	-5.58516	-4.20438	-0.32465
H	-6.60430	-2.99217	-1.13812
H	-5.34904	-3.87453	-2.04006
C	6.31344	-2.95768	-1.19548
H	7.00962	-3.45303	-0.51211
H	6.85222	-2.77035	-2.12976
H	5.47660	-3.63299	-1.40023

SCF energy: -1187.49759135 hartree
Zero-point correction: 0.392521 hartree
Enthalpy correction: 0.499013 hartree
Free Energy correction: 0.199530 hartree
Quasiharmonic Free Energy correction: 0.216757 hartree

6a

C	-4.03841	-1.64402	-0.80623
C	-2.77656	-2.23588	-0.89195
C	-4.13677	-0.34260	-0.29525
C	-2.98009	0.32534	0.12515
C	-1.62510	-1.57540	-0.47607
C	-0.53936	0.53570	0.45893
C	0.69353	-0.01723	0.89008
C	1.90802	0.73779	0.65306
C	-0.60667	1.93106	0.28422
C	0.27047	2.87164	0.30760
C	1.90981	2.20150	0.70498
C	3.06942	2.86502	0.14373
C	4.10909	2.16721	-0.39956
C	4.13415	0.74322	-0.33383
C	3.05741	0.05261	0.21052
H	3.07034	-1.02737	0.21709
H	1.67634	2.57534	1.71019
H	-0.66018	-2.05418	-0.58282

H	-3.04485	1.33440	0.52449
C	-1.71250	-0.27239	0.04987
C	0.98560	-2.50785	1.70832
C	0.82556	-1.37767	1.29383
C	1.15745	-3.87557	2.18399
H	2.12413	-4.28369	1.86500
H	1.12194	-3.92423	3.27985
H	0.36917	-4.53347	1.79751
C	0.24799	4.35519	0.46364
H	0.72398	4.67598	1.40162
H	0.78096	4.85687	-0.35522
H	-0.78553	4.71151	0.46449
H	-2.69605	-3.23733	-1.30694
H	4.95369	2.69582	-0.83882
H	-4.93057	-2.16333	-1.12580
N	-5.35983	0.35491	-0.17013
C	-6.63176	-0.05663	-0.49752
C	-7.71718	0.97984	-0.23204
H	-8.47021	0.53594	0.42607
H	-7.35419	1.90831	0.22023
H	-8.21226	1.21863	-1.17861
H	-5.27396	1.28758	0.20913
O	-6.90225	-1.15355	-0.96657
N	5.27161	0.11402	-0.86804
H	5.94376	0.74011	-1.28975
C	5.59205	-1.23060	-0.90215
O	4.89005	-2.11119	-0.42965
C	6.90290	-1.54357	-1.61084
H	7.54239	-0.67022	-1.77479
H	7.44994	-2.28112	-1.01825
H	6.68205	-2.00060	-2.58194
H	3.11016	3.95033	0.17918

SCF energy: -1187.41718818 hartree
Zero-point correction: 0.391039 hartree
Enthalpy correction: 0.495425 hartree
Free Energy correction: 0.200235 hartree
Quasiharmonic Free Energy correction: 0.219980 hartree

6a-*annul*

C	4.21186	-1.43421	-1.00711
C	2.96888	-2.02857	-1.22967
C	4.26958	-0.24639	-0.26064
C	3.09055	0.31122	0.24388
C	1.79183	-1.47633	-0.73255
C	0.63275	0.39636	0.50311
C	-0.71278	-0.25558	0.55744
C	-1.76232	0.51865	0.09264
C	0.58583	1.71884	0.78018
C	-0.43391	2.56731	0.62367
C	-1.48736	1.99325	-0.31838
C	-2.74036	2.80430	-0.51516
C	-3.95086	2.23652	-0.60669
C	-4.13386	0.79622	-0.42600
C	-3.08543	-0.00903	-0.07540
H	-3.25470	-1.05923	0.11636
H	-1.03969	1.92384	-1.32984
H	0.83950	-1.95453	-0.92864
H	3.12155	1.21676	0.84591
C	1.83972	-0.28185	0.00996
C	-1.01924	-2.74197	1.37276
C	-0.88626	-1.59695	0.98856
C	-1.18239	-4.11517	1.83712
H	-0.36999	-4.75843	1.47623
H	-1.18377	-4.16948	2.93347
H	-2.12913	-4.54113	1.48344
C	-0.67005	3.82076	1.41404
H	-0.63903	4.72267	0.78503
H	-1.66097	3.80494	1.88946
H	0.09371	3.93020	2.18924
H	-2.62751	3.87682	-0.64893
H	2.92466	-2.94700	-1.80931
H	-4.83025	2.84917	-0.80096
H	5.12406	-1.87295	-1.38546
N	-5.45204	0.35210	-0.60809
N	5.47570	0.42974	0.03156
C	-5.96080	-0.93185	-0.50779
C	6.76541	0.09835	-0.31846
C	-7.44308	-1.04692	-0.83552
H	-7.96671	-0.08672	-0.88457
H	-7.55551	-1.55503	-1.79969
H	-7.91865	-1.67450	-0.07747
C	7.82595	1.05972	0.20443
H	8.45269	0.53131	0.93055
H	8.47000	1.35353	-0.62916
H	7.42345	1.96063	0.67852
H	-6.11390	1.07017	-0.86791
H	5.36271	1.26807	0.58446
O	-5.29011	-1.90462	-0.20305
O	7.06884	-0.88314	-0.98213

SCF energy: -1187.43470494 hartree
Zero-point correction: 0.392484 hartree
Enthalpy correction: 0.497709 hartree
Free Energy correction: 0.200504 hartree
Quasiharmonic Free Energy correction: 0.220784 hartree

6b

C	5.03562	1.29262	0.55984
C	4.33402	2.39503	1.04156
C	4.34299	0.23676	-0.04871
C	2.94802	0.28576	-0.15986
C	2.94877	2.45330	0.92705
C	0.75493	1.51448	0.21464
C	-0.09719	0.38626	0.31351

C	-1.50231	0.52641	0.03952
C	0.25018	2.84411	0.09499
C	-1.07176	3.01096	-0.28390
C	-2.01218	1.79931	-0.42028
C	-3.42054	1.91408	-0.68945
C	-4.28085	0.86493	-0.49375
C	-3.77056	-0.38893	-0.05306
C	-2.41190	-0.53681	0.19270
H	-2.01899	-1.49312	0.52624
H	-1.36510	2.17980	-1.38110
H	2.38465	3.31566	1.26296
H	2.43414	-0.53054	-0.64349
C	2.23890	1.39038	0.34190
C	0.73066	-1.99243	1.10906
C	0.36187	-0.89225	0.75163
C	1.28483	-3.28961	1.47939
H	0.57091	-4.10204	1.29623
H	2.18729	-3.48349	0.88729
H	1.55479	-3.31822	2.54274
C	-1.68404	4.36843	-0.55080
H	-2.11239	4.46591	-1.55718
H	-2.48975	4.58248	0.16573
H	-0.89827	5.11673	-0.43802
H	-3.81267	2.86274	-1.03916
H	4.87653	3.21406	1.50647
H	-5.34188	0.96932	-0.67041
H	6.11973	1.24962	0.65130
N	-4.59312	-1.51063	0.14990
N	5.12104	-0.83625	-0.55368
C	-5.95486	-1.64708	-0.04383
C	4.72848	-2.10285	-0.90851
C	-6.49587	-3.03632	0.26338
H	-6.86899	-3.48126	-0.66500
H	-5.76395	-3.71659	0.70990
H	-7.34788	-2.93495	0.94148
C	5.86256	-3.01039	-1.36997
H	6.85573	-2.55263	-1.32085
H	5.85862	-3.91582	-0.75550
H	5.66752	-3.31725	-2.40245
H	-4.10514	-2.33362	0.47651
H	6.11476	-0.65558	-0.58296
O	-6.68433	-0.74919	-0.43693
O	3.57010	-2.50203	-0.87889

SCF energy: -1187.40835091 hartree
Zero-point correction: 0.389131 hartree
Enthalpy correction: 0.493117 hartree
Free Energy correction: 0.203835 hartree
Quasiharmonic Free Energy correction: 0.219140 hartree

6c

C	4.30107	-2.01096	0.03799
C	3.34942	-2.85668	0.60579
C	3.92475	-0.70060	-0.29892
C	2.61773	-0.26415	-0.05346
C	2.04863	-2.42594	0.85050
C	0.25583	-0.70964	0.75089
C	-0.17808	0.62738	0.95808
C	-1.48668	1.01460	0.48105
C	-0.74509	-1.67322	0.62366
C	-2.02345	-1.65294	0.49038
C	-2.63483	0.08892	0.48296
C	-3.79885	0.48767	-0.32144
C	-3.80349	1.65561	-1.05601
C	-2.71937	2.55042	-0.94169
C	-1.61600	2.26392	-0.16475
H	-0.78136	2.95487	-0.12664
H	-2.93805	-0.14756	1.51151
H	1.31657	-3.08770	1.30087
H	2.33348	0.74322	-0.34022
C	1.66324	-1.11146	0.52763
C	1.44447	2.53648	1.78950
C	0.72242	1.65707	1.36398
C	2.33153	3.57273	2.30722
H	2.13160	3.77346	3.36742
H	3.38421	3.27627	2.22091
H	2.20296	4.51766	1.76473
C	-3.07413	-2.67541	0.79374
H	-3.73471	-2.36315	1.61862
H	-3.70010	-2.90721	-0.07760
H	-2.58974	-3.60535	1.10242
H	3.63680	-3.87210	0.86567
H	-4.66642	1.90501	-1.65649
H	5.31246	-2.34174	-0.15015
N	4.80578	0.22629	-0.90136
C	6.12589	0.06518	-1.25998
C	6.74925	1.28424	-1.92904
H	7.68919	1.51730	-1.42087
H	6.99350	1.03003	-2.96581
H	6.11245	2.17472	-1.92729
H	4.39265	1.12463	-1.10970
O	6.76893	-0.95915	-1.07958
N	-4.92015	-0.35527	-0.24148
C	-6.14849	-0.23764	-0.86762
H	-4.82648	-1.14043	0.38406
O	-6.43372	0.64411	-1.66322
H	-2.75359	3.48335	-1.49781
C	-7.15597	-1.30744	-0.46799
H	-7.91957	-0.85560	0.17506
H	-7.65799	-1.66454	-1.37073
H	-6.71762	-2.16077	0.05953

SCF energy: -1187.41375492 hartree
Zero-point correction: 0.391428 hartree
Enthalpy correction: 0.495594 hartree
Free Energy correction: 0.202564 hartree
Quasiharmonic Free Energy correction: 0.221280 hartree

6c-*annul*

C	3.91947	-2.78192	0.14871
C	2.89626	-3.44808	-0.52238
C	3.78928	-1.41722	0.44620
C	2.62447	-0.72884	0.08509
C	1.74772	-2.76630	-0.90623
C	0.33285	-0.73515	-0.96096
C	0.09478	0.74843	-0.85705
C	-1.13535	1.12197	-0.35129
C	-0.79903	-1.38824	-1.28533
C	-2.07526	-1.03705	-1.12005
C	-2.17105	0.00628	-0.00542
C	-3.55068	0.51172	0.38626
C	-3.80659	1.83202	0.55033
C	-2.76645	2.80769	0.31299
C	-1.51010	2.48203	-0.09761
H	-0.76936	3.25385	-0.28229
H	-1.77316	-0.45278	0.91847
H	0.96284	-3.26702	-1.46462
H	2.53477	0.31819	0.32967
C	1.59277	-1.40175	-0.59367
C	2.00577	2.45846	-1.45180
C	1.10293	1.68909	-1.18880
C	3.13742	3.34276	-1.70341
H	3.51913	3.22694	-2.72588
H	2.86181	4.39584	-1.56876
H	3.95101	3.11003	-1.00523
C	-3.17712	-1.30808	-2.10697
H	-3.99095	-1.92585	-1.70206
H	-3.63955	-0.36560	-2.43057
H	-2.77307	-1.82509	-2.98199
H	3.00956	-4.50198	-0.76179
H	-4.78478	2.15529	0.87701
H	4.82780	-3.31400	0.42535
N	4.86655	-0.80296	1.12791
C	5.12698	0.53543	1.31746
C	6.42017	0.82535	2.06936
H	7.02019	-0.06195	2.29496
H	7.02146	1.51891	1.47428
H	6.17393	1.33107	3.00861
H	5.57674	-1.44305	1.45484
O	4.39617	1.43999	0.93749
H	-3.01835	3.85306	0.47194
N	-4.45183	-0.52621	0.66031
C	-5.74864	-0.44407	1.13712
H	-4.08651	-1.45749	0.51724
C	-6.42748	-1.78898	1.35519
H	-7.33691	-1.82548	0.74741
H	-5.80293	-2.65359	1.10928
H	-6.73414	-1.86114	2.40331
O	-6.32008	0.61035	1.36587

SCF energy: -1187.43627485 hartree
Zero-point correction: 0.393102 hartree
Enthalpy correction: 0.497995 hartree
Free Energy correction: 0.205810 hartree
Quasiharmonic Free Energy correction: 0.221618 hartree

6d

C	4.19604	-2.58249	0.12699
C	3.20804	-3.33720	-0.49977
C	3.93746	-1.25020	0.48235
C	2.68724	-0.68362	0.21079
C	1.96771	-2.77539	-0.78646
C	0.33659	-0.89740	-0.69872
C	0.06699	0.50007	-0.84347
C	-1.24510	0.97716	-0.54190
C	-0.71978	-1.79884	-0.88717
C	-2.04252	-1.38844	-0.76648
C	-2.33203	0.03590	-0.28167
C	-3.63141	0.56250	0.13663
C	-3.83675	1.92691	0.18027
C	-2.77892	2.81295	-0.12111
C	-1.52336	2.36325	-0.45507
H	-0.71603	3.05953	-0.65082
H	-2.02365	-0.83668	0.53311
H	1.18590	-3.34182	-1.27962
H	2.50047	0.33716	0.50641
C	1.69423	-1.44138	-0.43558
C	1.92816	2.22332	-1.56942
C	1.06510	1.43310	-1.24503
C	3.03025	3.12428	-1.88469
H	3.45837	2.89897	-2.86972
H	2.70454	4.17149	-1.89610
H	3.82145	3.01633	-1.13280
C	-3.15119	-2.31931	-1.21230
H	-3.59314	-2.92537	-0.40664
H	-3.95579	-1.79811	-1.74381
H	-2.67455	-3.03653	-1.88712
H	3.41551	-4.36783	-0.77560
H	-4.80759	2.30286	0.46731
H	5.17110	-3.02004	0.33467
N	4.97855	-0.54353	1.13433
C	5.12534	0.81115	1.31647
C	6.41778	1.21823	2.01393
H	7.07809	0.38224	2.26570
H	6.95966	1.91542	1.36749
H	6.16493	1.75645	2.93277
H	5.75657	-1.11734	1.42824
O	4.30251	1.64788	0.96692
H	-2.96870	3.88128	-0.06445
N	-4.62099	-0.35814	0.52605
C	-5.86533	-0.11224	1.08411
H	-4.40285	-1.33175	0.38674

C	-6.66842	-1.37056	1.38516	SCF energy: -1187.39790182 hartree
H	-7.07442	-1.28819	2.39683	Zero-point correction: 0.389022 hartree
H	-7.51774	-1.42149	0.69521	Enthalpy correction: 0.492993 hartree
H	-6.09663	-2.30053	1.30374	Free Energy correction: 0.203882 hartree
O	-6.31315	1.00026	1.31041	Quasiharmonic Free Energy correction: 0.219582 hartree

Computed structures of $[8]_A$GNR, PDA **1**, PDA **1-annul** for frequency calculations

$[8]_A$GNR (computed structure described in Fig. A22)
PDA **1**
PDA **1-*annu***

$[8]_A$GNR

C	0.55650	16.86421	0.00769
C	4.28665	14.69804	0.00487
C	4.28755	13.30577	0.00353
C	3.09106	12.57962	0.00300
C	1.85091	13.28860	0.00376
C	1.85480	14.71814	0.00519
C	3.09202	15.39450	0.00571
C	0.59830	15.43700	0.00604
C	-0.61884	14.71890	0.00525
C	-1.86482	15.43164	0.00600
C	-3.10666	14.73148	0.00513
C	-4.29501	15.47334	0.00592
C	-4.28927	16.87115	0.00756
C	-3.09121	17.56216	0.00841
C	-1.86934	16.86058	0.00764
C	-0.61436	13.27708	0.00371
C	4.27513	10.38040	0.00110
C	4.27487	9.00167	-0.00020
C	3.08018	8.26456	-0.00099
C	1.84959	8.97740	-0.00036
C	1.85069	10.41043	0.00098
C	3.08314	11.12013	0.00167
C	0.60892	11.12761	0.00162
C	-0.61094	10.41311	0.00090
C	-1.85300	11.12990	0.00147
C	-3.08307	10.41550	0.00065
C	-4.27928	11.14949	0.00106
C	-4.28300	12.52904	0.00246
C	-3.09407	13.27091	0.00348
C	-1.85737	12.56247	0.00290
C	0.60789	12.56785	0.00306
C	-0.62298	17.54879	0.00847
C	-0.61040	0.35788	-0.00521
C	-4.27571	2.54089	-0.00549
C	-4.27516	3.91784	-0.00477
C	-3.07934	4.65705	-0.00397
C	-1.84841	3.94599	-0.00419
C	-1.84876	2.51345	-0.00489
C	-3.07991	1.80160	-0.00542
C	-0.61007	1.79529	-0.00498
C	0.61078	2.51158	-0.00476
C	1.84958	1.79342	-0.00514
C	3.08067	2.50516	-0.00522
C	4.27647	1.76572	-0.00586
C	4.27613	0.38877	-0.00610
C	3.08018	-0.35071	-0.00570
C	1.84928	0.36080	-0.00537
C	0.61087	3.94917	-0.00411
C	-4.27513	6.84602	-0.00219
C	-4.27516	8.22347	-0.00105
C	-3.08067	8.96273	-0.00054
C	-1.84886	8.25321	-0.00108
C	-1.84848	6.82072	-0.00224
C	-3.07938	6.10825	-0.00285
C	-0.60943	6.10298	-0.00272
C	0.61057	6.81947	-0.00218
C	1.84948	6.10070	-0.00278
C	3.08032	6.81201	-0.00234
C	4.27580	6.07327	-0.00319
C	4.27604	4.69585	-0.00426
C	3.08063	3.95641	-0.00448
C	1.84961	4.66800	-0.00381
C	0.61010	8.25843	-0.00100
C	-0.60960	4.66486	-0.00368
C	0.61040	-0.35788	-0.00521
C	-0.61022	8.97306	-0.00043
C	4.27571	-2.54089	-0.00549
C	4.27516	-3.91784	-0.00477
C	3.07934	-4.65705	-0.00397
C	1.84841	-3.94599	-0.00419
C	1.84876	-2.51345	-0.00489
C	3.07991	-1.80160	-0.00542
C	0.61007	-1.79529	-0.00498
C	-0.61078	-2.51158	-0.00476
C	-1.84958	-1.79342	-0.00514
C	-3.08067	-2.50516	-0.00522
C	-4.27647	-1.76572	-0.00586
C	-4.27613	-0.38877	-0.00610
C	-3.08018	0.35071	-0.00570
C	-1.84928	-0.36080	-0.00537
C	-0.61087	-3.94917	-0.00411
C	4.27513	-6.84602	-0.00219
C	4.27516	-8.22347	-0.00105
C	3.08067	-8.96273	-0.00054
C	1.84886	-8.25321	-0.00108
C	1.84848	-6.82072	-0.00224
C	3.07938	-6.10825	-0.00285
C	0.60943	-6.10298	-0.00272
C	-0.61057	-6.81947	-0.00218
C	-1.84948	-6.10070	-0.00278
C	-3.08032	-6.81201	-0.00234
C	-4.27580	-6.07327	-0.00319
C	-4.27604	-4.69585	-0.00426
C	-3.08063	-3.95641	-0.00448
C	-1.84961	-4.66800	-0.00381
C	0.60960	-4.66486	-0.00368
C	-0.55650	-16.86421	0.00769
C	-4.28665	-14.69804	0.00487
C	-4.28755	-13.30577	0.00353
C	-3.09106	-12.57962	0.00300

C	-1.85091	-13.28860	0.00376
C	-1.85480	-14.71814	0.00519
C	-3.09202	-15.39450	0.00571
C	-0.59830	-15.43700	0.00604
C	0.61884	-14.71890	0.00525
C	1.86482	-15.43164	0.00600
C	3.10666	-14.73148	0.00513
C	4.29501	-15.47334	0.00592
C	4.28927	-16.87115	0.00756
C	3.09121	-17.56216	0.00841
C	1.86934	-16.86058	0.00764
C	0.61436	-13.27708	0.00371
C	-4.27513	-10.38040	0.00110
C	-4.27487	-9.00167	-0.00020
C	-3.08018	-8.26456	-0.00099
C	-1.84959	-8.97740	-0.00036
C	-1.85069	-10.41043	0.00098
C	-3.08314	-11.12013	0.00167
C	-0.60892	-11.12761	0.00162
C	0.61094	-10.41311	0.00090
C	1.85300	-11.12990	0.00147
C	3.08307	-10.41550	0.00065
C	4.27928	-11.14949	0.00106
C	4.28300	-12.52904	0.00246
C	3.09407	-13.27091	0.00348
C	1.85737	-12.56247	0.00290
C	0.61022	-8.97306	-0.00043
C	-0.60789	-12.56785	0.00306
C	0.62298	-17.54879	0.00847
C	-0.61010	-8.25843	-0.00100
H	1.47901	17.43129	0.00842
H	5.22961	15.23783	0.00526
H	5.24203	12.79458	0.00285
H	3.12600	16.47659	0.00672
H	-5.25429	14.96952	0.00530
H	-5.23284	17.40988	0.00816
H	-3.07539	18.64908	0.00968
H	5.23393	10.88403	0.00172
H	5.23236	8.49593	-0.00056
H	-5.23575	10.64166	0.00026
H	-5.24188	13.03304	0.00277
H	-0.62627	18.63591	0.00974
H	-5.23345	2.03529	-0.00602
H	-5.23247	4.42383	-0.00481
H	5.23424	2.27127	-0.00610
H	5.23342	-0.11729	-0.00652
H	-5.23262	6.34001	-0.00248
H	-5.23293	8.72850	-0.00047
H	5.23355	6.57893	-0.00301
H	5.23357	4.19018	-0.00485
H	5.23345	-2.03529	-0.00602
H	5.23247	-4.42383	-0.00481
H	-5.23424	-2.27127	-0.00610
H	-5.23342	0.11729	-0.00652
H	5.23262	-6.34001	-0.00248
H	5.23293	-8.72850	-0.00047
H	-5.23355	-6.57893	-0.00301
H	-5.23357	-4.19018	-0.00485
H	-1.47901	-17.43129	0.00842
H	-5.22961	-15.23783	0.00526
H	-5.24203	-12.79458	0.00285
H	-3.12600	-16.47659	0.00672
H	5.25429	-14.96952	0.00530
H	5.23284	-17.40988	0.00816
H	3.07539	-18.64908	0.00968
H	-5.23393	-10.88403	0.00172
H	-5.23236	-8.49593	-0.00056
H	5.23575	-10.64166	0.00026
H	5.24188	-13.03304	0.00277
H	0.62627	-18.63591	0.00974

SCF energy: -4978.77060971 hartree
Zero-point correction: 1.249321 hartree
Enthalpy correction: 1.324765 hartree
Free Energy correction: 1.143176 hartree

PDA **1**

C	-6.45855	4.35630	0.30470
C	-7.56343	5.13226	-0.08147
C	-8.76276	4.47391	-0.39894
C	-8.83647	3.08685	-0.36071
C	-7.71700	2.29811	-0.01358
C	-6.52943	2.97340	0.34450
C	-7.36076	-1.58267	-0.13638
C	-6.64070	-2.59094	0.52370
C	-7.00828	-3.92856	0.40413
C	-8.10781	-4.29981	-0.38167
C	-8.83171	-3.29403	-1.04107
C	-8.46353	-1.96044	-0.92604
C	-2.88915	4.15778	-0.80763
C	-2.15573	4.72784	0.24302
C	-1.68803	3.89340	1.26949
C	-1.93233	2.52676	1.24202
C	-2.64515	1.95105	0.17764
C	-3.13081	2.78626	-0.83940
C	-2.22648	-1.93519	0.29818
C	-3.15270	-2.54466	-0.56590
C	-3.43327	-3.90056	-0.45490
C	-2.79238	-4.69249	0.51065
C	-1.82912	-4.09785	1.33949
C	-1.55158	-2.73787	1.23182

C	8.40650	-4.48221	-1.25953
C	7.24565	-5.12104	-0.79303
C	6.28723	-4.35220	-0.11300
C	6.45772	-2.98939	0.07089
C	7.60414	-2.33091	-0.42443
C	8.58321	-3.11708	-1.07080
C	7.50884	1.52155	0.12254
C	6.74026	2.63537	-0.26089
C	7.23173	3.92544	-0.11303
C	8.50415	4.15115	0.43498
C	9.26700	3.04431	0.83566
C	8.77514	1.75130	0.68837
C	2.64552	-4.14110	-0.61055
C	2.92119	-2.78463	-0.76950
C	2.67513	-1.88180	0.27359
C	2.17348	-2.36852	1.49092
C	1.89362	-3.72065	1.64587
C	2.11660	-4.62380	0.59512
C	2.24723	1.97686	-0.14827
C	1.71836	2.93957	0.72240
C	1.93501	4.29785	0.50069
C	2.67382	4.72583	-0.61120
C	3.18851	3.76321	-1.49364
C	2.98303	2.40769	-1.26595
H	-5.53865	4.86468	0.57126
H	-5.66252	2.40874	0.65770
H	-6.41705	-4.68369	0.91145
H	-9.67179	-3.58986	-1.66106
H	-3.27082	4.77911	-1.61145
H	-4.15913	-4.37060	-1.10946
H	9.17532	-5.04702	-1.77772
H	9.48511	-2.63720	-1.44293
H	6.64097	4.78316	-0.41835
H	10.24574	3.18504	1.28380
H	2.83864	-4.81966	-1.43513
H	3.32503	-2.42005	-1.70919
H	1.50086	5.02189	1.18252
H	5.40332	-4.84989	0.26923
H	5.70715	-2.42909	0.61219
H	-3.69922	2.35625	-1.65838
H	-1.14139	4.34442	2.09103
H	-9.64249	5.04089	-0.68771
H	3.73966	4.10769	-2.36288
H	9.36682	0.91475	1.04696
H	-3.65234	-1.95321	-1.32479
H	-0.81059	-2.28625	1.88249
H	-1.28647	-4.69353	2.06629
H	-5.78106	-2.32301	1.12832
H	-9.01061	-1.20664	-1.48446
H	1.50216	-4.10511	2.58208
C	-8.53100	-5.72806	-0.57058
O	-9.49354	-5.99541	-1.27518
C	-7.39983	6.61731	-0.14912
O	-6.30277	7.13412	0.02100
C	-1.82955	6.18991	0.31084
O	-0.96317	6.58627	1.08140
C	-3.19146	-6.13292	0.63192
O	-4.12199	-6.57212	-0.03332
H	2.00891	-1.67845	2.31333
C	1.75083	-6.06296	0.80083
O	1.05472	-6.38574	1.75656
C	2.92936	6.17637	-0.91371
O	3.51907	6.49235	-1.93645
C	6.97680	-6.57851	-0.99244
O	5.90735	-7.07036	-0.65441
C	8.98029	5.56493	0.58302
O	8.26801	6.49883	0.24827
C	8.05116	-7.44478	-1.62787
H	8.28165	-7.10283	-2.64417
H	7.69271	-8.47458	-1.66882
H	8.98300	-7.40517	-1.05145
C	-2.59183	7.15623	-0.57343
H	-2.42159	6.93557	-1.63450
H	-2.24709	8.17030	-0.36361
H	-3.67213	7.09011	-0.39292
C	-2.44963	-7.02468	1.60894
H	-2.83122	-8.04264	1.51137
H	-2.61380	-6.68062	2.63820
H	-1.36672	-7.01318	1.44189
C	-8.61685	7.47929	-0.43923
H	-9.41167	7.30323	0.29509
H	-9.03099	7.25187	-1.42913
H	-8.31885	8.52858	-0.40901
C	-7.74393	-6.82209	0.12658
H	-8.17702	-7.78734	-0.14174
H	-7.79085	-6.69812	1.21593
H	-6.68437	-6.80230	-0.15498
C	2.25491	-7.09769	-0.18502
H	1.94562	-8.08733	0.15595
H	3.34726	-7.06227	-0.27849
H	1.83513	-6.92009	-1.18324
C	10.36537	5.81716	1.15816
H	10.44682	5.42285	2.17840
H	10.54511	6.89337	1.17366
H	11.14024	5.32800	0.55585
C	2.45537	7.22618	0.07317
H	2.93165	7.07890	1.05049
H	1.37192	7.17600	0.23408
H	2.72474	8.21148	-0.31122
H	1.13322	2.61878	1.57803
C	-6.93710	-0.15403	-0.02203
C	-7.86999	0.84927	-0.05135

H	-8.90256	0.51977	-0.13915
C	-5.53833	0.07123	0.07049
C	-4.31945	0.16933	0.10644
C	-2.94158	0.48472	0.16082
C	-1.94312	-0.47066	0.24035
C	-0.57787	-0.09365	0.25653
C	0.61981	0.15134	0.20629
C	1.97954	0.52479	0.07651
C	2.98046	-0.42436	0.10095
C	4.35760	-0.11748	0.00770
C	5.57763	-0.03342	-0.01412
C	6.98705	0.13447	-0.05290
H	5.75102	2.48335	-0.67887
C	7.85472	-0.90234	-0.28333
H	3.36924	1.67414	-1.96702
H	-1.58379	1.89546	2.05327
H	-9.76974	2.59395	-0.62182
H	8.89426	-0.61922	-0.42976

SCF energy: -3608.89483372 hartree
Zero-point correction: 1.133001 hartree
Enthalpy correction: 1.214160 hartree
Free Energy correction: 1.001313 hartree

PDA **1-*annul***

C	5.55520	-5.25313	1.71968
C	4.16291	-4.97648	1.80309
C	3.67404	-3.79295	1.27296
C	4.52512	-2.84697	0.65423
C	5.92960	-3.13106	0.58284
C	6.40944	-4.35335	1.12831
C	6.80568	-2.19046	-0.01186
C	6.33775	-0.99399	-0.52655
C	7.25648	-0.00422	-1.13940
C	7.04822	1.37469	-0.96705
C	7.91186	2.30503	-1.53884
C	9.01081	1.88611	-2.30221
C	9.22200	0.50946	-2.47700
C	8.36086	-0.41843	-1.90786
C	4.94017	-0.72572	-0.45503
C	1.33468	-3.34482	-2.73928
C	-0.04451	-3.00916	-2.75883
C	-0.52265	-2.09342	-1.83906
C	0.32153	-1.48225	-0.88236
C	1.71029	-1.84484	-0.84884
C	2.18039	-2.77989	-1.81451
C	2.58597	-1.25880	0.12511
C	2.07862	-0.31928	1.02006
C	2.91412	0.36262	2.05147
C	2.95886	1.76814	2.09551
C	3.70731	2.42882	3.06177
C	4.42638	1.70670	4.02629
C	4.37326	0.30575	3.99421
C	3.62941	-0.35673	3.02070
C	4.04440	-1.60780	0.11152
C	-3.87403	3.98840	2.65162
C	-3.83387	5.26959	2.08230
C	-4.60197	5.51871	0.93470
C	-5.38648	4.51740	0.37681
C	-5.42041	3.22727	0.93745
C	-4.65365	2.98195	2.08707
C	-6.30397	2.18523	0.33883
C	-5.84707	0.92731	-0.05549
C	-6.76316	-0.01101	-0.64159
C	-8.14370	0.34614	-0.79263
C	-9.04508	-0.57911	-1.36760
C	-8.62638	-1.82355	-1.80314
C	-7.25428	-2.16873	-1.66980
C	-6.35453	-1.29186	-1.11005
C	-4.39471	0.56267	0.03092
C	-0.87236	1.76169	-4.34087
C	-1.62001	1.16723	-3.32658
C	-1.29509	1.37668	-1.97701
C	-0.20848	2.21433	-1.67246
C	0.53378	2.81032	-2.68364
C	0.21646	2.58949	-4.03282
C	-2.13115	0.75818	-0.90710
C	-1.61680	-0.10963	0.05307
C	-2.49673	-0.66870	1.03923
C	-2.03550	-1.58370	2.02806
C	-2.88393	-2.10800	2.97435
C	-4.25680	-1.74848	2.99526
C	-4.73495	-0.87555	2.03332
C	-3.89211	-0.32605	1.03670
C	-0.17208	-0.50958	0.04711
C	-3.51857	1.07018	-0.90258
C	0.70242	0.03818	0.95933
H	5.95273	-6.17696	2.12753
H	7.47427	-4.56541	1.07187
H	7.72482	3.36229	-1.37915
H	10.06879	0.19291	-3.07719
H	1.73502	-4.05255	-3.45828
H	3.75316	3.51266	3.09135
H	-3.30135	3.76760	3.54726
H	-4.68295	2.00292	2.55350
H	-10.09298	-0.31602	-1.47900
H	-6.90020	-3.13468	-2.01549
H	-1.14349	1.57060	-5.37461
H	-2.45171	0.51616	-3.58123
H	-2.48955	-2.80295	3.70879
H	-9.61938	1.90091	-0.48463

C	-8.57193	1.63286	-0.37348
C	-7.67851	2.52243	0.16329
H	-4.56579	6.51110	0.49716
H	-5.97199	4.72469	-0.51497
H	3.23077	-3.04737	-1.81869
H	-1.57738	-1.84698	-1.86771
H	2.60822	-3.60518	1.34537
H	7.86950	-2.41160	-0.02934
H	4.56316	0.19631	-0.88655
H	-5.78858	-0.61905	2.05503
H	-5.31253	-1.57936	-1.02835
H	-8.01505	3.50155	0.49080
H	2.41313	2.34185	1.35089
H	3.59199	-1.44103	3.02131
H	4.90967	-0.28101	4.73358
H	6.21903	1.72141	-0.35727
H	8.52416	-1.47833	-2.08113
H	-3.89186	1.74915	-1.66322
H	1.36904	3.46399	-2.45425
C	9.97232	2.84093	-2.94490
O	10.92099	2.42271	-3.59149
C	3.18649	-5.91454	2.45040
O	2.00237	-5.62366	2.53291
C	-1.01464	-3.59433	-3.74208
O	-2.18623	-3.24534	-3.74741
C	5.21525	2.47254	5.04610
O	5.23152	3.69402	5.02837
H	0.03877	2.40958	-0.63404
H	0.33082	0.76279	1.67843
C	1.06076	3.25334	-5.07880
O	2.01665	3.94426	-4.75904
C	-5.22198	-2.27788	4.01635
O	-6.39093	-1.92393	4.01171
C	-3.01121	6.38889	2.64513
O	-3.00304	7.48618	2.10751
C	-9.64453	-2.74632	-2.40520
O	-10.81176	-2.40170	-2.51469
C	-2.18702	6.13706	3.89770
H	-2.82597	5.83540	4.73637
H	-1.65854	7.05545	4.15854
H	-1.45872	5.33303	3.73738
C	-0.51298	-4.62983	-4.73446
H	0.27602	-4.21376	-5.37275
H	-1.34832	-4.95201	-5.35831
H	-0.08839	-5.49877	-4.21735
C	5.99409	1.70364	6.10086
H	6.50493	2.41845	6.74802
H	6.73400	1.03894	5.63916
H	5.32678	1.07874	6.70656
C	3.69741	-7.23432	3.00410
H	4.44895	-7.07010	3.78591
H	4.17111	-7.83580	2.21884
H	2.85572	-7.78702	3.42455
C	9.74544	4.33418	-2.77897
H	10.53402	4.86859	-3.31118
H	9.76353	4.62161	-1.72076
H	8.76981	4.63213	-3.18135
C	0.70831	3.05236	-6.54361
H	1.42266	3.60710	-7.15414
H	-0.30630	3.40905	-6.75762
H	0.74540	1.99096	-6.81688
C	-9.19647	-4.11943	-2.87736
H	-8.42690	-4.03744	-3.65452
H	-10.06071	-4.65091	-3.27918
H	-8.76458	-4.69862	-2.05226
C	-4.71520	-3.26215	5.05737
H	-3.91344	-2.81970	5.66102
H	-4.30588	-4.16253	4.58344
H	-5.54511	-3.54135	5.70856
H	-0.99063	-1.87162	2.03173

SCF energy: -3685.36777794 hartree
Zero-point correction: 1.153329 hartree

References

[1] Allen, M. J.; Tung, V. C.; Kaner, R. B. *Chem. Rev.* **2010**, *110*, 132–145.

[2] Nakada, K.; Fujita, M.; Dresselhaus, G.; Dresselhaus, M. S. *Phys. Rev. B* **1996**, *54*, 17954–17961.

[3] Dutta, S.; Pati, S. K. *J. Mater. Chem.* **2010**, *20*, 8207–8223.

[4] We are proposing the use of a modified nomenclature for the armchair (A) or zigzag (Z) topologies of graphene nanoribbons, in which the A or Z letters are subscripted in front of the GNR acronym. The established convention for GNR width, indicated by the number of carbons within the GNR width, is placed in between brackets at the front of the $_{A}$GNR or $_{Z}$GNR terms. Thus, $N = 8$ armchair graphene nanoribbons are designated as $[8]_{A}$GNR rather than the current designation (8-AGNR), while $N = 11$ zigzag graphene nanoribbons would be designated as $[11]_{Z}$GNR (instead of 11-ZGNR). However, the current nomenclature for graphene nanoribbons with 2D "chirality" can be retained, as it is defined by the [n,m] numerals (n = zigzag edge repeat carbons, m = armchair edge repeat carbons) in front of the GNR abbreviation.

[5] Son, Y.-W.; Cohen, M. L.; Louie, S. G. *Phys. Rev. Lett.* **2006**, *97*, 216803.

[6] Kimouche, A.; Ervasi, M. M.; Drost, R.; Halonen, S.; Harju, A.; Joensuu, P. M.; Sainio, J.; Liljeroth, P. *Nat. Commun.* **2015**, 10177.

[7] Yang, W.; Lucotti, A.; Tommasini, M.; Chalifoux, W. A. *J. Am. Chem. Soc.* **2016**, *138*, 9137–9144.

[8] Jänsch, D.; Ivanov, I.; Zagranyarski, Y.; Duznovic, I.; Baumgarten, M.; Turchinovich, D.; Li, C.; Bonn, M.; Müllen, K. *Chem. Eur. J.* **2017**, *23*, 4870–4875.

[9] Zhang, H.; Lin, H.; Sun, K.; Chen, L.; Zagranyarski, Y.; Aghdassi, N.; Duhm, S.; Li, Q.; Zhong, D.; Li, Y.; Müllen, K.; Fuchs, H.; Chi, L. *J. Am. Chem. Soc.* **2015**, *137*, 4022–4025.

[10] Tour, J. M. *Chem. Mater.* **2014**, *26*, 163–171.

[11] Sommer, B.; Sonntag, J.; Ganczarczyk, A.; Braam, D.; Prinz, G.; Lorke, A.; Geller, M. *Sci.*

Rep. **2015**, *5*, 7781.

[12] Kosynkin, D. V.; Higginbotham, A. L.; Sinitskii, A.; Lomeda, J. R.; Dimiev, A.; Price, B. K.; Tour, J. M. *Nature* **2009**, *458*, 872–876.

[13] Li, X.; Wang, X.; Zhang, L.; Lee, S.; Dai, H. *Science* **2008**, *319*, 1229–1232.

[14] Cai, J.; Ruffieux, P.; Jaafar, R.; Bieri, M.; Braun, T.; Blankenburg, S.; Muoth, M.; Seitsonin, A. P.; Saleh, M.; Feng, X.; Müllen, K.; Fasel, R. *Nature* **2010**, *466*, 470–473.

[15] Ruffieux, P.; Wang, S.; Yang, B.; Sánchez-Sánchez, C.; Liu, J.; Dienel, T.; Talirz, L.; Shinde, P.; Pignedoli, C. A.; Passerone, D.; Dumslaff, T.; Feng, X.; Müllen, K.; Fasel, R. *Nature* **2016**, *531*, 489–492.

[16] Yang, X.; Dou, X.; Rouhanipour, A.; Zhi, L.; Räder, J.; Müllen, K. *J. Am. Chem. Soc.* **2008**, *130*, 4216–4217.

[17] Narita, A.; Verzhbitskiy, I. A.; Frederickx, W.; Mali, K. S.; Jensen, S. A.; Hansen, M. R.; Bonn, M.; De Feyter, S.; Casiraghi, C.; Feng, X.; Müllen, K. *ACS Nano* **2014,** *8*, 11622–11630.

[18] Yang, W.; Lucotti, A.; Tommasini, M.; Chalifoux, W. A. *J. Am. Chem. Soc.* **2016,** *138,* 9137–9144.

[19] Gao, J.; Uribe-Romo, F. J.; Saathoff, J. D.; Arslan, H.; Crick, C. R.; Hein, S. J.; Itin, B.; Clancy, P.; Dichtel, W. R.; Loo, Y-L. *ACS Nano*, **2016**, *10*, 4847–4856.

[20] Park, I. S.; Park, H. J.; Kim, J.-M. *ACS Appl. Mater. Interfaces* **2013**, *5*, 8805–8812.

[21] Lauher, J. W.; Fowler, F. W.; Goroff, N. S. *Accts. Chem. Res.* **2008**, *41*, 1215–1229.

[22] Ishijima, Y.; Okaniwa, M.; Oaki, Y.; Imai, H. *Chem. Sci.* **2017**, *8*, 647–653.

[23] Luo, L.; Wilhelm, C.; Young, C. N.; Grey, C. P.; Halada, G. P.; Xiao, K.; Ivanov, I. N.; Howe, J. Y.; Geohegan, D. B.; Goroff, N. S. *Macromolecules* **2011***, 44*, 2626–2631.

[24] Luo, L.; Resch, D.; Wilhelm, C.; Young, C. N.; Halada, G. P.; Gambino, R. J.; Grey, C. P.; Goroff, N. S. *J. Am. Chem. Soc.* **2011**, *133*, 19274–19277.

[25] Levesque, I.; Néabo, J. R.; Rondeau-Gagné, S.; Vigier-Carrière, C.; Diagle, M.; Morin, J.-F. *Chem. Sci.* **2014**, *5*, 831–836.

[26] Suzuki, M.; Comito, A.; Khan, S. I.; Rubin, Y. *Org. Lett.* **2010**, *12*, 2346–2349.

[27] Suzuki, M.; Khosrowabadi Kotyk, J. F.; Khan, S. I.; Rubin, Y. *J. Am. Chem. Soc.* **2016**, *138*, 5939–5956.

[28] Jordan, R. S.; Wang, Y.; McCurdy, R. D.; Yeung, M. T.; Marsh, K. L.; Khan, S. I.; Kaner, R. B.; Rubin, Y. *Chem* **2016**, *1*, 78–90.

[29] Prall, M.; Krüger, A.; Shreiner, P. R.; Hopf, H. *Chem. Eur. J.* **2001**, *7*, 4386–4394.

[30] Zimmerman, G. *Eur. J. Org. Chem.* **2001**, 457–471.

[31] (a) Becke, A. D. *J. Chem. Phys.* **1993**, *98*, 5648−5652. (b) Lee, C.; Yang, W.; Parr, R. G. *Phys. Rev. B* **1988**, *37*, 785−789. (c) Stephens, P. J.; Devlin, F. J.; Chabalowski, C. F.; Frisch, M. J. *J. Phys. Chem.* **1994**, *98*, 11623−11627. (d) Vosko, S. H.; Wilk, L.; Nusair, M. *Can. J. Phys.* **1980**, *58*, 1200−1211.

[32] All calculations described here were performed using Gaussian 09: Frisch, M. J.; Trucks, G. W.; Schlegel, H. B.; Scuseria, G. E.; Robb, M. A.; Cheeseman, J. R.; Scalmani, G.; Barone, V.; Mennucci, B.; Petersson, G. A.; Nakatsuji, H.; Caricato, M.; Li, X.; Hratchian, H. P.; Izmaylov, A. F.; Bloino, J.; Zheng, G.; Sonnenberg, J. L.; Hada, M.; Ehara, M.; Toyota, K.; Fukuda, R.; Hasegawa, J.; Ishida, M.; Nakajima, T.; Honda, Y.; Kitao, O.; Nakai, H.; Vreven, T.; Montgomery, J. A., Jr.; Peralta, J. E.; Ogliaro, F.; Bearpark, M.; Heyd, J. J.; Brothers, E.; Kudin, K. N.; Staroverov, V. N.; Kobayashi, R.; Normand, J.; Raghavachari, K.; Rendell, A.; Burant, J. C.; Iyengar, S. S.; Tomasi, J.; Cossi, M.; Rega, N.; Millam, N. J.; Klene, M.; Knox, J. E.; Cross, J. B.; Bakken, V.; Adamo, C.; Jaramillo, J.; Gomperts, R.; Stratmann, R. E.; Yazyev, O.; Austin, A. J.; Cammi, R.; Pomelli, C.; Ochterski, J. W.; Martin, R. L.; Morokuma, K.; Zakrzewski, V. G.; Voth, G. A.; Salvador, P.; Dannenberg, J. J.; Dapprich, S.; Daniels, A. D.; Farkas, Ö.; Foresman, J. B.; Ortiz, J. V.; Cioslowski, J.; Fox, D. J. *Gaussian 09, Revision B.01*; Gaussian, Inc.: Wallingford, CT, 2009.

[33] See Experimental and Appendix A for further details.

[34] Osowska, K.; Lis, T.; Szafert, S. *Eur. J. Org. Chem.* **2008**, 4598–4606.

[35] Tanphibal, P.; Tashiro, K.; Chirachanchai, S. *Macromol. Rapid Commun.* **2016**, *37*, 685– 690.

[36] Wegner, G. *J. Polym. Sci. Pol. Lett.* **1971**, *9*, 133-144.

[37] Wegner, G. *Makromol. Chem.* **1972**, *154*, 35–48.

[38] Nava, A. D.; Thakur, M.; Tonelli, A. E. *Macromolecules* **1990**, *23*, 3055–3063.

[39] Cholli, A. L.; Sandman, D. J. *Bull. Mater. Sci.* **1999**, *22*, 691–695.

[40] Colthup, N. B.; Daly, L. H.; Wiberley, S. E. *Introduction to Infrared and Raman Spectroscopy*, 3rd ed.; Academic Press: San Diego, 1990.

[41] de Souza, F. A. L.; Ambrozio, A. R.; Souza, E. S.; Cipriano, D. F.; Scopel, W. L.; Freitas, J. C. C. *J. Phys. Chem. C* **2016**, *120*, 27707–27716.

[42] Clar, E.; Ironside, C. T.; Zander, M. J. *J. Chem. Soc.* **1959**, 142–147.

[43] Talyzin, A. V.; Luzan, S. M.; Leifer, K.; Akhtar, S.; Fetzer, J.; Cataldo, F.; Tsybin, Y. O.; Tai, C. W.; Dzwilewski, A.; Moons, E. *J. Phys. Chem. C* **2011**, *115*, 13207–13214.

[44] Hansen, P. E. *Org. Magn. Reson.* **1979**, *12*, 109–142.

[45] The same curve fitting analysis for PDA **2a** is available in the Supporting Information. Those for PDAs **2b** and **2c** are very similar to that of PDA **2a**, and are not provided.

[46] Ryu, S.; Maultzsch, J.; Han, M. Y.; Kim, P.; Brus, L. E. *ACS Nano* **2011**, *5*, 4123–4130.

[47] Graf, D.; Molitor, F.; Ensslin, K.; Stampfer, C.; Jungen, A.; Hierold, C.; Wirtz, L. *Nano Lett.* **2007**, *7*, 238–242.

[48] Ferrari, A. C.; Robertson, J. *Phys. Rev. B*. **2000**, *61*, 14095–14107.

[49] Bottari, G.; Herrans, M. Á.; Wibmer, L.; Volland, M.; Rodrígues-Pérez, L.; Guldi, D. M.; Hirsch, A.; Martín, N.; D'Souza, F.; Torres, T. *Chem. Soc. Rev.* **2017**, *46,* 4464–4500.

[50] Tanphibal, P.; Tashiro, K.; Chirachanchai, S. *Macromol. Rapid Commun.* **2016**, *37*, 685–690.

[51] Osowska, K.; Lis, T.; Szafert, S. *Eur. J. Org. Chem.* **2008**, 4598–4606.

[52] Alajtal, A. I.; Edwards, H. G. M.; Elbagerma, M. A.; Scowden, I. J. *Spectrochim. Acta Mol. Biomol. Spectrosc.* **2010**, *76*, 1-5.

[53] Spartan, Wavefunction, Inc. Irvine, CA. Except for molecular mechanics and semi-empirical models, the calculation methods used in Spartan have been documented in: Y. Shao, L.F.

Molnar, Y. Jung, J. Kussmann, C. Ochsenfeld, S.T. Brown, A.T.B. Gilbert, L.V. Slipchenko, S.V. Levchenko, D.P. O'Neill, R.A. DiStasio Jr., R.C. Lochan, T. Wang, G.J.O. Beran, N.A. Besley, J.M. Herbert, C.Y. Lin, T. Van Voorhis, S.H. Chien, A. Sodt, R.P. Steele, V.A. Rassolov, P.E. Maslen, P.P. Korambath, R.D. Adamson, B. Austin, J. Baker, E.F.C. Byrd, H. Dachsel, R.J. Doerksen, A. Dreuw, B.D. Dunietz, A.D. Dutoi, T.R. Furlani, S.R. Gwaltney, A. Heyden, S. Hirata, C-P. Hsu, G. Kedziora, R.Z. Khalliulin, P. Klunzinger, A.M. Lee, M.S. Lee, W.Z. Liang, I. Lotan, N. Nair, B. Peters, E.I. Proynov, P.A. Pieniazek, Y.M. Rhee, J. Ritchie, E. Rosta, C.D. Sherrill, A.C. Simmonett, J.E. Subotnik, H.L. Woodcock III, W. Zhang, A.T. Bell, A.K. Chakraborty, D.M. Chipman, F.J. Keil, A.Warshel, W.J. Hehre, H.F. Schaefer, J. Kong, A.I. Krylov, P.M.W. Gill and M. Head-Gordon, *Phys. Chem. Chem. Phys*. **2006,** *8,* 3172–3191.

[54] Becke, A. D. *J. Chem. Phys.* **1993**, *98*, 5648−5652.

[55] Lee, C.; Yang, W.; Parr, R. G. *Phys. Rev. B* **1988**, *37*, 785−789.

[56] Stephens, P. J.; Devlin, F. J.; Chabalowski, C. F.; Frisch, M. J. *J. Phys. Chem.* **1994**, *98*, 11623−11627.

[57] Vosko, S. H.; Wilk, L.; Nusair, M. *Can. J. Phys.* **1980**, *58*, 1200−1211.

[58] Bauschlicher, C. W., Jr.; Partridge, H. *J. Chem. Phys.* **1995**, *103,* 1788-1791.

[59] Wong, M. W. *Chem. Phys. Lett.* **1996**, *256*, 391-399.

[60] Zhao, Y.; Truhlar, D. G. *Phys. Chem. Chem. Phys.* **2008**, *10*, 2813-2818.

[61] Ribeiro, R. F.; Marenich, A. V.; Cramer, C. J.; Truhlar, D. G. *J. Phys. Chem. B* **2011**, *115*, 14556-14562.

[62] Frisch, M. J.; Trucks, G. W.; Schlegel, H. B.; Scuseria, G. E.; Robb, M. A.; Cheeseman, J. R.; Scalmani, G.; Barone, V.; Mennucci, B.; Petersson, G. A.; Nakatsuji, H.; Caricato, M.; Li, X.; Hratchian, H. P.; Izmaylov, A. F.; Bloino, J.; Zheng, G.; Sonnenberg, J. L.; Hada, M.; Ehara, M.; Toyota, K.; Fukuda, R.; Hasegawa, J.; Ishida, M.; Nakajima, T.; Honda, Y.; Kitao, O.; Nakai, H.; Vreven, T.; Montgomery, J. A., Jr.; Peralta, J. E.; Ogliaro, F.;

Bearpark, M.; Heyd, J. J.; Brothers, E.; Kudin, K. N.; Staroverov, V. N.; Kobayashi, R.; Normand, J.; Raghavachari, K.; Rendell, A.; Burant, J. C.; Iyengar, S. S.; Tomasi, J.; Cossi, M.; Rega, N.; Millam, N. J.; Klene, M.; Knox, J. E.; Cross, J. B.; Bakken, V.; Adamo, C.; Jaramillo, J.; Gomperts, R.; Stratmann, R. E.; Yazyev, O.; Austin, A. J.; Cammi, R.; Pomelli, C.; Ochterski, J. W.; Martin, R. L.; Morokuma, K.; Zakrzewski, V. G.; Voth, G. A.; Salvador, P.; Dannenberg, J. J.; Dapprich, S.; Daniels, A. D.; Farkas, Ö.; Foresman, J. B.; Ortiz, J. V.; Cioslowski, J.; Fox, D. J. *Gaussian 09, Revision B.01*; Gaussian, Inc.: Wallingford, CT, 2009.

[63] Legault, C. Y. *CYLview, 1.0 b*; *Université de Sherbrooke* (http://www.cylview.org), 2009.

[64] Watts, K. S.; Dalal, P.; Tebben, A. J.; Cheney, D. L.; Shelley, J. C. J. Chem. Inf. Model. 2014, 54, 2680.

[65] Zimmerman, G. *Eur. J. Org. Chem.* **2001**, 457-471.

[66] Prall, M.; Krüger, A.; Schreiner, P. R.; Hopf, H. *Chem. Eur. J.* **2001**, *7,* 4386-4394.

Chapter 2: Synthesis of *N* = 12 Armchair Graphene Nanoribbons via the Topochemical Polymerization and Subsequent Aromatization of a Diacetylene Precursor

Section 2.1: Abstract

We have developed a synthetic approach to graphene nanoribbons using butadiyne-containing monomers that are initially polymerized to polydiacetylenes via topochemical polymerization in the crystal. Subsequent aromatization of the isolated polydiacetylenes at surprisingly mild temperatures affords graphene nanoribbons ~1.36 nm in width with a 1.4 eV bandgap. These transformations take place solely in the solid-state in contrast to published on-surface or in-solution methods. This synthetic approach is well suited for electronic device fabrication processes because it only requires UV light or heating, and no external chemical reagents.

Section 2.2: Introduction

Although graphene is characterized by an exceptionally high carrier mobility (>200,000 $cm^2\ V^{-1}\ s^{-1}$), its zero bandgap has prevented application to logic devices such as field-effect transistors (FETs), the essential devices behind modern electronics.[1] Graphene nanoribbons (GNRs), which are narrow ribbons (≤ 10 nm) of graphene, enable bandgap tuning through their edge structure and ribbon width, offering the exciting prospect of workable molecular electronics.[2,3] GNRs have swiftly gained prominence thanks to the development of a number of

synthetic approaches and chemical modifications.[4,5,6] These synthetic approaches fall into either "top-down" or "bottom-up" strategies.[7] Top-down approaches include the chemical unzipping of carbon nanotubes and cutting of single sheets of graphene with an electron beam.[8,9,10,11,12] These methods demonstrate high material throughput but often produce mixtures of different GNRs and struggle to achieve ribbon widths below 10 nm. In contrast, bottom-up strategies allow the construction of ribbons from small molecular precursors by taking advantage of the precise control that classical synthetic chemistry can afford.[13]

To date, only two variations of "bottom-up" approaches to GNR synthesis have been developed: 1) via on-surface aryl radical generation and coupling to form oligoarene backbone polymers, which are subsequently cyclodehydrogenated to produce GNRs, and 2) in-solution synthesis of oligoarene backbone polymers, which are then oxidized to GNRs using chemical oxidants. On-surface synthesis provides excellent control over nanoribbon structure, giving access to a range of widths and edge functionalizations.[14,15,16,17,18] These approaches display extraordinary synthetic control, but can usually only produce tiny amounts of materials on very specific substrates, requiring high-cost equipment and conditions such as ultra-high-vacuum scanning probe microscopy. In contrast, solution-phase synthesis can produce large amounts (up to grams) of GNRs, but typically requires the use of transition metal catalysts, and in-solution oxidation using chemical oxidants.[19,20,21,22,23,24]

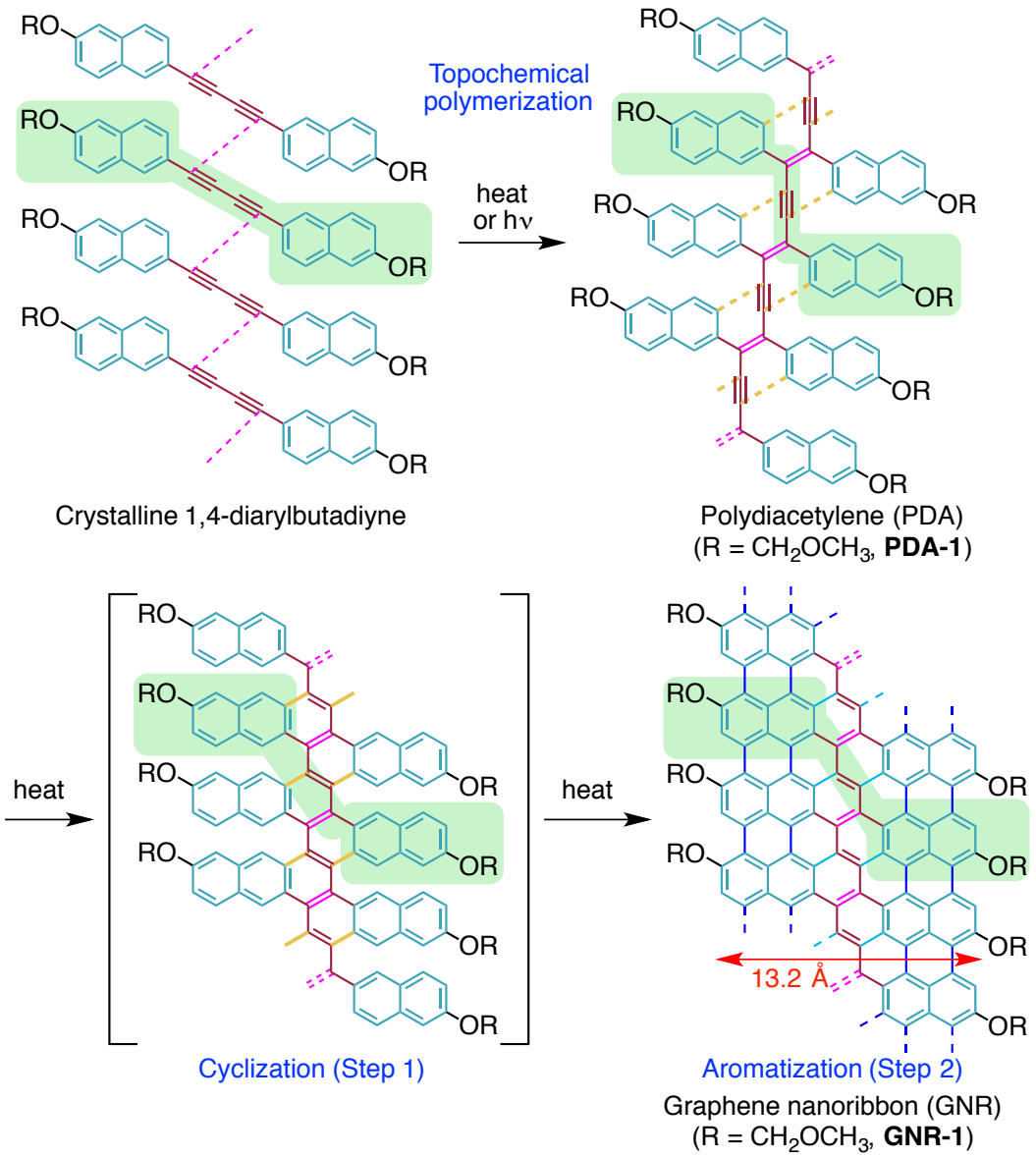

Scheme 2.1. Synthetic approach to GNRs via the topochemical polymerization of polyacetylenes. Our approach consists of a 3 step process including 1) crystallization of suitable monomers into a solid-state structure suitable for topochemical polymerization, 2) initiation of polymerization using heat or UV light, 3) subsuquent heating to promote cyclization of the polydiacetylene backbone and cyclodehydrogenation to produce GNRs.

Inspired by our recent forays into the controlled synthesis of 1D carbon nanostructures through the aromatization of polydiacetylene polymers with defined topology,[25,26] we have translated this concept to a process that would allow the bottom-up construction of GNRs in only three simple steps: 1) Synthesis and crystallization of monomeric precursors to achieve tight intermolecular distances between terminal butadiyne carbons in the crystal (C1-C4 ≃ 3.6 Å or less), 2) crystal-to-crystal topochemical polymerization to polydiacetylene molecules, and 3) exhaustive cyclization and aromatization to graphene nanoribbons (Scheme 2.1). Specifically, we show that 1,4-bis(6-methoxymethyloxynaphthalen-2-yl)butadiyne (**1**) undergoes topochemical polymerization to the corresponding polydiacetylene (**PDA-1**). Heating of **PDA-1** under an inert atmosphere at unusually mild temperatures (150-300 ˚C) provides putative graphene nanoribbons with an average width of ~1.36 nm and an optical band gap of 1.4 eV. The chemical and morphological properties of these GNRs are confirmed by Raman, UV-vis-NIR, XPS, electron diffraction, SEM and TEM. As opposed to previous "bottom-up" synthetic approaches to GNRs, both the monomer-to-PDA and PDA-to-GNR conversion processes occur in solid-state without the need for any additional reagents. Such features are desirable for ultimate device applications as they can be more readily incorporated into the fabrication of electronics. Proof-of-concept patterning of microscopic features of GNRs is demonstrated via selective adsorption. Finally, preliminary electrical property measurements of these GNRs indicate that they are indeed conductive.

Section 2.3: Results and Discussion

Monomer design and synthesis

The key to our process was the design of a monomer suitable to 1) undergo topochemical polymerization to the corresponding PDA polymer and 2) facilitate complete cyclization of the PDA backbone and aromatic substituents to a GNR. From our initial hypothesis, we rationalized that aryl substituents on the PDA backbone could undergo aromatization steps via a series of intramolecular dienyne electrocyclizations (Scheme 2.1).[27,28,29] Despite previous reports on diaryl-substituted PDAs, literature on their cyclization and aromatization is non-existent to the best of our knowledge.[30,31] Since naphthalene is less stabilized by aromaticity than benzene, and therefore more reactive, we chose to synthesize dinaphthylbutadiyne-based monomers that should have a higher propensity for solid-state reactions.[32] For the topochemical polymerization of butadiynes to be feasible under mild conditions, several factors must be satisfied in the crystalline state.[33] First among these is achieving a tight (≤ 3.6 Å) C1-C4 packing distance between adjacent butadiyne units. Accordingly, several diarylbutadiynes (**1-4**) were synthesized and their solid-state packing was investigated by single crystal X-ray diffraction (Fig. 2.1).[34]

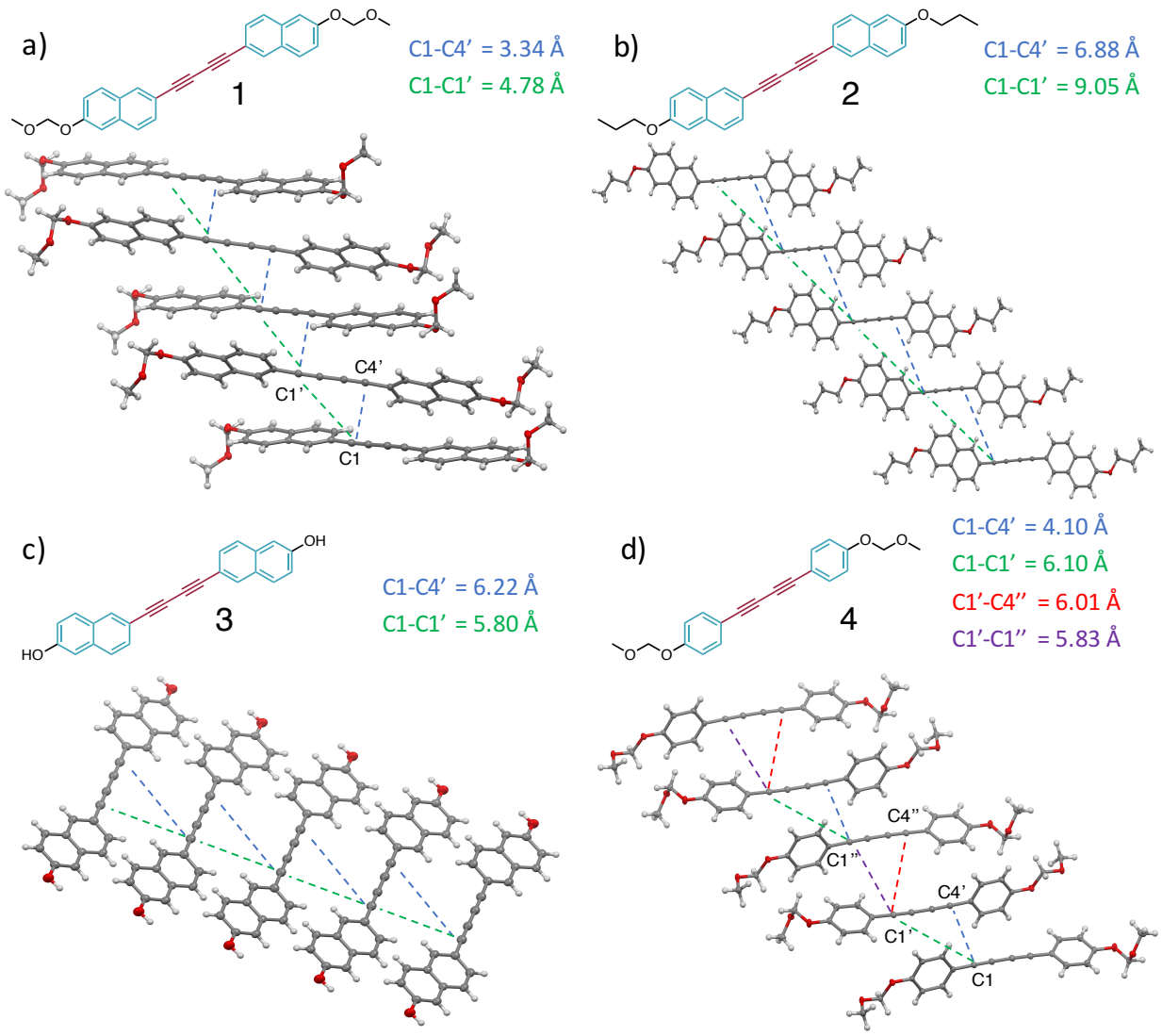

Figure 2.1. Solid-state packing parameters for synthesized diarylbutadiynes. C1-C4 and C1-C1 distance are displayed in blue and green respectively for compounds **1-3** (a)-(c). Compound **4** (d) displays two repeating C1-C4 distances highlighted in blue and red, with its C1-C1 distances shown in green and purple.

As can be seen from the X-ray crystallographic data, compound **1** organizes its butadiyne units within one key parameter for a topochemical polymerization to occur, namely the close C1-C4 carbon distance (Fig. 2.1a). Compound **1** has perfect inversion symmetry with respect to the

center of the butadiyne unit and has a tight C1-C4 distance of 3.34 Å. However, it also has a highly unusual zig-zag relationship between molecules along the stacking axis, with the angle between the two mean planes defined by the two different pairs of symmetrically related diyne units being 63.8°. To investigate how the methoxymethyl (MOM) group affects this organization, diynes **2** and **3** were also synthesized. Interestingly, replacement of the MOM group with the isosteric propyl group dramatically changes the packing structure to a herringbone arrangement, which more than doubles the C1-C4 distance to 6.9 Å (Fig. 2.1b). We attribute the efficient packing of diyne **1** in the crystal to the bent shape of its MOM side-chain, due to the anomeric effect between the two oxygen atoms, which allows for tighter packing of the monomer units overall. Removal of the MOM groups to give the corresponding dinaphthol **3** also dramatically changes the stacking pattern and increases the C1-C4 distance to 6.2 Å (Fig. 2.1c). Thus, both compounds **2** and **3** highlight the indispensable presence of the MOM group on the butadiyne organization of the dinaphthyl system **1** within crystals. We also synthesized the diphenyl butadiyne **4** containing two MOM groups for comparison. While diyne **4** contains an aryl-MOM motif similar to that of diyne **1**, it does not result in a solid-state packing structure amenable to topochemical polymerization (Fig. 2.1d). Furthermore, we isolated another polymorph of diyne **1** that does not contain ideal packing parameters, and topochemical polymerization did not occur (Fig. B1). These results highlight the high sensitivity of the crystalline-state organization to small structural perturbations.

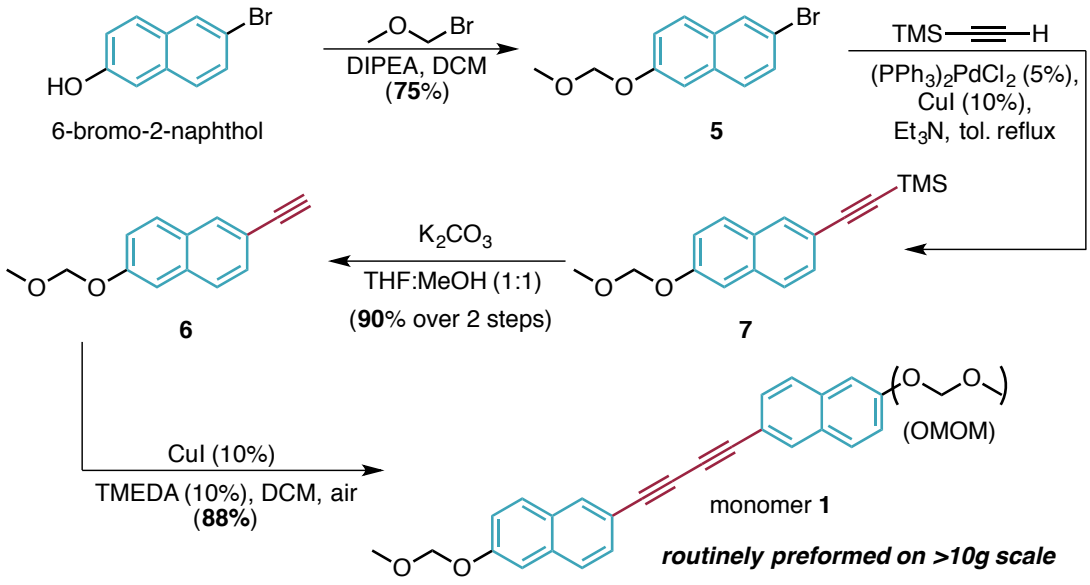

Scheme 2.2. Synthesis of monomer **1**. Monomer **1** is prepared in four steps in 60% overall yield from commercially available 6-bromo-2-naphthol. Specific procedures and characterization data for all compounds is provided in the Supplementary Information.

The synthesis of diyne monomer **1** is concise and can be readily applied to a large scale. This compound was synthesized in four steps with 60% overall yield from commercially available 6-bromo-2-naphthol (Scheme 2.2). Some key features of the synthesis are that only one column chromatography separation step was needed and that the final product could be obtained as a bulk crystalline solid after recrystallization from acetonitrile/water. Importantly, the bulk crystals contain the same crystalline state packing motif as the single crystal and are suitable for topochemical polymerization by either UV irradiation or thermal energy.

Topochemical polymerization of monomer 1

Crystals of **1** polymerize spontaneously at room temperature upon exposure to UV light. The polymerization proceeds slowly at room temperature but can be accelerated via thermal annealing at 115 ˚C (below the melting temperature of **1** at 137-138 °C) or irradiation with 254 nm light, which imparts a deep green/black color to the crystals. Upon dissolution in chloroform to wash away unreacted monomer, **PDA-1** is recovered. The **PDA-1** appears in forms of fibers, or sheets comprised of aggregated fibers if collected on a filter, and displays a deep blue color characteristic of the PDA backbone, with broad absorption peaks at 620 and 670 nm (Fig. 2.2a). The polymer was found to form stable blue dispersions upon sonication in chloroform and can be processed onto virtually any substrate. The structure of the polymer was also characterized using Raman spectroscopy (Fig. 2.2b). The Raman spectrum of **PDA-1** displays two characteristic stretches at 1450 and 2100 cm^{-1} corresponding to the internal alkene and alkyne stretching modes of the PDA polymer backbone, respectively. The chemical structure is further confirmed by x-ray photoelectron spectroscopy (XPS). The high-resolution C1s spectrum for **PDA-1** shows prominent peaks at 284.5, 286.3, and 288.0 eV, which represent C-C, C-O, and O-C-O bonded carbons, respectively (Fig. B2).[35,36,37,38] Note that since the alkyne and alkene carbons are very close in binding energy, they appear as one peak centered around 284.4 eV. A π-π* shake-up feature is also seen around 289.2 eV, which provides evidence of a π-conjugated system.

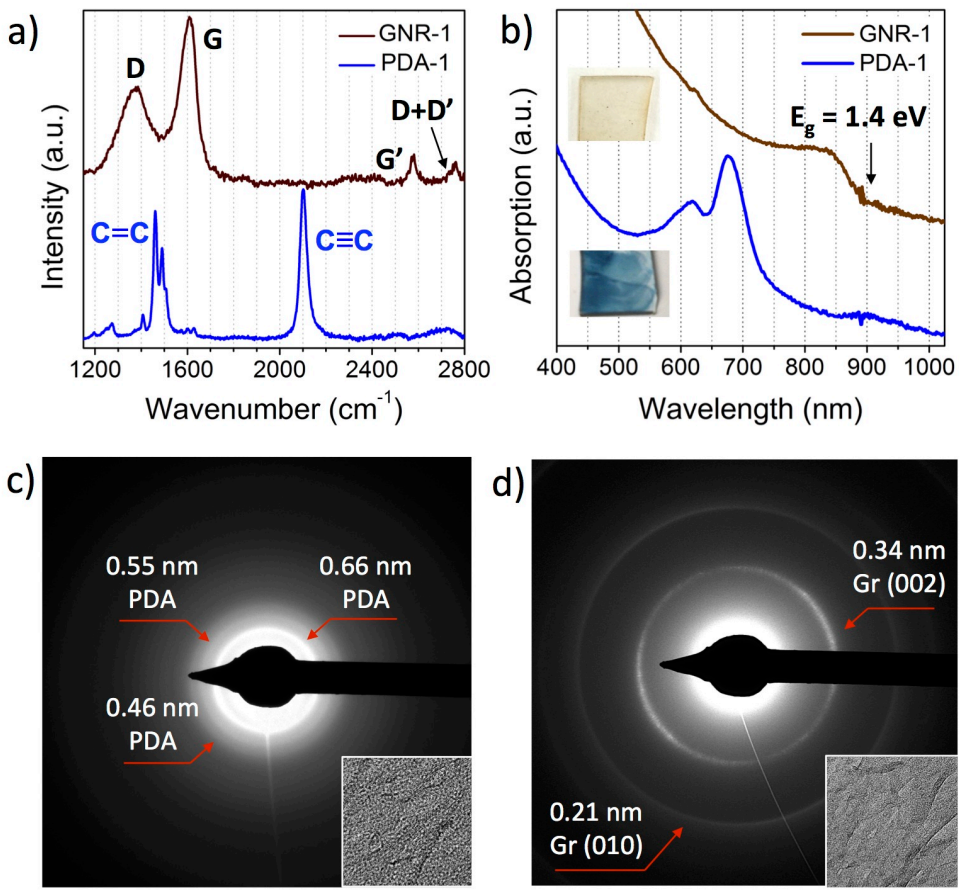

Figure 2.2. Chemical and crystallographic characterization of **PDA-1** and **GNR-1**. (a) Raman and (b) UV-vis-NIR spectra of **PDA-1** and **GNR-1**, respectively. Pictures in (b) illustrate the color change upon the conversion from **PDA-1** (bottom blue film) vs. **GNR-1** (top brownish black film). (c) and (d) Selected-area electron diffraction (SAED) patterns of **PDA-1** and **GNR-1**, respectively. Insets are the TEM images of the areas where diffraction patterns were collected.

GNR formation and characterization

Heating polymer **PDA-1** at relatively moderate temperatures (e.g. 300 ˚C for 8 h) under inert atmosphere such as argon or in vacuum led to the loss of the characteristic blue color, with the material taking on a deep brown-to-black color. Raman spectroscopy of this material showed

it to be graphitic in nature and consistent with "bottom-up" synthesized GNRs from other groups (Fig. 2.2b). The backbone alkene and alkyne stretches at 1450 and 2100 cm^{-1} corresponding to **PDA-1** are completely absent after heating and are replaced by the characteristic G and D peaks of graphene-based materials. Compared to large area graphene, the G peak is up-shifted to 1610 cm^{-1} and has a larger full width at half peak height due to quantum confinement effects that relax the Raman selection rules, which has also been observed in previous GNR reports.[20,39,40] The D peak at 1380 cm^{-1} arises as a result of the confinement of π-electronics into a finite domain.[20,39,40] The breadth of the G and D peaks could also indicate the presence of non-sp^2 carbon species, due to a small amount of defects formed during the aromatization process.

XPS analysis allowed us to confirm the presence of small amount of defects in the GNR (Fig. B2). First, the C1s spectrum for **GNR-1** is devoid of the oxygen bound components, evidenced by the complete disappearance of the C-O and O-C-O peaks at 286.3 and 288.0 eV, respectively. This indicates that the MOM substituents on **PDA-1** are removed in the aromatization process to **GNR-1**. Additionally, aside from the sp^2 C peak at 284.4 eV and the π-π* shake-up feature around 289.6 eV, a small shoulder can be seen at ≈ 286 eV, which can be attributed to amorphous sp^3 carbon. This may be due to the creation of a small amount of defect sites in the formed GNRs, and explains the breadth of the D and G bands seen in the Raman spectra (Fig. 2.2b).

UV-vis-NIR spectroscopy also confirms the PDA-to-GNR conversion (Fig. 2.2a). Absorption peaks at 620 and 675 nm characteristic to **PDA-1** have been replaced with a peak at around 840 nm after the heating step. An optical band gap of 1.4 eV can be calculated from the absorption edge at 890 nm for the GNR.

The GNR formation is further verified via selected-area electron diffraction (SAED). Due to the small size of the **PDA-1** or **GNR-1** fibers, and their susceptibility to electron beam damage, it is extremely challenging to collect diffraction patterns on individual ribbons. Hence, areas containing clusters of **PDA-1** fibers or GNRs were chosen (insets to Fig. 2.2c and 2.2d), which yield ring-like patterns due to the combination of diffraction spots in all orientations. SAED patterns of **PDA-1** show three diffraction rings with d-spacings of 0.66, 0.55, and 0.46 nm (Fig. 2.2c) and do not correspond to any diffraction peak from the monomer (see Fig. B3 for comparison), demonstrating the formation of a different compound. The SAED patterns of clusters of **GNR-1** show two sharp rings at 0.34 and 0.21 nm that are characteristic of the graphene (002) and (010) spacings, which crystallographically confirm the graphitic nature of the **GNR-1**.

Although the PDA-to-GNR aromatization process was carried out at 300 ˚C, it can also proceed at lower temperatures (e.g. <200 ˚C), but at a slower rate. Fig. A4a shows the UV-vis-NIR spectra of films of monomer, **PDA-1**, and **PDA-1** after 8 h of annealing under argon at various temperatures. The absorption peaks characteristic of **PDA-1** (620 and 675 nm) start to diminish in intensity at temperatures as low as 200 ˚C. The absorption associated with **GNR-1** at 840 nm starts to appear after annealing at 250 ˚C, indicating full aromatization of the polymer. The peak further grows in intensity when the thermal treatment is carried out at 300 ˚C.

In order to monitor the PDA-to-GNR conversion, a film of **PDA-1** was annealed at 200 ˚C for various amounts of time and its absorption monitored by UV-vis-NIR spectroscopy (Fig. B4b). The PDA absorption peaks are still present (albeit lower in intensity) after 8 h of heating in argon under 200 ˚C. However, after increasing the annealing time to 24 h, the 840 nm peak associated with GNR formation coexists with the **PDA-1** absorptions. This provides

evidence that the backbone of the polydiacetylene is aromatized under prolonged heating even at relatively mild temperatures.

Note that since the topochemical polymerization and aromatization processes here are activated by UV or thermal energy, both the monomer-to-PDA and the PDA-to-GNR processes proceed in the solid-state. This feature holds a significant advantage over other "bottom-up" syntheses of GNR that are solution-based, due to the elimination of reagents and its compatibility with electronic device fabrication processes. Subsequent work will also examine the suitability of this process to self-assembled monolayers of diyne **1** or similarly substituted congeners.

Microscopic analysis of GNRs

The successful transformation of **PDA-1** to **GNR-1** is further confirmed through SEM and TEM characterization. Fig. 3a shows a bundle of ribbon-like structures in which the larger ribbon (~10 nm in width) splits into finer features as small as <2 nm in width. Higher resolution image zooming-in on a section that is about 5 nm in width reveals two thin ribbons (<2 nm) laying adjacent to each other, with a width similar to the calculated **GNR-1** width of 1.32 nm based on the molecular structure (Scheme 2.1). In fact, **GNR-1** processed from **PDA-1** fibers that are only mildly sonicated tend to form sheet-like structures as a result of the aggregation of many GNRs (Fig. B5). The fine nanoscaled ribbon features are evident in TEM images (Fig. B5d,e). Higher resolution images allow the observation of the individual **GNR-1** constituents (Fig. B5f), where each bundle comprises GNRs oriented parallel with respect to each other. Such aggregates are frequently observed in literature reports on solution-processed GNRs.[20,21] A line profile across these bundles (e.g. the yellow line on Fig. B5f) reveals periodic repeating distances (Fig. B5g) that are averaged to 1.36 nm (averaged over >30 ribbons across multiple areas), which

is very similar to the calculated GNR width of 1.32 nm (Scheme 2.1), further confirming the formation of GNRs.

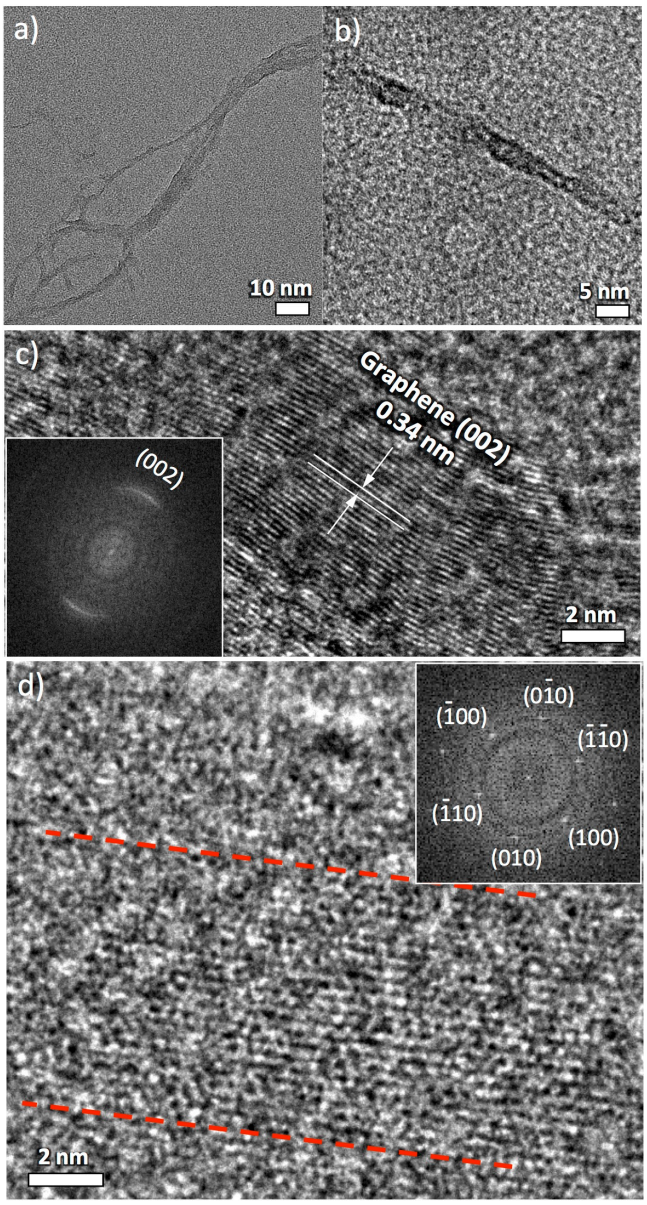

Figure 2.3. TEM characterization of **GNR-1**. TEM images of (a) a bundle of GNRs; (b) Two adjacent individual GNRs. (c) High resolution TEM image of a GNR stack showing the characteristic (002) graphene interlayer spacing. Inset is the FFT pattern of the lattice fringes. (d) High resolution TEM image revealing the well-ordered basal plane of the GNR. The

corresponding FFT pattern along index is shown in the inset.

Stacks of GNRs assembled via co-facial π-π interactions are also observed in TEM. Fig. 1.3c shows such a stack with a characteristic (002) graphitic inter-layer spacing of 0.34 nm. Resolving the atomic structure of graphitic materials on a TEM without spherical aberration correction features is extremely challenging, and we were not able to achieve such feat for individual GNRs. However, we found that although the majority of GNRs observed are <2 nm in width (Fig. 2.3a, b, and Fig. B5f, g), occasionally there are larger area GNRs in the TEM sample that are about 7.8 nm wide, which allowed us to resolve the hexagonal atomic lattice of its basal plane (Fig. 2.3d). Fast Fourier Transform (FFT) pattern of the high resolution TEM image (inset to Fig. 2.3d) agrees with the crystal structure of the graphene basal plane, confirming full aromatization. The 7.8 nm width of such graphene ribbons indicates that approximately 6 original GNRs have possibly fused together. Although this will need further investigation, such edge-to-edge fusion could provide a unique path for a controlled synthesis of larger GNRs.[41,42]

Patterning and Electrical Measurements

Microscopic patterning is an integral part of virtually all modern electronic device fabrication. Here, we demonstrate the possibility of patterning **GNR-1** ribbons into microscale features by selective adsorption. The patterning steps are summarized in Fig. B6. In short, we used photolithography to create desired microscopic features on SiO_2/Si wafers, and treated these features with a monolayer of octadecyltrichlorosilane (OTS) prior to photoresist liftoff. These patterned substrates were dip-coated in a heavily sonicated chloroform dispersion of **PDA-1**. Due to the higher binding affinity that these organic polymers have for hydrocarbon-terminated surfaces over oxide surfaces, the **PDA-1** fibers selectively adsorbed on the OTS-covered

microscale features. The **PDA-1**-coated substrates were then thermally aromatized to **GNR-1**. Fig. 2.4a and b show GNR films patterned in star and line shapes, respectively. Feature resolution as small as 10 μm can be readily achieved (Fig. 2.4b). Reverse coverage is also possible by treating the areas outside of the patterns with OTS instead. Fig. 2.4c shows a substrate with such inverted patterns where the "UCLA CHEM" shapes are left intact, while all other surfaces are covered with GNRs. Note that due to the small size of GNRs, these micron-sized, photolithographically patterned features are several orders of magnitude larger than the dimension of **GNR-1**. The feature sizes can be further scaled down by incorporating e-beam or nano-imprint lithography. Our demonstration here serves as proof-of-concept illustrating the possibility of selectively depositing single or few GNRs at desired locations on a substrate or potentially in circuits.

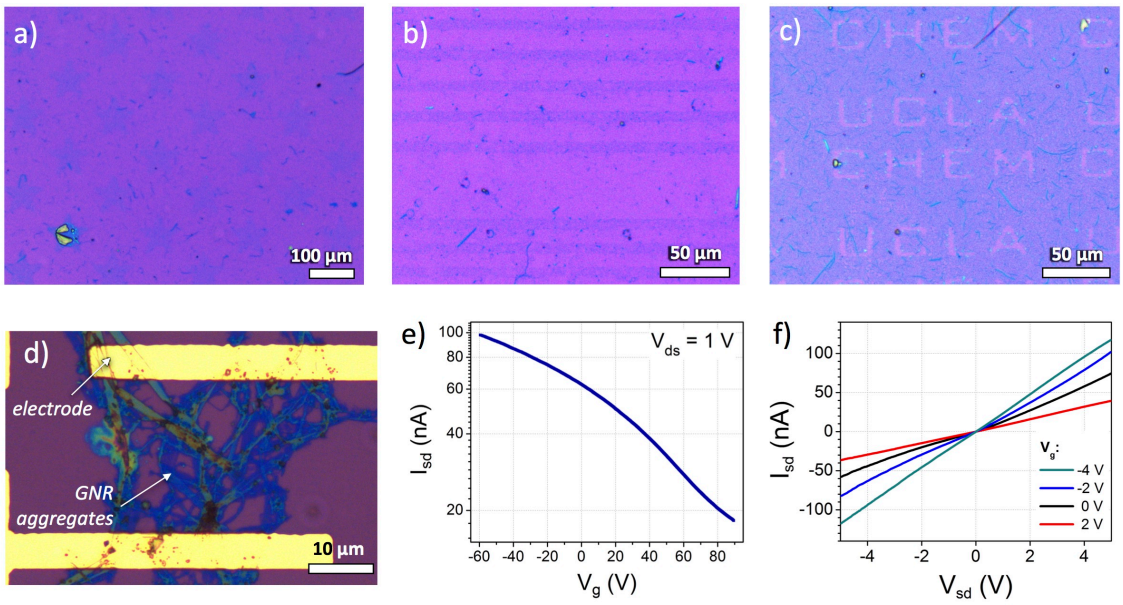

Figure 2.4. Patterning and electrical property characterization. (a)-(c) Optical microscope images of stars, lines, and "UCLA CHEM" patterns comprised of GNR thin films obtained by selective-area adsorption of PDA followed by solid-state aromatization. (d) Optical microscope

image of a GNR transistor. (e) Transfer characteristics of a GNR transistor at V_{sd} = 1 V. (f) Drain current (I_{sd}) vs. source-drain voltage (V_{sd}) under different gate modulation voltages.

In order to probe the electrical properties of the topochemically synthesized GNRs, bottom contact, back-gate field-effect transistors were fabricated. A dispersion of PDA in chloroform was drop-casted onto an OTS-coated SiO_2/Si wafer with microelectrodes fabricated by photolithography, followed by thermally-induced aromatization to GNR. Fig. 1.4d illustrates a representative device. The transfer characteristic indicates the GNR here is heavily p-doped with a Dirac point around or slightly beyond 85 V (Fig. 2.4e). We were not able to scan beyond this voltage due to instrument limitations. The heavily shifted Dirac point could be attributed to the presence of the OTS adhesion layer and solvent molecules trapped between the GNR and the dielectric layer, issues frequently observed on bottom-contact devices.[43] Fig. 2.4f demonstrates the gate modulation behavior of the transistor where the drain current (I_{sd}) changes under different gate voltages (V_g). The low-field field-effect mobility expression[44] is used here for mobility calculations:

$$\mu = \frac{dI_{sd}}{dV_g} \times \frac{L}{W \cdot C_i \cdot V_{sd}}$$

where channel length L is 24 μm, channel width W is integrated based on the GNR aggregate coverage between the electrodes, and capacitance C_i for OTS-treated 300 nm-thick SiO_2 dielectric layer is 10 nF/cm.[2,45] The devices show an average mobility μ of ~0.15 $cm^2 V^{-1} s^{-1}$, with an I_{on}/I_{off} of about 5 (based on the assumption that the Dirac point is at around 85 V). The mobility value is comparable to several previous reports.[4,39] Note that due to the small size of the GNRs, it is extremely challenging to fabricate field-effect transistors based on single ribbons to

probe their intrinsic properties. There are millions of randomly stacked GNRs within our channel area. The tremendous amounts of junctions between GNRs create significant contact resistance, which greatly decreases the drain current (I_{sd}). The contact resistance may also be attributed to a much lowered I_{on}, which leads to a low I_{on}/I_{off}. In addition, due to the collective effect of millions of GNR within the channel, it is possible that the electrical property is approaching bulk, which could contribute to bulk graphene-like low I_{on}/I_{off} ratio. Note that the purpose of our electrical property measurements here is to complement the spectroscopic and microscopic characterization of the GNRs, which demonstrates that they are indeed electrically active, further confirming the aromatization of **PDA-1** to **GNR-1**. We are currently working on further probing the intrinsic properties of individual GNRs.

Section 2.4: Conclusion

In conclusion, we are describing here a bottom-up approach to GNRs having defined width (~1.36 nm) and bandgap (1.4 eV) starting from very simple diacetylenes such as dinaphthyl diyne derivative **1**. This process relies on the in-crystal topochemical polymerization of dinaphthyl diyne **1** to the polydiacetylene polymer **PDA-1**, which can be isolated and manipulated in stable suspensions. Subsequent aromatization at relatively mild temperatures efficiently converts **PDA-1** to **GNR-1**. This approach should ultimately lend itself to nanofabrication methods on a large scale using relatively inexpensive procedures.

Acknowledgements

We thank Prof. X. Duan (UCLA) for help with his probe station for transistor

measurements, the UCLA Nanoelectronics Research Facility for cleanroom access, and the Electron Imagining Center for Nanomachines at the California NanoSystems Institute for TEM and Raman usage.

We thank Dr. Simon Kervyn for preliminary experiments towards this work, and Prof. Sarah Tolbert for helpful discussions on the XPS results. This work was supported by the National Science Foundation through an International Collaboration grant to Y.R. (NSF-CHE-1125054), and for instrumentation grants NSF-CHE-9871332 (X-ray) and NSF-CHE-9974928 (NMR). Y.W. was also supported by a National Science Foundation—Graduate Research Fellowship.

Section 2.5: Experimental

Synthetic procedures for all compounds are described in the Supporting Information. Topochemical polymerization of the monomer was carried out by irradiation of the crystals directly with a quartz-filtered medium-pressure Hg Hanovia lamp. The crystals were irradiated for 3 days after which time dissolution in chloroform and filtration provided the PDA in an average 5% yield based on weight. **PDA-1** was converted to **GNR-1** by annealing in a programmable tube furnace at various temperatures up to 300 ˚C under inert atmosphere (i.e. in vacuum or under argon flow) for various amounts of time. A 10 ˚C/min ramping rate was used to reach the target temperature.

UV-vis-NIR spectra of thin films deposited on glass or quartz substrates were collected on a Shimadzu UV-3101 PC UV-vis-NIR Scanning Spectrophotometer. Raman was performed on a Reinshaw 1000 instrument using a 50x objective lens and an excitation wavelength of 514 nm. Scanning electron microscope (SEM) samples were prepared by drop-casting a

chloroform dispersion of PDA after sonication, followed by the aromatization step described in the previous section. SEM images were collected on a JEOL JSM-6700 Field Emission scanning electron microscope. Transmission electron microscope (TEM) samples were prepared by brushing a Cu TEM grid with a lacey carbon support against the surface of a substrate containing the SEM sample, hence mechanically transferring some GNRs onto the TEM grid. TEM imagining was performed on a FEI Tecnai G^2 TF20 transmission electron microscope operating at 200 kV accelerating voltage. We chose 200 kV instead of the more commonly used 80 kV in order to resolve the atomic structure of the graphene basal plane since our TEM is not equipped with spherical aberration correction. Electron beam damage to the GNR is minimized via low dose techniques commonly practiced on highly beam sensitive polymer or biological samples.[46,47]

Photolithography patterning steps of the GNR are depicted in Fig. S4. In short, a photomask with desired patterns was aligned to a SiO_2/Si wafer coated with AZ 5214 photoresist and exposed to UV irradiation (6 s, 8 mW) using a Karl Suss MA6 aligner. After exposing the patterns by developing the substrate in the AZ developer, the wafer pieces were treated with oxygen plasma (200 W, 10 s) to create a hydroxyl-terminated SiO_2 surface. The samples were then soaked in a 1% OTS chloroform solution for 3 h and rinsed repeatedly with copious amount of chloroform, followed by a 10 min baking step at 150 ˚C in air. Finally, the remaining photoresist was removed with acetone, and substrate rinsed with acetone then isopropanol. The patterned substrates were dip coated in a heavily sonicated chloroform dispersion of PDA, and dried with nitrogen flow. The sample was then annealed in a tube furnace at 300 ˚C for 8 h under argon flow to convert the PDA to GNR.

Field-effect transistors were fabricated by first defining the source and drain electrode

areas using photolithography followed by metal deposition (5/40 nm Ti/Au) on a heavily p-doped Si wafer (as back gate electrode) with a 300 nm SiO_2 layer (as dielectric layer). Liftoff of the photoresist affords a SiO_2/Si wafer covered with microelectrodes. The surface was treated with OTS (as described previously) to improve the adhesion between the active material and the substrate. A PDA/chloroform dispersion was drop-casted onto these electrodes, allowed to soak for ~30 sec, and the excess dispersion removed with gentle nitrogen flow. The sample was then annealed for 8 h at 300 ˚C under argon flow. The FET measurements were carried out in a Lake Shore probe station.

Accession numbers: Crystallographic data has been deposited in the Cambridge Crystallographic Data Center (CCDC) under the numbers: CCDC 1485224-1485228.

General Procedures: Unless stated otherwise, reactions were performed under an argon atmosphere in flame-dried glassware. Tetrahydrofuran (THF), methylene chloride (CH_2Cl_2), diethyl ether (Et_2O), toluene (C_7H_8), and acetonitrile (CH_3CN) were passed through activated alumina columns prior to use. Chemical reagents were obtained from commercial sources and used without further purification. Reaction temperatures were controlled using an IKA magnetic temperature modulator. Procedures were performed at room temperature (~23 ˚C) unless otherwise indicated. Column chromatography was performed on Silicycle (Siliflash P60) silica gel 60 (240-400 mesh). Thin layer chromatography and preparative layer chromatography utilized pre-coated plates from E. Merck (silica gel 60 PF254, 0.25 mm or 0.5 mm).

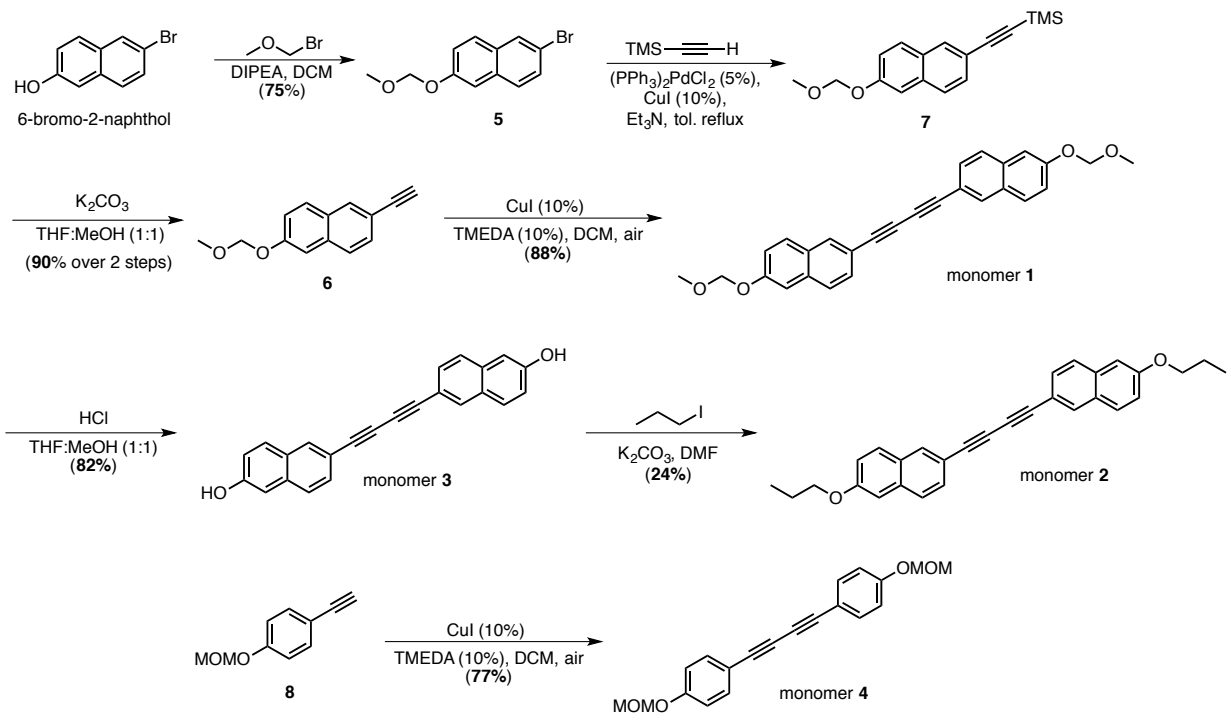

Scheme B1: Overview of the synthetic reactions for all compounds described. Specific synthetic details are described below.

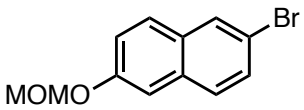

2-Bromo-6-(methoxymethoxy)naphthalene (5)

2-Bromo-6-hydroxynaphthol (10 g, 45 mmol, 1 eq) was added to a round bottom flask and DCM (200 mL, 0.23 M) was added. To the resulting solution was added N,N-diisopropylethylamine (15.7 mL, 90 mmol, 2 eq) followed by bromomethyl methyl ether (4.4 mL, 54 mmol, 1.2 eq) in one portion under argon. The resulting mixture was allowed to stir at room temperature until the SM had been consumed (TLC). Upon completion of the reaction the

mixture was diluted with water and the layers separated. The aqueous layer was extracted with fresh DCM (2 x 50 mL) and the organics combined. The organic layer was washed with 0.5M HCl, brine, dried over $MgSO_4$, filtered and concentrated *in-vacuo*. The crude residue was purified using by filtration over SiO_2 (Hex:$CHCl_3$ or DCM) to produce 9.3 g (75%) of the product (**5**) as a tan/white solid. ^{1}H NMR (400 MHz, $CDCl_3$): 3.53 (s, 3H, CH_3), 5.29 (s, 2H, CH_2), 7.24 (dd, *J* = 8.9, 2.4 Hz, 1H, CH), 7.36 (d, *J* = 2.4 Hz, 1H, CH), 7.50 (dd, *J* = 8.8, 2 Hz, 1H, CH) 7.60 (d, *J* = 8.8 Hz, 1H, CH), 7.67 (d, *J* = 8.9 Hz, 1H, CH), 7.92 (d, *J* = 2 Hz, 1H, CH); ^{13}C NMR (100 MHz, $CDCl_3$): 56.2, 94.5, 109.9, 117.6, 120.0, 128.5, 128.7, 129.6, 129.7, 130.5, 132.9, 155.3; HRMS (DART): calculated for $C_{12}H_{11}BrO_2$ ($M^{\bullet+}$): 265.9942; measured: 265.9939.

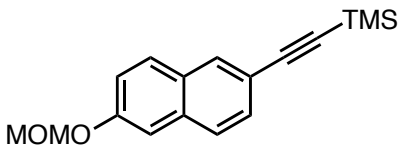

2-Trimethylsilethynyl-6-(methoxymethoxy)naphthalene (6)

2-Bromo-6-(methoxymethoxy)naphthalene (**5**) (8.5 g, 31.8 mmol, 1 eq) was added to a schlenk flask followed by addition of toluene (96 mL, 0.33 M) and triethylamine (8.9 mL, 64 mmol, 2.0 eq). Bis(triphenylphosphine)palladium chloride (1.1 g, 1.6 mmol, 0.05 eq) and copper(I) iodide (610 mg, 3.2 mmol, 0.1 eq) was added in succession and the mixture was sparged with argon for 30 min at room temperature. After the sparging had completed trimethylsilylacetylene (9 mL, 64 mmol, 2 eq) was added, the flask flushed with argon, sealed and heated to 110 °C until the SM had been consumed by 1H NMR analysis. After cooling to room temperature the mixture was filtered over celite and the filter cake washed with fresh

toluene (2 x 50 mL). The crude product **6** (9 g) was recovered as a deep brown/red oil and used directly in the next step without further purification. ^{1}H NMR (400 MHz, $CDCl_3$): 0.27 (s, 9H, CH_3), 3.51 (s, 3H, CH_3), 5.28 (s, 2H, CH_2), 7.21 (dd, *J* = 9.0, 2.4 Hz, 1H, CH), 7.34 (d, *J* = 2.4 Hz, 1H, CH) 7.46 (dd, *J* = 8.5, 1.6 Hz, 1H, CH), 7.65 (d, *J* = 8.5 Hz, 1H, CH), 7.69 (d, *J* = 9.0 Hz, 1H, CH), 7.92 (d, *J* = 1.6 Hz, 1H, CH); ^{13}C NMR (100 MHz, $CDCl_3$): 0.1, 56.2, 93.9, 94.4, 105.6, 109.8, 118.5, 119.6, 126.9, 128.9, 129.2, 129.4, 131.8, 134.1, 155.8; HRMS (DART): calculated for $C_{17}H_{20}O_2Si$ ($M^{\bullet+}$): 284.1227; measured: 284.1226.

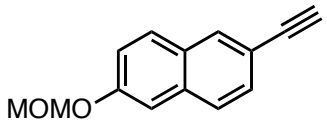

2-Ethynyl-6-(methoxymethoxy)naphthalene (7)

2-Trimethylsilethynyl-6-(methoxymethoxy)naphthalene (**6**) (9 g, 31.6 mmol, 1 eq) was added to a round bottom flask and dissolved in 150 mL (0.2 M) of a 1:1 mixture of THF and MeOH. Solid potassium carbonate (414 mg, 3 mmol, 0.1 eq) was added in a single portion and the mixture allowed to stir at room temperature. After stirring for ~30 min TLC indicated consumption of the starting material. The mixture was concentrated *in vacuo* to remove the solvents. The crude residue was partitioned between Et_2O and H_2O and the layers were separated. The aqueous phase was extracted with fresh Et_2O (3 x 50 mL), organics combined and dried over $MgSO_4$, filtered and concentrated *in vacuo* to provide a crude residue that was purified by flash column chromatography on SiO_2. The product (**7**) (6.2 g, 90% over 2 steps) was recovered as a tan crystalline solid. ^{1}H NMR (400 MHz, $CDCl_3$): 3.10 (s, 1H, CH), 3.52 (s, 3H, CH_3), 5.29 (s, 2H, CH_2), 7.23 (dd, *J* = 8.9, 2.4 Hz, 1H, CH), 7.36 (d, *J* = 2.4 Hz, 1H, CH), 7.48

(dd, *J* = 8.5, 1.7 Hz, 1H, CH) 7.67 (d, J= 8.5 Hz, 1H, CH), 7.72 (d, *J* = 8.9 Hz, 1H, CH), 7.95 (d, 1.7 Hz, 1H, CH); ^{13}C NMR (100 MHz, $CDCl_3$): 56.2, 76.9, 84.1, 94.4, 109.8, 117.4, 119.7, 127.2, 128.8, 129.1, 129.4, 132.1, 134.2, 155.9 ; HRMS (DART): calculated for $C_{14}H_{12}O_2$ (M+H): 213.0910; measured: 213.0908.

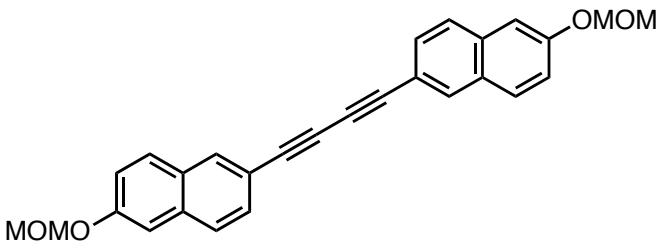

1,4-Bis(6-(methoxymethoxy)naphthalen-2-yl)buta-1,3-diyne (1)

2-Ethynyl-6-(methoxymethoxy)naphthalene (**7**) (6.2 g, 29 mmol, 1 eq) was added to a round bottom flask and dissolved in DCM (100 mL, 0.33 M). Copper(I) iodide (550 mg, 2.9 mmol, 0.1 eq) was added followed by TMEDA (434 μL, 2.9 mmol, 0.1 eq). Air was bubbled through the mixture for ca. 30 minutes. The resulting solution was allowed to stir overnight open to the air. In the morning, TLC indicated consumption of SM. The mixture was diluted with water, the layers separated, aqueous washed with fresh DCM (2 x 50 mL), organics combined, washed with dilute (0.5 M) HCl, brine, dried over $MgSO_4$, filtered and concentrated *in vacuo* to produce the crude product. The crude product was purified by recrystallization from ACN/H_2O by hot filtration to give the product (**1**) as deep gold needles (5.5 g, 88%). **NOTE: the crystals undergo spontaneous topochemical polymerization under ambient light to the corresponding polydiacetylene polymer. To inhibit the extent of polymerization, exposure to light should be minimized and the crystals stored in a covered vessel at -20 °C.** ^{1}H NMR (400 MHz, $CDCl_3$): 3.53 (s, 3H, CH_3), 5.30 (s, 2H, CH_2), 7.25 (dd, *J* = 8.9, 2.4 Hz, 1H, CH),

7.37 (d, *J* = 2.4 Hz, 1H, CH), 7.52 (dd, *J* = 8.5, 1.6 Hz, 1H, CH) 7.69 (d, *J* = 8.5, 1H, CH), 7.73 (d, *J* = 8.9 Hz, 1H, CH), 8.01 (d, *J* = 1.6 Hz, 1H, CH); ^{13}C NMR (100 MHz, $CDCl_3$): 56.2, 74.0, 82.2, 94.4, 109.9, 117.1, 119.9, 127.3, 128.8, 129.1, 129.5, 132.8, 134.4, 156.1; HRMS (DART): calculated for $C_{28}H_{22}O_4$ ($M^{\bullet+}$): 422.1512; measured: 422.1521. mp. 137-138 ºC.

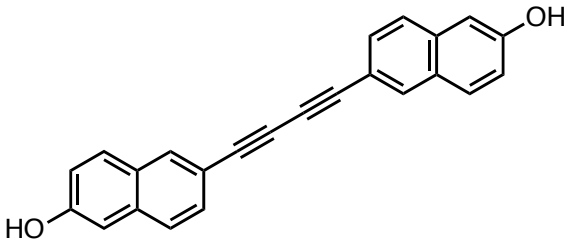

6,6'-(Buta-1,3-diyne-1,4-diyl)bis(naphthalen-2-ol) (3)

1,4-Bis(6-(methoxymethoxy)naphthalen-2-yl)buta-1,3-diyne (**1**) (118 mg, 0.3 mmol, 1 eq) was dissolved in 40 mL of THF:MeOH (1:1) in a round bottom flask. Concentrated HCl (37%, 1 mL) was added, the flask capped, and allowed to stir at room temperature until consumption of SM by TLC (ca. 2 days). The reaction was concentrated *in vacuo*, residual water was azeotroped using ACN x 2, and the crude residue was purified by crystallization from ACN by hot-filtration to give 80 mg (82%) of the product (**3**) as tan crystals. ^{1}H NMR (400 MHz, CD_3OD): 7.10 (1H, s), 7.11 (dd, *J* = 8, 2 Hz, 1H, CH), 7.42 (dd, *J* = 8.5, 1.5 Hz, 1H, CH), 7.62 (d, *J* = 8.5 Hz, 1H, CH), 7.72 (dd, *J* = 8, 2 Hz, 1H, CH) 7.96 (d, *J* = 1.5 Hz, 1H, CH); ^{13}C NMR (100 MHz, $CDCl_3$): 74.2, 82.9, 110.1, 117.0, 120.4, 127.7, 129.2, 129.7, 130.6, 133.8, 136.5, 158.1; HRMS (DART): calculated for $C_{24}H_{14}O_2$ ($M^{\bullet+}$): 334.09883; measured: 334.09733.

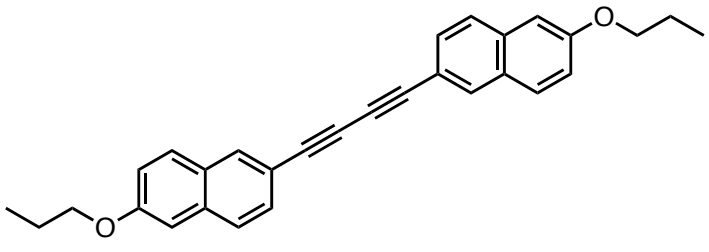

1,4-Bis(6-propoxynaphthalen-2-yl)buta-1,3-diyne (2)

6,6'-(Buta-1,3-diyne-1,4-diyl)bis(naphthalen-2-ol) **(3)** (100 mg, 0.3 mmol, 1 eq) was added to a round bottom flask and potassium carbonate (166 mg, 1.2 mmol, 4 eq) was added followed by DMF (3 mL). Iodopropane (153 mg, 0.9 mmol, 3 eq) was added in a single portion and the mixture was allowed to stir at room temperature. DMF was added as necessary to maintain stirring. The mixture was allowed to stir until the reaction was complete as judged by TLC. When the reaction was complete the mixture was diluted with water (10 x DMF volume) and the solid filtered. Purification of the crude precipitate using flash column chromatography gave 31mg (24%) of the product as a tan solid. ^{1}H NMR (400 MHz, $CDCl_3$): 1.08 (t, J = 7.5 Hz, 3H, CH_3), 1.88 (m, 2H, CH_2), 4.09 (t, J = 6.5 Hz, 2H, CH_2), 7.10 (d, J = 2.4 Hz, 1H, CH), 7.17 (dd, J = 8.9, 2.4 Hz, 1H, CH) 7.5 (dd, J = 8.5, 1.6 Hz, 1H, CH), 7.66 (d, J = 8.5 Hz, 1H, CH), 7.70 (d, J = 8.9, 1H, CH), 7.99 (d, J = 1.6 Hz, 1H, CH); ^{13}C NMR (100 MHz, $CDCl_3$): 10.6, 22.5, 69.6, 73.8, 82.3, 106.6, 116.5, 119.9, 126.9, 128.3, 129.1, 129.4, 132.8, 134.7, 158.3; HRMS (DART): calculated for $C_{24}H_{14}O_2$ ($M^{\bullet+}$): 418.19273; measured: 418.19135.

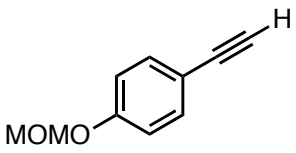

1-Ethynyl-4-(methoxymethoxy)benzene (8)

Compound 8 was prepared as described previously, see Arakawa, Y., Kang, S., Nakajima, S., Sakajiri, K., Cho, Y., Kawauchi, S., Watanabe, J., Konishi, G-I. (2013) Diphenyltriacetylenes: novel nematic liquid crystal materials and analysis of their nematic phase-transition and birefringence behaviours. *J. Mater. Chem. C*, *1*, 8094-8102.

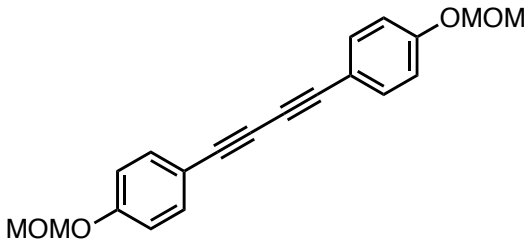

1,4-Bis(4-(methoxymethoxy)phenyl)buta-1,3-diyne (4)

1,4-Bis(4-(methoxymethoxy)phenyl)buta-1,3-diyne was prepared in a Hay coupling analogous to compound (**1**). Utilizing (**8**) (2.6 g, 16 mmol, 1 eq), CuI (304 mg, 1.6 mmol, 0.1 eq), TMEDA (186 mg, 1.6 mmol, 0.1 eq) and DCM (50 mL) provided 2.0 g (77%) of the desired product (**4**) as an orange crystalline solid after workup as described above. ^{1}H NMR (400 MHz, $CDCl_3$): 3.48 (s, 3H, CH_3), 5.19 (s, 2H, CH_2), 6.99 (d, J = 8.7 Hz, 2H, CH), 7.45 (d, J = 8.7 Hz, 2H, CH); ^{13}C NMR (100 MHz, $CDCl_3$): 56.2, 73.1, 81.2, 94.2, 115.1, 116.3, 134.0, 157.9; HRMS (DART): calculated for $C_{20}H_{18}O_4$ ($M^{\bullet+}$): 322.11996; measured: 322.11870.

Section 2.6: Appendix B

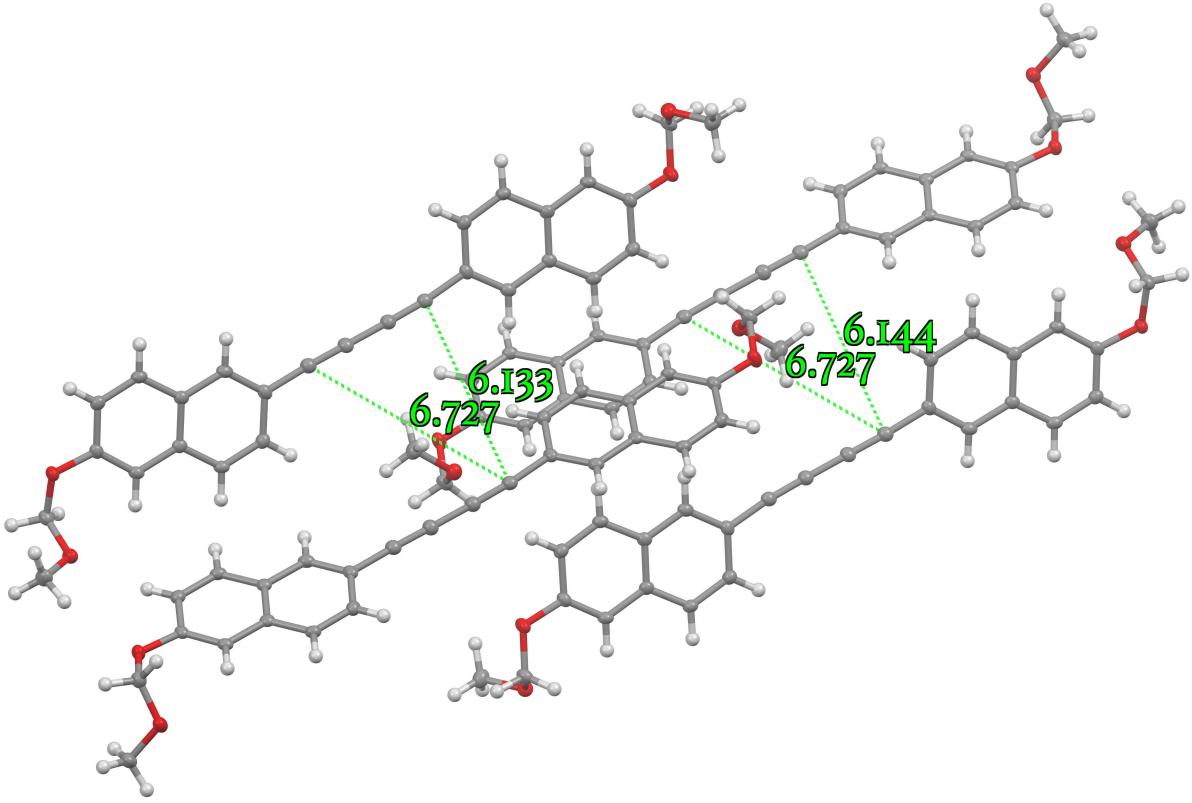

Figure B1. X-ray crystal structure of the unreactive polymorph of monomer **1**. C1-C4' distance of 6.727 Å and C1-C1' distance of 6.133 Å highlighted on structure. Crystals of this polymorph do not undergo topochemical polymerization even when treated with UV light.

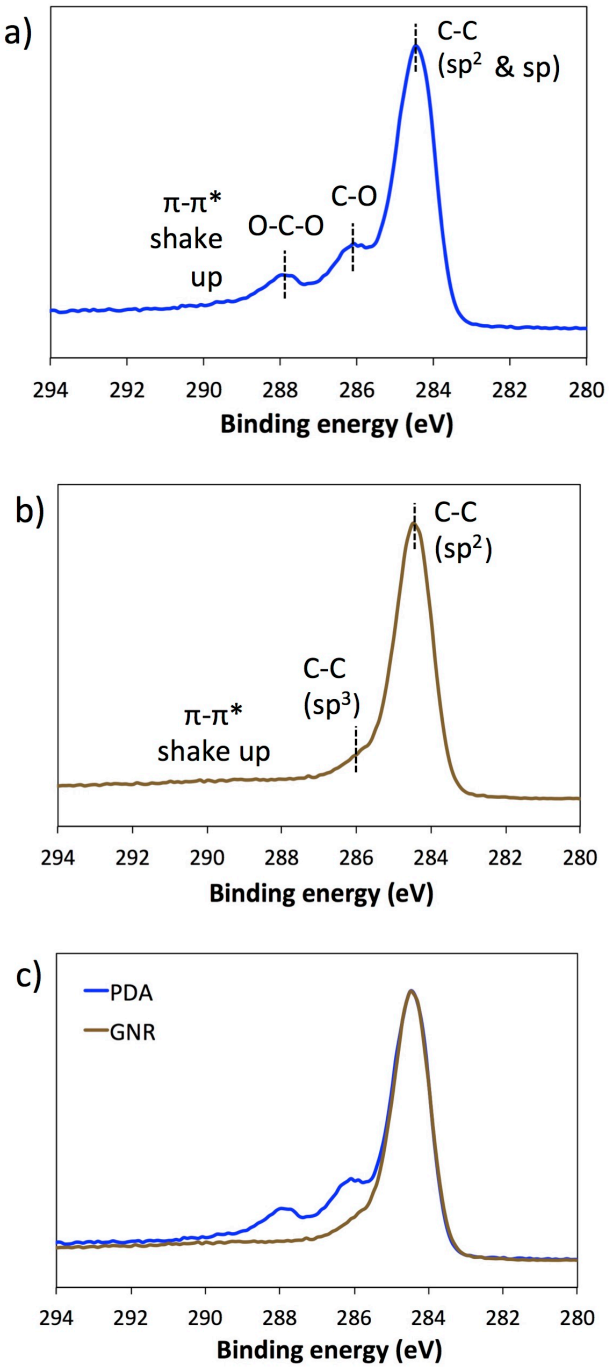

Figure B2. XPS C1s spectra of (a) **PDA-1**, (b) **GNR-1**, and (c) **PDA-1** and **GNR-1** spectra overlapped for comparison.

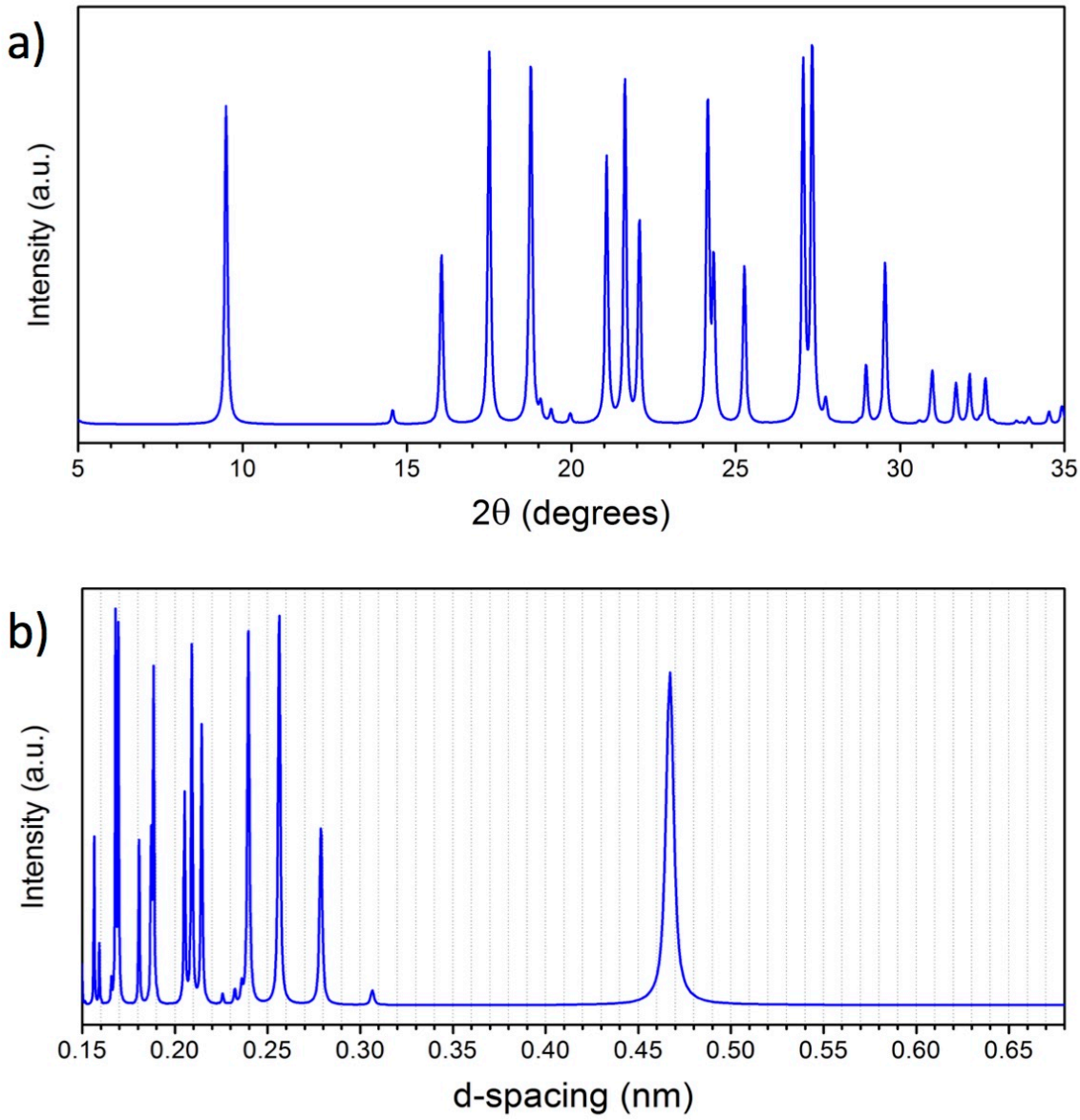

Figure B3. Powder XRD pattern simulated from single crystal XRD data of the **monomer-1** plotted in (a) reciprocal spacing and (b) d-spacing. None of the SAED diffraction spacing values obtained for **PDA-1** (0.46, 0.55, 0.66 nm, see Fig. 2c) matches up with any of the monomer peaks, indicating its full topological conversion to **PDA-1**.

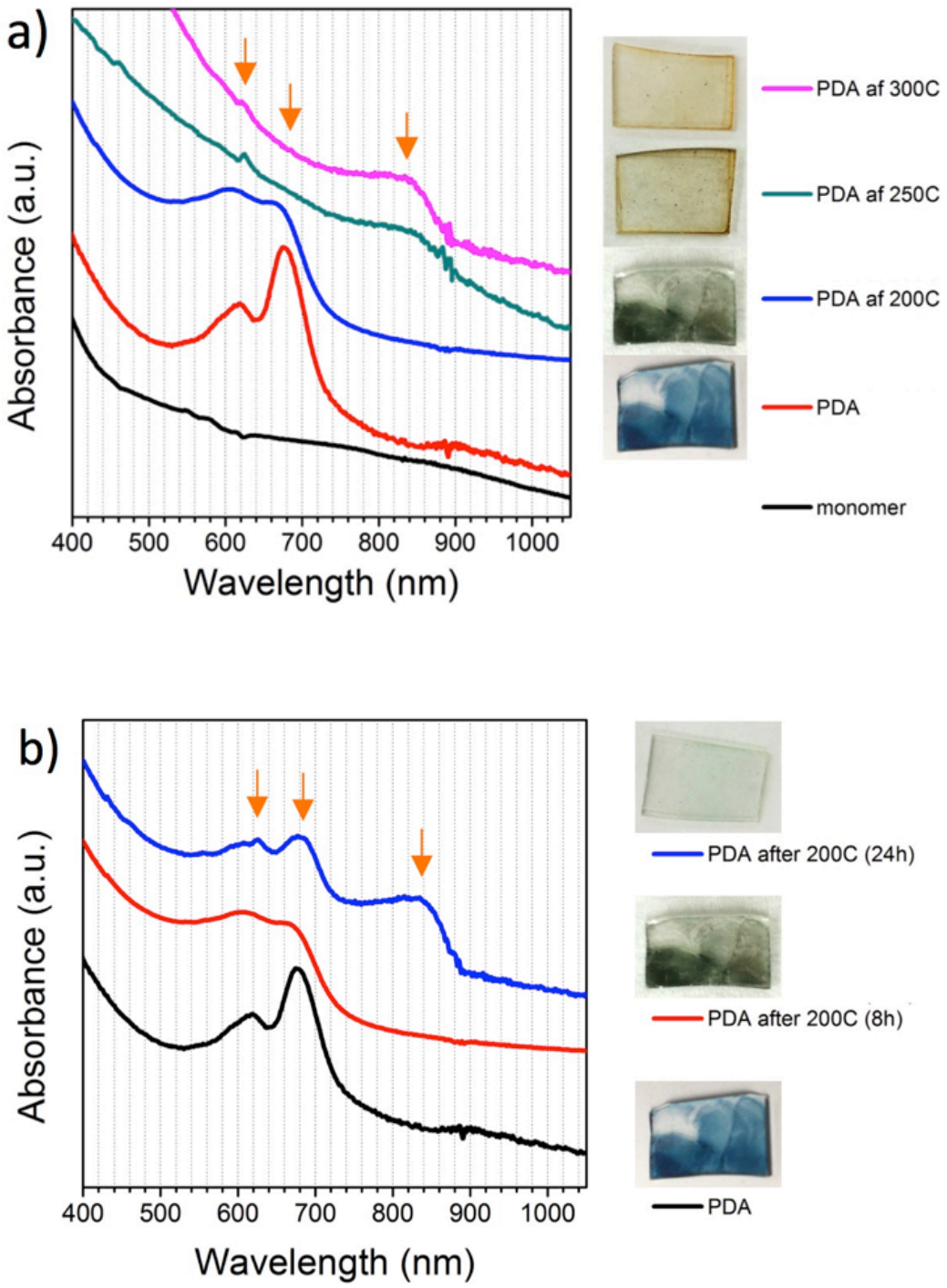

Figure B4. UV-vis-NIR spectra monitoring the **PDA-1** to **GNR-1** aromatization process (a) under 8 h of annealing at different temperatures and (b) at 200 °C over various durations.

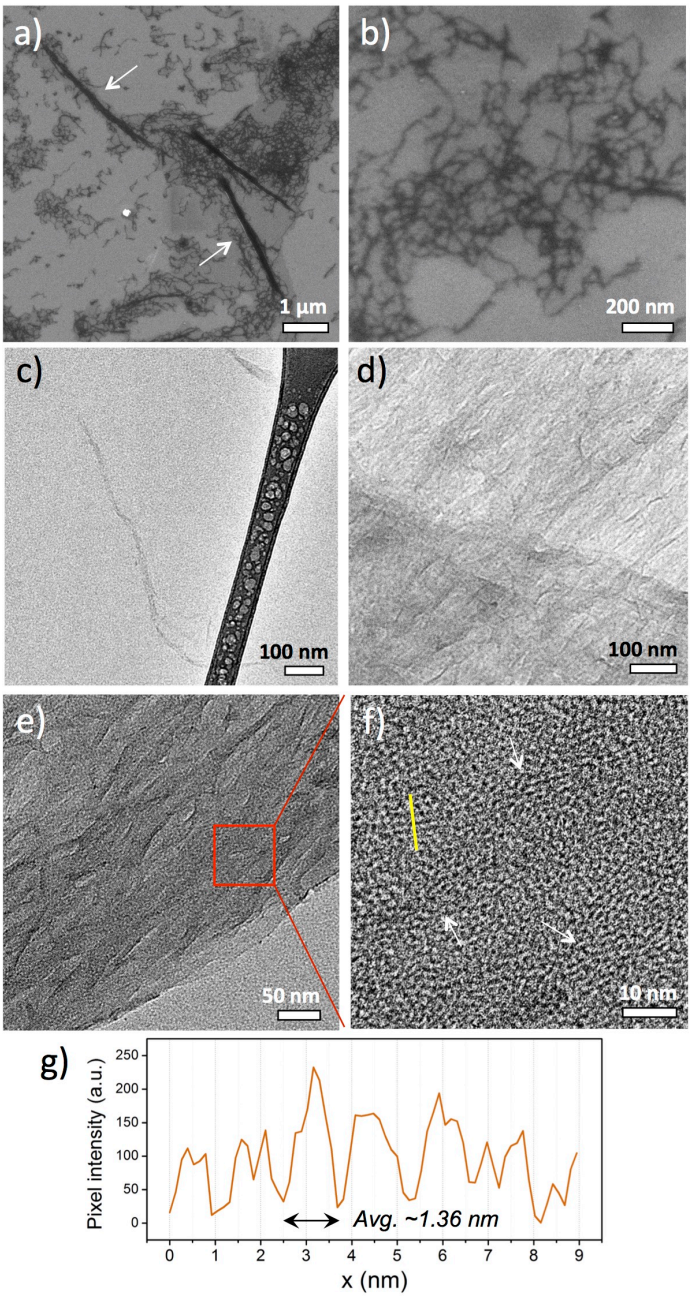

Figure B5. SEM and TEM characterization of **GNR-1**. (a) and (b) are SEM images showing the aggregated fibers of **GNR-1**. Scarce amount of large fibers such as the ones indicated by white arrows in (a) are present on the substrates, but can be disassembled into smaller entities by extensive sonication. TEM images in (c)-(f) show **GNR-1** under different magnifications. (c) shows a thin bundle of **GNR-1**. Larger sheets can also be observed (d and e), which show fiber-

like internal structures. A higher magnification TEM image (f) reveals these sheets are comprised of aggregates of GNRs. Line profile across the **GNR-1** bundles (g) allowed us to calculate the average width of these thin ribbons, which is ~1.36 nm, agreeing with the width calculated based on chemical structures.

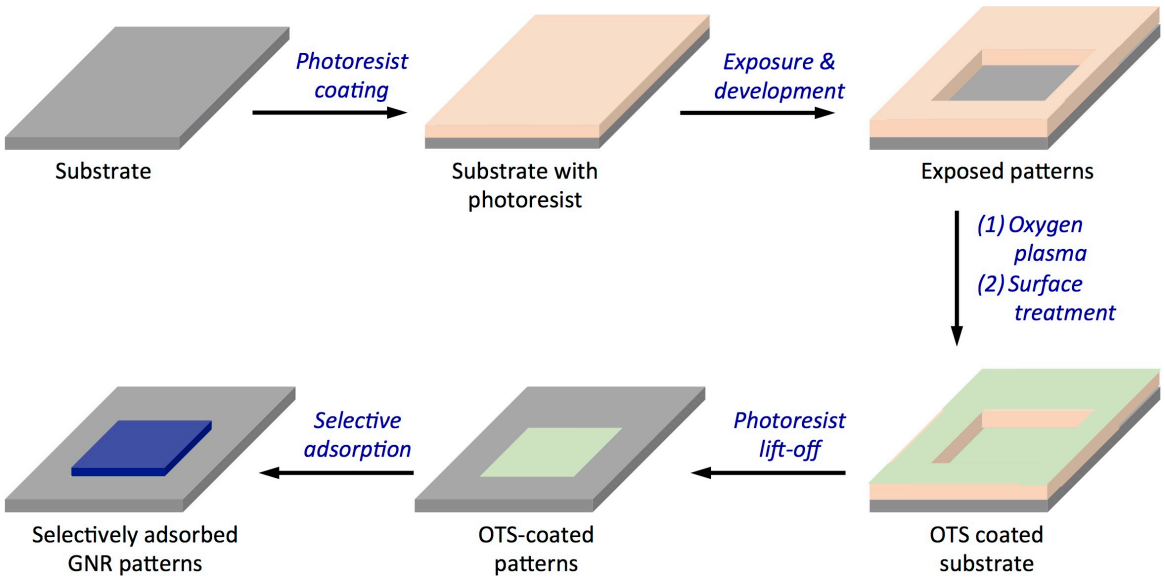

Figure B6. Schematic diagram showing the patterning steps for achieving selective adsorption of GNR.

References

[1] Novoselov, K. S., Fal'Ko, V. I., Colomobo, L., Gellert, P. R., Schwab, M. G., Kim, K. (2012). A roadmap for graphene. Nature *490*, 192-200.

[2] Wakabayashi, K., Fujita, M., Ajiki, H., Sigrist, M. (1999). Electronic and magnetic properties of nanographite ribbons. Phys. Rev. B. *59*, 8271-8282.

[3] Gao, J., Uribe-Romo, F.J., Saathoff, J.D., Arslan, H., Crick, C.R., Hein, S.J., Itin, B., Clancy, P., Dichtel, W.R., Loo, Y.-L. (2016). Ambipolar Transport in Solution-Synthesized Graphene Nanoribbons. ACS Nano. DOI: 10.1021/acsnano.6b00643

[4] Xu, W., Lee, T.-W. (2016) Recent Progress on Fabrication Techniques of Graphene Nanoribbons. Mater. Horizons. DOI: 10.1039/c5mh00288e

[5] Schwierz, F. (2010) Graphene transistors. Nat. Nanotechnol. *5*, 487-496.

[6] Yazyev, O.V. (2013). A Guide to the Design of Electronic Properties of Graphene Nanoribbons. Acc. Chem. Res. *46*, 2319-2328.

[7] Tour, J. M. (2014) Top-down versus bottom-up fabrication of graphene-based electronics. Chem. Mater. *26,* 163–171.

[8] Kosynkin, D. V., Higginbotham, A. L., Sinitskii, A., Lomeda, J. R., Dimiev, A., Price, B. K., Tour, J. (2009) Longitudinal unzipping of carbon nanotubes to form graphene nanoribbons. Nature *458,* 872–876.

[9] Kato, T., Hatakeyama, R. (2012) Site- and alignment-controlled growth of graphene nanoribbons from nickel nanobars. Nat. Nanotechnol. *7,* 651–656.

[10] Sommer, B., Sonntag, J., Ganzarczyk, A., Braam, D., Prinz, G., Lorke, A., Geller, M. (2015) Electron-beam induced nano-etching of suspended graphene. Sci. Rep. *5,* 7781.

[11] Jaison, M. J., Narayanan, T. N., Prem Kumar, T., Pillai, V. K. (2015) A single-step room-temperature electrochemical synthesis of nitrogen-doped graphene nanoribbons from carbon nanotubes. J. Mater. Chem. A *3,* 18222–18228.

[12] Li, Y.-S., Liao, J.-L., Wang, S.-Y., Chiang, W.-H. (2016) Intercalation-assisted longitudinal unzipping of carbon nanotubes for green and scalable synthesis of graphene nanoribbons. Sci. Rep. *6,* 22755.

[13] Chen, L., Hernandez, Y., Feng, X., Müllen, K. (2012) From nanographene and graphene nanoribbons to graphene sheets: Chemical synthesis. Angew. Chemie. - Int. Ed. *51,* 7640–7654.

[14] Cai, J. *et al.* (2010) Atomically precise bottom-up fabrication of graphene nanoribbons. Nature *466,* 470–3.

[15] Sakaguchi, H., Kawagoe, Y., Hirano, Y., Iruka, T., Yano, M., Nakae, T. (2014) Width-controlled sub-nanometer graphene nanoribbon films synthesized by radical-polymerized chemical vapor deposition. Adv. Mater. *26,* 4134–4138.

[16] Basagni, A., Sedona, F., Pignedoli, C. A., Cattelan, M., Nicolas, L., Casarin, M., Sambi, M. (2015) Molecules-oligomers-nanowires-graphene nanoribbons: A bottom-up stepwise on-surface covalent synthesis preserving long-range order. J. Am. Chem. Soc. *137,* 1802–1808.

[17] Kawai, S., Siato, S., Osumi, S., Yamaguchi, S., Foster, A. D., Spijker, P., Meyer, E. (2015) Atomically controlled substitutional boron-doping of graphene nanoribbons. Nat. Commun. *6,* 8098.

[18] Nguyen, G. D. *et al.* (2016) Bottom-up synthesis of $N = 13$ sulfur-doped graphene nanoribbons. J. Phys. Chem. C doi:10.1021/acs.jpcc.5b09986

[19] Yang, X., Dou, X., Rouhanipour, A., Zhi, L., Rader, H. J., Mullen, K. (2008) Two-dimensional graphene nanoribbons. J. Am. Chem. Soc. *130,* 4216–7.

[20] Narita, A. *et al.* (2014) Synthesis of structurally well-defined and liquid-phase-processable graphene nanoribbons. Nat. Chem. *6,* 126–32.

[21] Vo, T. H., Shekhriev, M., Kunkel, D. A., Morton, M. D., Berglund, E., Kong, L., Wilson, P. M., Dowben, P. A., Enders, A., Sinitskii, A. (2014) Large-scale solution synthesis of narrow graphene nanoribbons. Nat. Commun. *5,* 3189.

[22] Narita, A. *et al.* (2014) Bottom-up synthesis of liquid-phase-processable graphene nanoribbons with near-infrared absorption. ACS Nano *8,* 11622–11630.

[23] Liu, J. Li, B-W., Tan, Y., Giannakopoulos, A., Sanchez-Sanchez, C., Belijonne, D., Ruffieux, P., Fasel, R., Feng, X., Mullen, K. (2015) Towards cove-edged low band gap graphene nanoribbons. J. Am. Chem. Soc. *137,* 6097–6103.

[24] Schwab, M. G. *et al.* (2015) Bottom-up synthesis of necklace-like graphene nanoribbons. Chem. - An Asian J. *10,* 2134–2138.

[25] Suzuki, M., Comito, A., Khan, S. I., Rubin, Y. (2010) Nanochannel array within a multilayered network of a planarized dehydro[24]annulene. Org. Lett. *12,* 2346–2349.

[26] Suzuki, M. Khosrowabadi Kotyk, J. F., Khan, S. I., Rubin, Y. (2016) Directing the Crystallization of Dehydro[24]annulenes into Supramolecular Nanotubular Scaffolds. J. Am. Chem. Soc. *138*, 5939–5956..

[27] Tinnemans, A. H. A., Laarhoven, W. H. (1976) Synthesis and spectroscopic properties of 1,4-diarylbutenynes. J. Chem. Soc. Perkin 2, 1104.

[28] Tinnemans, A. H. A., Laarhoven, W. H. (1976) Photocyclisations of 1,4-diarylbut-1-en-3-ynes. Part II. Mechanism of the reaction. J. Chem. Soc. Perkin 2, 1111.

[29] Tinnemans, A. H. A., Laarhoven, W. H. (1976) Photocyclisations of 1,4-diarylbut-1-en-3-ynes. Part III. Scope and limitations of the reaction. J. Chem. Soc. Perkin 2, 1115.

[30] Rondeau-Gagné, S., Morin, J.-F. (2014) Preparation of carbon nanomaterials from molecular precursors. Chem. Soc. Rev. *43,* 85–98.

[31] Levesque, I., Neabo, J. R., Rondeau-Gange, S., Vigier-Carriere, C., Daigle, M., Morin, J-F. (2014) Layered graphitic materials from a molecular precursor. *Chem. Sci.* **5,** 831–836.

[32] Herndon, W. C., Ellzey, M. L. Jr., (1974) Resonance theory. V. Resonance energies of benzoid and nonbenzoid π systems. J. Am. Chem. Soc. *96,* 6631-6642.

[33] Wegner, G. (1972) Topochemical polymerization of monomers with conjugated triple bonds. Makromol. Chem. *154*, 35-48.

[34] The synthetic details for compounds **2-4** are included in Supporting Information.

[35] Hontoria-Lucas, C., Lopez-Peinado, A. J., Lopez-Gonzalez, J. de D., Rojas-Cervantes, M. L., Martin-Arnada, R. M. (1995). Study of oxygen-containing groups in a series of graphite oxides: physical and chemical characterization. Carbon, *33*, 1585.

[36] Dietrich, P. M., Horlacher, T., Girard-Lauriault, P-L., Gross, T., Lippitz, A., Min, H., Wirth, T., Castelli, R., Seeberger, P. H., Unger, W. E. S. (2011). Adlayers of dimmanoside thiols on glod: surface chemical analysis Langmuir, *27*, 4808.

[37] Wepasnick, K. A., Smith, B. A., Schrote, K. E., Wilson, H. K., Diegelmann, S. R., Fairbrother, D. H. (2011). Surface and structural characterization of multi-walled carbon nanotubes following different oxidative treatments. Carbon, *49*, 24.

[38] Biniak, S., Szymanski, G., Siedlewski, J., Swiatkowski, A. (1997). The characterization of activated carbons with oxygen and nitrogen surface groups. Carbon, *35,* 1799.

[39] Sokolov, A.N., Yap, F.L., Liu, N., Kim, K., Ci, L.J., Johnson, O.B., Wang, H.L., Vosgueritchian, M., Koh, A.L., Chen, J.H., Park, J., Bao, Z. (2013). Direct growth of aligned graphitic nanoribbons from a DNA template by chemical vapour deposition. Nat Commun. *4*: 2402.

[40] Ferrari, A.C., Basko, D.M. (2013). Raman spectroscopy as a versatile tool for studying the properties of graphene. Nat. Nanotechnol. *8*, 235-246.

[41] Huang, H., Wie, D., Sun, J., Liang Wong, S., Ping Feng, Y., Castro Neto, A. H., Wee, A. T. S. (2012). Spatially resolved electronic structures of atomically precise armchair graphene nanoribbons. Sci. Reports. *2*, 983.

[42] Basagni, A., Sedona, F., Pignedoli, C. A., Cattelan, M., Nicolas, L., Casarin, M., Sambi, M. (2015) Molecules-oligomers-nanowires-graphene nanoribbons: A bottom-up stepwise on-surface covalent synthesis preserving long-range order. J. Am. Chem. Soc. *137*, 1802.

[43] Wang, Y., Tran, H.D., Liao, L., Duan, X.F., Kaner, R.B. (2010). Nanoscale Morphology, Dimensional Control, and Electrical Properties of Oligoanilines. J. Am. Chem. Soc. *132*, 10365-10373.

[44] Lembke, D., Kis, A. (2012). Breakdown of High-Performance Monolayer MoS2 Transistors. ACS Nano *6*, 10070-10075.

[45] Oh, J.H., Lee, H.W., Mannsfeld, S., Stoltenberg, R.M., Jung, E., Jin, Y.W., Kim, J.M., Yoo, J.-B., and Bao, Z. (2009). Solution-processed, high-performance n-channel organic microwire transistors. Proc. Nat. Acad. Sci. *106*, 15, 6065-6070.

[46] Martin, D.C., Thomas, E.L. (1995). Experimental high-resolution electron-microscopy of polymers. Polymer *36*, 1743-1759.

[47] Martin, D.C., Chen, J.H., Yang, J.Y., Drummy, L.F., Kubel, C. (2005). High resolution electron microscopy of ordered polymers and organic molecular crystals: Recent developments and future possibilities. J. Polym. Sci. Pol. Phys. *43*, 1749-1778.

Chapter 3: Synthesis, Annulation and Oligomerization of Diaryl Enediynes

Section 3.1: Introduction

We recently described the successful development of a new synthetic approach to graphene nanoribbons (GNRs) that takes advantage of a strategic pericyclic cyclization of diaryl substituted polydiacetylene polymers.[1,2] Key to this process is the thermal engagement of the polydiacetylene enyne backbone in dienyne cyclizations to form annulated aromatic rings, en route to GNRs (Figure 3.1a). This specific pericyclic reaction, formally named the Hopf cyclization after its pioneer Henning Hopf, has been studied in many systems and is well understood in the context of simple systems to give new aromatic rings upon heating (Figure 3.1b,c).[3,4,5]

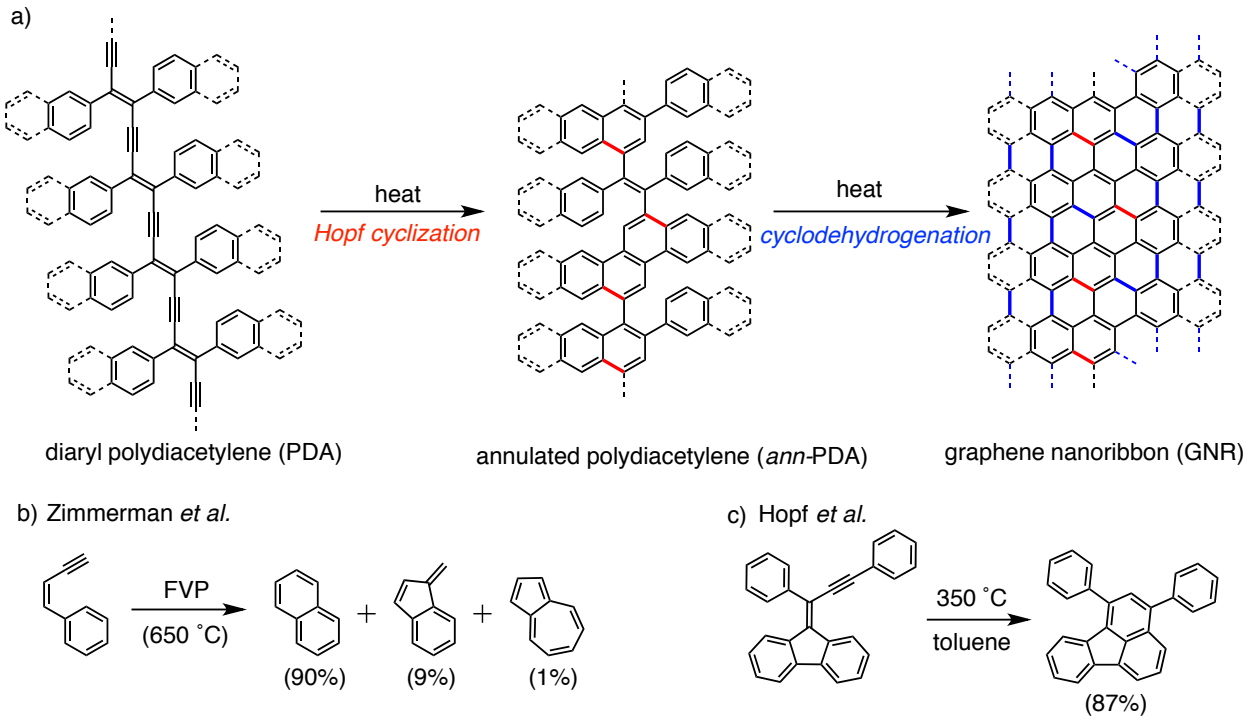

Figure 3.1. a) Overview of our approach to armchair graphene nanoribbons via thermal reactions of polydiacetylene polymer precursors. b,c) Specific examples of Hopf-type pericyclic reactions with systems containing aromatic rings.

To aid in our understanding of the Hopf cyclization within our polymers, we designed a small molecule model system that incorporates a *trans*-enediyne unit at its core, to model the cyclization of an individual monomer unit within our PDA polymers (Figure 3.2). Synthetically, our approach to these models would follow a symmetric retrosynthetic disconnection of its internal stilbene-like double bond to produce two equivalent aryl ynones (**1**). In the forward synthesis, these aryl ynones could be coupled in a formal McMurry coupling furnishing the target *trans*-enediyne **2**.[6] One benefit of this synthesis is the expedience in which ynones can be constructed through two simple steps starting from the corresponding aryl aldehydes, using a carbonyl addition and subsequent oxidation.

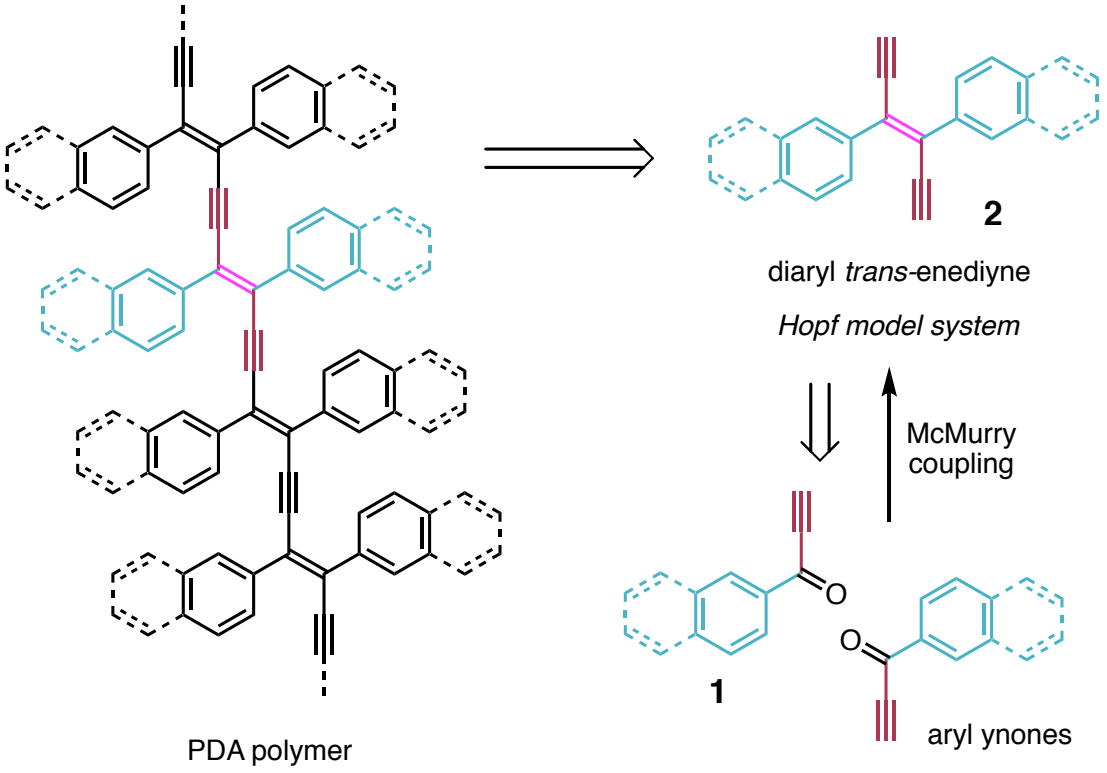

Figure 3.2. Retrosynthetic strategy towards *trans*-enediyne model systems **2**.

Section 3.2: Results and Discussion

Synthesis of a di-naphthyl-trans-enediyne and thermal cyclization

With the synthetic plan towards diaryl *trans*-enediynes shown in Figure 3.2, efforts were undertaken to synthesize naphthyl ynone precursor **1** that would function as a platform for the key McMurry coupling dimerization. The synthesis began with the addition of the lithium acetylide of 4-tert-butylphenylacetylene to the known aldehyde 6-triisopropylsilyloxy-2-naphthaldehyde (**3**). This produced the corresponding naphthyl propargylic alcohol **4** in 56% yield. Mild oxidation of the propargylic alcohol **4** with manganese dioxide produced the corresponding naphthyl ynone **5** in 90% yield and high purity. With ynone **5** in hand, the McMurry coupling was attempted. A number of different coupling conditions were tested, but unfortunately all reactions produced an intractable mixture of products (Table 3.1).[7,8]

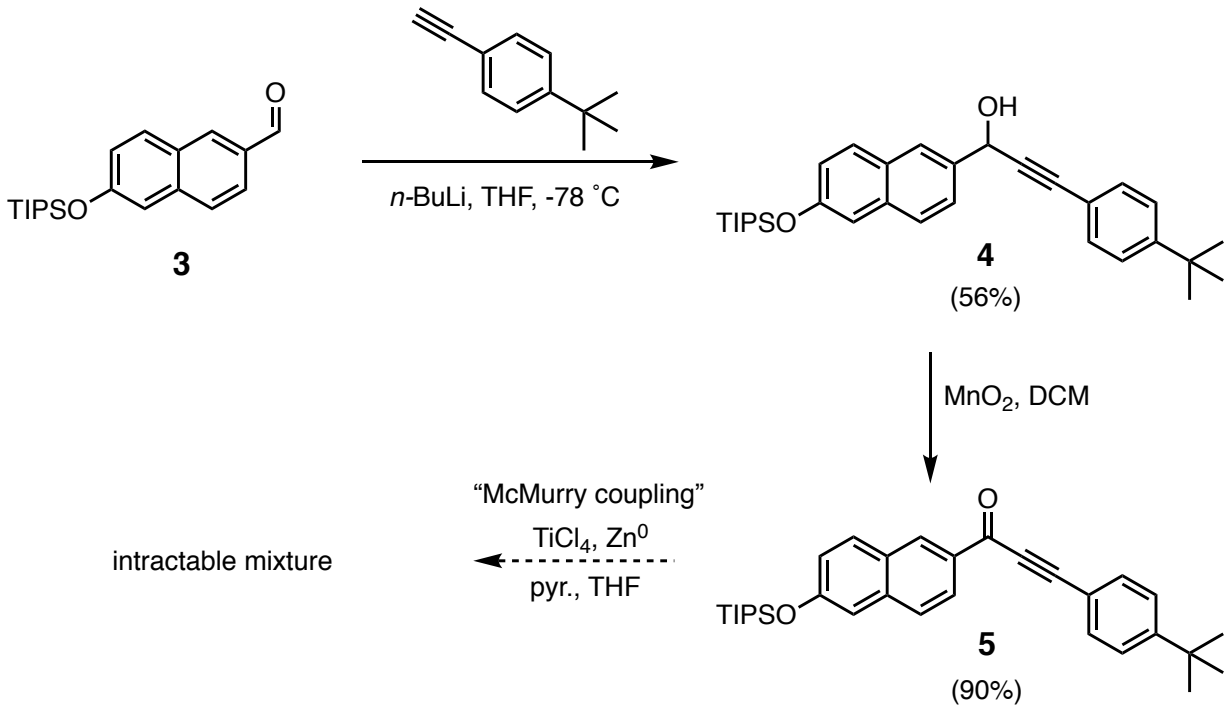

Figure 3.3. Synthesis of naphthyl ynone **5** and its attempted McMurry coupling.

While our initial strategy towards diaryl *trans*-enediynes did not prove fruitful, Mathews *et al.* had reported the dimerization of propargylic bromides in the presence of LiHMDS and HMPA to provide *trans*-enediynes (Figure 3.4).[9] This method produced enediynes in good to high yield and displayed selectivity for (*E*) products when bulky substituents on the propargyl bromide were used. Reconsidering our synthesis, we surmised that propargylic alcohol **4** could easily be converted to the corresponding propargylic bromide by treatment with phosphorous tribromide (PBr_3) under water free conditions. Upon treatment of compound **4** with 1.5 equivalents (eq) of PBr_3 at 0 ˚C a single product was formed in 86% yield. ^{1}H NMR analysis of the product of the reaction detailed a loss of the characteristic ^3J coupling (6 Hz) between the propargylic methine and hydroxyl protons, reflecting the loss of the hydroxyl group. Interestingly, close analysis of the ^{13}C NMR spectrum showed a carbon with a resonance of 203.5 ppm, proving that this compound was not the intended propargylic bromide, but instead, the allenic bromide **6** formed by an S_N2' attack of the internal alkyne.

Table 3.1. Conditions used for the attempted McMurry coupling of ynone **5**.

Entry #	Conditions	Yield	Ref.
1	5 eq $TiCl_4$, 10 eq Zn, 2.5 eq pyridine, 0.04 M THF	N/A	7
2	1 eq $TiCl_4$, 2 eq Et_3N, 0.05M CH_2Cl_2, 0˚C	N/A	7
3	2 eq $TiCl_4$, 4 eq Zn, 0.25 M THF, 0˚C to reflux	N/A	8

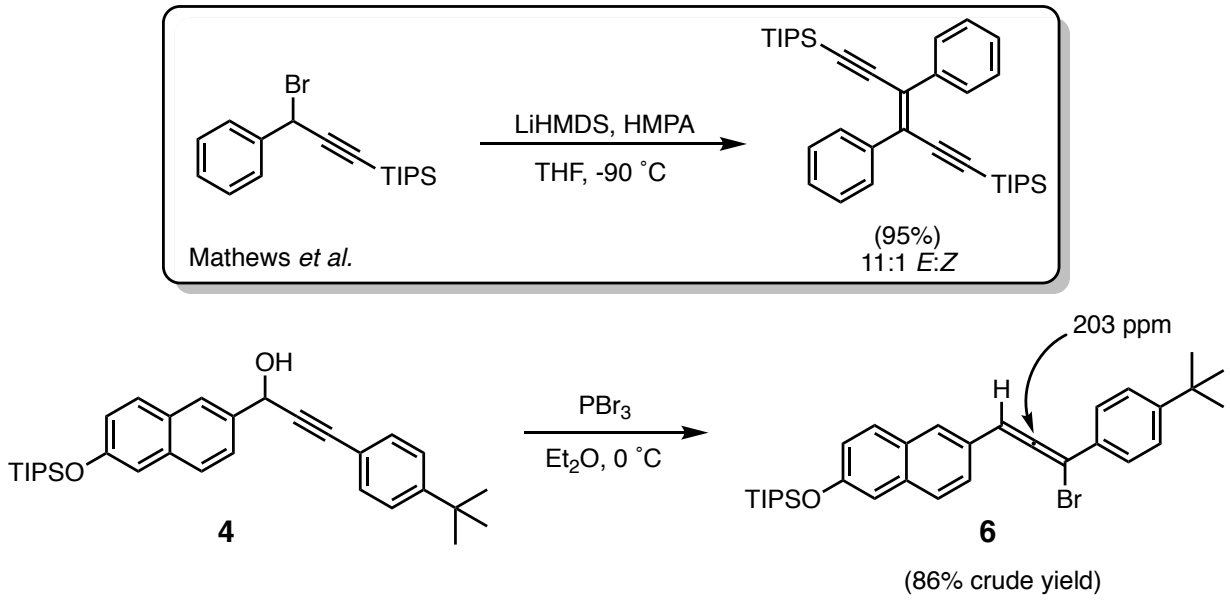

Figure 3.4. Synthetic route to *trans*-enediynes reported by Mathews *et al.* and unforeseen conversion of propargylic alcohol **4** to allenic bromide **6**.

Following closely the reported synthesis by Mathews *et al.*, we thought that protection of the terminal acetylenic carbon with a bulky triisopropylsilyl (TIPS) group should direct the incoming bromide nucleophile away from the alkyne terminus and towards the benzylic methine, preventing formation of the allene. To test our hypothesis, propargylic alcohol **7** was prepared in 69% yield in a preparation analogous to that of **4** (Figure 3.5). Treatment of compound **7** with PBr_3 provided clean conversion to the corresponding propargylic bromide **8**. Compound **8** is unstable on all tested chromatographic supports (SiO_2, alumina), likely due to rapid heterolysis of the C–Br bond. Although we were unable to purify compound **8**, conversion of propargyl alcohol **7** to bromide **8** is highly efficient and clean, therefore the decision was made to carry compound **8** into the dimerization reaction. Treatment of bromide **8** with 1.1 eq of LiHMDS and 1.1 eq of HMPA at –90 ˚C produced bis-naphthyl *trans*-enediyne **9** with excellent selectivity (19:1 *E*:*Z*) in 80% overall yield over two steps.

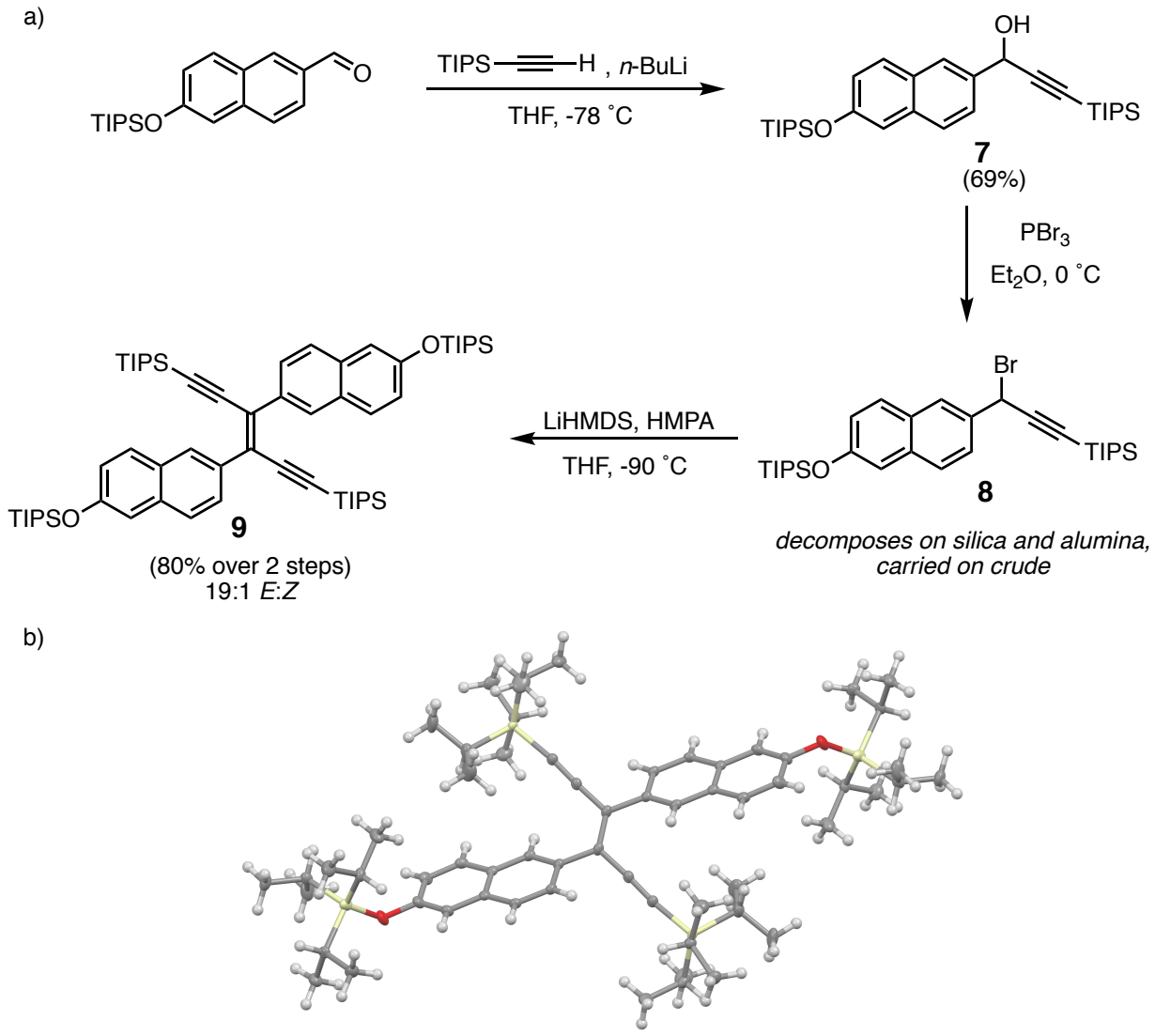

Figure 3.5. a) Synthetic route and b) X-ray crystal structure of dinaphthyl *trans*-enediyne **9**.

With dinaphthyl *trans*-enediyne **9** in hand, studies were undertaken to assess the propensity and selectivity of thermally-promoted Hopf cyclizations (Figure 3.6). Two different regioselective Hopf cyclizations are possible for compound **9** depending on whether the alpha (C1) or beta (C3) carbons of the naphthalene ring engage with the pendant enyne system. Tinnemans and Laarhoven have shown experimentally that upon photochemical irradiation, 2-substituted naphthalenes undergo Hopf cyclization at their alpha (C1) positions, although thermal and photochemical Hopf

cyclizations are believed to be mechanistically distinct.[10,11] Heating of compound **9** for 10 h at 300 ˚C produced the alpha-cyclization product **10** in 17% yield after purification by preparative thin layer chromatography (SiO_2, eluting with 10% $CHCl_3$ in hexanes). During the course of the reaction, the TIPS group initially attached to the alkyne group undergoing cyclization is lost. The low yield (17%) of compound **10** may not adequately reflect the efficiency of the reaction due to the preponderance of intermolecular byproducts produced from performing this reaction as a neat melt. In the future, it would be ideal to attempt the reaction using a gas-phase technique such as flash vacuum pyrolysis (FVP) to prevent intermolecular reactions from occurring (*vide infra*). This could provide better insight into the true efficiency of this reaction process.

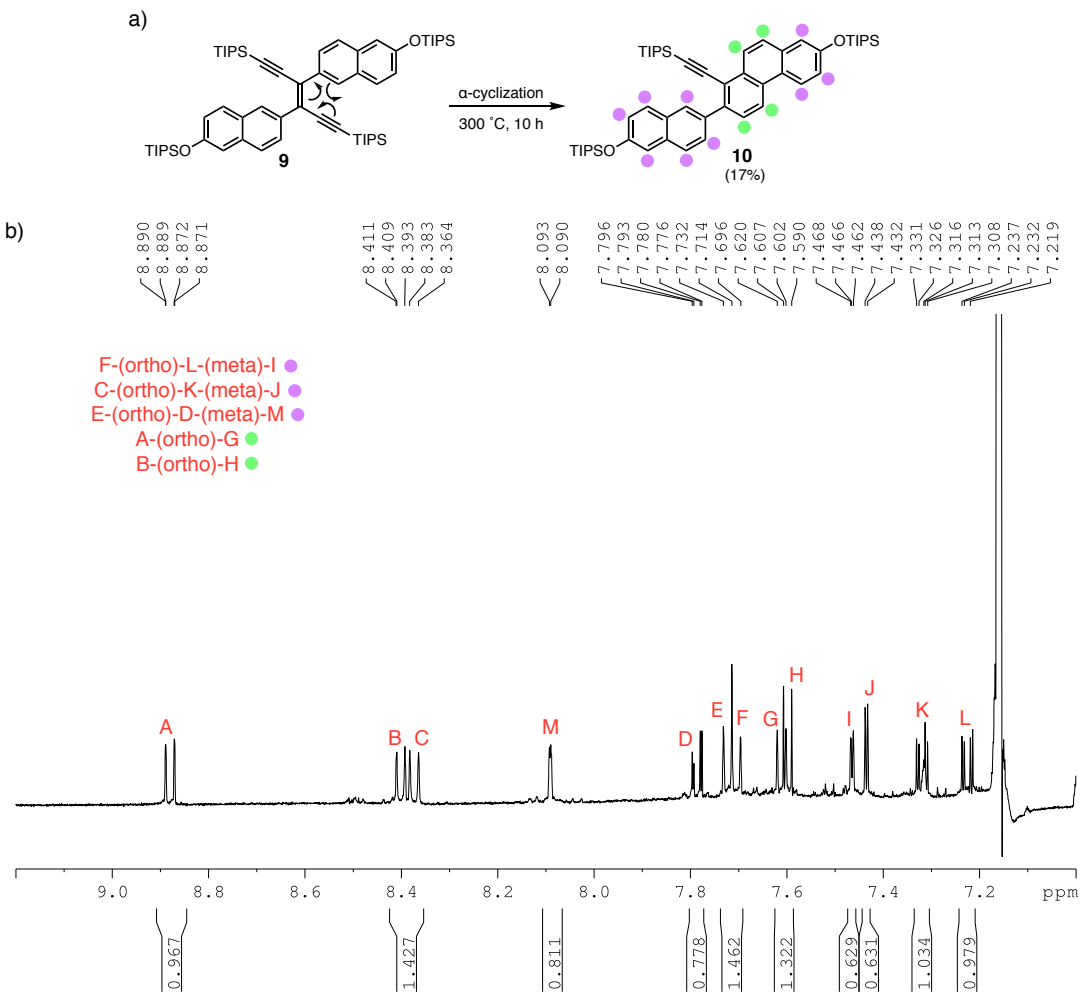

Figure 3.6. a) Experimental Hopf cyclization of dinaphthyl *trans*-enediyne **9** and b) ^{1}H NMR spectrum in C_6D_6.

Photochemical cyclization of di-naphthyl-trans-enediynes to diethynyl[5]helicenes

With access to preparative amounts of di-naphthyl *trans*-enediyne **9**, we sought to investigate the photochemical cyclization to complement the thermal study above. To facilitate separation of the isomeric products by silica gel chromatography, the bulky, non-polar TIPS protecting groups on the naphthol functions were replaced with methoxymethyl groups (MOM)

using two steps (Figure 3.7). Irradiation of bis-MOM-naphthyl *trans*-enediyne **12** with a 365 nm lamp overnight in hexanes produced a mixture of (*E*) **12** and (*Z*) **13** isomers of the starting enediyne as well as a product that had undergone a single cyclization. Careful analysis of the ^{1}H NMR spectrum of the cyclized compound showed it to be diethynyl[5]helicene **14**. The cyclization pathway is actually the well-known photochemical isomerization of *trans*-enediyne **12** to *cis*-enediyne **13** followed by photochemically promoted stilbene cyclization (Mallory reaction).[12] The Mallory reaction appears to be the most favorable cyclization kinetically and we never observed any photochemical Hopf cyclization under these conditions.

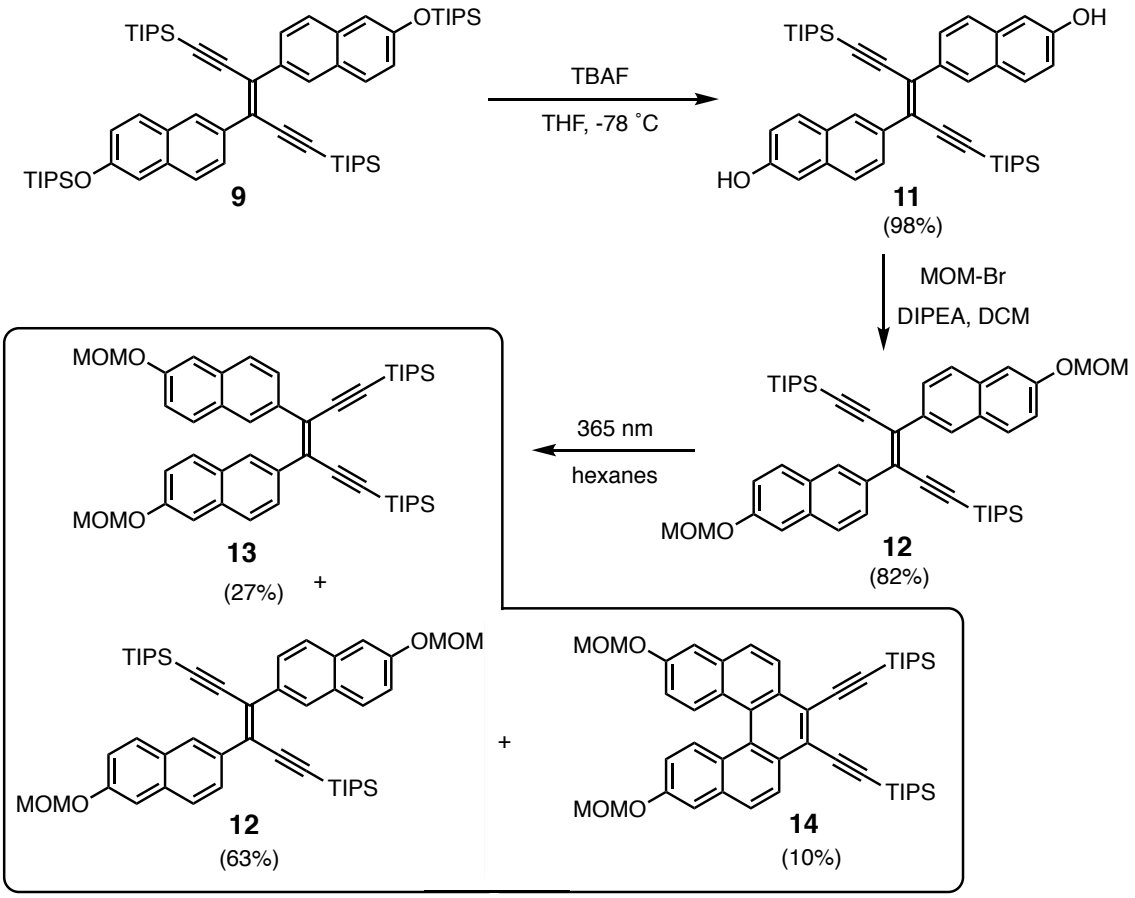

Figure 3.7. Synthesis of bis-MOM-naphthyl *trans*-enediyne **12** and photochemical cyclization to helicene **14**.

After our initial attempts to promote photochemical Hopf cyclization did not prove successful, we refocused our efforts on the optimization of the conversion of diaryl *trans*-enediynes to diethynyl[5]helicenes. *To our knowledge, this is the first example of a diaryl trans-enediyne undergoing a Mallory type cyclization*. An important improvement to the Mallory reaction was advanced by Katz *et al.,* who found that addition of iodine as a stoichiometric oxidant, with the use of propylene oxide to scavenge hydrogen iodide formed in the reaction, greatly improves the yield of this transformation.[13,14] Application of Katz's conditions to our system gave a greatly improved yield (76%) and allowed us to produce gram quantities of diethynyl[5]helicene **14**, which was used in the studies described later (Figure 3.8). It is important to note that diethynyl[5]helicene exists as a racemic pair of (*P*) and (*M*) atropisomers as no stereochemical templating occurs during the photocyclization.

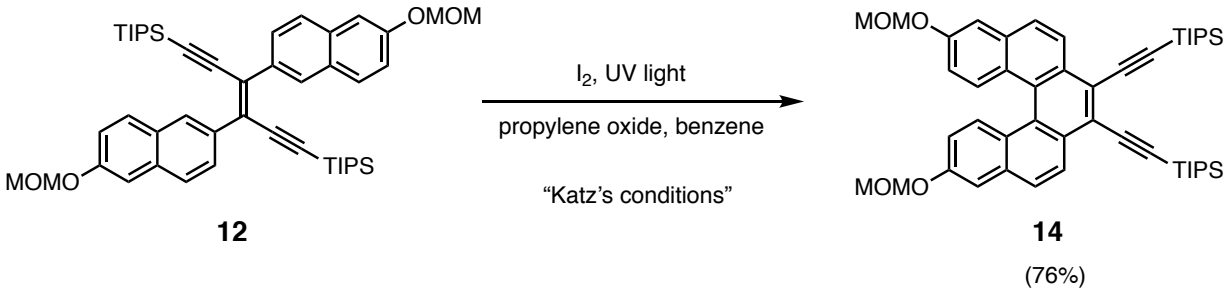

Figure 3.8. Photochemical cyclization of *trans*-enediyne **12** to diethynyl[5]helicene **14** using Katz's conditions.

Synthesis of diphenyl trans-enediynes, and their thermal, photochemical, and acid promoted cyclizations.

Access to a diphenyl *trans*-enediyne would follow an analogous route to the one developed for the formation of dinaphthyl *trans*-enediyne **9**. The addition of the lithium acetylide of triisopropylacetylene to 4-(triisopropylsilyloxy)benzaldehyde (**15**) provided propargylic alcohol

16 in 92% yield. This substrate was readily brominated and dimerized under the conditions developed by Mathews *et al.* to provide diphenyl *trans*-enediyne in high yield (78% yield over two steps) with complete selectivity for the (*E*) isomer.

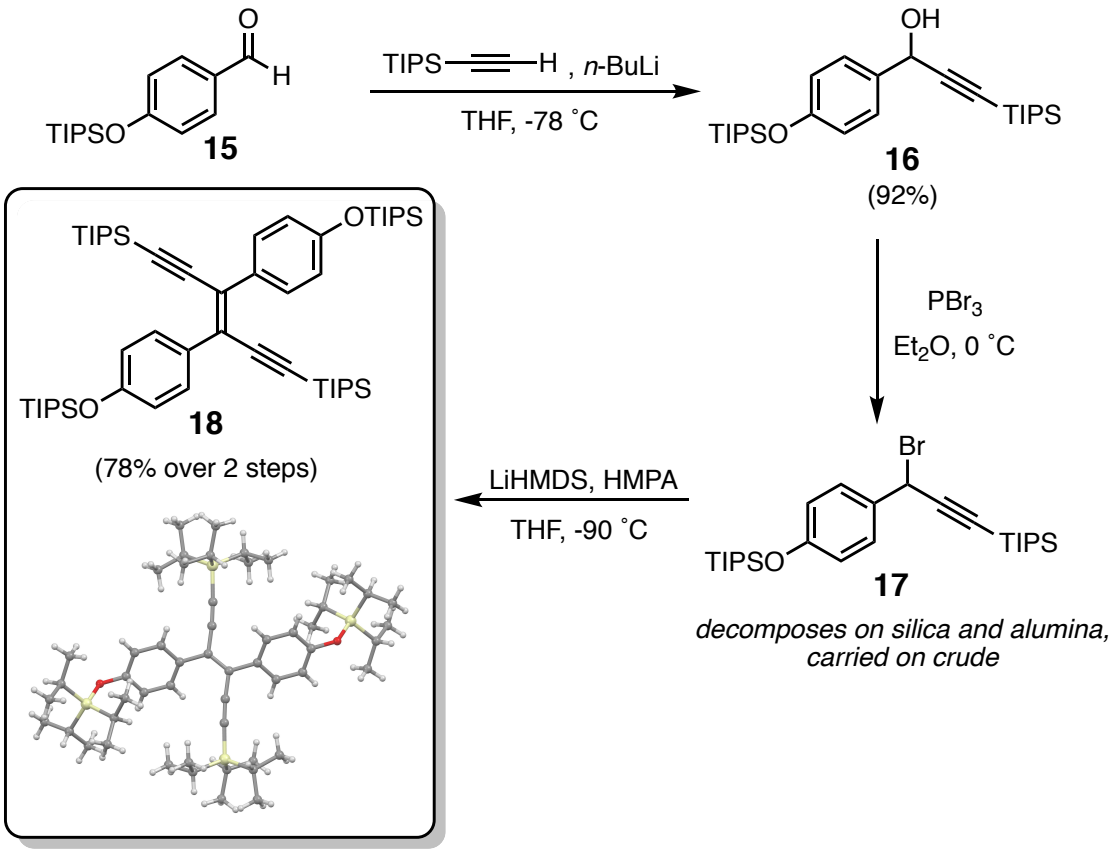

Figure 3.9. Synthesis and single crystal X-ray structure of diphenyl-*trans*-enediyne **18**.

Diphenyl *trans*-enediyne **18** was subjected to thermal and photochemical cyclizations conditions analogous to those described above for dinaphthyl *trans*-enediyne **9** (Figures 3.10 and 3.11). Heating of compound **18** in a sealed tube as a neat melt at 340 ˚C overnight produced the corresponding Hopf cyclization product **20** in 18% yield. Again, analogous to the thermal cyclization of compound dinaphthyl *trans*-enediyne **9**, the TIPS protecting group of the reacting

alkyne was lost. Although the yield for cyclization product **19** is low, it is the major compound of the crude mixture. Similar to compound **10**, the yield of this reaction most likely reflects competing intermolecular reaction pathways, such as oligomerization, and does not reflect the true efficiency of the process.

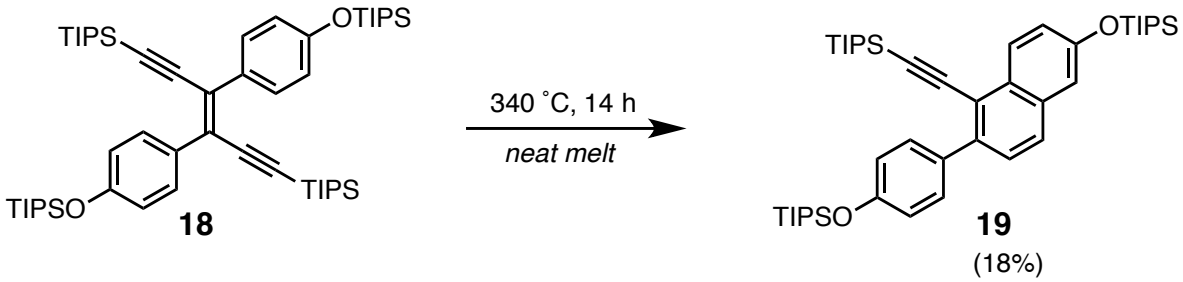

Figure 3.10. Thermal cyclization of diphenyl-*trans*-enediyne **18**.

Flash vacuum pyrolysis (FVP) is a synthetic technique that utilizes the dilute, gas-phase heating of molecules to preference intramolecular reaction pathways over intermolecular ones. During the course of his career, the lab of Larry Scott has championed the use of FVP for the synthesis of polycyclic aromatic hydrocarbons with unusual ring fusions and topology, typically via high-temperature pericyclic reactions.[15] Taking inspiration from the work of Scott, we believed that FVP may present ideal reaction conditions to probe the Hopf cyclization of compound **18** in a more suitable environment then a neat melt. Accordingly, crystalline **18** was placed at the end of a tube furnace, packed with quartz Raschig rings and held at a temperature of 700 ˚C, and the solid was slowly moved into the hot-zone to promote sublimation. We quickly noted that compound **18** did not readily sublime under vacuum, but instead melted and charred when placed in the hot-zone (Table 3.2, entry 1). To overcome the low volatility of compound **18**, the solution-spray flash vacuum pyrolysis (SSFVP) method was attempted.[16] This method utilizes a sprayed benzene

aerosol of the compound to be first frozen then sublimed quickly to facilitate the evaporation of compounds with high molecular weight and or low volatility. When SSFVP was utilized, we were able to successfully transfer amounts of **18** through the hot-zone held at 700 ˚C. Interestingly, at this temperature we only observed *cis*-*trans* isomerization of the internal stilbene-bond and no cyclization. When the hot-zone was heated further to 900 ˚C and SSFVP used, a large amount of an insoluble reflective-black material coated the inside of the tube and the quartz rings within it. The small amount of material that did condense beyond the hot-zone again only showed *cis*-*trans* isomerization and no Hopf products. We believe that the high molecular weight (885.67 g/mol) of compound **18** most likely contributes to its low volatility and makes FVP difficult. In the future, derivatives with lower molecular weights, and higher volatility, may provide better success in these types of experiments.

Table 3.2. FVP and SSFVP conditions used for the attempted thermal Hopf cyclization of compound **18**.

Entry	Conditions	Result
1	FVP (700 ˚C, 1 mTorr)	Material melted and charred within the tube
2	SSFVP (700 ˚C, 1 mTorr)	Isolated mixture of (*E*) and (*Z*) isomers of **18**, no Hopf cyclization to **19**
3	SSFVP (900 ˚C, 1 mTorr)	Isolated mixture of (*E*) and (*Z*) isomers of **18**, no Hopf cyclization, majority of material decomposed in tube to a black shiny solid.

Inspired by our initial success in the photochemical cyclization of dinaphthyl *trans*-enediynes, we believed that diphenyl *trans*-enediyne should undergo similar reactivity in a smooth

fashion. Photochemical cyclization of **18** using Katz's conditions gave the corresponding diethynylphenanthrene **20** in 92% yield (Figure 3.11). This proves to be an interesting access point to diethynylphenanthrenes that contrasts with their more classical preparation from the addition of Grignard reagents to phenanthrene quinone.[17] The high yield of this process allows for the generation of large amounts of diethynylphenanthrenes and we utilized this process to supply material for experiments described in below.

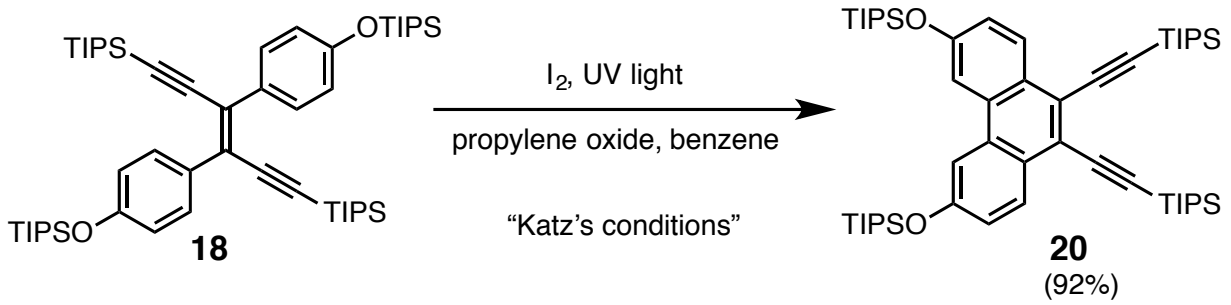

Figure 3.11. Photochemical cyclization of compound **20**

During the course of the previously mentioned cyclization experiments, the idea surfaced to test whether a strong Brønsted acid would promote cyclization of the enediyne via a different mechanism. Taking inspiration from the work of Swager, we hypothesized that strong Brønsted acids could protonate the alkyne function, leading to strongly electrophilic carbocations.[18] Importantly, we believed that the large steric bulk of the TIPS group may direct protonation away from the Si atom, giving an intermediate vinylic carbocation that would undergo a subsequent Friedel-Crafts reaction with the pendant aryl ring to give a hypothetical cyclization product (***hyp-23***) similar to that observed during thermal cyclization (Figure 3.12).

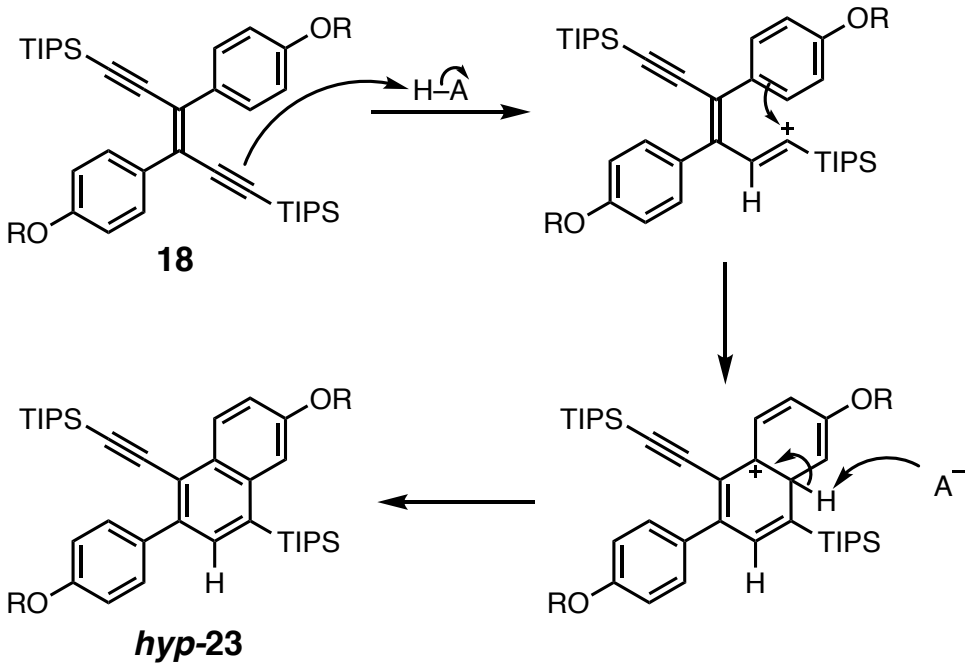

Figure 3.12. Intended mechanistic pathway for the acid-promoted cyclization of diphenyl *trans*-enediyne **18**.

Prior to conducting the key acid-catalyzed cyclization, the TIPS protecting groups on the two phenolic oxygens were removed and replaced with methyl groups using two synthetic steps (Figure 3.13a). Removal of the TIPS groups using TBAF and reaction of the resulting free phenols with methyl iodide under basic conditions produced bis(4-methoxyphenyl)-*trans*-enedinye **22**. Treatment of compound **22** with TfOH at –78 ˚C produced a single compound (**23**) in 60% yield. ^{1}H NMR analysis of this product showed that it had indeed undergone a cyclization event between one alkyne unit and one aryl ring, but structural assignment was difficult due to the lack of any distinctive NMR features. Thankfully, a single crystal suitable for X-ray analysis was grown and provided insight into the product structure and the regioselectivity of the cyclization (Figure 3.13b). The X-ray crystal structure of compound **23** proved that it was not the intended naphthalene product, but instead, benzofulvene **23**. Mechanistically, the pathway to benzofulvene **23** is similar

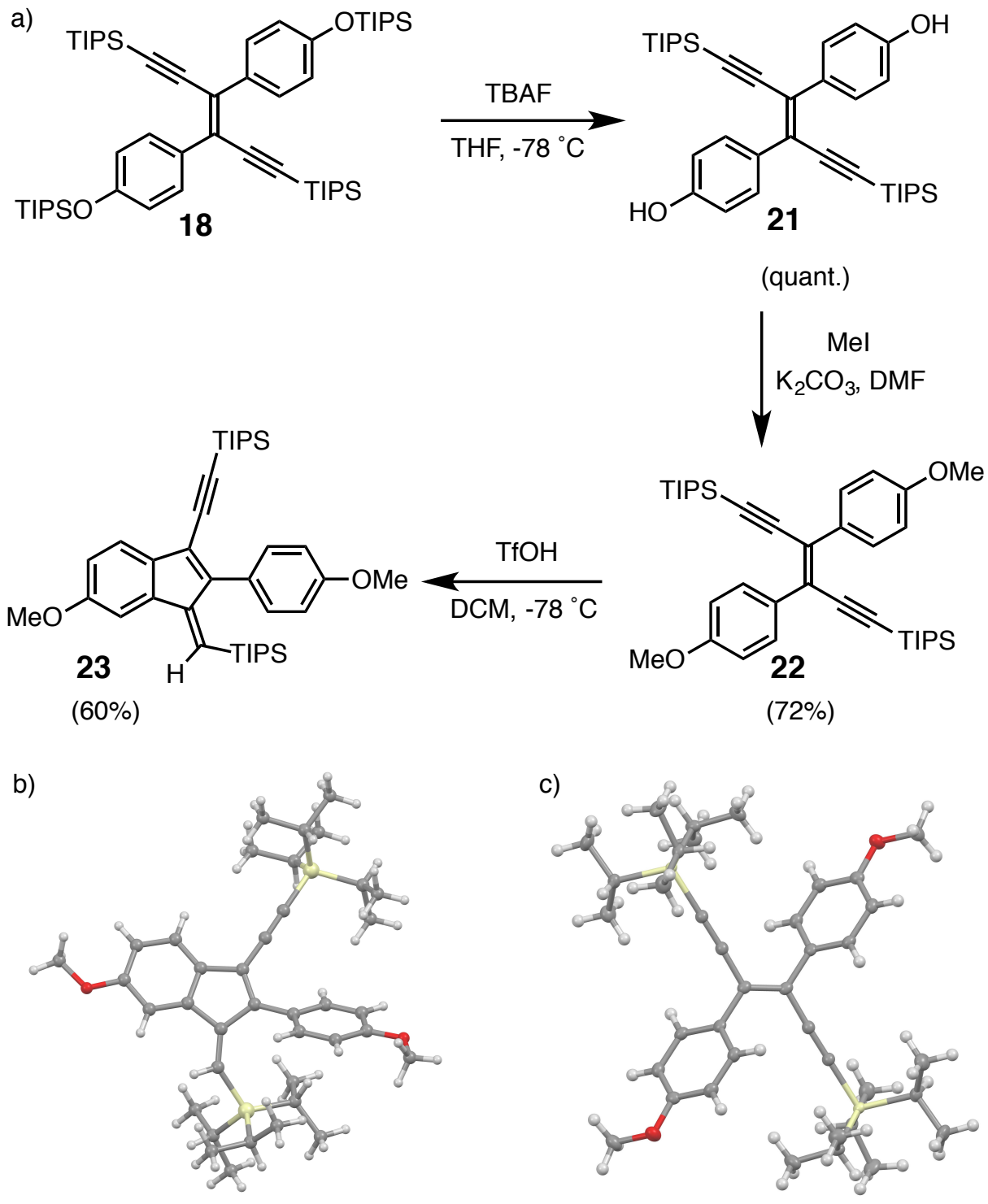

Figure 3.13. a) Synthesis of bis(4-methoxyphenyl)-*trans*-enediyne **22** and its acid catalyzed cyclization to ethynylbenzofulvene **23**. b,c) Single crystal X-ray structures of compounds **22** and **23**.

to that described in Figure 3.12, except that the initial protonation of the alkyne group occurs proximal to the TIPS group, not distal as we had hypothesized. One fascinating physical feature of compound **23** is that it is a deep orange solid. The near-visible absorption band for this molecule is unique compared to the other compounds discussed here, and the bathochromic shift of its absorption is most likely due to torsional strain around the benzofulvene exocyclic double bond (Figure 3.14). The X-ray crystal structure reveals a fairly large torsion angle (29˚) along the fulvene bond. Similar effects on visible-light absorption correlated to alkene torsional strain have been observed in a number of similar systems.[19,20]

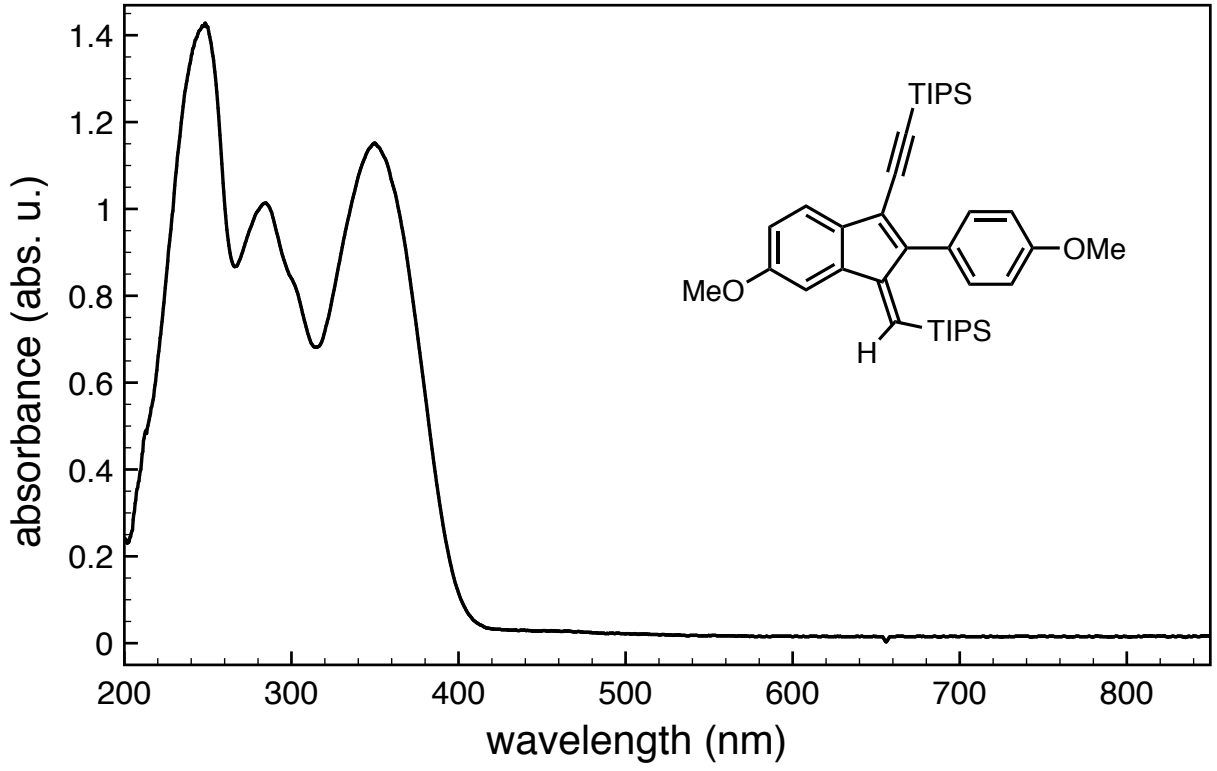

Figure 3.14. UV-Vis spectrum of compound **23** in hexanes.

In brief, diphenyl *trans*-enediynes are able to undergo three distinct annulation reactions depending on the reaction conditions. Importantly, in all annulation reactions, either one or both alkynes survive the transformation unaltered. These remaining alkyne groups should allow further annulations to occur if they can be promoted to react further. Further development of these processes could lead to syntheses of chrysenes, triphenylenes, dibenzofulvenes and possibly other complex polycyclic aromatic hydrocarbons.

Theoretical development of a synthetic route to armchair graphene nanoribbons via Bergman polymerization.

In the course of our work on the synthesis of diethynyl[5]helicene **14**, we were intrigued by the idea that formal Bergman polymerization of such a compound could in principle give access to substituted poly-phenylene polymers, which would be ideal access points for $_A$GNRs (Figure 3.15a). In 1994, Tour *et al.* reported the synthesis of polyphenylene and polynaphthylene polymers from simple *cis*-enediynes via high-temperature Bergman polymerization.[21,22] In the course of their work, preliminary kinetic experiments appeared to indicated a step-growth mechanism for the polymerization. Also, infrared spectroscopic analysis of their polymers seemed to imply that the polymer backbone only contained 1,4-disubstituted benzene rings (Figure 3.15b). In 2003, the group of Adam Matzger reported the synthesis of a simple polynaphthylene polymer via two mechanistically distinct routes, namely a nickel catalyzed Kumada coupling, and a Bergman polymerization under the same conditions as used by Tour.[23] Utilizing a combination of pyrolytic GC-MS, solid-state NMR, and MALDI-TOF MS, they concluded that, contrary to Tour, the backbone of the poly-naphthylene produced via Bergman polymerization likely contains a complex mixture of 1,4-benzene, benzofulvene and stilbene-like linkages (Figure 3.15c).

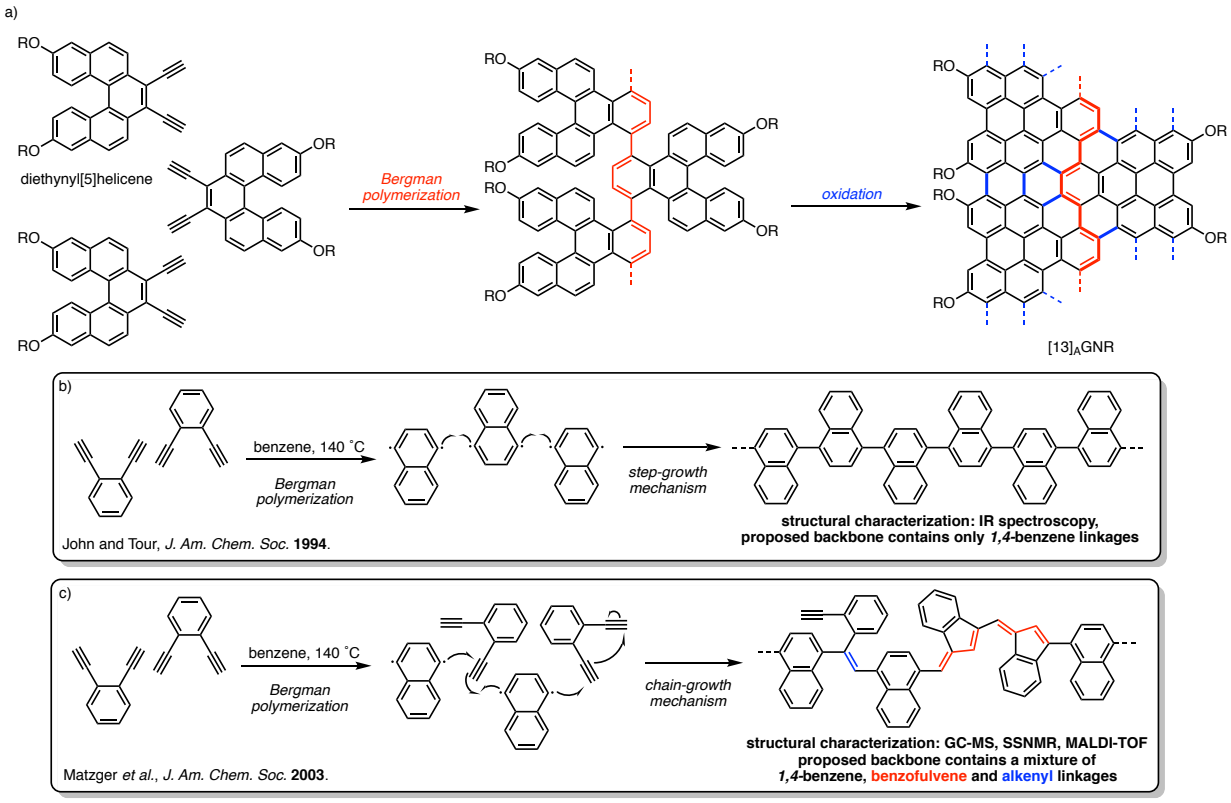

Figure 3.15. a) Theoretical approach to [13]$_A$GNRs via Bergman polymerization of diethynyl[5]helicenes. b,c) Previous contradicting studies on the true nature of polynaphthylene polymers produced through Bergman polymerization.

Our approach to $_A$GNRs via *cis*-enediynes would only be successful if the polymerization reaction was completely selective in producing a polymer with 1,4-benzene linkages in the backbone. Any amount of benzofulvene or alkenyl linkages along the polymer backbone would inhibit oxidative cyclization to a pristine $_A$GNR. With large quantities of bis-MOM diethynyl[5]helicene **14** in hand, we decided to attempt the Bergman cyclization induced polymerization of this compound and examine the resulting polymer by NMR spectroscopy. Deprotection of the alkynyl TIPS groups using TBAF furnished the expected diethynyl[5]helicene **24** in 94% yield (Figure 3.16a). This material was heated overnight in benzene at 180 ˚C to produce

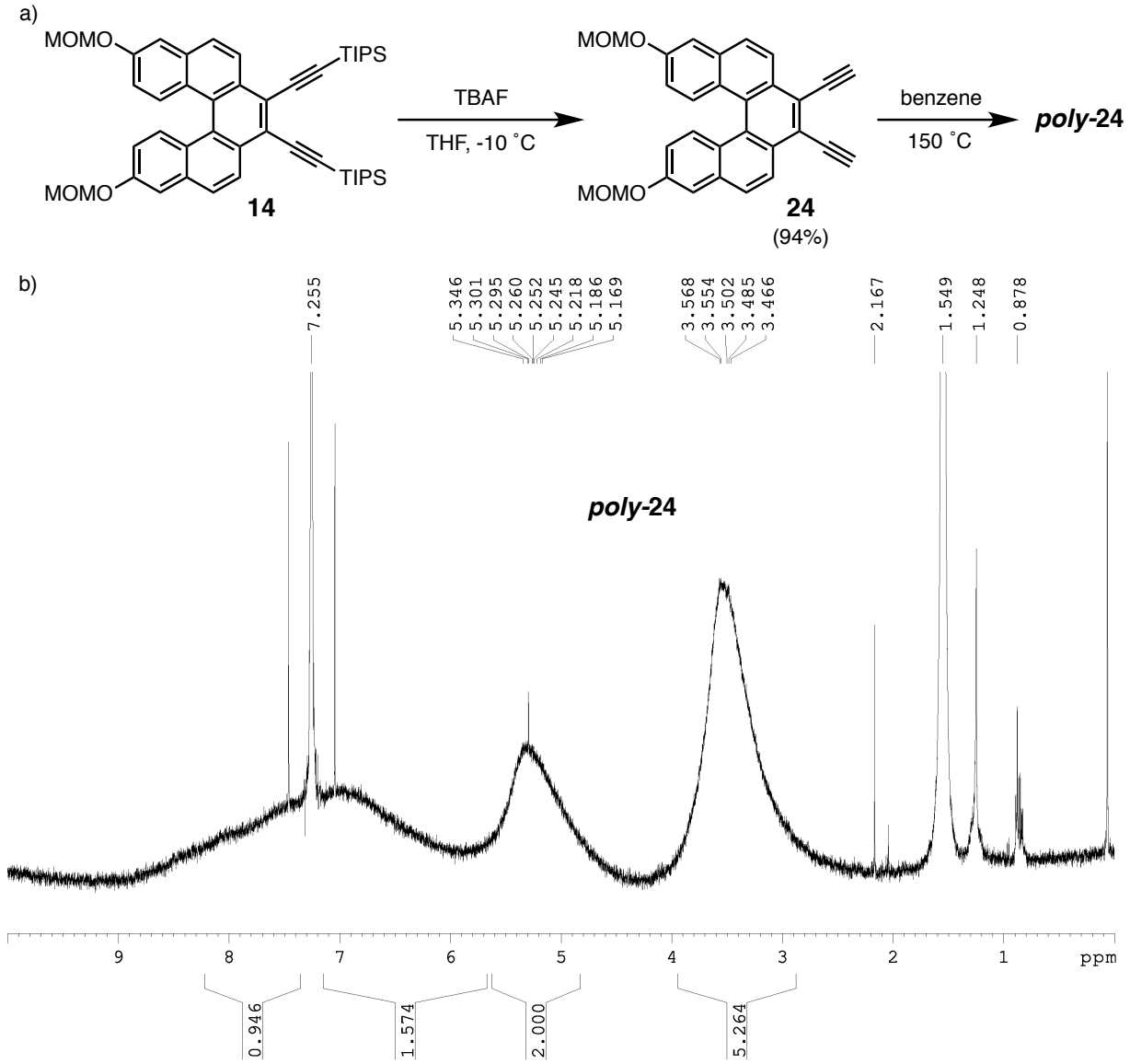

Figure 3.16. a) Synthesis of diethynyl[5]helicene **24** and its corresponding polymer ***poly*-24** and b) the ^{1}H NMR spectrum of ***poly*-24**.

polymer ***poly*-24**. ^{1}H NMR analysis of ***poly*-24** showed only three extremely broad peaks that correspond to the four helicene aryl protons, and the methylene and methyl group of the MOM protecting group (Figure 3.16b). As noted above, the photocyclization of *trans*-enediynes produces

a racemic mixture of (*P*) and (*M*) [5]helicenes. Accordingly, ***poly*-24** is likely an atactic polymer with a random distribution of the (*P*) and (*M*) [5]helicenes along its length. Because of this, we are unable to confidently determine whether the broad nature of our NMR spectrum is due to the atacticicity or backbone linkages of the polymer.

Taking the contrasting views of Tour and Matzger, as well as our preliminary NMR data from the polymerization of diethynyl[5]helicene into account, we saw a unique opportunity to contribute to the understanding of the mechanistic process behind the Bergman polymerization. We anticipated that early termination of the polymerization using a good hydrogen radical donor such as 1,4-cyclohexadiene, could allow us to isolate small oligomers that would provide a unique window into the polymerization process. In planning these oligomerization experiments we decided that the diethynyl[5]helicenes would not be ideal substrates to form oligomers due to the unnecessary complication of spectra from mixtures of (*P*) and (*M*) atropisomers. Having recently developed a concise synthesis of diethynylphenanthrenes from diphenyl-*trans*-enediynes, we believed that they presented a great opportunity to investigate this question in a relevant system.

Synthesis and structural determination of oligomers formed during Bergman polymerization.

In the preceding section, we described the conceptual development of a synthetic route to $_{A}$GNRs via Bergman polymerization of aryl *cis*-enediynes (Figure 3.15a) as well as the controversial nature behind the discrete mechanism of polymerization. To this end, we sought to use a *cis*-enediyne monomer that would allow our results to be easily understood in the context of the previous reports by Tour and Matzger. To begin, the simple *cis*-enediyne 1,2-diethynyl-4,5-dipropoxybenzene (**28**) was prepared in four synthetic steps from catechol in 61% overall yield (Figure 3.17). This specific monomer was chosen to produce polymers structurally similar to those

made by Tour and Matzger. Also, the *n*-propyloxy groups were used to provide better solubility to the intermediate oligomers, so that they could be separated using chromatography.

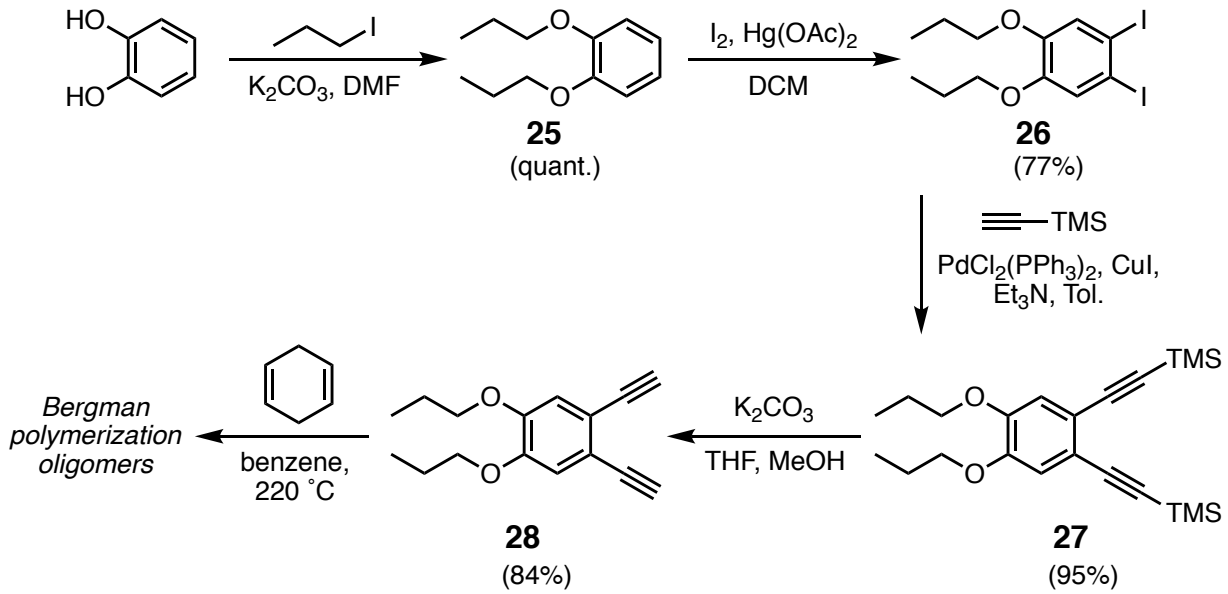

Figure 3.17. Synthesis of *cis*-enediyne **28** from catechol and oligomerization conditions.

With *cis*-enediyne **28** in hand, 1,4-cyclohexadiene (CHD) was chosen as the H atom donor in the reaction due to its well understood reactivity and history of use in the Bergman reaction.[24,25] Compound **28** was heated with 1.5 eq CHD as a degassed solution in benzene at 220 ˚C overnight in a pressure tube. In the morning, removal of the volatiles and purification over silica gel chromatography gave a series of mixed fractions that contained compounds resulting from the reaction of one *cis*-enediyne unit (monomer adducts), two *cis*-enediyne units (dimers) and higher oligomers (trimers and larger). The main component within the monomeric adducts was the simple Bergman product naphthalene **29**. Most interesting was the fraction containing the dimers which showed two predominant products. The dimeric products were separated by preparative TLC and their structures elucidated using NMR spectroscopy (Figure 3.18a).

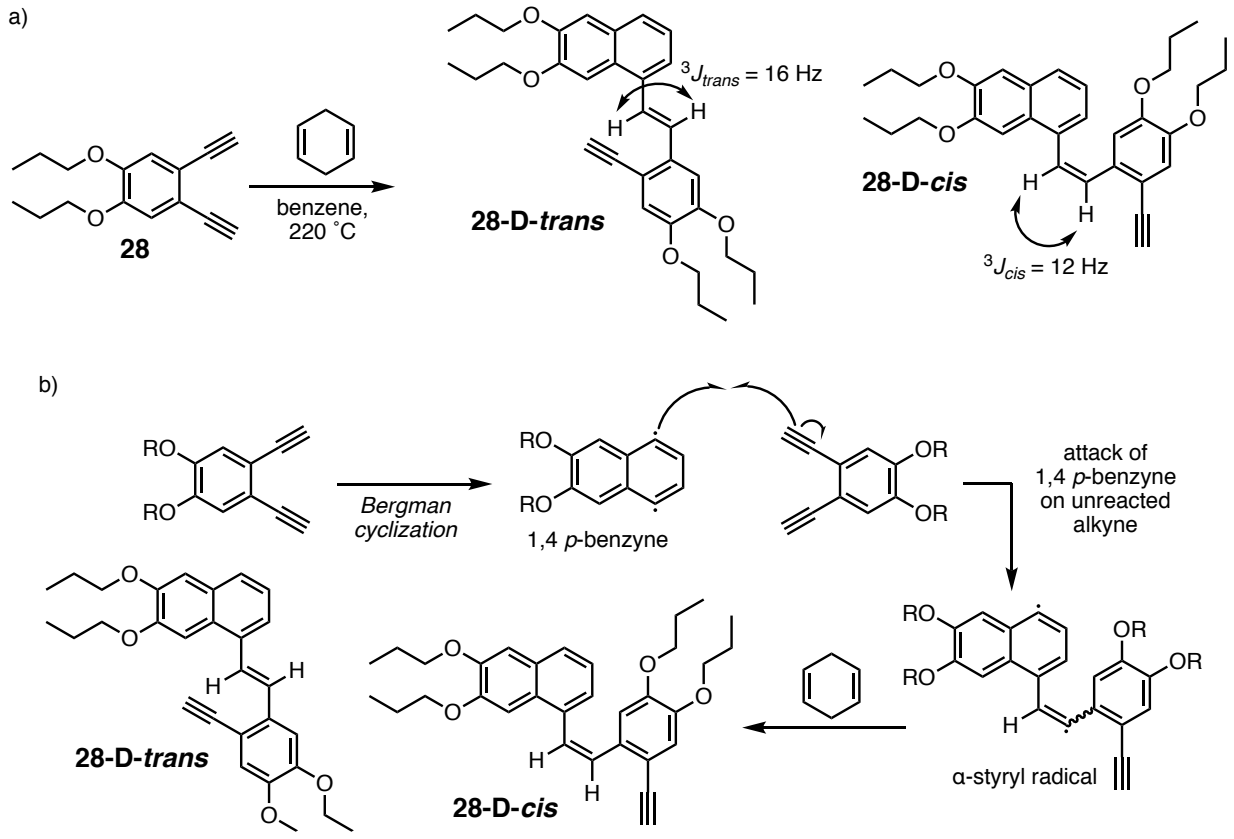

Figure 3.18. a) Synthesis and structures of dimeric products (**28-D-*trans*** and **28-D-*cis***) and b) the mechanistic route explaining their formation.

Careful structural assignment of the dimeric products proves them to be *cis* (**28-D-*cis***) and *trans* (**28-D-*trans***) isomers of an oxygenated styrylnaphthalene. The mechanism to explain the formation of these dimers is fascinating. The first step of the mechanism is the Bergman cyclization of an individual monomer to produce the 1,4-benzyne biradical. Then, the 1,4 *p*-benzyne biradical undergoes intermolecular addition to the alkyne of an unreacted monomer, giving an α-styryl radical intermediate. This intermediate undergoes radical termination of its styryl and aryl radicals with CHD to give the observed products. As stated above, dimers **28-D-*cis*** and **28-D-*trans*** are the predominant dimeric products. In direct support of this mechanism, previous reports have documented that heteroatom radicals undergo addition on aryl acetylenes producing α-styryl

radicals with good selectivities.[26] This mechanism implies a chain-growth pathway for polymerization and not the step-growth as asserted by Tour.[21]

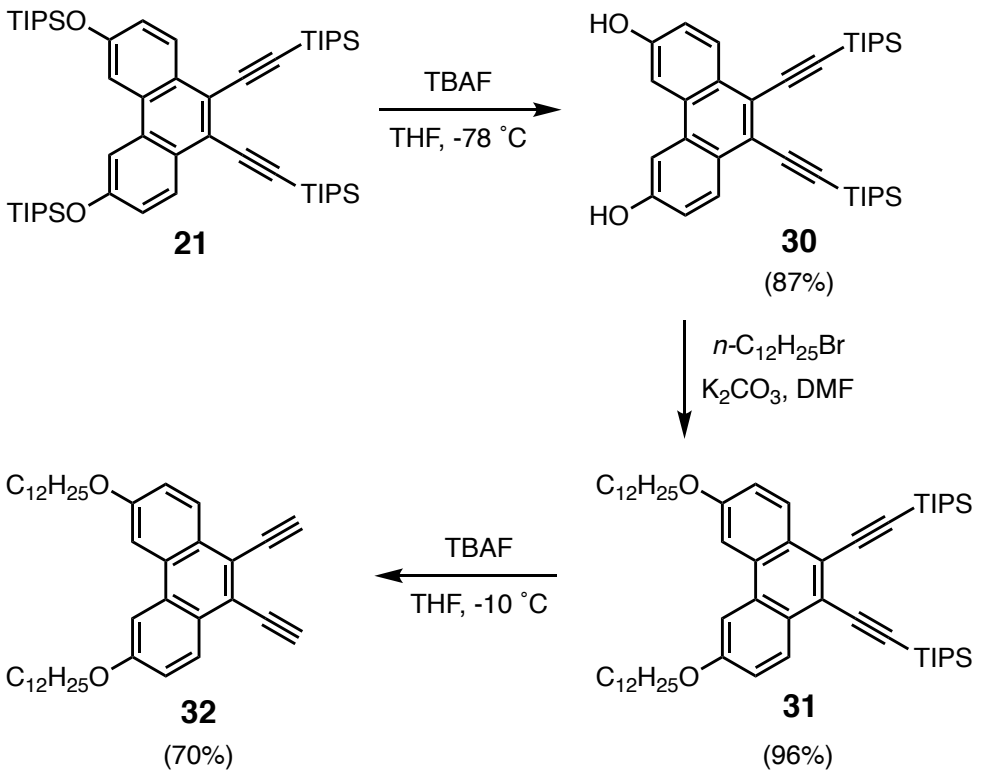

Figure 3.19. Synthesis of diethynylphenanthrene **32**.

Inspired by our success with the isolation of dimeric products of this simple system, we forayed into the oligomerization of a more complex system based on diethynylphenanthrene **21**. To do so, we synthesized didodecyl-diethynylphenanthrene **32** from tetra-TIPS-diethynylphenanthrene **21** in three synthetic steps and 58% overall yield (Figure 3.19). Large dodecyl chains were used to provide adequate solubility to the oligomers and aid in chromatographic separation. Monomer **32** was subjected to polymerization conditions similar to that for compound **28**, reacting with 5 eq of CHD at 180 ˚C in benzene overnight. This produced a complex mixture of oligomers

that was subjected to initial flash column chromatography on SiO_2 to separate the mixture into three smaller fractions containing monomeric, dimeric and higher products, which were each further purified by preparative TLC.

The major product of the mixture containing monomer adducts was the intended triphenylene **33** as well as a small amount of 9-ethynyl-10-vinylphenanthrene **34** (Figure 3.20a). Compound **34** is quite interesting from a mechanistic point of view and provides a window into the oligomerization reaction conditions. The formation of 9-ethynyl-10-vinylphenanthrene **34** likely occurs through the addition of two hydrogen atom radicals to the alkyne producing a net hydrogenation of one of the carbon-carbon π-bonds. The formation of this product demonstrates that at 180˚C, 1,4-cyclohexadiene undergoes decomposition to hydrogen radicals at a significant rate. Previous studies have measured an appreciable rate of thermal decomposition of CHD, although at much higher temperatures (250˚C to 620 ˚C).[27] In contrast to the stereoisomeric dimer products produced in the simpler system, a single dimer product (**35**) was isolated in the reaction of **32**. 2D NMR techniques (COSY, TOCSY, NOESY, HSQC, and HMBC) were utilized to elucidate the exact structure of dimer **35**. Specifically, key NOESY and HMBC correlations were essential to determine which of two regioisomeric products (**35** or ***regio*-35**) had formed (Figure 3.20b). The mechanism behind the formation of dimer **35** is analogous to that of pathway B above and is depicted in Figure 3.20b. An initially formed 1,4-benzyne biradical undergoes intermolecular addition to the alkyne of another monomer producing an intermediate α-styryl radical. Addition of this radical to a π-bond of a neighboring aryl ring produces a new six-membered ring and a corresponding resonance-stabilized radical. Finally, a formal H atom transfer gives isolated dimer **35**. The group of Alabugin has demonstrated the addition of carbon-centered radicals to pendant aryl rings to be kinetically favorable in both theory and experiment.[28]

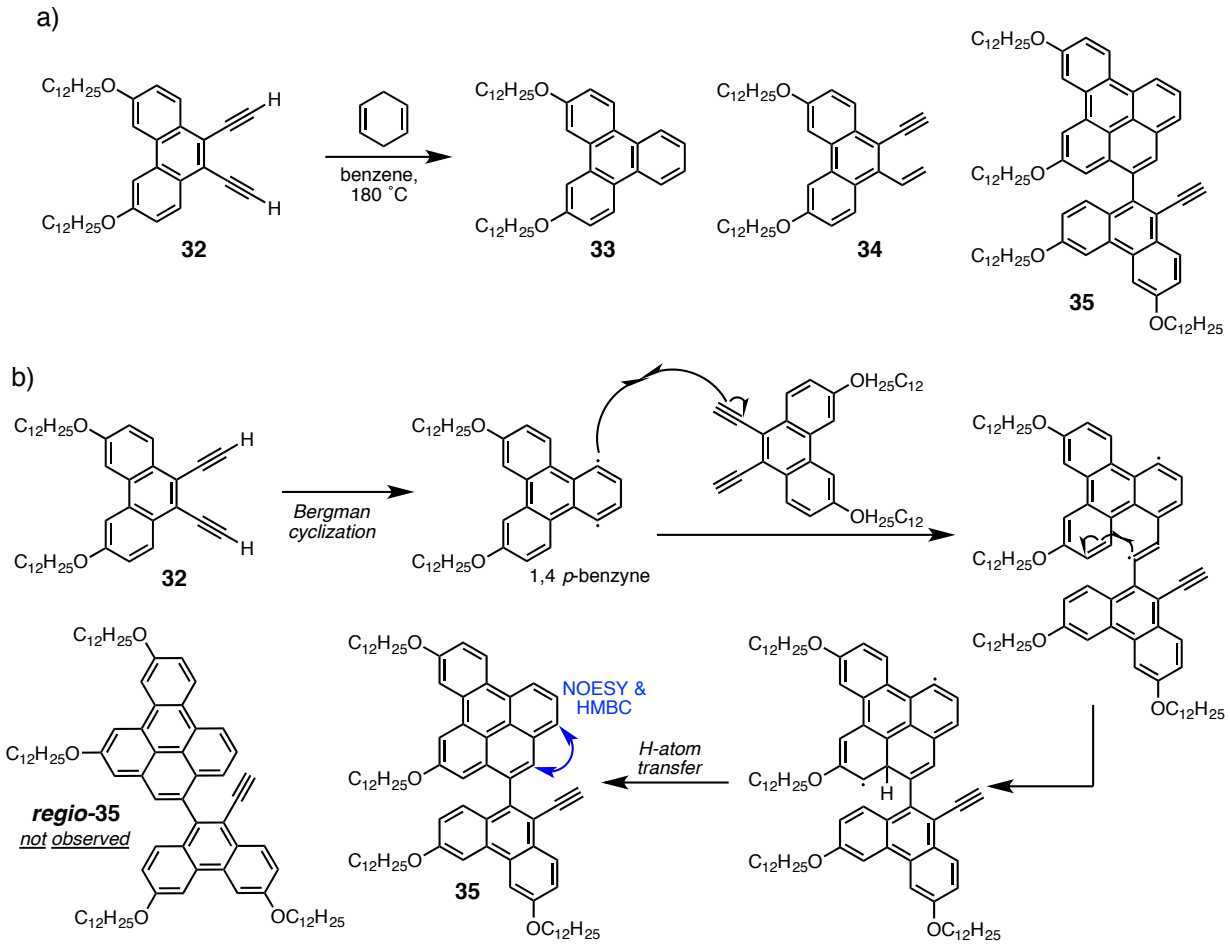

4

Figure 3.20. a) Oligomerization of diethynylphenanthrene **32** and b) proposed mechanism for the formation of dimeric product **35**.

Taking into account the formation of dimer products **28-D-*trans***, **28-D-*cis***, and benzophenanthrene **35**, it is possible to make some fundamental conclusions about the Bergman polymerization process:

(1) The process does not occur via a step-growth mechanism, but rather a chain-growth mechanism, in contrast to the conclusion by Tour. The dimeric products isolated herein

have all undergone reaction of 1,4-benzyne with an unreacted *cis*-enediyne moiety, which the formation of dimer **35** demonstrates conclusively. If a step-growth mechanism was operative, we would expect that the dimers resulting from combination of two individual 1,4-benzyne radicals (i.e. either binaphthyl and bitriphenylene) would be the predominantly isolated dimeric products. *This is not the case.* Thus, even without the presence of CHD, we can be confident that the reaction takes place via a chain-growth mechanism.

(2) The polymer produced should not contain a polyphenylene type backbone consisting of only six membered rings, but an assortment of phenyl, benzofulvyl, and styryl units. Due to the chain-growth mechanism of this process, a definite structure for the polymer cannot be elucidated easily. The formed polymer likely contains a complex polymer backbone with a random assortment of *p*-phenyl, benzofulvyl and styryl linkages, leading to the complex nature of its NMR spectra (e.g. Figure 3.16b), complicating any definite structural assignment at this point.

(3) Due to the lack of a well-defined and predictable structure, the Bergman polymerization cannot be used to form $_{A}$GNRs as proposed.

Our results, taken together with the report by the group of Matzger demonstrate that Bergman polymerization is not likely to be a successful access point to $_{A}$GNRs.[23] This synthetic approach could be successful if 1,4-benzyne biradicals formed in the Bergman reaction could be trapped in high yield with a suitable cross-coupling partner, for example a halogen, triflate, or boronate group, to carry out metal-catalyzed cross coupling reactions. This would produce monomer units that could still provide access to the targeted intermediate polymers en route to $_{A}$GNRs. Future work in the group will focus on this goal.

Section 3.3: Conclusion

In conclusion, diaryl *trans*-enediynes have proven to be a versatile platform for the formation of differentially annulated PAHs. The regioselectivity of the annulation can be controlled via the reaction conditions. These transformations currently allow expedient access to diethynyl [5]helicenes and phenanthrenes and may allow for the formation of even larger fused-aromatic systems. We also proposed a possible new approach to $_A$GNRs via the Bergman polymerization of *o*-diethynyl aromatic compounds. Confusion in the literature over the exact mechanism and backbone structure of the polymerization led us to investigate these questions through early termination of the polymerization and analysis of the formed oligomers. Structural elucidation of these oligomers illuminated the true nature of the polymerization mechanism and structure of the polymer backbone. We have concluded that our results show that the Bergman polymerization cannot act as an access point to $_A$GNRs in its current form.

Section 3.4: Outlook

The results reported above have led to the answering of some specific questions and the development of many more. Due to the work already concluded, we are proposing future studies that may prove fruitful in the near future. One major idea is to utilize the facile synthesis of diaryl *trans*-enediynes as a new access point to diaryl PDA polymers for graphitization to GNRs (Figure 3.21). Recently, the group of Yang Qin described the development of new molybdenum catalysts that formed soluble polydiacetylenes from alkyne metathesis of *trans*-enediynes.[29] Utilizing an alkyne metathesis strategy would allow us to avoid the necessity of solid-state polymerization reactions to form PDA polymers. This would allow much more freedom in the design of PDA

polymers and could allow for the specific incorporation of heteroatoms and solubilizing groups. Current PDA polymers produced from solid-state polymerization typically display abysmal solubility in common solvents, which is a major hindrance to their application in device manufacturing. This new access point to PDA polymers may solve some of the current limitations with our recently developed diarylbutadiyne to GNR process.

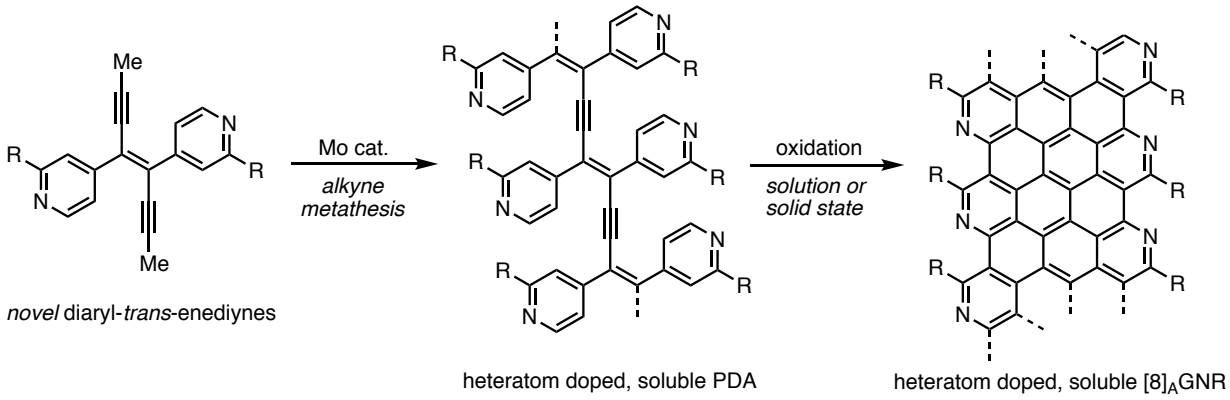

Figure 3.21. Proposed synthesis of heteroatom doped $[8]_A$GNRs via alkyne metathesis of diaryl-*trans*-enediynes.

Diaryl-*trans*-enediynes could also be used as access points to GNRs with novel edges and structures via Hay polymerization and oxidation (Figure 3.22). Hay polymerization of diaryl-*trans*-enediynes would produce polytriacetylene polymers (PTA), a polymer class much less explored then their polydiacetylene brethren. Oxidation of these PTA polymers, either in solution or in the solid-state, would produce an interesting new class of GNRs with novel *fjord* edges that are yet unreported in the literature. The *fjord* edge also provides an interesting opportunity for heteroatom incorporation to provide GNRs that contain metal binding cavities. Metal doping of these GNRs could provide a ground-breaking way to tune the inherent GNR bandgap and also provide GNRs that act as sensors for specific metal or organic cations.

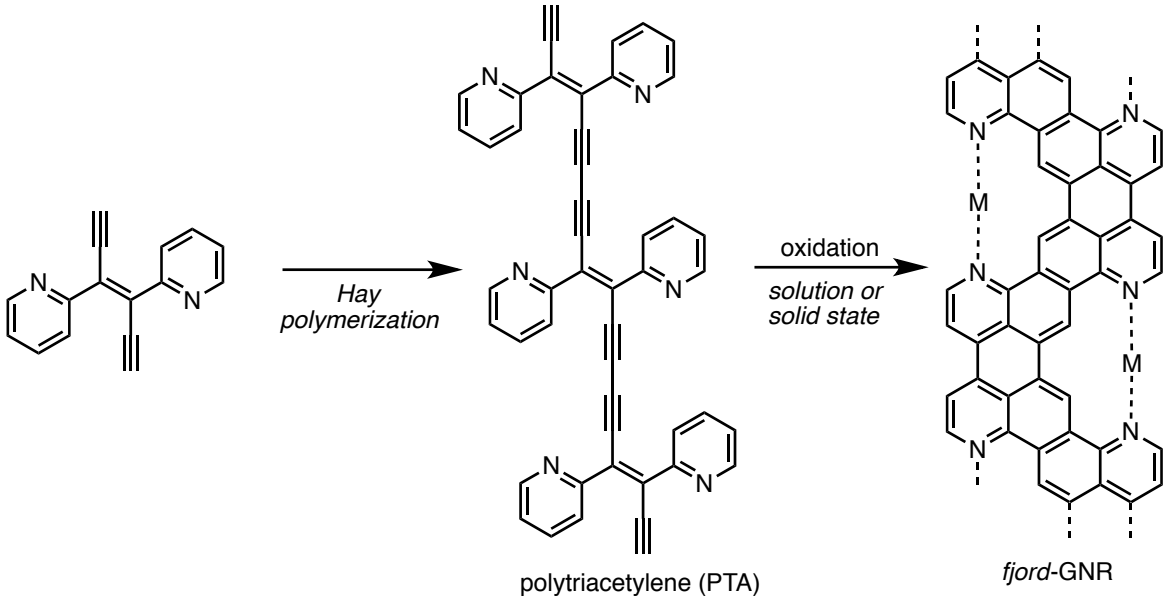

Figure 3.22. GNRs with novel edges (*fjord*-GNR) formed from polymerization of diaryl-*trans*-enediynes and subsequent oxidation.

Section 3.5: Experimental

General Procedures: Unless stated otherwise, reactions were performed under an argon atmosphere in flame-dried glassware. Tetrahydrofuran (THF), methylene chloride (CH_2Cl_2), diethyl ether (Et_2O), toluene (C_7H_8), and acetonitrile (CH_3CN) were passed through activated alumina columns prior to use. Chemical reagents were obtained from commercial sources and used without further purification. Reaction temperatures were controlled using an IKA magnetic stirplate with a temperature modulator and oil bath. Procedures were performed at room temperature (~23 ˚C) unless otherwise indicated. Column chromatography was performed on Silicycle (Siliflash P60) silica gel 60 (240-400 mesh). Thin layer chromatography utilized pre-coated plates from E. Merck (silica gel 60 PF254, 0.25 mm).

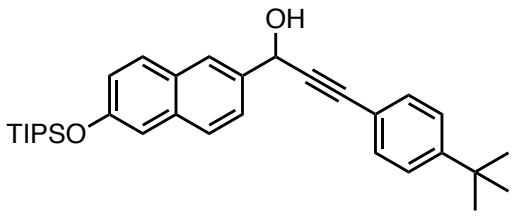

3-(4-(*Tert*-butyl)phenyl)-1-(6-((triisopropylsilyl)oxy)naphthalen-2-yl)prop-2-yn-1-ol (4)

To a flame-dried round bottom flask equipped with a stir bar was added 1-(*tert*-butyl)-4-ethynylbenzene (2.3 g, 14.5 mmol, 1.9 eq) followed by THF (15 mL). The mixture was cooled to -78 ˚C and a 1.8M solution of *n*-BuLi (6.4 mL, 11.6 mmol, 1.5 eq) in hexanes was added dropwise at -78 ˚C. The mixture was allowed to stir for 10 min. and then 6-((triisopropylsilyl)oxy)-2-naphthaldehyde (20.6 g, 62.7 mmol, 1 eq) was added as a solution in THF (15 mL) dropwise at -78 ˚C. The resulting mixture was allowed to stir at -78 ˚C for 10 min. and then allowed to warm to room temperature. Upon reaching room temperature the mixture was quenched by the addition

of saturated NH_4Cl (100 mL). The mixture was diluted with Et_2O and then transferred to a separatory funnel. The layers were separated and the aqueous layer extracted with fresh Et_2O twice. The organics were pooled, washed with water x3, brine x3, dried over $MgSO_4$, filtered and concentrated *in vacuo* to produce a crude oil which was purified by filtration over SiO_2 eluting with a gradient of 0% to 100% $CHCl_3$ in hexanes. This produced 2.1 g (56%) of the product **4** as a light yellow oil. ^{1}H NMR (500 MHz, $CDCl_3$) δ 8.07 – 7.90 (m, 1H), 7.81 – 7.70 (m, 2H), 7.66 (dd, *J* = 8.5, 1.8 Hz, 1H), 7.44 (d, *J* = 8.5 Hz, 1H), 7.35 (d, *J* = 8.5 Hz, 2H), 7.23 (d, *J* = 2.4 Hz, 1H), 7.15 (dd, *J* = 8.7, 2.4 Hz, 1H), 5.81 (d, *J* = 6 Hz, 1H), 2.29 (d, *J* = 6 Hz, 1H), 1.32 (m, 12H), 1.13 (d, *J* = 7.4 Hz, 18H). ^{13}C NMR (126 MHz, $CDCl_3$) δ 154.52, 152.06, 136.06, 134.74, 131.65, 129.75, 128.88, 127.48, 125.57, 125.48, 125.21, 122.63, 119.57, 114.59, 88.26, 87.08, 65.53, 31.74, 31.31, 18.11, 12.86. HRMS (DART) Calculated for $C_{32}H_{43}O_2Si$ $[M+H]^+$: 487.30268, found 487.29969.

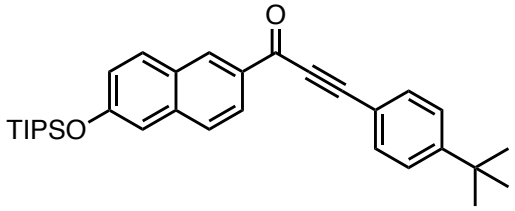

3-(4-(*tert*-Butyl)phenyl)-1-(6-((triisopropylsilyl)oxy)naphthalen-2-yl)prop-2-yn-1-one (5)

3-(4-(*tert*-butyl)phenyl)-1-(6-((triisopropylsilyl)oxy)naphthalen-2-yl)prop-2-yn-1-ol (**4**) (2 g, 4.3 mmol, 1 eq) was added to a round bottom flask with a stir bar and dissolved in DCM (22 mL, 0.2M). Manganese dioxide (1.13 g, 12.9 mmol, 3 eq) was added in a single portion and the reaction was allowed to stir at room temperature until judged complete by TLC. Upon completion of the reaction the mixture was filtered over celite and concentrated *in vacuo*. The crude residue was subjected to chromatography over SiO_2 eluting with a gradient of 0% to 4% EtOAc in hexanes.

This produced 1.8 g (90%) of the product **5** as a yellow oil. ^{1}H NMR (500 MHz, $CDCl_3$) δ 8.74 – 8.68 (m, 1H), 8.15 (dd, *J* = 8.6, 1.7 Hz, 1H), 7.91 (d, *J* = 8.8 Hz, 1H), 7.74 (d, *J* = 8.7 Hz, 1H), 7.70 – 7.64 (m, 2H), 7.50 – 7.44 (m, 2H), 7.25 (d, *J* = 2.4 Hz, 1H), 7.21 (dd, *J* = 8.8, 2.4 Hz, 1H), 1.36 (m, 12H), 1.14 (d, *J* = 7.5 Hz, 18H). ^{13}C NMR (126 MHz, $CDCl_3$) δ 178.04, 157.02, 154.55, 138.06, 133.07, 132.97, 132.72, 131.73, 128.01, 127.21, 125.91, 124.65, 123.26, 117.43, 114.78, 93.42, 87.08, 35.26, 31.23, 18.08, 12.88. HRMS (DART) Calculated for $C_{32}H_{41}O_2Si$ $[M+H]^+$: 485.28703, found 485.28397.

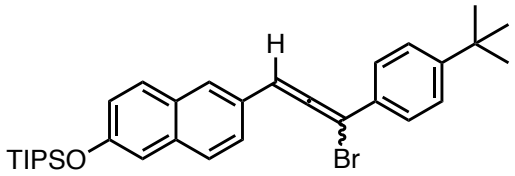

((6-(3-Bromo-3-(4-(*tert*-butyl)phenyl)propa-1,2-dien-1-yl)naphthalen-2-yl)oxy)triisopropylsilane (6)

3-(4-(*tert*-butyl)phenyl)-1-(6-((triisopropylsilyl)oxy)naphthalen-2-yl)prop-2-yn-1-ol (**4**) (30 mg, 0.06 mmol, 1 eq) was added to a flame-dried round bottom flask equipped with a stir bar and dissolved in dry Et_2O (4 mL, 0.015M). The mixture was cooled to 0 ˚C and then PBr_3 (26 mg, 0.09 mmol, 1.5 eq) was added dropwise. The mixture was allowed to stir for 30 min. at 0 ˚C after which the reaction quenched at 0 ˚C by dropwise addition of sat $NaHCO_3$ (2 mL). The mixture was transferred to a separatory funnel, the layers separated, and the aqueous layer extracted with fresh Et_2O twice. The organics were pooled, washed with sat $NaHCO_3$, brine, dried over $MgSO_4$, filtered and concentrated *in vacuo* to provide 29 mg (86% crude yield) of the product **6** as a clear oil. *Note: this aryl allenic bromide is unstable to all forms of chromatography tested (SiO_2 and*

alumina) making purification difficult. ^{1}H NMR (500 MHz, $CDCl_3$) δ 7.73 (d, *J* = 1.7 Hz, 1H), 7.70 (d, *J* = 8.9 Hz, 1H), 7.65 (d, *J* = 8.6 Hz, 1H), 7.57 (d, *J* = 8.5 Hz, 1H), 7.48 (dd, *J* = 8.6, 1.7 Hz, 1H), 7.38 (d, *J* = 8.5 Hz, 1H), 7.20 (d, *J* = 2.4 Hz, 1H), 7.14 (dd, *J* = 8.8, 2.4 Hz, 1H), 6.71 (s, 1H), 1.40 – 1.29 (m, 12H), 1.14 (d, *J* = 7.5 Hz, 18H). ^{13}C NMR (126 MHz, $CDCl_3$) δ 203.45, 154.65, 151.80, 134.72, 130.94, 129.50, 129.13, 127.53, 127.47, 127.44, 127.18, 125.44, 125.42, 122.62, 114.74, 102.67, 95.76, 65.89, 34.65, 31.25, 31.22, 18.02, 17.99, 17.97, 12.74. HRMS could not be obtained due to the instability of the compound.

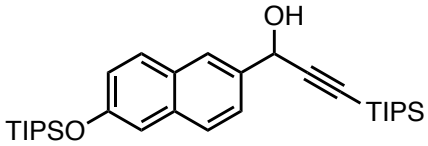

3-(Triisopropylsilyl)-1-(6-((triisopropylsilyl)oxy)naphthalen-2-yl)prop-2-yn-1-ol (7)

To a flame-dried round bottom flask equipped with a stir bar was added triisopropylsilylacetylene (12.6 g, 69 mmol, 1.1 eq) followed by THF (120 mL). The mixture was cooled to -78 ˚C and a 1.4M solution of *n*-BuLi (47 mL, 66 mmol, 1.05 eq) in hexanes was added dropwise at -78 ˚C. The mixture was allowed to stir for 10 min. and then 6-((triisopropylsilyl)oxy)-2-naphthaldehyde (20.6 g, 62.7 mmol, 1 eq) was added as a solution in THF (40 mL) dropwise at -78 ˚C. The resulting mixture was allowed to stir at -78 ˚C for 10 min. and then allowed to warm to room temperature. Upon reaching room temperature the mixture was quenched by the addition of saturated NH_4Cl (100 mL). The mixture was diluted with Et_2O and then transferred to a separatory funnel. The layers were separated and the aqueous layer extracted with fresh Et_2O twice. The organics were pooled, washed with water x3, brine x3, dried over $MgSO_4$, filtered and concentrated *in vacuo* to produce a crude oil which was purified by filtration over SiO_2 eluting

with a gradient of 0% to 100% $CHCl_3$ in hexanes. This produced 22.06 g (69%) of the product **7** as a light yellow oil. ^{1}H NMR (500 MHz, $CDCl_3$) δ 7.98 (dd, *J* = 1.7, 0.9 Hz, 1H), 7.71 (dd, *J* = 8.7, 3.2 Hz, 2H), 7.62 (dd, *J* = 8.6, 1.8 Hz, 1H), 7.22 (d, *J* = 2.5 Hz, 1H), 7.14 (dd, *J* = 8.8, 2.4 Hz, 1H), 5.60 (dd, *J* = 6.6, 0.7 Hz, 1H), 2.17 (d, *J* = 6.7 Hz, 1H), 1.42 – 1.26 (m, 3H), 1.26 – 0.99 (m, 39H). ^{13}C NMR (126 MHz, $CDCl_3$) δ 154.51, 135.83, 134.68, 129.74, 128.80, 127.34, 125.74, 125.31, 122.57, 114.54, 107.11, 88.29, 65.45, 18.78, 18.10, 12.86, 11.35. HRMS (DART) Calculated for $C_{31}H_{50}O_2Si_2$ [$M^{\bullet+}$]: 510.33439, found 510.32751.

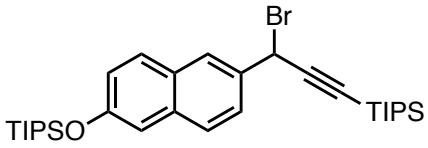

(3-Bromo-3-(6-((triisopropylsilyl)oxy)naphthalen-2-yl)prop-1-yn-1-yl)triisopropylsilane (8)

3-(triisopropylsilyl)-1-(6-((triisopropylsilyl)oxy)naphthalen-2-yl)prop-2-yn-1-ol (**7**) (4.2 g, 8.2 mmol, 1 eq) was added to a flame-dried round bottom flask equipped with a stir bar and dissolved in dry Et_2O (52 mL, 0.08M). The mixture was cooled to 0 ˚C and then PBr_3 (4.45 g, 16.4 mmol, 2 eq) was added dropwise. The mixture was allowed to stir for 30 min. at 0 ˚C after which the reaction quenched at 0 ˚C by dropwise addition of sat $NaHCO_3$ (30 mL). The mixture was transferred to a separatory funnel, the layers separated, and the aqueous layer extracted with fresh Et_2O twice. The organics were pooled, washed with sat $NaHCO_3$, brine, dried over $MgSO_4$, filtered and concentrated *in vacuo* to provide 4.58 g of the product **8** as a clear oil. *Note: this aryl propargylic bromide is unstable to all forms of chromatography tested (SiO_2 and alumina) making purification difficult. The crude material is typically of high purity and is carried on directly into the next step after drying overnight under high vacuum at room temperature.* ^{1}H NMR (500 MHz, $CDCl_3$) δ 8.00 (d, *J* = 1.8 Hz, 1H), 7.69 (dd, *J* = 8.7, 3.2 Hz, 2H), 7.62 (dd, *J* = 8.6, 1.9 Hz, 1H),

7.20 (d, J = 2.4 Hz, 1H), 7.14 (dd, J = 8.8, 2.4 Hz, 1H), 5.93 (s, 1H), 1.45 – 1.29 (m, 3H), 1.20 – 1.03 (m, 39H). ^{13}C NMR (126 MHz, $CDCl_3$) δ 155.08, 134.87, 134.16, 129.89, 128.63, 127.72, 126.68, 125.98, 122.86, 114.64, 104.15, 92.71, 38.43, 18.78, 18.10, 12.86, 11.39. HRMS could not be obtained due to the instability of the compound.

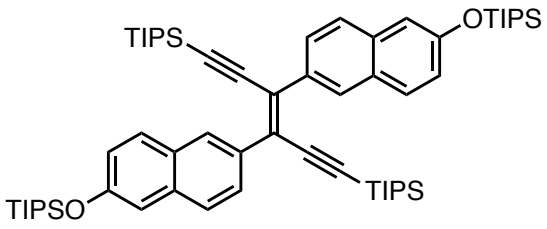

(*E*)-(3,4-Bis(6-((triisopropylsilyl)oxy)naphthalen-2-yl)hexa-3-en-1,5-diyne-1,6-diyl)bis(triisopropylsilane) (9)

Dry THF (20 mL) was added to a flame dried round bottom flask equipped with a stir bar and cooled to -10 ˚C. A 1M solution of LiHMDS in THF (8.8 mL, 8.8 mmol, 1.1 eq) was added followed by HMPA (1.58 g, 8.8 mmol, 1.1 eq). In a separate flask equipped with an addition funnel (3-bromo-3-(6-((triisopropylsilyl)oxy)naphthalen-2-yl)prop-1-yn-1-yl)triisopropylsilane (**8**) (4.58 g, 8 mmol, 1 eq) was dissolved in dry THF (60 mL) and cooled to -90 ˚C (hexanes: liq. N_2) *Note: The freezing point of THF is -108 ˚C and for this reason the cooling bath should be closely monitored to avoid excess liq. N_2 freezing the reactant solution.* The LiHMDS solution was transferred via cannula to the addition funnel and added dropwise to the cold solution of starting material at -90 ˚C over ca. 30 min. Once the addition was complete, the mixture was allowed to stir at -90 ˚C for 30 min. after which sat NH_4Cl (100 mL) was added to quench the reaction at -90 ˚C. The mixture was rapidly stirred and warmed to room temperature. The mixture was transferred to a separatory funnel and the layers separated. The aqueous layer was extracted with Et_2O twice, the organics were pooled, washed with brine thrice, dried over $MgSO_4$, filtered and concentrated

in vacuo to give a crude oil. Purification by column chromatography over SiO_2 eluting with a gradient of 0% to 100% $CHCl_3$ in hexanes provided 3.23 g (80% over two steps) of compound **9** as a crystalline solid. ^{1}H NMR (500 MHz, $CDCl_3$) δ 8.33 (d, *J* = 1.8 Hz, 1H), 7.99 (dd, *J* = 8.6, 1.9 Hz, 1H), 7.66 (dd, *J* = 21.0, 8.8 Hz, 2H), 7.21 (d, *J* = 2.4 Hz, 1H), 7.11 (dd, *J* = 8.8, 2.4 Hz, 1H), 1.39 – 1.27 (m, 3H), 1.15 (d, *J* = 7.4 Hz, 18H), 1.02 – 0.90 (m, 24H). ^{13}C NMR (126 MHz, $CDCl_3$) δ 154.36, 134.55, 134.43, 129.84, 129.28, 128.71, 128.53, 127.25, 125.85, 121.97, 114.35, 107.52, 101.88, 18.56, 17.99, 12.75, 11.25. HRMS (DART) Calculated for $C_{62}H_{97}O_2Si_4$ $[M+H]^+$: 985.65601, found 985.65048.

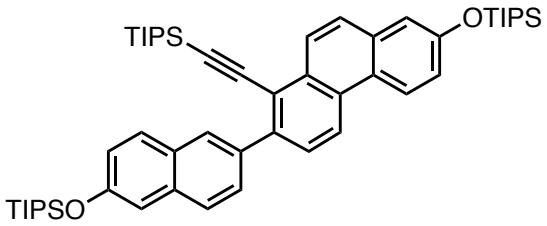

Triisopropyl((6-(1-((triisopropylsilyl)ethynyl)-7-((triisopropylsilyl)oxy)phenanthren-2-yl)naphthalen-2-yl)oxy)silane (10)

(*E*)-(3,4-bis(6-((triisopropylsilyl)oxy)naphthalen-2-yl)hexa-3-en-1,5-diyne-1,6-diyl)bis (triisopropylsilane) (**9**) (80 mg, 0.08 mmol, 1 eq) was placed in an alumina boat inside a quartz tube in a programmable tube furnace. The furnace was heated to 300 ˚C for 10 h under Ar flow. Upon cooling a large amount of material had distilled to outside the hot-zone. The material remaining in the boat and the material that had sublimed into the tube were collected using $CHCl_3$ and the solution concentrated *in vacuo* to produce a crude residue which was purified by preparative TLC eluting with 10% $CHCl_3$ in Hexanes to produce 12 mg (17%) of the product **10** as a yellow solid. To assist in structural assignment ^{1}H NMR was collected in $CDCl_3$ as well as C_6D_6. ^{1}H NMR (500 MHz, $CDCl_3$) δ 8.62 (d, *J* = 8.7 Hz, 1H), 8.57 (d, *J* = 9.0 Hz, 1H), 8.50 (d, *J*

= 9.1 Hz, 1H), 8.11 – 8.04 (m, 1H), 7.83 – 7.73 (m, 4H), 7.71 (d, *J* = 8.5 Hz, 1H), 7.34 (s, 1H), 7.32 – 7.27 (m, 2H), 7.15 (dd, *J* = 8.8, 2.4 Hz, 1H), 1.35 (tdd, *J* = 8.4, 5.8, 3.8 Hz, 6H), 1.17 (t, *J* = 5.8 Hz, 39H), 0.97 (d, *J* = 5.5 Hz, 18H). ^{1}H NMR (500 MHz, C_6D_6) δ 8.88 (d, *J* = 9.0 Hz, 1H), 8.39 (dd, *J* = 13.9, 8.8 Hz, 2H), 8.09 (d, *J* = 1.7 Hz, 1H), 7.79 (dd, *J* = 8.3, 1.8 Hz, 1H), 7.71 (t, *J* = 8.8 Hz, 2H), 7.60 (dd, *J* = 8.8, 6.2 Hz, 2H), 7.45 (dd, *J* = 14.8, 2.6 Hz, 2H), 7.35 – 7.28 (m, 2H), 7.23 (dd, *J* = 8.7, 2.5 Hz, 1H), 1.30 (ddd, *J* = 15.9, 8.2, 6.1 Hz, 5H), 1.18 (dd, *J* = 7.2, 3.2 Hz, 48H). ^{13}C NMR (126 MHz, $CDCl_3$) δ 155.12, 154.16, 143.12, 136.65, 134.04, 133.56, 132.31, 129.77, 129.34, 128.98, 128.65, 128.38, 128.07, 127.89, 126.37, 125.84, 124.91, 124.41, 122.60, 122.24, 121.49, 119.98, 116.71, 114.55, 104.68, 99.97, 31.74, 22.81, 18.71, 18.13, 14.27, 12.90, 11.40. HRMS (DART) Calculated for $C_{53}H_{77}O_2Si_3$ $[M+H]^+$: 829.52314, found 829.52413.

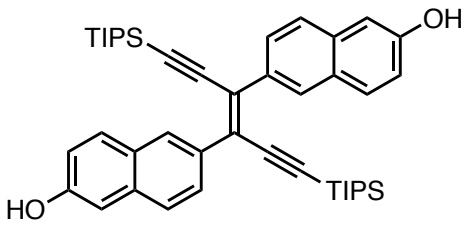

(*E*)-6,6'-(1,6-Bis(triisopropylsilyl)hexa-3-en-1,5-diyne-3,4-diyl)bis(naphthalen-2-ol) (11)

(*E*)-(3,4-bis(6-((triisopropylsilyl)oxy)naphthalen-2-yl)hexa-3-en-1,5-diyne-1,6-diyl)bis (triisopropylsilane) (**9**) (1.05 g, 1.06 mmol, 1 eq) was added to a round bottom flask equipped with a stir bar, dissolved in THF (20 mL, 0.05M) and cooled to -78 ˚C. To this mixture was added a 1M solution of TBAF in THF (2.2 mL, 2.2 mmol, 2.1 eq). The mixture was stirred at -78 ˚C until judged complete by TLC. Once complete, the mixture was diluted with sat NH_4Cl and allowed to warm to room temperature. The mixture was diluted with Et_2O, transferred to a separatory funnel and the layers separated. The aqueous layer was extracted twice with fresh Et_2O, organics pooled, washed twice with brine, dried over $MgSO_4$, filtered and concentrated *in vacuo* to produce a crude

product that was purified by chromatography over SiO_2 eluting with a gradient of 50% to 100% hexanes:DCM to provide 700 mg (98%) of the product **11** as a yellow crystalline solid. ^{1}H NMR (500 MHz, $CDCl_3$) δ 8.34 (d, *J* = 1.7 Hz, 1H), 8.04 (dd, *J* = 8.6, 1.8 Hz, 1H), 7.72 (d, *J* = 8.8 Hz, 1H), 7.64 (d, *J* = 8.6 Hz, 1H), 7.15 (d, *J* = 2.5 Hz, 1H), 7.09 (dd, *J* = 8.8, 2.6 Hz, 1H), 4.96 (s, 1H), 1.04 – 0.91 (m, 21H). ^{13}C NMR (126 MHz, $CDCl_3$) δ 153.92, 134.74, 134.48, 130.59, 129.19, 129.01, 128.53, 127.90, 125.68, 117.79, 109.48, 107.61, 102.29, 18.72, 11.40. HRMS (DART) Calculated for $C_{44}H_{57}O_2Si_2$ $[M+H]^+$: 673.38916, found 673.38603.

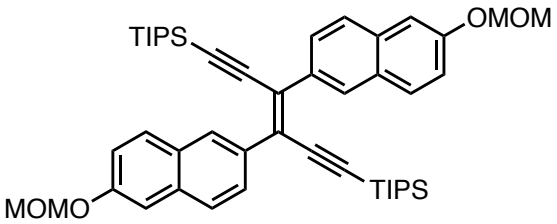

(*E*)-(3,4-Bis(6-(methoxymethoxy)naphthalen-2-yl)hexa-3-en-1,5-diyne-1,6-diyl)bis(triisopropylsilane) (12)

(*E*)-6,6'-(1,6-bis(triisopropylsilyl)hexa-3-en-1,5-diyne-3,4-diyl)bis(naphthalen-2-ol) (**11**) (700 mg, 1.04 mmol, 1 eq) was added to a round bottom flask equipped with a stir bar followed by DCM (20 mL, 0.05M). DIPEA (2 g, 16 mmol, 16 eq) was added followed by bromomethyl methyl ether (1 g, 8 mmol, 8 eq) in one portion under Ar. The mixture was allowed to stir at room temperature until judged complete by TLC. Upon completion of the reaction the mixture was diluted with water and DCM and the layers separated. The aqueous layer was extracted twice with DCM, the organics pooled, and washed with dilute HCl, sat $NaHCO_3$, dried over $MgSO_4$, filtered and concentrated *in vacuo*. The crude residue was purified by chromatography over SiO_2 eluting with a gradient of 0% to 100% $CHCl_3$ in hexanes to provide 650 mg (82%) of the product **12** as a yellow solid. ^{1}H NMR (500 MHz, $CDCl_3$) δ 8.35 (d, *J* = 1.9 Hz, 1H), 8.07 (dd, *J* = 8.6, 1.8 Hz,

1H), 7.72 (dd, J = 15.8, 8.7 Hz, 2H), 7.39 (d, J = 2.3 Hz, 1H), 7.26 (s, 1H), 7.20 (dd, J = 8.9, 2.5 Hz, 1H), 5.32 (s, 2H), 3.55 (d, J = 0.7 Hz, 3H), 1.04 – 0.92 (m, 21H). ^{13}C NMR (126 MHz, $CDCl_3$) δ 155.62, 135.13, 134.34, 130.14, 129.13, 129.06, 128.87, 127.71, 126.34, 119.03, 109.83, 107.63, 102.41, 94.70, 56.29, 18.73, 11.42. HRMS (DART) Calculated for $C_{48}H_{65}O_4Si_2$ $[M+H]^+$: 761.44159, found 761.43932.

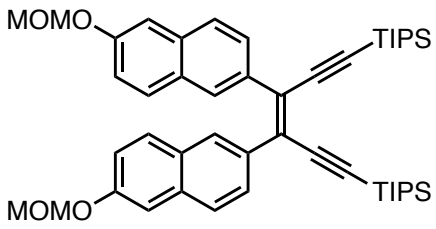

(*Z*)-(3,4-Bis(6-(methoxymethoxy)naphthalen-2-yl)hexa-3-en-1,5-diyne-1,6-diyl)bis(triisopropylsilane) (13)

(*E*)-(3,4-bis(6-(methoxymethoxy)naphthalen-2-yl)hexa-3-en-1,5-diyne-1,6-diyl)bis(triisopropylsilane) (**12**) (130 mg, 0.17 mmol, 1 eq) was dissolved in spectroscopic grade hexanes (60 mL, 2.8 mM) and irradiated with a long-wave UV (365 nm) lamp overnight. In the morning ^{1}H NMR analysis showed a mixture of 63% (*E*) isomer **12**, 27% (*Z*) isomer **13**, and 10% phenanthrene **14**. After stirring under irradiation for 40 h the mixture showed the same ratio by ^{1}H NMR therefore the mixture was concentrated and the crude residue purified by column chromatography on SiO_2 eluting with a gradient of 0% to 5% EtOAc in Hexanes. This provided 32 mg (25%) of compound **13** as a light yellow solid. ^{1}H NMR (500 MHz, CD_2Cl_2) δ 7.88 (d, J = 1.8 Hz, 1H), 7.58 (d, J = 8.9 Hz, 1H), 7.40 (d, J = 8.7 Hz, 1H), 7.26 (d, J = 2.4 Hz, 1H), 7.17 (dd, J = 8.6, 1.8 Hz, 1H), 7.14 (dd, J = 8.9, 2.5 Hz, 1H), 5.25 (s, 2H), 3.47 (s, 3H), 1.29 – 1.23 (m, 3H), 1.15 (d, J = 3.7 Hz, 18H). ^{13}C NMR (126 MHz, CD_2Cl_2) δ 156.05, 134.37, 134.17, 130.04, 129.88,

129.40, 129.01, 128.52, 126.45, 119.56, 110.09, 109.05, 100.28, 94.87, 56.33, 30.10, 19.02, 11.84. HRMS (DART) Calculated for $C_{48}H_{65}O_4Si_2$ $[M+H]^+$: 761.44159, found 761.44032.

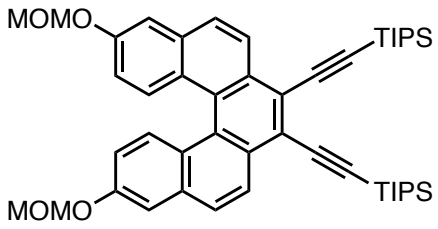

((8,13-Bis(methoxymethoxy)dibenzo[*c*,*g*]phenanthrene-3,4-diyl)bis(ethyne-2,1-diyl))bis(triisopropylsilane) (14)

(*E*)-(3,4-bis(6-(methoxymethoxy)naphthalen-2-yl)hexa-3-en-1,5-diyne-1,6-diyl)bis(triisopropylsilane) (**12**) (400 mg, 0.52 mmol, 1 eq) was added to a borosilicate photochemical reactor flask equipped with a stirbar and dissolved in benzene (700 mL, .004 M). Iodine (133 mg, 0.52 mmol, 1.0 eq) was added and the mixture was sparged with Ar for 20 min. Then propylene oxide (8 mL) was added. A jacketed quartz immersion well with a Hanovia lamp was placed inside the reactor and a rapid water flow was used to cool the immersion well. The lamp was turned on and the mixture allowed to react until judged complete by ^{1}H NMR. Upon completion of the reaction the mixture was transferred to a separatory funnel and washed with 10% sodium thiosulfate solution. The organic layer was dried over $MgSO_4$, filtered and concentrated *in vacuo* to provide the crude product which was purified by chromatography over SiO_2 eluting with a gradient of 0% to 20% EtOAc in hexanes to provide 303 mg (76%) of the product **14** as a yellow crystalline solid. ^{1}H NMR (500 MHz, $CDCl_3$) δ 8.56 (d, J = 8.9 Hz, 1H), 8.23 (d, J = 9.2 Hz, 1H), 7.90 (d, J = 8.8 Hz, 1H), 7.50 (d, J = 2.6 Hz, 1H), 6.96 (dd, J = 9.2, 2.6 Hz, 1H), 5.38 – 5.30 (m, 2H), 3.56 (s, 3H), 1.35 – 1.20 (m, 21H). ^{13}C NMR (126 MHz, $CDCl_3$) δ

155.89, 134.34, 131.04, 130.94, 127.80, 126.98, 126.15, 125.11, 122.71, 116.68, 110.41, 104.19, 101.61, 94.68, 56.40, 19.07, 11.71. HRMS (DART) Calculated for $C_{48}H_{63}O_4Si_2$ $[M+H]^+$: 759.42594, found 759.42469.

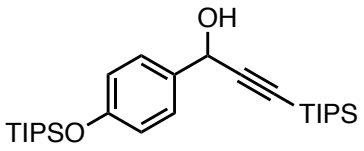

3-(Triisopropylsilyl)-1-(4-((triisopropylsilyl)oxy)phenyl)prop-2-yn-1-ol (16)

To a flame-dried round bottom flask equipped with a stir bar was added triisopropylsilylacetylene (3.9 g, 21.6 mmol, 1.2 eq) followed by THF (24 mL). The mixture was cooled to -78 ˚C and a 1.9M solution of *n*-BuLi (9.5 mL, 18 mmol, 1 eq) in hexanes was added dropwise at -78 ˚C. The mixture was allowed to stir for 10 min. and then 4-((triisopropylsilyl)oxy)benzaldehyde (5 g, 18 mmol, 1 eq) was added as a solution in THF (12 mL) dropwise at -78 ˚C. The resulting mixture was allowed to stir at -78 ˚C for 10 min. and then allowed to warm to room temperature. Upon reaching room temperature the mixture was quenched by the addition of saturated NH_4Cl (100 mL). The mixture was diluted with Et_2O and then transferred to a separatory funnel. The layers were separated and the aqueous layer extracted with fresh Et_2O twice. The organics were pooled, washed with water x3, brine x3, dried over $MgSO_4$, filtered and concentrated *in vacuo* to produce a crude oil which was purified by filtration over SiO_2 eluting with a gradient of 0% to 100% $CHCl_3$ in hexanes. This produced 7.62 g (92%) of the product **16** as a light yellow oil. ^{1}H NMR (500 MHz, $CDCl_3$) δ 7.48 – 7.37 (m, 2H), 6.97 – 6.75 (m, 2H), 5.42 (d, J = 6.4 Hz, 1H), 2.06 (d, J = 6.5 Hz, 1H), 1.35 – 1.15 (m, 3H), 1.09 (d, J = 9.3 Hz, 39H). ^{13}C NMR (126 MHz, $CDCl_3$) δ 156.35, 133.39, 128.23, 119.99, 107.41, 87.82, 64.93, 18.75, 18.05, 12.80, 11.33. HRMS (DART) Calculated for $C_{22}H_{35}O_2Si_2$ $[M+H]^+$: 461.32656, found 461.32722.

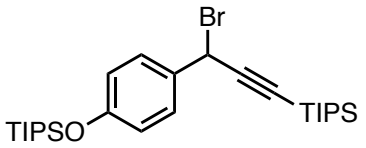

(3-Bromo-3-(4-((triisopropylsilyl)oxy)phenyl)prop-1-yn-1-yl)triisopropylsilane (17)

3-(triisopropylsilyl)-1-(4-((triisopropylsilyl)oxy)phenyl)prop-2-yn-1-ol (**16**) (7.33 g, 15.9 mmol, 1 eq) was added to a flame-dried round bottom flask equipped with a stir bar and dissolved in dry Et_2O (100 mL, 0.16M). The mixture was cooled to 0 ˚C and then PBr_3 (8.6 g, 31.8 mmol, 2 eq) was added dropwise. The mixture was allowed to stir for 30 min. at 0 ˚C after which the reaction quenched at 0 ˚C by dropwise addition of sat $NaHCO_3$ (50 mL). The mixture was transferred to a separatory funnel, the layers separated, and the aqueous layer extracted with fresh Et_2O twice. The organics were pooled, washed with sat $NaHCO_3$, brine, dried over $MgSO_4$, filtered and concentrated *in vacuo* to provide 7.87 g of the product **17** as a clear oil. *Note: this aryl propargylic bromide is unstable to all forms of chromatography tested (SiO_2 and alumina) making purification difficult. The crude material is typically of high purity and is carried on directly into the next step after drying overnight under high vacuum at room temperature.* ^{1}H NMR (500 MHz, $CDCl_3$) δ 7.49 – 7.42 (m, 2H), 6.87 – 6.81 (m, 2H), 5.77 (s, 1H), 1.33 – 1.19 (m, 3H), 1.17 – 1.03 (m, 39H). ^{13}C NMR (126 MHz, $CDCl_3$) δ 156.83, 131.66, 129.29, 120.20, 104.45, 92.32, 38.04, 18.75, 18.60, 18.04, 12.81, 11.37. HRMS could not be obtained due to the instability of the compound.

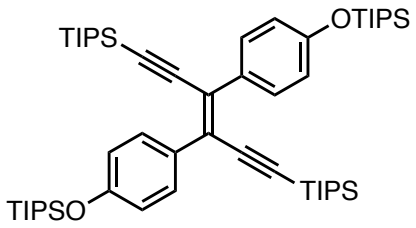

(*E*)-(3,4-Bis(4-((triisopropylsilyl)oxy)phenyl)hexa-3-en-1,5-diyne-1,6-diyl)bis(triisopropylsilane) (18)

Dry THF (80 mL) was added to a flame dried round bottom flask equipped with a stir bar and cooled to -10 ˚C. A 1M solution of LiHMDS in THF (16.5 mL, 16.5 mmol, 1.1 eq) was added followed by HMPA (2.96 g, 16.5 mmol, 1.1 eq). In a separate flask equipped with an addition funnel (3-bromo-3-(4-((triisopropylsilyl)oxy)phenyl)prop-1-yn-1-yl)triisopropylsilane (**17**) (7.87 g, 15 mmol, 1 eq) was dissolved in dry THF (200 mL) and cooled to -90 ˚C (hexanes: liq. N_2) *Note: The freezing point of THF is -108 ˚C and for this reason the cooling bath should be closely monitored to avoid excess liq. N_2 freezing the reactant solution.* The LiHMDS solution was transferred via cannula to the addition funnel and added dropwise to the cold solution of starting material at -90 ˚C over ca. 1h. Once the addition was complete, the mixture was allowed to stir at -90 ˚C for 30 min. after which sat NH_4Cl (200 mL) was added to quench the reaction at -90 ˚C. The mixture was rapidly stirred and warmed to room temperature. The mixture was transferred to a separatory funnel and the layers separated. The aqueous layer was extracted with Et_2O twice, the organics were pooled, washed with brine thrice, dried over $MgSO_4$, filtered and concentrated *in vacuo* to give a crude oil. Purification by column chromatography over SiO_2 eluting with a gradient of 0% to 100% $CHCl_3$ in hexanes provided the a crystalline solid which could be further purified by recrystallization from hot IPA to provide 5.51 g (78% over two steps) of product **18** as off-white crystals. ^{1}H NMR (500 MHz, $CDCl_3$) δ 7.86 – 7.77 (m, 2H), 6.85 – 6.78 (m, 2H), 1.32 – 1.22 (m, 3H), 1.11 (d, J = 7.5 Hz, 19H), 1.02 (s, 21H). ^{13}C NMR (126 MHz, $CDCl_3$) δ 156.00,

132.10, 130.78, 127.57, 119.02, 107.90, 101.48, 18.76, 18.06, 12.82, 11.50. HRMS (DART) Calculated for $C_{54}H_{92}O_2Si_4$ $[M+H]^+$: 885.62471, found 885.62207.

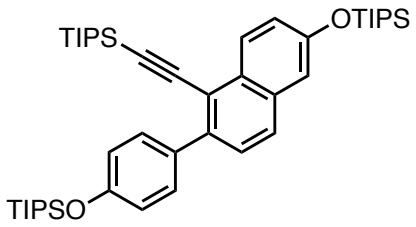

Triisopropyl(4-(1-((triisopropylsilyl)ethynyl)-6-((triisopropylsilyl)oxy)naphthalen-2-yl)phenoxy)silane (19)

(*E*)-(3,4-bis(4-((triisopropylsilyl)oxy)phenyl)hexa-3-en-1,5-diyne-1,6-diyl)bis(triisopropylsilane) (**18**) (145 mg, 0.16 mmol, 1 eq) was added to a small pressure tube. The tube was flushed with Ar, sealed and heated to 340 ˚C overnight. In the morning the material was subjected to chromatography over SiO_2 eluting with a gradient of 0% to 20% $CHCl_3$ in hexanes. The product was further purified by preparative TLC eluting multiple times with hexanes and 10% $CHCl_3$ in hexanes. This produced 21 mg (18%) of the product **19** as a yellow solid. ^{1}H NMR (500 MHz, $CDCl_3$) δ 8.46 – 8.34 (m, 1H), 7.70 – 7.62 (m, 1H), 7.61 – 7.51 (m, 2H), 7.43 (d, J = 8.5 Hz, 1H), 7.24 – 7.16 (m, 2H), 6.98 – 6.87 (m, 2H), 1.43 – 1.24 (m, 6H), 1.20 – 1.02 (m, 54H). ^{13}C NMR (126 MHz, $CDCl_3$) δ 155.41, 154.11, 140.78, 133.79, 133.19, 130.84, 129.71, 128.32, 128.02, 127.20, 123.01, 119.16, 117.94, 114.67, 104.45, 99.25, 18.72, 18.00, 17.98, 12.74, 12.73, 11.40. HRMS (DART) Calculated for $C_{45}H_{73}O_2Si_3$ $[M+H]^+$: 729.49129, found 729.48824.

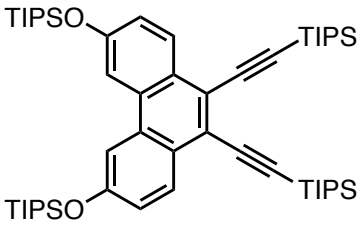

((9,10-Bis((triisopropylsilyl)ethynyl)phenanthrene-3,6-diyl)bis(oxy))bis(triisopropylsilane) (20)

(*E*)-(3,4-bis(4-((triisopropylsilyl)oxy)phenyl)hexa-3-en-1,5-diyne-1,6-diyl)bis (triisopropylsilane) (**18**) (2.2 g, 2.48 mmol, 1 eq) was added to a borosilicate photochemical reactor flask equipped with a stirbar and dissolved in benzene (700 mL, .004 M). Iodine (757 mg, 2.98 mmol, 1.2 eq) was added and the mixture was sparged with Ar for 20 min. Then propylene oxide (37 mL) was added. A jacketed quartz immersion well with a Hanovia lamp was placed inside the reactor and a rapid water flow was used to cool the immersion well. The lamp was turned on and the mixture allowed to react until judged complete by ^{1}H NMR. Upon completion of the reaction the mixture was transferred to a separatory funnel and washed with 10% sodium thiosulfate solution. The organic layer was dried over $MgSO_4$, filtered and concentrated *in vacuo* to provide the crude product which was purified by chromatography over SiO_2 eluting with a gradient of 0% to 20% $CHCl_3$ in hexanes to provide 2.04 g (92%) of the product **20** as an off-tan solid. ^{1}H NMR (500 MHz, $CDCl_3$) δ 8.41 (d, J = 8.9 Hz, 1H), 7.86 (d, J = 2.4 Hz, 1H), 7.23 (dd, J = 8.9, 2.3 Hz, 1H), 1.46 – 1.32 (m, 3H), 1.26 – 1.19 (m, 21H), 1.17 (d, J = 7.4 Hz, 18H).

^{13}C NMR (126 MHz, $CDCl_3$) δ 155.78, 130.75, 129.37, 126.41, 121.99, 121.31, 111.32, 104.48, 100.48, 19.06, 18.12, 13.03, 11.71. HRMS (DART) Calculated for $C_{54}H_{91}O_2Si_4$ $[M+H]^+$: 883.60906, found 883.60637.

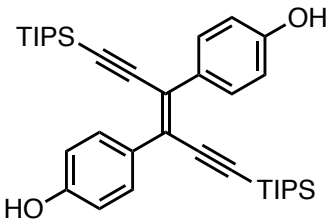

(E)-4,4'-(1,6-Bis(triisopropylsilyl)hexa-3-en-1,5-diyne-3,4-diyl)diphenol (21)

(E)-(3,4-bis(4-((triisopropylsilyl)oxy)phenyl)hexa-3-en-1,5-diyne-1,6-diyl)bis(triisopropylsilane) (**18**) (2.5 g, 2.8 mmol, 1 eq) was added to a round bottom flask equipped with a stir bar, dissolved in THF (28 mL, 0.1M) and cooled to -78 ˚C. To this mixture was added a 1M solution of TBAF in THF (6.2 mL, 6.2 mmol, 2.2 eq). The mixture was stirred at -78 ˚C until judged complete by TLC. Once complete, the mixture was diluted with sat NH_4Cl and allowed to warm to room temperature. The mixture was diluted with Et_2O, transferred to a separatory funnel and the layers separated. The aqueous layer was extracted twice with fresh Et_2O, organics pooled, washed twice with brine, dried over $MgSO_4$, filtered and concentrated *in vacuo* to produce a crude product that was purified by chromatography over SiO_2 eluting with a gradient of 50% to 100% hexanes:DCM and then 0% to 8% MeOH:DCM to provide 1.6 g (quant.) of the product **21** as an off yellow oil. ^{1}H NMR (500 MHz, $CDCl_3$) δ 7.81 (d, J = 8.8 Hz, 2H), 6.77 (d, J = 8.7 Hz, 2H), 4.94 (s, 2H), 1.01 (s, 21H). ^{13}C NMR (126 MHz, $CDCl_3$) δ 155.44, 131.99, 131.01, 127.74, 114.55, 107.63, 101.79, 18.74, 11.46. HRMS (DART) Calculated for $C_{36}H_{53}O_2Si_2$ $[M+H]^+$: 573.35786, found 573.35430.

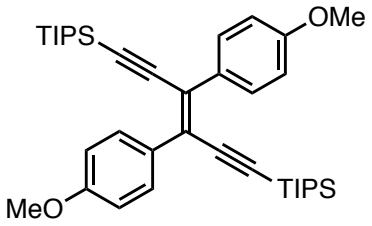

(*E*)-(3,4-Bis(4-methoxyphenyl)hexa-3-en-1,5-diyne-1,6-diyl)bis(triisopropylsilane) (22)

(E)-4,4'-(1,6-bis(triisopropylsilyl)hexa-3-en-1,5-diyne-3,4-diyl)diphenol (**21**) (1.6 g, 2.8 mmol, 1 eq) was dissolved in DMF (60 mL, 0.05M) in a round bottom flask equipped with a stir bar and K_2CO_3 (5.4 g, 39 mmol, 14 eq) was added followed by MeI (4 g, 28 mmol, 10 eq). The resulting mixture was gently heated to 60 ˚C until the reaction was complete as judged by TLC. Upon completion of the reaction, the mixture was cooled and diluted with water (300 mL) and Et_2O (200 mL). The layers were separated and the aqueous layer extracted twice with Et_2O. The organic layers were pooled, washed thrice with water, thrice with brine, dried over $MgSO_4$, filtered and concentrated *in vacuo* to produce a crude product which was purified by chromatography over SiO_2 using a gradient of 0% to 100% $CHCl_3$ in hexanes. This provided 1.2 g (71%) of the product **22** as a white crystalline solid. ^{1}H NMR (500 MHz, $CDCl_3$) δ 7.95 – 7.84 (m, 2H), 6.95 – 6.81 (m, 2H), 3.83 (s, 3H), 1.02 (m, 21H). ^{13}C NMR (126 MHz, $CDCl_3$) δ 159.44, 131.84, 130.78, 127.82, 113.11, 107.73, 101.59, 55.43, 18.76, 11.48. HRMS (DART) Calculated for $C_{38}H_{56}O_2Si_2$ $[M+H]^+$: 601.38916, found 601.38671.

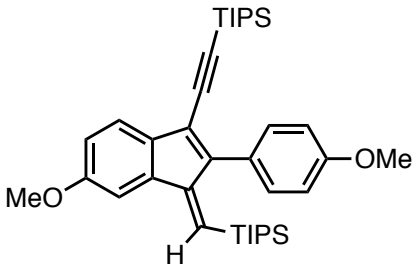

(*Z*)-Triisopropyl((6-methoxy-2-(4-methoxyphenyl)-1-((triisopropylsilyl)methylene)-1*H*-inden-3-yl)ethynyl)silane (23)

(*E*)-(3,4-bis(4-methoxyphenyl)hexa-3-en-1,5-diyne-1,6-diyl)bis(triisopropylsilane) (**22**) (12 mg, 0.02 mmol, 1 eq) was added to a round bottom flask, dissolved in DCM (2 mL) flushed with Ar, and cooled to -78 ˚C. TfOH (1 drop) was added via syringe at -78 ˚C which immediately caused a blue ppt to form. The ppt proceeded to dissolve over 5 min. producing a deep green solution. The mixture continued to darken and was quenched after 10 min by the addition of sat $NaHCO_3$ followed by extraction with DCM. The organic layer was dried over $MgSO_4$, filtered and concentrated *in vacuo* to provide a crude residue which was purified by preparative TLC eluting multiple times with 10% $CHCl_3$ in hexanes. This provided 7 mg (60%) of the product **23** as an orange oil which produced deep orange crystals upon sitting. ^{1}H NMR (500 MHz, $CDCl_3$) δ 7.38 – 7.32 (m, 2H), 7.28 (d, *J* = 8.1 Hz, 1H), 7.15 (d, *J* = 2.3 Hz, 1H), 6.93 – 6.83 (m, 4H), 3.89 (s, 3H), 3.84 (s, 3H), 1.03 (s, 21H), 0.96 (d, *J* = 7.5 Hz, 18H), 0.62 (p, *J* = 7.5 Hz, 3H). ^{13}C NMR (126 MHz, $CDCl_3$) δ 159.28, 159.05, 154.50, 145.19, 139.18, 133.58, 131.63, 131.24, 128.56, 127.34, 119.96, 113.16, 112.40, 106.35, 101.79, 101.71, 55.79, 55.53, 19.49, 18.61, 13.02, 11.26. HRMS (DART) Calculated for $C_{38}H_{57}O_2Si_2$ $[M+H]^+$: 601.38916, found 601.38515.

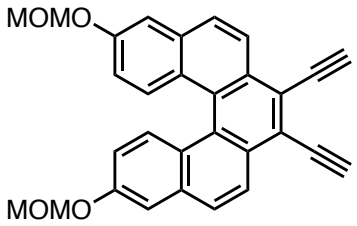

3,4-Diethynyl-8,13-bis(methoxymethoxy)dibenzo[*c*,*g*]phenanthrene (24)

((8,13-bis(methoxymethoxy)dibenzo[*c*,*g*]phenanthrene-3,4-diyl)bis(ethyne-2,1-diyl))bis(triisopropylsilane) (**14**) (24 mg, 0.031 mmol, 1 eq) was added to a round bottom flask equipped with a stir bar, dissolved in THF (7 mL, 0.005M) and cooled to -10 ˚C. To this mixture was added a 1M solution of TBAF in THF (62 µL, 0.062 mmol, 2 eq). The mixture was stirred at -10 ˚C until judged complete by TLC. Once complete, the mixture was diluted with sat NH_4Cl and allowed to warm to room temperature. The mixture was diluted with Et_2O, transferred to a separatory funnel and the layers separated. The aqueous layer was extracted twice with fresh Et_2O, organics pooled, washed twice with brine, dried over $MgSO_4$, filtered and concentrated *in vacuo* to produce a crude product that was purified by chromatography over SiO_2 eluting with a gradient of 0% to 20% EtOAc in hexanes to provide 13 mg (94%) of the product **24** as a yellow brown solid. ^{1}H NMR (500 MHz, $CDCl_3$) δ 8.44 (d, *J* = 8.8 Hz, 1H), 8.26 (d, *J* = 9.2 Hz, 1H), 7.91 (d, *J* = 8.8 Hz, 1H), 7.51 (d, *J* = 2.7 Hz, 1H), 6.98 (dd, *J* = 9.2, 2.7 Hz, 1H), 5.35 (d, *J* = 1.3 Hz, 2H), 3.83 (s, 1H), 3.57 (s, 3H). ^{13}C NMR (126 MHz, $CDCl_3$) δ 156.08, 134.54, 130.92, 130.50, 128.15, 127.25, 126.02, 124.74, 122.56, 116.84, 110.46, 94.66, 86.63, 81.10, 56.44. HRMS (DART) Calculated for $C_{30}H_{22}O_4$ [$M^{\bullet+}$]: 446.15126, found 446.14899.

Bergman polymerization procedure for the synthesis of *poly*-24

3,4-diethynyl-8,13-bis(methoxymethoxy)dibenzo[*c*,*g*]phenanthrene (**24**) (50 mg, 0.11 mmol, 1 eq) was added to a Schlenk bomb and dissolved in benzene (0.5 mL, .22M). The mixture was freeze-pump-thawed three times and then sealed and heated to 140 ˚C. After heating for 2.5 h TLC indicates complete consumption of starting material. The mixture was concentrated and the crude polymer dissolved in DCM and filtered through a 0.2 micron syringe filter to remove insolubles. The filtrate was concentrated and dissolved in DCM and the polymer precipitated by addition of methanol giving a mixture resembling chocolate milk. The polymer was filtered over a fine fritted funnel. This precipitation procedure was repeated thrice to provide the 34 mg (68%) of the polymer as a brown solid. ^{1}H NMR analysis was attempted in Chloroform-*d* and yielded a broad spectra with only three definable peaks corresponding to the helicene protons, and the methylene and methyl protons of the MOM group. ^{13}C NMR was unable to obtain due to the significant line broadening of the aryl region. Most likely due to the non-uniform structure of the polymer.

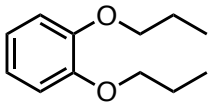

1,2-Di-*n*-propoxybenzene (25)

Catechol (1.0 g, 9 mmol, 1 eq) and potassium carbonate (6.2 g, 45 mmol, 5 eq) were added to a round bottom flask followed by DMF (15 mL, 0.6M). Propyl iodide (3.3 g, 20 mmol, 2.2 eq) was added and the mixture heated to 70 ˚C until the reaction was complete as indicated by TLC (typically overnight). Upon completion of the reaction the mixture was diluted with water (150 mL) and extracted with Et_2O three times. The organics were combined and washed with water

three times, brine three times, dried over $MgSO_4$, filtered and concentrated *in vacuo* to give 1.72 g (quant.) of the product **25** as a deep red oil in adequate purity suitable for the next step. ^{1}H NMR (500 MHz, $CDCl_3$) δ 6.89 (d, J = 1.1 Hz, 2H), 3.97 (t, J = 6.7 Hz, 2H), 2.58 – 1.71 (m, 2H), 1.04 (t, J = 7.4 Hz, 3H). ^{13}C NMR (126 MHz, $CDCl_3$) δ 149.35, 121.15, 114.28, 70.89, 22.79, 10.64. HRMS (DART) Calculated for $C_{12}H_{19}O_2$ $[M+H]^+$: 195.13796, found 195.13786.

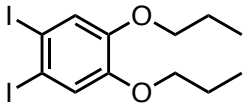

1,2-Diiodo-4,5-dipropoxybenzene (26)

1,2-dipropoxybenzene (**25**) (1.7 g, 8.8 mmol, 1.0 eq) was added to a round bottom flask with a stir bar and dissolved in DCM (100 mL, 0.08M). To the mixture was added iodine (4.9 g, 19.3 mmol, 2.2 eq) as well as $Hg(OAc)_2$ (6.15 g, 19.3 mmol, 2.2 eq) and the mixture was allowed to stir at room temperature. After stirring for 4 hours TLC indicates completion of the reaction. The mixture was diluted with 10% sodium thiosulfate solution (150 mL) transferred to a separatory funnel and shaken vigorously. The layers were separated, and the aqueous layer extracted with fresh DCM twice. The organics were combined, washed with 10% sodium thiosulfate, water, and brine, dried over $MgSO_4$, filtered and concentrated *in vacuo* to give a crude oil. Purification over a plug of SiO_2 eluting with 1:1 Hexanes:$CHCl_3$ gave the 3.03 g (77%) of the product **26** as a gold oil. ^{1}H NMR (500 MHz, $CDCl_3$) δ 7.25 (s, 1H), 3.90 (t, J = 6.6 Hz, 2H), 1.82 (sext, J = 6.7 Hz, 2H), 1.02 (t, J = 7.4 Hz, 3H). ^{13}C NMR (126 MHz, $CDCl_3$) δ 149.90, 123.96, 96.13, 71.08, 70.96, 22.57, 10.55. HRMS (DART) Calculated for $C_{12}H_{16}I_2O_2$ $[M^{\bullet+}]$:445.923417, found 445.92216.

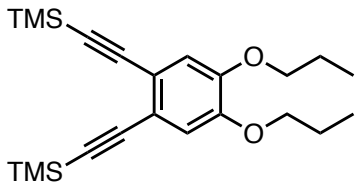

((4,5-Dipropoxy-1,2-phenylene)bis(ethyne-2,1-diyl))bis(trimethylsilane) (27)

1,2-diiodo-4,5-dipropoxybenzene (**26**) (3 g, 6.7 mmol, 1 eq) was added to a Shlenck tube with a stir bar followed by $PdCl_2(PPh_3)_2$ (235 mg, 0.34 mmol, .05 eq), CuI (127 mg, 0.67 mmol, 0.1 eq), and triethylamine (2.7 g, 26.8 mmol, 4 eq). Toluene (20 mL, 0.33M) was added and the mixture was sparged with Ar for 20 min. After sparging was complete, trimethylsilylacetylene (2.6 g, 26.8 mmol, 4 eq) was added and the mixture was sealed under Ar and allowed to stir at room temperature overnight. In the morning, analysis by ^{1}H NMR showed the reaction to be complete. The mixture was filtered over celite and concentrated *in vacuo*. Purification of the crude residue by filtration over SiO_2 eluting with a gradient of 0% to 40% $CHCl_3$ in Hexanes gave 2.5 g (95%) of the product **27** as a clear red oil. ^{1}H NMR (500 MHz, $CDCl_3$) δ 6.91 (s, 2H), 3.94 (t, J = 6.7 Hz, 4H), 1.83 (dtd, J = 14.0, 7.4, 6.6 Hz, 4H), 1.03 (t, J = 7.4 Hz, 6H), 0.26 (s, 18H). ^{13}C NMR (126 MHz, $CDCl_3$) δ 149.05, 118.74, 116.24, 103.61, 96.44, 70.53, 22.45, 10.41, -1.08. HRMS (DART) Calculated for $C_{22}H_{35}O_2Si_2$ $[M+H]^+$: 387.21700, found 387.21583.

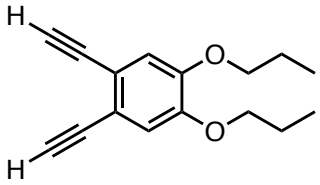

1,2-Diethynyl-4,5-dipropoxybenzene (28)

((4,5-dipropoxy-1,2-phenylene)bis(ethyne-2,1-diyl))bis(trimethylsilane) (**27**) (8 g, 20.7 mmol, 1 eq) was added to a round bottom flask equipped with a stir bar and dissolved in 1:1

MeOH:THF (100 mL, 0.2M). Potassium carbonate (7.1 g, 51.7 mmol, 2.5 eq) was added in one portion and the mixture allowed to stir at room temperature until the reaction was complete as indicated by TLC. Upon completion of the reaction the mixture was concentrated *in vacuo* and partitioned between water:Et_2O. The layers were separated, and the aqueous extracted with fresh Et_2O twice. The organics were pooled and washed with brine, dried over $MgSO_4$, filtered and concentrated *in vacuo* to give a crude residue which was purified by column chromatography over SiO_2 eluting with a gradient of 0% to 20% DCM in hexanes. This provided 4.2 g (84%) of the product **28** as a crystalline orange solid. ^{1}H NMR (500 MHz, $CDCl_3$) δ 6.96 (s, 2H), 3.96 (t, J = 6.6 Hz, 4H), 3.25 (s, 2H), 1.84 (dtd, J = 14.0, 7.4, 6.6 Hz, 4H), 1.04 (t, J = 7.4 Hz, 6H). ^{13}C NMR (126 MHz, $CDCl_3$) δ 149.52, 117.93, 116.73, 82.32, 79.54, 70.75, 22.55, 10.54. HRMS (DART) Calculated for $C_{16}H_{19}O_2$ $[M+H]^+$: 243.13796, found 243.13636.

Oligomerization of 1,2-diethynyl-4,5-dipropoxybenzene (28)

1,2-diethynyl-4,5-dipropoxybenzene (**28**) (750 mg, 3.1 mmol, 1 eq) was added to a small pressure tube and dissolved in benzene (20 mL, 0.15 M). 1,4-Cyclohexadiene (372 mg, 4.6 mmol, 1.5 eq) was added in a single portion and the mixture freeze-pump-thawed three times. The tube was then sealed and heated to 220 ˚C for two days. The mixture was then cooled and concentrated *in vacuo*. The crude residue was fractionated by column chromatography over SiO_2 eluting with a gradient of 0% to 100% $CHCl_3$ in hexanes and then 0% to 15% MeOH in $CHCl_3$. This provided three major fractions that contained mixtures of monomeric adducts (least polar), dimeric adducts (medium polarity) and higher oligomers (high polarity). The isolated mixtures were further purified by individual preparative TLC to give compounds of suitable purity for NMR analysis.

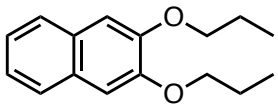

2,3-Dipropoxynaphthalene (29)

This compound was isolated as the major component of the monomeric mixture. 230 mg was recovered during column chromatography which contained small impurities. An analytical sample was purified by preparative TLC. ^{1}H NMR (500 MHz, $CDCl_3$) δ 7.70 – 7.63 (m, 2H), 7.32 (dd, *J* = 6.1, 3.2 Hz, 2H), 7.13 (s, 2H), 4.09 (t, *J* = 6.6 Hz, 4H), 1.94 (dtd, *J* = 14.0, 7.4, 6.6 Hz, 4H), 1.10 (t, *J* = 7.4 Hz, 6H). ^{13}C NMR (126 MHz, $CDCl_3$) δ 149.54, 129.37, 126.34, 124.06, 108.02, 70.42, 22.61, 10.66. HRMS (DART) Calculated for $C_{16}H_{21}O_2$ $[M+H]^+$: 245.15361, found 245.15241.

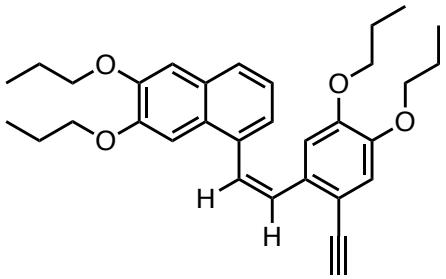

(*Z*)-1-(2-Ethynyl-4,5-dipropoxystyryl)-6,7-dipropoxynaphthalene (28-D-*cis*)

Compound **28-D-*cis*** was isolated as the less polar of the dimeric adducts. Purification by preparative TLC, eluting multiple times with 30% $CHCl_3$ in hexanes provided 11 mg of the title compound as a clear residue. ^{1}H NMR (500 MHz, CD_2Cl_2) δ 7.58 (dd, *J* = 7.9, 1.5 Hz, 1H), 7.28 – 7.23 (m, 1H), 7.22 (t, *J* = 1.3 Hz, 1H), 7.21 (s, 1H), 7.15 (d, *J* = 12.2 Hz, 1H), 7.12 (s, 1H), 7.02 (d, *J* = 12.2 Hz, 1H), 6.89 (s, 1H), 6.31 (s, 1H), 4.04 (t, *J* = 6.6 Hz, 2H), 3.88 (t, *J* = 6.7 Hz, 2H), 3.83 (t, *J* = 6.7 Hz, 2H), 3.36 (s, 1H), 2.91 (t, *J* = 7.0 Hz, 2H), 1.88 (dt, *J* = 7.5, 6.7 Hz, 2H), 1.84 – 1.77 (m, 2H), 1.74 (dt, *J* = 7.5, 6.7 Hz, 2H), 1.31 – 1.21 (m, 2H), 1.08 (t, *J* = 7.4 Hz, 3H), 1.03

(t, J = 7.4 Hz, 3H), 0.97 (t, J = 7.4 Hz, 3H), 0.66 (t, J = 7.4 Hz, 3H). ^{13}C NMR (126 MHz, CD_2Cl_2) δ 149.90, 149.74, 149.13, 148.10, 134.31, 133.21, 130.06, 129.94, 128.94, 126.98, 126.18, 124.75, 124.11, 116.70, 113.94, 113.60, 108.37, 106.00, 82.74, 80.74, 70.79, 70.51, 69.93, 22.91, 22.85, 22.82, 22.22, 10.68, 10.66, 10.52, 10.08. HRMS (DART) Calculated for $C_{32}H_{39}O_4$ $[M+H]^+$: 487.28429, found 487.28123.

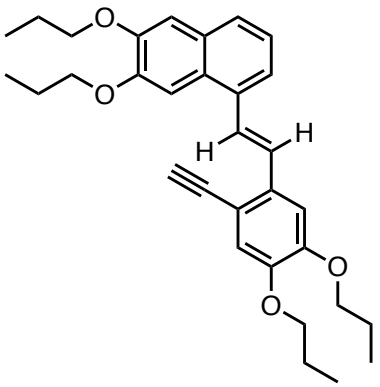

(*E*)-1-(2-Ethynyl-4,5-dipropoxystyryl)-6,7-dipropoxynaphthalene (28-D-*trans*)

Compound **28-D-*trans*** was isolated as the more polar of the dimeric adducts. Purification by preparative TLC, eluting multiple times with 30% $CHCl_3$ in hexanes provided 10 mg of the title compound as a clear residue. ^{1}H NMR (500 MHz, CD_2Cl_2) δ 7.71 (d, J = 16.0 Hz, 1H), 7.63 (d, J = 8.1 Hz, 1H), 7.60 (d, J = 7.2 Hz, 1H), 7.55 (d, J = 16 Hz, 1H), 7.47 (s, 1H), 7.33 (t, J = 7.7 Hz, 1H), 7.28 (s, 1H), 7.17 (s, 1H), 7.02 (s, 1H), 4.09 (dt, J = 10.2, 6.6 Hz, 6H), 3.98 (t, J = 6.6 Hz, 2H), 3.34 (s, 1H), 2.10 – 1.74 (m, 8H), 1.21 – 0.98 (m, 12H). ^{13}C NMR (126 MHz, CD_2Cl_2) δ 150.60, 150.01, 149.81, 149.10, 133.95, 133.90, 130.25, 129.29, 127.43, 126.80, 126.73, 124.31, 122.59, 117.55, 113.78, 110.21, 108.73, 105.03, 82.64, 80.97, 71.15, 71.10, 70.92, 70.55, 30.09, 23.03, 23.00, 22.96, 22.93, 10.73, 10.71, 10.65, 10.62. HRMS (DART) Calculated for $C_{32}H_{39}O_4$ $[M+H]^+$: 487.28429, found 487.28174.

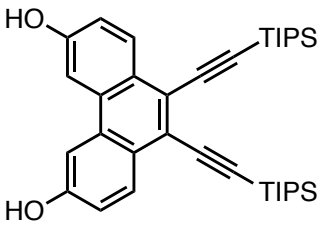

9,10-Bis((triisopropylsilyl)ethynyl)phenanthrene-3,6-diol (30)

((9,10-bis((triisopropylsilyl)ethynyl)phenanthrene-3,6-diyl)bis(oxy))bis-(triisopropylsilane) (**21**) (2.04 g, 2.3 mmol, 1 eq) was added to a round bottom flask equipped with a stir bar, dissolved in THF (50 mL, 0.05M) and cooled to -78 ˚C. To this mixture was added a 1M solution of TBAF in THF (4.6 mL, 4.6 mmol, 2 eq). The mixture was stirred at -78 ˚C until judged complete by TLC. Once complete, the mixture was diluted with sat NH_4Cl and allowed to warm to room temperature. The mixture was diluted with Et_2O, transferred to a separatory funnel and the layers separated. The aqueous layer was extracted twice with fresh Et_2O, organics pooled, washed twice with brine, dried over $MgSO_4$, filtered and concentrated *in vacuo* to produce a crude product that was purified by chromatography over SiO_2 eluting with a gradient of 50% to 100% hexanes:DCM and then 0% to 8% MeOH:DCM to provide 1.16 g (87%) of the product **30** as an off yellow oil. ^{1}H NMR (500 MHz, $CDCl_3$) δ 8.43 (d, J = 8.9 Hz, 1H), 7.83 (d, J = 2.5 Hz, 1H), 7.19 (dd, J = 8.9, 2.5 Hz, 1H), 5.60 (s, 1H), 1.22 (q, J = 4.9 Hz, 21H). ^{13}C NMR (126 MHz, $CDCl_3$) δ 155.21, 130.86, 129.75, 126.31, 121.22, 117.62, 107.18, 104.31, 100.69, 19.04, 11.68. HRMS (DART) Calculated for $C_{36}H_{51}O_2Si_2$ $[M+H]^+$: 571.34221, found 571.33864.

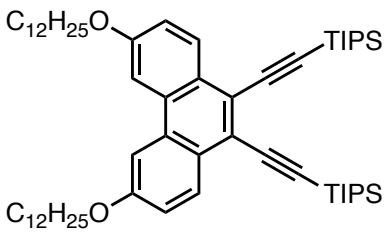

((3,6-Bis(dodecyloxy)phenanthrene-9,10-diyl)bis(ethyne-2,1-diyl))bis(triisopropylsilane) (31)

9,10-bis((triisopropylsilyl)ethynyl)phenanthrene-3,6-diol (**30**) (600 mg, 1.05 mmol, 1 eq) was dissolved in DMF (30 mL, 0.03M) in a round bottom flask equipped with a stir bar and K_2CO_3 (2 g, 14.7 mmol, 14 eq) was added followed by bromododecane (2.6 g, 10.5 mmol, 10 eq). The resulting mixture was gently heated to 60 ˚C until the reaction was complete as judged by TLC. Upon completion of the reaction, the mixture was cooled and diluted with water (150 mL) and Et_2O (100 mL). The layers were separated and the aqueous layer extracted twice with Et_2O. The organic layers were pooled, washed thrice with water, thrice with brine, dried over $MgSO_4$, filtered and concentrated *in vacuo* to produce a crude product which was purified by chromatography over SiO_2 using a gradient of 0% to 50% DCM in hexanes. This provided 920 mg (96%) of the product **31** as a clear light yellow oil. ^{1}H NMR (500 MHz, $CDCl_3$) δ 8.46 (d, J = 9.0 Hz, 1H), 7.88 (d, J = 2.5 Hz, 1H), 7.28 (dd, J = 9, 2.4 Hz, 1H), 4.17 (t, J = 6.5 Hz, 2H), 1.88 (p, J = 6.7 Hz, 2H), 1.59 – 1.46 (m, 2H), 1.40 – 1.14 (m, 36H), 0.95 – 0.83 (m, 3H). ^{13}C NMR (126 MHz, $CDCl_3$) δ 158.68, 130.88, 129.36, 126.18, 121.10, 117.06, 105.71, 104.52, 100.44, 68.46, 32.07, 29.83, 29.80, 29.77, 29.60, 29.54, 29.51, 26.28, 22.84, 22.81, 19.06, 14.27, 11.69. HRMS (DART) Calculated for $C_{60}H_{99}O_2Si_2$ $[M+H]^+$: 907.71781, found 907.71267.

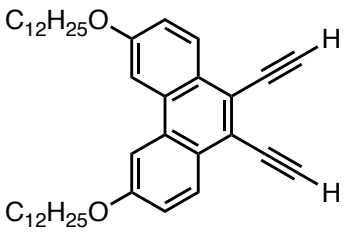

3,6-Bis(dodecyloxy)-9,10-diethynylphenanthrene (32)

((3,6-bis(dodecyloxy)phenanthrene-9,10-diyl)bis(ethyne-2,1-diyl))bis(triisopropylsilane) (**31**) (920 mg, 1.01 mmol, 1 eq) was added to a round bottom flask equipped with a stir bar, dissolved in THF (20 mL, 0.05M) and cooled to -10 ˚C. To this mixture was added a 1M solution of TBAF in THF (2.1 mL, 2.1 mmol, 2.1 eq). The mixture was stirred at -10 ˚C until judged complete by TLC. Once complete, the mixture was diluted with sat NH_4Cl and allowed to warm to room temperature. The mixture was diluted with Et_2O, transferred to a separatory funnel and the layers separated. The aqueous layer was extracted twice with fresh Et_2O, organics pooled, washed twice with brine, dried over $MgSO_4$, filtered and concentrated *in vacuo* to produce a crude product that was purified by chromatography over SiO_2 eluting with a gradient of 0% to 50% DCM: hexanes to provide 423 mg (70%) of the product **32** as a white solid. ^{1}H NMR (500 MHz, $CDCl_3$) δ 8.37 (d, J = 9.0 Hz, 2H), 7.89 (d, J = 2.5 Hz, 2H), 7.29 (dd, J = 9.0, 2.4 Hz, 2H), 4.18 (t, J = 6.6 Hz, 4H), 3.74 (s, 2H), 1.94 – 1.84 (m, 4H), 1.56 – 1.49 (m, 4H), 1.41 – 1.23 (m, 32H), 0.91 – 0.85 (m, 6H). ^{13}C NMR (126 MHz, $CDCl_3$) δ 158.99, 131.05, 129.15, 125.55, 120.99, 117.46, 105.61, 85.67, 81.37, 68.52, 32.07, 29.83, 29.80, 29.77, 29.76, 29.61, 29.51, 26.27, 22.84, 18.29, 14.28. HRMS (DART) Calculated for $C_{42}H_{58}O_2$ [$M^{\bullet+}$]: 594.44313, found 594.44079.

Oligomerization of 3,6-bis(dodecyloxy)-9,10-diethynylphenanthrene (32)

3,6-bis(dodecyloxy)-9,10-diethynylphenanthrene (**32**) (60 mg, 0.1 mmol, 1 eq) was placed in a small Schlenk bomb, dissolved in benzene (670 μL, 0.15M) and 1,4-cyclohexadiene (40 mg, 0.5 mmol, 5 eq) was added in a single portion. The mixture was freeze-pumped-thaw thrice before sealing under Ar. The mixture was subsequently heated to 180 ˚C overnight. In the morning the mixture was cooled and evaporated to give a crude residue which was subjected to initial column chromatography on SiO_2 eluting with a gradient of 0% to 40% DCM in Hexanes. The mixed

fractions were separated based on polarity into least polar (monomer adducts), moderately polar (dimer adducts) and most polar (trimers and higher oligomers). The fractions were further separated by individual purification by preparative TLC eluting with 30% DCM in Hexanes.

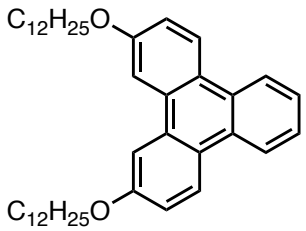

2,11-Bis(dodecyloxy)triphenylene (33)

Compound **33** was isolated as the major component of the least polar mixed fractions (monomer adducts). 24 mg of triphenylene **33** was isolated as a clear oil. 1H NMR (500 MHz, $CDCl_3$) δ 8.55 (d, *J* = 9.1 Hz, 2H), 8.52 (dd, *J* = 6.3, 3.4 Hz, 2H), 7.96 (d, *J* = 2.6 Hz, 2H), 7.56 (dd, *J* = 6.2, 3.2 Hz, 2H), 7.28 (dd, *J* = 9.1, 2.6 Hz, 2H), 4.19 (t, *J* = 6.6 Hz, 4H), 2.00 – 1.80 (m, 4H), 1.60 – 1.51 (m, 4H), 1.45 – 1.23 (m, 32H), 0.96 – 0.70 (m, 6H). ^{13}C NMR (126 MHz, $CDCl_3$) δ 158.49, 131.14, 129.06, 126.36, 125.06, 124.18, 122.85, 116.07, 107.16, 68.46, 32.08, 29.84, 29.80, 29.79, 29.64, 29.59, 29.51, 26.30, 22.85, 14.28. HRMS (DART) Calculated for $C_{42}H_{58}O_2$ [$M^{\bullet+}$]: 594.44313, found 594.44079.

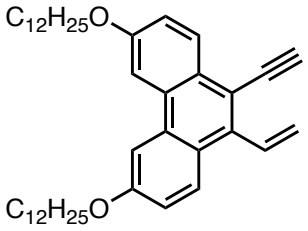

3,6-Bis(dodecyloxy)-9-ethynyl-10-vinylphenanthrene (34)

Compound **34** was isolated as the minor component of the least polar mixed fractions (monomer adducts). 3 mg of alkene **34** was isolated as a clear residue. ^{1}H NMR (500 MHz, CD_2Cl_2) δ 8.41 (d, J = 9.0 Hz, 1H), 8.19 (d, J = 9.1 Hz, 1H), 7.97 (d, J = 2.6 Hz, 1H), 7.95 (d, J = 2.5 Hz, 1H), 7.32 – 7.24 (m, 3H), 5.85 (dd, J = 11.5, 1.8 Hz, 1H), 5.76 (dd, J = 17.8, 1.8 Hz, 1H), 4.20 (td, J = 6.6, 1.4 Hz, 4H), 3.70 (s, 1H), 2.01 – 1.84 (m, 4H), 1.39 – 1.18 (m, 36H), 0.89 (t, J = 6.7 Hz, 6H). ^{13}C NMR (126 MHz, CD_2Cl_2) δ 158.51, 158.17, 137.45, 134.18, 131.45, 130.23, 128.62, 128.27, 125.74, 124.48, 121.90, 117.28, 116.77, 113.49, 105.45, 105.20, 85.64, 81.40, 68.38, 68.35, 31.92, 29.67, 29.62, 29.45, 29.38, 29.35, 26.08, 22.69, 13.87. HRMS (DART) Calculated for $C_{42}H_{61}O_2$ $[M+H]^+$: 597.46661, found 597.46300.

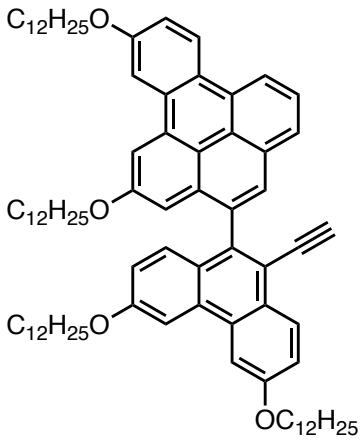

4-(3,6-Bis(dodecyloxy)-10-ethynylphenanthren-9-yl)-2,11-bis(dodecyloxy)benzo[*e*]pyrene (35)

Compound **35** was isolated as the major component of the moderate polarity mixed fractions (dimer adducts). 4 mg of dimer **35** was isolated as a clear residue. ^{1}H NMR (500 MHz,

$CDCl_3$) δ 8.85 – 8.81 (m, 1H), 8.79 (d, *J* = 9.2 Hz, 1H), 8.51 (d, *J* = 8.9 Hz, 1H), 8.35 (d, *J* = 2.4 Hz, 1H), 8.19 (d, *J* = 2.6 Hz, 1H), 8.15 – 8.10 (m, 1H), 8.09 (d, *J* = 2.5 Hz, 1H), 8.06 (s, 1H), 8.05 (d, *J* = 2.7 Hz, 1H), 7.98 (t, *J* = 7.7 Hz, 1H), 7.39 (dd, *J* = 8.9, 2.5 Hz, 2H), 7.35 (d, *J* = 9.1 Hz, 1H), 7.15 (d, *J* = 2.3 Hz, 1H), 6.95 (dd, *J* = 9.1, 2.5 Hz, 1H), 4.26 (td, *J* = 6.6, 1.6 Hz, 4H), 4.15 (t, *J* = 6.5 Hz, 2H), 3.98 – 3.82 (m, 2H), 3.01 (s, 1H), 1.94 (dt, *J* = 13.2, 6.5 Hz, 4H), 1.86 (p, *J* = 6.7 Hz, 2H), 1.55 (m, 2H) 1.50 – 1.07 (m, 72H), 0.88 (m, 12H). ^{13}C NMR (126 MHz, $CDCl_3$) δ 158.87, 158.57, 158.41, 157.59, 139.75, 136.21, 133.37, 131.67, 131.58, 131.01, 130.95, 130.53, 130.31, 129.93, 129.12, 128.58, 126.63, 126.24, 125.76, 125.49, 124.45, 123.58, 120.05, 117.38, 116.89, 116.82, 116.59, 109.76, 108.88, 107.32, 105.69, 85.04, 81.40, 68.60, 68.52, 68.46, 68.36, 32.07, 32.06, 29.85, 29.81, 29.72, 29.68, 29.66, 29.62, 29.60, 29.58, 29.51, 29.50, 29.34, 26.33, 26.27, 26.18, 22.84 (d, *J* = 2.0 Hz), 14.27 (d, *J* = 2.0 Hz), 10.33, 1.17. HRMS (MALDI-TOF) Calculated for $C_{84}H_{116}O_4$ [$M^{\bullet+}$]: 1188.8874, found 1188.8651.

Section 3.6: Appendix C

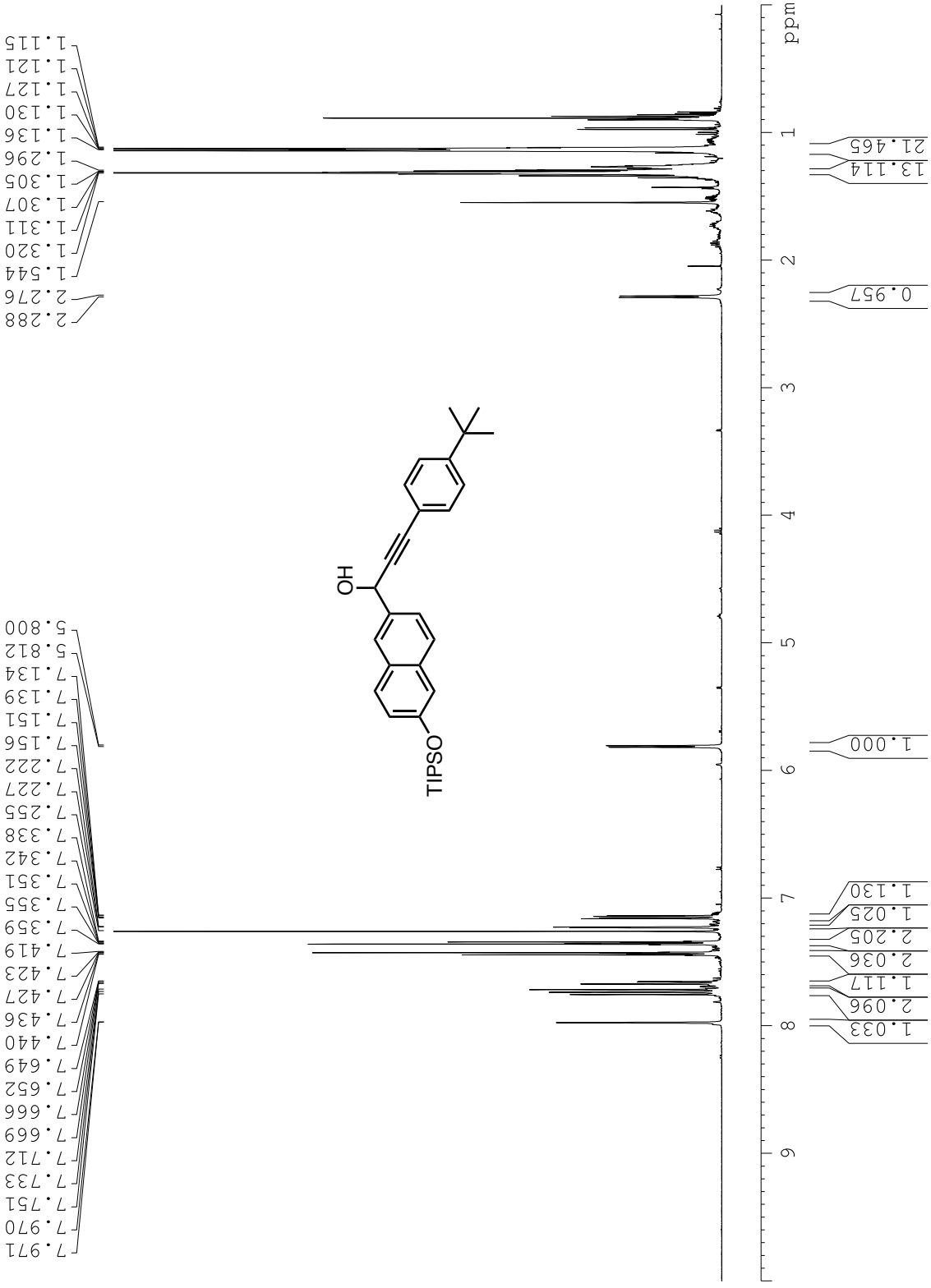

Figure C1. ^{1}H NMR spectrum of compound **4**.

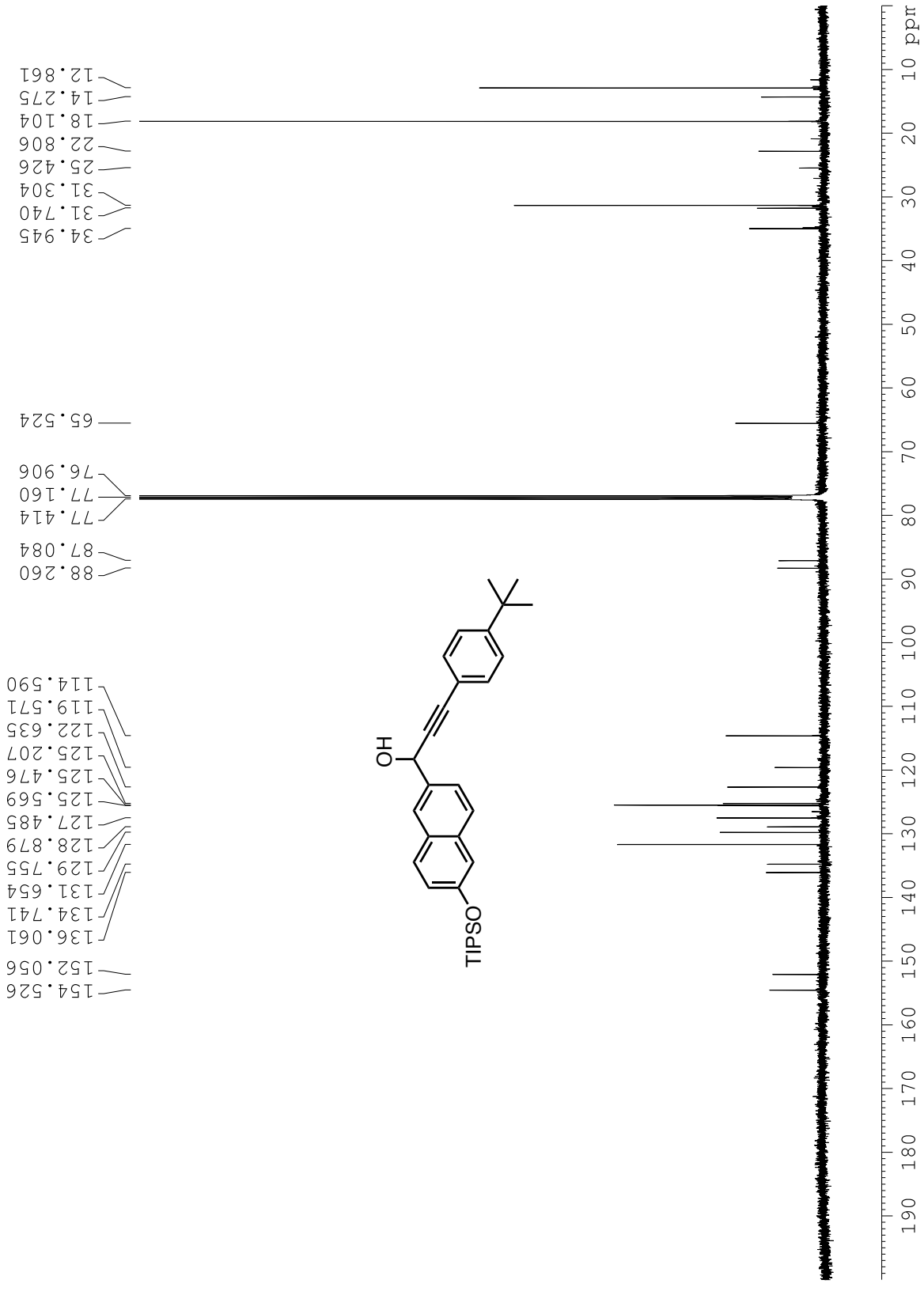

Figure C2. ^{13}C NMR spectrum of compound **4**.

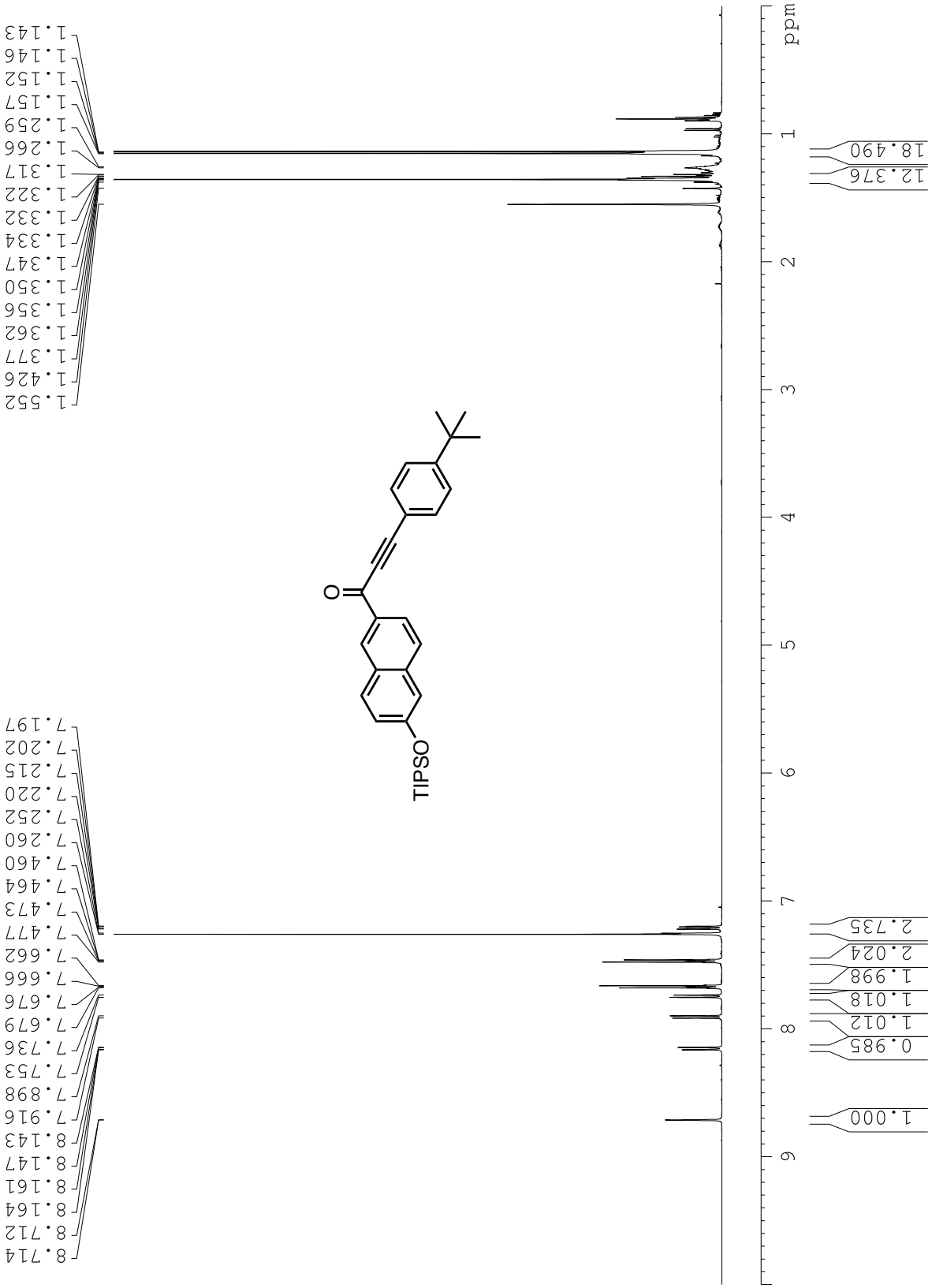

Figure C3. ^{1}H NMR spectrum of compound **5**.

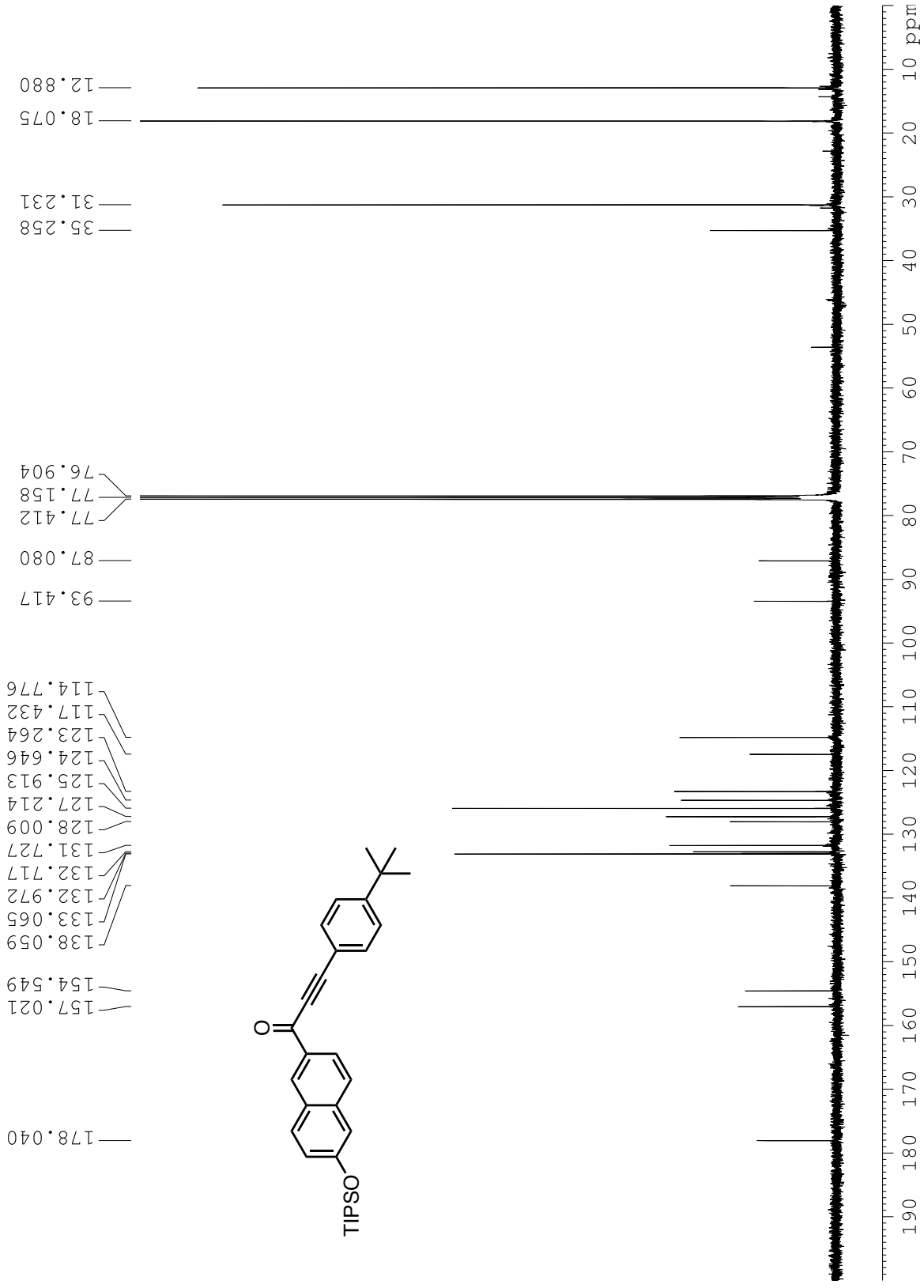

Figure C4. ^{13}C NMR spectrum of compound **5**.

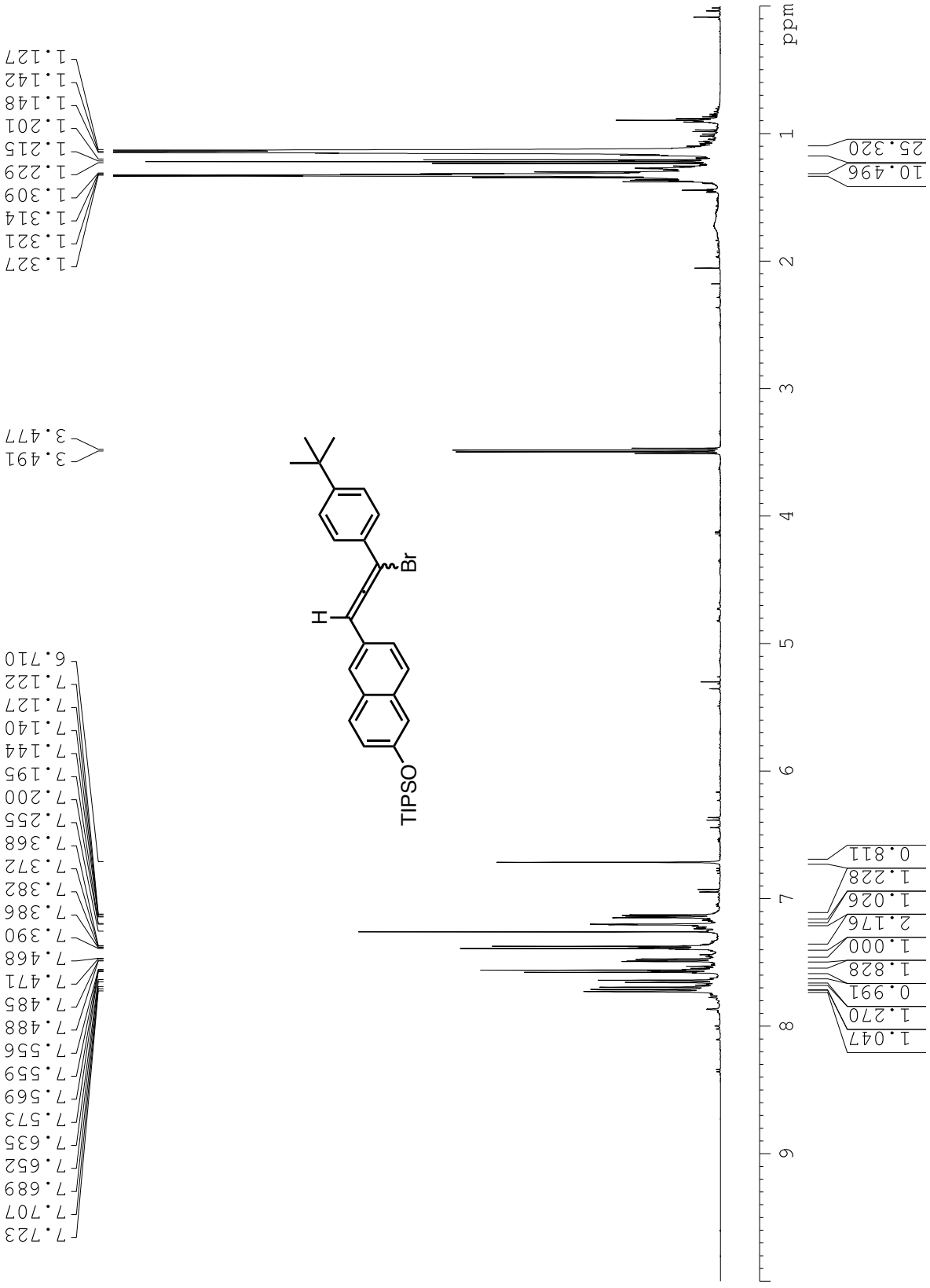

Figure C5. ^{1}H NMR spectrum of compound **6**.

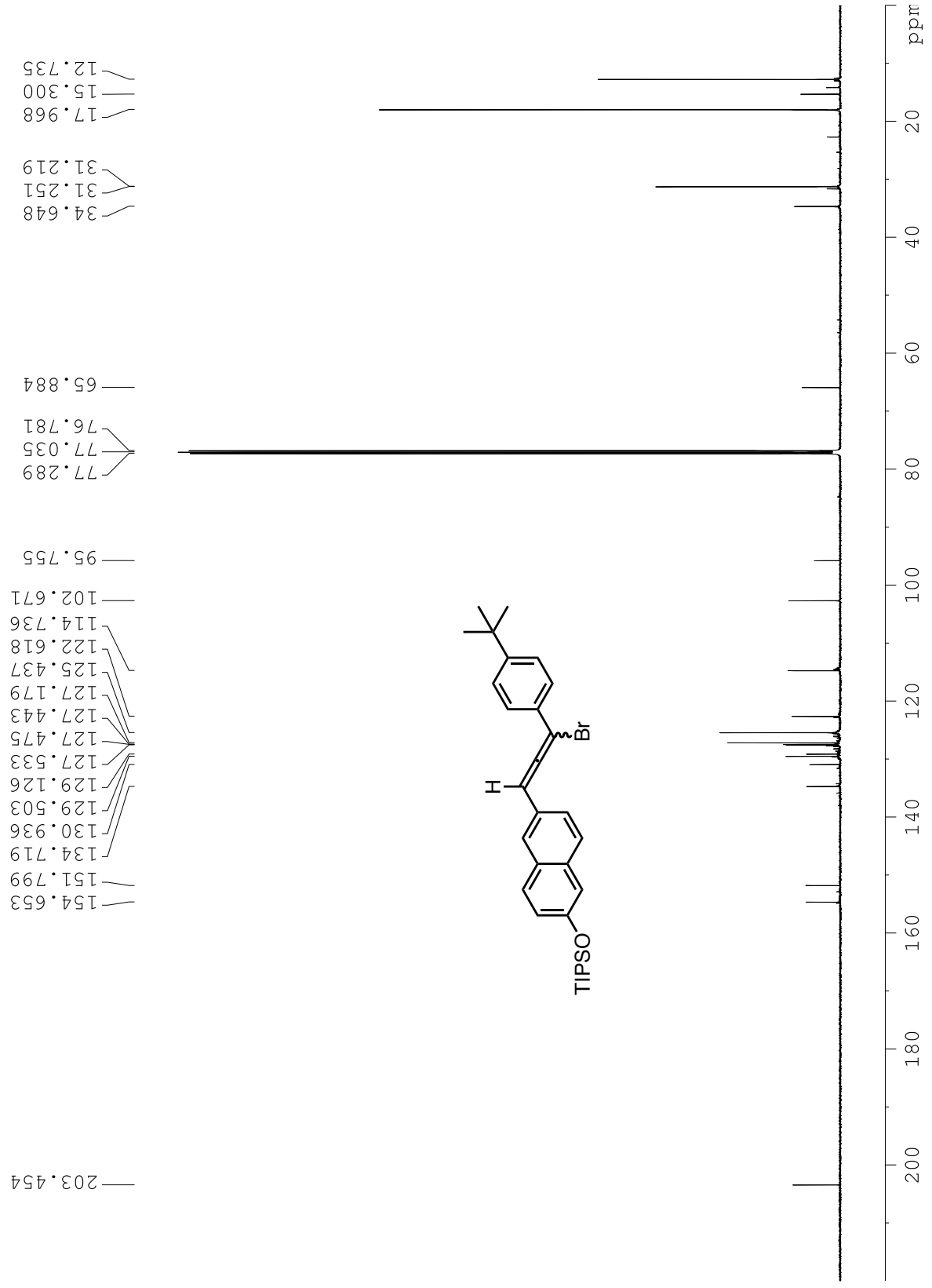

Figure C6. ^{13}C NMR spectrum of compound **6**.

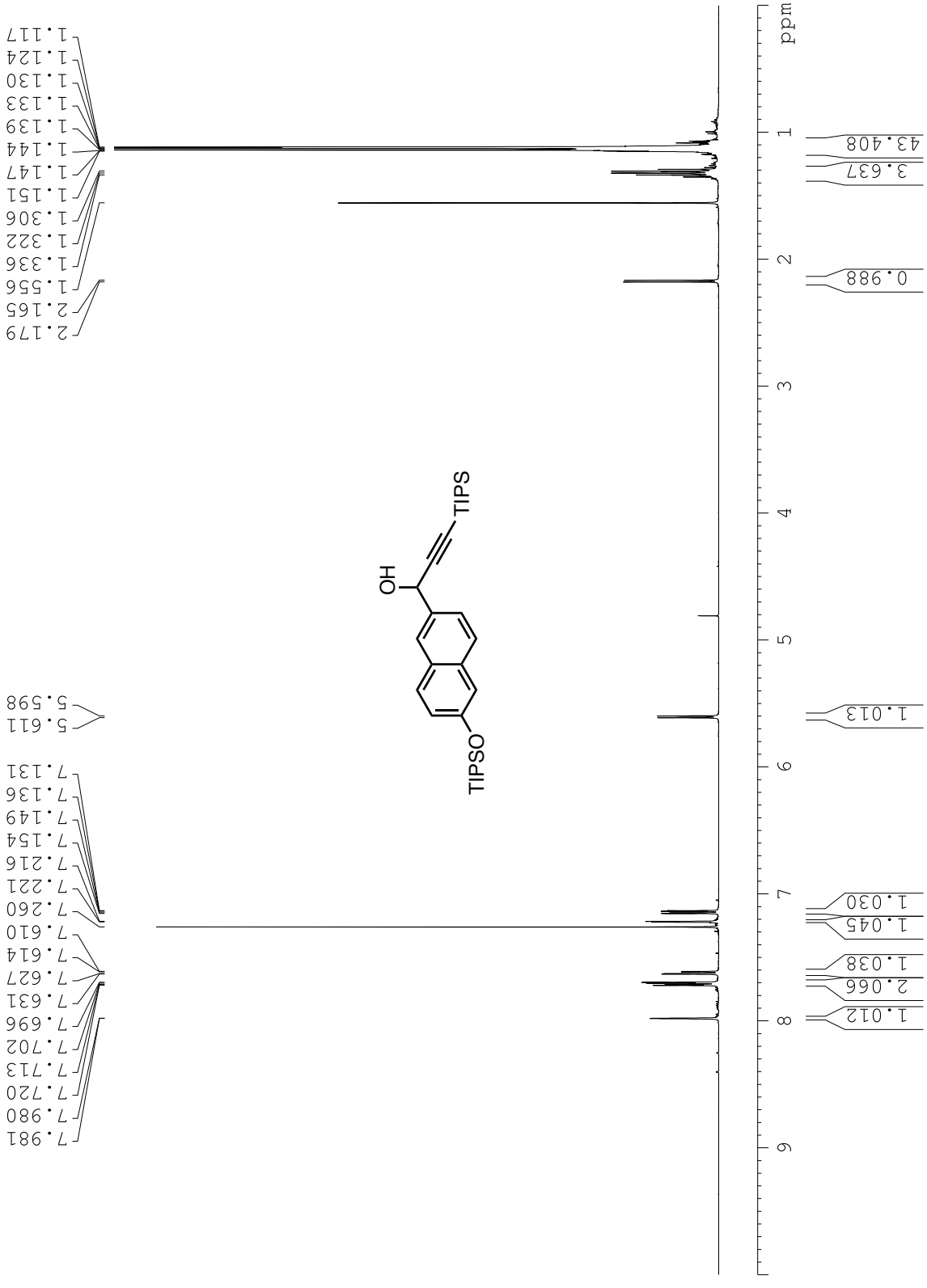

Figure C7. ^{1}H NMR spectrum of compound **7**.

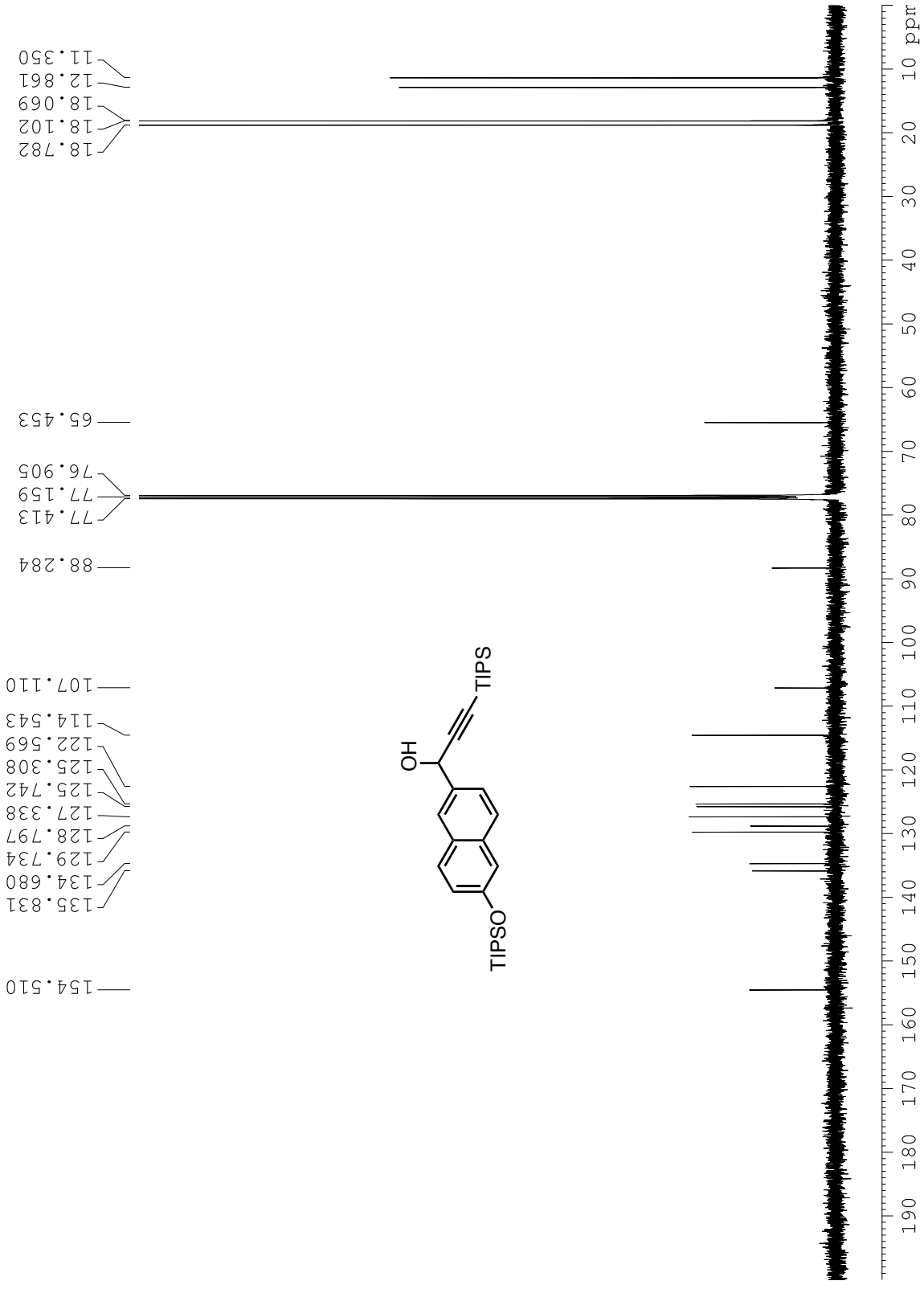

Figure C8. ^{13}C NMR spectrum of compound **7**.

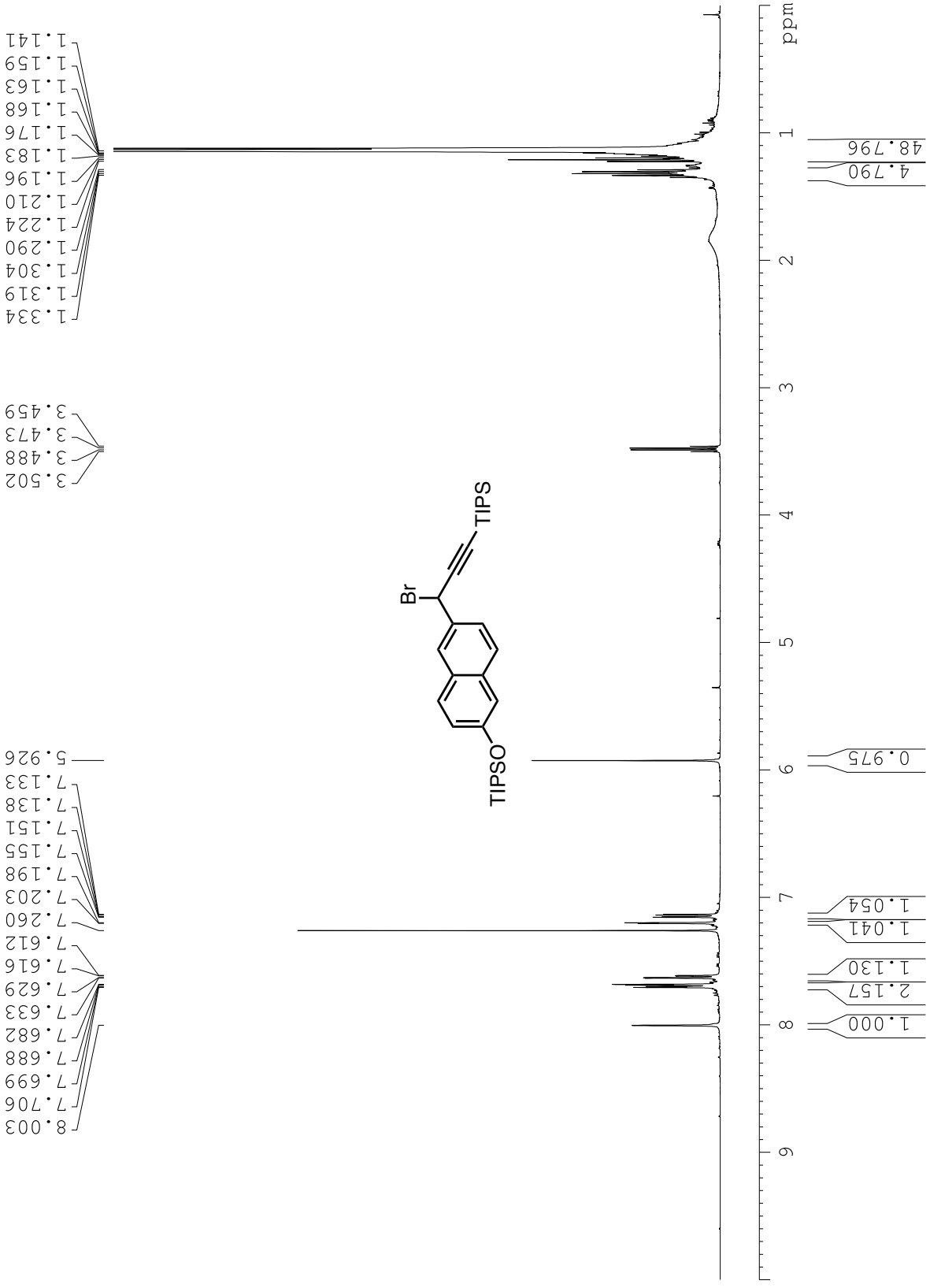

Figure C9. ^{1}H NMR spectrum of compound **8**.

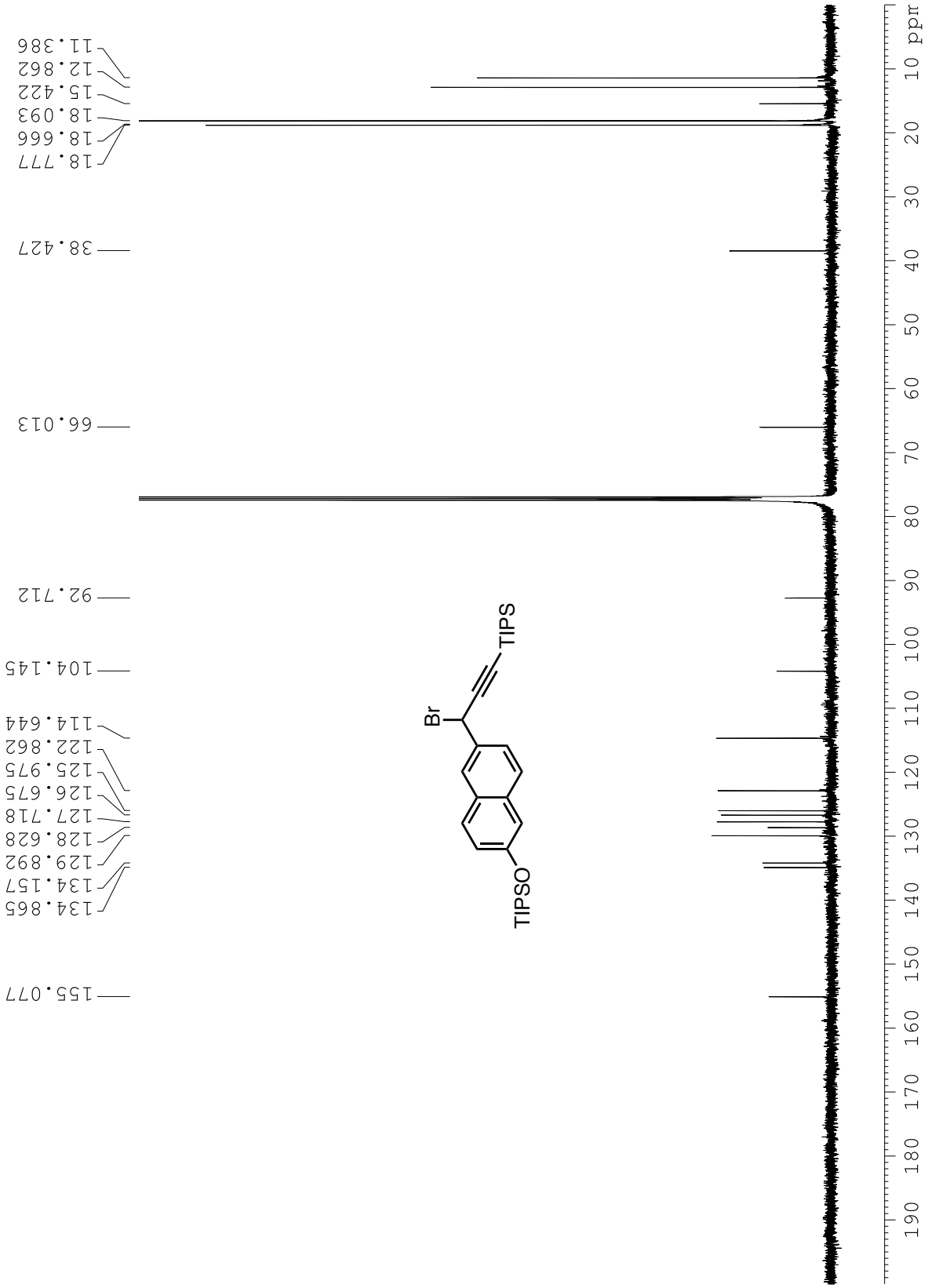

Figure C10. ^{13}C NMR spectrum of compound **8**.

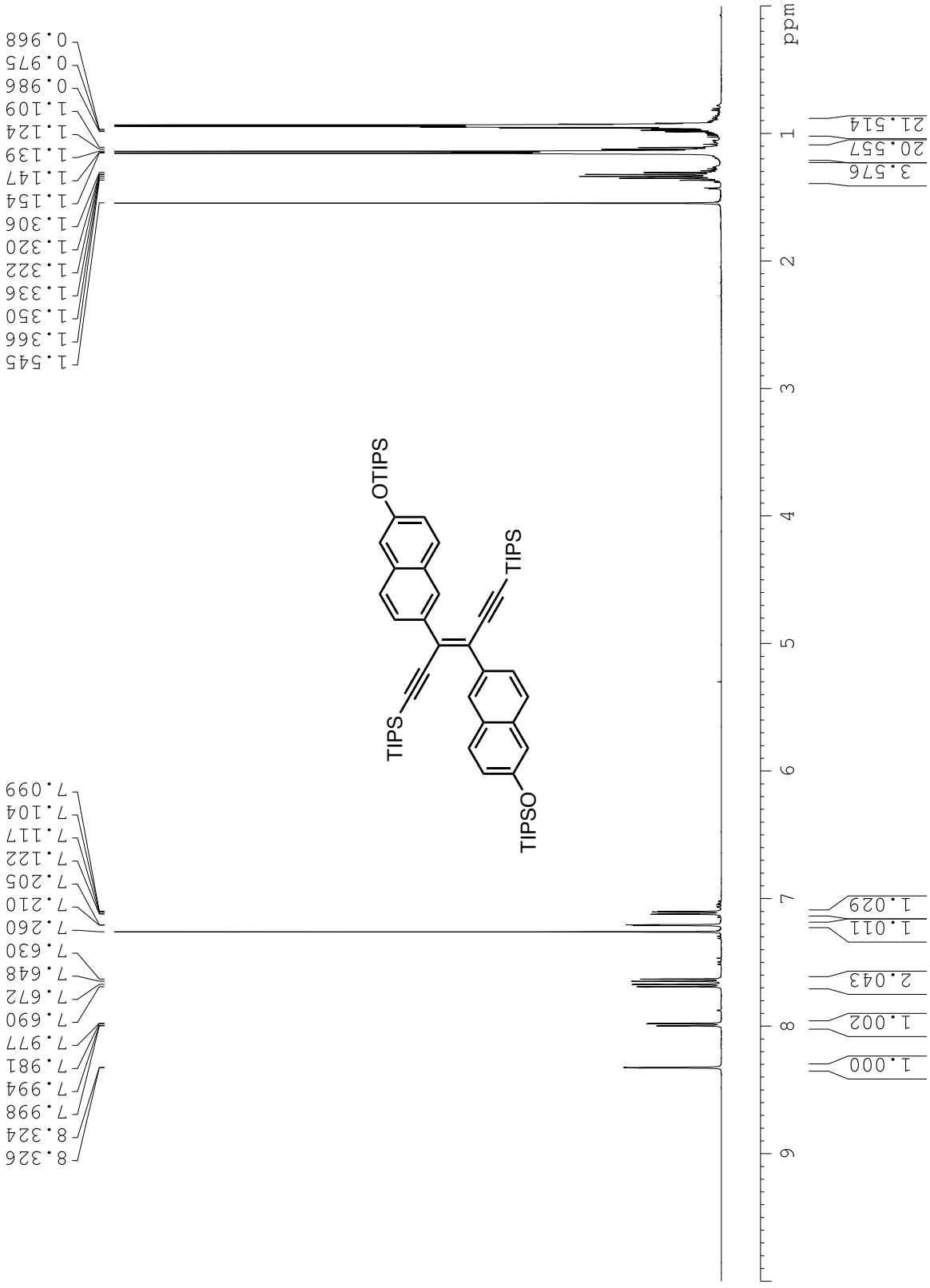

Figure C11. ^{1}H NMR spectrum of compound **9**.

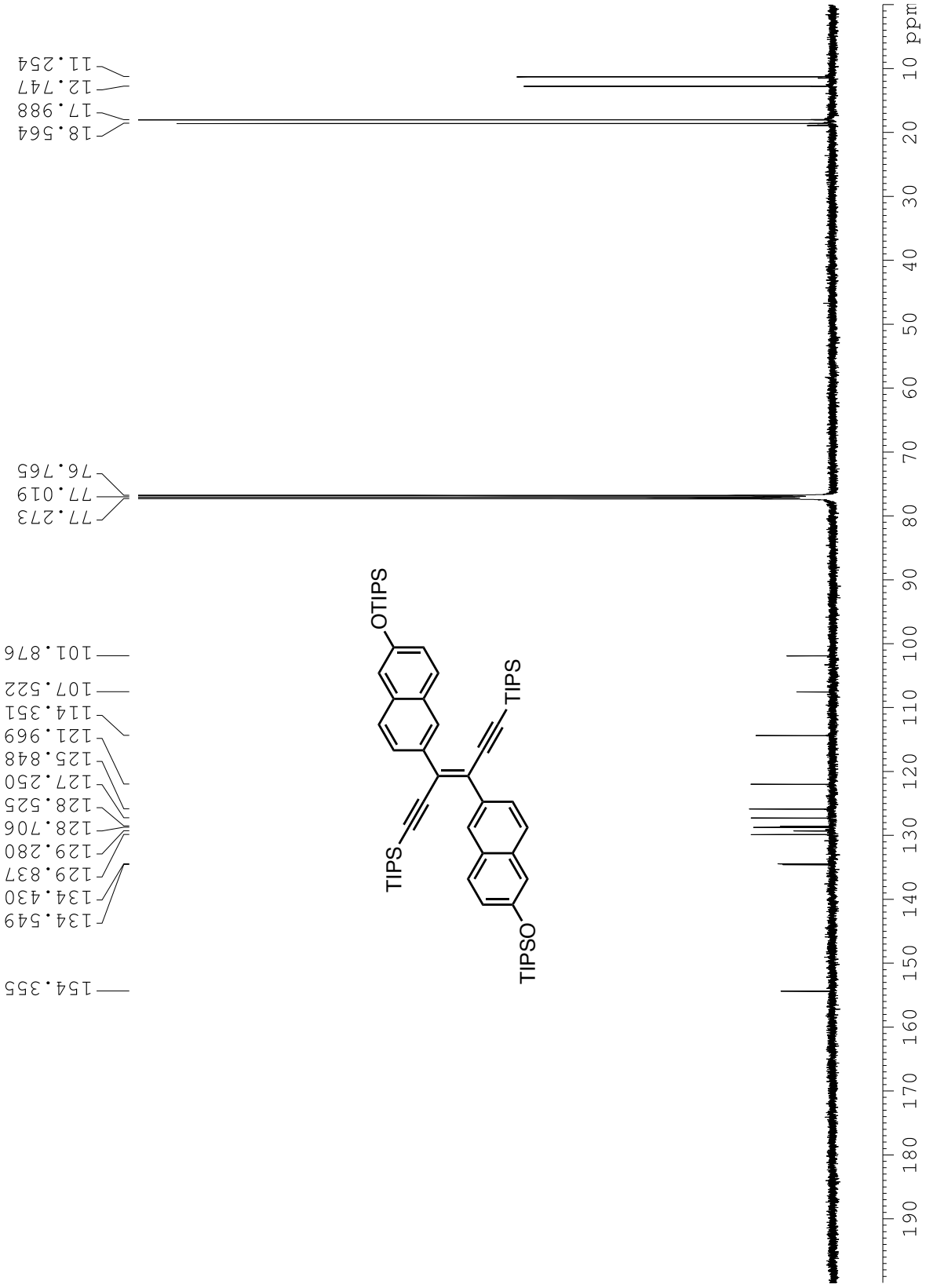

Figure C12. ^{13}C NMR spectrum of compound **9**.

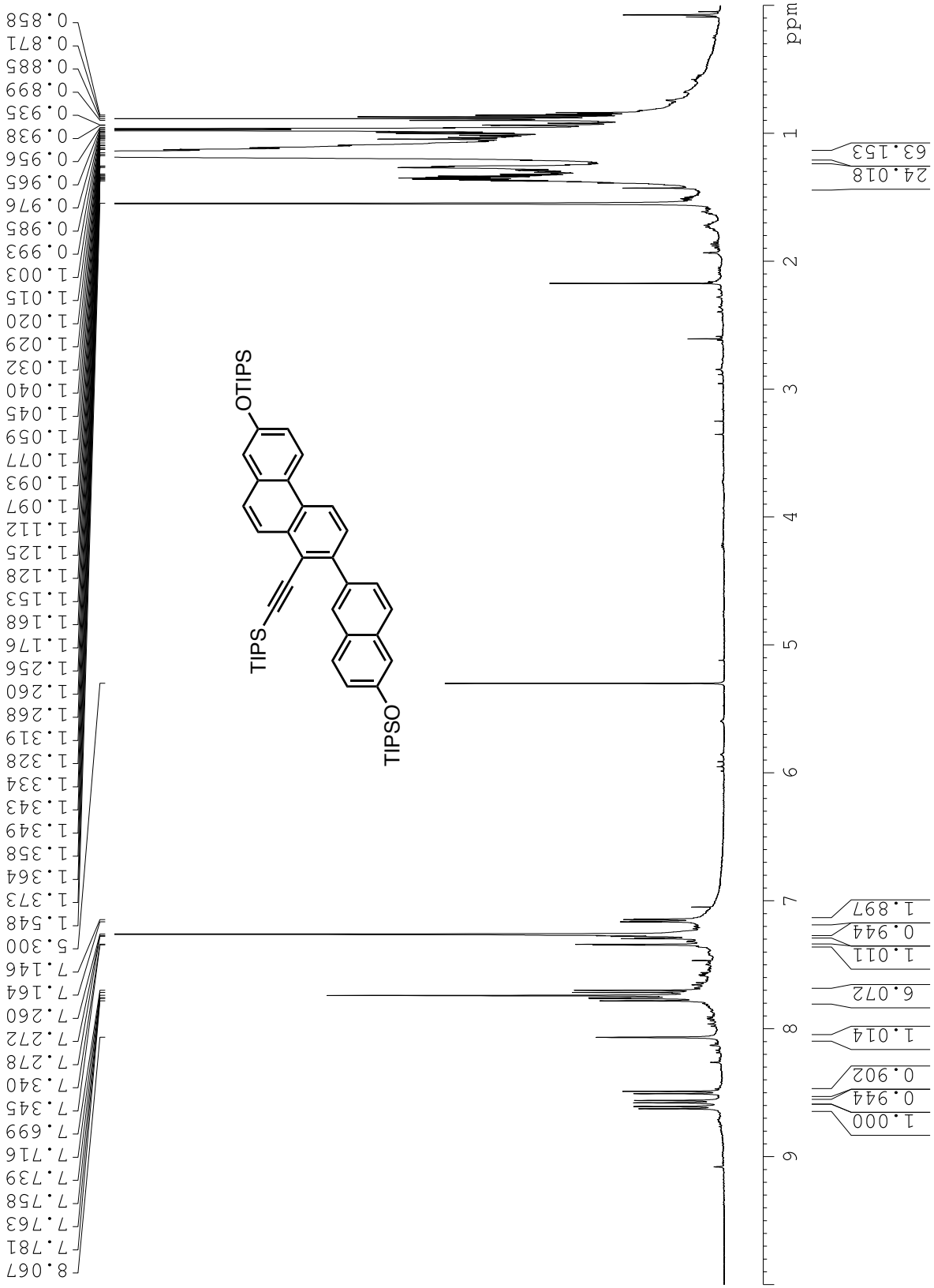

Figure C13. ^{1}H NMR spectrum of compound **10**.

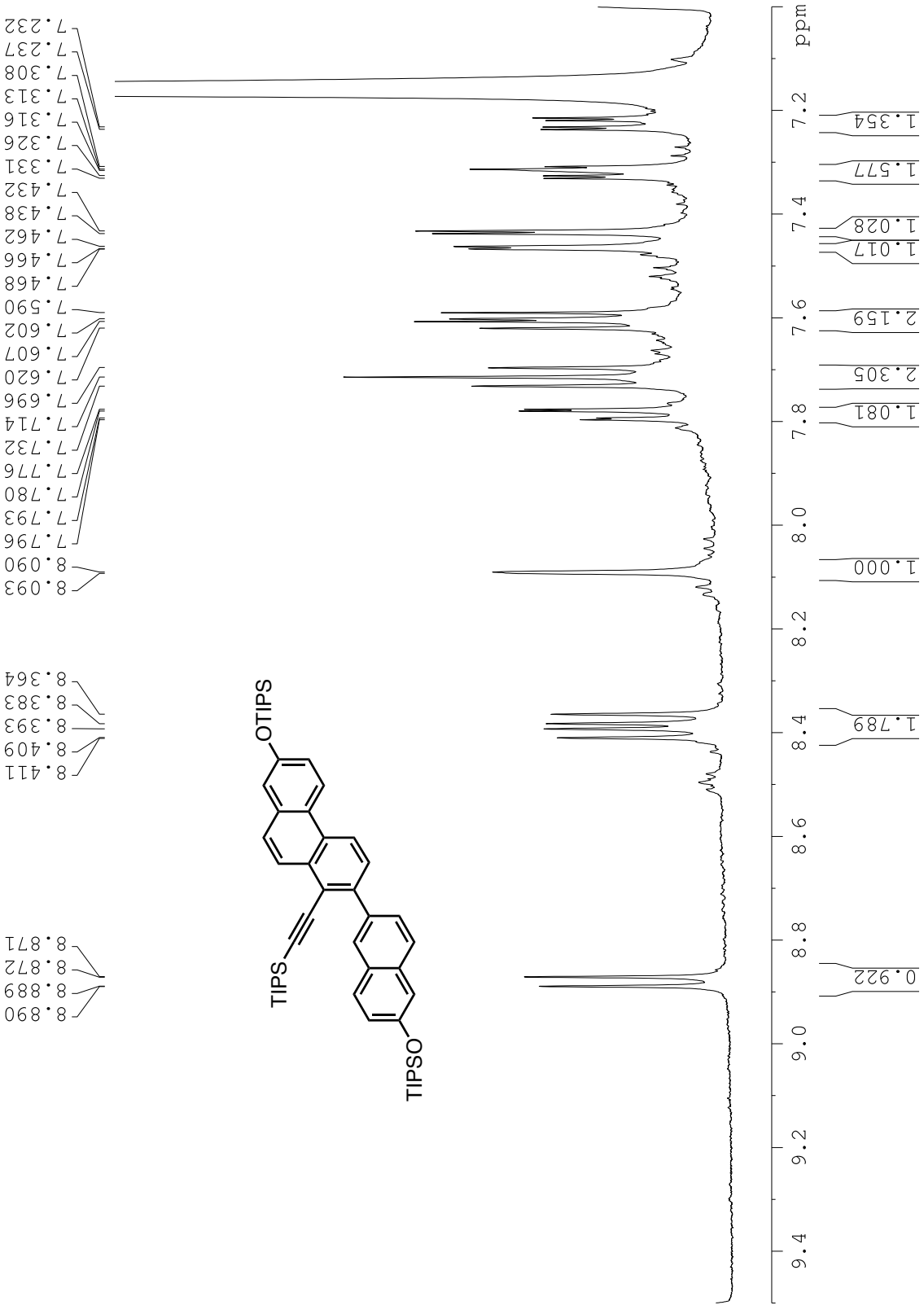

Figure C14. ^{1}H NMR spectrum of aryl region of compound **10** in C_6D_6.

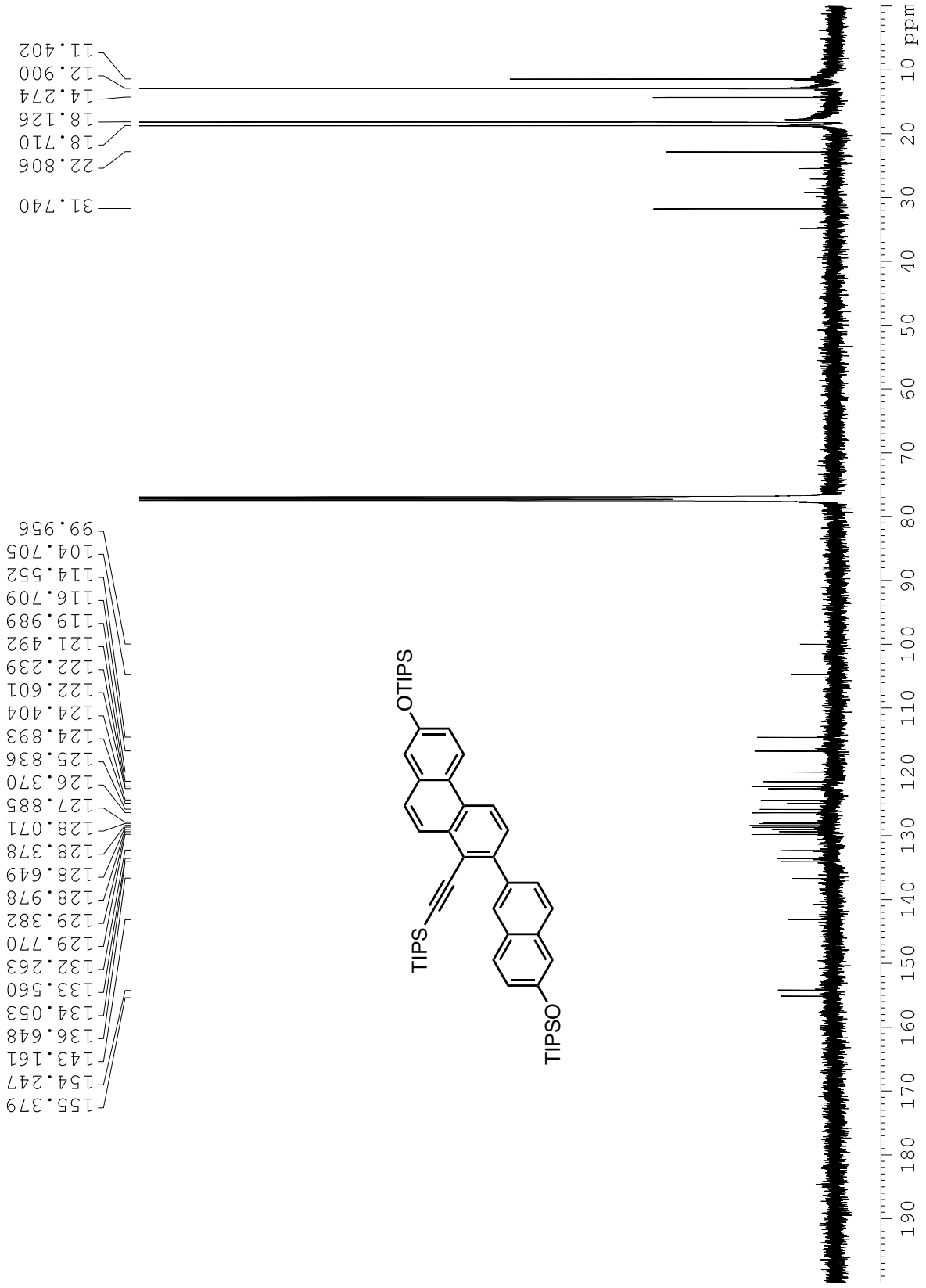

Figure C15. ^{13}C NMR spectrum of compound **10**.

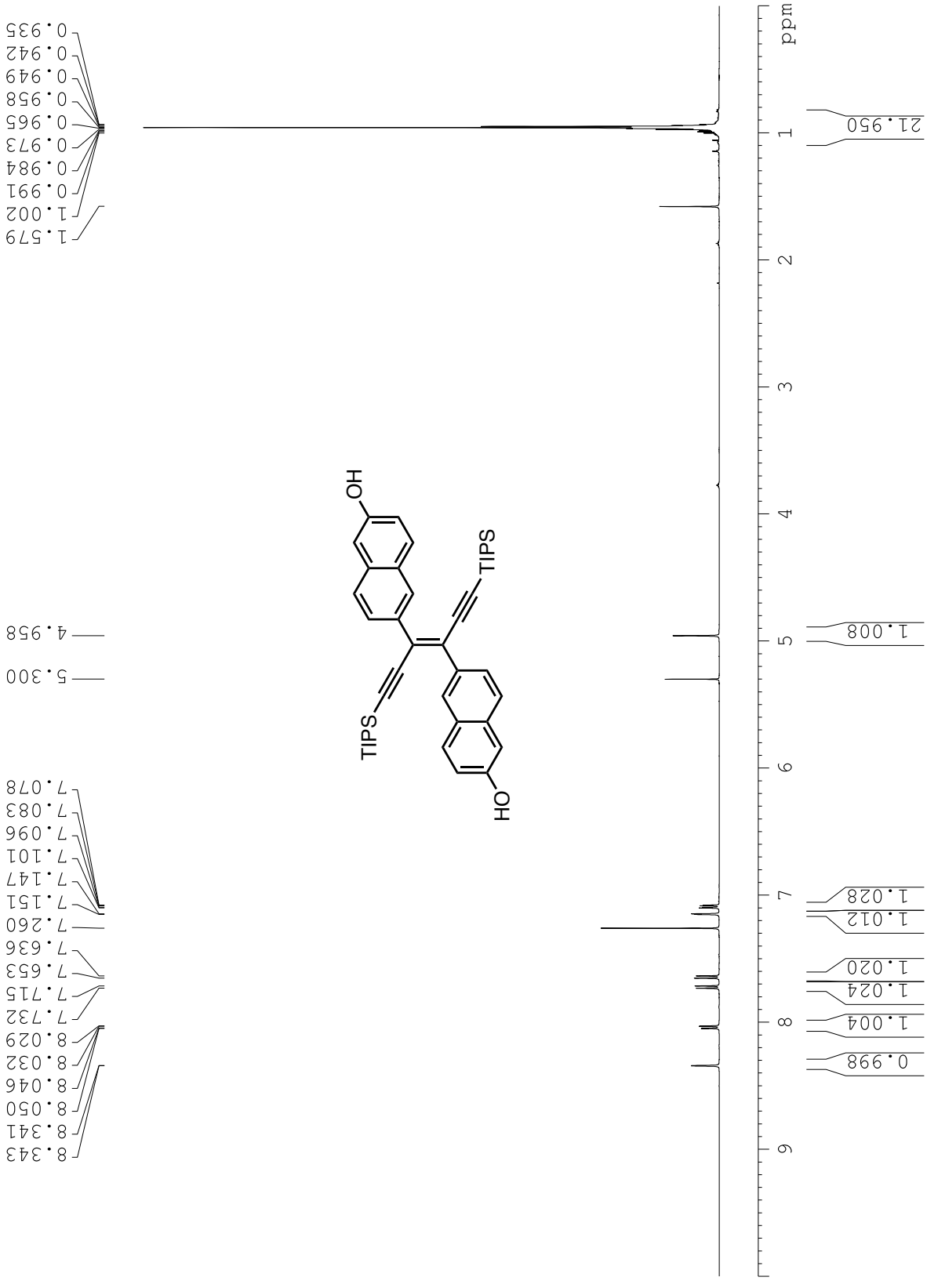

Figure C16. ^{1}H NMR spectrum of compound **11**.

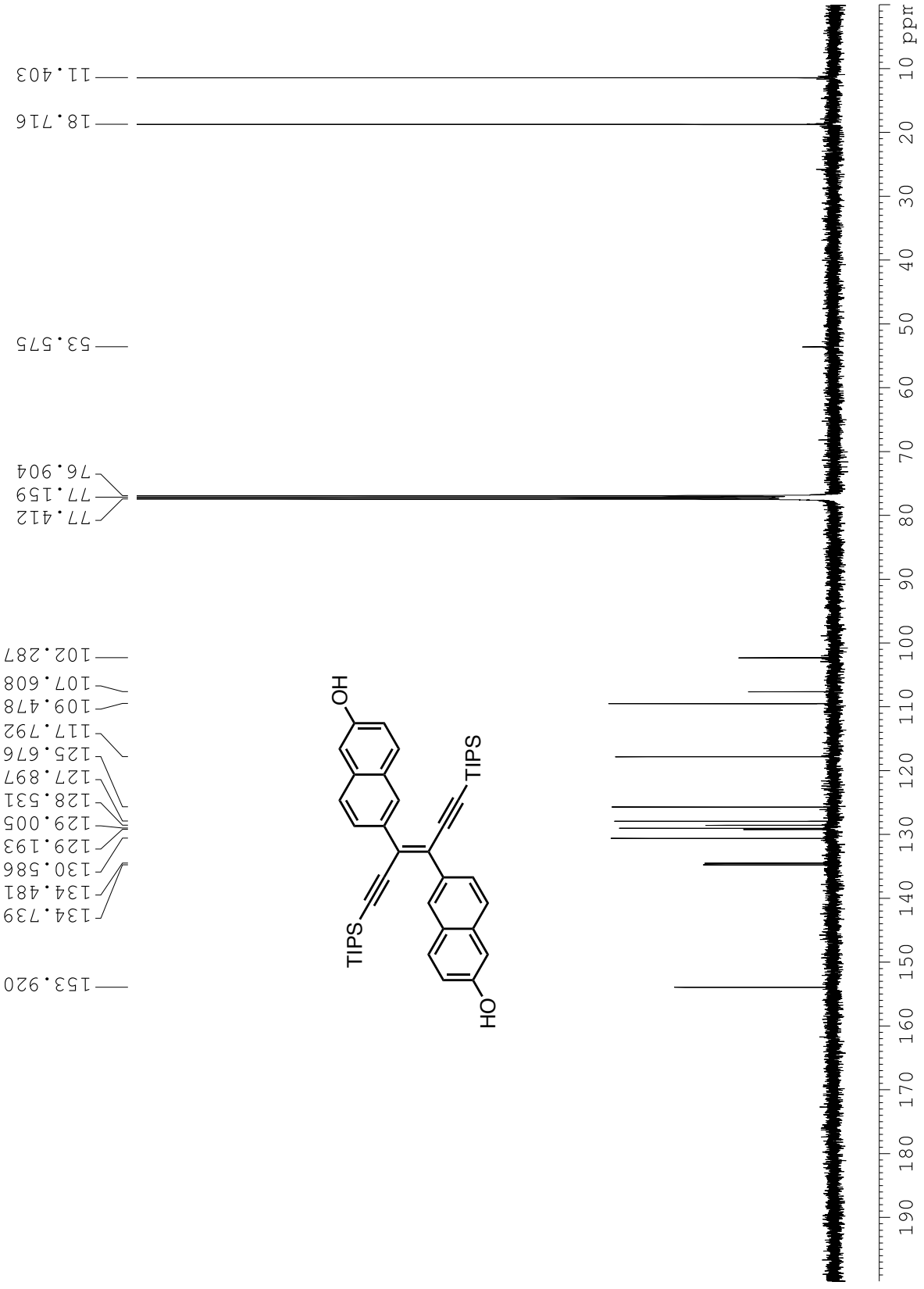

Figure C17. ^{13}C NMR spectrum of compound **11**.

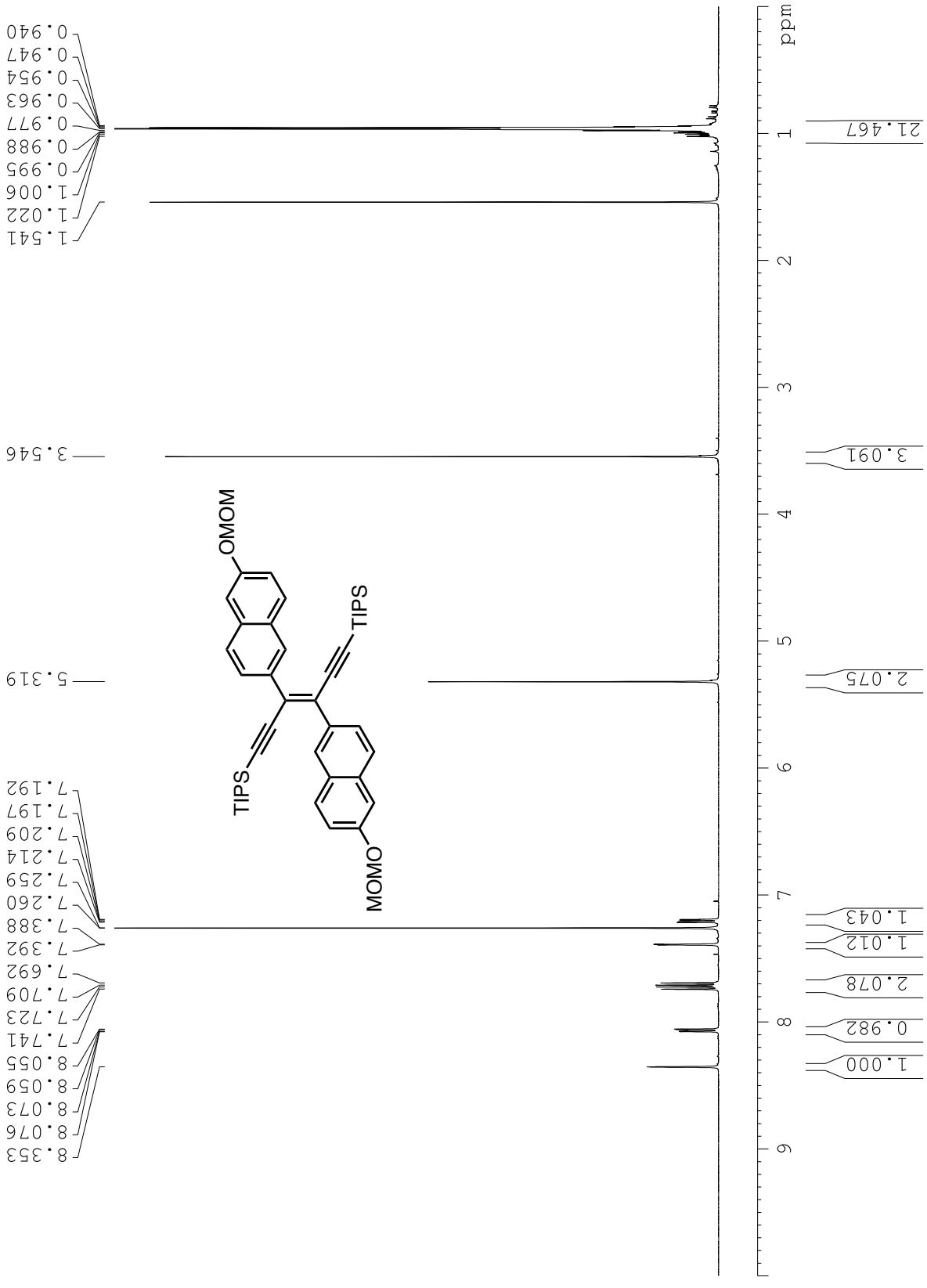

Figure C18. ^{1}H NMR spectrum of compound **12**.

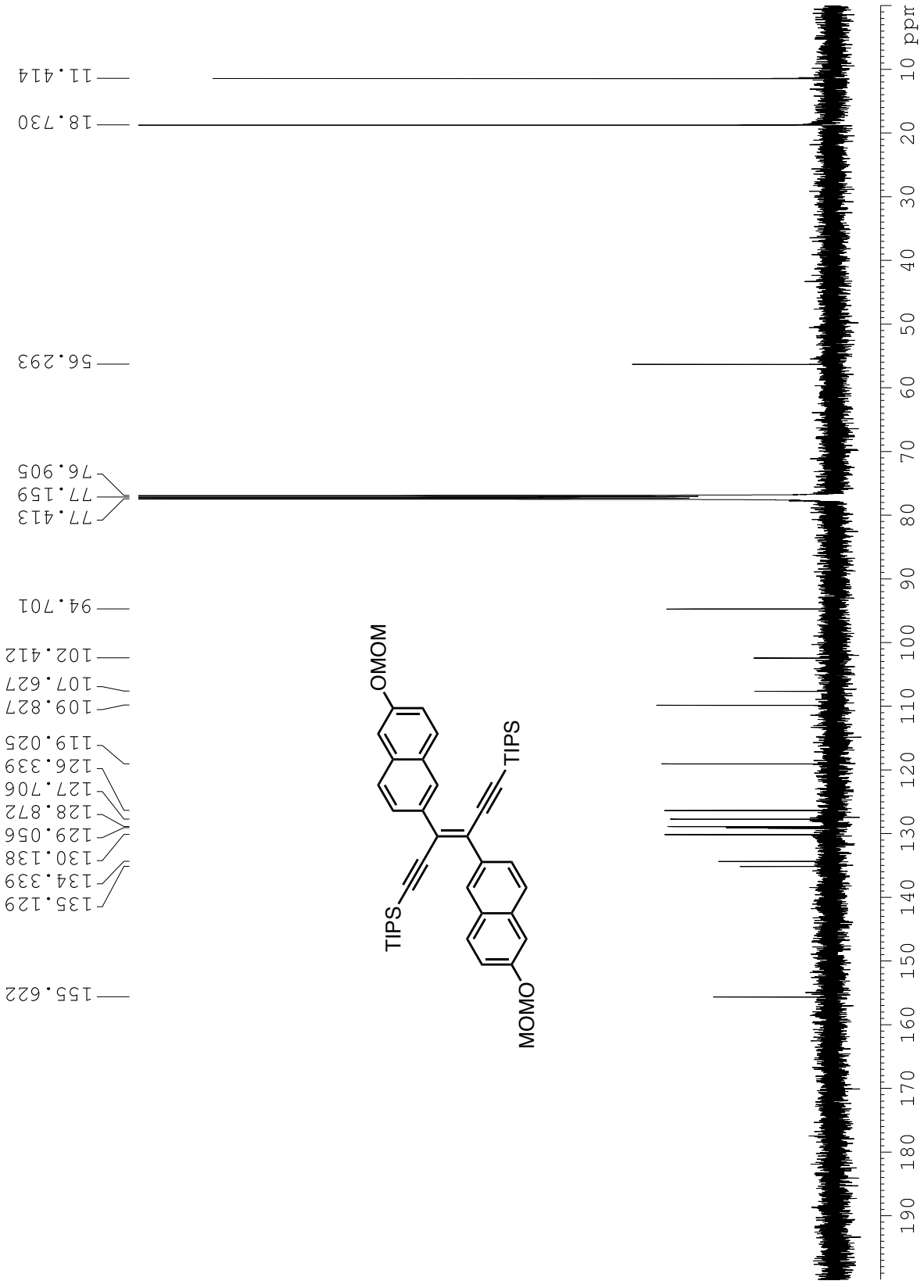

Figure C19. ^{13}C NMR spectrum of compound **12**.

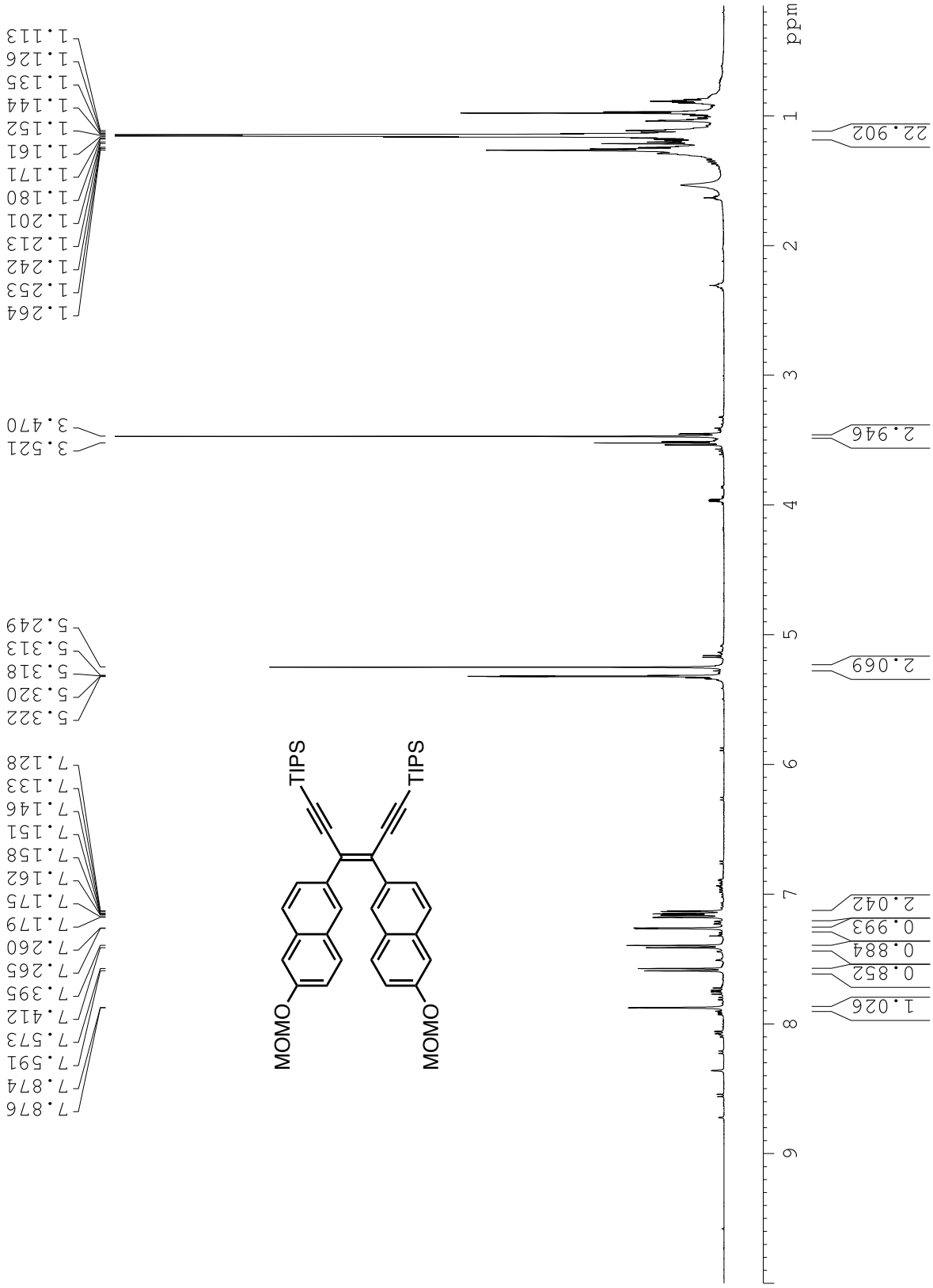

Figure C20. ^{1}H NMR spectrum of compound **13**.

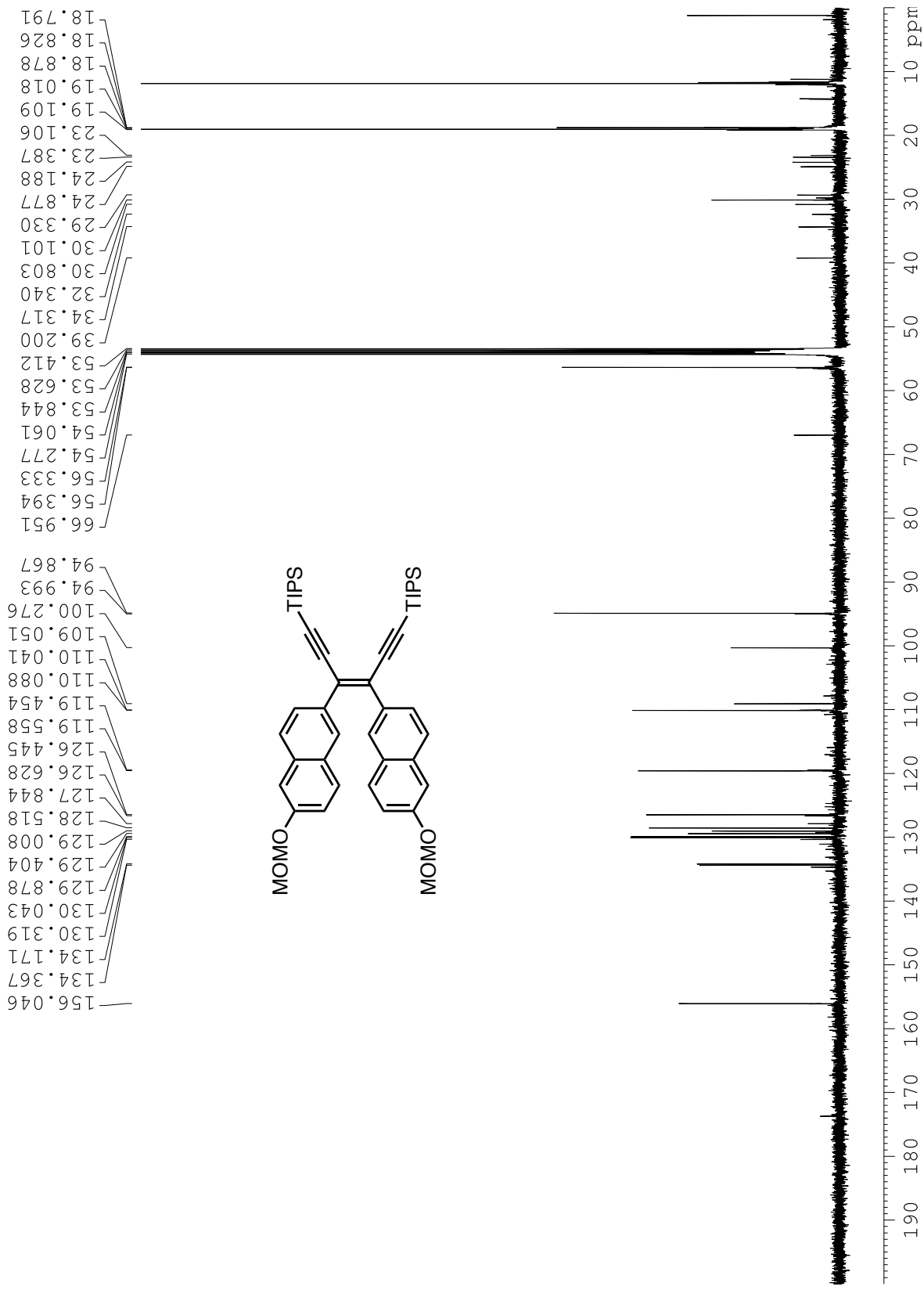

Figure C21. ^{13}C NMR spectrum of compound **13**.

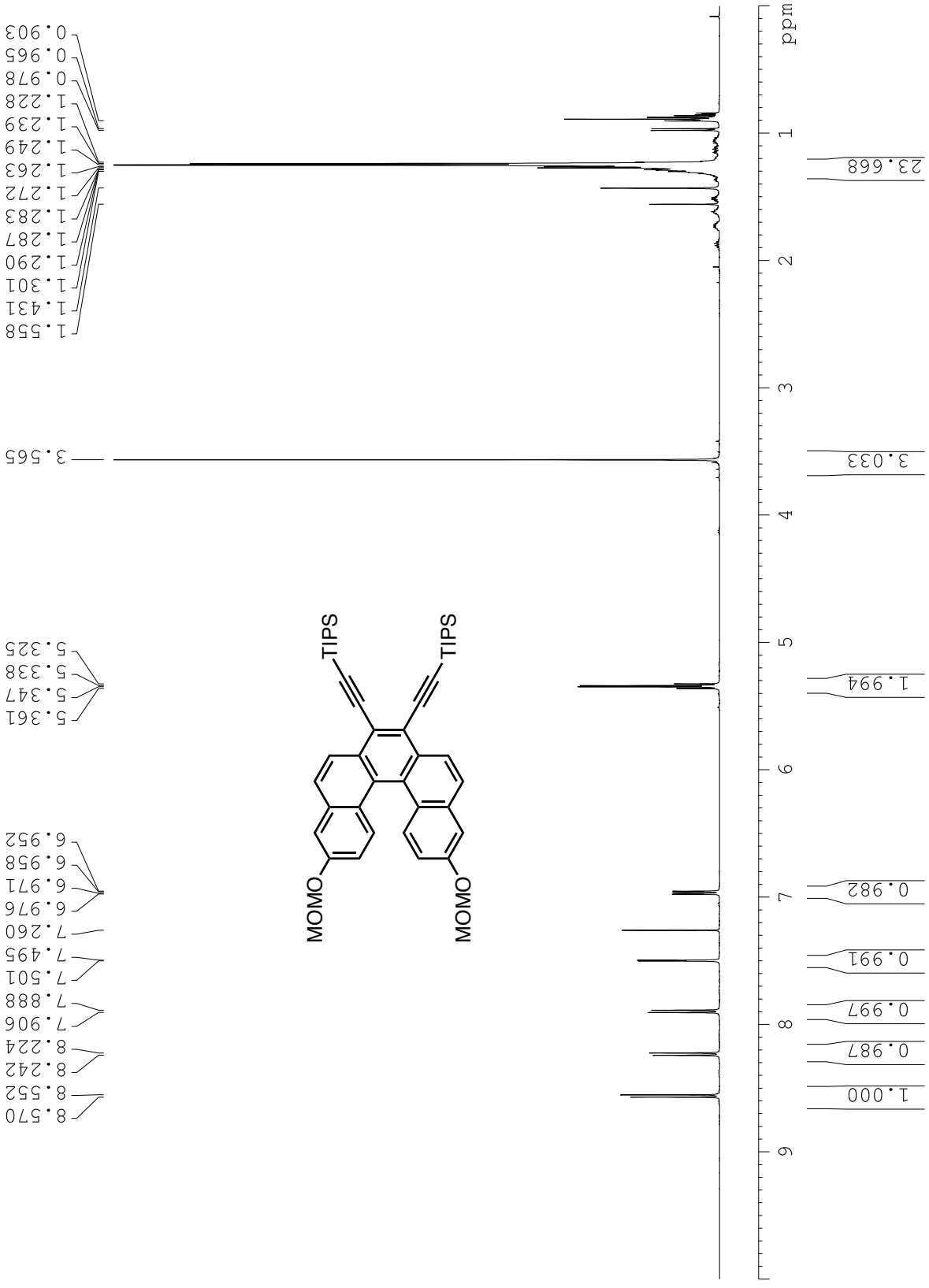

Figure C22. ^{1}H NMR spectrum of compound **14**.

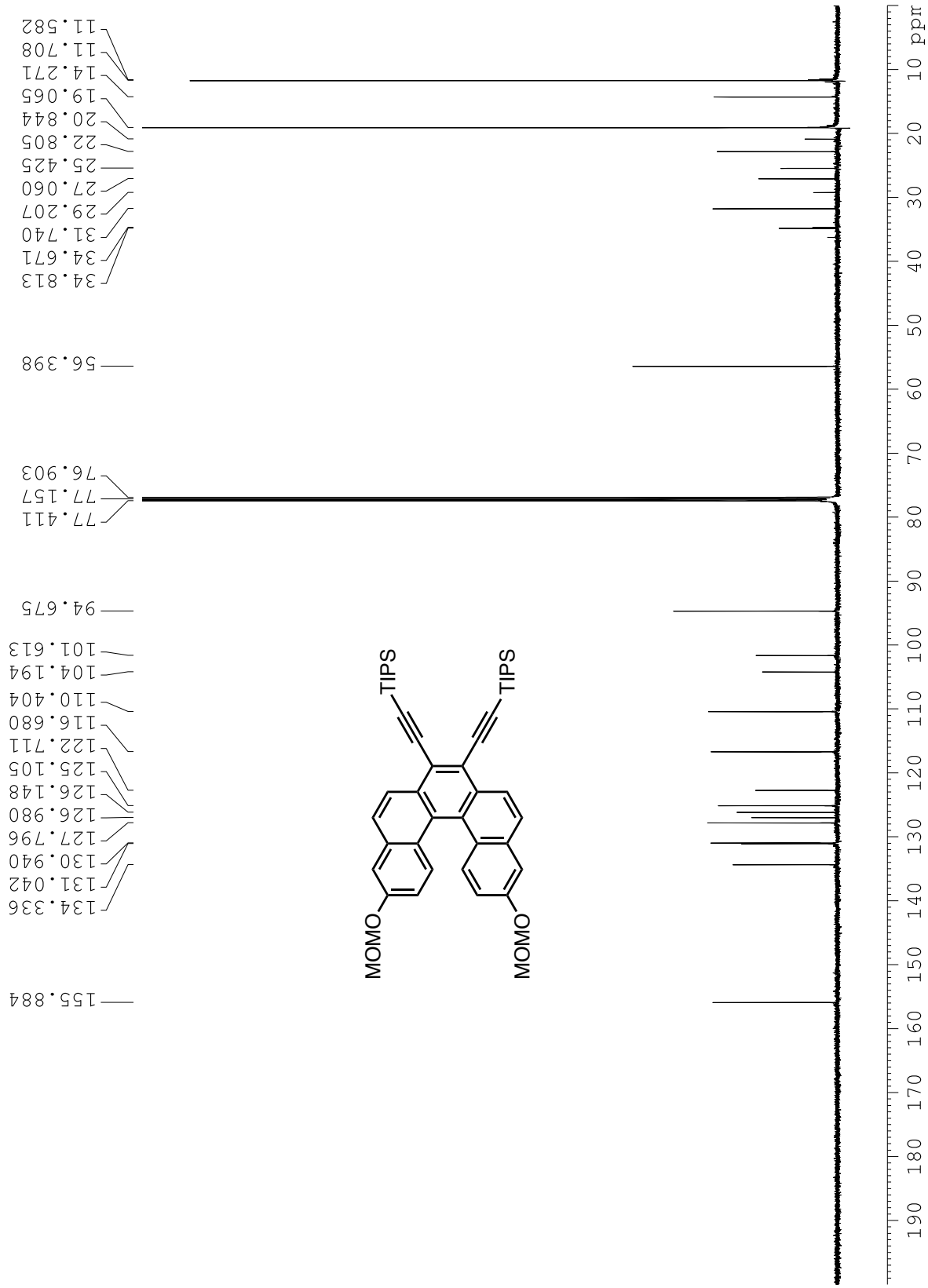

Figure C23. ^{13}C NMR spectrum of compound **14**.

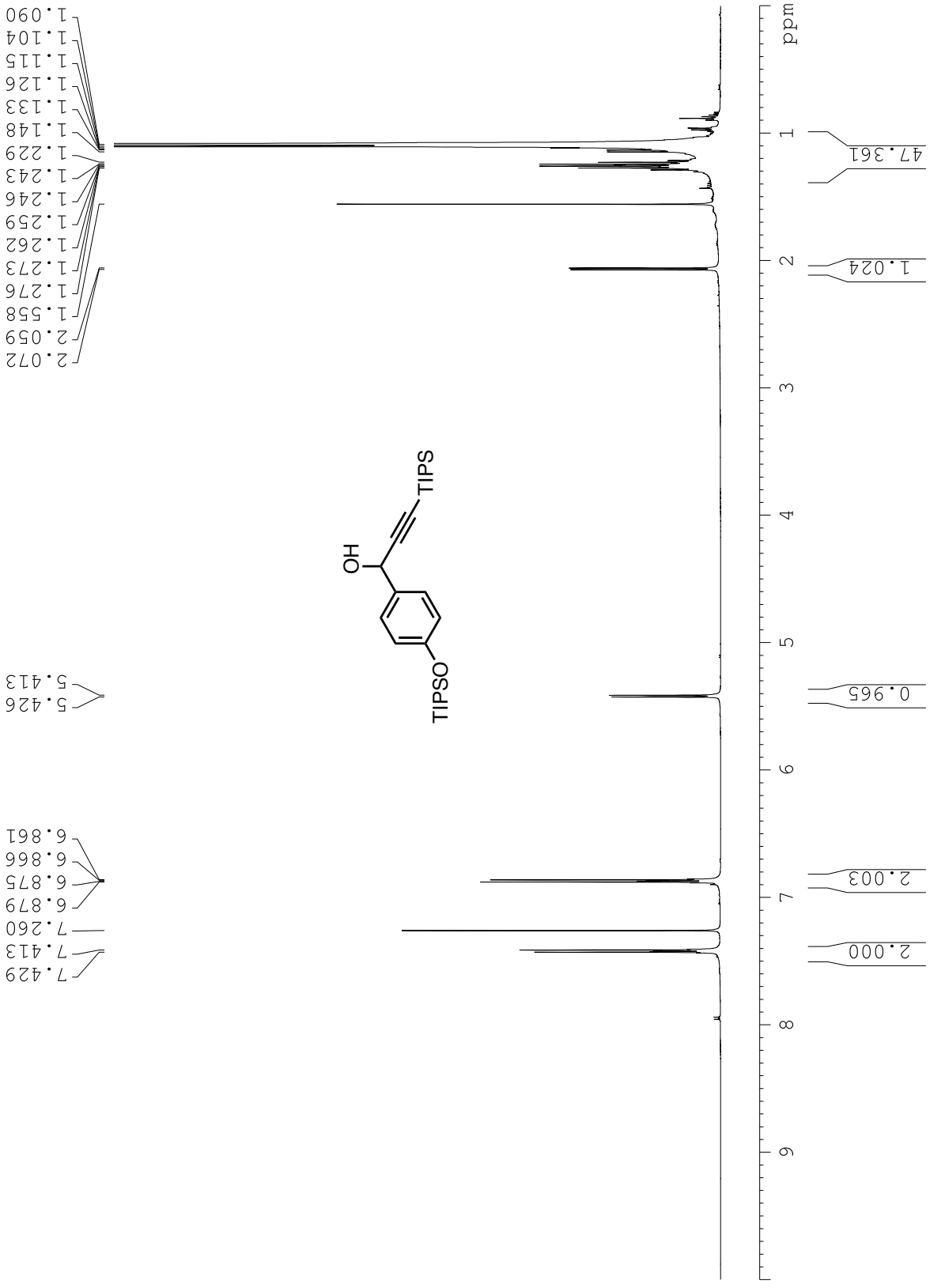

Figure C24. ^{1}H NMR spectrum of compound **16**.

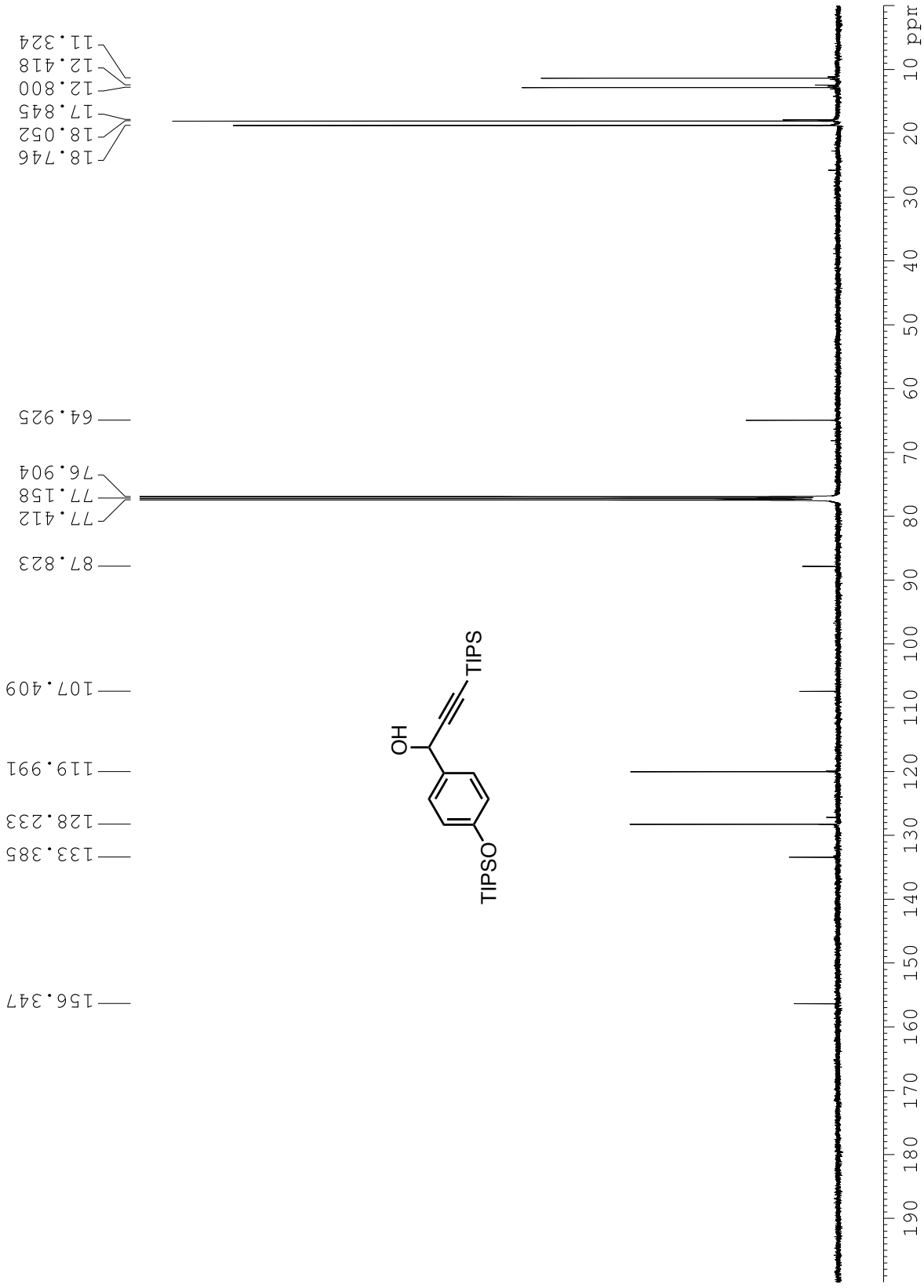

Figure C25. ^{13}C NMR spectrum of compound **16**.

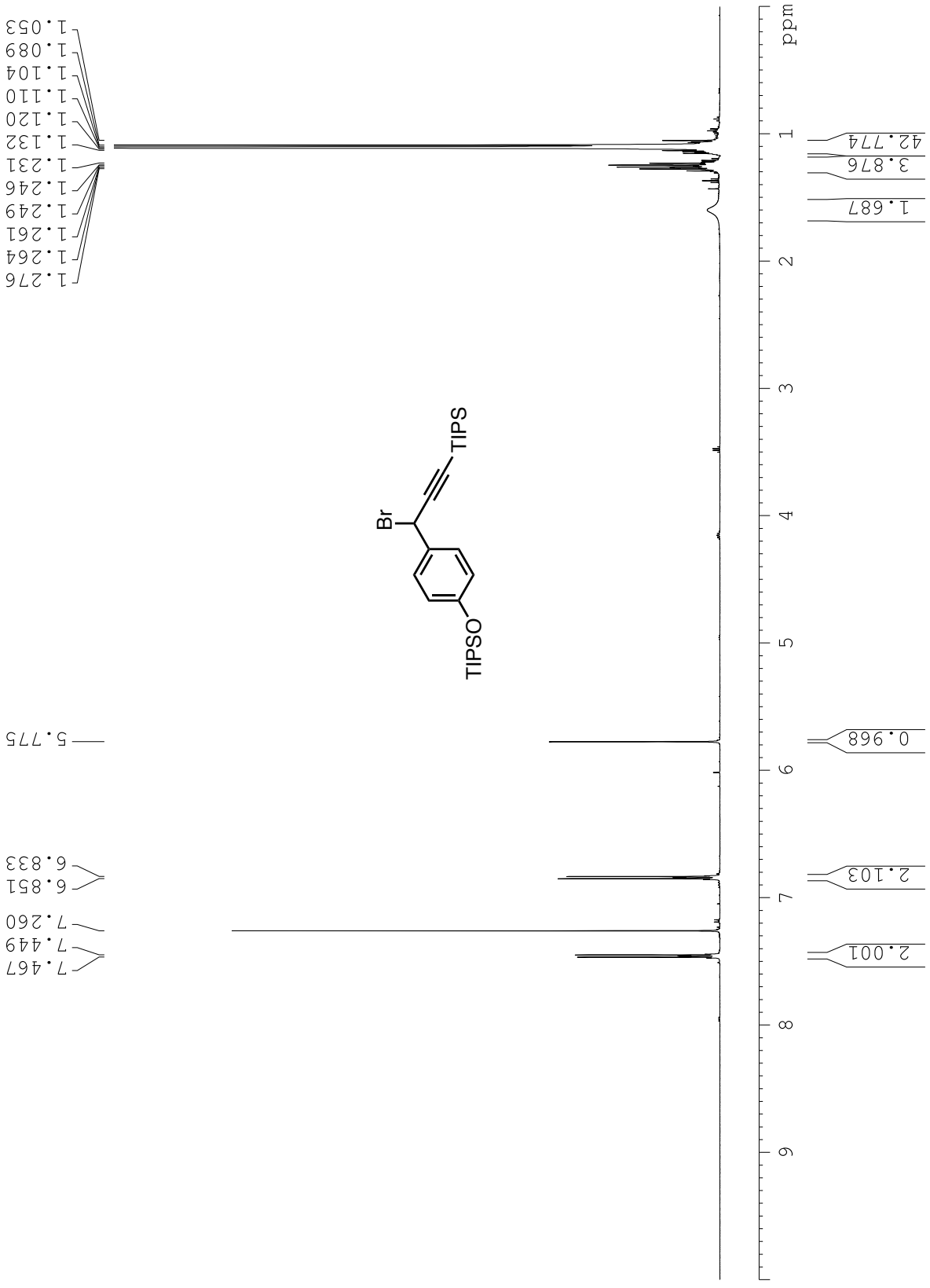

Figure C26. ^{1}H NMR spectrum of compound **17**.

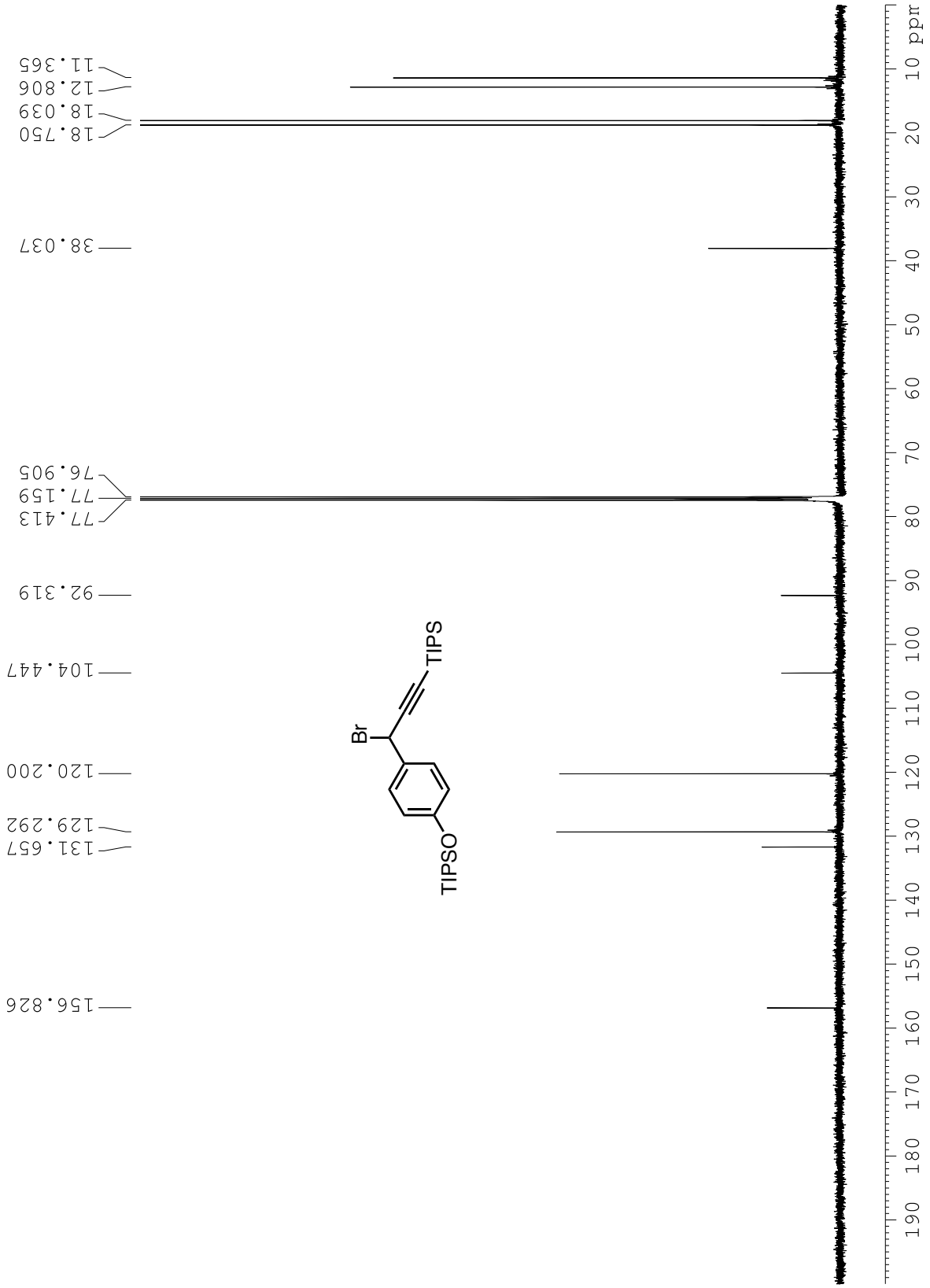

Figure C27. ^{13}C NMR spectrum of compound **17**.

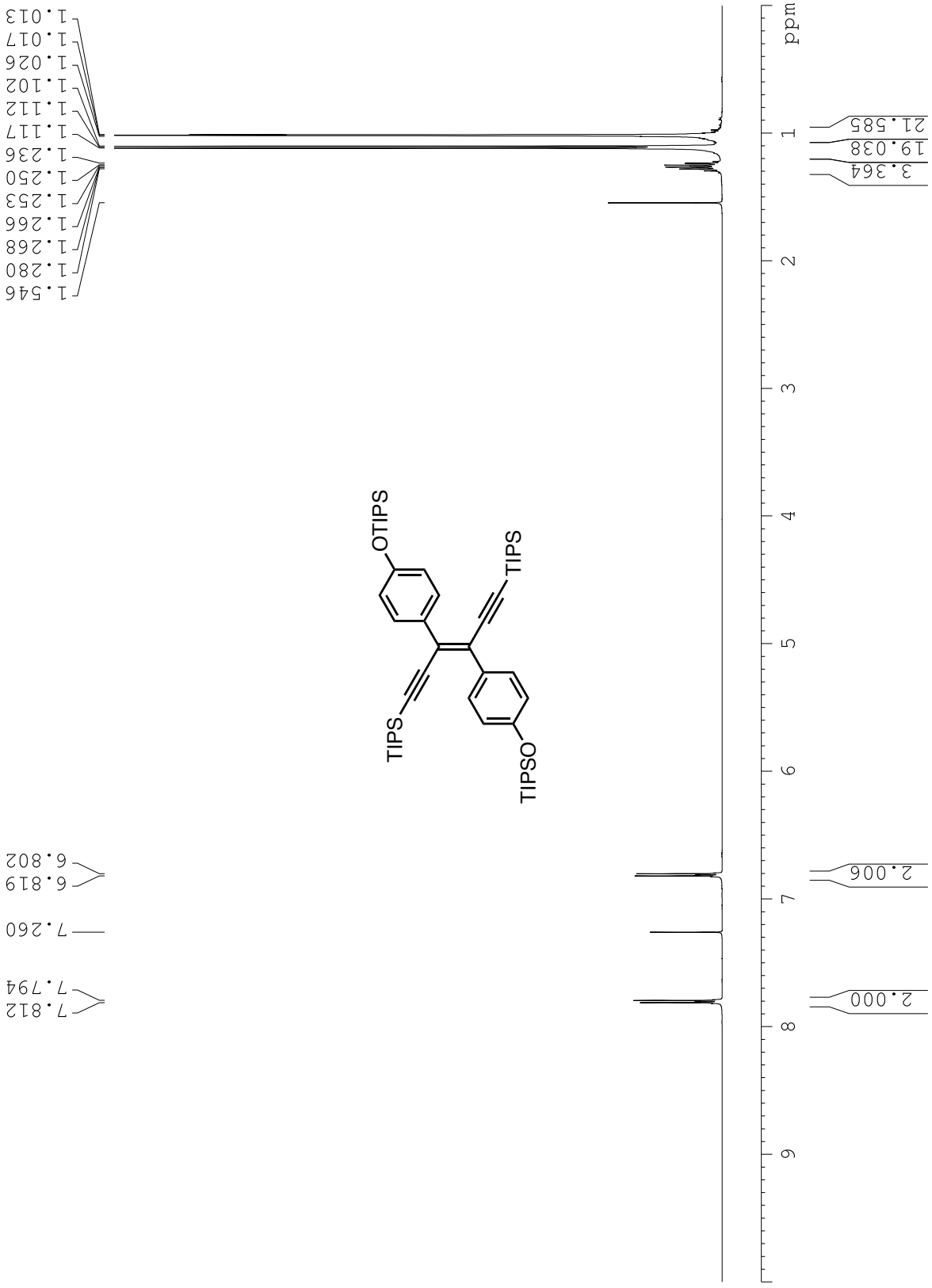

Figure C28. ^{1}H NMR spectrum of compound **18**.

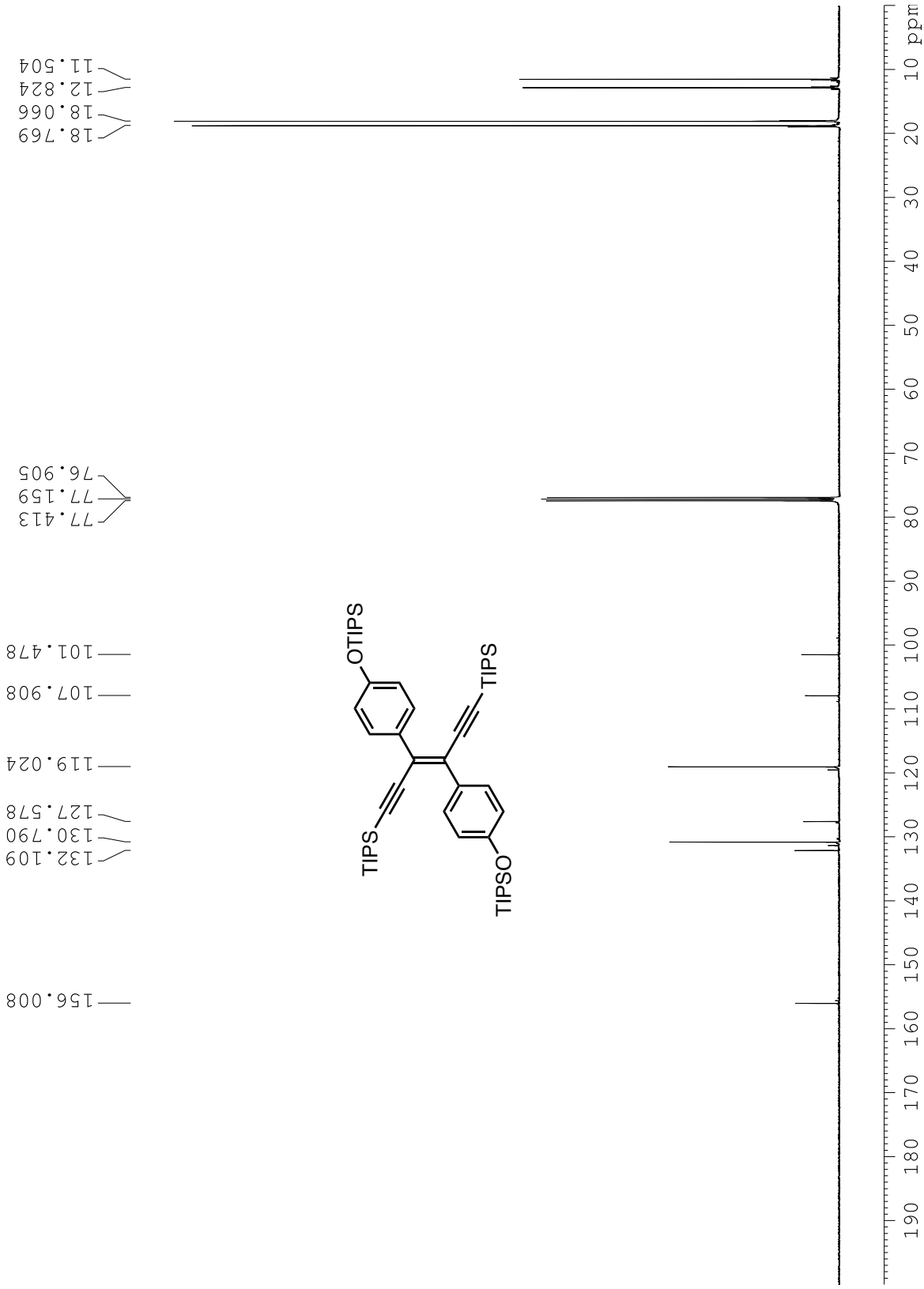

Figure C29. ^{13}C NMR spectrum of compound **18**.

Figure C30. ^{1}H NMR spectrum of compound **19**.

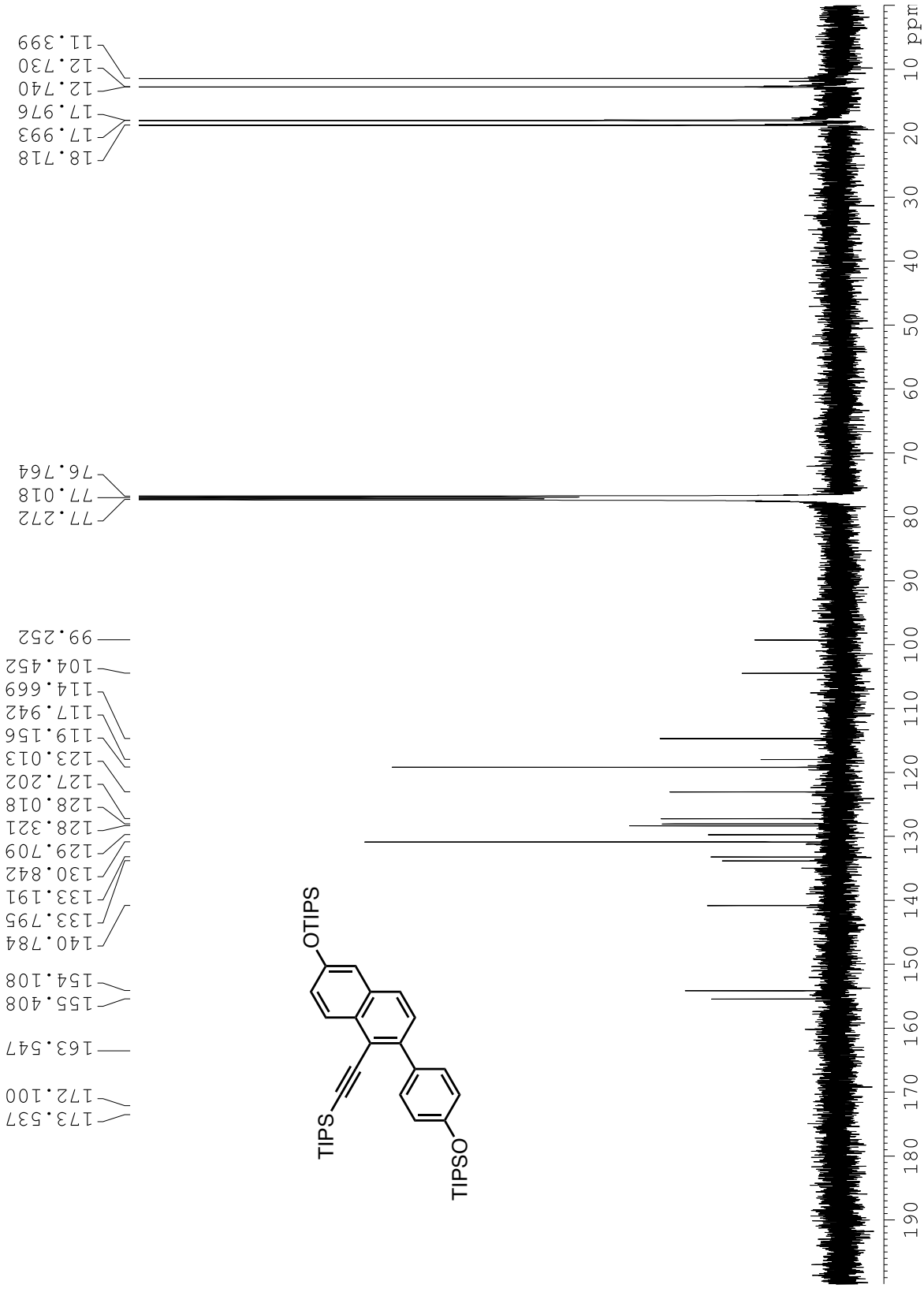

Figure C31. ^{13}C NMR spectrum of compound **19**.

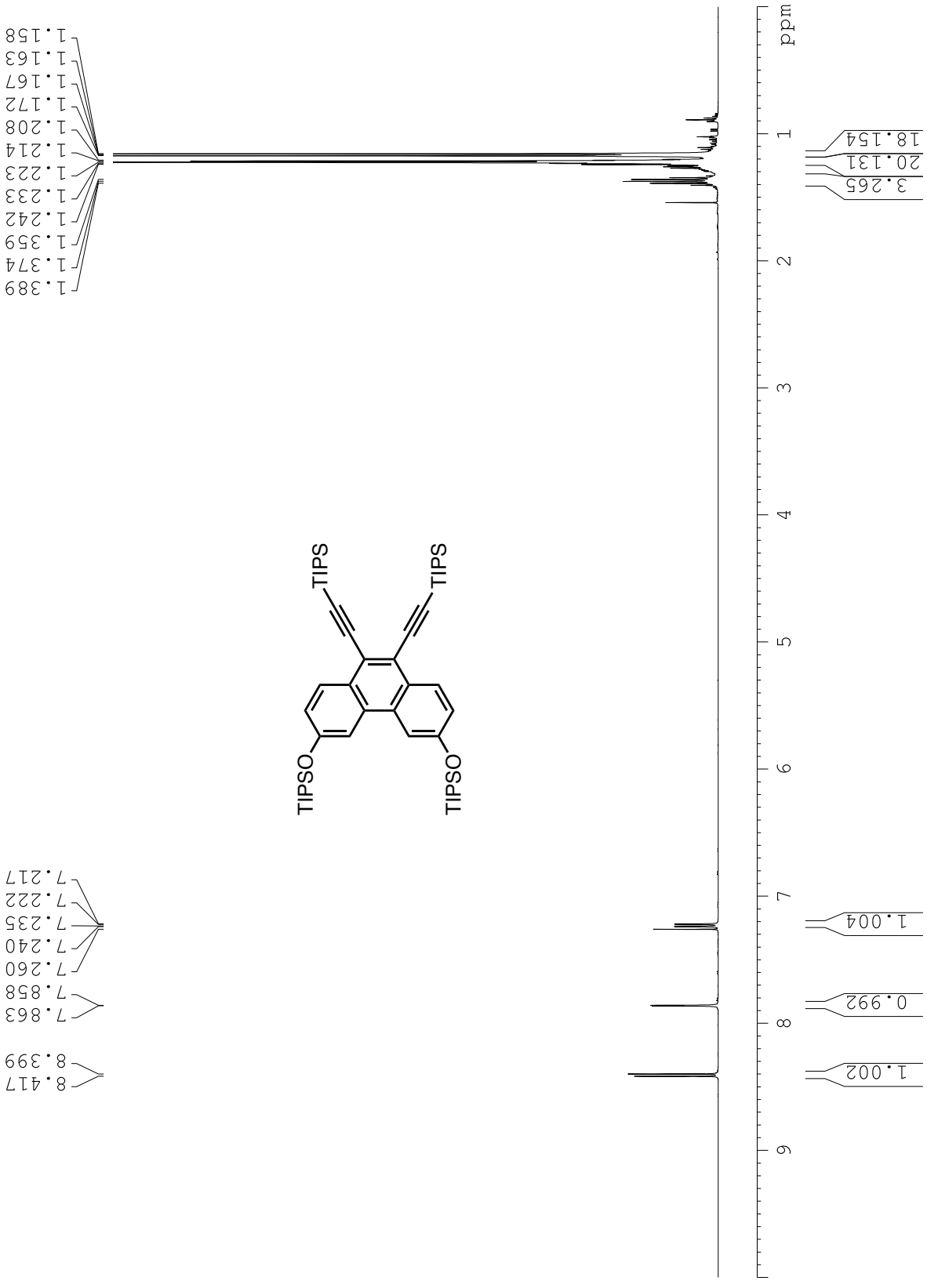

Figure C32. ^{1}H NMR spectrum of compound **20**.

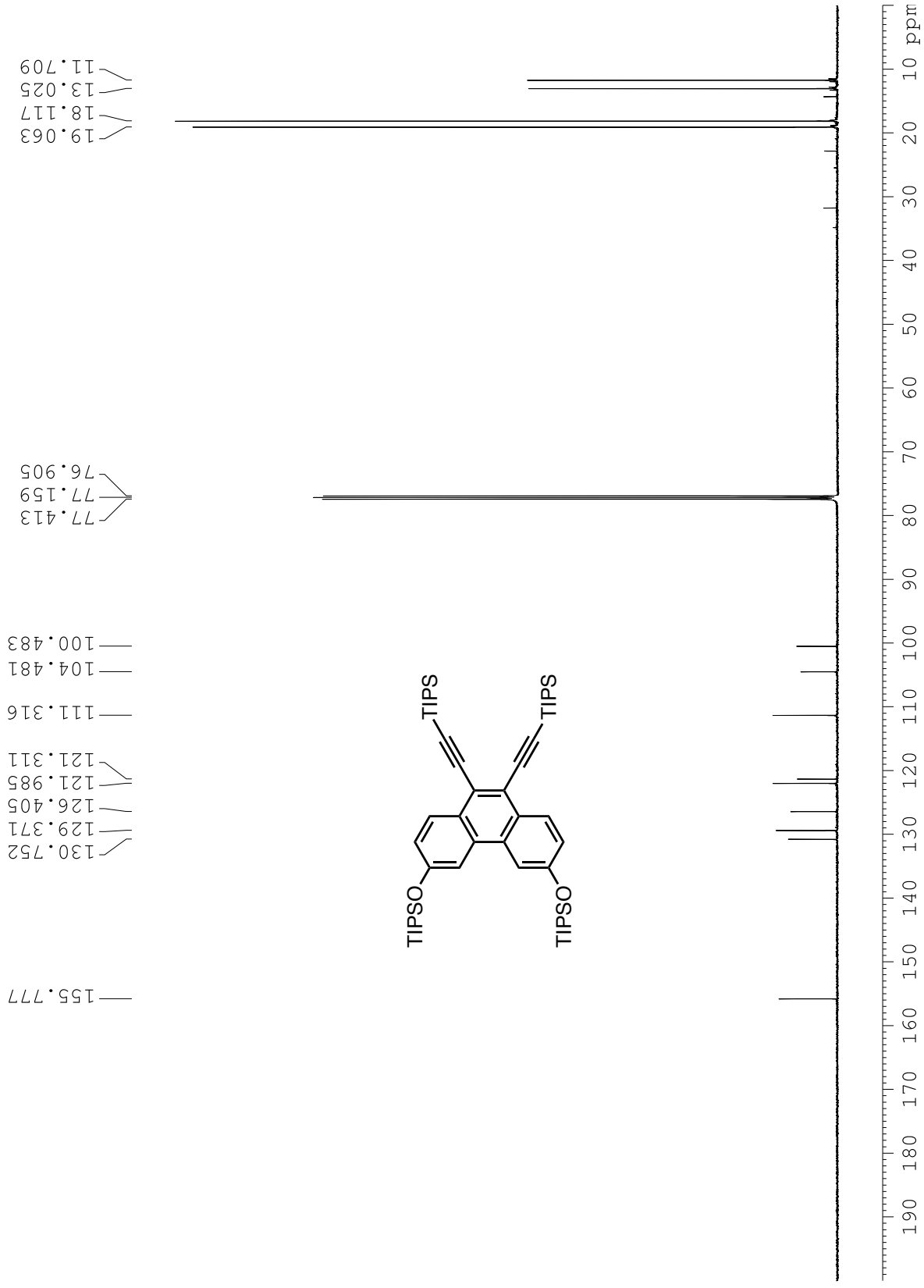

Figure C33. ^{13}C NMR spectrum of compound **20**.

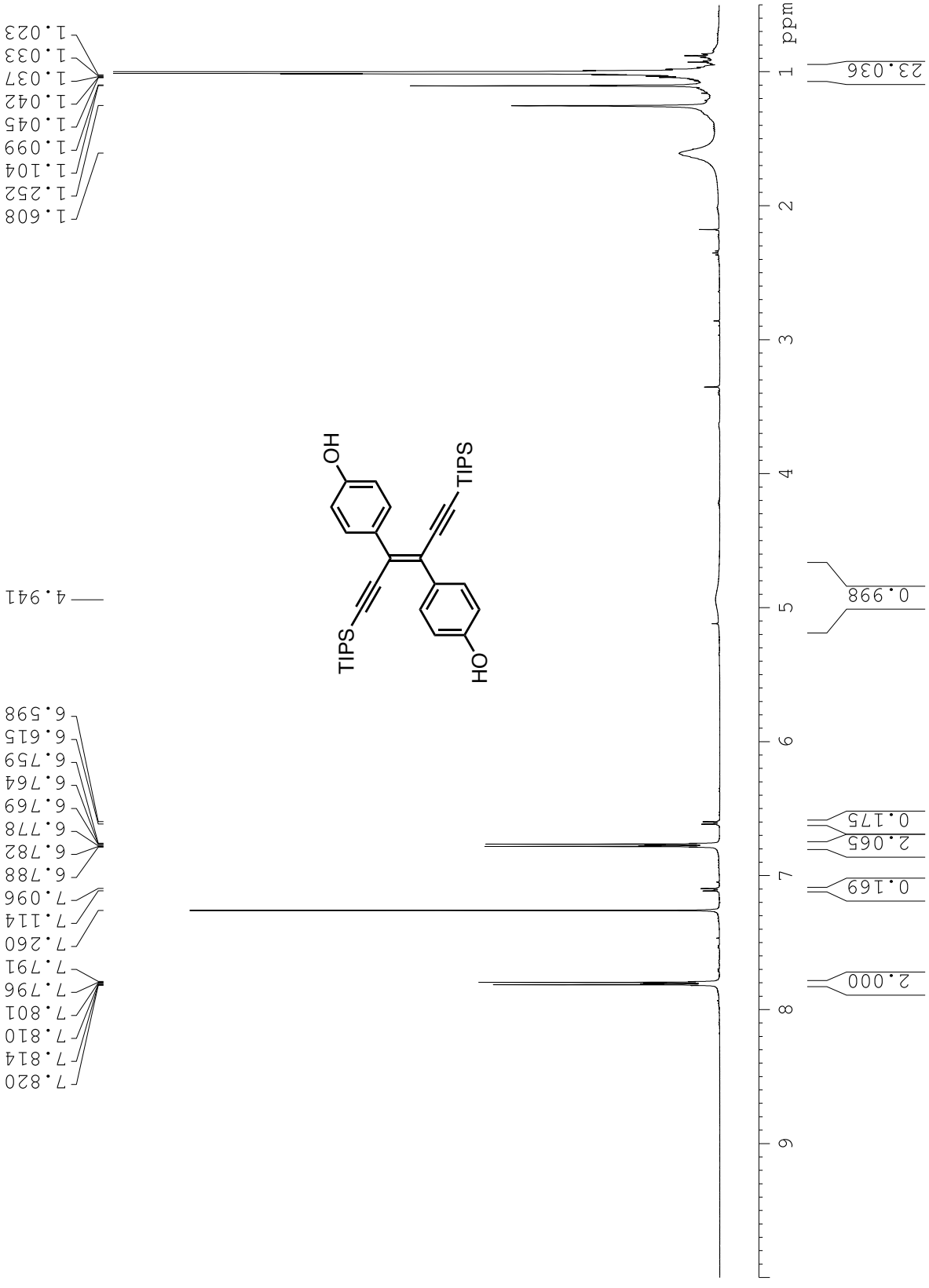

Figure C34. ^{1}H NMR spectrum of compound **21**.

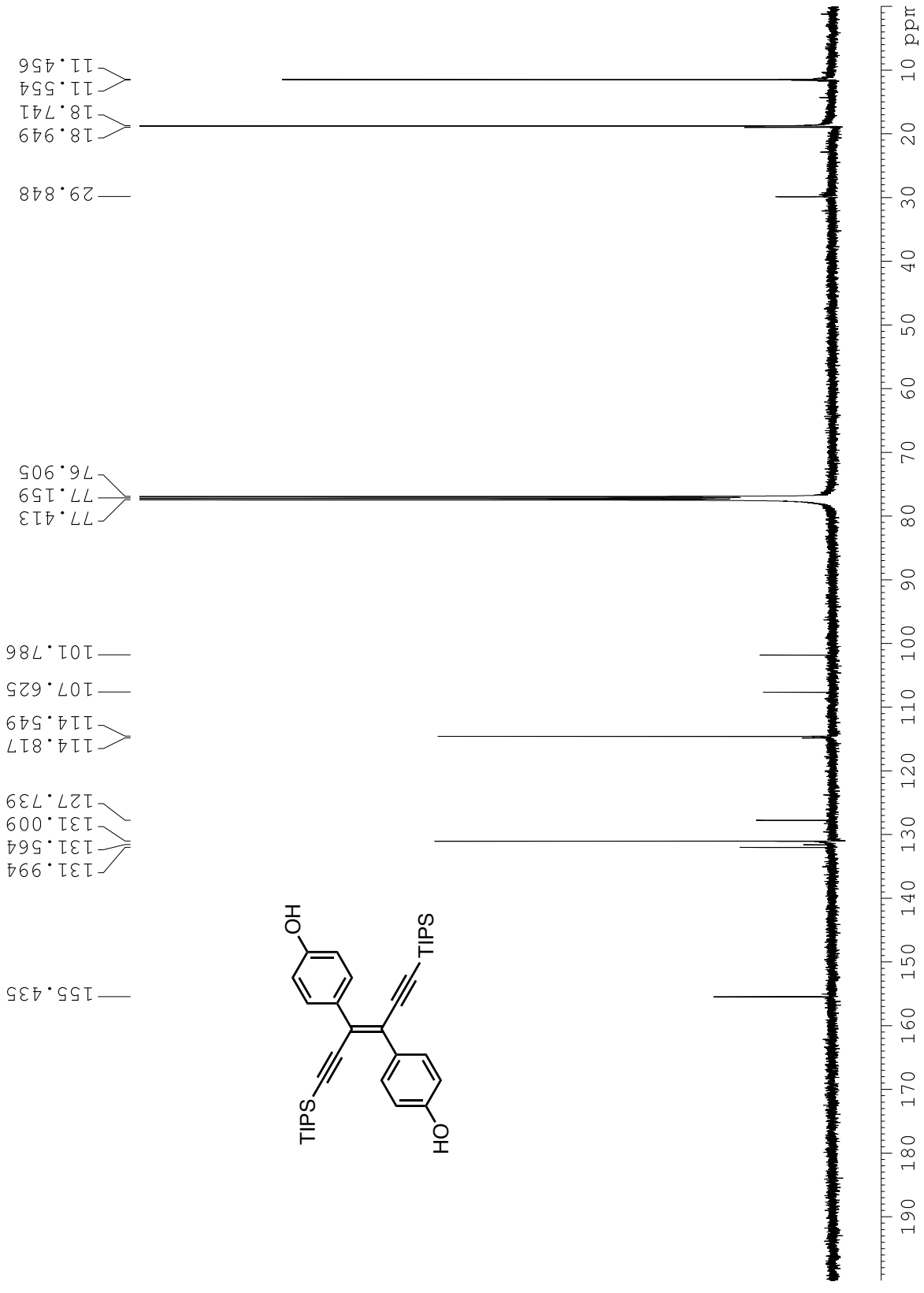

Figure C35. ^{13}C NMR spectrum of compound **21**.

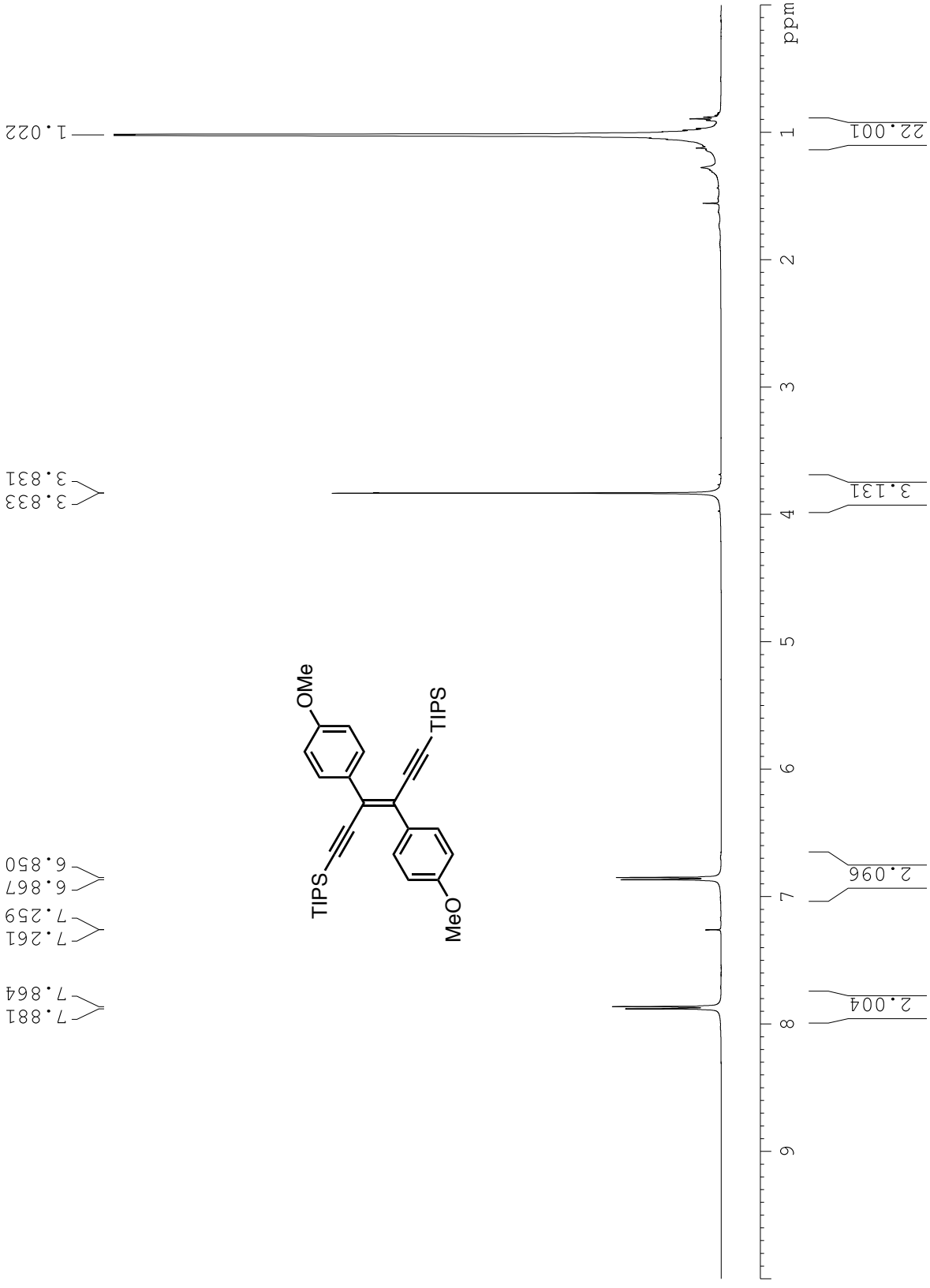

Figure C36. ^{1}H NMR spectrum of compound **22**.

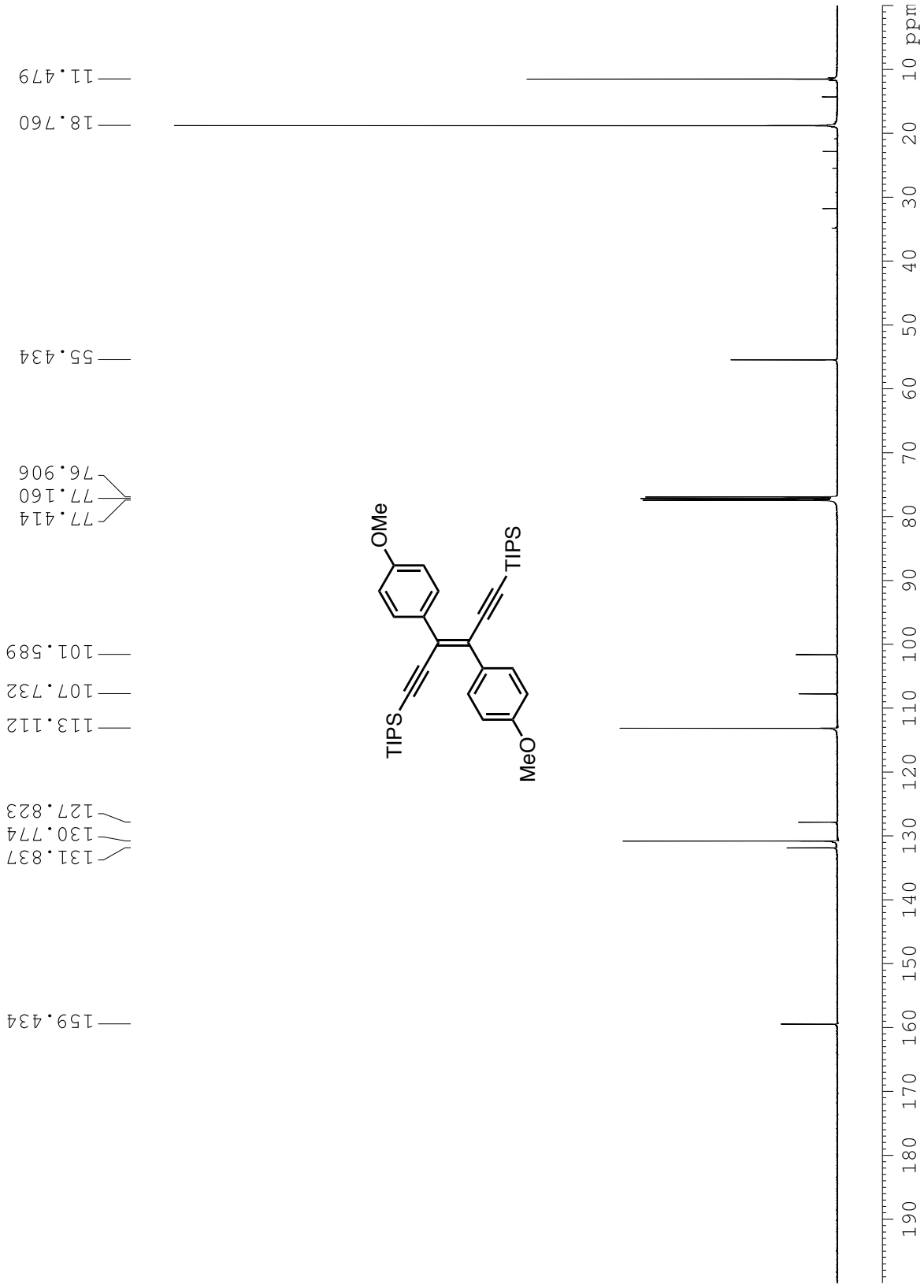

Figure C37. ^{13}C NMR spectrum of compound **22**.

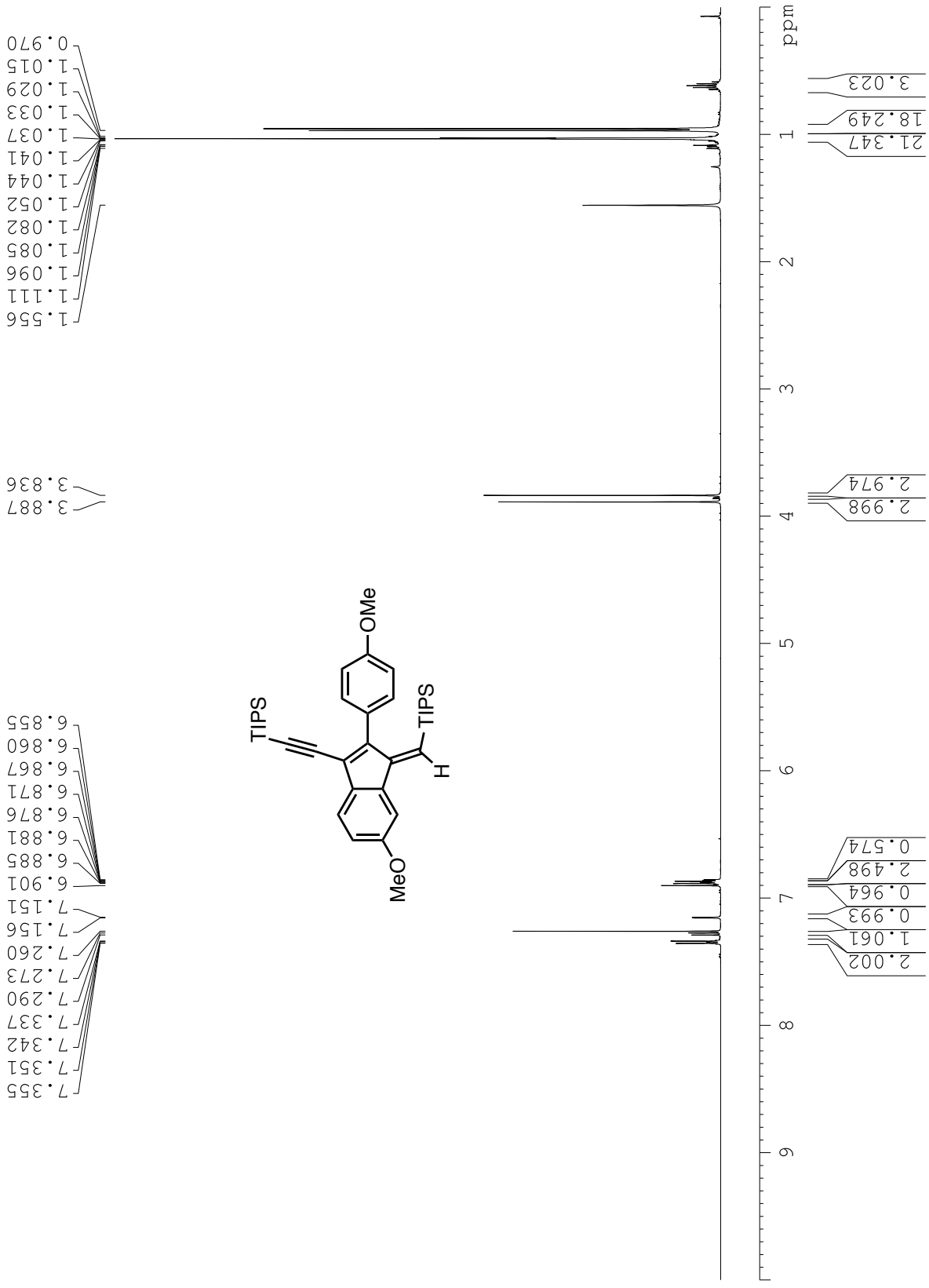

Figure C38. ^{1}H NMR spectrum of compound **23**.

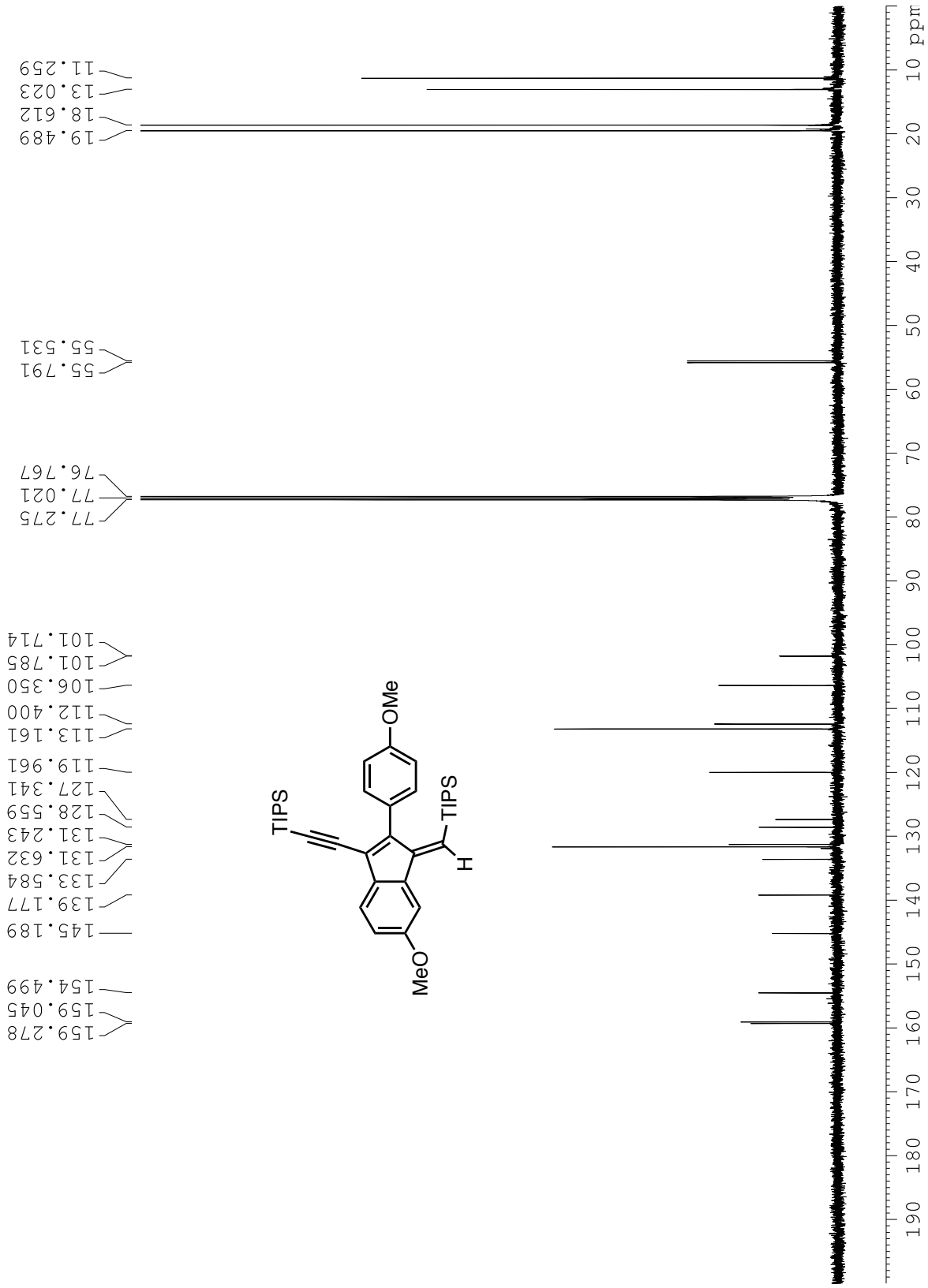

Figure C39. ^{13}C NMR spectrum of compound **23**.

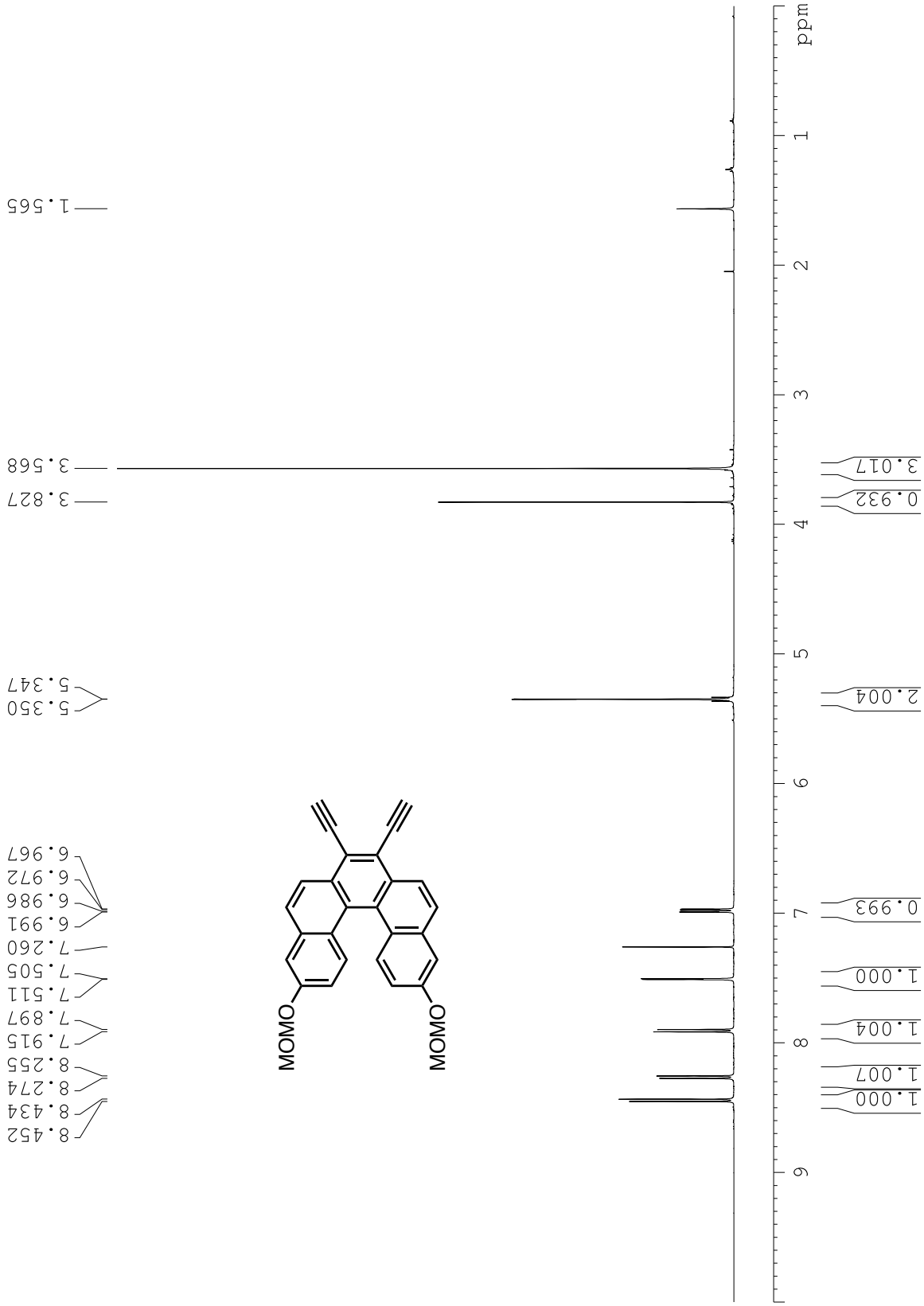

Figure C40. ^{1}H NMR spectrum of compound **24**.

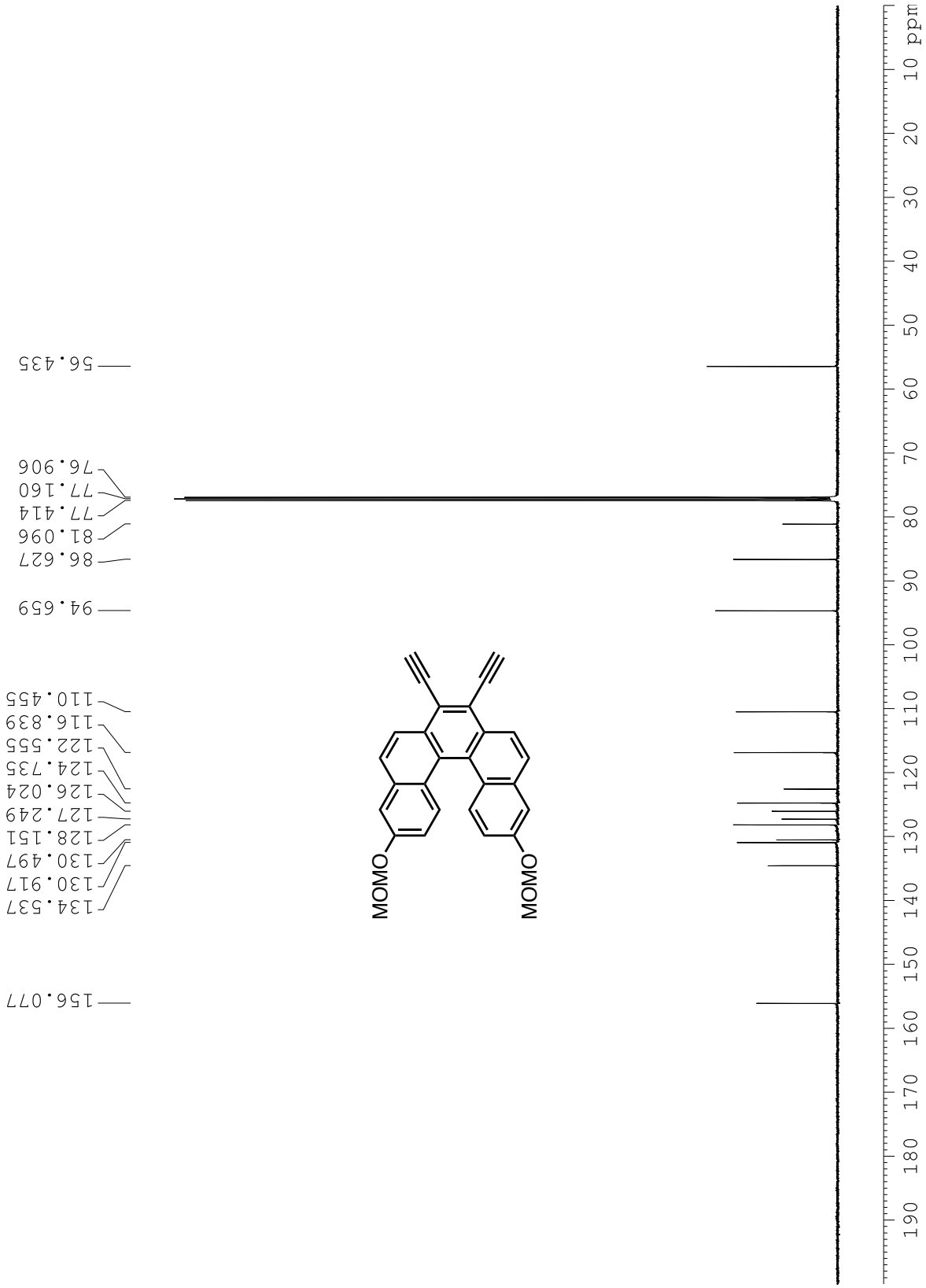

Figure C41. ^{13}C NMR spectrum of compound **24**.

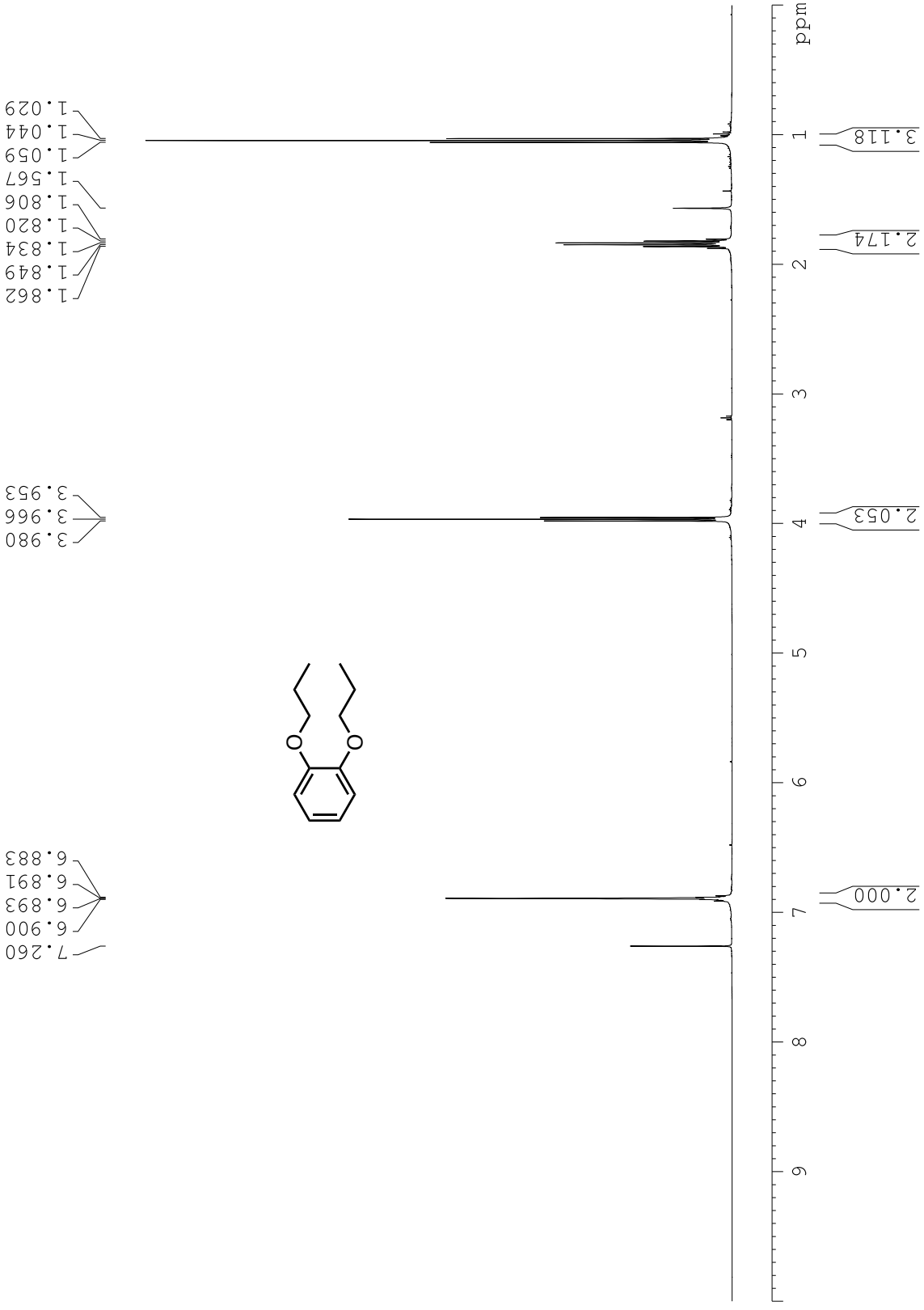

Figure C42. ^{1}H NMR spectrum of compound **25**.

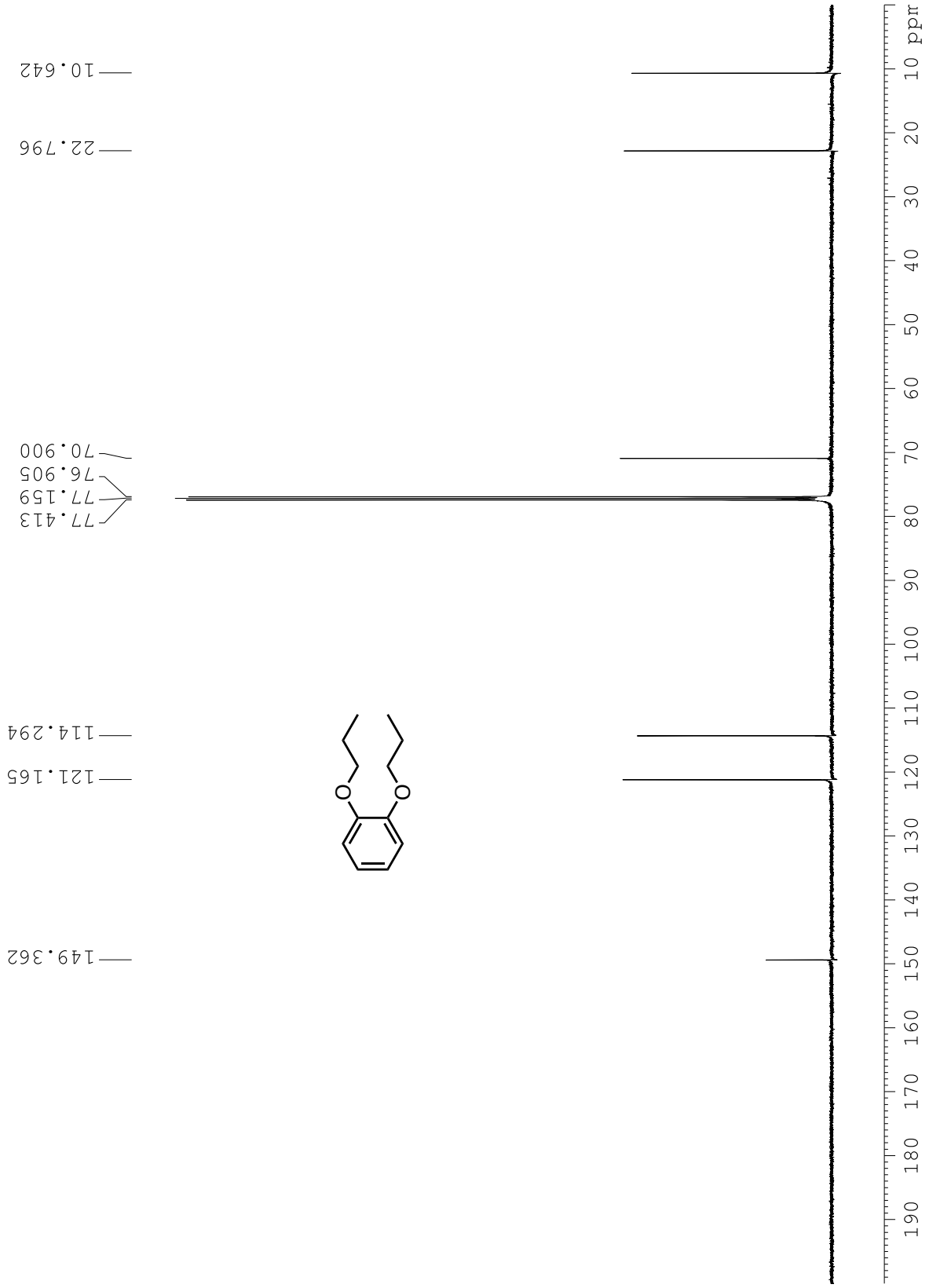

Figure C43. ^{13}C NMR spectrum of compound **25**.

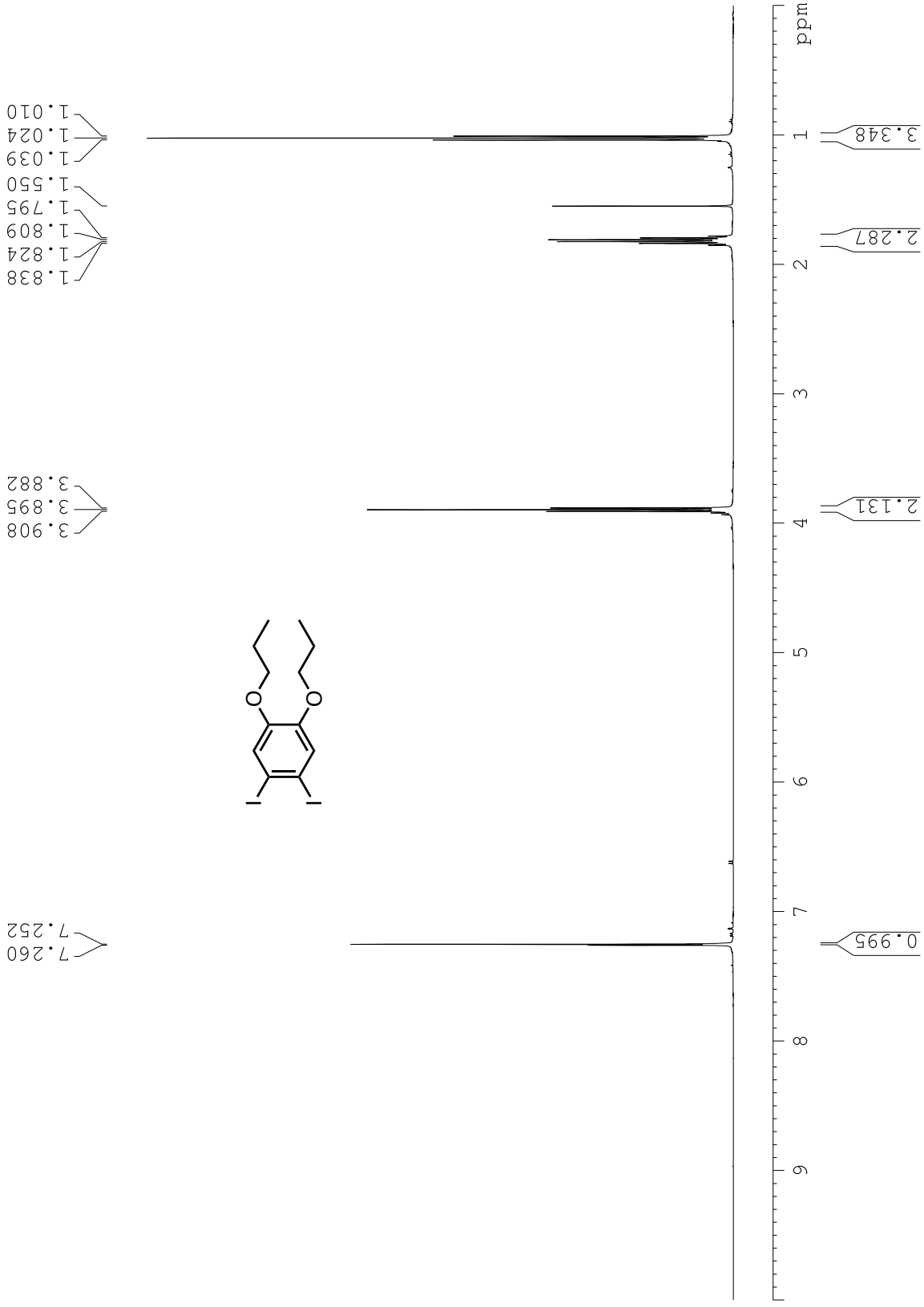

Figure C44. ^{1}H NMR spectrum of compound **26**.

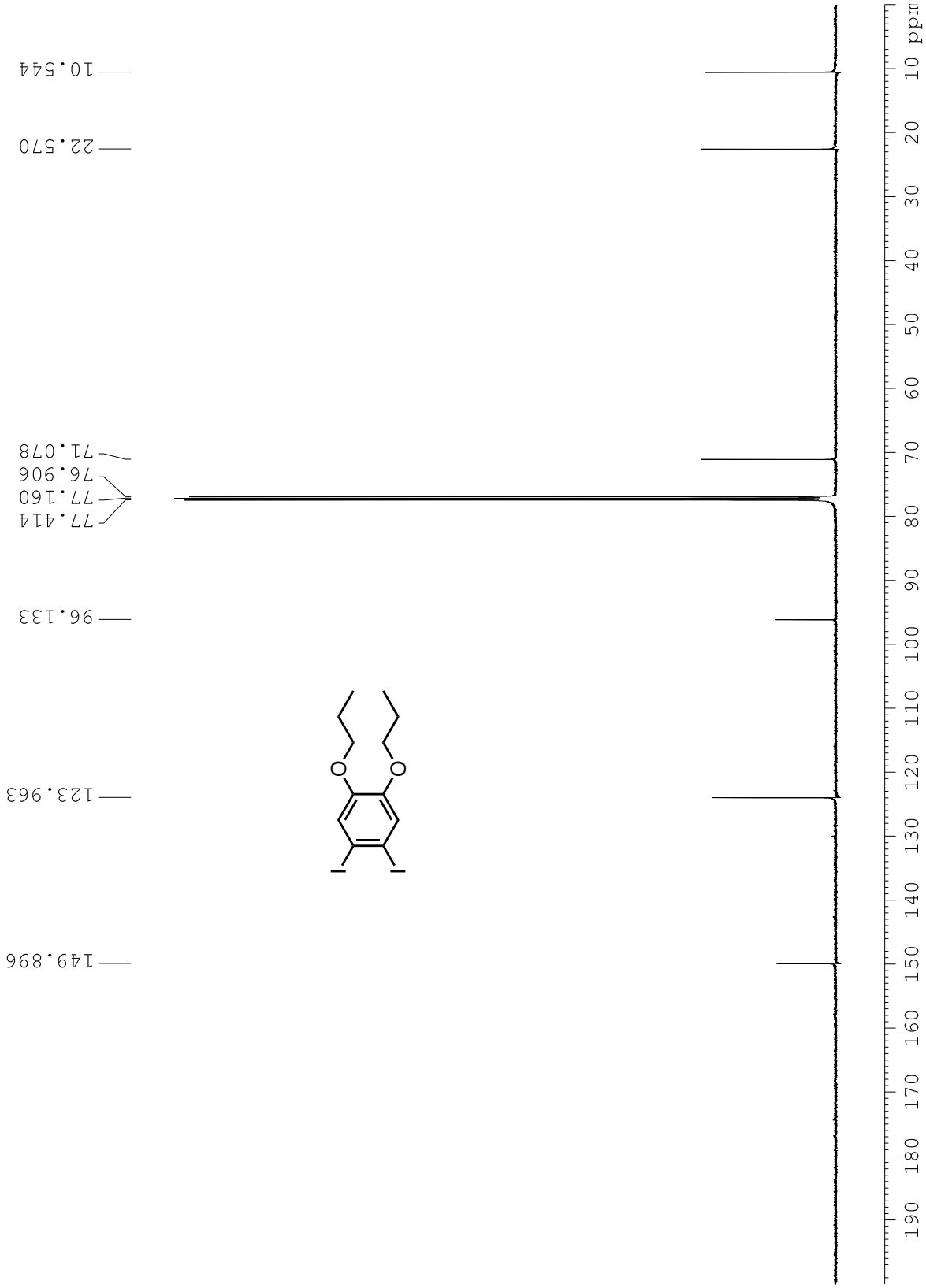

Figure C45. ^{13}C NMR spectrum of compound **26**.

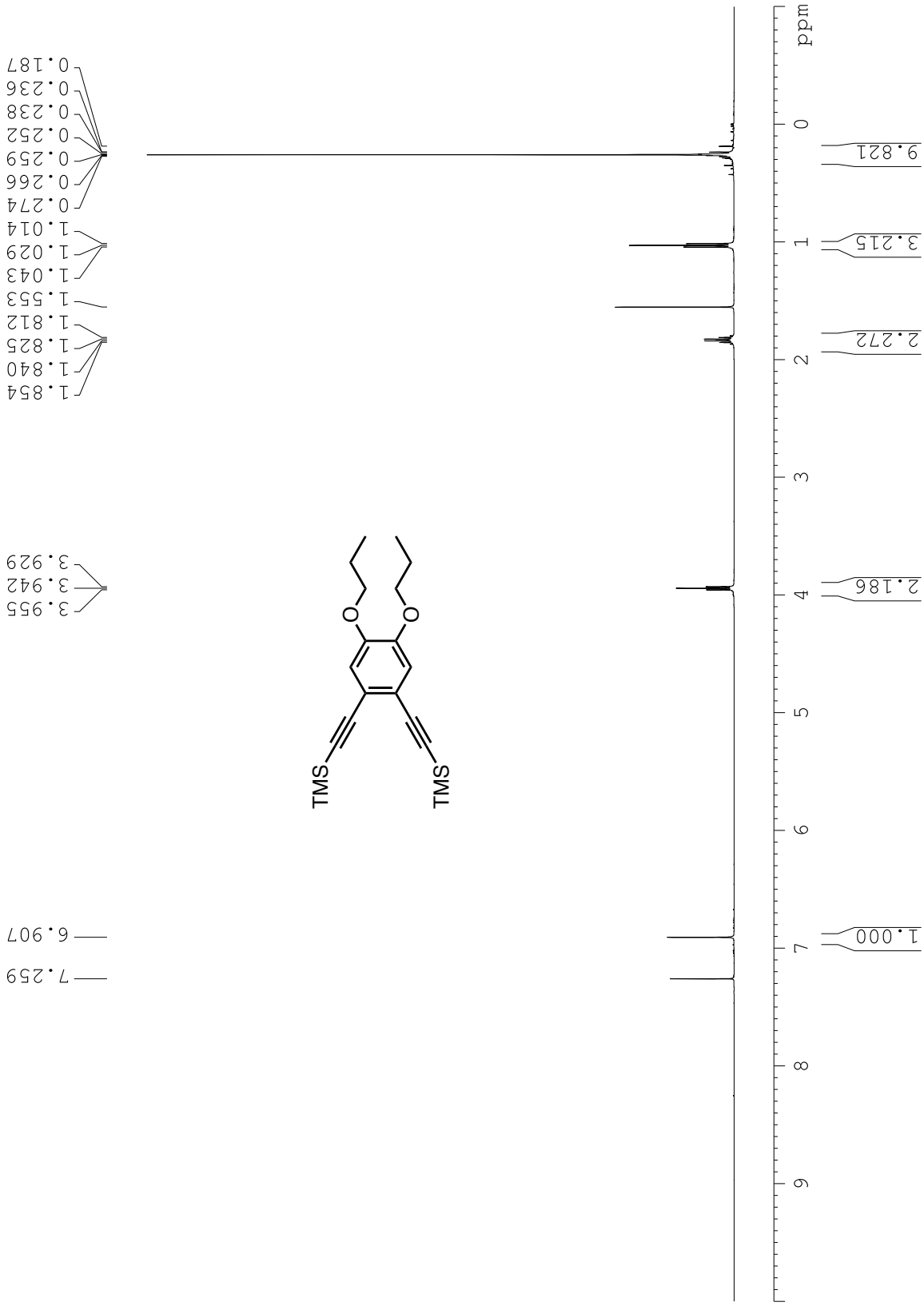

Figure C46. ^{1}H NMR spectrum of compound **27**.

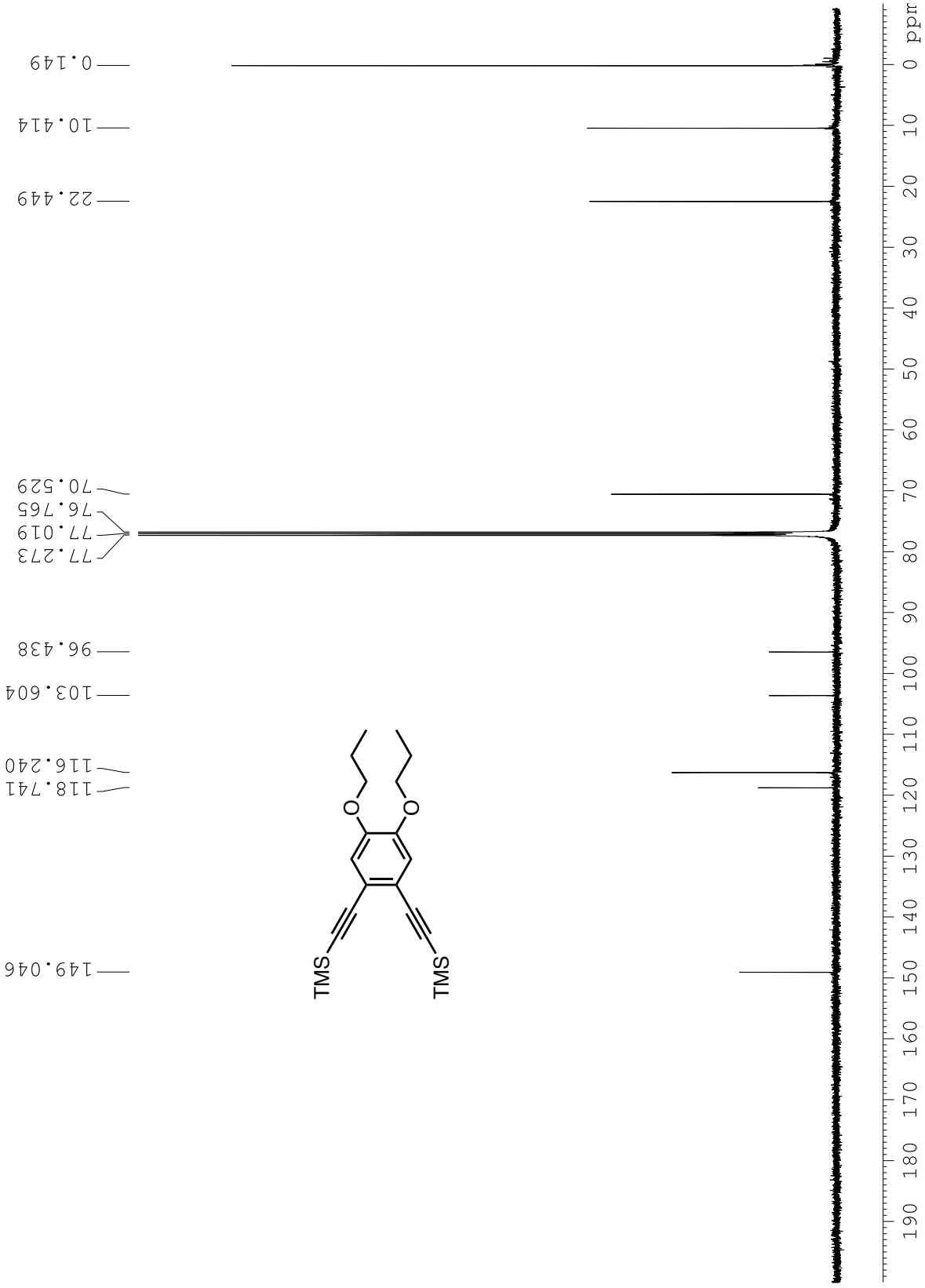

Figure C47. ^{13}C NMR spectrum of compound **27**.

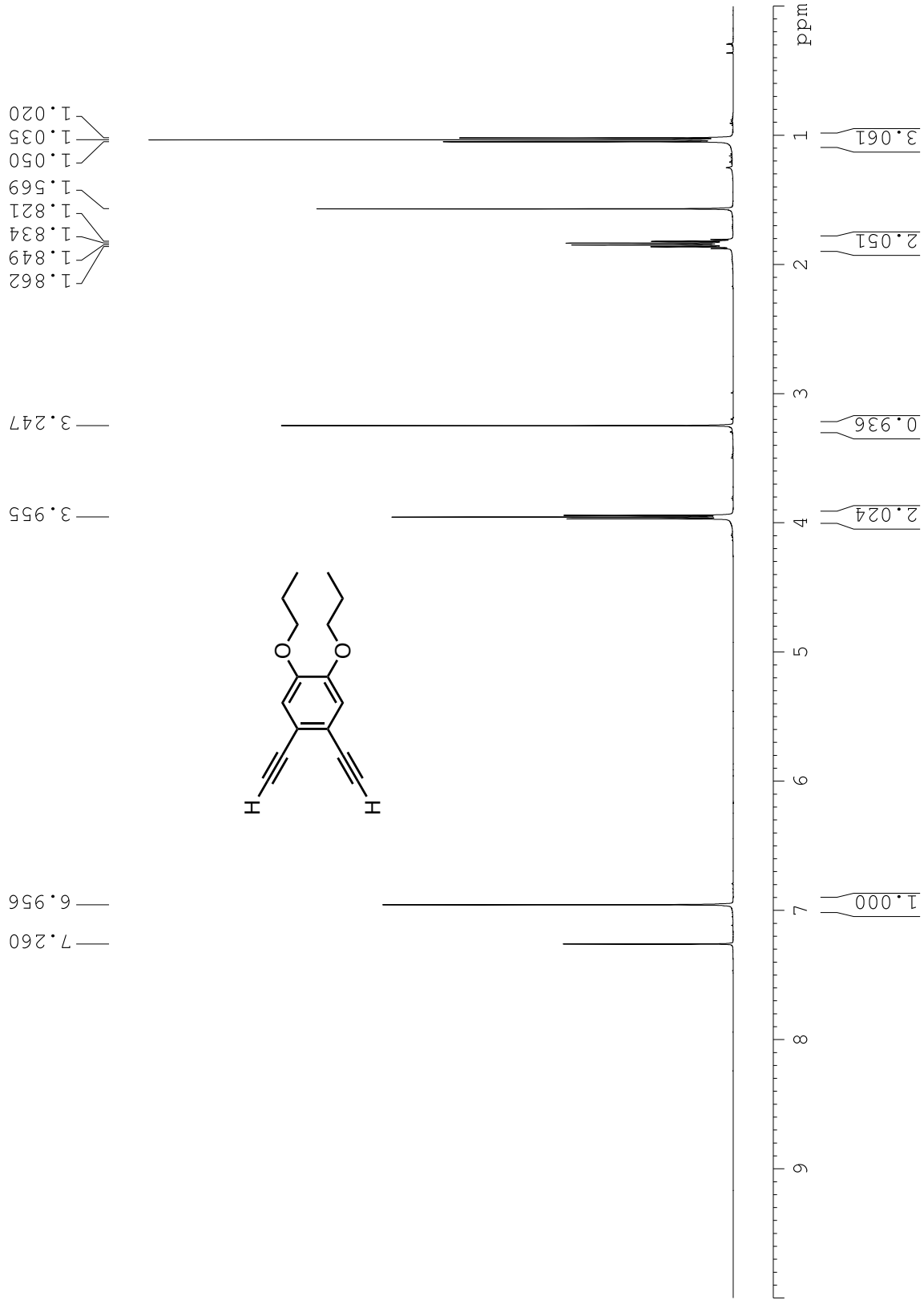

Figure C48. ^{1}H NMR spectrum of compound **28**.

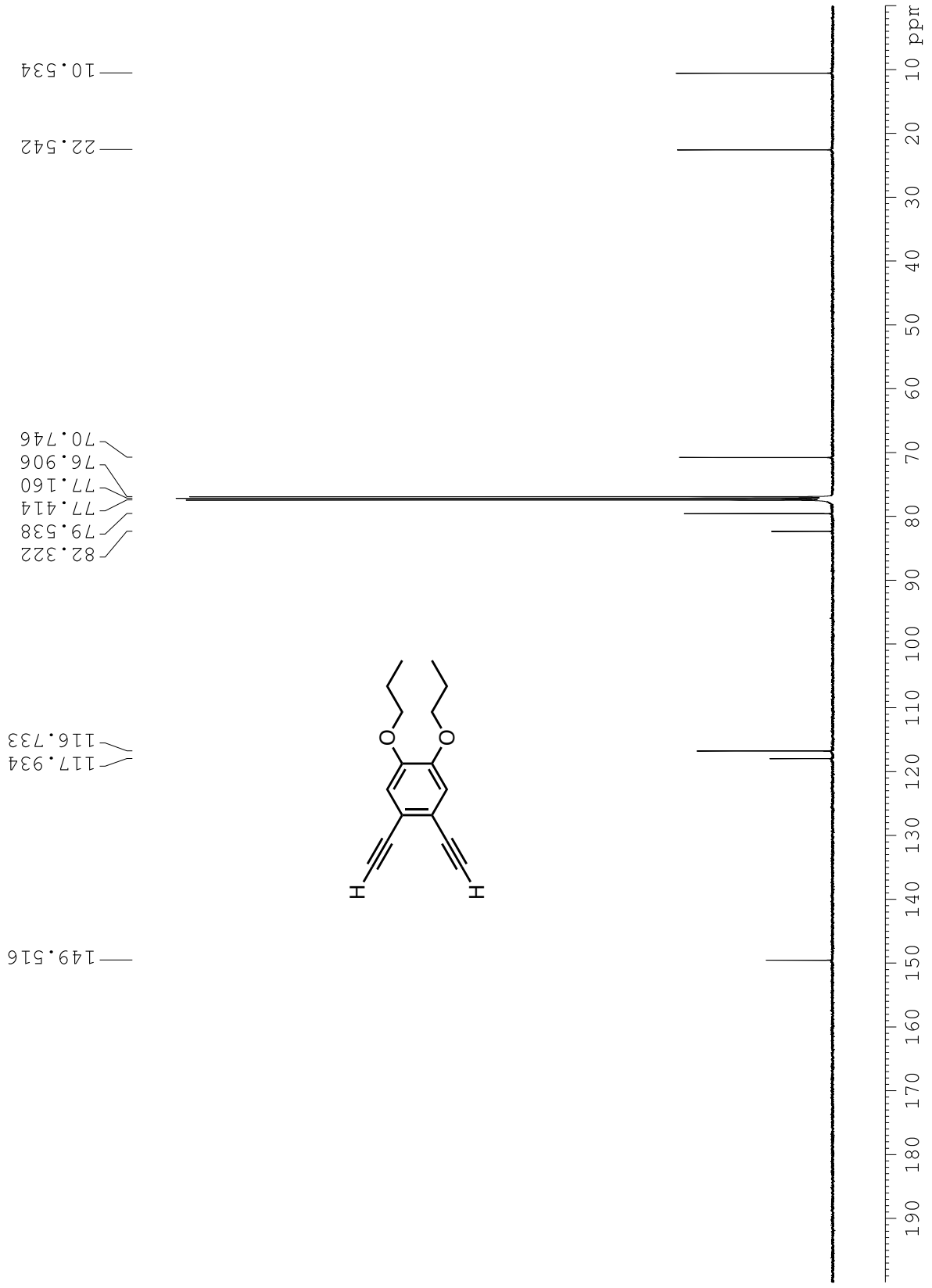

Figure C49. ^{13}C NMR spectrum of compound **28**.

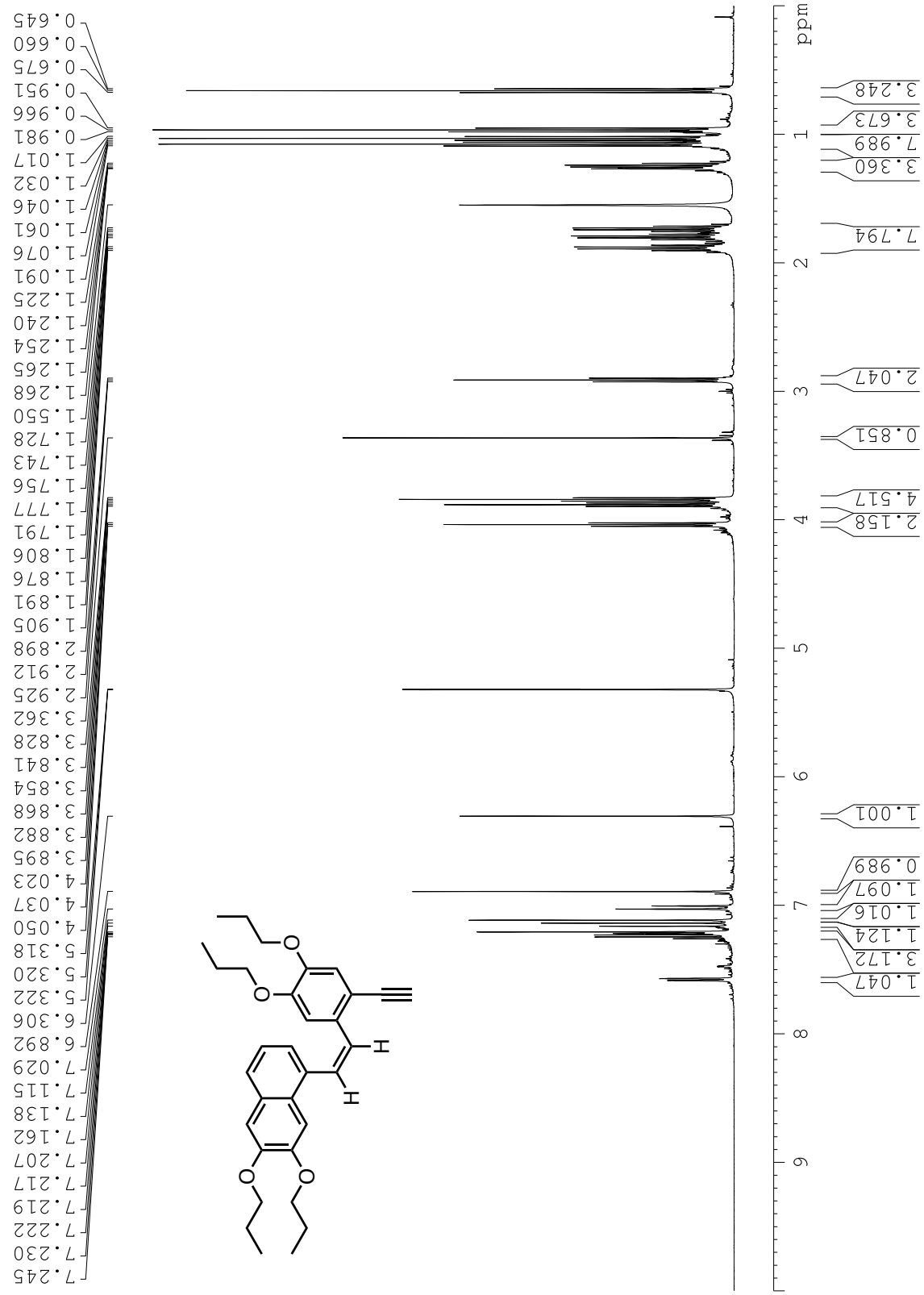

Figure C50. ^{1}H NMR spectrum of compound **28-D-*cis***.

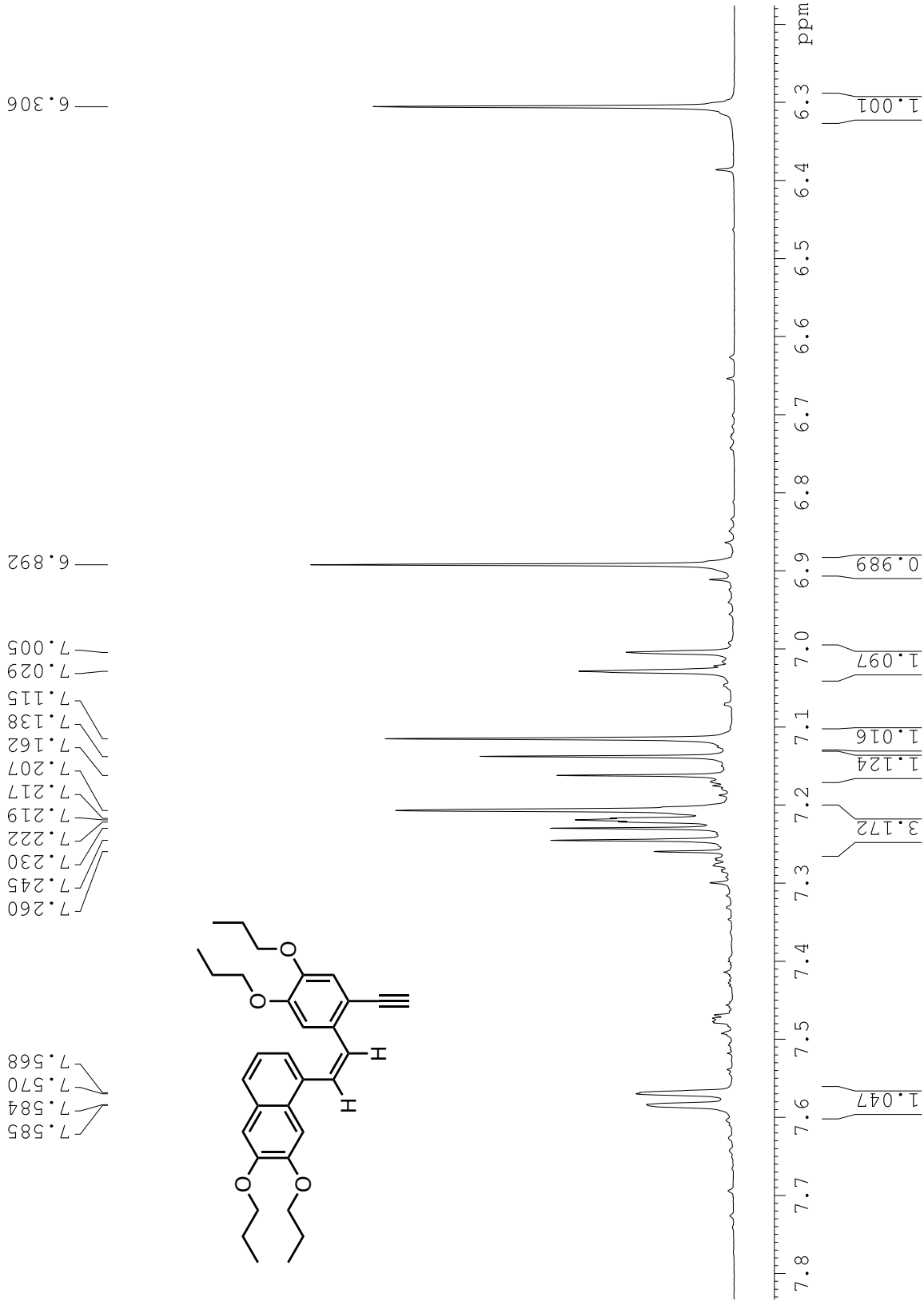

Figure C51. ^{1}H NMR spectrum of the aryl region compound **28-D-*cis***.

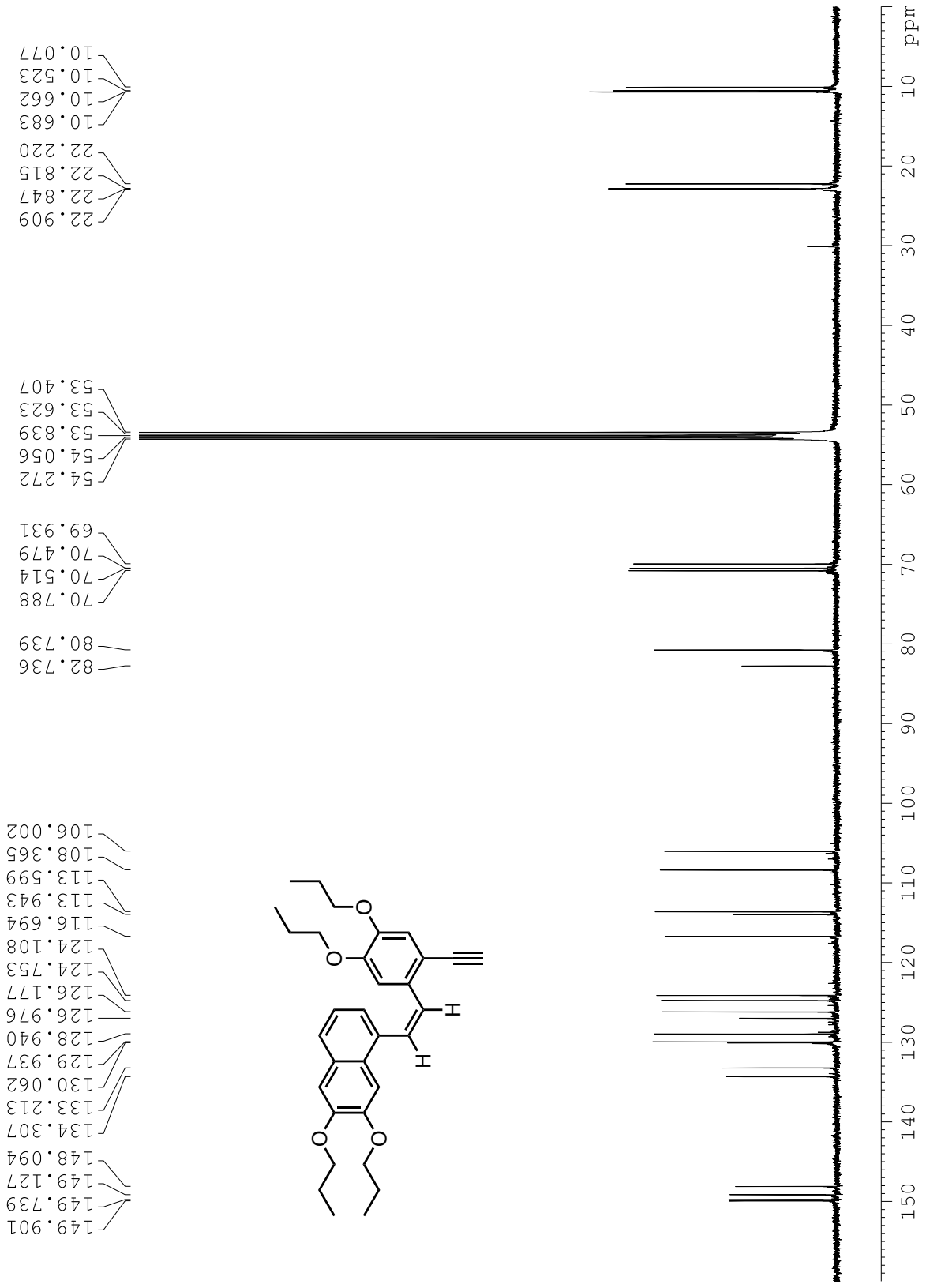

Figure C52. ^{13}C NMR spectrum of compound **28-D-*cis***.

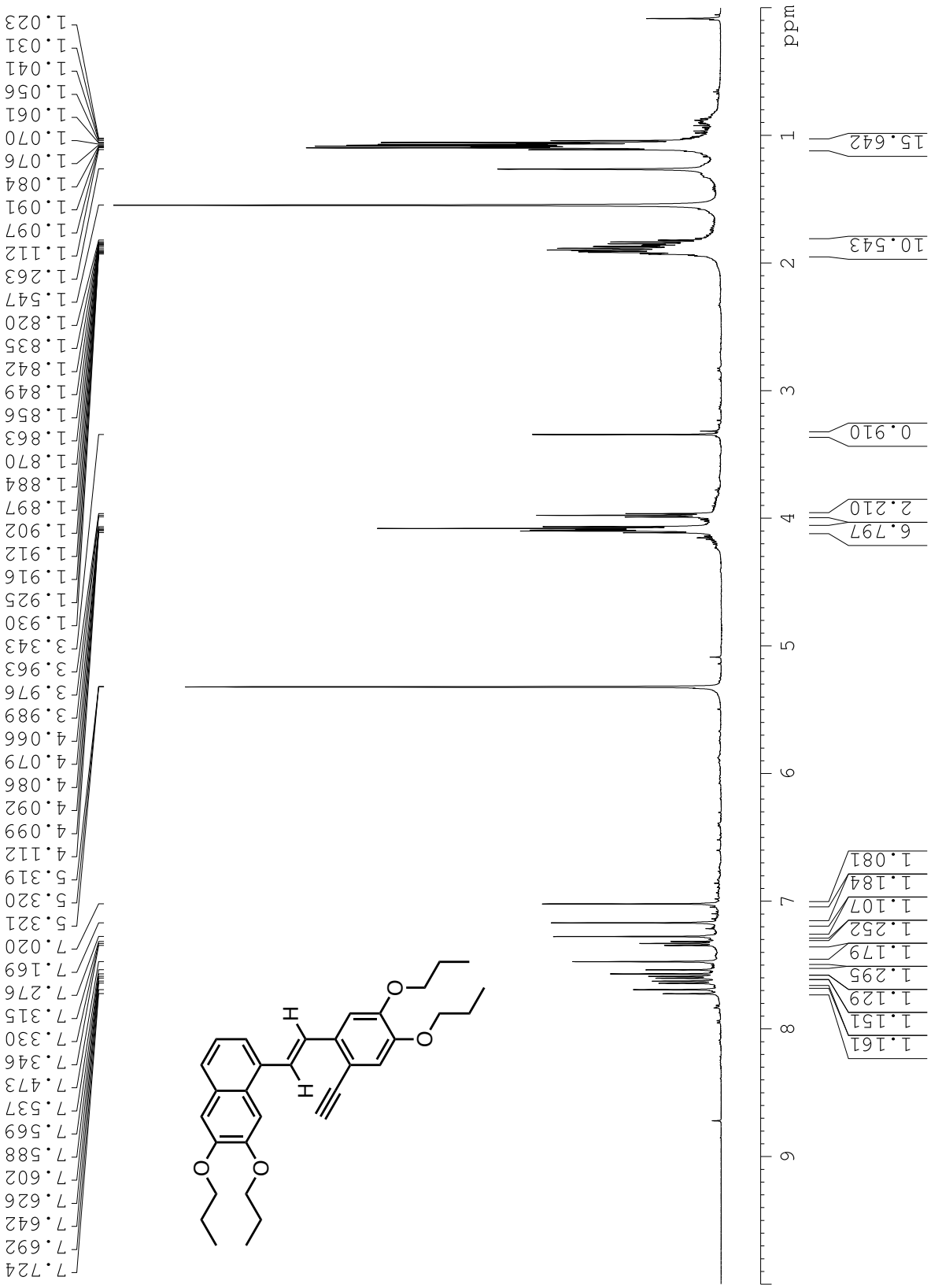

Figure C53. ^{1}H NMR spectrum of compound **28-D-*trans***.

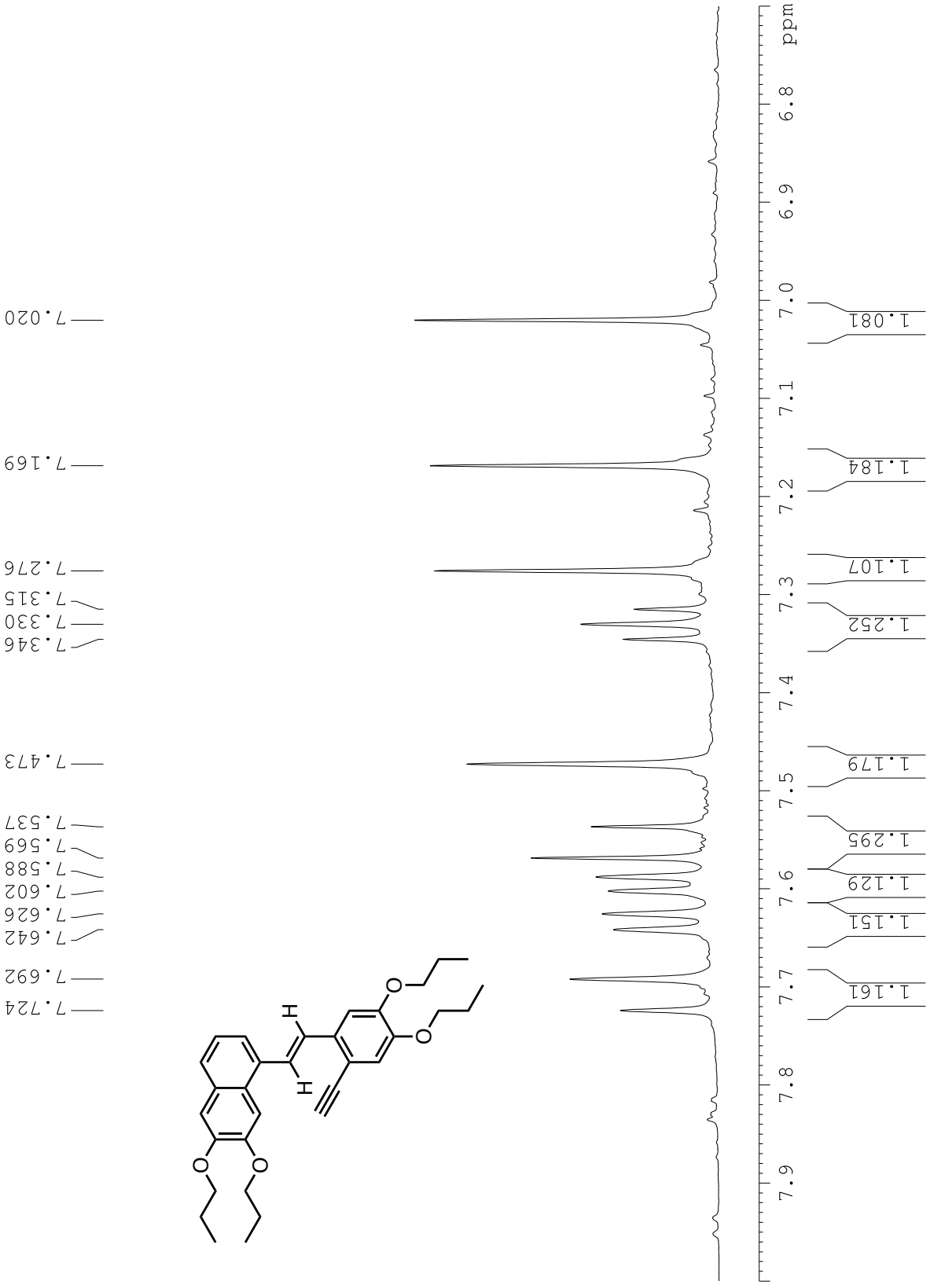

Figure C54. ^{1}H NMR spectrum of the aryl region of compound **28-D-*trans***.

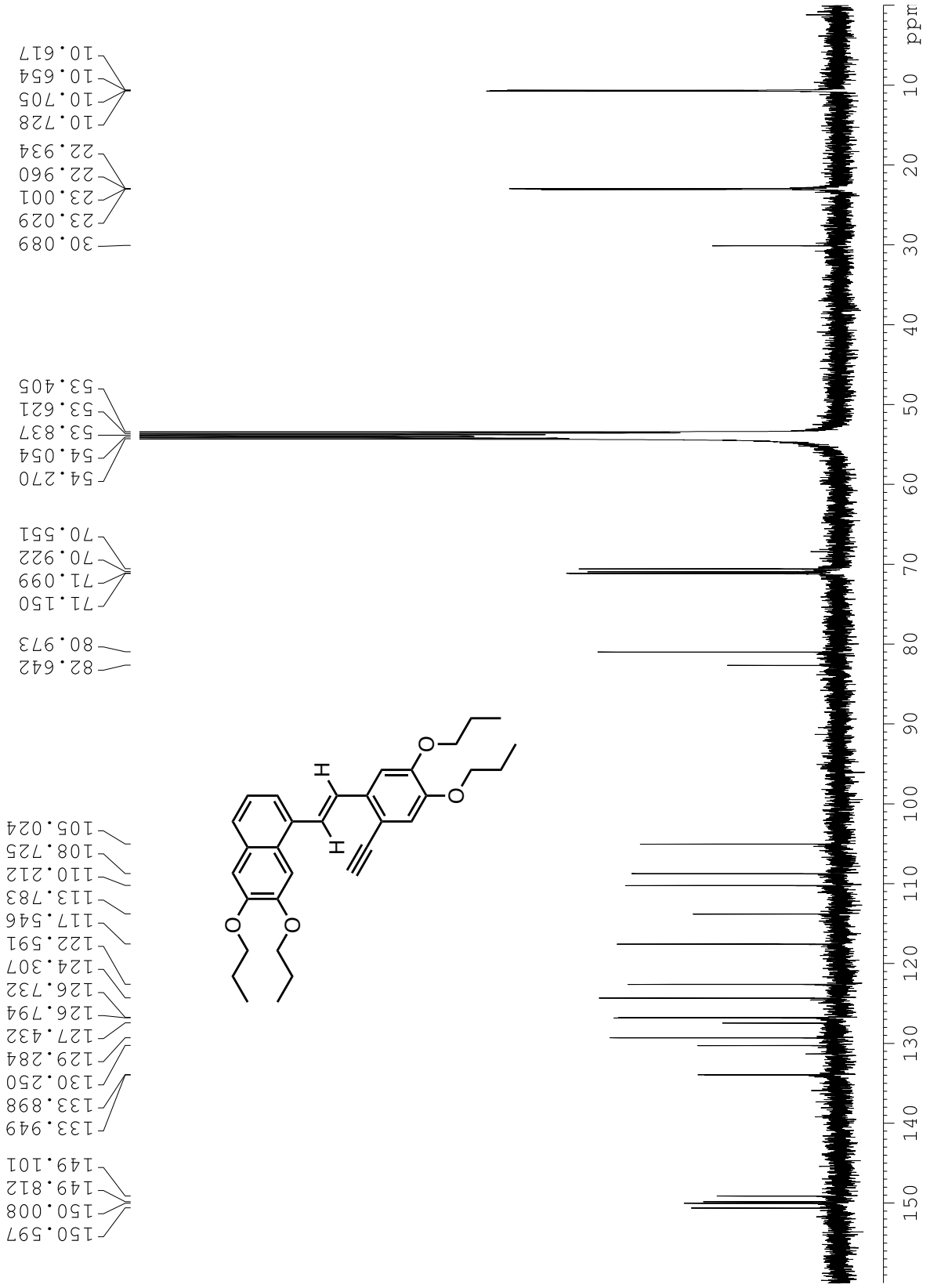

Figure C55. ^{13}C NMR spectrum of compound **28-D-*trans***.

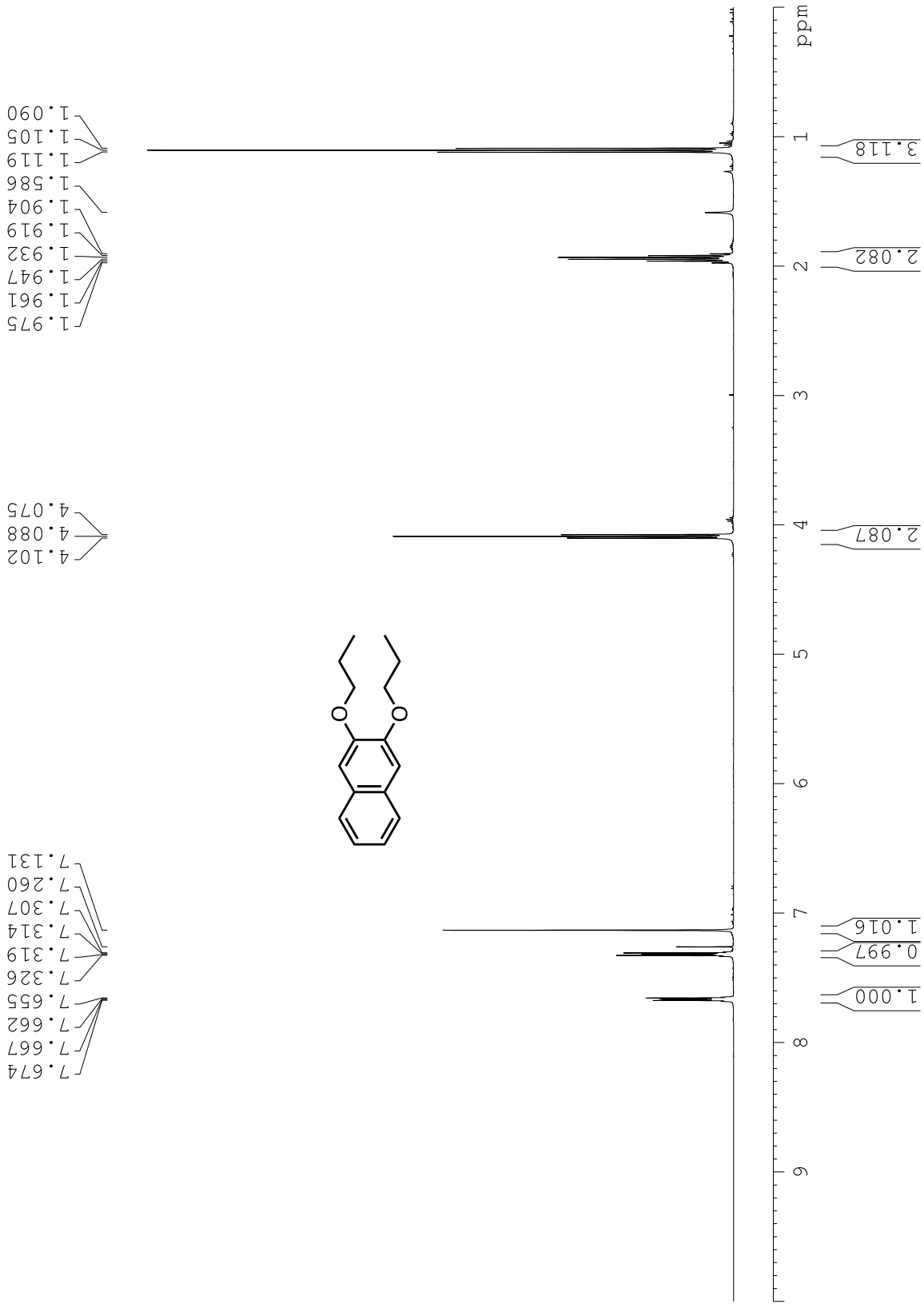

Figure C56. ^{1}H NMR spectrum of compound **29**.

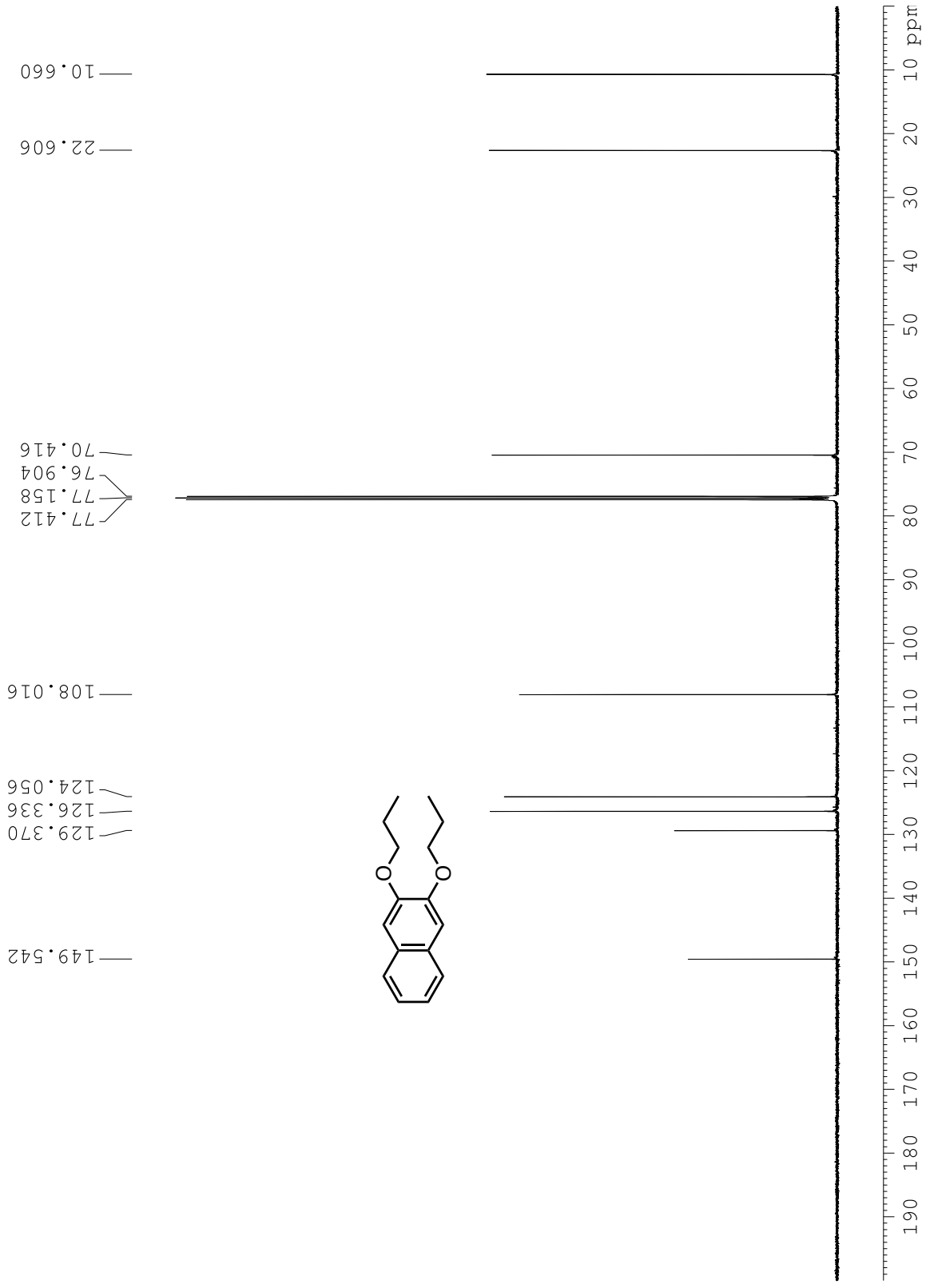

Figure C57. ^{13}C NMR spectrum of compound **29**.

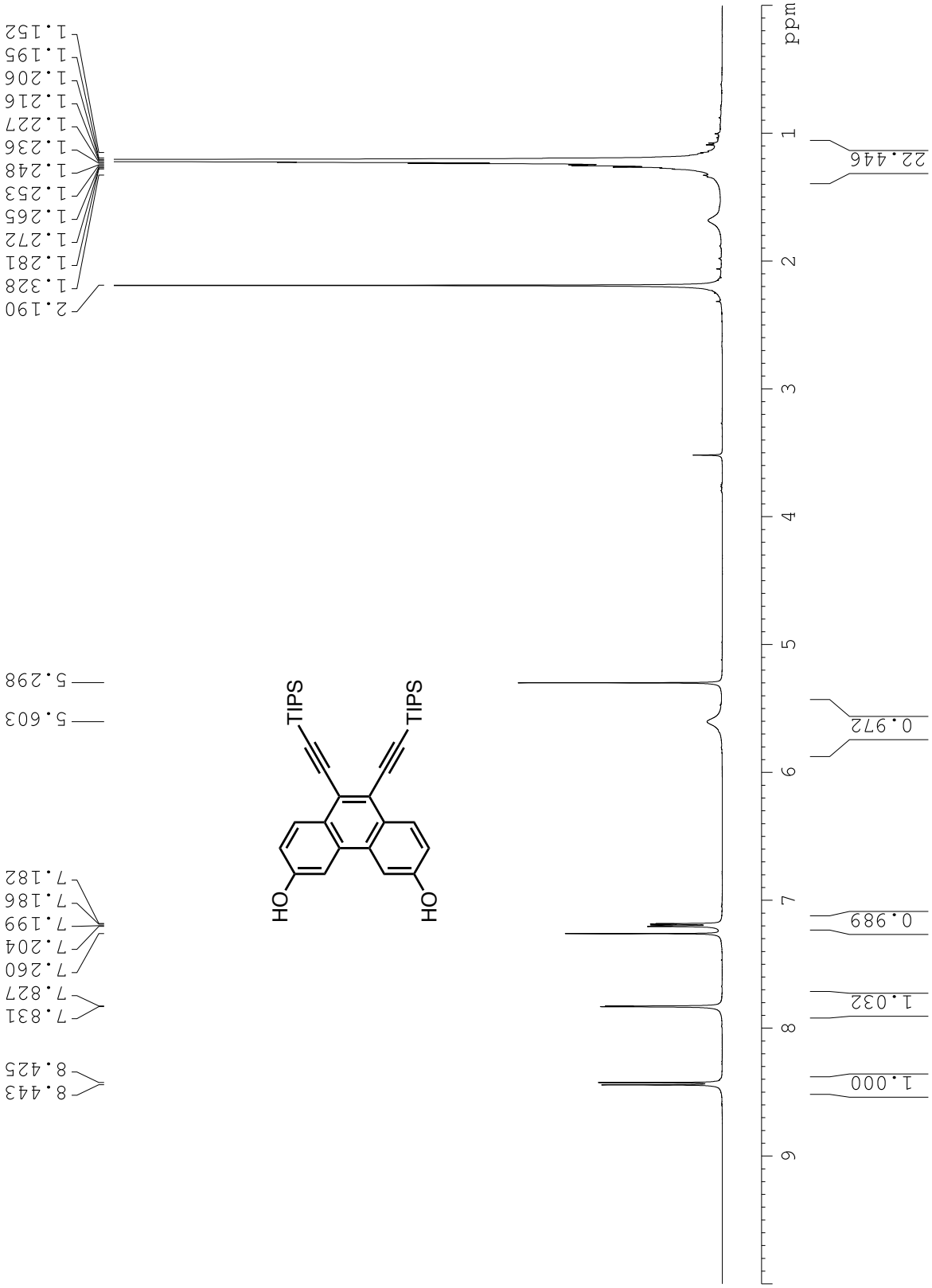

Figure C58. ^{1}H NMR spectrum of compound **30**.

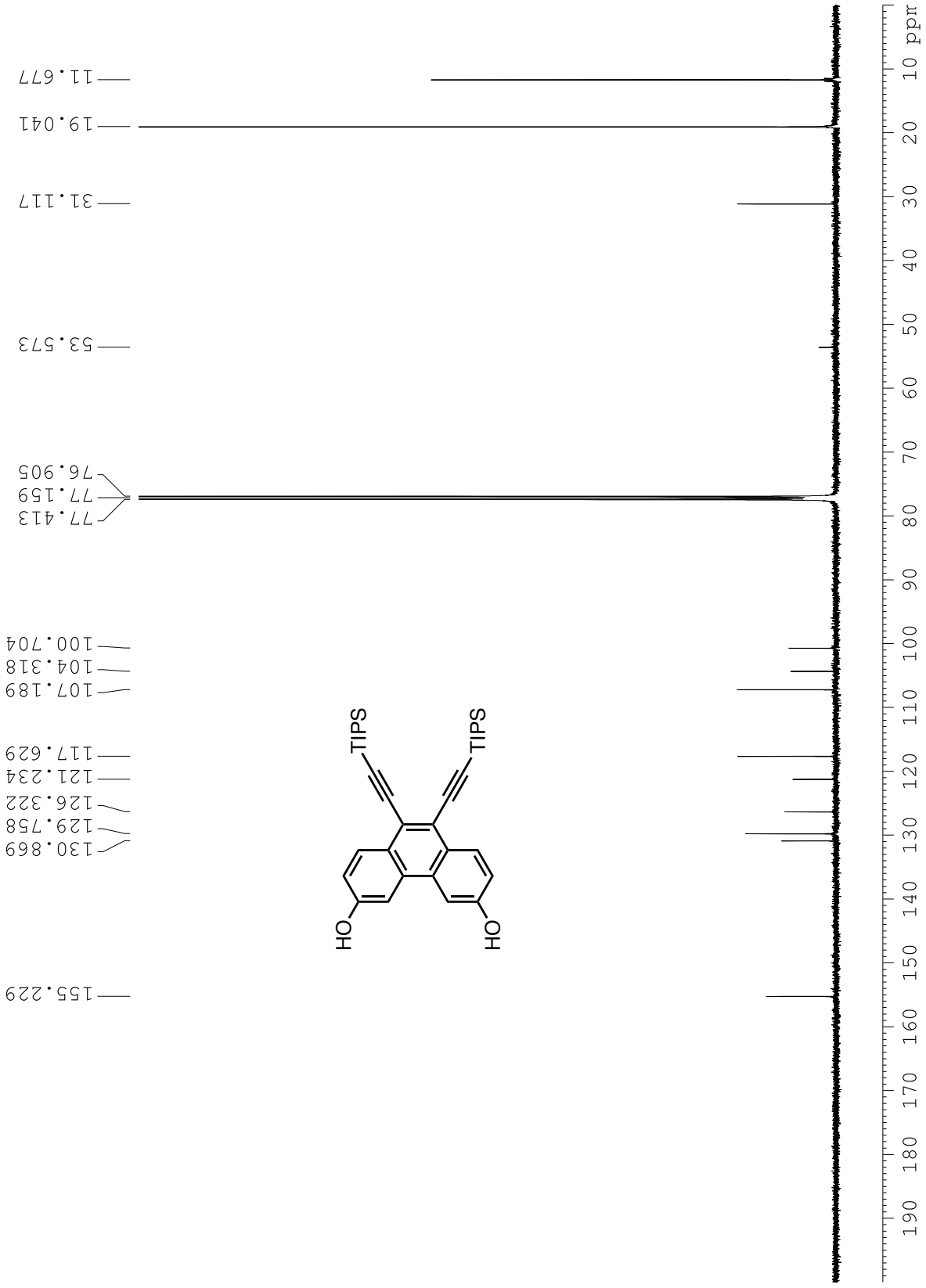

Figure C59. ^{13}C NMR spectrum of compound **30**.

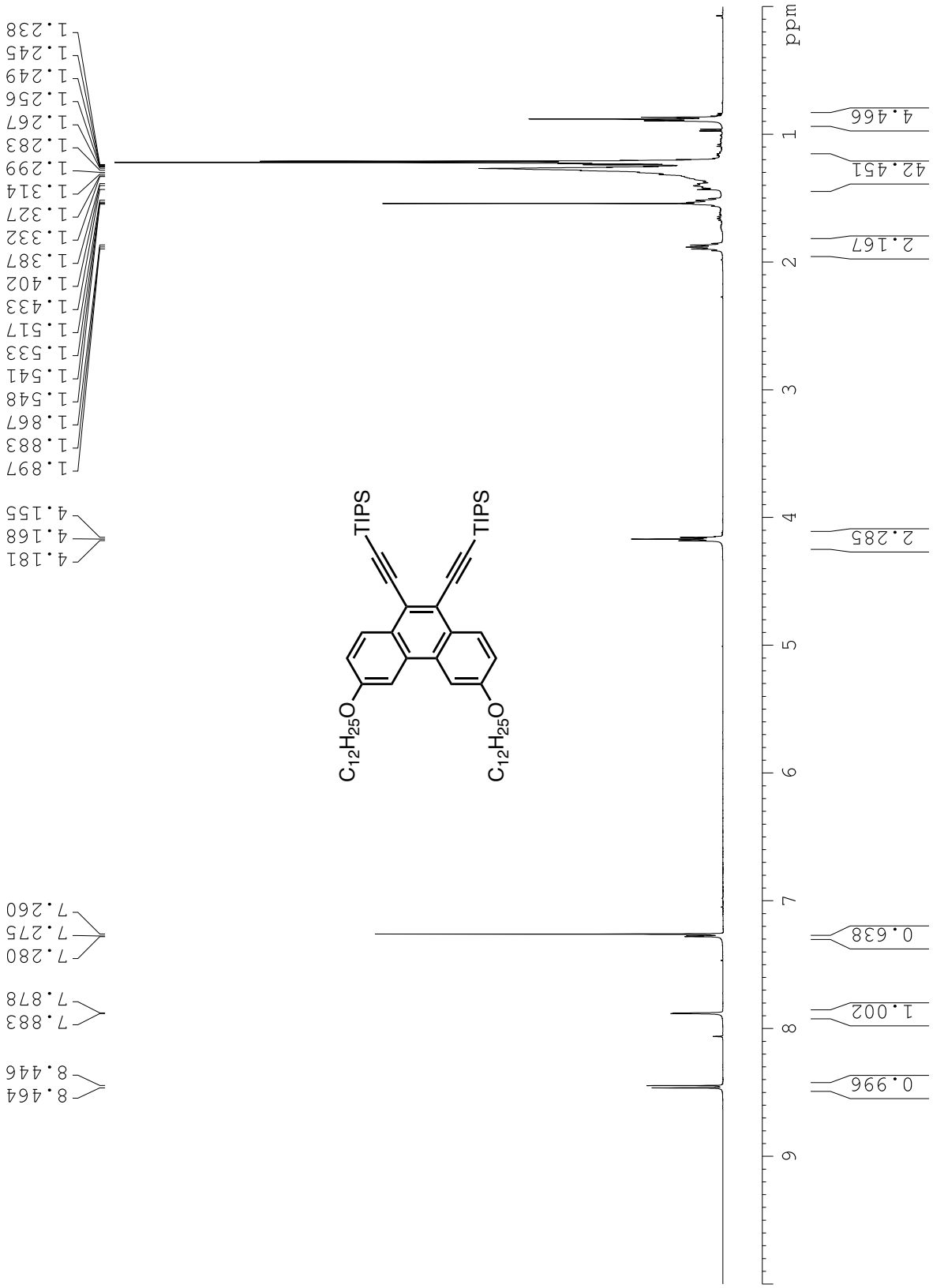

Figure C60. ^{1}H NMR spectrum of compound **31**.

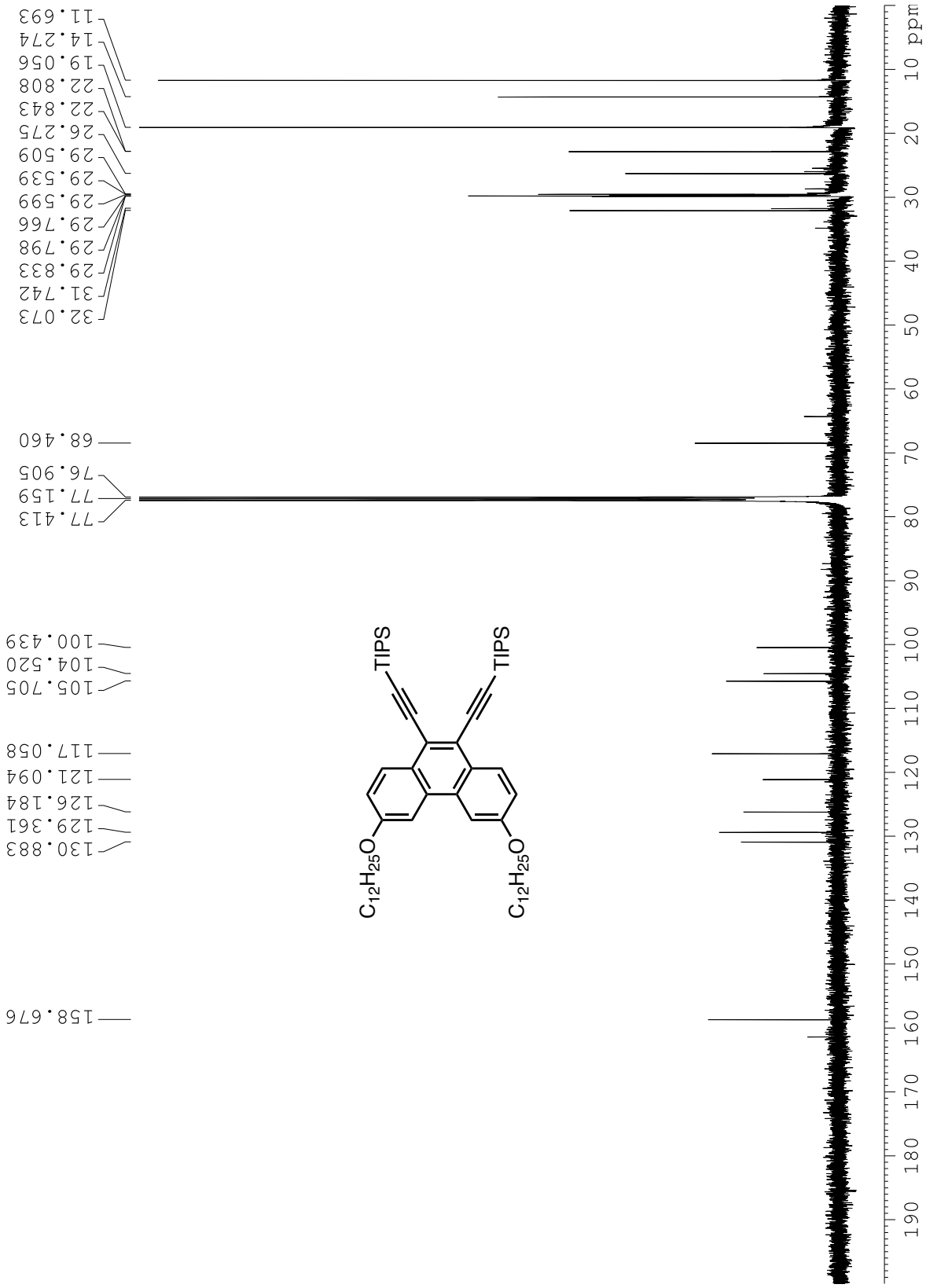

Figure C61. ^{13}C NMR spectrum of compound **31**.

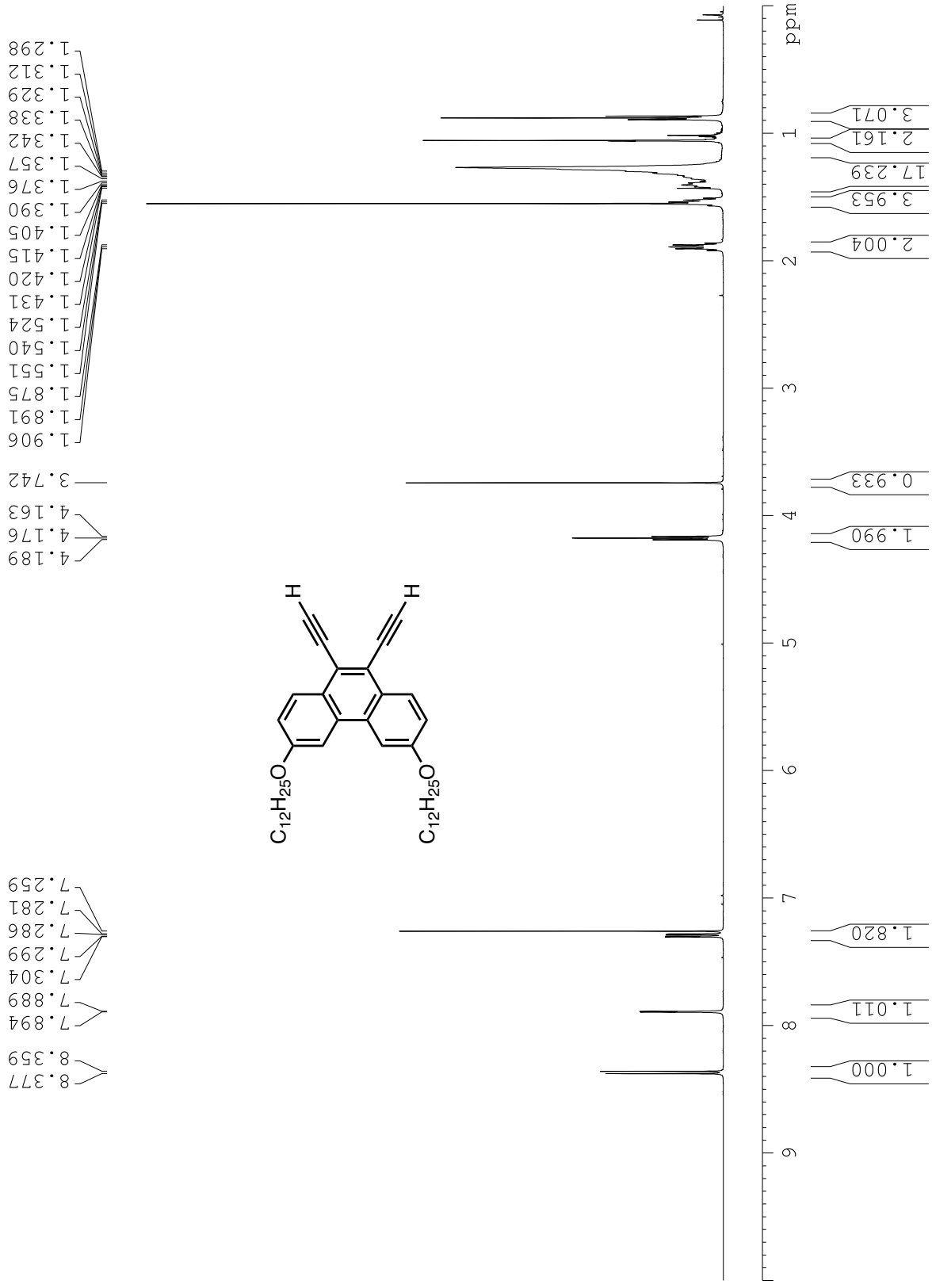

Figure C62. ^{1}H NMR spectrum of compound **32**.

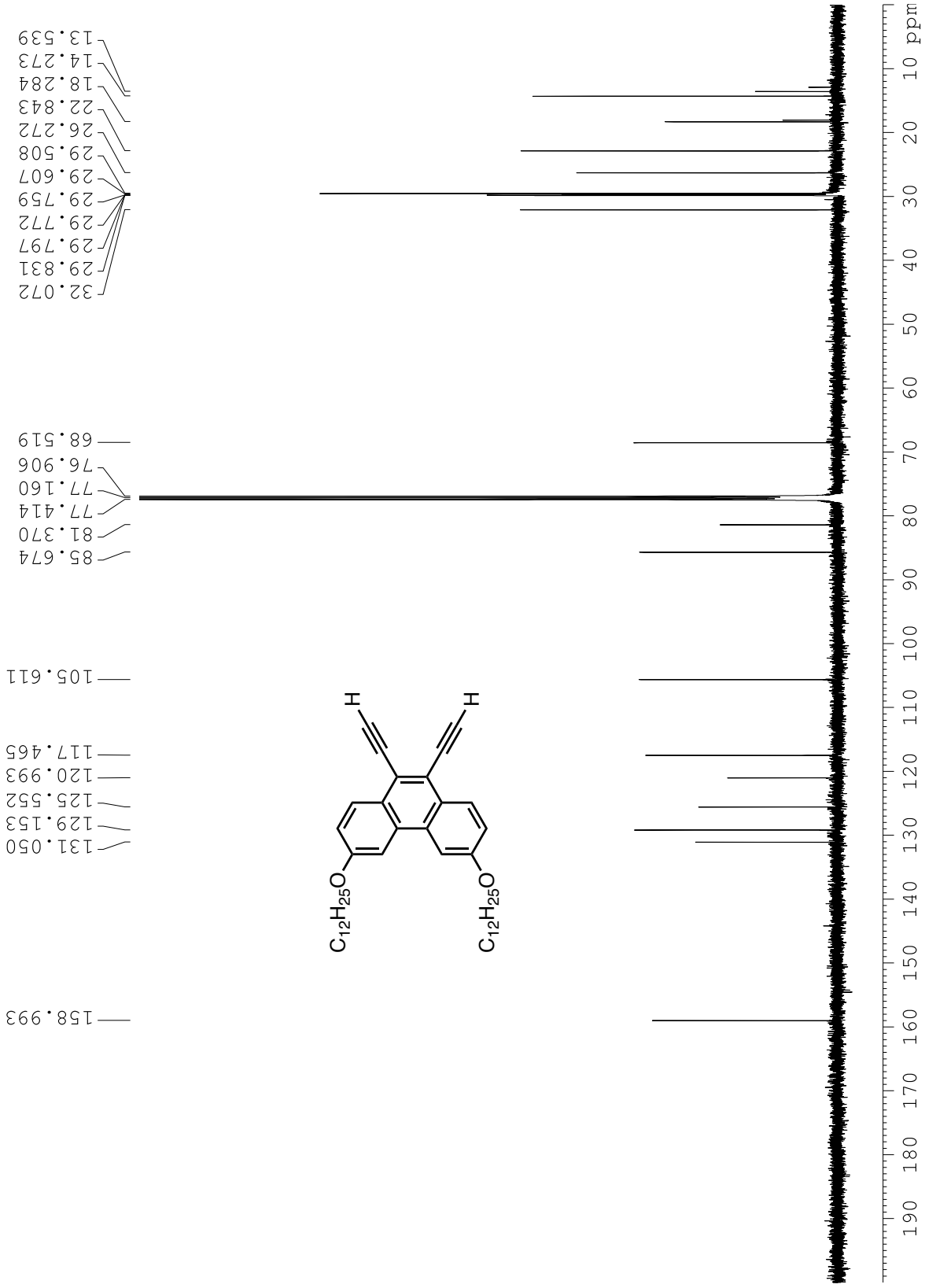

Figure C63. ^{13}C NMR spectrum of compound **32**.

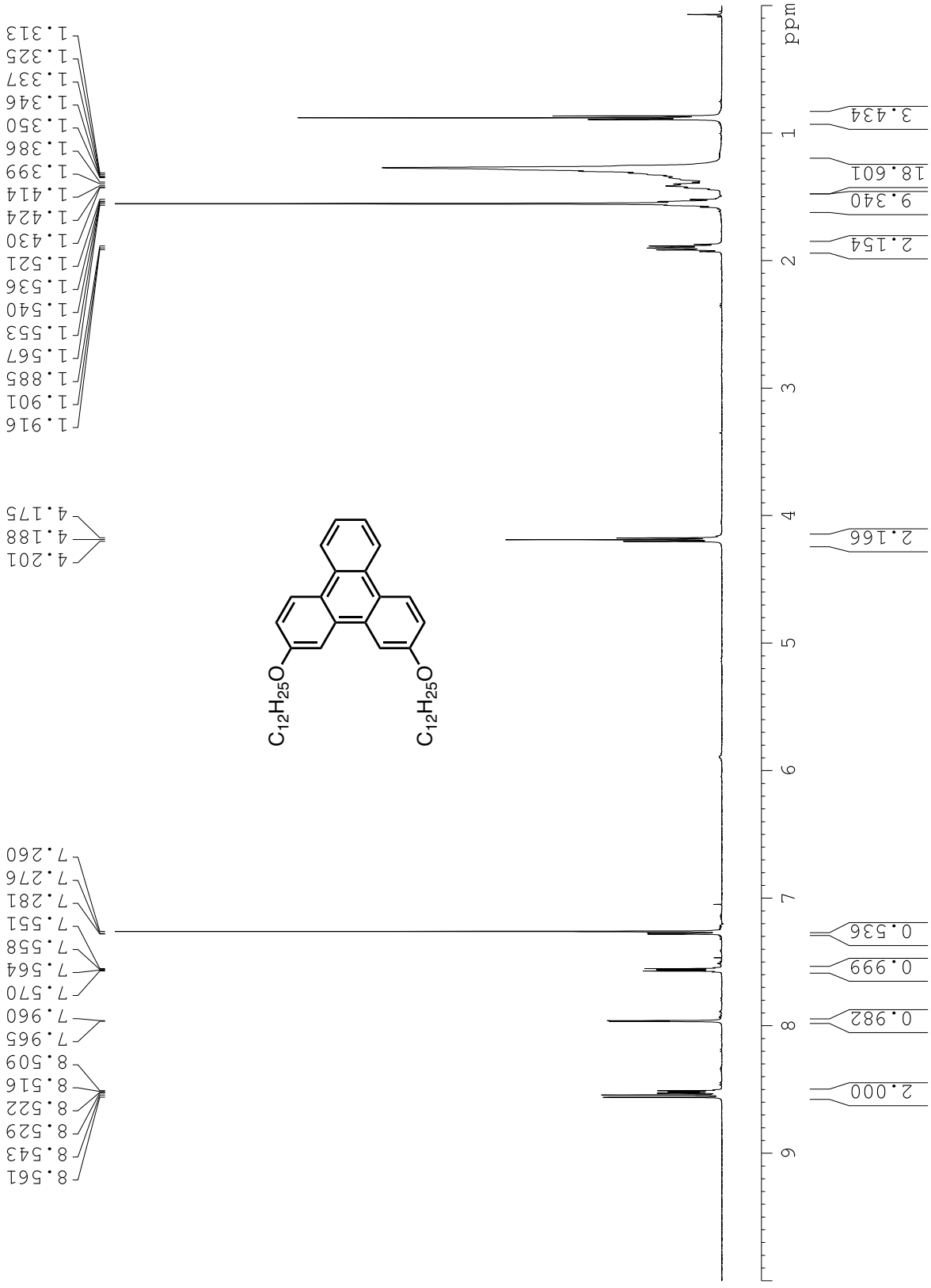

Figure C64. ^{1}H NMR spectrum of compound **33**.

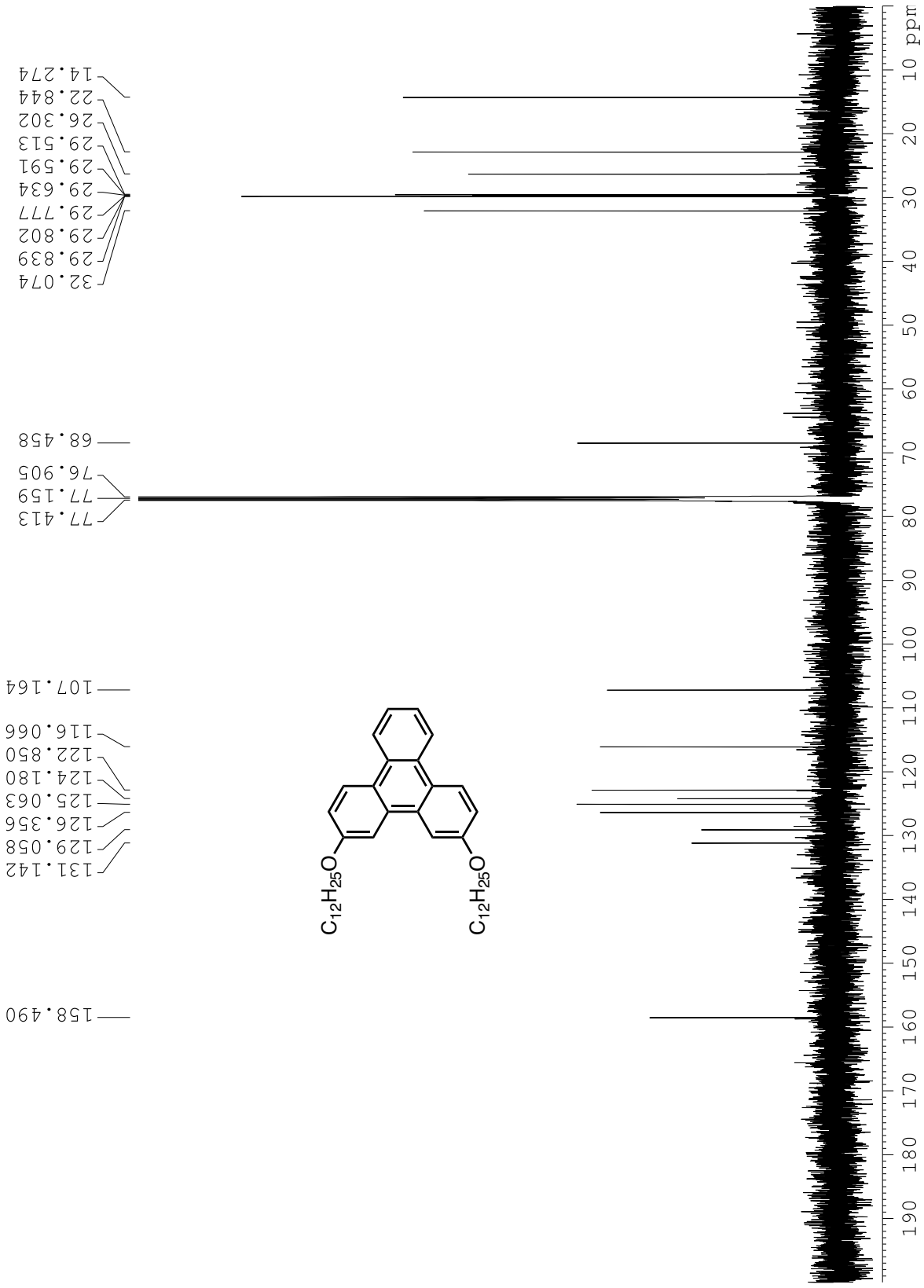

Figure C65. ^{13}C NMR spectrum of compound **33**.

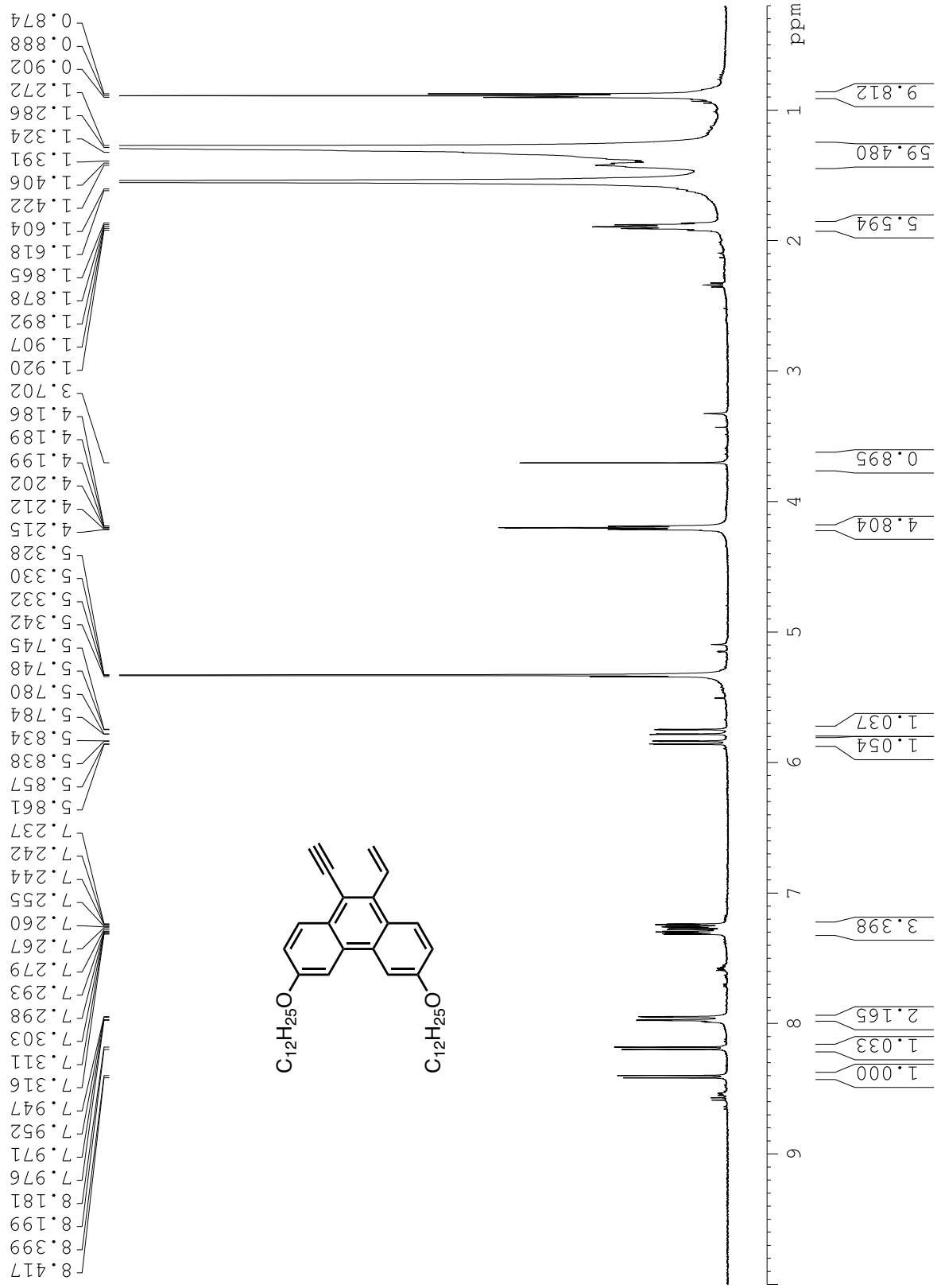

Figure C66. ^{1}H NMR spectrum of compound **34**.

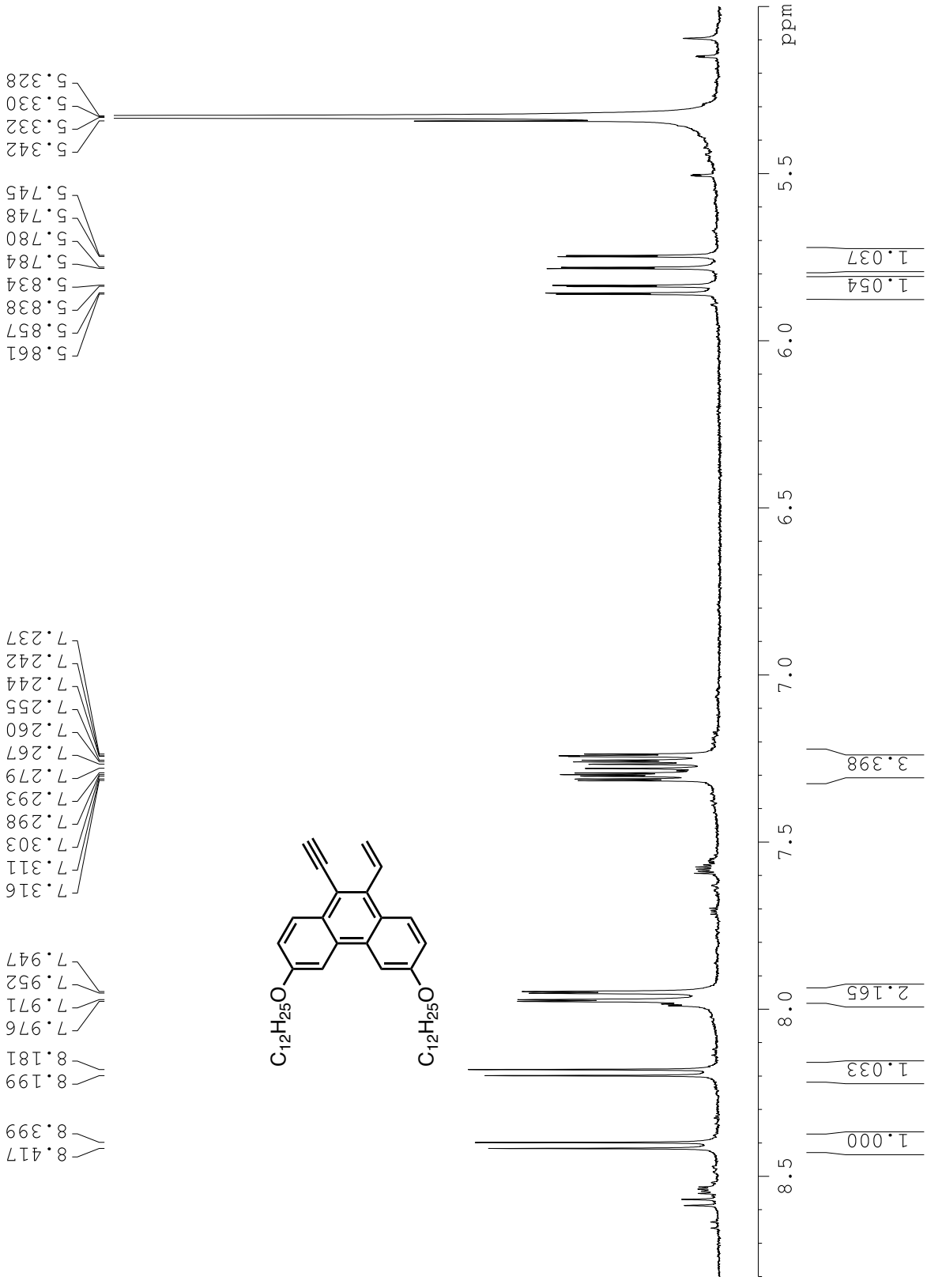

Figure C67. ^{1}H NMR spectrum of the aryl region of compound **34**.

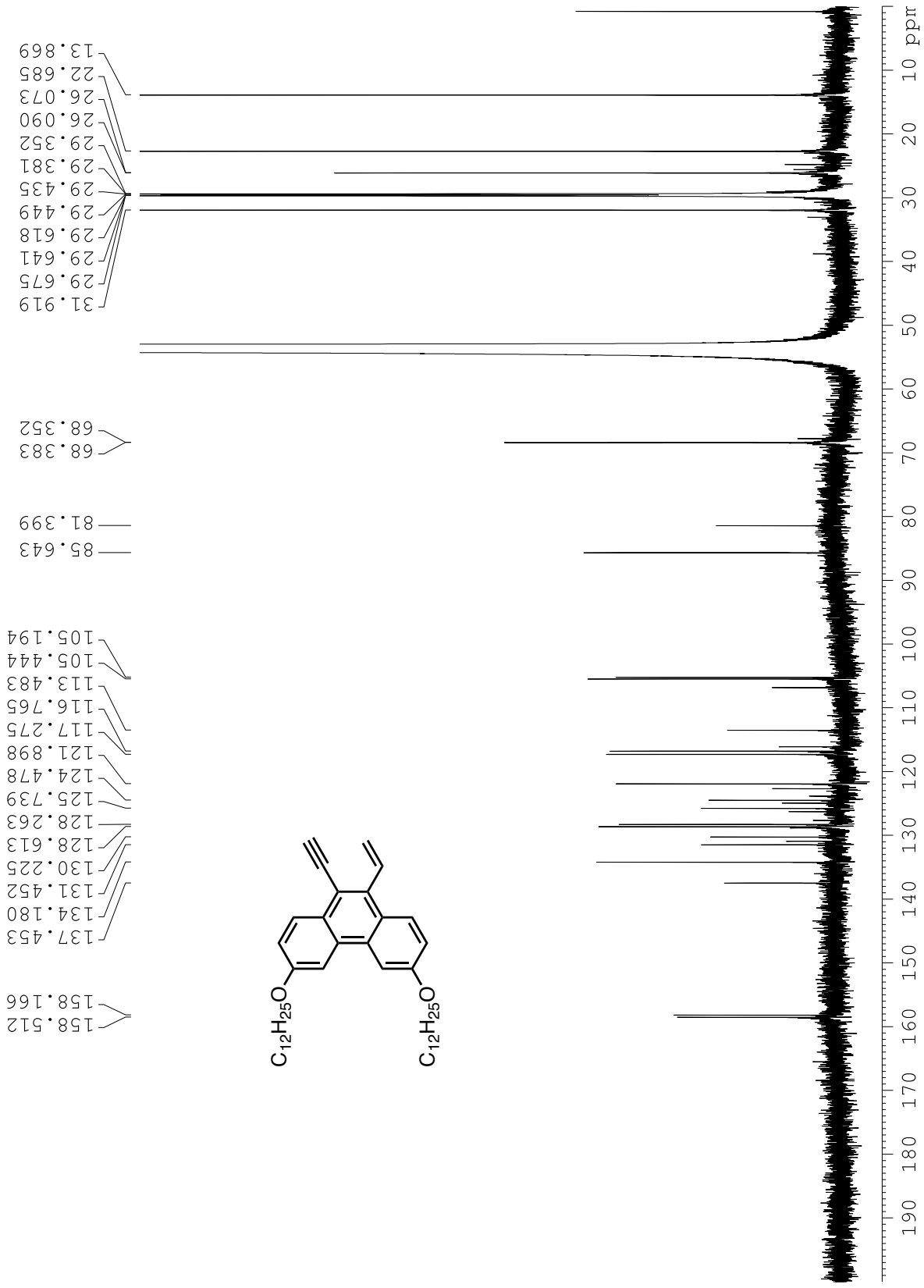

Figure C68. ^{13}C NMR spectrum of compound **34**.

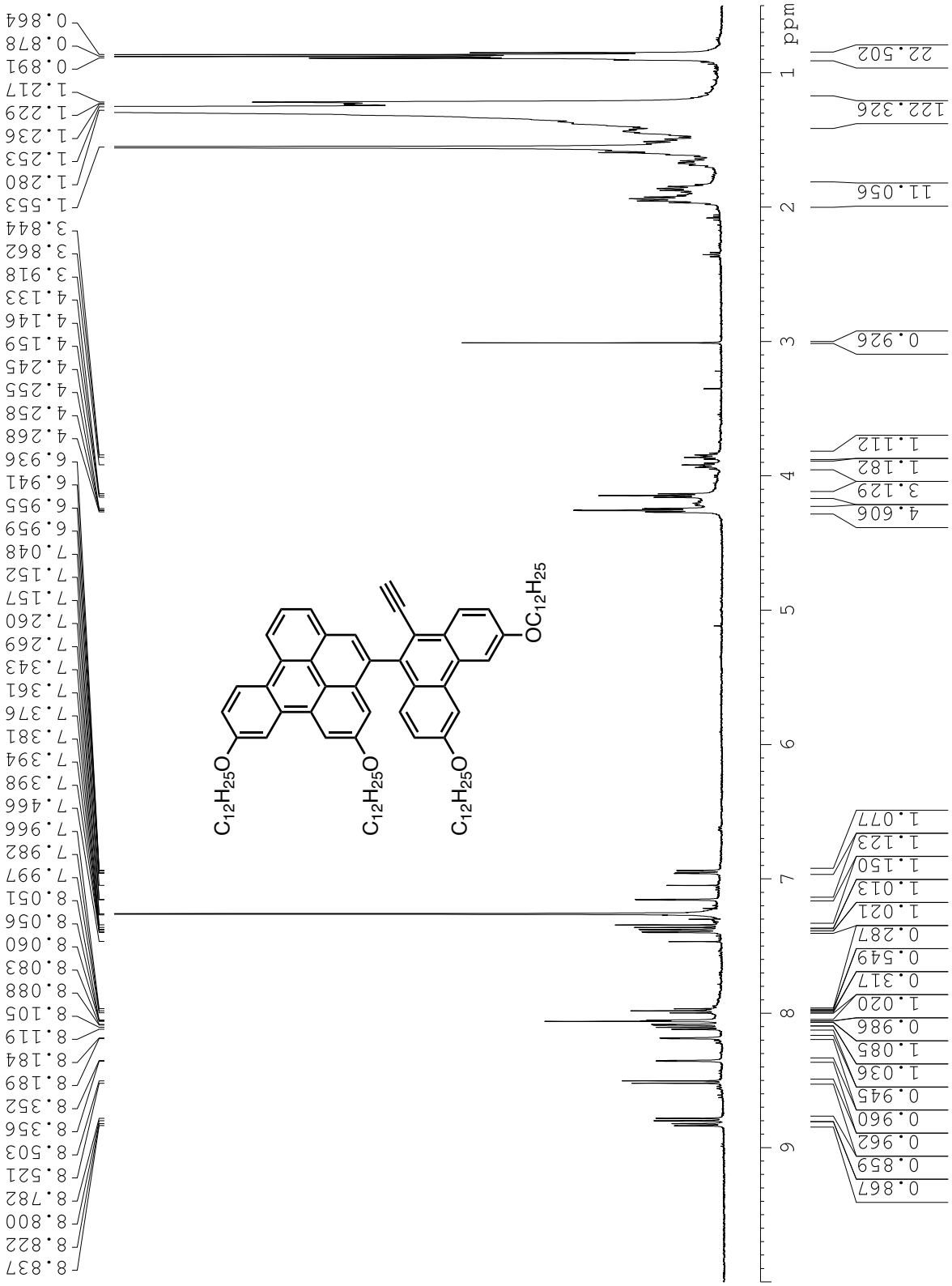

Figure C69. ^{1}H NMR spectrum of compound **35**.

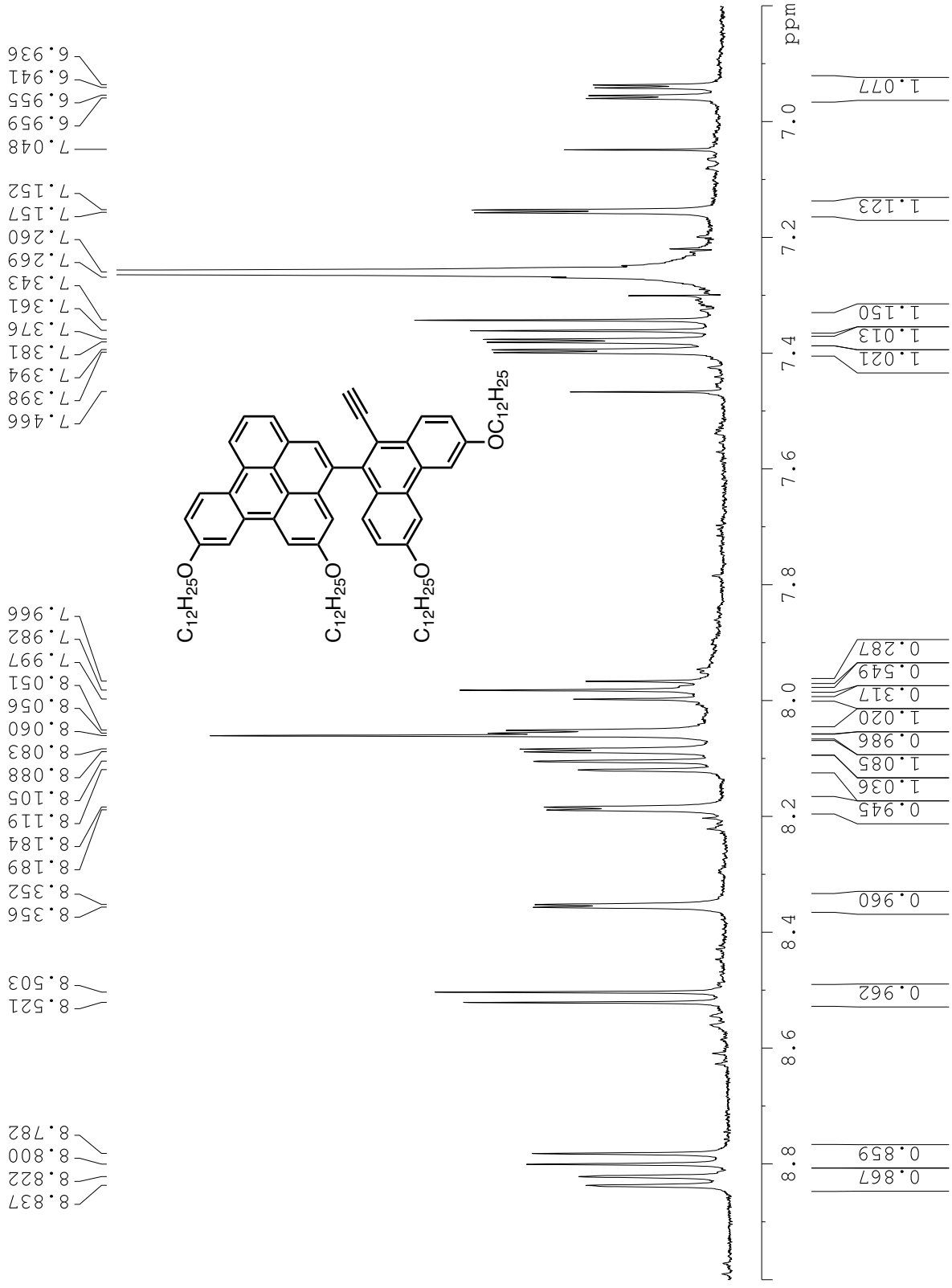

Figure C70. ^{1}H NMR spectrum of the aryl region of compound **35**.

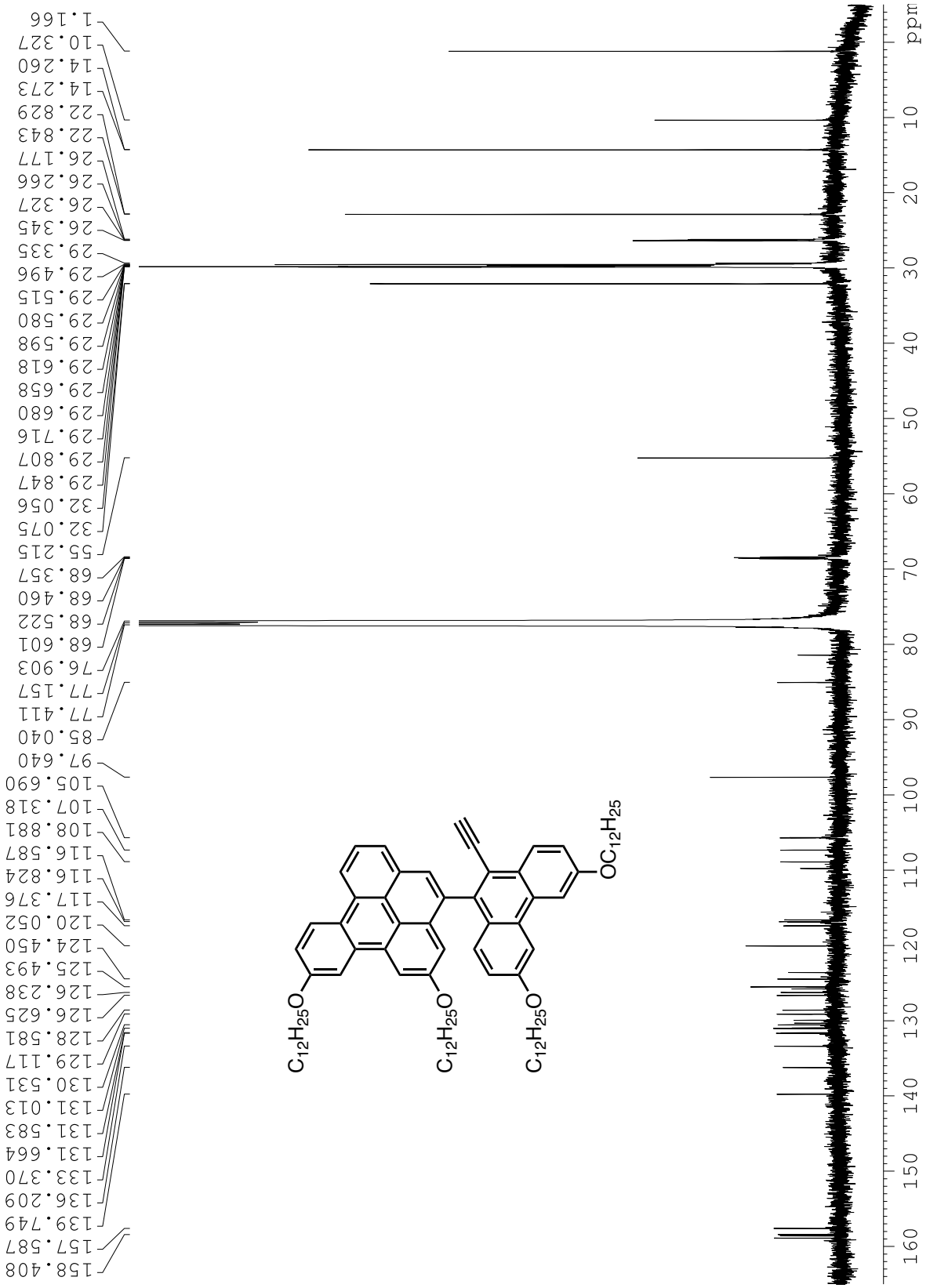

Figure C71. ^{13}C NMR spectrum of compound **35**.

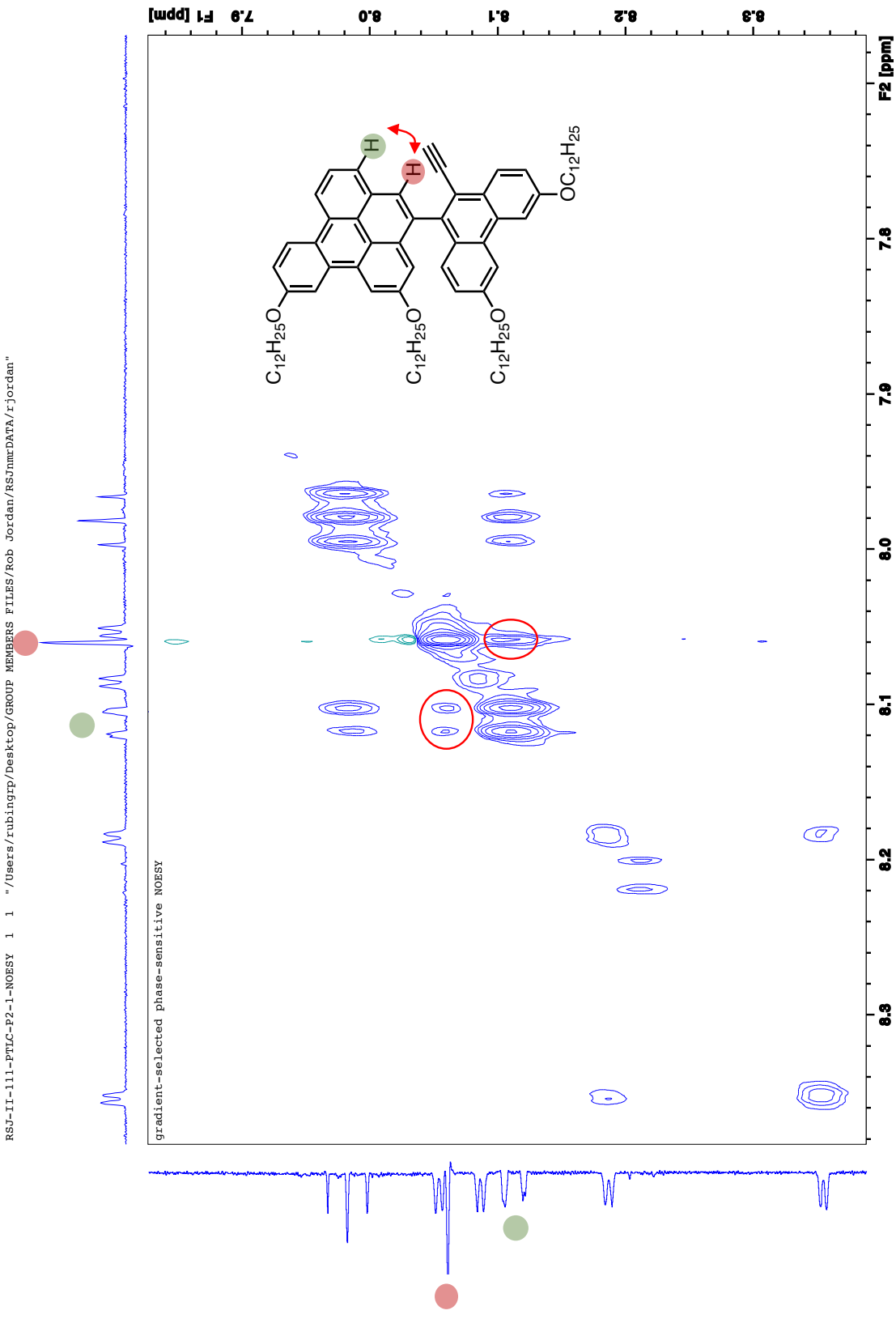

Figure C72. NOESY NMR spectrum of compound **35** with key correlation highlighted.

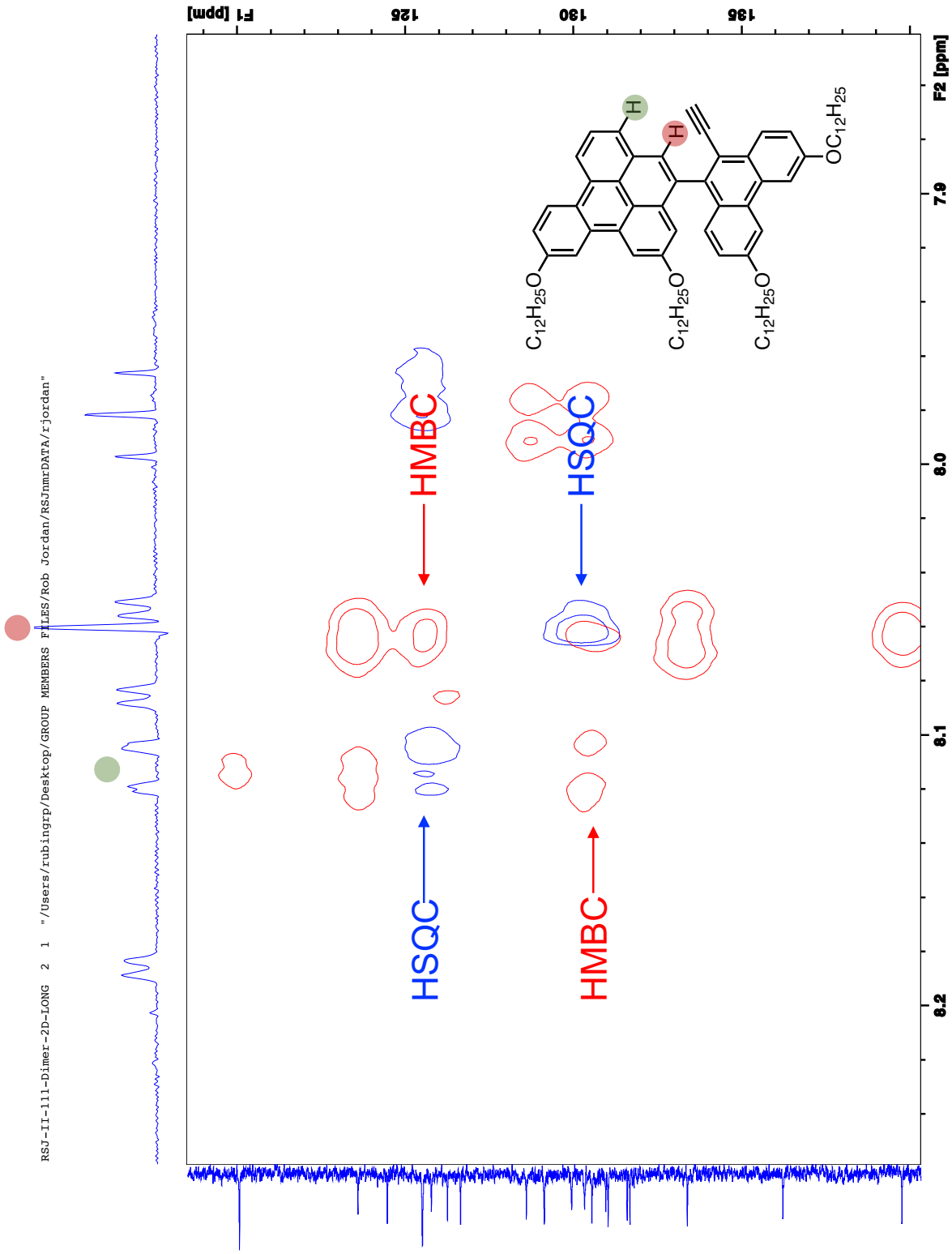

Figure C72. Combined HSQC and HMBC NMR spectrum of compound **35** with key correlations highlighted.

References

[1] Jordan, R. S.; Wang, Y.; McCurdy, R. D.; Yeung, M. T.; Marsh, K. L.; Khan, S. I.; Kaner, R. B.; Rubin, Y. *Chem* **2016**, *1*, 78–90.

[2] Jordan, R. S.; Li, Y. L.; Lin, C-W.; McCurdy, R. D.; Lin, J. B.; Brosmer, J. L.; Marsh, K. L.; Houk, K. N.; Kaner, R. B.; Rubin Y. *J. Am. Chem. Soc. Submitted.* Chapter 1 of this dissertation.

[3] Hitt, D. M; O'Connor, J. M. *Chem. Rev.* **2011**, *111*, 7904-7922.

[4] Hofmann, J.; Schulz, K.; Altmann, A.; Findeisen, M.; Zimmermann, G. *Liebigs Ann./Recueil* **1997**, *12*, 2541-2548.

[5] Berger, H.; Hopf, H.; Dix, I.; Jones, P. G. *Eur. J. Org. Chem.* **2004**, *16*, 3401-3403.

[6] McMurry, J. E. *Chem. Rev.* **1989**, *89*, 1513-1524.

[7] Duan, X-F.; Zeng, J.; Lü, J-W.; Zhang, Z-B. *J. Org. Chem.* **2006**, *71*, 9873-9876.

[8] Kise, N.; Takenaga, Y.; Ishikawa, Y.; Morikami, Y.; Sakurai, T. *Tetrahedron Lett.* **2012**, *53*, 1940-1945.

[9] Jones, G. B.; Wright, J. M.; Plourde, G. W. II, Hynd, G.; Huber, R. S.; Mathews, J. E. *J. Am. Chem. Soc.* **2000**, *122*, 1937-1944.

[10] Tinnemans, A. H. A.; Laarhoven, W. H. *J. Chem. Soc. Perkin Trans. II*, **1976**, 1111-1115.

[11] Prall, M.; Krüger, A.; Schreiner, P. R.; Hopf, H. *Chem. Eur. J.* **2001**, *7*, 4386-4394.

[12] Jørgensen, K. B. *Molecules* **2010**, *15*, 4334-4358.

[13] Sudhakar, A.; Katz, T. J.; *Tetrahedron Lett.* **1986**, *27*, 2231-2234.

[14] Sudhakar, A.; Katz, T. J.; Yang, B. *J. Am. Chem. Soc.* **1986**. *108*, 2790-2791.

[15] Scott, L. T. *J. Org. Chem.* **2016**, *81*, 11535-11547.

[16] Rubin, Y.; Lin, S. S.; Knobler, C. B.; Anthony, J.; Boldi, A. M.; Diederich, F. *J. Am. Chem. Soc.* **1991**, *113*, 6943-6949.

[17] Baidossi, W.; Schumann, H.; Blum, J. *Tetrahedron* **1996**, *52*, 8349-8364.

[18] Goldfinger, M. B.; Swager, T. M. *J. Am. Chem. Soc.* **1994**, *116*, 7895-7896.

[19] Molins, E.; Miravitlles, C.; Espinosa, E.; Ballester, M. *J. Org. Chem.* **2002**, *67*, 7175-7178

[20] Liebman, J. F.; Greenberg, A. *Chem. Rev.* **1976**, *76*, 311-365.

[21] John, J. A.; Tour, J. M. *J. Am. Chem. Soc.* **1994**, *116*, 5011-5012.

[22] John, J. A.; Tour, J. M. *Tetrahedron,* **1997**, *53*, 15515-15534

[23] Johnson, J. P.; Bringley, D. A.; Wilson, E. E.; Lewis, K. D.; Beck, L. W.; Matzger, A. J. *J. Am. Chem. Soc.* **2003**, *125*, 14708-14709.

[24] Lockhart, T. P.; Comita, P. B.; Bergman, R. G. *J. Am. Chem. Soc.* **1981**, *103*, 4082-4090

[25] Grissom, J. W.; Calkins, T. L.; Egan, M. *J. Am. Chem. Soc.* **1993**, *115*, 11744-11752.

[26] Benati, L.; Capella, L.; Montevecchi, P. C.; Spagnolo, P. *J. Org. Chem.* **1995**, *60*, 7941-7946.

[27] Benson, S. W.; Shaw, R. *T. Faraday Soc.* **1967**, *63*, 985-992.

[28] Pati, K.; dos Passos Gomes, G.; Harris, T.; Hughes, A.; Phan, H.; Banerjee, T.; Hanson, K.; Alabugin, I. V. *J. Am. Chem. Soc.* **2015**, *137*, 1165-1180.

[29] Hu, K.; Yang, H.; Zhang, W.; Qin, Y. *Chem. Sci.* **2013**, *4*, 3649.